Reinforced Concrete Columns Under Seismic Lateral Force and Varying Axial Load

A Thesis
Presented for the Degree
of
Doctor of Philosophy in Civil Engineering
at the
University of Canterbury
Christchurch
New Zealand

By Xinrong Li

October, 1994

ABSTRACT

The project is carried out with the intention to study the strength and ductility of reinforced concrete columns subjected to simulated seismic horizontal loading and varying axial load.

First, an extensive review of previous research on the behaviour of reinforced concrete members and hysteretic modelling is provided.

Then, the experimentally investigation which involves testing a total of nine reinforced concrete specimens under simultaneously cyclic lateral loading and varying axial load is carried out. The first series of six reinforced concrete column units were tested to obtain the variations in flexural hysteretic behaviour with fluctuation in axial load level. In the second phase of experimental investigation, three specimens were tested to study the shear strength of reinforced concrete columns subjected to cyclic lateral loading and varying axial load with emphasis placed on the study of degrading concrete shear resisting mechanisms and comparisons with the present design code equations for shear strength.

Following the experimental program, the mechanisms of shear resistance and the factors affecting the shear strength are considered. In particular, the effects of alternating tension and compression axial load on the shear resisting mechanisms are studied. On the basis of experimental results, proposals are made for predicting shear strength of reinforced concrete column of ductility and limited ductility.

Next, the theoretical work was undertaken to investigate the elastic and post-yield flexural rigidities of reinforced concrete sections. The equations for determining the elastic and post-yield flexural regidities are presented. Also, a moment-curvature hysteretic model including varying axial loading effect is proposed. The theoretical predictions for the moment-curvature hysteresis relationship were found to compare well with the experimental results.

Finally, an example is given of inelastic dynamic response analysis of reinforced concrete frame using the proposed moment-curvature model which includes the effects of varying axial load on the yield moment, and loading and unloading stiffness of the structural members.

ACKNOWLEDGEMENTS

The research reported in this thesis was carried out at the Department of Civil Engineering, University of Canterbuty, New Zealand, under the overall guidance of its Head, Professor R. Park(former Head), and Dr. N. Cooke.

I wish to sincerely thank Professor R. Park, my senior supervisor, for his invaluable help, and guidance and encouragement, and Dr. H. Tanaka, co-supervisor of the project, for his helpful advice and opinions given on numerous occasions.

Special thanks are given to Emeritus Professor T. Paulay for his constant personal interest and fruitful discussions, to Dr. A. Carr for his assistance in the computer work, and to Professor M.J.N. Priestley for his fruitful discussion and comments.

Thanks are extended to the technical staff of the Department of Civil Engineering under the management of Mr G.E. Hill. In particular, thanks are due to Messrs N. Dixon, and J. Maley and G. Hill, for their valuable contributions to the experimental work; Mr. R Allen for his contribution of manufacturing the test frames; Mr H.H. Crowther for his assistance with purchase of the materials; Messrs P.J. Coursey and B. Hutchinson for their support with computer facilities. Thanks are also given to Mrs. V. Grey for drawing some of the figures in the thesis, and to Mr. M. Roestenbury for his photographic assistance.

The financial support and scholarship provided by the Ministry of External Relation and Trade, and the New Zealand Concrete Society and the University of Canterbury, are greatly acknowledged.

I wish to thank my fellow post-graduate student and visitors for their discussions and friendship. In particular, Drs. P.C.Chuang, L.L Dodd, Bing Li, J Restrepo, and Messrs. J. Maffei, S. Hakuto, Widodo, Y. Sato.

Finally, I wish to express my sincere gratitude to my wife, my son and my parents for their constant support, encouragement and understanding during the past years.

TABLES OF CONTENTS

NOTATION

A_b = Area of reinforcing bar

A_c = Area of core concrete of column section

A_e = Effective shear area of section

A_g = Gross area of column section

A_s = Area of longitudinal reinforcement

A_{sh} = Area of hoop bars and supplementary cross-tie confining reinforcement in one principal direction of column section

A_t = Area of longitudinal reinforcement

A_{te} = Area of stirrups required by code to tie the longitudinal bars

A_v = Area of shear reinforcement parallel to the direction of shear force

b = Overall width of rectangular column section

b_c = Width concrete core, measured to the centre-line of perimeter hoop

b_w = Width of web of concrete section

c = Depth of compression zone

c = Concrete cover thickness, measured to the centre-line of perimeter hoop

d = Effective depth of column section

d_b = Diameter of reinforcing bar

d' = Distance between the centre of extreme reinforcing bars

D = Overall diameter of circular column section of depth of column section

D' = Distance between centres of the periphery hoops

E_c = Modulus of elasticity for concrete

$(EI)_e$ = Effective flexural stiffness of the column section

$(EI)_{el}$ = Elastic flexural rigidity of column section

$(EI)_g$ = Elastic stiffness of gross section

$(EI)_{py}$ = Post-yield second slope rigidity

$(EI)_{re}$ = Inelastic reloading section stiffness

E_s = Modulus of elasticity for steel

E_{sh} = Strain hardening modulus for steel

E_{sec} = Secant modulus of confined concrete at maximum strength

E_u = Initial concrete modulus of elasticity at the onset of unloading

$(EI)_{un}$ = Inelastic unloading section stiffness

f = Section type factor

f_c = Concrete stress

f'_c = Concrete Compressive strength

f'_{cc} = Compressive strength of confined concrete

f_l = Transverse confining stress

f'_l = Effective transverse confining stress

f_{new} = Concrete stress on reloading curve

f_s = Steel stress

f_{su} = Ultimate strength of steel

f'_t = Tensile strength of concrete

f_y = Yield strength of steel

f_{yh} = Yield strength of transverse reinforcement

F_i = Horizontal static load at level i

F_t = Horizontal static load at top storey

g = Acceleration of gravity

G = Shear modulus

h = Overall depth of rectangular column section
or Storey height

h_i = distance between opposing of potentiometers

h" = Dimension of concrete core of section measured to outside of peripheral hoop

h_b = Overall beam depth

h_c = Concrete core dimension, measured to the centre-line of perimeter hoop

H = Applied lateral load

H^+_i = Theoretical lateral load corresponding to M^+_i

H^-_i = Theoretical lateral load corresponding to M^-_i

H^+_{max} = Theoretical lateral load corresponding to M^+_i

H^-_{max} = Theoretical lateral load corresponding to M^-_i

H_{max} = Maximum experimental lateral load

H^+_u = Theoretical ultimate lateral load

I = Moment of inertia of the gross concrete section

I_e = Effective second moment of area of section

I_g = Second moment of area of gross section

l_i = gauge length

L = Effective height of column

L = Live load

L_p = Equivalent plastic hinge length

L_r = Reduced live load

L_s = Live load at serviceability

m = Mass per unit length

M = Bending moment

M_b = Bending moment at balance failure point

M_{exp} = Experimental maximum bending moment

M_i = Ideal flexural strength calculated using code approach

M^+_i = Ideal flexural strength calculated using code approach corresponding applied maximum compression axial load

M^-_i = Ideal flexural strength calculated using code approach corresponding applied maximum

tension axial load

M_m = Flexural moment of column at ten times yield curvature

M_{max} = Maximum bending moment

M^+_{max} = Maximum bending moment in compression axial load cycle

M^-_{max} = Maximum bending moment in tension axial load cycle

M_0 = Flexural yield moment at zero axial load

M_{up} = Moment corresponding to axial load of two-third axial compression capacity

M_y = Flexural yield moment of concrete member

M'_y = Moment calculated at the first yield of longitudinal reinforcement, or when the extreme compressive fibre strain reaches 0.002, whichever is smaller

M^* = Bending moment in a previous loading step

N = Column axial load

P = Applied axial load

P_b = Axial load at balance failure point

P_e = Axial compression load on column due to design gravity and seismic loading

P_{max} = Maximum compression axial load applied to column

P_{min} = Maximum tension axial load applied to column

P_t = Axial tension capacity of column

P_{un} = Axial load at the onset of unloading

P_{up} = Applied axial load

P* = Axial load applied in a previous loading step

R = Ratio of maximum compressive strength of confined concrete to unconfined concrete

R = Risk factor

R_l = Reduction factor for live load

R_m = Bending moment reduction factor

R_v = Axial force reduction factor

s' = Clear spacing between hoop bars in which arching action of concrete develops

s_h = Centre-to-centre spacing of hoop sets

S = Structural type factor

t = Time

T = Natural period of vibration

v_b = Basic shear stress carried by concrete

v_c = Shear stress carried by the concrete mechanisms

v_{cf} = Residual concrete shear stress

v_{cr} = Average shear stress at onset of diagonal cracking

v_{cu} = Average shear stress resisted by the concrete at ultimate

v_u = Shear stress at maximum lateral load

v^-_{cu} = Shear stress resited by the concrete under tension axial load

v^-_{cf} = Shear stress resisted by the concrete under tension axial load at failure

V = Total applied shear force

V = Total horizontal seismic shear force at base

V_{ACI} = Shear strength calculated the equations of the American Code ACI 317-89

V_{Ang} = Shear strength calculated by the equations due to Ang et al[A7]

V_c = Shear resistance of concrete member provided by concrete mechanisms

V_{ci} = Initial shear strength of concrete component

V_f = Residual shear strength of concrete component

V_{cl} = Shear strength of concrete component for limited ductility

V_{col} = Column design shear force

V_{cu} = Shear resisted by the concrete at ultimate

V_{exp} = Maximum experimental shear strength

V^+_{max} = Maximum shear force in compression axial loading direction

V^-_{max} = Maximum shear force in tension axial loading direction

$V_{Priestley}$ = Shear strength calculated by the equations due to Priestley et al[P23]

V_n = Shear strength of column

V_{NZS} = Shear strength specified by code provisions of NZS 3101:1982 for outside plastic hinge region

V^p_{NZS} = Shear strength specified by code provisions of NZS 3101:1982 for inside plastic hinge region

V_i = Shear strength specified by code provisions

V^+_{if} = Shear force corresponding to ideal flexural strength M^+_i

V^-_{if} = Shear force corresponding to ideal flexural strength M^-i

V^+_{io} = Shear force corresponding to development of flexural overstrength

V_p = Shear strength enhancement due to column axial load

V_r = Shear force at failure under compression axial load

V^-_r = Shear at failure under tension axial load

V_s = Shear force carried by transverse reinforcement

V_u = Shear force at ultimate load

V^-_u = Ultimate shear force under tension axial loads

V'_y = Shear force at the first yield

y_i = Distance from centre of gauge length to the top of column base

α = a coefficient

β = a coefficient

Δ = Lateral displacement of column

Δ_c = Column deflection

Δ_f = Column deflection due to flexure

Δ_{fi} = Column deflection due to flexure

Δ_p = Lateral displacement of column due to plastic deformation along the member

Δ_s = Column deflection due to shear

Δ_{slip} = Column deflection due to bar slip at the base

Δ_y = Lateral displacement of column at yield

Δ_{yi}, Δ_{y2} = lateral displacement at 0.75 of ideal flexural strength in the positive and negative lateral loading direction

Δ'_y = Lateral displacement at the first yield

Δ'_{yf} = Displacement at the first yield due to flexure

Δ'_{ys} = Displacement at the first yield due to shear

δ_{Ei} = Observed vertical displacement

δ_{Wi} = Observed vertical displacement

δ_{slip} = Displacement due to bar slip at column base

ε_c = Concrete compressive strain

ε_{cc} = Strain at maximum confined strength of concrete

ε_{cu} = Ultimate concrete compressive strain

ε_{Ei}, ε_{Wi} = Longitudinal strain of column section

ε_k = Contact strain in concrete model

ε_{ro} = Concrete strain at reloading reversal

ε_{un} = Unloading strain of concrete

ε_{pl} = Plastic strain in concrete model

ε_{sh} = Steel strain at commencement of strain hardening of steel

ε_{spall} = Compressive strain at which unconfined cover concrete spalls

ε_{su} = Ultimate strain of steel

ε_y = Yield strain of steel

θ = Angle of inclination of diagonal strut to the longitudinal axis

θ_i = Average rotation of column section over the gauge length

θ_p = Equivalent plastic hinge rotation

λ_1, λ_1 = Coefficients

μ_n = Nominal displacement ductility factor

ρ_s = Volumetric transverse reinforcement ratio

ρ_t = Total longitudinal reinforcement ratio

ρ_w = Tensile reinforcement ratio

ϕ = Column curvature

ϕ = Strength reduction factor

ϕ_i = Average column curvature over gauge length

ϕ_m = Curvature at ten times yield curvature

ϕ_{un} = Curvature at onset of unloading

ϕ_y = Yield curvature

ϕ'_y = Curvature calculated at the first yield of longitudinal tension steel, or when the extreme compressive fibre strain of concrete reaches 0.002, whichever is smaller

ϕ_{max} = Maximum curvature

ϕ^* = Curvature at a previous loading step

$\delta 1$, $\delta 2$ = Diagonal displacement of column panel

γ_i, γ_1, γ_2 = Shear deformation of column panel

ω = Dynamic magnification factor

Chapter 1

Introduction

1.1 GENERAL

The principle performance criteria used for the design of multistorey structures for earthquake forces expected during the useful life of the building, as adopted in many seismic design codes, are:

☞ to resist minor earthquakes without damage.

☞ to resist moderate earthquakes without structural damage, but perhaps with some non-structural damage.

☞ to resist major earthquakes without collapse, but perhaps with structural and non-structural damage.

These criteria have arisen because it is uneconomical to design a structure to remain elastic during major earthquake attack. When a structure responds elastically to ground motions during a severe earthquake, the maximum response acceleration may be several times the maximum ground acceleration depending on the stiffness of the structure and the magnitude of damping[P1]. The structure would need

to be designed for very high strength in order to respond elastically to such high inertia load. By contrast, when a structure is designed in which some of its members will experience certain amount of post-elastic excursion associated with permanent deformation and stiffness and strength deterioration, the lateral inertia forces induced in the structure for the same ground acceleration will be significantly reduced.

Most building codes recommend design seismic forces which are generally much less than the inertia force induced if structures responded in the elastic range to severe earthquake. The strengths of structures are a fraction, as low as about one-sixth or less than that corresponding to elastic response, and to expect the structure to survive an earthquake by large inelastic deformations and energy dissipation corresponding to material distress[P6].

To enable the structures to dissipate seismic energy through inelastic deformation at the critical regions of members, and to increase damping and lengthen the fundamental period of vibration of structure so as to reduce the response during earthquake, it is required that the structure to be properly designed and detailed. The ductile design method was therefore developed to ensure that the inelastic deformation demand for the members could be met. The capacity design approach due to Park and Paulay[P6,P12] is a well developed ductile design strategy. In capacity design of a moment resisting frame, a beam sidesway mechanism is chosen for the mechanism of inelastic deformation, in which the inelastic deformations of the structure occur mainly by flexural yielding of the beams, rather than by flexural yielding of the columns. The chosen regions of yielding are designed for adequate strength and ductility to resist design seismic actions. The remainder of the structure is then designed for amplified actions to ensure the flexural yield does not occur[P4].

In a beam sidesway mechanism, the plastic hinges will normally be located at the ends of beams. However, some plastic hinges of columns may be inevitable during a very large earthquake because to eliminate the possibility of plastic hinging in columns would require columns very much stronger than the beams[P6]. Also, at the base of columns of multistorey frame, the plastic hinging in column can help to complete the inelastic deformation mechanisms. In the bridge structures, it is neither feasible nor desirable to locate the plastic hinge in the superstructure, and hence the columns tend to be the primary source of energy dissipation[P23]. Furthermore, with the uncertainties of earthquake loading and overall structural response, it is difficult, if not possible, to avoid inelastic deformation in the columns. The aim of the design procedure for these columns is, therefore, to provide sufficient deformation capacity and shear strength to ensure that the columns behave in ductile manner under seismic actions and no shear failure occurs.

1.2 REVIEW OF PREVIOUS RESEARCH ON THE DUCTILE BEHAVIOUR OF REINFORCED CONCRETE COLUMNS

1.2.1 Previous Studies

During the past ,twenty years, extensive research has been aimed at the design method of reinforced concrete columns to achieve sufficient ductility and to suppress the shear failure. It is now generally accepted that adequate ductility of a reinforced concrete column can be achieved by means of providing sufficient transverse reinforcement in the plastic hinge regions to confine the core concrete of the section, to prevent premature buckling of the longitudinal reinforcement and to provide adequate shear reinforcement. However, the provisions of various seismic design codes indicate that significantly different approach exist for the detailing of confining steel in the plastic hinge regions[P8]. Based on the considerations of maintaining of the axial load capacity of the section after the cover concrete has spalled, the ACI code 318:89[A3] prescribes the quantity of confining steel for columns with axial load level greater than about 10% of the axial compression strength.

During the last 20 years extensive testing and analysis have been carried out to investigate the strength and ductility of reinforced concrete columns subjected to simulated seismic loading, in New Zealand particularly, and to verify the effect of confinement of transverse reinforcement on the available ductility of the column.

Gill et al[G1] and Potangaroa et al[P19] conducted tests on full size square and octagonal reinforced concrete columns with various quantities of confining reinforcement. The constant compression axial load level studied ranged from $0.21f'_cA_g$ to $0.7f'_cA_g$, and shear span to depth ratio was about 2.2. The hoops provided in test columns were designed according to the recommendation of the draft New Zealand concrete design code DZ 3101:1978[D2]. The test columns demonstrated very ductile behaviour and reached displacement ductility factors of at least 6, indicating the adequacy of the amount of confining steel proposed by draft code provisions. It was observed that considerable enhancement of flexural strength over that calculated on the basis of ACI stress block, and the larger maximum concrete strain at the extreme compression fibre of the concrete core. The degree of strength enhancement was found to depend on the axial load level.

Ang et al[A6] conducted the tests on octagonal and square columns of more slender aspect ratio(4.0), as continuation of Gill's and Potangaroa's works[G1,P19], to study influence of the change in aspect ratio on the section ductility. All of the test columns effectively reached displacement ductility factor

of at least 8. It was observed that the extreme concrete fibre strains at first crushing were about 0.008 to 0.01, which are much larger than that assumed in normal code design procedure for calculate of flexural strength. Flexural strength of the columns exceeded theoretical predictions based on ACI stress block, with an extreme fibre compression strain of 0.003, by between 18% and 90%.

The deformation capacity is a very important properties of structural member in the seismic design. The term "ductility" has been used by many investigators to represent the ability of a structure to undergo large amplitude cyclic deformation in the inelastic range with a substantial reduction in the strength. Ductility factors can be expressed as the ratio of the maximum available deformation(displacement, rotation or curvature) to the yield deformation. When calculating ductility factor of a reinforced concrete member, it is essential to adequately define the yield deformation since reinforced concrete member normally exhibits nonlinear behaviour even at very low stress stage. Park[P2] compared several alternative definitions to estimate the yield deformation. He suggested that the yield deformation should be estimated from an equivalent elasto-perfectly plastic system with elastic stiffness which includes the effects of cracking and with the same ultimate load as the real system. The maximum available deformation should be estimated as that post-peak deformation when the load carrying capacity has reduced by a small specified amount, or when the reinforcement fractures or buckles, whichever occurs first. This definition has been conventionally used in New Zealand in the evaluation of ductility of test assemblages from laboratory testing.

Zahn et al[Z2] tested four reinforced concrete columns with 400mm square cross section to investigate the effects of loading along a section diagonal causing biaxial bending on the column behaviour. The column contained approximately the quantity of transverse reinforcement recommended by the current New Zealand code NZS 3101:1982[S14], and with constant compression axial load ranged from $0.23f'_cA_g$ to $0.48f'_cA_g$. The test columns exhibited satisfactory behaviour with displacement ductility exceeding about 8. They concluded that no special detailing requirements need to be develop to cater for the biaxial loading column.

Mander et al[M2] conducted test on four hollow rectangular reinforced concrete columns with effective shear span length of 3.2m, and a 750mm square cross section and 120mm wall thickness. The columns were tested as cantilever in single bending curvature. The applied axial load was $0.1f'_cA_g$ to $0.5f'_cA_g$. The amount of transverse steel present in the plastic hinge regions of the test columns were 53% to 83% of that required by the New Zealand concrete design code[S14] for full ductile design. It was concluded that the provisions of the current New Zealand code NZS 3101:1982[S14] can be used to detail the transverse reinforcement in the flange of hollow column in the same manner as for solid column.

Tanaka et al[T3,T4] conducted simulated seismic load tests on eight square reinforced concrete columns,

to investigate the effectiveness of alternative end anchorage details for transverse reinforcement in column. The constant compression axial load was $0.2f'_cA_g$. The transverse reinforcement in the specimens involved perimeter hoops with 135-deg hooks, crossties with 90 and/or 180-deg hooks, and "U' or "J' shaped crossties and perimeter hoops with tension splices. It was indicated that the interior cross tie with a 90-deg hook at one end and 180-deg standard hook at the other end behaved satisfactorily only before the yielding of cross tie and spalling of cover concrete. The perimeter hoops formed "U' bars lapped in the cover concrete must not be used because of the rapid reduced effectiveness in confining concrete when loss of cover concrete occurred.

Priestley and Park[P22] in reviewing the results from both experimental and analytical studies at the University of Canterbury concluded that the columns designed in accordance with detailing requirements of New Zealand concrete code[S14] demonstrated ductile behaviour and can reach dependable displacement ductility factors of at least 6. The prediction of the flexural strength of confined columns on the basis of the ACI concrete compressive stress block, which assumes a mean stress of $0.85f'_c$, an extreme fibre concrete strain of 0.003, was inevitably conservative. They suggested that flexural strength enhancement above the moment predicted by ACI method can be estimated by an empirical equation developed by Ang et al[A6]. In this equation the strength enhancement due to confinement, for columns containing about the New Zealand code NZS 3101:1982[S14] recommended quantities of transverse reinforcement, is related only to the axial load ratio. The test results reported by Sheikh et al[S11] indicated that the strength enhancement observed in their tests were much lower than that predicted by Ang's equation. Some of the columns with axial load in range of 0.6 to $0.78f'_cA_g$ did not even reach the ACI moment capacity. However their tests were for a member without a stub near the critical section. Sakai and Sheikh[S7] commented that flexural strength enhancement in the columns tested at the University of Canterbury may come from significant contribution of the stubs near the critical section, which simulated the presence of a beam or foundation member. Sheikh and Khoury[S10] demonstrated that a stub can provide additional confinement to the adjacent section, and increase section moment capacity by more than 20%.

While extensive research has been conducted on the behaviour of reinforced concrete columns under uni-directional and bi-directional cyclic loading. The information on the effects of fluctuations in axial load, which can be generated in the columns of structure under earthquake attack, on the response of the column is very limited. A few work in this area is listed below.

Abram[A1] carried out an experimental study on ten reinforced concrete column specimens to investigate the effects of variations in axial force on the flexural behaviour. The test specimens were deflected in single bending curvature. In this study, the axial load applied to the columns was varied directly with either the moment at critical section or the lateral deflection. The range of variation in axial load was $0.07f'_cA_g$ in tension to $0.32f'_cA_g$ in compression. The results of this experimental study

demonstrated that variation in axial load can significantly effect the strength, stiffness and deformation capacity of reinforced concrete columns. Due to the effects of axial force variation on stiffness, more shear force will be attracted to the stiffer and strong column. The shear strength should be provided in accordance with the more realistic distribution.

Kreger and Linbeck[K3] reported three tests conducted on one-half scale reinforced concrete columns. Of the two of specimens tested, the relationship between the lateral load and axial column load applied was coupled and in direct proportion to each other. The other specimen was subjected to uncoupled lateral load and axial load. It was shown that the behaviour of the column depended greatly on the histories of the axial force. The observed response of the reinforced concrete columns under varying axial load was significantly different from those of columns subjected to reversals of lateral load under constant axial force.

Li et al[L1] tested a series of quarter-scale reinforced concrete cantilever columns under varying axial column load and bidirectional lateral reversals. The axial load applied was varied proportional to the lateral resistance of the columns. The lateral load-displacement hysteresis loops for the columns tested were observed to have a non-symmetrical characteristics.

Saadeghvaziri and Foutch[S1] reported the results of an analytical investigation in which nonproportional variations in axial load and lateral were considered. Several types of variation of axial load histories were investigated. The results indicated that under nonproportional variations in axial force and lateral load, the hysteresis curves were not Masing type, showing considerable pinching effect. The lateral shear-displacement hysteresis loops demonstrated anomalies referred to as "negative energy" dissipation capacity. The cause of this abnormal behaviour was explained as due to the axial deformation and axial hysteresis energy. They commented that axial deformation could have significant effect on the total energy dissipation capacity of structural system. Under fluctuating axial force, considerably alternate yielding in tension and compression could occur.

More recently, Saadeghvaziri et al[S2] carried out an analysis on the influence of vertical ground motion on the dynamic response of highway bridge. Vertical motion generates fluctuating axial force in the columns. This analytical studies showed that hysteresis loops of column and piers are very unstable and asymmetric, owing to uncoupled variations in the axial load. They demonstrated significant fluctuation in the stiffness and strength of the columns. As a result of compressive axial load the column stiffness increased. Consequently, the amount of lateral shear and moment carried by the column increased. This in return, increased the possibility of failure in the column. On the other hand, tensile axial force reduced the shear and moment capacity of the cross-section, which may lead to shear failure or yielding of column under bending moments that are much lower than the anticipated design capacity.

1.3 REVIEW OF PREVIOUS RESEARCH ON THE SEISMIC SHEAR BEHAVIOUR OF REINFORCED CONCRETE MEMBERS

1.3.1 Previous Studies

As noted previously the formation of plastic hinges in some columns of structures cannot be avoided during earthquake excitation even for the building designed to achieve a beam-sidesway mechanism. This makes it important to insure that columns are capable of behaving in a ductile manner. While the columns develop their maximum flexural capacity, the premature shear failure, either within the plastic hinge regions or elsewhere, must be prevented because of its unstable hysteretic behaviour under cyclic loading and serious consequences. In the slender columns, the behaviour is primarily controlled by flexure. In short columns, however, high shear forces are required to fully develop the flexural capacity of the member and the members loaded cyclically with high shear forces generally exhibit degradation of load carrying capacity, In this case, the shear may become critical. In the capacity design, the design column shear forces across the column are obtained from the equilibrium of the forces corresponding to the development of the flexural overstrength[P12]. Consequently the design column shear force is not directly related to the design horizontal inertia loading specified by the code, but depends on the maximum feasible flexural strength that can be developed in the plastic hinges of the column[P20].

Shear failure of short columns are sometimes reported to occur in recent earthquakes. The columns shear failures reported in both the 1968 Tokachi-Oki Earthquake in Japan[A9] and the 1971 San Fernaado Earthquake in California[J1] highlighted the possible shear problem under seismic actions. More recently, shear failure of columns and piers(Figs.1.1 to 1.3) was reported in the 1992 Erzincan Earthquake, Turkey[J3]. Fig.1.4 shows the latest examples of shear failure in the column of frame structure, during the 1994 Northridge Earthquake of Los Angeles[B4]. The post-earthquake observations have indicated that the short columns damaged during earthquakes were suffered large deformation and shear distress. The shear failure was explained as due to unexpected high seismic forces and poor detailing of transverse reinforcement. If the shear strength of the column is really greater than the maximum probable flexural strength, the column should have not failed in shear before yielding. This indicated that the shear strength of the column in reality might have been less than, or degraded under earthquake excitation below, the anticipated value . This has warranted the need for further research on the shear strength of columns, especially when the column is subjected to complex loading histories.

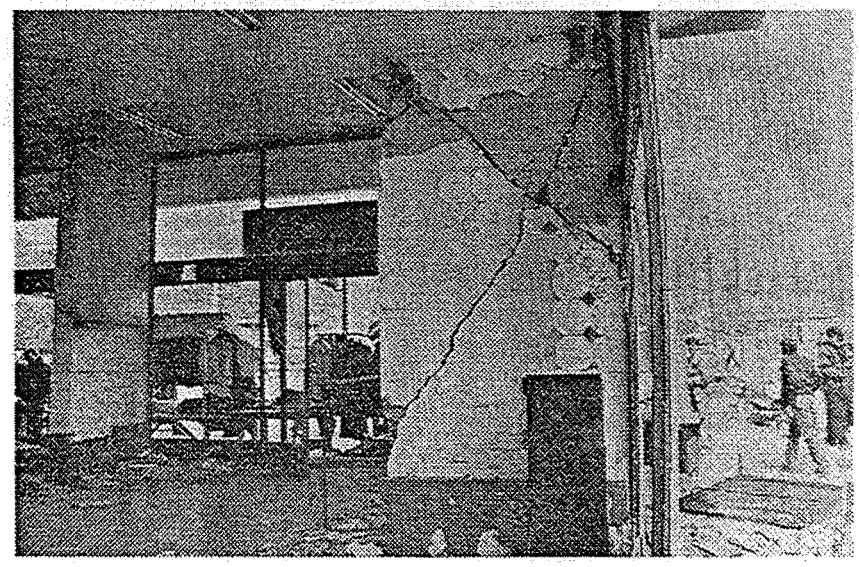

Fig.1.1: Shear failure of a column in the first floor of building(Erzincan Earthquake[J3])

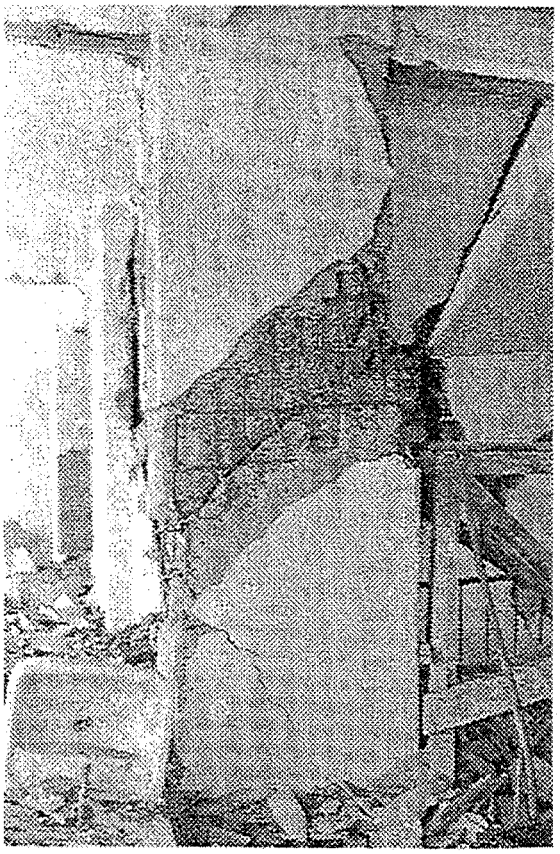

Fig.1.2: Shear failure at mod-height of reinforced concrete column(Erzincan Earthquake[J3])

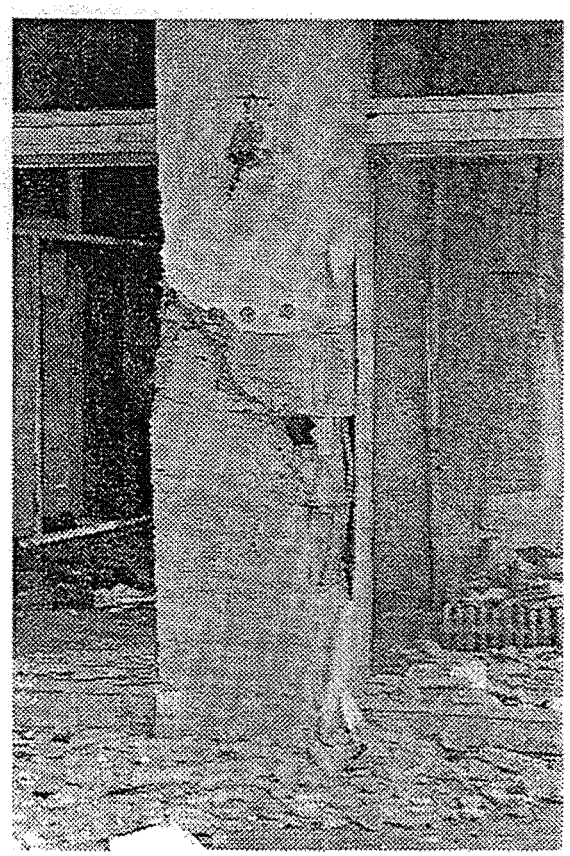

Fig.1.3: Shear failure in a column of building(Erzincan Earthquake[J3])

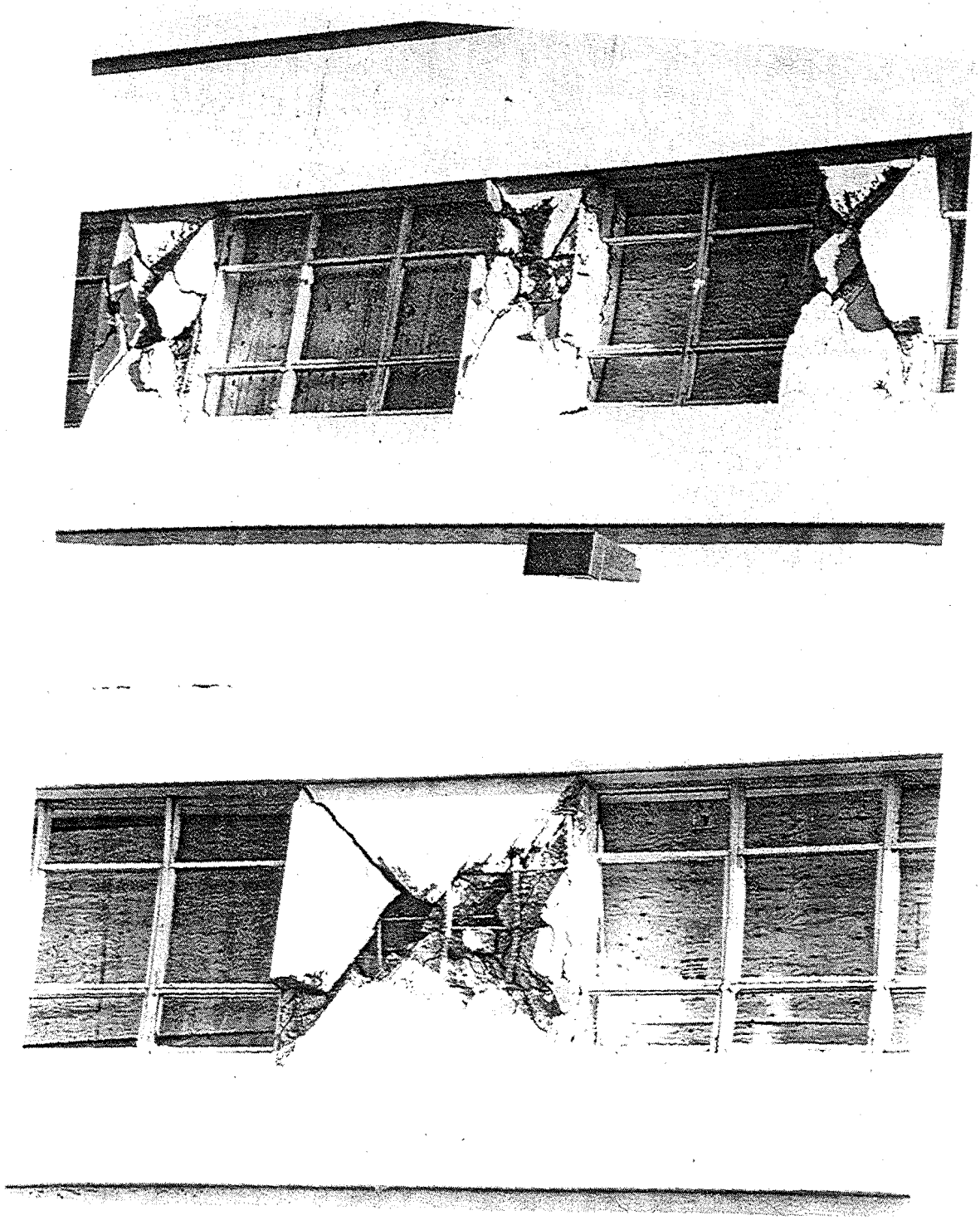

Fig.1.4: Shear failure in the reinforced concrete floor piers, St John's Hospital, Northridge earthquake 1994[B4], photo courtesy of D Bull.

Extensive research work has been conducted during past 20 years regarding the shear behaviour of reinforced concrete members. However most of it has concerned uniaxial loading. There have been only limited studies on the influence of multi-directional loading on shear behaviour of reinforced concrete columns. Also, very limited test data is available on the effect of varying axial load on the shear behaviour of reinforced concrete columns. In following sections, a number of experimental studies concerning with the shear behaviour of reinforced concrete columns will be reviewed, to reflect the main aspects affecting the characteristic of reinforced concrete columns.

The early experimental investigation was most concentrated on the mechanisms of shear transfer in the reinforced concrete. The laboratory tests were carried out on the reinforced concrete beams with or without web reinforcement by Mattock, et al[M8] and Fenwick et al[F1,F3], and the test specimens were monotonically loaded to failure[B3, L4]. The progress and research on the shear mechanisms in reinforced concrete since 1960 was summarized by ASCE-ACI Task Committee 426 in A State-of-the - Art report[A3], based on the review of over 2000 references dealing with various aspects of shear strength and behaviours. The main types of shear transfer are recognized to consist of (1) shear stress in the uncracked concrete; (2) aggregate interlock shear transfer; (3) dowel shear of longitudinal reinforcement; (4) shear reinforcement.

Early studies on reinforced concrete members under shear reversal have been limited to members with no axial load. To determine the effects of axial force on the shear strength of reinforced concrete members, Viest and Baldwin[V1] conducted tests on a knee frame. The applied axial compression load in terms of ratio of axial force to the shear ranged from 0 to 6. It was found that axial load had some effect on the shear strength capacity. Both diagonal cracking shear strength and ultimate shear strength increased with axial compression load. The test results also indicated that at shear compression failure, the compatibility of strains and equilibrium of forces were affected by the axial compression load.

The test results reported by Haddadin et al[H1] on reinforced concrete members with web reinforcement, subjected to axial force in addition to shear and bending, indicated that the crack width was significantly affected by the axial forces. They concluded that the effectiveness of web reinforcement in resisting shear was not altered by the presence of axial force in the members. Even with the presence of tension axial force, the effectiveness of web reinforcement was not reduced. They also showed that the effectiveness of web reinforcement in increasing shear strength is greater in the case of diagonal tension failure than at shear compression failures.

Yamada and Furui[Y2] investigated the influence of shear span ratio, axial load level, and web reinforcement on the behaviour of tied columns. It was shown that when the axial compression load was

increased, or when either shear span ratio or web reinforcement reduced, the ductility of the column decreased significantly. The shear resistance increased with an increase in axial compression load or a decrease in shear span ratio. Later Yamada[Y1] studied the mode of failures and found that there existed a critical shear span ratio between brittle shear of short column and ductile bending of long column. The value of critical shear span ratio was a function of reinforcing index, $\rho_t f_y/f'_c$, and axial load level, where ρ_t is total longitudinal reinforcement ratio. Hirosawa et al[H2] reviewed a number of Japanese column tests and concluded that the axial load could enhance the shear strength of the columns. They suggested that the effect of axial loads could be accounted for by including a term of $\alpha(N/A_g)$ in the shear carried by concrete, where N is the axial force, α is a coefficient.

The influence of longitudinal steel ratio on the shear resistance of reinforced concrete beams was experimentally investigated by Elzanaty et al[E1]. The tension longitudinal reinforcement ratio, $\rho_w = A_s/b_w d$, in the test beams ranged from 0.6 to 3.3%, and concrete compressive strength ranged from 21 to 79MPa. The shear strength of test beams without stirrup increased with increasing ρ_w for all concrete strength. The comparison of their results with ACI code equations [A3] for shear strength showed that the code equation underestimates the importance of longitudinal steel for high ρ_w value, and overestimates its effect when ρ_w is low. For the concrete compressive strength of about 40MPa, the code equation becomes unconservative as the longitudinal steel ratio, ρ_w, is less than 1.4%.

Wight et al[W3] tested twelve specimens, representing that part of a column between the points of contraflexure above and below a story level, subjected to large transverse displacement reversals. The main variables included axial load(0 to $0.15f'_cA_g$), the transverse reinforcement ratio(0.33 to 1.47%) and deflection level. It was found in this study the decay in shear strength as a result of loading into inelastic range and cycling the inelastic deflection was related to a change in the shear carrying mechanism of the member. The rate of shear strength decay was a function of axial load, amount of transverse reinforcement and displacement level. The presence of a compressive axial load slowed the decay in the strength and stiffness with cycle. It was suggested that the transverse reinforcement must be designed to carry the entire shear if the member is expected to resist large shear reversal in the inelastic range. It was also emphasized the importance of effective confinement to core concrete, since the loads applied to a reinforced concrete members are ultimately carried by the concrete and if the concrete does not stay intact, the strength of the reinforcement cannot be developed.

While a large number of studies was conducted on the shear strength of reinforced concrete with various patterns of uni-directional cyclic loading, the experimental investigations were also carried out to examine the effect of deformation path on the shear strength and deterioration of reinforced concrete columns. A large test program was subsequently conducted in the University of Texas at Austin to investigate behaviour of short reinforced concrete column under uni-directional and multi-directional load histories. Jirsa et al[J2] and Maruyama et al[M5] conducted test on four short columns. the

specimen simulated a short column framing into a stiff floor system. All specimen had an identical geometry with an aspect ratio of 1.5. The principle variable included loading histories and axial load level(0 to $0.2f'_cA_g$). The two of the specimens were tested with alternating axial tension and compression axial load in addition to lateral load in the two orthogonal directions.

The results indicated that the level and mode of axial load greatly effected the shear behaviour of the member. The presence of constant compressive axial force increased the initial stiffness and the maximum lateral capacity of the column. But the compressive axial load increased the rate of degradation of shear strength for the deflections greater than the deflection at which the maximum shear strength of the column was achieved, and also decreased the deflection at which degradation initiated. It was commented based on limited data that the application of axial tension alternating with compression influenced member performance only while the tension or compression was applied. They concluded that the application of axial tension alternating with compression was no more severe than the constant compression axial load. The comparisons indicated previous loading in either direction of simultaneous loading histories did not significantly affect the ultimate shear strength of the column. However, shear strength deterioration was much more severe under loading histories.

Woodward et al[W6] conducted tests on 12 specimens to investigate the effect of varying amounts of transverse and longitudinal reinforcement on the behaviour of short reinforced concrete columns. The specimens were tested in double bending curvature, representing a structural column bounded by stiff framing members. It was observed that the degradation began at the deflection level where the maximum lateral load was achieved and continued with both cycling and increased deflections. The shear capacity was most dependent on the capacity of the concrete to resist shear before inclined cracking. After diagonal cracking, the shear resistance of the column was strongly related to the effectiveness of aggregate interlock. Therefore, the primary function of the transverse reinforcement was to control the width of the inclined cracks to maintain the effectiveness of the aggregate interlock. The bond degradation was also observed to relate to the boundary and loading conditions imposed on the teste specimens.

Umehara et al[U1] investigated the shear strength of bidirectionally loaded rectangular short columns as compared with square columns. The variables in this study and loading histories were similar to those in previous studies by Maruyama et al[M5] and Woodward et al[W6]. Their tests showed that the maximum shear strength of the short column was not significantly influenced by previous loading in perpendicular directions unless the deformation in that direction exceeded the deflection corresponding to the maximum shear strength of the column under uni-directional loading. Based on 20 tests they concluded that the shear capacity of columns under diagonal uniaxial loading could be estimated using a circle of ellipse curve.

Zagajeski et al[Z1] tested seven short reinforced concrete column subjected axial load cyclic shear reversals. Each specimen represents the component of a one bay two storey in a typical spandrel wall frame. The specimen was deflected in a double bending curvature with aspect ratio of 1.5, and subjected to compression axial load(0.21 to $0.3f'_cA_g$). Three distinct failure modes were identified in the tests, a shear compression failure, a bond failure, and a diagonal tension failure. High nominal shear stress($0.7\sqrt{f'_c}$ to $0.87\sqrt{f'_c}$MPa) were developed and maintained while the model columns experienced significant inelastic deformation. It was observed that the maximum shear achieved under monotonic loading was slightly higher than that under cyclic incremental loading. Relative story rotation ductilities greater than 6 were observed in specimens under monotonic loading, and greater than 4 were observed in specimens under cyclic incremental loading before brittle shear failure. The test indicated that presence of transverse reinforcement can improve the ductile behaviour of the column. The presence of relatively high axial force can enhance the cyclic shear resistance. It was also noted that the magnitude of the axial load should be less than, or at most equal to, the balance point axial load, and sufficient transverse reinforcement should be provided.

Aschheim and Moehle[A10] reviewed experimental tests recently conducted on both circular and square reinforced concrete columns and concluded that column shear strength (a) increases with increasing amount of transverse steel, (b) increases with increase in compression axial load, and (c) decrease with increasing displacement demand and with multi-directional loading.The deformability of the column (a) decreases as shear demand increase, (b) decreases with decreasing transverse steel ratio, and (c) decreases with multi-directional loading. An increase in axial load can result in more brittle failure of a column once failure commences.

The major aspect affecting the shear behaviour of reinforced concrete members is generally recognised. The effectiveness of each parameter on the shear strength is far from fully understood. Previous experimental studies indicated that the shear strength increased with concrete compressive strength f'_c. Provisions for the shear strength in the current codes, such as the ACI code[A3] and the New Zealand Code[S14], are mainly based on experimentally derived equations. The basic data used in deriving these equations were conducted on the members with low concrete compressive strength. The current ACI code and the New Zealand Code relate the shear strength to the concrete compressive strength, f'_c, with a power equal to 0.5, while some investigators[Z6, P18] based on their test results pointed out that increase in shear strength is proportional to f'_c with a power close to 0.3. Ahmad et al[A4] found that a better correlation can be achieved by using a power of 0.333 to determine the effect of concrete strength on the shear strength. The results from tests, conducted by Elzanaty et al[E1] on the reinforced concrete beams using concrete with compressive strength ranging from approximately 20 to 83 MPa, indicated the current ACI code[A3] equations for shear strength was quite conservative for lower concrete strength(below 30MPa), and became unconservative for medium-to-high concrete strength. This trend became more significant for the members with low longitudinal reinforcement ratio. The reduced

effect of concrete strength on the shear resistance was attributed to the decreased shear force carried by aggregate interlock with increase in f'_c, because the crack surface became distinctly smoother for higher concrete strength.

While a large number of tests have been concentrated on confirming the effect of the amount of transverse reinforcement on the flexural behaviour of the column to achieve required ductility, as reviewed in previous section, the experimental investigations on the shear strength of reinforced concrete members has been extensively conducted at the University of Canterbury since 1970. O'Leary[O1] tested ten reinforced concrete beams subjected to shear and tension axial force. The ratio of applied axial force to shear force remained approximately constant throughout each test. It was found that the crack patterns of the beams with axial tension were similar to those in shear span of beams with no axial force and of similar shear span ratio. The inclination of critical diagonal crack to the longitudinal axis was around 45-deg. Within the range of tests, the amount of axial tension applied did not substantially effect the diagonal cracking load. But axial tension did decrease the member stiffness. It was also concluded that the stirrup spacing had little influence on the shear resistance of the test beams provided that more than one stirrup crossed the critical diagonal crack.

Ang et al[A7,A8] reported the results of a compressive test program investigating the shear strength and ductility of squat circular columns subjected to different levels of axial compression and uni-directional cyclic displacement of gradually increasing amplitude. The results indicated that the maximum experimental shear strength was the function of axial load level, the column aspect ratio, and the amount of transverse spiral reinforcement. It further confirmed the dependence of shear strength as a function of flexural displacement ductility factor. From experimental observations of the columns subjected to uniaxial cyclic loading, it was found that the existing design equations for the shear strength are inconsistent and very conservative for the initial shear strength. The shear strength reduced with increasing flexural displacement ductility factor in excess of 2. They developed a model to represent the influence of flexural ductility on shear strength of concrete shear resisting mechanism. The shear strength of concrete component is expressed by bilinear function. An initial shear strength before degradation is applicable for low ductility level, a final shear strength after significant degradation applicable for high ductility levels. For moderate ductility levels the shear strength is represented by a degrading straight line. The displacement ductility factor at which degradation started is assumed to be 2.0.

Consequently, Wong et al[W4,W5] tested sixteen circular reinforced concrete column with aspect ratio of 2.0 and different spiral reinforcement content under various displacement patterns and axial compression intensities. The results from this study further confirmed the findings of previous research[A7]. It was found that the influence of various biaxial displacement patterns on the reduction of initial shear strength and ductility capacity of squat columns was not significant. However, the biaxial

displacement pattern led to more severe degradation of shear strength and stiffness and hence energy dissipation. The displacement ductility level at which shear strength decay occurred during biaxial displacement was about one unit less than that of identical column subjected to uniaxial loading pattern.

Priestley et al[P23] examined the aspects relating to the shear strength of circular and rectangular columns under seismic loading in their large test program on assessment and retrofit of bridge columns susceptible to shear failure. It was recognized that the shear strength of the concrete mechanisms gradually degrades with flexural ductility demand. The shear strength model, developed by Ang et al(1985) to represent the interaction between flexural ductility and shear strength, was further refined. The effect of axial force on enhancing shear strength was modeled by arch action forming an inclined strut along the column height. An innovation in modeling of shear strength is that they separated the shear strength enhancement provided by axial compression force from the conventional "concrete contribution' of shear strength. It was shown that the proposed model give significantly improved prediction of shear strength than other existing shear strength methods.

1.3.2 Conclusions

The past research has led to understanding of the behaviour of reinforced concrete failing in shear to the extent that a fairly realistic description of shear behaviour can be presented. The main parameters affecting the shear strength of columns are: concrete compressive strength, shear span ratio, axial force, the amount of transverse reinforcement crossing the critical diagonal cracks, and the longitudinal reinforcement content.

The general tendency in a codified design procedure for shear strength assumes a portion of the shear resistance to be resisted by transverse reinforcement. This portion of shear resistance is accomplished by an assumed truss analogy. The rest of shear resistance of all mechanisms other than the truss mechanism is assigned to a term, known as the concrete mechanisms. This assumption is for the convenience of designers. The shear resistance of the concrete mechanisms includes contributions from shear transfer in the uncracked concrete compression zone, aggregate interlock across diagonal cracks, as well as dowel action of longitudinal reinforcement. When establishing a predictive equation for the shear strength, the difficulty arises in assessing the effect of each parameter on the shear strength, due to the interactions between various shear resisting mechanism and change of shear carrying mechanism during cyclic loading. Before cracking, the shear force is mainly carried by the concrete. The formation of diagonal cracks reduces the compression area while the shear deformation along the cracks calls on the aggregate interlock action and dowel force. The effectiveness of aggregate interlock along an inclined crack is related to the restraint of transverse reinforcement on the crack width. The concrete strength, which the shear capacity of the column will ultimately rely on, is also affected by the degree

of confinement.

The current design code provisions for shear strength have largely been based on the results of reinforced concrete beams failing in shear. Moreover, most of previous tests considered only monotonic loading. The codes apply these results with much caution when predicting the shear strength of reinforced concrete columns, and hence result in some conservatism. The research on shear strength of reinforced concrete column with a realistic distribution of longitudinal reinforcement along the sides of section is very limited. The effects of axial force on the failure mechanism and shear resistance are still not fully understood. The research on the effect of varying axial load on the shear strength of reinforced concrete column is very limited.

1.4 REVIEW OF PREVIOUS RESEARCH ON THE HYSTERETIC MODELLING OF REINFORCED CONCRETE MEMBERS

1.4.1 Previous Studies

The accurate inelastic response analysis of reinforced concrete structure requires reliable models which can simulate the strength, stiffness and energy dissipation characteristics of the members and joints. Structures subjected to strong ground motions generally undergo nonlinear deformation. The post-elastic deformations are always accompanied by the deterioration of member stiffness, and degradation of load capacity as well as energy dissipation capacity. The hysteresis behaviour of reinforced concrete columns varies considerably, depending on the member properties and imposed loading histories. It may be affected by many factors such as cracking of concrete, opening and closing of cracks, yielding of the reinforcing steel, bond deterioration and bar slip. Various hysteresis models have been developed to describe these aspects of the behaviour of columns. No one hysteresis model can consider every aspect of reinforced concrete hysteretic response accurately[S3].

A brief review is presented in this section to reflect the feature of different hysteresis models and to highlight the aspect of hysteretic modelling affecting the response histories.

The elastic-perfectly plastic model, initially developed for perfectly elasto-plastic materials shown in Fig.1.5, is not suitable for reinforced concrete members where the inelastic deformations are expected.

Due to its simplicity this model has been used by many investigators to give the general response of reinforced concrete structure, although no degradation of stiffness or strength variation is considered in the model.

Clough[C1] developed a model(Fig.1.6) to represent degrading stiffness due to cracking. The strain hardening characteristics was also considered by a post-yield stiffness which is greater than zero. This model is suitable for flexural dominated elements which show stable hysteresis loops and strength enhancement due to strain hardening.

Takeda et al[T2] developed an improved degrading stiffness model(Fig.1.7) on the basis of experimental observations. This model included the stiffness change at flexural cracking, yielding, and unloading strength degradation as well as stiffness deterioration during reloading. This trilinear degrading model become later the basis on which many variations have been made to allow for different feature of the response.

Takeda's model was simplified by Riddel et al[R1] and Saiidi et al[S6], the latter is known as "Q-Hyst" model as shown in Fig.1.8. The modified Takeda models use a bilinear relationship for the primary curve, and the unloading slope is a function of the maximum deformation experienced in previous loading excursion.

The above mentioned models for the cyclic behaviour of reinforced concrete members have assumed that predominant deformation component is caused by flexure. However pinching of the force-displacement hysteresis loops is a common feature of the cyclic behaviour of reinforced concrete. The pinching effect is due to the fact that cracks formed in one loading direction remain open in the initial stages of a load reversal. It also occurs in the members where the shear deformation becomes significant, for example, in the response of short column.

The pinching effect caused by shear and bond deterioration was incorporated in a modified Takeda model by Takayanagi et al[T1], which has a reduced stiffness range between the unloading and reloading branches(Fig.1.9). It also considered the strength decay characteristics.

Roufaiel et al[R2] modified the Takeda model to include strength and stiffness degradations as well as pinching effects. The shear effects on hysteretic behaviour is reflected by a reduced stiffness in reloading slope. The degree of pinching is related to the magnitude of shear stress at the section under consideration, and expressed in terms of shear span ratio. The member model explicitly accounts for the finite size of inelastic regions. The strength decay occurs at the critical curvature at which the concrete reaches the ultimate strain. The strength drop-off is assumed to be proportional to the amount

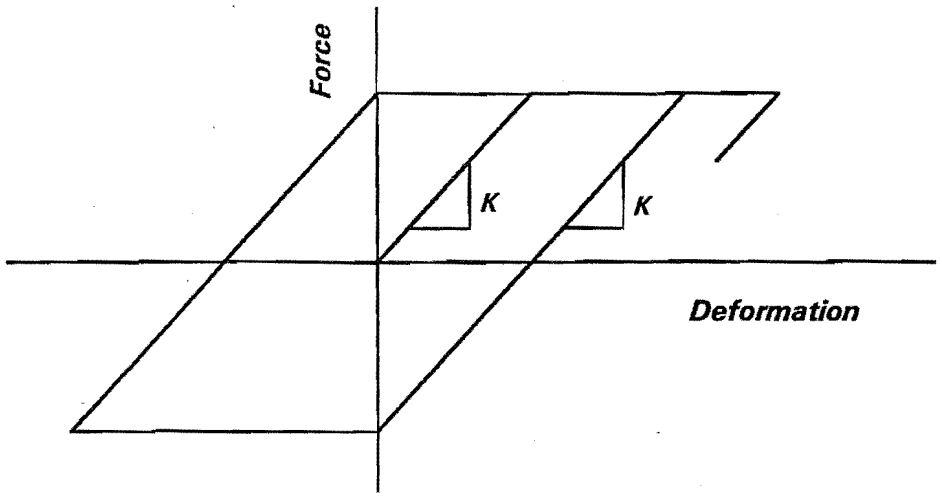

Fig.1.5: Elasto-plastic model

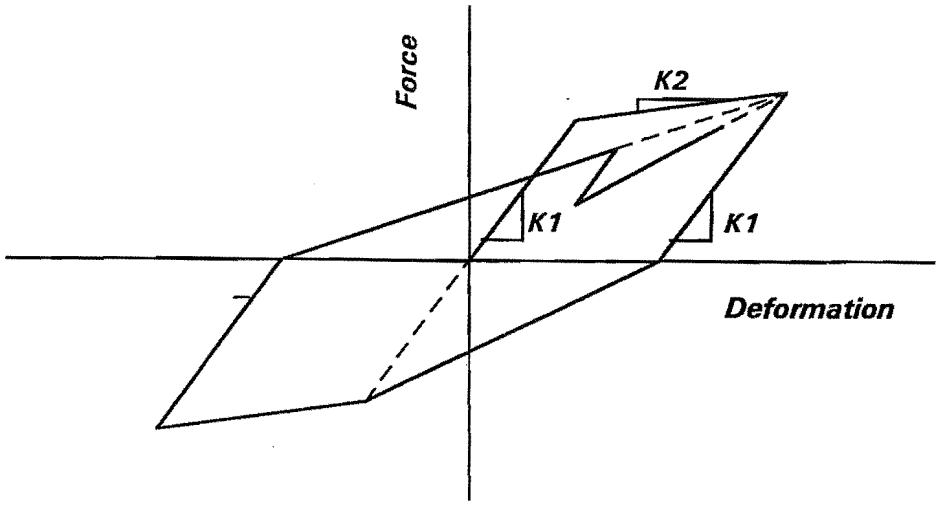

Fig.1.6: Stiffness degrading model by Clough[C1].

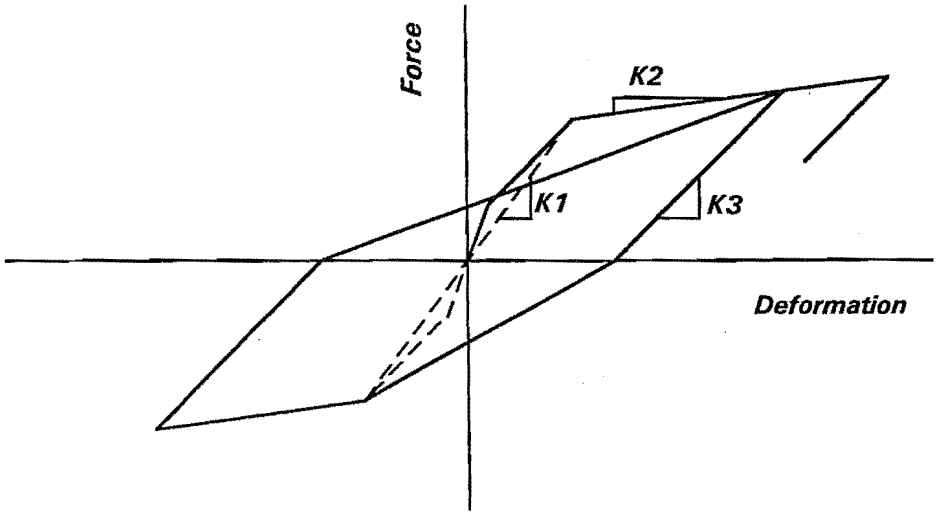

Fig.1.7: Stiffness degrading model by Takeda[T2]

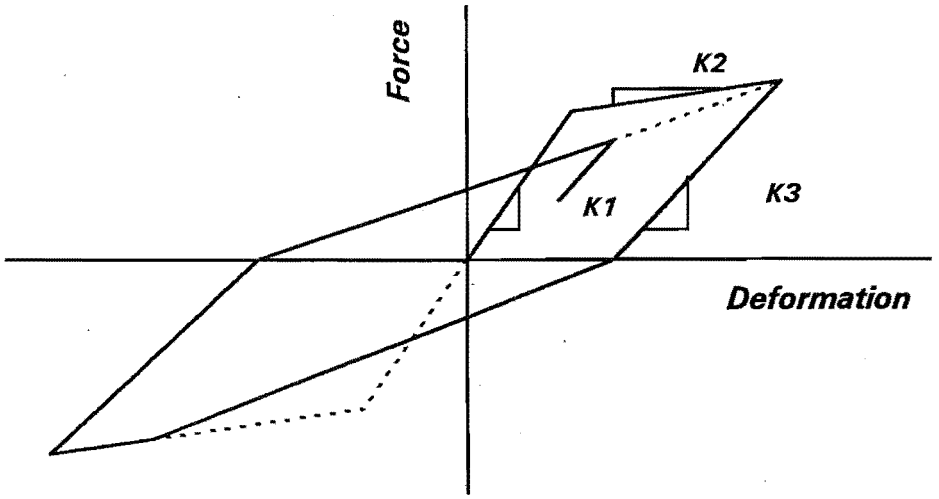

Fig.1.8: Q-hyst model

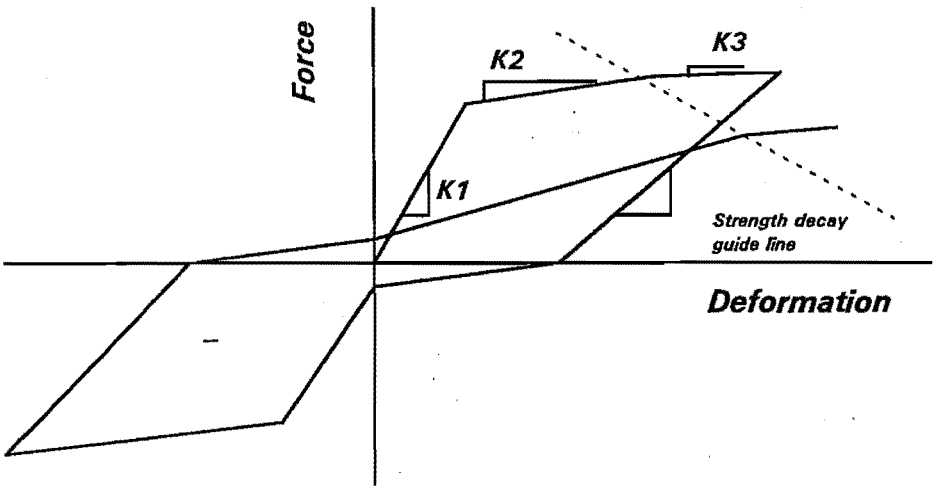

Fig.1.9: Hysteretic model with pinching and strength decay

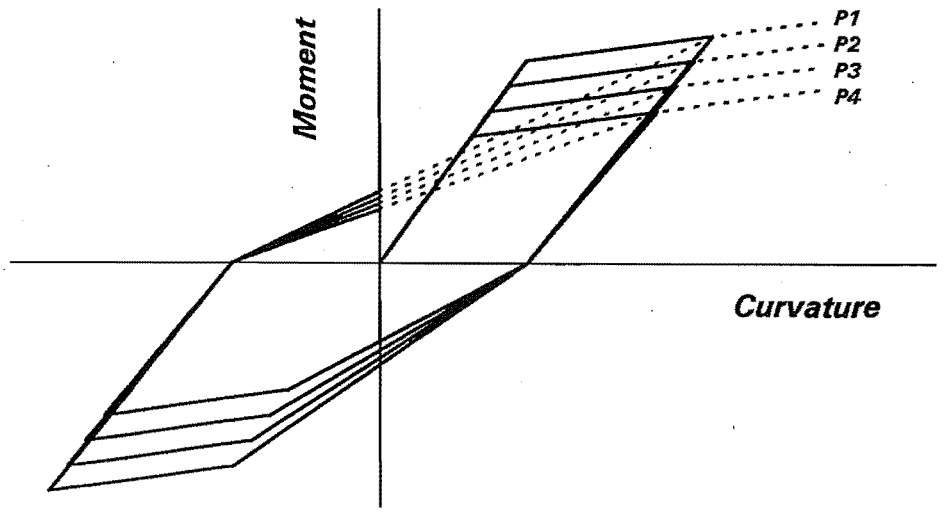

Fig.1.10: Axial force-moment interaction model

by which the critical curvature has been exceeded. The model was found to be capable of reproducing the results of experiments on reinforced concrete members.

Because of the complication of inelastic behaviour of reinforced concrete members, it appears the accuracy of the various hysteretic models depends on how close they account for the aspects affecting the response. When more factors are taken into account, the model becomes more sophisticated and normally more realistic. Saiidi[S5] compared the dynamic response histories by using five different hysteretic models in the analysis of a simple reinforced concrete specimen to earthquake. It was found that the degrading stiffness models(Takeda, Clough, and Q-hyst) generally give a better prediction of observed response than that obtained by using simple elasto-plastic and bilinear models. This indicates that the stiffness degradation feature of hysteretic response is essential in predicting reinforced concrete response. Otani[O2] compared several models that simulated the flexural dominant behaviour. It was found that the maximum response was not as sensitive to detail differences in hysteretic rules of these models, but rather is influenced by more the basic characteristics of hysteresis loops, such as stiffness properties to define the primary curve and the fatness of hysteresis loop. Otani concluded that models with detailed hysteretic rules do not produce significantly different response than those with simple rules provided that the basic properties are the same.

The elastic-perfectly plastic model, Takeda's model and its modified versions, all construct their primary curve assuming that the axial load remains at a constant level. In the response analysis the level of axial force assigned to each individual members is generally obtained from gravity load elastic analysis. The axial force in the member of structure during response to lateral force is significantly different from that under gravity load. Also, some members will undergo large variations in the level of axial force due to overturning moment or in some cases vertical acceleration. The dynamic response of structure may be greatly affected by the level of axial force, because the yield strength and stiffness of the member are directly related to the level of axial force.

The axial force-flexure interaction effects was included in modified Takeda's model first by Takayanagi et al[T1]. The model consists of a set of trilinear primary curves(Fig.1.10), each corresponding to a specific level of axial load, and computed following Takeda's rules corresponding to the concurrent level of axial load.

Saatcioglu et al[S4] developed a degrading stiffness column element model to represent wall elements in the modelling of coupled shear walls. A set of modified Takeda hysteretic loops, corresponding to different level of axial force, is used as a guide in predicting change in stiffness due to axial force effects. The stiffness is updated for the subsequent time increment based on the axial force computed for the current time increment. If there is a change in the axial load, the hysteresis loop is directed

towards the corresponding moment-rotation loop. The modified model with axial force-flexure interaction was used in the response analysis of a twenty storey coupled wall structure. The results indicated that the maximum force in the walls can be affected significantly by the axial force. When the effect of axial force was ignored the maximum shear and moment in the base wall was underestimated by as much as 50 per cent. The varying axial force also affected the sequence of yielding and yielding pattern. The analyses were also conducted to investigate the effect of beam strength reduction on dynamic response. The results indicated that effects of strength decay in the coupling beams was significant, increasing the horizontal displacement of the structure and the coupling beams ductility demands.

Keshavarzian et al[K2] developed a procedure to include the effect of varying axial load on the hysteretic behaviour of reinforced concrete members. The primary curve was prescribed by simplified Takeda hysteretic model for the critical section under a constant axial load level. The current section stiffness was continually adjusted through the established moment-curvature relationship. They conducted an analysis on the reinforced concrete coupled shear walls under static and dynamic loads using developed procedure. It was found that fluctuation of axial force in coupled shear wall structure had a significant effect on the maximum force and deformation that the individual wall experiences. Ignoring the effect of varying axial load on flexural strength and stiffness may result in underestimate of the maximum shear and moment in individual members by up to 50 percent, depending on the degree of coupling.

1.4.2 Conclusions

The inelastic cyclic behaviour of reinforced concrete members is influenced by many factors, such as member properties and loading histories. The deterioration of member stiffness and the degradation of load carrying capacity are related to the development of cracking in the concrete and yielding of reinforcement. In hysteretic modelling, these features should be considered. In addition, attention should be paid on the pinching effect on hysteretic behaviour due to shear deformation, bond slip and crack opening. Several hysteretic models have been developed to represent this behaviour. Few models considered the interaction effects of flexure-shear-axial force. The effects of fluctuating axial force on the hysteretic behaviour and response histories of structure need to be further studied.

1.5 AIMS OF THE RESEARCH

The structural column is one of the most important structural elements of a structures. Failure of a column can cause serious consequences. Therefore, extensive studies have been conducted on understanding the inelastic cyclic behaviour of reinforced concrete column under different loading

conditions. As a result of these studies significant improvements in design practice have been achieved. Provisions for ductility are now incorporated in design codes. The behaviour of reinforced concrete column under load reversal is influenced by many factors, such as loading histories, degree of concrete confinement, strain hardening and bond deterioration. Previous experimental studies have revealed that the axial load has a significant effect on the inelastic behaviour of reinforced concrete columns. Flexural strength, stiffness, ductility, and energy dissipation capacity of the column are all affected by the presence of axial load[P6]. When investigating the effects of axial force, most previous research work has assumed that the axial load remains constant at a particular chosen level. Very little research has been done to investigate the performance of reinforced concrete columns under the influence of varying axial load level.

The major objective of this research is to experimentally investigate the behaviour of reinforced concrete columns subjected to simulated seismic horizontal loading under varying axial load. The aim is to obtain a better understanding of the parameters affecting the overall performance of columns under complex loading histories.

A further objective is to formulate a mathematical hysteretic model for reinforced concrete members, based on the evidence from test results and taking into account the effects of varying axial load on the hysteretic behaviour. This model is to be used for studies of the inelastic dynamic response of reinforced concrete structures.

The experimental investigation involves testing a total of nine full size column specimens under simultaneously cyclic lateral loading and varying axial load. All column units were tested as cantilevers projecting from a stiff foundation block. The main variable was the axial load history.

The axial force induced by seismic lateral force in the column of a moment resisting frame is equal to the summation of shear forces in the beams above the level under consideration, as shown in Fig.1.11. It is evident that the exterior column will undergo large change in axial force, when the frame is subjected to lateral load reversal[P17]. For the columns in a low story, which receive axial load reversal from all the floors above, the variations in axial force could be quite significant. For a frame-wall system such as shown in Fig.1.12, the variation in axial force may be generated by the overturning moment[3]. The fluctuating axial force can also be generated by vertical acceleration. This has been overlooked in the past due to the assumption that the maximum vertical acceleration is small and always smaller than the maximum acceleration in the horizontal direction. The reports on recent earthquakes indicate that not only is the maximum acceleration in the vertical direction significant, but also that there have been earthquakes where the maximum acceleration in the vertical direction has exceeded that in the horizontal direction[H4].

The nature of axial load histories in a column can be very complicated. The seismic induced axial force may be approximately proportional to the bending moment when the frame responds mainly elastically in the first mode of vibration. The yielding of the members and the simultaneous occurrence of vertical and horizontal seismic motions, will add to the complication in the response. It is unrealistic to attempt to simulate the real axial load histories in a column. Instead, arbitrarily predetermined axial load patterns were used in the experimental program to study the influence of axial load variation on the behaviour of reinforced concrete columns. The axial load pattern used for each test specimen is described in detail in Chapter 2 and Chapter 4.

The first series of tests consisted of six column units with aspect ratio of 4.13. Of particular interest in this test program was the flexural response and hysteretic behaviour of reinforced concrete column under cyclic flexure and varying axial load. Past test results have indicated that the columns provided with the amounts of transverse reinforcement according to the current New Zealand code[S14] can achieve satisfactory ductile behaviour[P22]. The confinement effects were not a main concern in this study. The transverse reinforcement provided in the test specimens was designed in accordance with the requirements of the current New Zealand code provisions[S14]. The main objective of these tests was to obtain the variations in flexural hysteretic behaviour with fluctuation in axial load level.

In the second phase of experimental investigation, three column specimens were tested to study the shear strength of reinforced concrete columns subjected to cyclic lateral loading and varying axial load, with emphasis placed on the study of degrading concrete shear resisting mechanism and comparisons with the present design code equations for shear strength.The presence of tensile axial force increases the widening of diagonal cracks. Unsymmetric shear deformation with repeated abrasion will increase the degradation in concrete shear resisting mechanism. It was expected that the variations in axial load would have a greater effect on the response of the column dominated by shear than that dominated by flexure.

1.6 FORMAT OF THE THESIS

The thesis starts in Chapter 1 with some general aspects of seismic design philosophies. A literature review on the behaviour of reinforced concrete members and hysteretic modelling is provided.

Chapter 2 describes the details of design parameters, construction of test specimens, instrumentation, testing procedure, and the measured material properties of the first series test specimens.

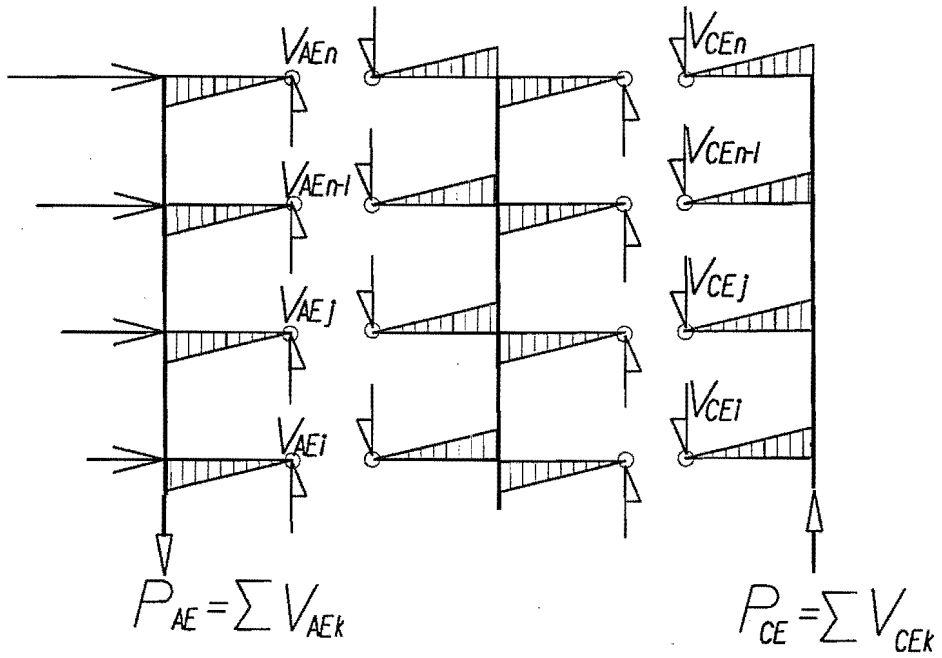

Fig.1.11: Column axial force due to seismic action

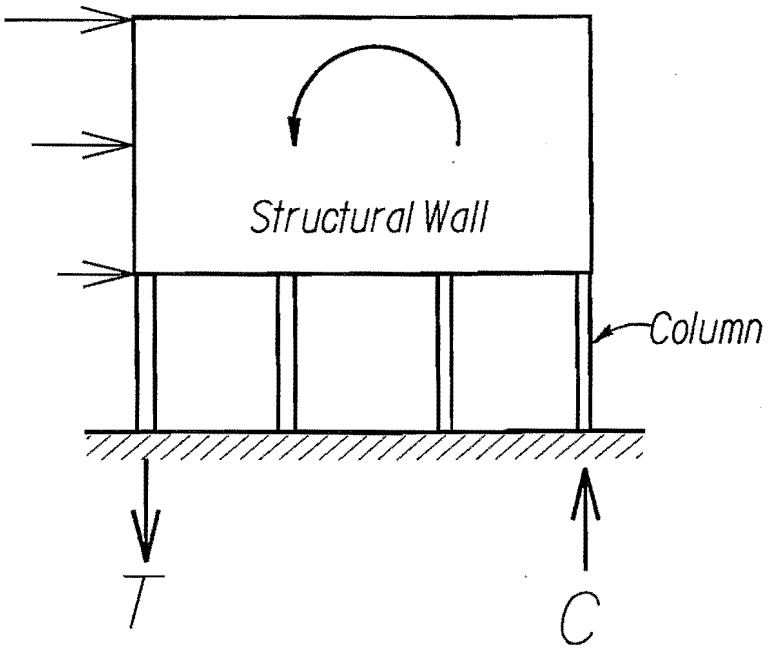

Fig.1.12: Column axial force resulting from overturning moment of structural system

Chapter 3 reports the general observations from six column units tested in the first section and describes the test results.

Chapter 4 gives the details of the three column units tested in the second series. The instrumentation, testing procedure, and measured material properties.

Chapter 5 presents the general observations and test results from the three column units of the second series. Comparisons of experimental shear strength with present code provisions and other available shear strength predictive models are given in this chapter.

Chapter 6 gives a summary of shear strength mechanism and important parameters affecting the shear strength of reinforced concrete columns. The effects of variations in tension and compression on the shear resistance mechanism are studied. Based on the experimental and analytical work, proposals for the seismic design of reinforced concrete columns are made.

Chapter 7 reports the theoretical investigation on the section stiffness of reinforced concrete columns. Based on the experimental information from Chapter 3 and Chapter 5, a hysteretic model for reinforced concrete members, taking into account the effect of varying axial load is developed.

Chapter 8 gives an example of inelastic dynamic response analysis to reflect the effects of varying axial load on the response histories of a reinforced concrete frame.

Chapter 9 summarizes the main conclusions of the research project and gives the recommendations for the further research work.

Chapter 2

Experimental Investigation of the Flexural Behaviour of Reinforced Concrete Columns Under Varying Axial Load
___ Test Series 1

2.1 INTRODUCTION

The variations of axial load in the columns of a moment resisting frame is inevitable in the event of a major earthquake. The experimental investigations of the behaviour of reinforced concrete columns under varying axial loading conditions have not been conducted in New Zealand, while only a limited information on the topic has been reported overseas. There is a need to carry out such research to obtain a better understanding of the seismic behaviour of reinforced concrete columns under this more complex loading condition. The aim of this series of tests is to investigate experimentally the influence of variation in axial load on the behaviour of reinforced concrete columns. This chapter describes the design, construction and instrumentations of six reinforced concrete columns. The measured material properties used and the testing procedure are also presented in this chapter. The experimental results and the evaluation of the results will be presented in the following chapter.

2.2 DESIGN OF THE COLUMN UNITS

2.2.1 Details of the Column Units

The test program consisted of six reinforced concrete column units tested under cyclic lateral load while simultaneously subjected to varying axial load levels. All column units had the same overall dimensions. The column unit consisted of a 1.0x0.9x0.96 m concrete base, which simulated a rigid foundation for the column and supports the loading frames, and the column portion which was the main region of the test. The cross section of the column was 400x400 mm. The distance from the column base to the

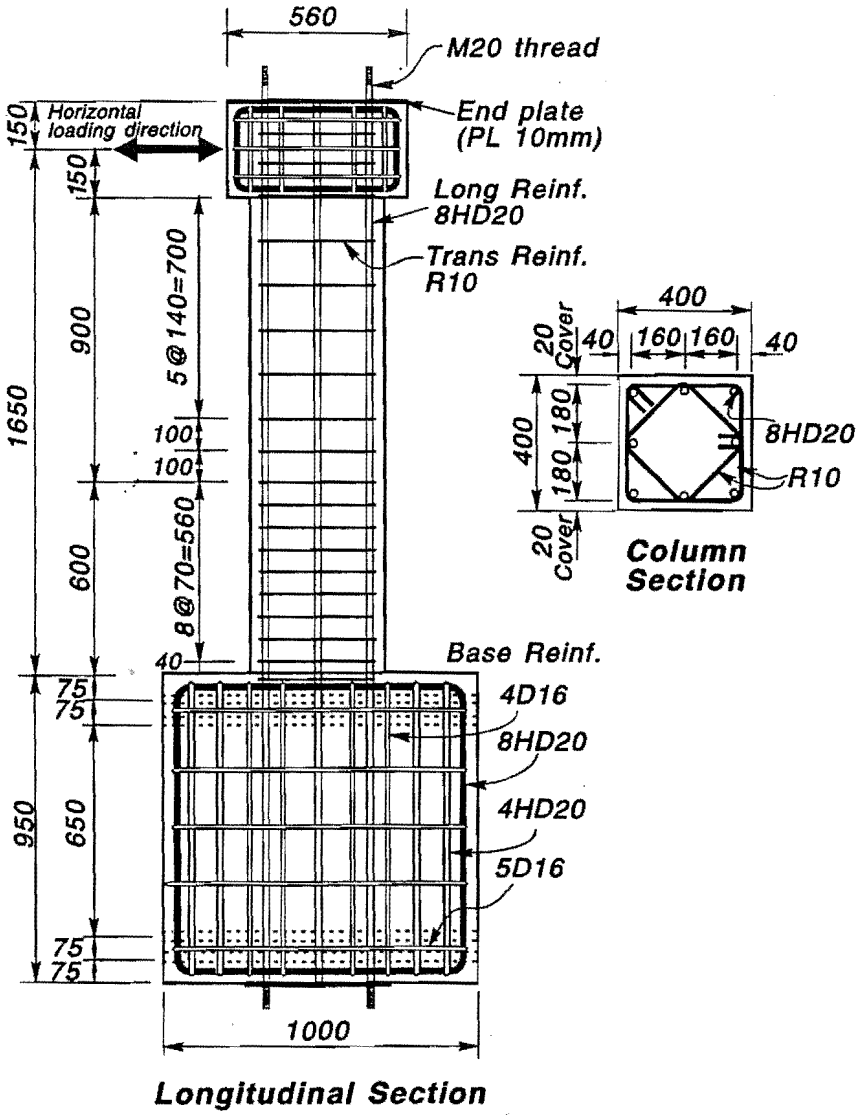

Fig.2.1: Details of reinforcement of Units 1, 2 and 3

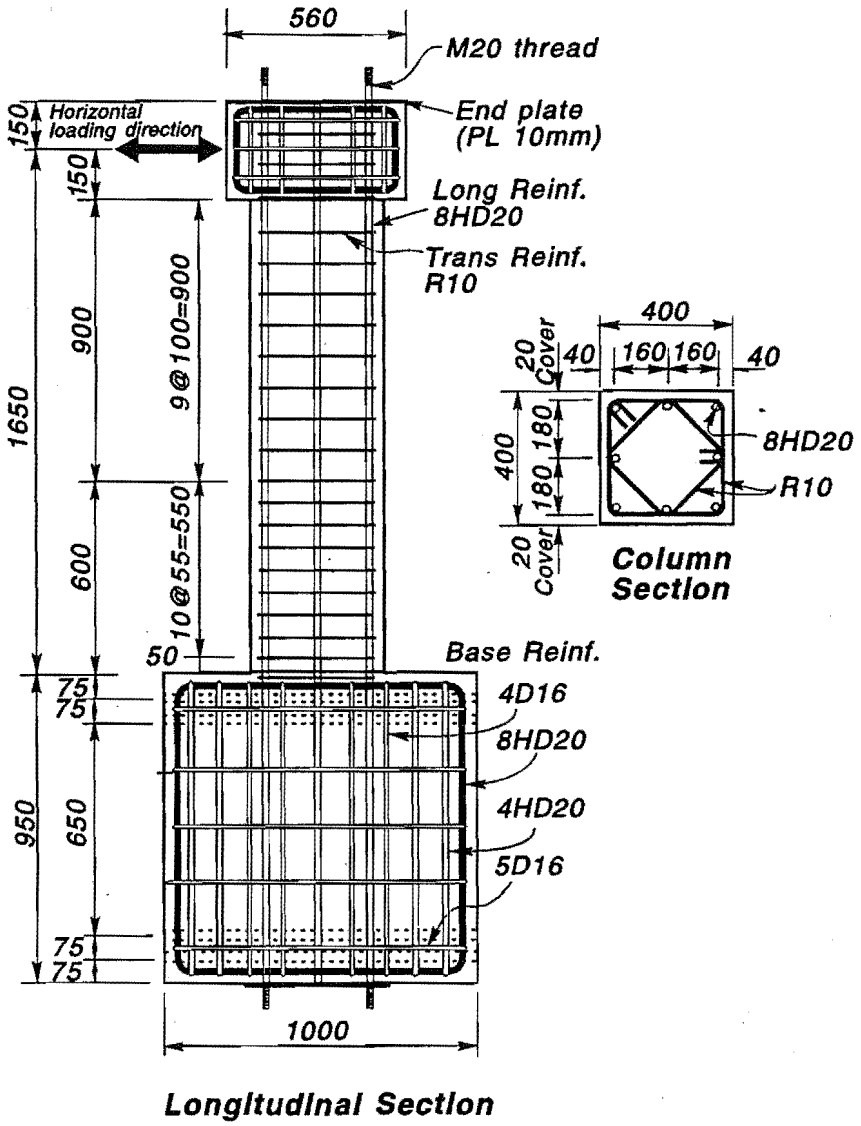

Fig.2.2: Details of reinforcement of Units 4, 5 and 6

point of the application of lateral load was 1.65m, giving an aspect ratio of 4.13. The column dimension represented approximately an one-half to two-third scale model of a typical column in a structure. The overall dimensions of the column units and the cross section, and the arrangement of longitudinal and transverse reinforcement in the column and column base, are shown in Figs.2.1 and 2.2. The column units were tested as a cantilever column, which simulated the first floor column in a building or the pier

in a bridge between adjoining footing and contraflexural point. The main variable for the column units was the type of applied axial load histories. Other variable included the level of axial compression and magnitude of axial tension applied.

Each column units contained eight 20 mm diameter Grade 430 deformed steel as the longitudinal reinforcement, which were evenly distributed along the sides of the section, resulting in a longitudinal reinforcement ratio, ρ_t, of 1.57%. The transverse reinforcement in the column units consisted of 10 mm diameter Grade 300 plain round bar in form of square and octagonal hoops. All hoops had a standard 135-deg end hook with a $8d_b$ extension tail. The concrete was provided by a local ready-mix supplier. A graded aggregate with maximum size of 10 mm was used. The target compressive concrete strength for the column portion was 30 MPa.

Due to its roles in acting as foundation and resisting the action induced by applied loads, the concrete base was provided with heavy reinforcement to ensure it would remain in the elastic range during the tests. Grade 430 deformed bars were used as main reinforcement for the column base and Grade 300 plain round bars were used as confinement hoops. Concrete with higher strength than that for column portion was used for the column base. The target compressive concrete strength was 45MPa for the base block.

Constant compression axial load, at $0.3f'_cA_g$ and $0.5f'_cA_g$, was applied to Units 1 and 4, respectively. These column units were to act as comparison specimens. For Units 2, and 3, the maximum axial compression and the maximum axial tension applied were $0.3f'_cA_g$(=1536kN) and $0.05f'_cA_g$(=256kN), respectively. For Units 5, and 6, the maximum axial compression and tension were $0.5f'_cA_g$(=2856kN) and $0.1f'_cA_g$ (=572kN), respectively.

2.2.2 Quantity of Transverse Reinforcement Required for Concrete Confinement and to Prevent Premature Buckling of Longitudinal Reinforcement in the Plastic Hinge Regions

In the design of a ductile reinforced concrete column, an important aspect is to provide the regions of the member where plastic hinging is expected to occur with sufficient transverse reinforcement to confine the compressed concrete core, to prevent premature buckling of longitudinal bars and to prevent shear failure so as to ensure adequate ductility. To confine the compressed concrete, the current New Zealand concrete design code NZS 3101:1982[S14] specifies that, in potential plastic hinge regions of reinforced concrete column of ductile structure when rectangular hoops with or without cross ties are used, the total area of transverse reinforcement A_{sh} in each of the transverse directions with spacing s_h should not be less than

$$A_{sh} = 0.3 s_h h'' \left(\frac{A_g}{A_c} - 1\right) \frac{f'_c}{f_{yh}} \left[0.5 + 1.25 \frac{P_e}{\phi f'_c A_g}\right] \qquad (2.1a)$$

or

$$A_{sh} = 0.12 s_h h'' \frac{f'_c}{f_{yh}} \left[0.5 + 1.25 \frac{P_e}{\phi f'_c A_g}\right] \qquad (2.1b)$$

whichever is greater, where A_{sh} = the area of transverse reinforcement in each of transverse direction(A_{sh} =3.414A_b in the case of the reinforcing detail used for the six column units), A_b = transverse bar area, h" = is the dimension of concrete core of the section measured perpendicular to the direction of the hoop bars to the outside of the perimeter hoop(mm), s_h = the centre to centre spacing of hoop sets(mm), A_g = the gross area of column cross section(mm^2), A_c = the area of concrete core of the section measured to outside of peripheral transverse steel(mm^2), f'_c = the concrete compressive strength(MPa), f_{yh} = the yield strength of transverse reinforcement(MPa), P = the axial compression load due to gravity and seismic loading, and ϕ = the strength reduction factor.

In determining the amount of transverse reinforcement for the confinement of concrete for the test specimens, the maximum compression axial loads applied to each column unit were used to determine the axial load ratio. The net thickness of the cover concrete for the six columns was 20mm. The strength reduction factor, ϕ, was taken as unity. It can be shown that the amount of the transverse reinforcement for all column units was governed by Eq.2.1b.

It is also necessary to ensure that an adequate quantity of hoop and supplementary cross-ties are presented in the potential plastic hinge regions to provide the necessary lateral forces to the longitudinal steel to prevent premature buckling. The New Zealand code[S14] recommends that the area of one leg of a stirrup tie in beams and a hoop or supplementary cross-tie in columns should not be less than one-sixteenth of the area of the longitudinal bars reliant on the tie if the spacing is 100mm and the steel yield strengths of longitudinal and transverse steel are the same. This requirement in general may be expressed as

$$A_{te} = \frac{1}{16} \frac{\sum A_b f_y}{f_{yh}} \frac{s_h}{100} \qquad (2.2)$$

where ΣA_b = sum of areas of longitudinal bars reliant on the tie(mm^2), f_y = yield strength of longitudinal bars(MPa), the other notation are as defined previously. Therefore, to prevent premature buckling of the compressed longitudinal bars, the quantity of transverse reinforcement should not be

less than

$$A_{sh} = \sum A_{te} \qquad (2.3)$$

The transverse reinforcement provided in the column units was checked against that required by Eq.2.3 and found that the amount of transverse reinforcement required by Eq.2.3 was not critical.

In order to prevent premature buckling of longitudinal reinforcement and to confine compressed concrete, the code provisions of NZS3101:1982[S14] also requires that the centre to centre spacing of transverse reinforcement in the potential plastic hinge regions should not exceed the smaller of one-fifth of the least lateral dimension of cross section, six times longitudinal bar diameter, or 200mm. According these requirements, the maximum permitted spacing of the hoop sets in the plastic hinge region was 80mm. For all column units tested, the actual spacings of transverse reinforcement, was as shown in Table 2.1. Note that the hoop spacings were governed by Eq.2.1b and hence less than 80mm.

2.2.3 Transverse Reinforcement required for Shear

The current New Zealand concrete design code of NZS 3101:1982[S14] adopts a capacity design approach to insure against shear failure. In this approach, it is required that ideal shear strength of the column V_i should at least be equal to the design shear force V_{col}, which is estimated from the probable critical moment gradients along columns[P12]. According to the current New Zealand concrete design code[S14], the shear strength of a reinforced concrete column is considered to be the sum of the contributions of the concrete shear resisting mechanism V_c, and the truss mechanism V_s involving transverse reinforcement and assuming a 45-deg critical diagonal crack pattern. Thus

$$V_i = V_c + V_s \qquad (2.4)$$

For the seismic design of ductile frames, inside the potential plastic hinge regions of columns, according to the New Zealand code[S14], the concrete contribution V_c to the shear strength is taken as zero when the axial compression load level $P \leq 0.1 f_c' A_g$. For the axial compression load level $P > 0.1 f_c' A_g$, V_c is taken as

$$V_c = 4 v_b b_w d \sqrt{\frac{P}{\phi f_c' A_g} - 0.1} \qquad (2.5)$$

where P = compression axial load; ϕ = strength reduction factor; f_c' = concrete compressive strength; A_g = gross area of column section; b_w = width of column section and d = effective depth of column section.

Also, inside the potential plastic hinge region V_c=0 if the axial load is tensile.

Outside the potential plastic hinge regions, when the axial load is compression V_c is given by

$$V_c = \left(1 + 3 \frac{P_e}{\phi f_c' A_g}\right) v_b b_w d \qquad (2.6)$$

The basic concrete shear stress, v_b, in Eqns.2.5 and 2.6 is given by

$$v_b = (0.07 + 10\rho_w)\sqrt{f_c'} \qquad (2.7)$$

where $\rho_w = A_t/(b_w d)$, and A_t = the area of longitudinal tension reinforcement. For the column, ρ_w can be taken as $0.5\rho_t$, where ρ_t is the total longitudinal reinforcement ratio. In cases of flexure with axial tension, the shear strength V_c outside the potential plastic hinge regions is assumed to be given by

$$V_c = \left(1 + 12 \frac{P}{f_c' A_g}\right) v_b b_w d \qquad (2.8)$$

The value of axial tension P is taken negative in Eq.2.8.

The shear strength provided by truss mechanism, assuming diagonal tension cracks at 45-deg to the longitudinal axis of the column, is given by

$$V_s = \frac{A_v f_{yh} d}{s_h} \qquad (2.9)$$

where A_v = total area of shear reinforcement parallel to the direction of shear force($A_v = (2+2/\sqrt{2})A_b$

in the case of the six columns tested); A_b = transverse bar area; s_h = the centre to centre spacing of the transverse reinforcement and f_{yh} = the yield strength of transverse reinforcement.

In designing the column units, the amount of transverse reinforcement determined based on the requirements in the Section 2.2.2 was checked against the shear strengths specified by the code provisions(Eqns.2.4 to 2.9). Two critical loading conditions, the maximum compression axial load and the maximum tension axial load applied to the column units, were considered in calculating concrete contribution to the shear strength. It was found that shear was not critical in all the column units, due to large aspect ratio and large concrete contribution to shear strength resulted from high axial compression level. Table 2.1 summarizes the details of all column units.

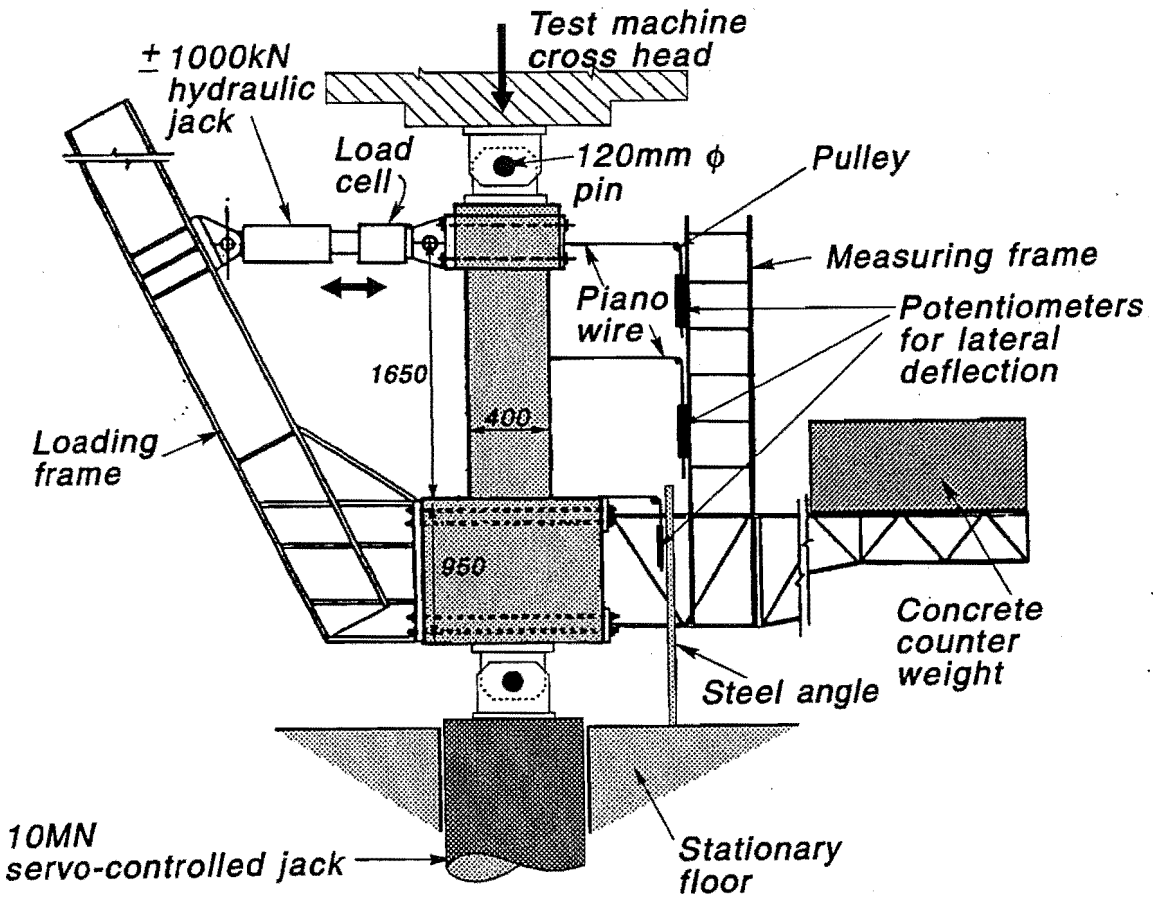

Fig.2.3: Test set-up for Units 1 to 6

2.3 TEST SET-UP

The schematic representation of the testing arrangement is illustrated in Fig.2.3. The loading frame was connected to the reinforced concrete base of the test specimen by twenty 25mm diameter high strength bolts. The inclined cantilever arm of the loading frame was linked to the load cell and then to the top concrete stub of the column. Reversed lateral loads were applied by a double acting hydraulic jack, which had a capacity of 1120kN in compression, 840kN in tension, and 400mm effective travel. The load imposed between the cantilever arm of the loading frame and the top stub of the column pushes or pulls laterally and results in the rotation of the concrete base of the column. Hence, a uniformally distributed shear force and linearly distributed bending moment with the maximum value being at the end of the column were induced in the test specimen. This actions was equivalent to that a cantilever column with horizontal load acting on the top of the column.

Table 2.1: Properties of Column Units

Unit	$(\frac{P}{f'_c A_g})^c$ (1)	$(\frac{P_e}{f'_c A_g})^t$ (2)	$(\frac{P}{f'_c A_g})^i$ (3)	Transverse Reinforcement			Longitudinal Bars	
				d_b (mm) (4)	s_h (mm) (5)	ρ_s % (6)	d_b (mm) (7)	ρ_t % (8)
1	0.3	-	0.3	R10	70	2.13	HD20	1.57
2	0.3	0.05	0.3	R10	70	2.13	HD20	1.57
3	0.3	0.05	0.3	R10	70	2.13	HD20	1.57
4	0.5	-	0.5	R10	55	2.70	HD20	1.57
5	0.5	0.1	0.5	R10	55	2.70	HD20	1.57
6	0.5	0.1	0.5	R10	55	2.70	HD20	1.57

(1). The maximum axial compression load

(2). The maximum tension axial load

(3). The axial compression load applied during initial loading cycles

(6). Volumetric ratio of transverse reinforcement, $\rho_s = (4+2\sqrt{2})A_b/h''s_h$, where h" = dimension of concrete core of section measured to outside of peripheral hoop

(8). Total longitudinal reinforcement ratio on gross section, $\rho_t = A_s/b_w d$

The 10MN servo-controlled hydraulic jack in the DARTEC universal testing machine was used to apply axial load. Two identical pin fittings were attached to each end of the column unit by an appropriate number of longitudinal bars. Fig.2.4 shows the details of the pin fitting, which were manufactured using T-shaped steel plates with a 100mm diameter pin anchored in the middle. A universal bearing was inserted between the pin and steel plate to facilitate the installation of the test specimen. The pin fitting was connected at one end to the testing machine. The other end was connected to the test specimen by end-threaded reinforcing bars, which comprised longitudinal column bars extending through the steel end plates and additional longitudinal bars embedded in the top stub and concrete base of the column. This set-up enabled both tension and compression axial load to be applied to the columns. The axial load applied by DARTEC machine was transferred through the pin fitting at each end to the test specimen.

Another steel frame bolted to the other side of the concrete base of the column was used as measuring frame to support the instrumentation devices, and as counterbalance to ensure that no initial bending moment was induced in the column at zero loading. Fig.2.5 shows the overall view of testing set-up.

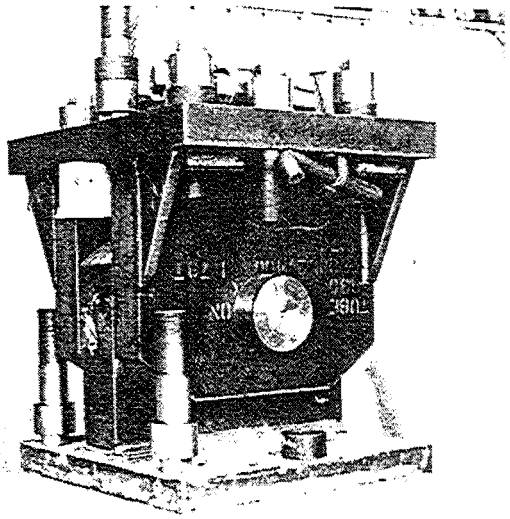

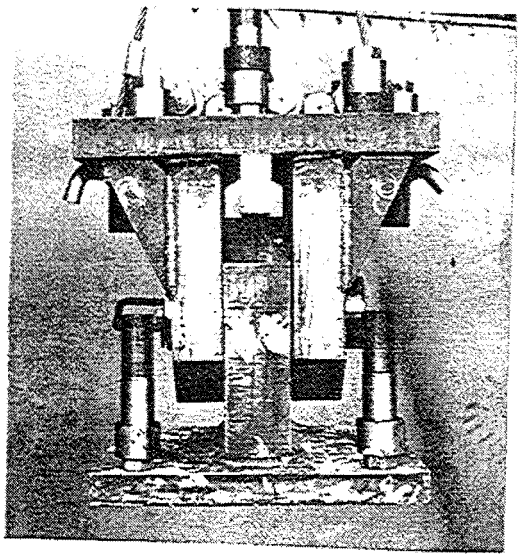

Fig.2.4: Pint fittings

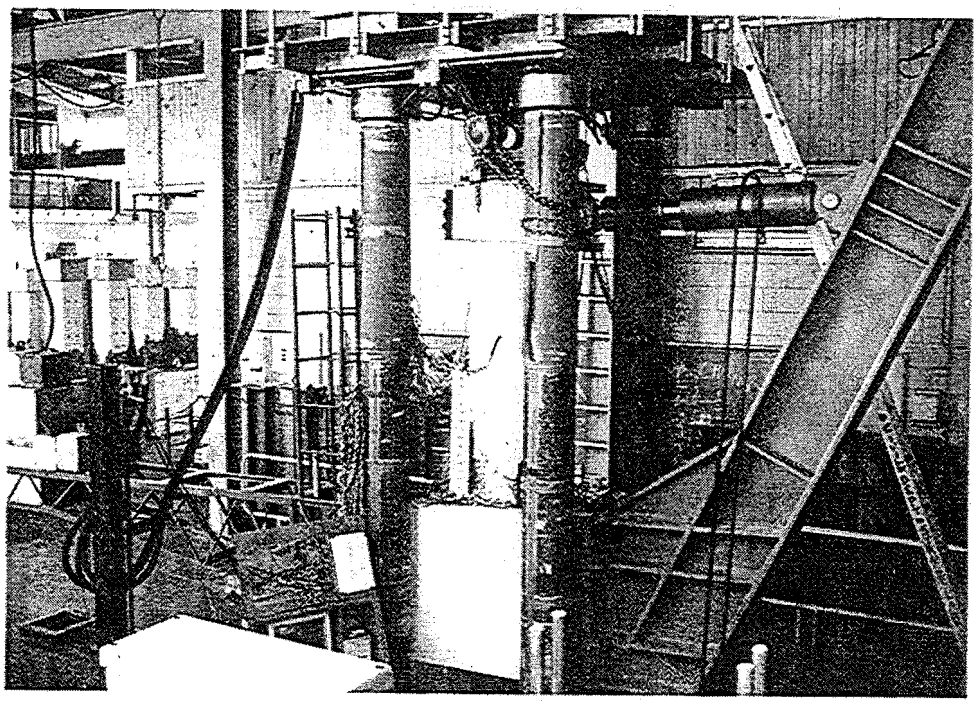

Fig.2.5: Overall view of test set-up

2.4 CONSTRUCTION OF THE COLUMN UNITS

The test specimens were fabricated within the laboratory with the assistance of the technicians. The reinforcing steel was supplied by a local steel firm. The hoops and most of the reinforcing bars were cut and bent by the firm. Some of the main longitudinal bars were cut in the laboratory to obtain more accurate dimensions.

The reinforcing cage for the column base was first fabricated. The Grade 430 deformed bars, bent in form of rectangular hoops, were used as main reinforcement for the column base. To ease the fabrication of the cage, the transverse loops were cut in form of U shapes so that they could be inserted from the two sides of the main cage and lap welded in the middle. Fig.2.6 shows a typical reinforcing steel cage for the column.

The column base, acting as support for the loading frame, had to accommodate 20 holes in four layers to allow the connection bolts to pass through. PVC tubes with 35 mm outside diameter were inserted in the reinforcing cage of the column base to form these holes. The positions of the tubes were held by 25 mm diameter steel bars passing through the base mould, as shown in Figs.2.6 and 2.7.

The longitudinal bars of the column unit were first welded to the bottom end steel plate. Portions of the longitudinal bars with threaded end were extended through the end plate to serve as connection bolts. The longitudinal bars were inserted through the reinforcing cage of the column base. The column hoops were placed in position from the tip of the longitudinal bars and tied to the longitudinal bars. The entire reinforcing cage was completed by welding the steel end plate to the top of the longitudinal bars(see Fig.2.6).

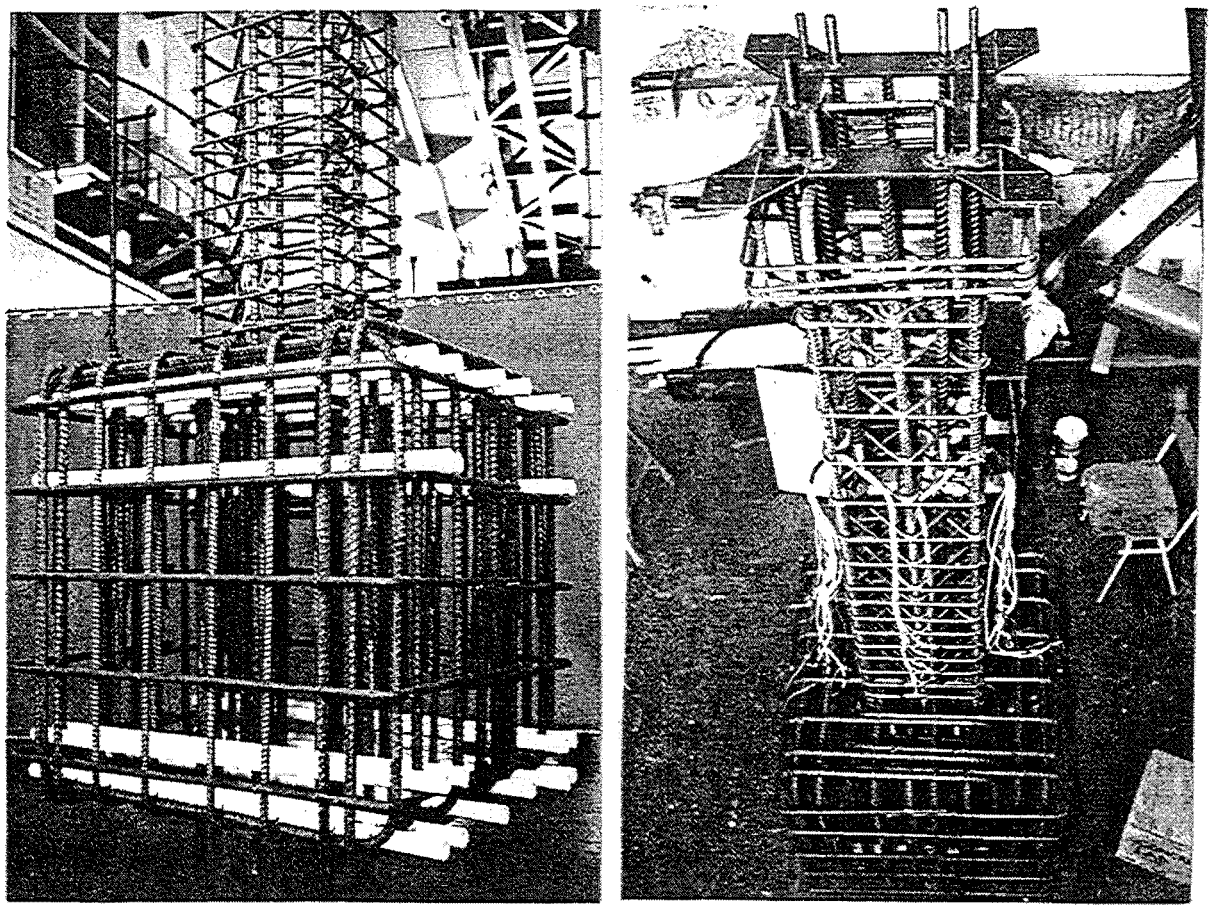

Fig.2.6: Typical Steel Reinforcing Cage

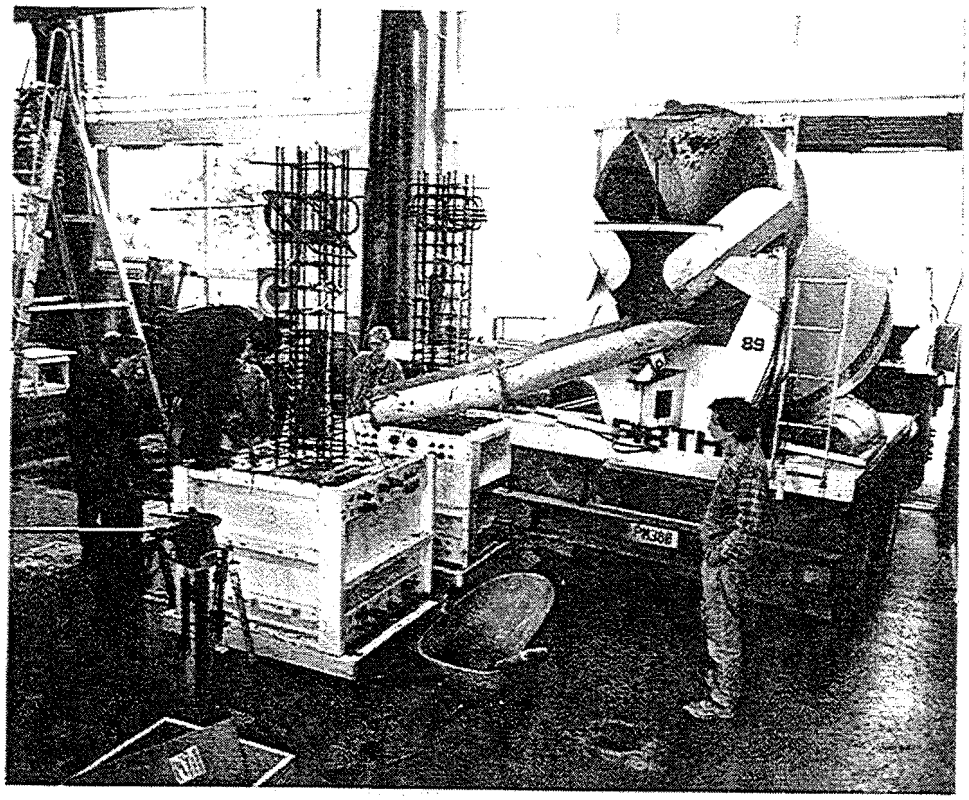

Fig.2.7: Casting of concrete for column base

Two separate mould were prepared for the column base and remaining portion, and hence the column units were constructed in pairs. Each side of the mould was made of 18 mm thick plywood sheet and stiffened with timber ribs. The sides were bolted together and held in position by steel brackets. The reinforcing steel bolts were attached outside the mould where is necessary to ensure that the dimensions of the specimen were not affected by possible movement or bowing during the concreting of the specimen. The internal face of the mould was painted and oiled to facilitate the removal of mould after curing. The edges of the joints were sealed with grey tact and covered with parcel tape to achieve a smooth surface.

The casting of the concrete was carried out in two stages. The first stage was the casting of the column base as shown in Fig.2.7, and the second stage was the casting of the column portion. Concrete cylinders were made from each batch of concrete for the estimate of the concrete strength.

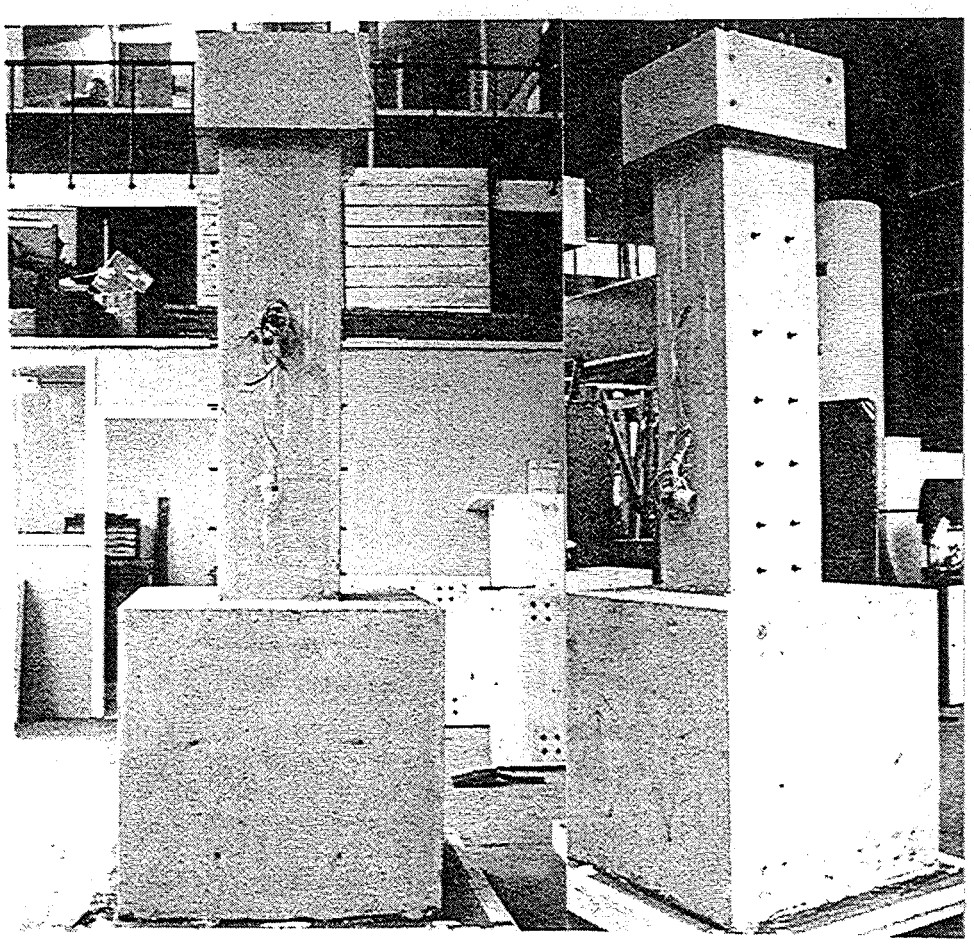

Fig.2.8: Completed column units before testing

After casting of the column base, it provided a base for the column mould. Before the column mould was erected on the base block, the concrete of the base has been cured for at least one week. The rough surface at the interface of the column portion and the column base was achieved with chemical retarder to ensure a good quantity construction joint. Fig.2.8 shows the column units after removal from column mould.

2.5 INSTRUMENTATION OF THE COLUMN UNITS

2.5.1 Measurement of Load

The lateral load applied to each test specimen by a hydraulic actuator was measured by a load cell as shown in Fig.2.3. Prior to the testing, the load cell was calibrated using an Avery Universal Testing machine. The load cell was only calibrated in compression. It was assumed that the sensitivity of the load cell in tension was equal to that obtained in compression.

2.5.2 Measurement of Displacements

The horizontal displacement of the columns units were measured by four 300 mm travel Sakae linear potentiometers, which were mounted on the measuring frame at the level of top, mid-height and bottom of the column units, as shown in Fig.2.3. The top horizontal displacement measured by the linear potentiometer and the horizontal load measured by a load cell were used to drive an X-Y plotter during testing to trace the load-displacement hysteresis responses.

Under loading actions, the concrete base will rotate about the centre of the bottom pin fitting. Hence, the end of the column will displace away from the centerline of application of the axial load, inducing a P-Δ moment at the critical section due to axial load. Therefore, a displacement transducer was mounted at the level just above the concrete base to monitor the displacement at end of the column which was used to evaluate the P-Δ effect. This potentiometer was attached to a steel angle fixed to the stationary floor.

The horizontal displacement measured at the various levels up the height of the column permitted the distribution of deflection of the column units to be determined.

All linear potentiometers were calibrated against a known displacement before testing.

2.5.3 Measurement of Column Curvature

The curvatures were measured using the conventionally used method at the University of Canterbury. Fourteen pairs of linear potentiometers of either 50mm or 30 mm travel were aligned vertically down the height of the columns. Fig.2.9 shows the arrangement of potentiometers mounted on steel brackets supported by 10mm diameter rods, which passed horizontally through the column. To minimize the influence due to the crushing of cover concrete, polystyrene pieces with 25 mm in depth and 30 mm in diameter were sleeved at both ends of the rods to create a clear space between the rods and surrounding concrete. The linear potentiometers measured the changes in length over the vertical gauge length concerned. The change in length can then be used to calculate the curvature distribution along column. Interpolation of the deformation measured by potentiometers also allowed the longitudinal strains at various position, for example, at the surface of core concrete, to be determined, assuming that plane sections of the column before bending remained plane after bending. The column elongation can also be readily calculated from the measurements of potentiometers. These calculations also assumed that the steel rods which supported the potentiometers remained straight after bending.

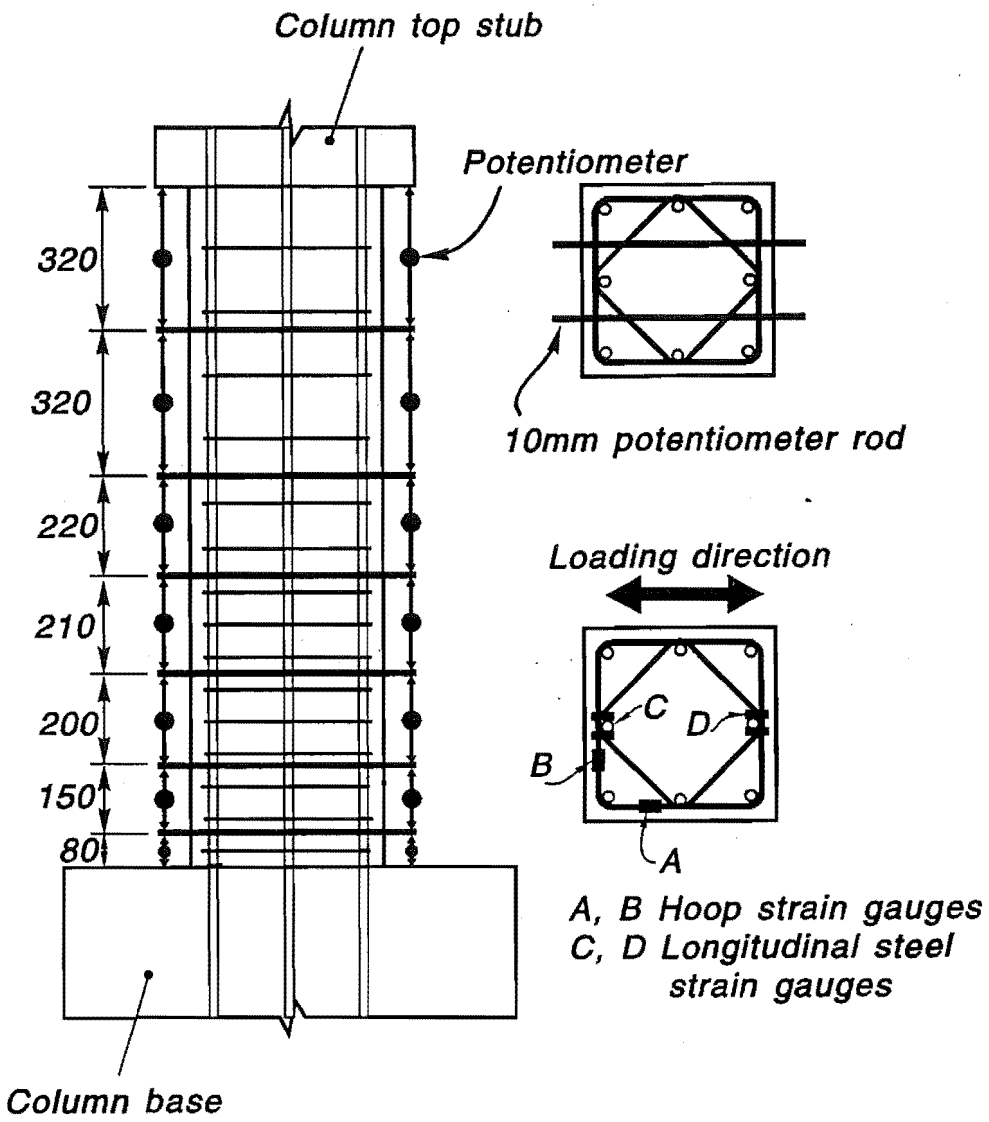

Fig.2.9: Position of Strain Gauges and Potentiometers

2.5.4 Measurement of Bar Slippage

Four clip gauges were placed on the column at plastic hinge regions to monitor the slippage of the longitudinal bars from concrete base, as shown in Fig.2.10a. These clip gauges were mounted on the first level steel bracket relative to steel studs which were welded to the longitudinal bars of the column 3-6mm above the surface of the concrete base. The difference between the displacement measured by these potentiometers and measured by first level potentiometer were used to calculate the longitudinal bar slip from base block. Fig.2.10 shows a close up view of these potentiometers. The clip gauges were used for units 2 and 3, and were replaced by the potentiometers for the rest of the column units, as it was found that the latter would give better performance for the measurements.

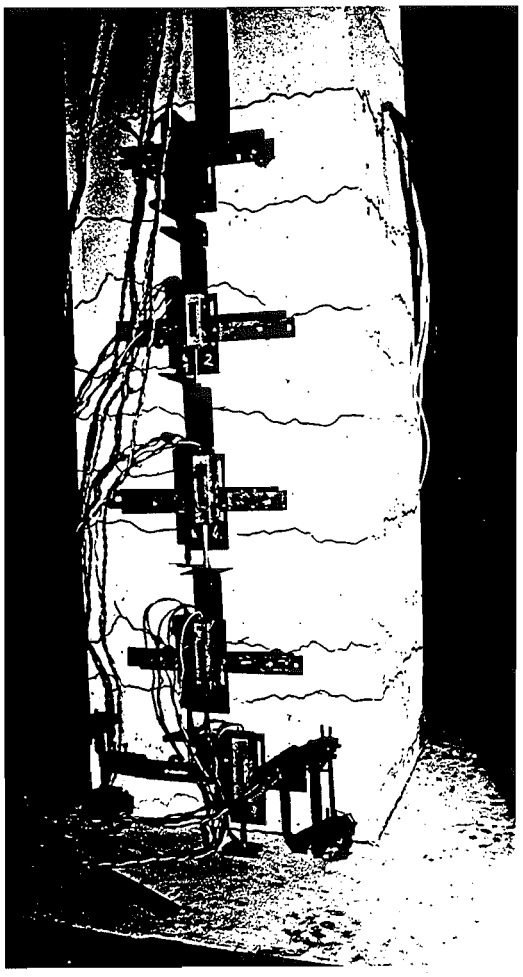

(a) Measurement of column curvature

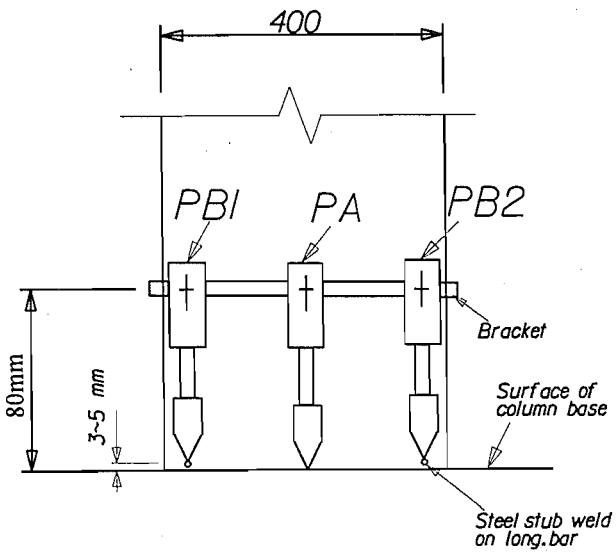

(b): Measurement of bar slip

Fig.2.10: Arrangement of Potentiometers

2.5.5 Measurement of Strains

Strain gauges were attached at various locations on the hoops and longitudinal reinforcement within potential plastic hinge regions. All gauges were the type SHOWA N11-FA-5 electrical resistance strain gauges with 5mm gauge length. For each gauge position on reinforcing bars, the strain gauges were placed in pairs on each opposite side of the bars so that the bar bending effect could be eliminated when calculating the axial strain of the hoop bars. All strain gauges on the hoops and longitudinal bars were attached before the fabrication of the reinforcing cage.

Strain Gauges on the Hoops

The strain gauges were placed in the directions parallel and perpendicular to the lateral loading direction on the square hoops of the columns, as shown in Fig.2.9. The strain gauges, marked A were used to

measure the strains mainly due to shear. The hoop strain gauges marked B on the square hoops were attached to measure the strains mainly due to confinement of the concrete. For Units 1,2 and 3, hoop strain gauges were placed on five levels of square hoops above the concrete base. Four levels of strain gauges were attached on every second hoop sets for Units 4, to Unit-6. This arrangement covered the measurement of the regions within 650mm from column base.

Strain Gauges on the Longitudinal Bars

Six levels of strain gauges were attached to the longitudinal bars at both sides of the column, as shown in Fig.2.9. These strain gauges covered a length of 860mm above the column base.

2.6 DATA ACQUISITION

The main data acquisition device used in the tests was the integral data logger unit consisting of 140 channels.

The scanning of the channels was controlled by a computer program, which allows the scan to be taken at any loading instant as directed from computer keyboard.

The displacement transducers and potentiometers used have been proved to behave in a sufficiently linear manner to justify using a constant calibration factor. Before the testing of each column unit, all transducers and potentiometers were calibrated against a known displacement to obtain calibration factors. The calibration factor for the load cell was found by calibration against a known load. The integers recorded by the datalogger were converted to numbers. The real measurements were then obtained by simply subtracting a zero-offset value and multiplying by the corresponding calibration factors.

2.7 MATERIAL PROPERTIES

In order to predict the strength of the column units accurately, it is required to determine the mechanical properties of the materials used. For each type of reinforcing steel, monotonic tensile test were carried out in accordance to the British Standard BS18: Part 2:1971 section 5[B2]. The steel specimens were cut from the reinforcing bars used for the column units.

The measured stress-strain relation for the HD20 longitudinal reinforcing steel is illustrated in Fig.2.11. The measured yield strength is about 7% higher than the specified yield strength for Grade 430. The measured stress-strain relationship for the R10 transverse reinforcing bar is shown in Fig.2.12. It can be seen that both deformed bar(HD20) and plain round bar(R10) show obviously yield point and yield plateau. The measured properties of reinforcing steel are given in Table2.2.

Table 2.2: Measured properties of reinforcing steel

Unit	Grade	f_y (MPa)	f_{su} (MPa)	E_s (MPa)	E_{sh} (MPa)	ε_y	ε_{sh}	ε_{su} (estimated)
1 to 6	R 10	362	476	182000	3510	0.0019	0.017	0.16
1	HD 20	450	593	218300	4785	0.0021	0.016	0.15
2 to 6	HD20	460	650	213400	6350	0.0022	0.013	0.15

Table 2.3: Concrete Strengths at Stage of Testing

Unit	Column Portion			Column Base Compressive Strength (Mpa)
	Test Age (days)	Comp. Strength (MPa)	Modulus of Rupture (MPa)	
1	96	33.2	4.8	53.7
2	94	32.0	5.4	40.0
3	116	32.0	5.6	40.0
4	110	35.7	6.2	44.0
5	125	35.5	6.1	45.8
6	143	35.7	5.6	45.0

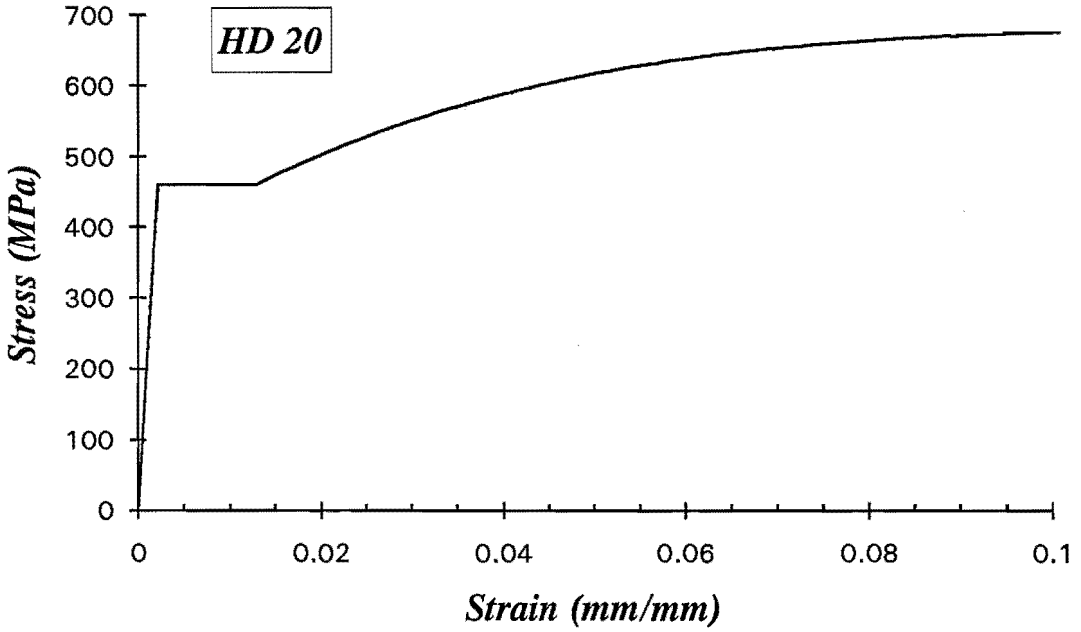

Fig.2.11: Stress-strain relation for longitudinal bas HD 20

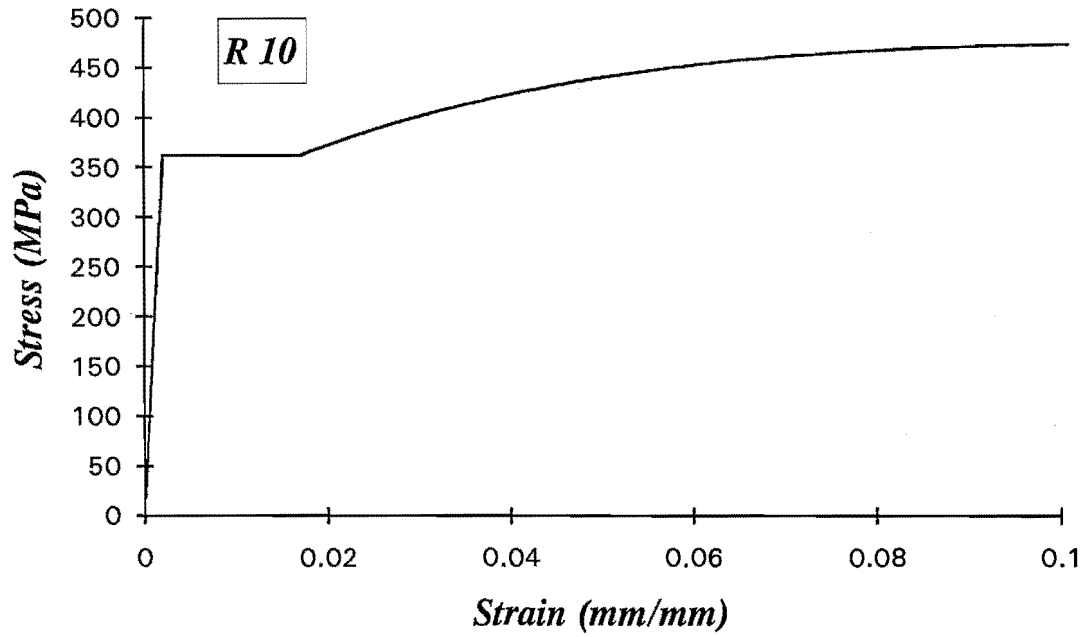

Fig.2.12: Stress-strain relation for transverse reinforcing steel R 10

The compression strength and the modulus of rupture of the concrete were obtained from 200×100mm diameter cylinder and 360×120×120mm prisms, respectively, tested according to the procedure specified in the New Zealand Standard 3112:Part 1986[S13]. These cylinders and prisms were tested at 28 days and at the stage when the column were tested. Table 2.3 lists the measured strengths on the day of testing each column. Each test result is the average value obtained from three concrete specimens.

2.8 LOADING HISTORIES

As mentioned before, the main variable for the column units tested was the applied axial loading histories. The column units were subjected to combined effects of simulating seismic lateral load and varying axial load with various intensity and frequency. The column units can be divided into three categories in terms of applied axial load pattern.

For Units 1 and 4

In the first type of axial loading pattern, an axial compression load with the value of $0.3f'_cA_g$(=1536kN) and $0.5f'_cA_g$(=2856kN), for Units 1 and 4, respectively, was applied and held constant through out the testing, while the columns were subjected to cyclic increments of lateral displacement, as shown in Fig.2.13. These two column units were to act as comparison specimens. The actions produced by this type of loading pattern are the most simple, idealized and commonly occur in the interior columns of a framed structure under the earthquake attack. This loading pattern was conventionally used by many investigators in the tests conducted on a great number of reinforced concrete columns in the past.

For Units 2 and 5

In the second type of axial loading pattern, the axial load applied was varied in direct proportion to the bending moment at the critical section of the column, as shown in Fig.2.14. This type of loading was applied to the Units 2 and 5. This loading actions could occur in the exterior columns of a moment resisting frame subjected to earthquake attack responding mainly in the first mode of vibration. The cyclic displacement history used for Units 2 and 5 in junction with this axial loading pattern is the same as that used for Units 1 and 4, as shown in Fig.2.13. With this type of axial loading pattern, it was also recognized that the variation in axial forces in the columns of a moment resisting frame would become

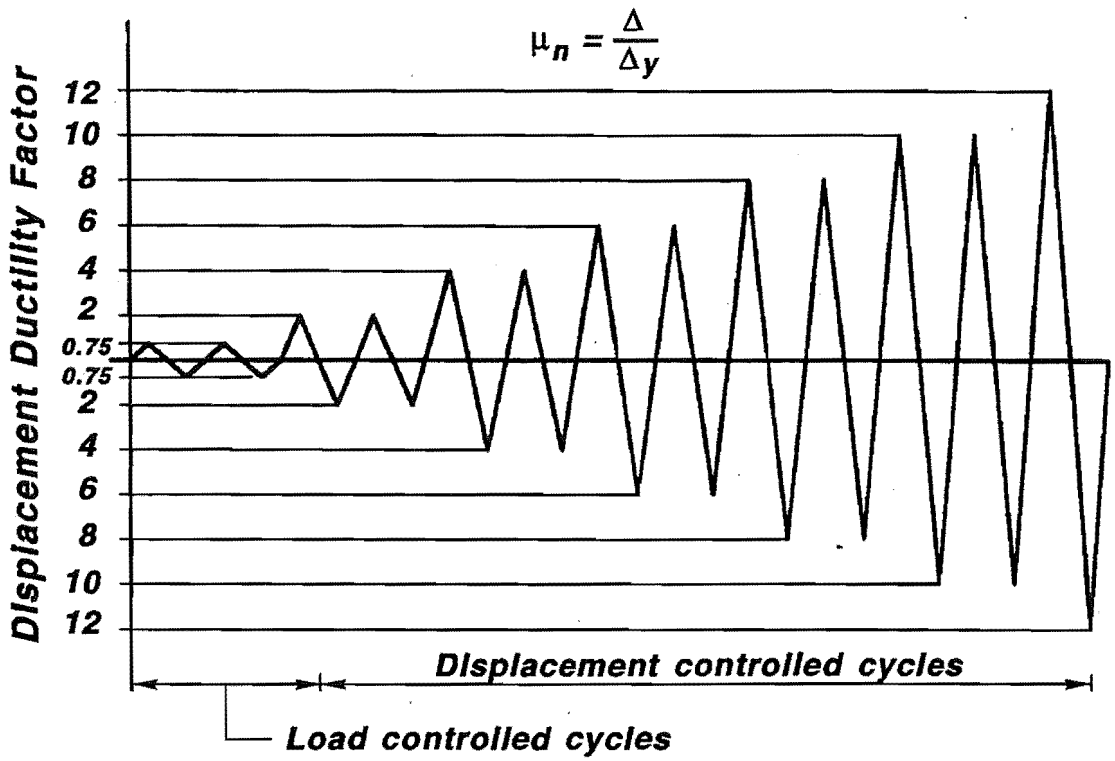

Fig.2.13: Sequence of imposed lateral displacements

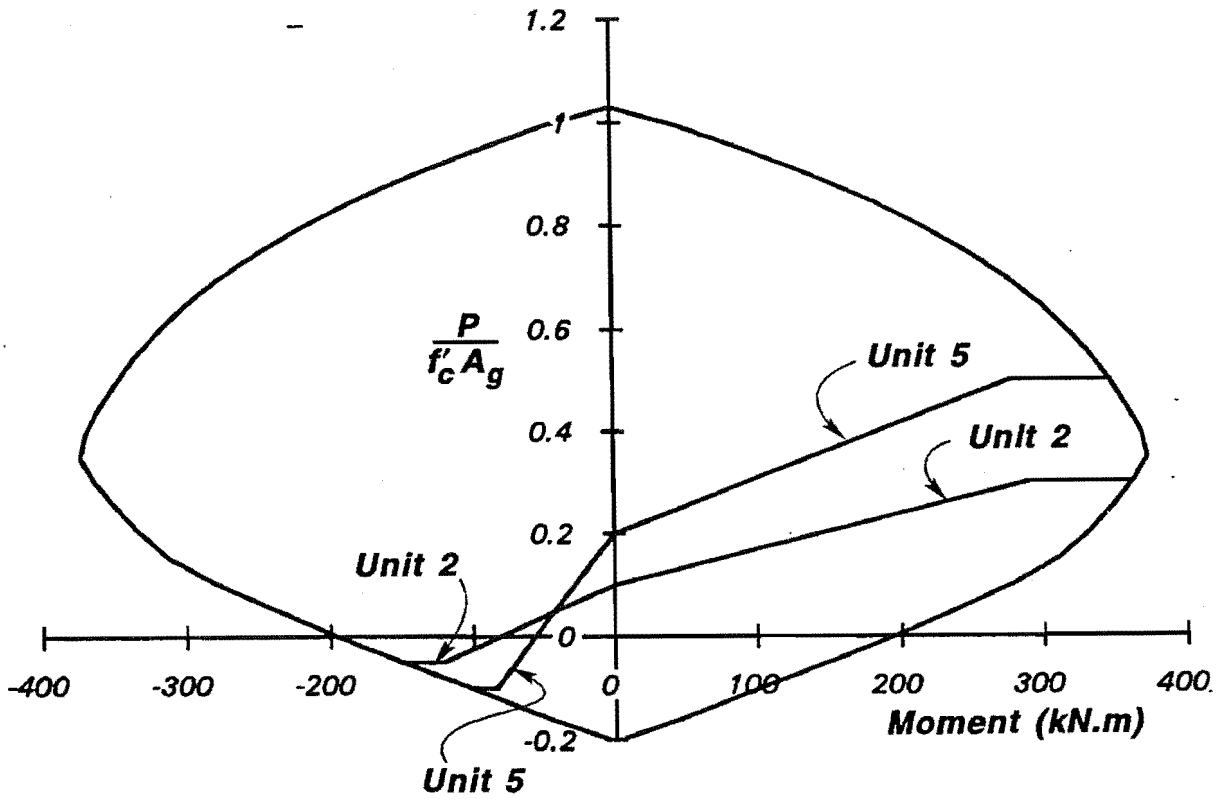

Fig.2.14: Axial load versus moment histories for Units 2 and 5

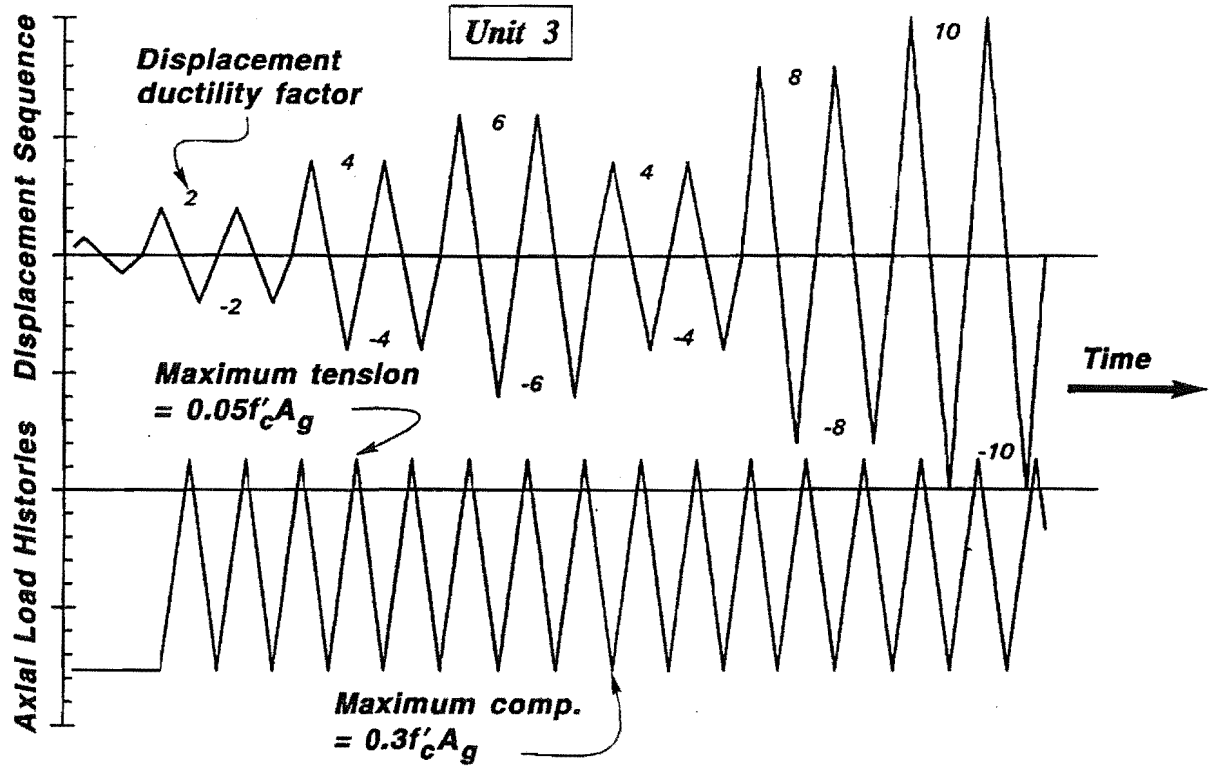

Fig.2.15: Axial and lateral displacement histories for Unit 3

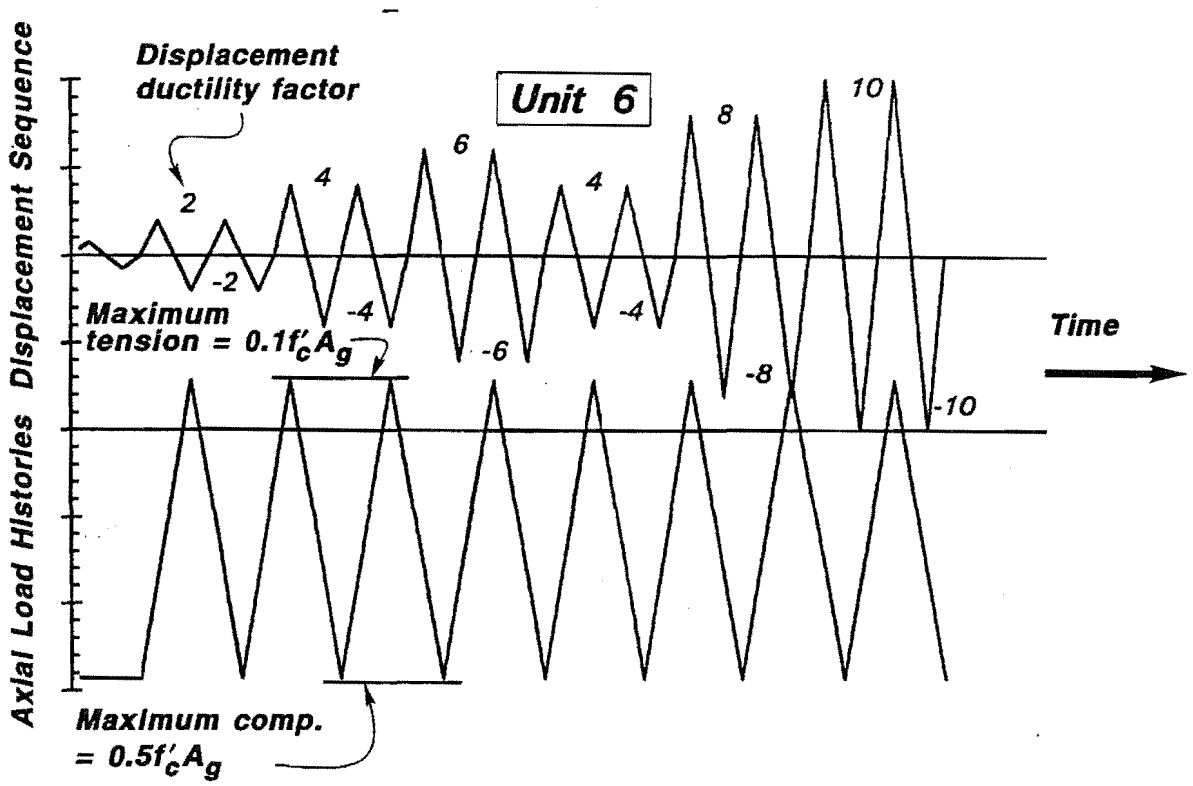

Fig.2.16: Axial and lateral displacement histories for Unit 6

very small after yielding of beams. It was therefore assumed that the axial load should be held unchanged after yielding of the column occurred. The post-yield range was defined as when $M > 0.8M_i$, where M = applied moment at the critical section of the column, M_i = ideal flexural strength of the column section calculated by using code approach and based on the measured material strengths.

When the applied moment at the critical section of the column was zero, the axial compression load was set to the level of $0.1f'_cA_g$ and $0.2f'_cA_g$, for Units 2 and 5, respectively. This neutral position was considered to be the level of axial force in the columns produced by gravity load. During the first loading cycle to 75% of the theoretical ultimate load H^+_u, in the establishment of the yield displacement Δ_y, the axial load was held constant at the level of maximum compression for these column units.

For Units 3 and 6

The third axial loading path used, is more complicated than first two types. The column units were assumed to be subjected to uncoupled variations in axial load and cyclic increments of lateral displacement. This situation might arise in the columns of a structure under the combined effects of vertical and horizontal earthquake motions. With regards to the uncoupled axial load pattern, two cases were selected to investigate the effect of change of magnitude, frequency and phasing of variation in axial load on the behaviour of the column units. Units 3 and 6 were tested using this type of axial loading pattern. The axial load applied to the column units followed independently the predetermined pattern while the units deformed with cyclic increment of lateral displacement. Figs.2.15 and 2.16 illustrate the axial and lateral displacement histories for the Unit-3 and Unit-6, respectively.

During the first loading cycle to 75% of the theoretical ultimate load H^+_u, in the establishment of the yield displacement Δ_y, the axial load was held constant at the level of maximum compression for these column units.

The maximum axial compression and the maximum axial tension loads set for Unit 3 were $0.3f'_cA_g$(= 1536kN) and $0.05f'_cA_g$(=256kN), respectively. For Unit 6, the maximum compression and tension loads were $0.5f'_cA_g$ (= 2856kN) and $0.1f'_cA_g$(=572kN), respectively.

It is to be noted that the axial load pattern imposed on each column unit was selected with the intention of investigating the effects of variations in axial load on the seismic behaviour of reinforced concrete columns. It was not intended to simulate the real variation of axial force which will occur in the columns of structures under earthquake motion.

2.9 TEST PROCEDURE

For all column units, the applied lateral loading followed the pattern conventionally used at the University of Canterbury. With the axial load held at the maximum compression axial load level for each column unit, the units were subjected to an initial loading cycle to 75% of the theoretical lateral load H^+_u to establish the yield displacement, Δ_y. H^+_u was calculated from the theoretical flexural strength of the column moment M^+_i, using the code approach, assuming a strength reduction factor ϕ=1.0, and based on the measured concrete and steel strengths. The experimental yield displacement Δ_y was found by extrapolating a straight line from the origin through the displacement at 75% H^+_u to the theoretical ultimate load H^+_u. The average of the values in both the positive and negative loading directions was taken as the experimental yield displacement.

Once the yield displacement was established, subsequent lateral loadings beyond the yield displacement were controlled by displacement increments to predetermined levels of nominal displacement ductility factor μ_n, where $\mu_n = \Delta/\Delta_y$, and Δ= lateral displacement at the top of the column. The post-yield loading pattern consisted of two complete cycles to nominal displacement ductility factors $\mu_n = \pm 2, \pm 4, \pm 6, \pm 4, \pm 8, \pm 10$ etc.

For Units 2 and 5, after establishment of the yield displacement, the lateral loading jack was operated under displacement control to each multiple value of Δ_y. The application of axial load was controlled by a computer(DARTEC APPLE) which monitored the relationship between the axial load and lateral load or the bending moment at the critical section of the column(equal to lateral load times the column height). The computer picked up the signal from hydraulic jack and displayed the value of axial load imposed on its screen. The corresponding lateral load based on the predetermined loading pattern was also displayed. On the other hand, a voltmeter was used to monitor the lateral load measured by the load cell. The feedback of the lateral load served as the command signal for the application of axial load. At any loading instant, when a displacement was applied, resulting in an increase or decrease in the lateral load, the updated value for the lateral load displayed on the voltmeter was compared with that shown on the computer. If there was any difference, the change was made by operating the computer keyboard to make these values match each other. In this way, the applied axial load followed the predetermined loading pattern.

A similar procedure was used for Units 3 and 6, in which uncoupled axial load patterns were applied. The predetermined loading history was interpreted into digital values for each loading step after the establishment of the experimental yield displacement. The lateral load was operated under displacement control while the variations in axial load were achieved by operating the computer keyboard.

Before the application of the lateral load, a complete set of readings were taken. These readings gave the initial zero readings for data reduction. Subsequently, complete sets of readings were recorded by the Data-Logger at reasonably small displacement increment intervals, including at every peak displacement ductility level.

During testing, all the cracks were marked at every peak displacement ductility level. The crack patterns were photographed, normally at each peak of nominal displacement ductility factor. Photographs of crack patterns were also taken during testing at intermediate loads in the case they were of particular interest. Photograph provided a visual record of the crack patterns at different load stage. The tests were terminated when serious buckling of longitudinal reinforcement or complete failure of the column occurred.

Chapter 3

Experimental Results and Observation of the Flexural Behaviour of Reinforced Concrete Columns Under Varying Axial Loading ___ Test Series 1

3.1 INTRODUCTION

The purpose of the first series of tests on six column specimens was to experimentally investigate the flexural behaviour of reinforced concrete column under the combined effects of reversed lateral load and varying axial load patterns. The experimental results and observations of the six reinforced concrete column units tested, Units 1 to 6, are reported in this chapter. The discussion on the performance of column units is made mainly with respect to the effect of the applied axial load. The presentations are given in the following form: general observations, lateral load-displacement hysteresis behaviour, measured curvature distributions and measured strain profiles.

3.2 GENERAL OBSERVATION

Each column unit was loaded to 75% of its theoretical ultimate lateral load, H^+_u, during the initial load cycles. The lateral strength, H^+_u,was obtained from the ideal flexural strength, M^+_i, which was calculated

using code[S14] approach with the measured material strengths and corresponding to the maximum compression axial load applied to each column unit. During the initial loading cycles, the maximum axial compression load for each column unit was applied and held constant. The experimental yield displacement, Δ_y, was then calculated as described in the Section 3.7.2 and the imposed lateral displacement pattern for the following loading cycles was determined. The general behaviour of the six column units tested are described below for the three applied axial loading patterns.

3.2.1 Units 1 and 4: Constant Compression Axial Load

The Units 1 and 4 were tested subjected to the cyclic increments of lateral displacement with the compression axial load held constant throughout the test. The constant compression axial load imposed to the column units was $0.3f'_cA_g$ and $0.5f'_cA_g$ for the Units 1 and 4, respectively.

For Unit 1, the flexural cracks first appeared near the column base and extended horizontally when the lateral load was about 70% of the theoretical ultimate lateral load. For Unit 4, with the higher axial compression load, the flexural cracks first appeared at a higher lateral load. The existing cracks became larger with further loading and some new cracks formed in the upper portion of the column. Figs.3.1 and 3.4 show the cracking patterns for the two column units at different stages of testing. Similar cracking patterns for both directions of lateral loading can be observed from these figures. The flexural cracks in the upper portions of the column became inclined at nominal displacement ductility factor of $\mu_n \geq 4$. The inclinations of the flexural/shear cracks to the column axis near the centre line were about 50 to 55-deg. The crack length in the Unit 1 was longer than that in the Unit 4. Some splitting cracks in the cover concrete of the plastic hinge regions were observed in Unit 4 at low displacement ductility level. The cover concrete started to spall during the cycle to $\mu_n=4$. On further loading to larger displacement ductility levels, most of the cover concrete in the plastic hinge regions spalled off. Incipient buckling of the longitudinal reinforcement in both the Units 1 and 4 took place at around $\mu_n=6$. Serious buckling of the longitudinal bars occurred in the Unit 4 before the end of testing.

For the two column units tested, no significant cracking was detected in the column base during the tests. This indicated that the column base remained in the elastic range and did provide extra confinement for the concrete in the plastic hinge regions of the column adjacent to the column base.

3.2.2 Units 2 and 5: Coupled Axial Load Patterns

The Units 2 and 5 were tested under cyclic lateral loading while simultaneously subjected to varying axial load. The axial load applied to these two column units was varied in direct proportion to the bending moment at the critical section of the column. Consequently, when the column was laterally loaded in the

positive lateral loading direction, a compression axial load was applied. Tension axial load was applied when the column was displaced in the negative lateral loading direction. Therefore, in the coordinates of the lateral load-displacement relation, the compression axial load occurred in one quadrant and the tension axial load occurred in the opposite quadrant. The maximum compression axial load applied to the Units 2 and 5 were $0.3f'_cA_g$ and $0.5f'_cA_g$, respectively. The maximum tension axial load applied to the Units 2 and 5 were $0.05f'_cA_g$ and $0.1f'_cA_g$, respectively.

Flexural cracks were formed in the initial positive and negative loading cycles on both sides of the column section. A few fine vertical cracks were observed early in the initial loading cycles for Unit 5. After completing the first loading cycle, the axial load varied in direct proportion with the bending moment at the critical section of the column. Two distinctive crack patterns were observed during the testing, as illustrated in Figs.3.2 and 3.5. In the positive lateral loading direction, where compression axial load was applied, the flexural cracks which formed were distributed mainly over the regions of length about 2 times the depth of column section. With further loading the flexural cracks lengthened and some cracks became inclined to the column axis.The inclined cracks did not became critical until the end of testing, indicating that shear was not significant in these column units. In the negative lateral loading direction, where tension axial load was applied, the cracks distributed over the entire height of the columns. In the plastic hinge regions, some cracks became slightly inclined to the column axis with further loading. In the upper portion of the column, the cracks extended horizontally over the full depth of the column section. For the Unit 5 with the higher tension axial load, the tension cracking was more significant than in the Unit 3. When the loading reversed from the positive lateral loading direction to the negative lateral loading direction, the previously opened cracks could not close due to the presence of tension axial load. The newly opened cracks crossed with those incompletely closed cracks. As a result, it was observed that flexure/tension cracks were formed over the full section depth in the plastic hinge regions when the loading was reversed from the positive loading direction to the negative loading direction.

The spalling and crushing of the cover concrete took place only on one side of the column during the positive lateral loading direction from about $\mu_n=4$. The crushing of the concrete was very significant in the Units 2 and 5. It was noted that crushing of the concrete extended into the core area at high displacement ductility level in the Units 2 and 5.

3.2.3 Units 3 and 6: Uncoupled Axial Load Patterns

The Units 3 and 6 were subjected to uncoupled variations in the axial load and cyclic flexure. The maximum compression axial load applied to the Units 3 and 6 was $0.3f'_cA_g$ and $0.5f'_cA_g$, respectively. The maximum tension axial load applied was $0.05f'_cA_g$ and $0.1f'_cA_g$, respectively.

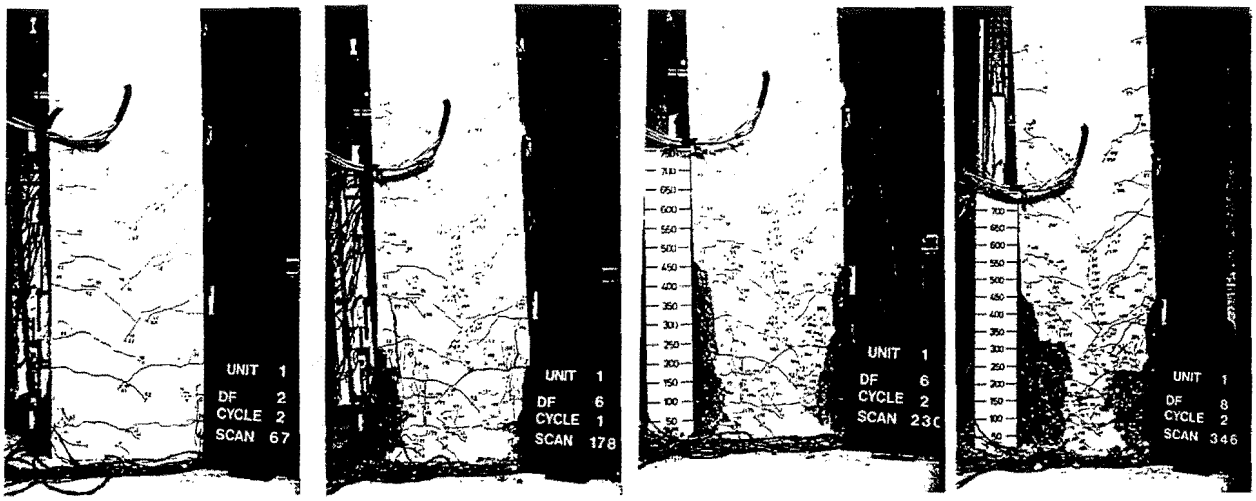

Fig.3.1: Cracking Patterns for Unit 1

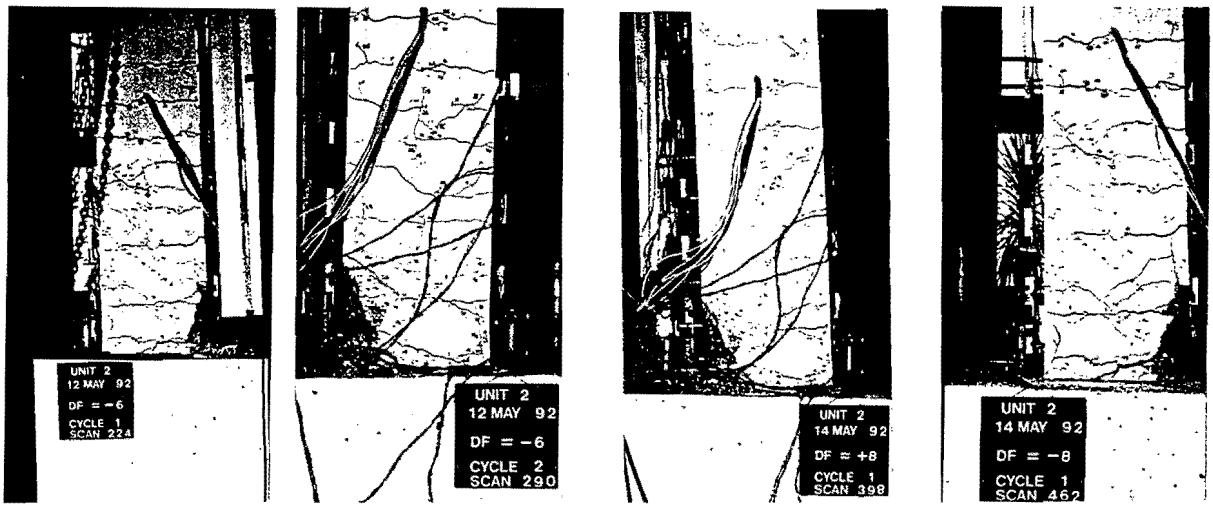

Fig.3.2: Cracking Pattern for Unit 2

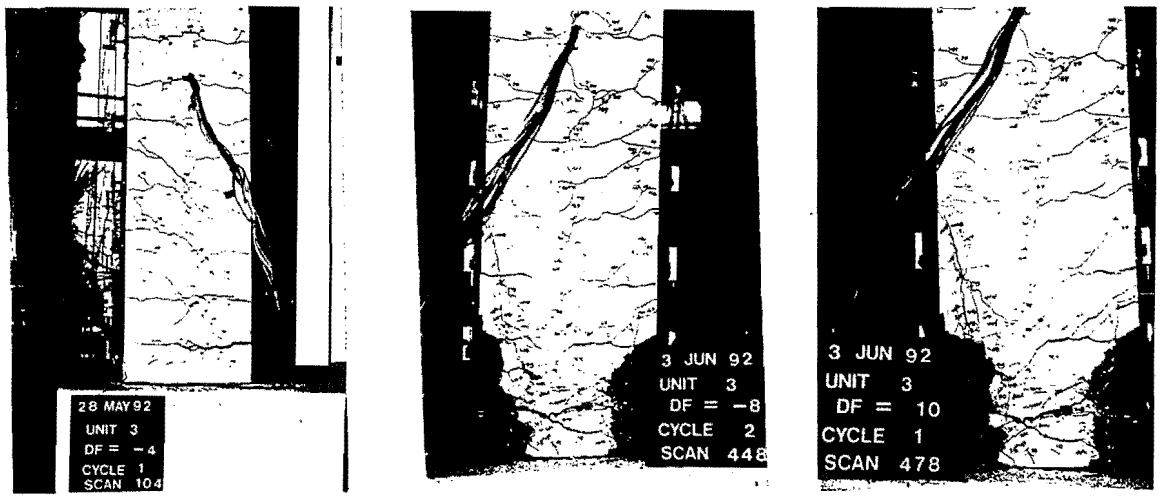

Fig.3.3 Cracking Pattern for Unit 3

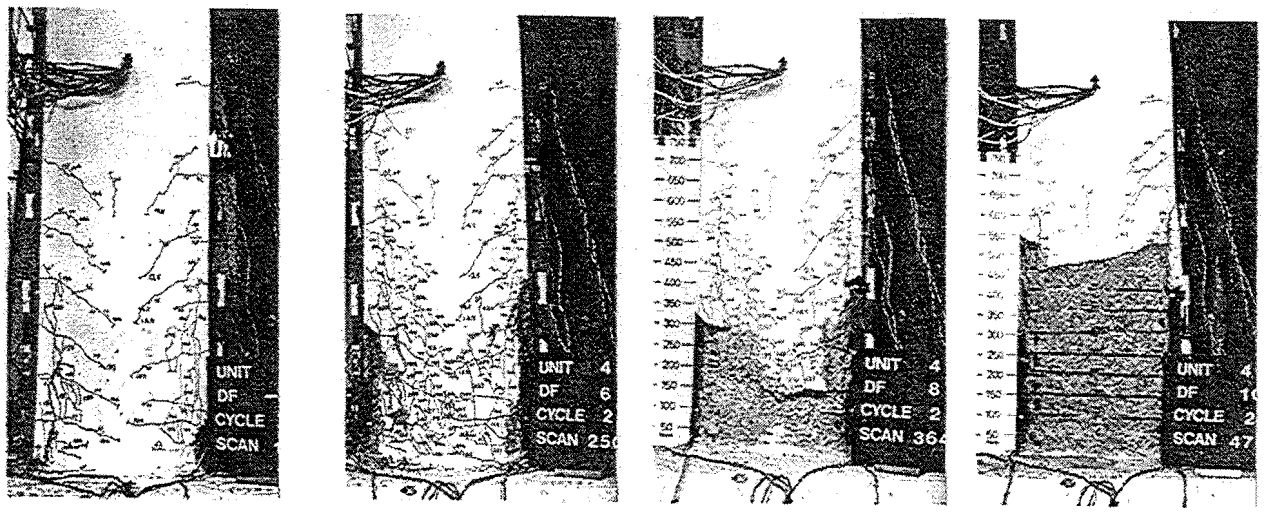

Fig.3.4: Cracking Patterns for Unit 4

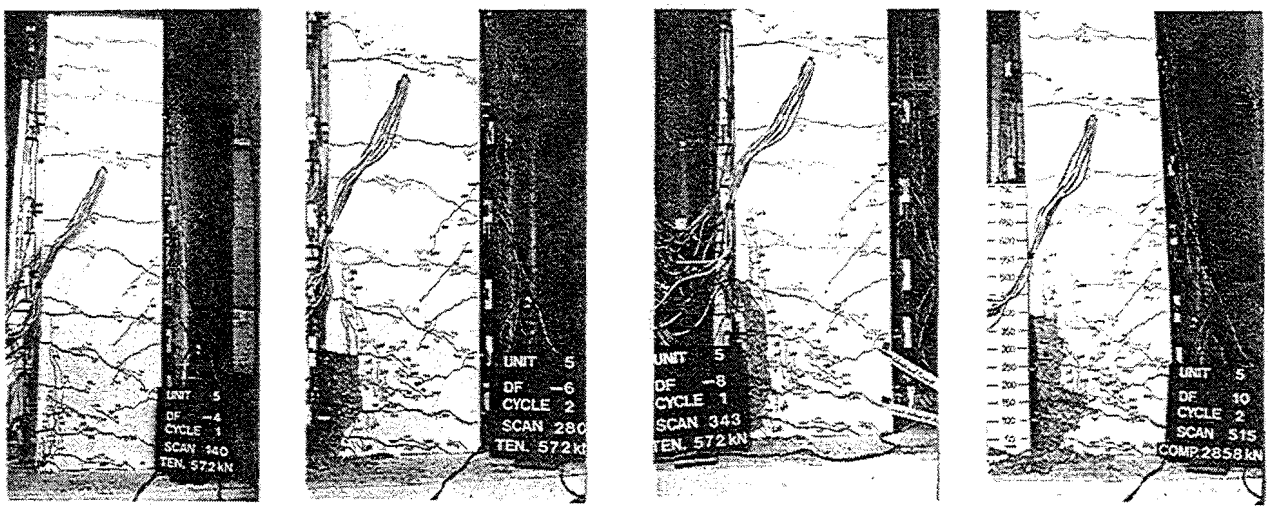

Fig.3.5: Cracking Pattern for Unit 5

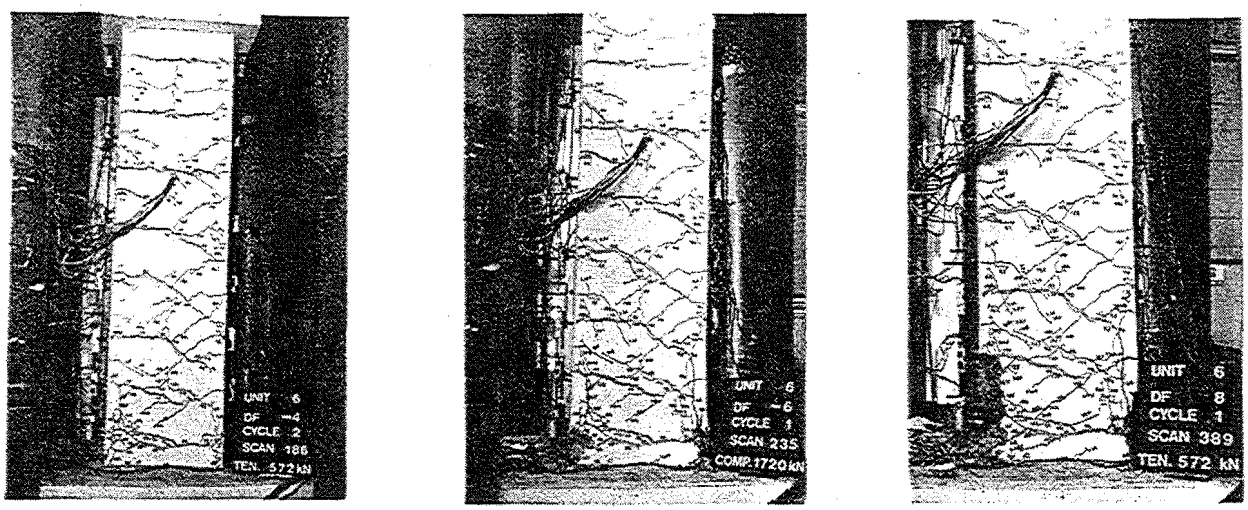

Fig.3.6 Cracking Pattern for Unit 6

The flexural cracking first took place in the plastic hinge regions in the initial loading cycle at about 65% of the theoretical ultimate lateral load, H^+_u, for Unit 3, and at slightly higher lateral load for the Unit 6. A few vertical cracks were observed in the regions adjacent to the column base in the Unit-6 at low displacement ductility levels. The flexural and tension cracks extended with further loading and distributed over the entire height of the columns in both loading directions. Figs.3.3 and 3.6 show the cracking patterns for the two column units at different stages of testing. The cracks in the upper portion of the columns extended horizontally through the section. These cracks were caused by the axial tension stress. The cracks in the plastic hinge regions were mainly caused by flexure. Under the influence of shear, these cracks became inclined to the column axis but were not critical until the end of the tests. It is apparent that shear was not significant in these columns. When the flexural/tension crack encountered the incompletely closed crack on the opposite side of the section, a full depth opened crack was formed in the plastic hinge regions. This was the case especially for the Unit 6 which had the higher tension axial load.

Spalling and crushing of the concrete took place on both sides of the column section. Serious buckling of the longitudinal reinforcement was observed at $\mu_n=10$, which terminated the tests.

Table 3.1: Theoretical Ideal Flexural Strengths and Measured Maximum Lateral Loads and Moments

Unit	Compression Axial Load				Tension Axial Load			
	M^+_i (kN.m) (a)	H^+_{max} (kN)	M^+_{max} (kN.m)	$\frac{M^+_{max}}{M^+_i}$	M^-_i (kN.m) (b)	H^-_{max} (kN.m)	M^-_{max} (kN)	$\frac{M^-_{max}}{M^-_i}$
1	345	237	408	1.18	/	/	/	/
2	356	227	389	1.09	150	134	206	1.37
3	356	235	405	1.13	150	94	152	1.02
4	348	280	493	1.42	/	/	/	/
5	348	255	456	1.30	105	94	134	1.28
6	348	240	427	1.22	105	82	120	1.14

Note:

(a). Ideal flexural strengths calculated at compression axial levels of $0.3f'_cA_g$ for Units 1, 2 and 3, and $0.5f'_cA_g$ for Units 4, 5 and 6.

(b). Ideal flexural strengths calculated at tension axial levels of $0.05f'_cA_g$ for Units 2 and 3, and $0.1f'_cA_g$ for Units 5 and 6.

3.3 Lateral Load-Displacement Hysteresis Behaviour

The experimental lateral load-displacement hysteresis loops for each column unit are presented in Figs.3.7 to 3.12. The deformation capacity of the column units is expressed in terms of both the nominal displacement ductility factor μ_n and the member interstorey drifts. The nominal displacement ductility factor is $\mu_n = \Delta/\Delta_y$, where Δ is the actual lateral displacement measured at the top of the column, and Δ_y is the experimental yield displacement. The interstorey drift is defined as the ratio of lateral displacement at the top of each column to the effective height of the column, that is, Δ/L(see Fig.3.19). For reference, the theoretical ultimate lateral load H^+_u calculated at the maximum compression axial load levels, and the maximum lateral loads obtained during the loading cycles are presented in the figures. The P-Δ effect due to axial load(see Fig.3.19) was taken into account and is plotted in the figures by a inclined line. For Units 3 and 6, in which an uncoupled axial load was applied, the axial compression or tension loads imposed on the columns at each peak of nominal displacement ductility levels are shown in these figures.

The flexural behaviour of the column units is discussed with reference to the lateral load-displacement hysteresis loops below for the three applied axial loading patterns. Table 3.1 contains some test results for the six column units tested.

3.3.1 Units 1 and 4: Constant Compression Axial Load

Figs.3.7 and 3.10 show the measured lateral load versus displacement hysteresis loops for the Units 1 and 4, respectively. The lateral load-displacement hysteresis loops were similar to those most commonly observed for the column tests conducted at the University of Canterbury during the past years. The detailing of the two column units satisfied the code[S14] requirements for ductile behaviour. As expected, both Units 1 and 4 exhibited a good energy dissipation capacity and limited reduction in strength up to the final stage of the testing. The maximum overstrength of $1.13H^+_u$ was observed for Unit 1 at $\mu_n=2$. The larger overstrength of $1.33H^+_u$ was observed at $\mu_n=4$ for the Unit 4, due to the higher compression axial load level. Although some strength degradation started at $\mu_n>4$, both column units sustained a margin over the theoretical lateral strength up to $\mu_n=8$. The degradation in the lateral load carrying capacity in the repeated loading cycles was small. No pinching of the hysteresis loops occurred in these two column units(see Figs.3.7 and 3.10).

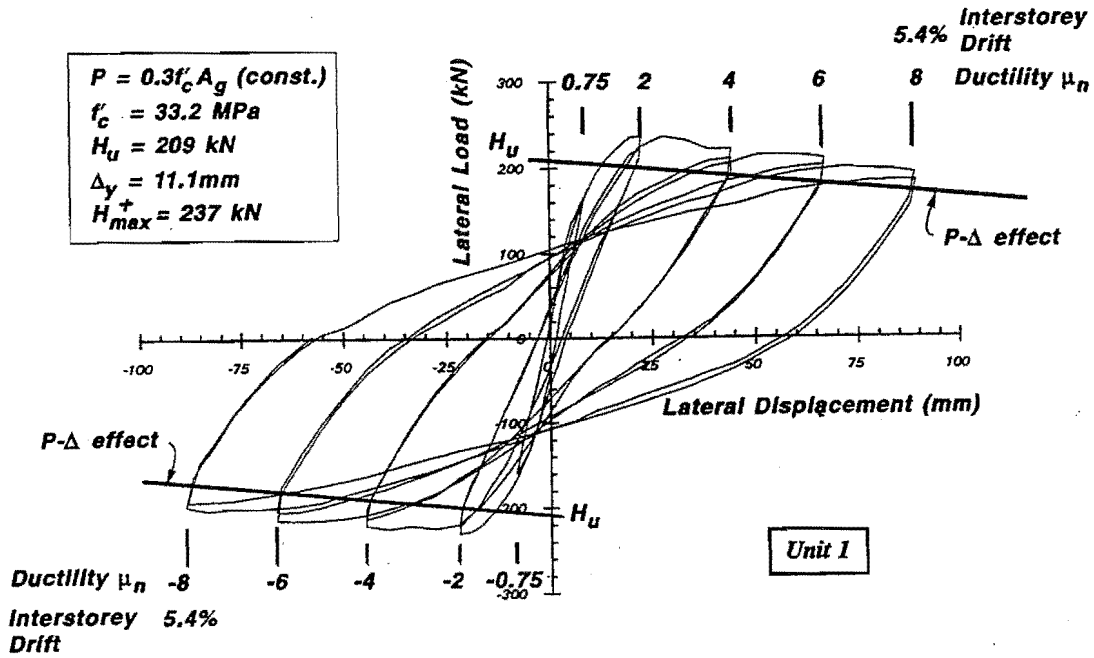

Fig.3.7: Experimental lateral load-displacement hysteresis loops for Unit 1

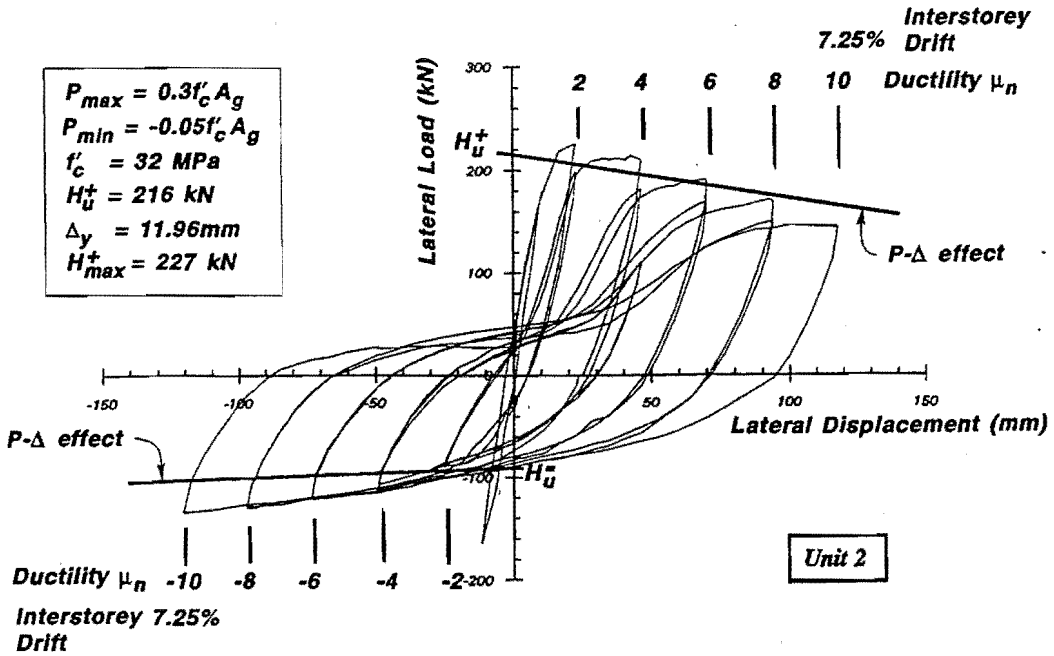

Fig.3.8: Experimental lateral load-displacement hysteresis loops for Unit 2

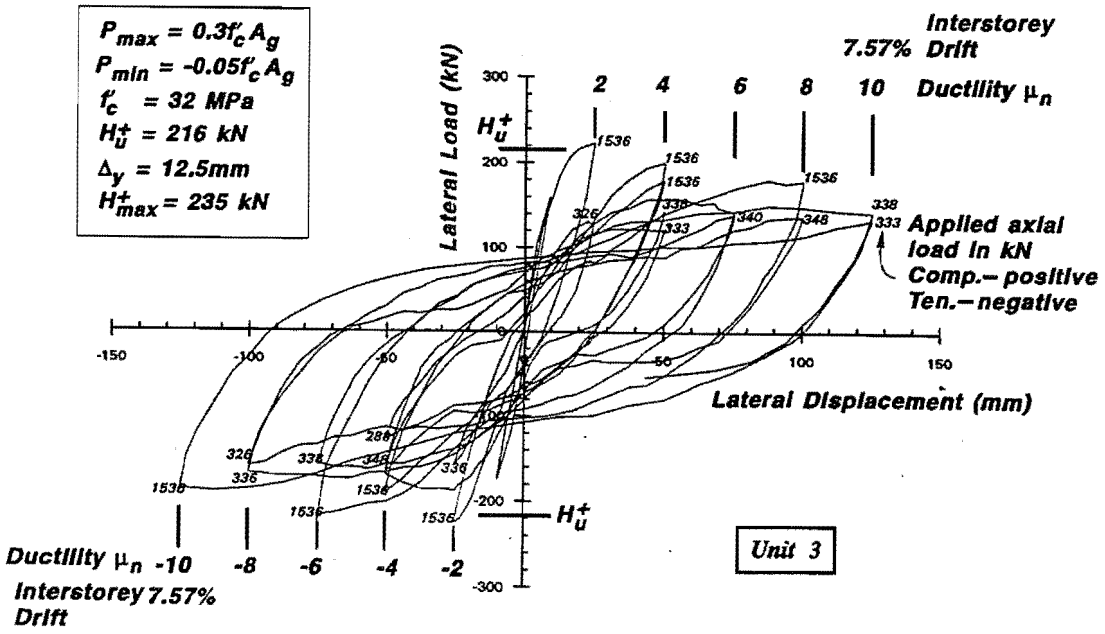

Fig.3.9: Experimental lateral load-displacement hysteresis loops for Unit 3

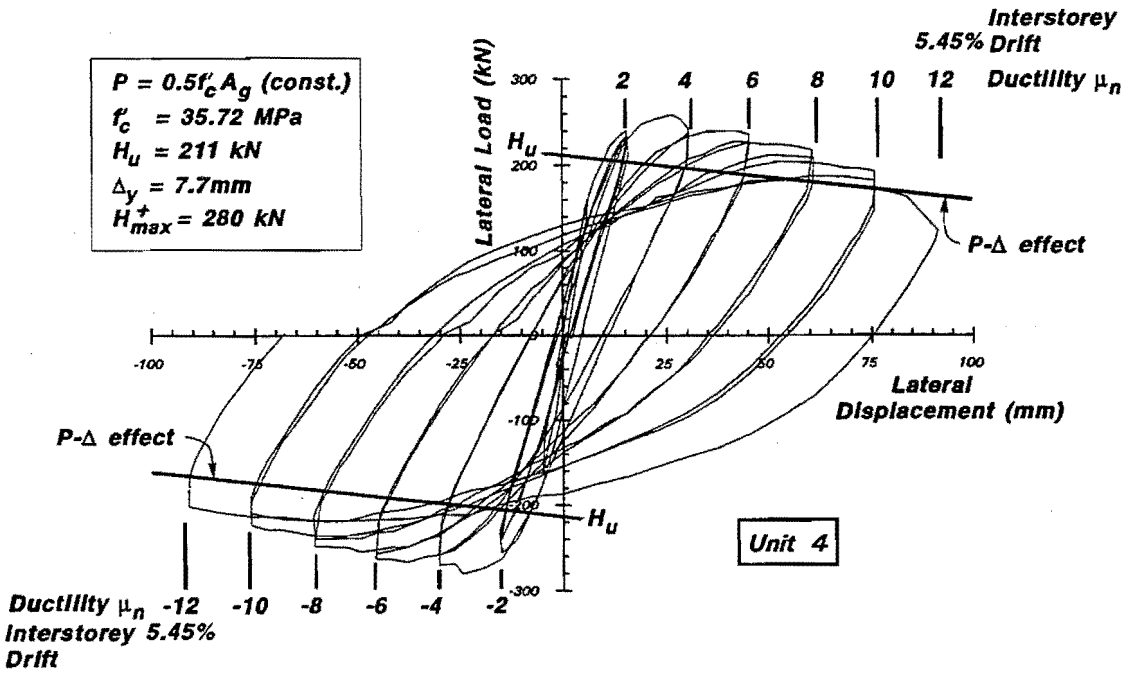

Fig.3.10: Experimental lateral load-displacement hysteresis loops for Unit 4

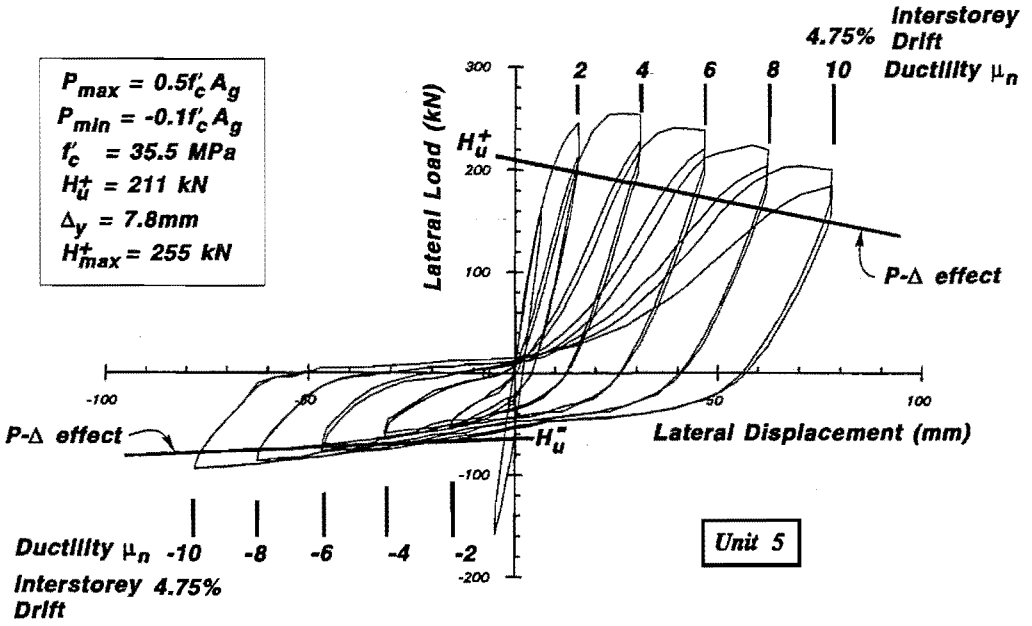

Fig.3.11: Experimental lateral load-displacement hysteresis loops for Unit 5

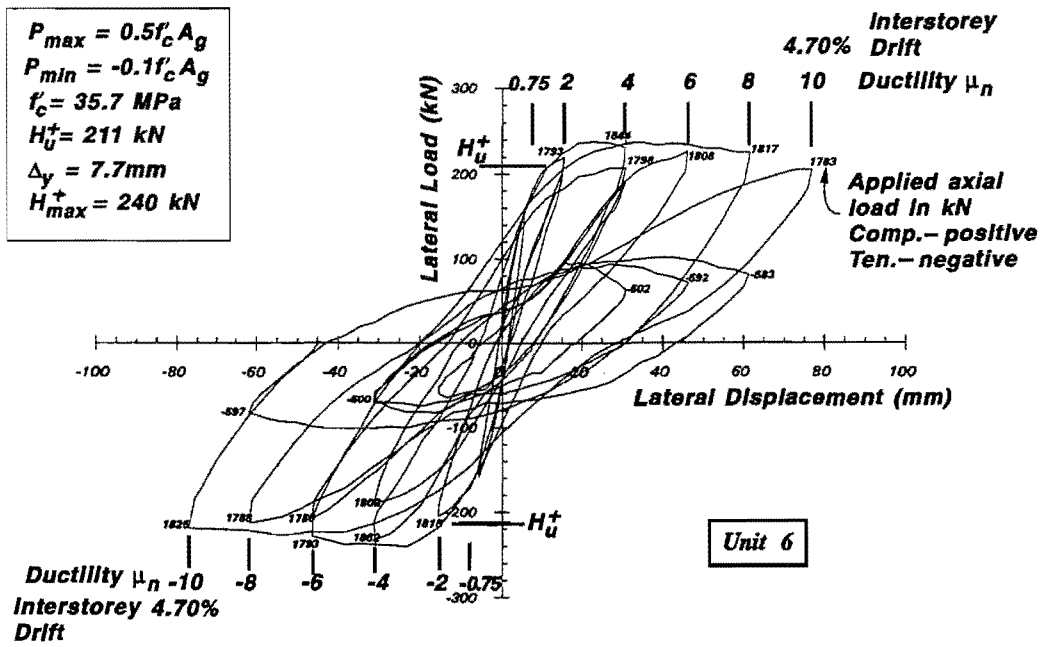

Fig.3.12: Experimental lateral load-displacement hysteresis loops for Unit 6

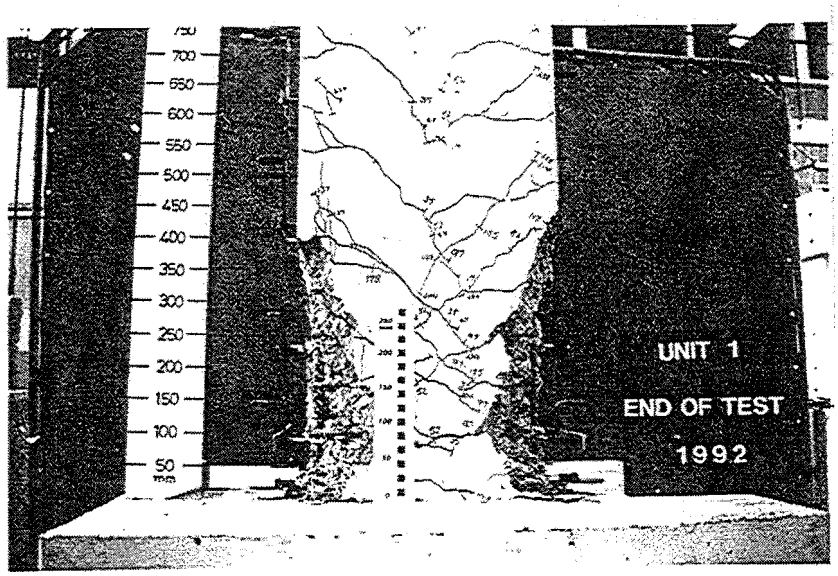

Fig.3.13: Appearance of Unit 1 at the end of testing

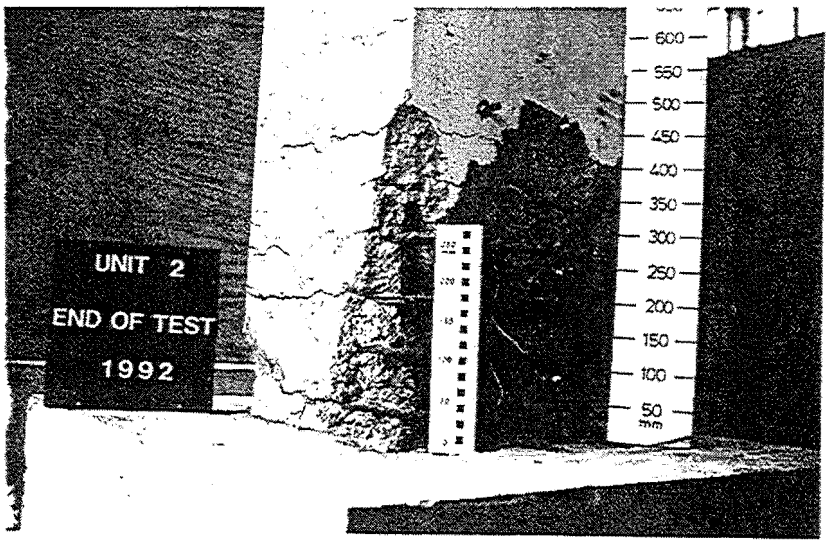

Fig.3.14: Appearance of Unit 2 at the end of testing

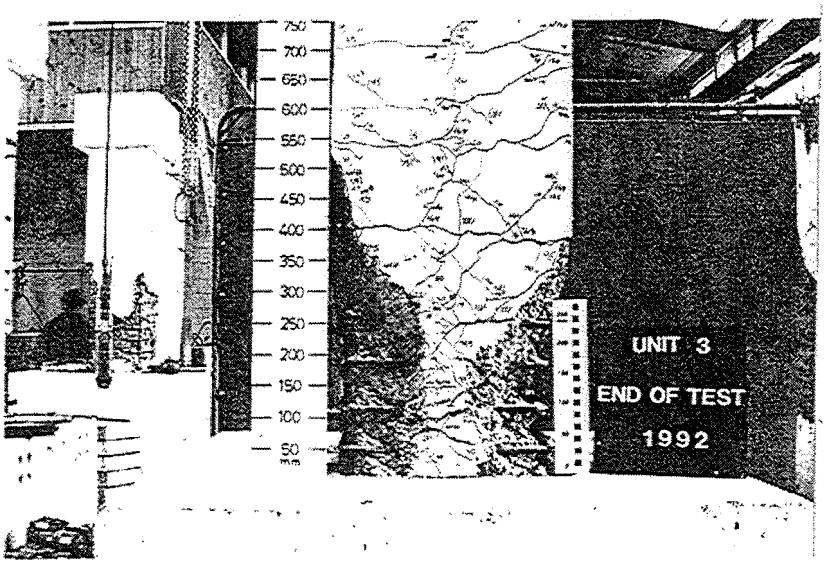

Fig.3.15: Appearance of Unit 3 at the end of testing

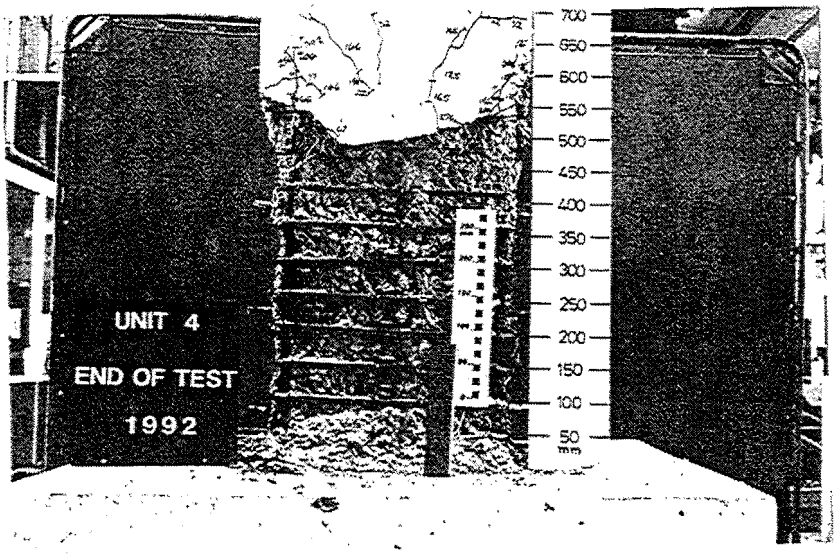

Fig.3.16: Appearance of Unit 4 at the end of testing

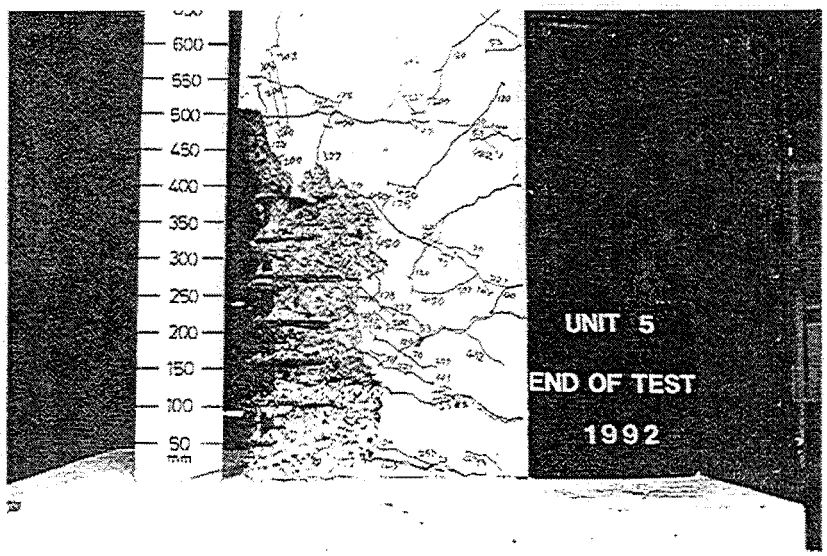

Fig.3.17: Appearance of Unit 5 at the end of testing

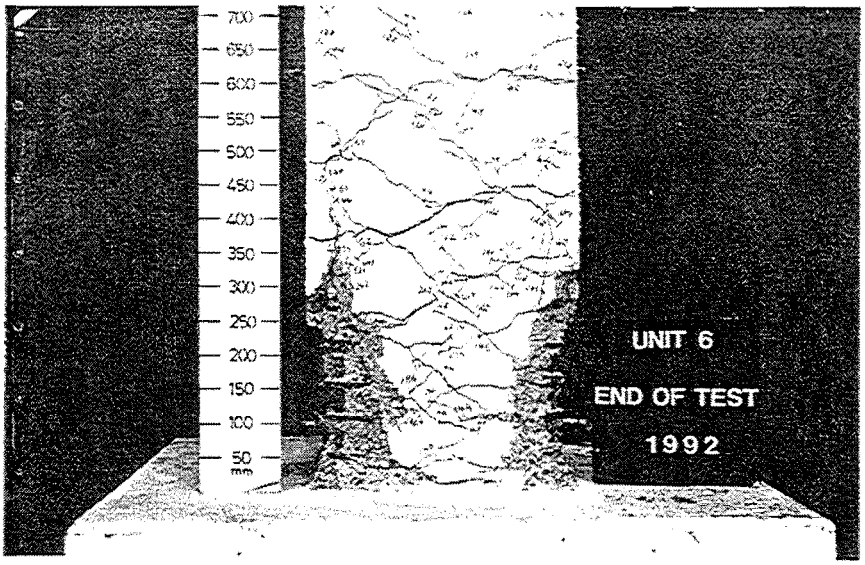

Fig.3.18: Appearance of Unit 6 at the end of testing

The inelastic deformation was caused mainly by flexural yielding, experimentally indicating a flexural dominated model. Crushing of compressed concrete and buckling of longitudinal bars occurred at nominal displacement ductility factor of $\mu_n \geq 6$. Figs.3.13 and 3.16 show the appearance of the two column units at the end of the testing. Both columns reached at least a nominal displacement ductility factor of $\mu_n = 8$, before the end of the tests.

3.3.2 Units 2 and 4: Coupled Axial Load Patterns

The lateral load-displacement hysteresis loops for the Units 2 and 5 are illustrated in Figs.3.8 and 3.11. The experimental yield displacement and the maximum lateral load measured during the tests are also included in these figures. The sloping line indicates the P-Δ effect due to axial load.

It is apparent that several features are common to these hysteresis curves. Both Figs.3.8 and 3.11 display a regular characteristic with decreasing stiffness as the imposed displacement ductility increased in the successive loading cycles. As was expected, the hysteresis loops for the two column units exhibited asymmetric shape, since the axial loads applied were completely different in the two lateral loading directions. The lateral load strength attained in the negative lateral loading direction was much smaller than that in the positive lateral loading direction, beacuse the tension axial load was applied in the former loading direction.

The effects of varying axial load on the response of the column can be found by comparing the hysteresis loops shown in Figs.3.8 and 3.11 with those in Figs.3.7 and 3.10. Considerable pinching on the hysteresis loops occurred when the load was reversed from the tension axial loading to the compression axial loading direction. This can be explained as follows. The pinching of the hysteresis loops is associated with the delay or incomplete closing of cracks under cyclic loading. The previously opened cracks with large width could not fully close when unloading to zero lateral load. Large residual plastic strains remained in the longitudinal reinforcement. It was evident that the presence of the tension axial load delayed the closing of opened cracks and increased the plastic strains in the longitudinal reinforcement. As the result, reloading into the positive loading direction met with little resistance in early stage. The column significantly softened during this stage. The lateral resistance increased after the cracked surfaces came into full contact. The pinching of the hysteresis loops was more prevalent in the Unit 5 than in Unit 2, because of the higher tension axial load applied to the Unit 5.

In the compression axial loading direction, the lateral load in both the Units 2 and 4 exceeded the theoretical strength H^+_u at nominal displacement ductility $\mu_n = 2.0$. For Unit 2, this was also the maximum lateral load measured during the testing, and strength degradation followed in the subsequently loading cycles. The lateral load had reduced to 22% less than the theoretical strength H^+_u at $\mu_n = 8$. The

strength degradation in the repeated loading cycles was very significant even at low displacement ductility levels. The maximum lateral load in the repeated loading cycles was $0.9H^+_u$ at $\mu_n=2$, and this reduced to $0.78H^+_u$ at $\mu_n=6$. Unit 5 reached its maximum lateral load of $1.21H^+_u$ at $\mu_n=4.0$, and sustained a lateral load of $0.96H^+_u$ at $\mu_n=10$. Although considerable pinching of the hysteresis loops also occurred in the case of Unit 5, the degradation in lateral load carrying capacity in Unit 2 was more significant than that in Unit 5. This may be attributed to the smaller quantity of the transverse confining reinforcement provided in the Unit 2 than in Unit 5. The centre to centre spacing of transverse reinforcement in the end regions was 70mm in Unit 2, and 55mm in Unit 5. It was observed during testing that the spalling and crushing of the concrete was more severe in the case of Unit 2. The core concrete became very loose during the reversed cyclic loading under large tension and compression strains. The crushing and spalling, which propagated into the concrete core at high displacement ductility levels in the case of Unit 2, greatly reduced the lateral load carrying capacity. Less crushing and spalling of concrete was observed in the case of Unit 5. The degradation of the strength of Units 2 and 5 during the varying axial load were more severe than that of Units 1 and 4.

In the tension axial load direction, both Units 2 and 5 attained a lateral load which greatly exceeded the theoretical ultimate load H^-_u, and the column units showed little degradation in the lateral load carrying capacity during the cyclic loading. In fact, the lateral load slightly increased as the imposed displacement ductility factor increased. It is to be noted that under tension axial load, the P-Δ effect tended to increase the lateral load capacity.

Figs.3.14 and 3.17 show the appearance of Units 2 and 5 at the end of testing. The failure of the Unit 2 was in flexure and was accompanied by serious buckling of the longitudinal bars before the end of testing. Buckling of longitudinal bars occurred at an earlier stage in Unit 5 than in Unit 2.

3.3.3 Units 3 and 6: Uncoupled Axial Load Patterns

Units 3 and 6 were subjected to uncoupled variations in axial load and cyclic lateral displacement. Figs.3.9 and 3.12 show the measured lateral load-displacement hysteresis loops for the Units 3 and 6, respectively. The lateral strength, H^+_u, calculated from the ideal flexural strength M^+_i and the maximum lateral load, H^+_{max}, measured during the testing are also included in these figures. The P-Δ effect is not shown because of the variations in the axial load at each peak of displacement ductility. Also shown in these figures are the axial loads imposed on the column units at each peak of displacement of the hysteresis loops.

It can be seen from Figs.3.9 and 3.12 that the uncoupled variations in axial load resulted in asymmetry of the lateral load-displacement hysteresis loops. Both Units 3 and 6 displayed an irregular hysteresis

behaviour with decreasing stiffness as the imposed displacement magnitude increased in successive loading cycles. It was found that the flexural strength of the columns developed at the peak displacement was not dependent on the axial loading sequence but was mainly dependent on the axial load level that was present in that loading sequence. When the imposed axial compression load was very low or when the axial load was in tension, the lateral load reached a very low value even at the initial low displacement ductility levels. The flexural strength capacity of the columns increased as the compression axial load increased to an appropriately high level in the following loading cycles. Hence the flexural strength followed that given by the interaction relationship between the axial load and bending moment.

Pinching of the hysteresis loops was observed at low displacement ductility levels when the axial load changed from the tension to compression.

The degradation in the strength was more pronounced for Unit 3 than that for Unit 6. The maximum lateral load of Unit 3 exceeded the theoretical ultimate load H^+_u at the nominal displacement ductility $\mu_n=2$ and finally reduced to $0.83H^+_u$ at $\mu_n=8$ in the positive lateral loading direction when the compression axial load attained the maximum value. However, the lateral load carrying capacity of Unit 6 maintained a good margin over the theoretical ultimate strength until a nominal displacement ductility factor of $\mu_n = 8$. This indicated that favourable effect of closely-placed transverse reinforcement on maintaining the flexural strength of the columns under repeated loading conditions. The strength degradation of Units 3 and 6 was more severe than that for their companion specimens, Units 1 and 4, which were subjected to constant compression axial load.

Figs.3.15 and 3.18 show the appearance of the two column units at the completion of the tests. The loose cover concrete has been removed to show the extent of spalling.

3.3.4 Monotonic Lateral Load-displacement Envelopes

From the experimental cyclic lateral load-displacement relations the monotonic lateral load-displacement envelopes for each column unit were constructed. The coordinates of the constructed monotonic lateral load-displacement envelopes for Units 1 and 4 are the average values of the cyclic lateral load-displacement relations, shown in Figs.3.7 and 3.10, at each peak displacement ductility in both the positive and negative lateral loading direction. For Units 2 and 5, the coordinates of the monotonic lateral load-displacement envelopes are the values of the cyclic lateral load-displacement curves(see Figs.3.8 and 3.11) at each peak displacement ductility in the compression axial load direction. For Units 3 and 6, these coordinates are the values at the peaks of the cyclic loading cycles where the maximum compression axial load was presented at that displacement ductility level. The constructed monotonic lateral load-displacement relations are shown in Fig.3.20.

The effects of the axial loading pattern on the behaviour of the column units can be found by comparing the constructed monotonic lateral load-displacement relations of the two groups of column units. Each of the two groups of column units contained the same amount of transverse reinforcement, and were tested under constant compression axial load(Units 1 and 4), and coupled(Units 2 and 5) and uncoupled(Units 3 and 6) varying axial load along with the cyclic lateral loading. The varying axial load patterns resulted in lower lateral load carrying capacity. The lateral load for the Units with varying axial load was about 8 to 17% less than that of companion units with constant axial load during the first loading cycles, and reduced up to 30% during the second loading cycles.

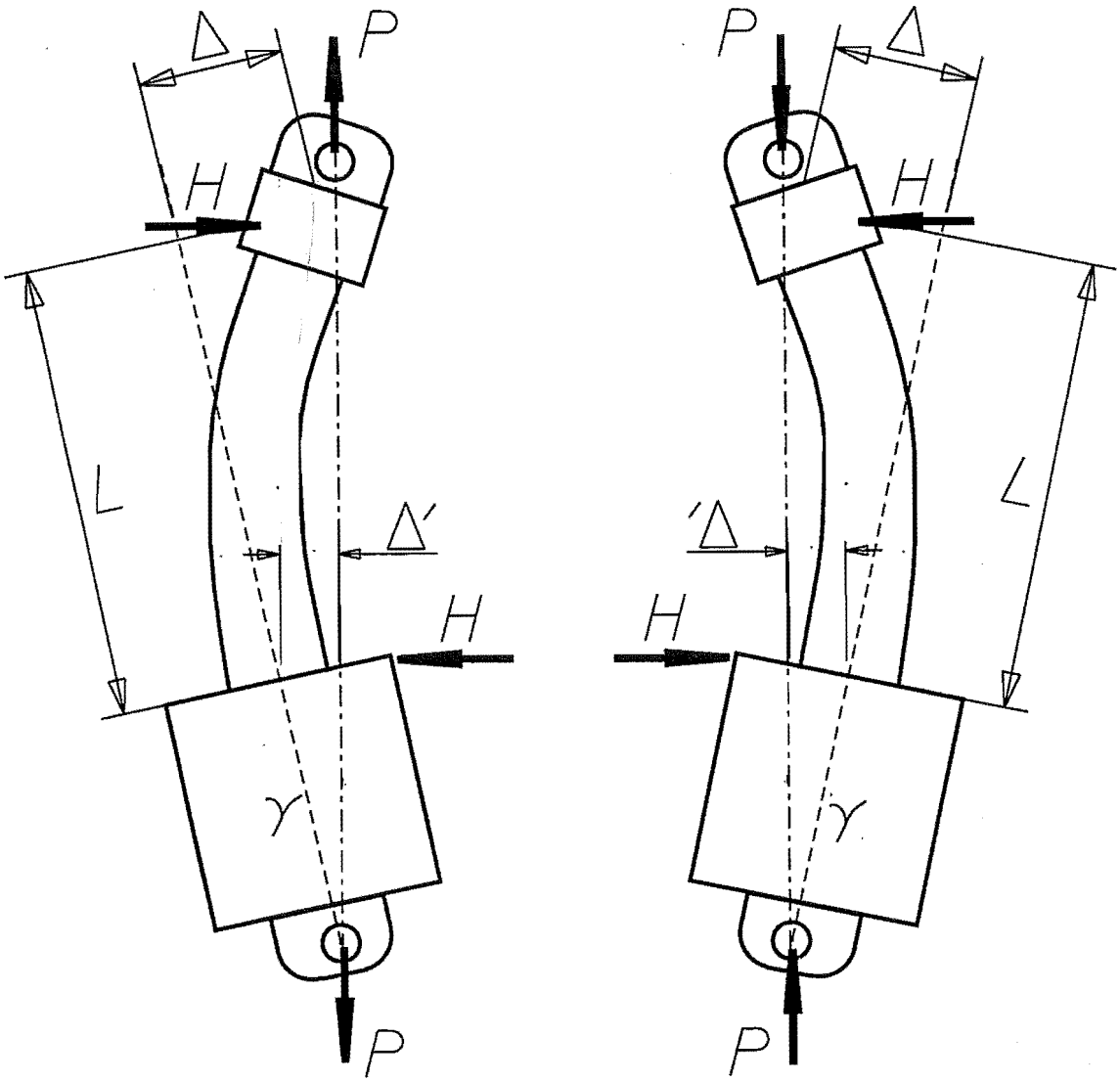

Fig.3.19: P-Δ effect due to axial load

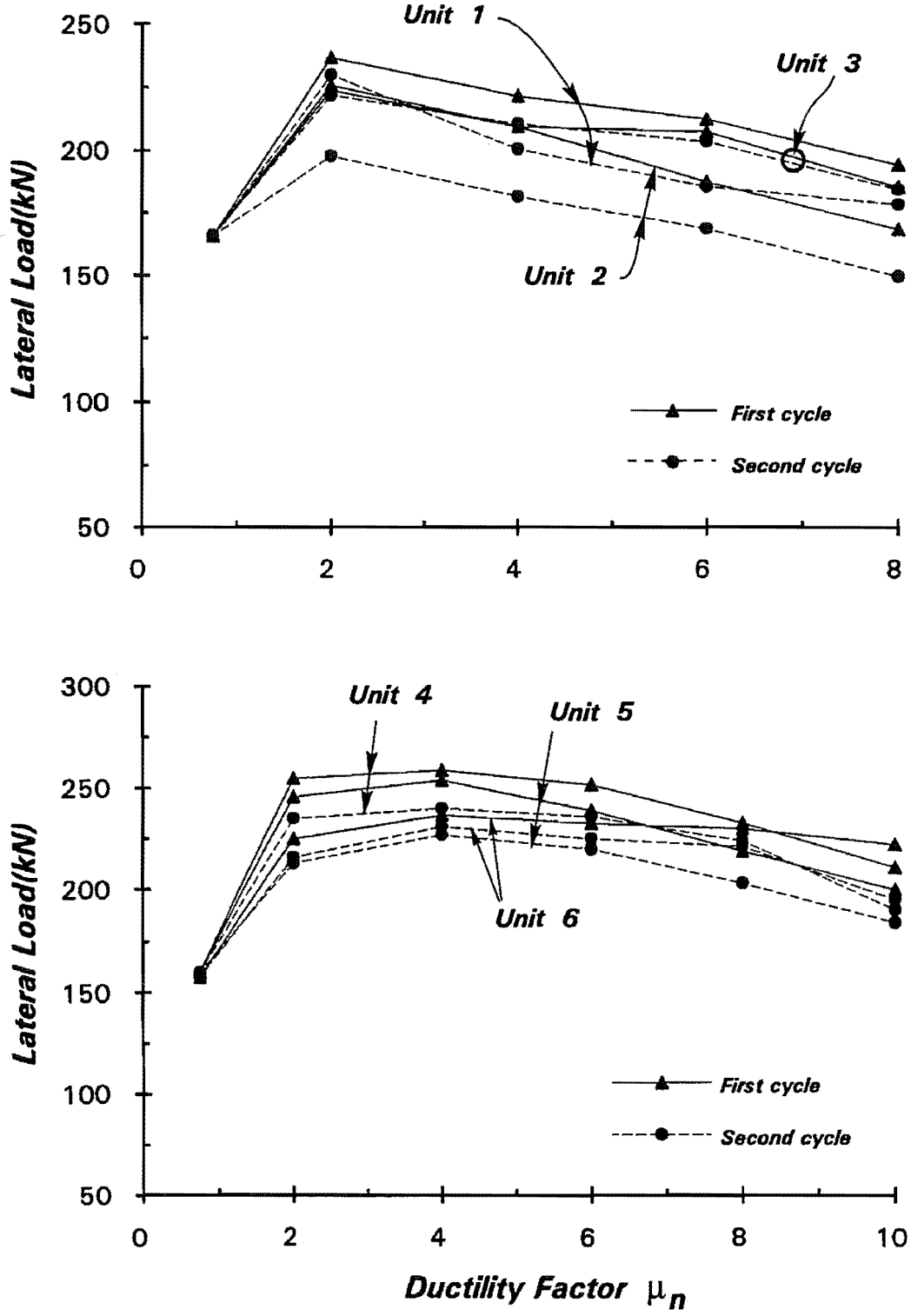

Fig.3.20: Constructed Monotonic Lateral Load-Displacement Relations

3.4 CURVATURE DISTRIBUTION

The experimental curvature was calculated from the readings of the linear potentiometers mounted on the columns, which measured the changes in various gauge lengths. The actual initial gauge length and the distance between the axes of opposing pairs of potentiometers were recorded before the test began. When placing the linear potentiometers, attention was paid to ensure that they were parallel to the column axis. Fig 3.21 shows the configuration of a typical pair of potentiometers. With the assumption that plane section remains plane after bending, and that the potentiometer rod remains straight, the average rotation, θ_i, over the gauge length can be computed as

$$\theta_i = \frac{\delta_{Ei} + \delta_{Wi}}{h_i} \qquad (3.1)$$

where δ_{Ei} and δ_{Wi} are the changes in the length of opposing pairs of vertical potentiometers. h_i is the distance between the opposing pair of the potentiometers. The average curvature(see Figs.3.21 and 3.22), ϕ_i, of each segment over the gauge length, l_i, is then given by

$$\phi_i = \frac{\theta_i}{l_i} \qquad (3.2)$$

The curvature profiles calculated by Eqns.3.1 and 3.2 for the six column units tested are shown in Figs.3.23 to 3.28. The experimental yield curvatures, ϕ_y, which will be further discussed in the next section, are also shown in these figures as vertical dashed lines. The average curvatures are plotted at the mid-point of the gauge length and successive points were connected by straight line, as shown in Fig.3.22.

The curvature distributions for Units 1 and 4 are seen to be symmetric as expected since the section was symmetrical about the axis of the bending and the compression axial load in each of these columns was held constant throughout the tests. Hence the loading actions were symmetric for each direction of displacement. Unsymmetric curvature distributions of Units 2 and 5 are seen in Figs.3.24 and 3.27. The curvature in the negative lateral loading direction was larger than that in the positive lateral loading direction.

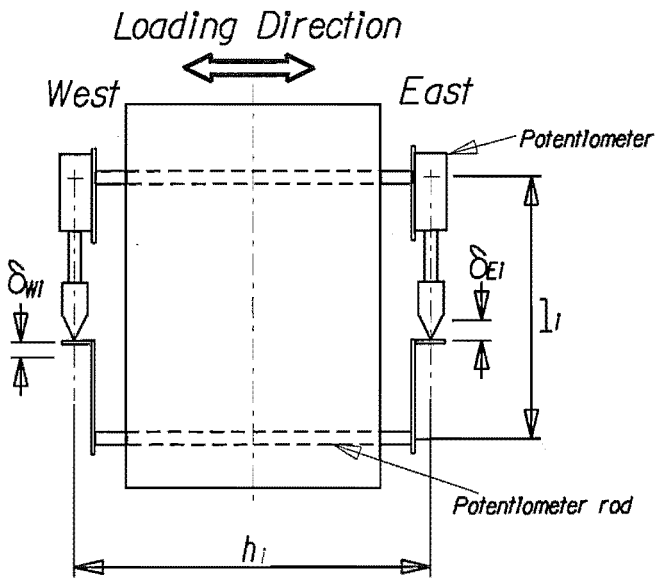

(a) Potentiometer Configuration

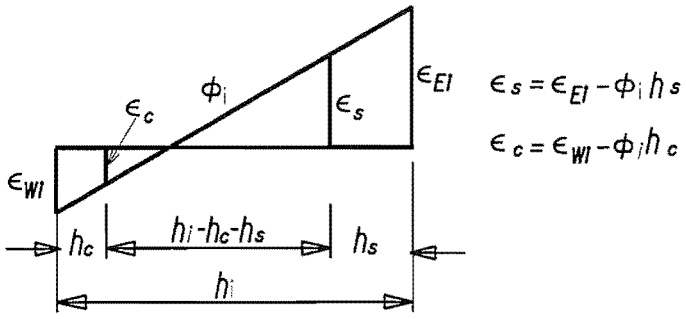

(b) Strain Distribution

Fig.3.21: Calculation of average curvature and concrete strain

The magnitude of the experimental curvature generally increased as the imposed displacement ductility increased. The curvatures at the first gauge level in some cases were unproportionally larger than those at other gauge levels. The curvature at the first gauge levels for the Unit 2 and Unit 5 when the tension axial load was applied was particularly large. It appeared that the columns yielded in the tension axial loading direction only in a small regions adjacent to the column base. The plastic curvatures were concentrated in these regions. To reach the same displacement at the top of the column as in the compression axial load direction, large rotations had to occur at these sections.

For the Units 1, 2, and 3 with a maximum compression axial load of $0.3f'_cA_g$, the plastic curvatures were observed to spread over the regions about 450mm above the column base. For the Units 4, 5 and 6, with a maximum axial compression load of $0.5f'_cA_g$, the plastic curvatures took place over regions about 600mm above column base, confirming that these regions require extra protection for confinement because of the high axial compression level. It is felt that the code specified length of 1.5 times the

column depth for the confined regions may not necessarily conservative for the columns with this axial compressive load level.

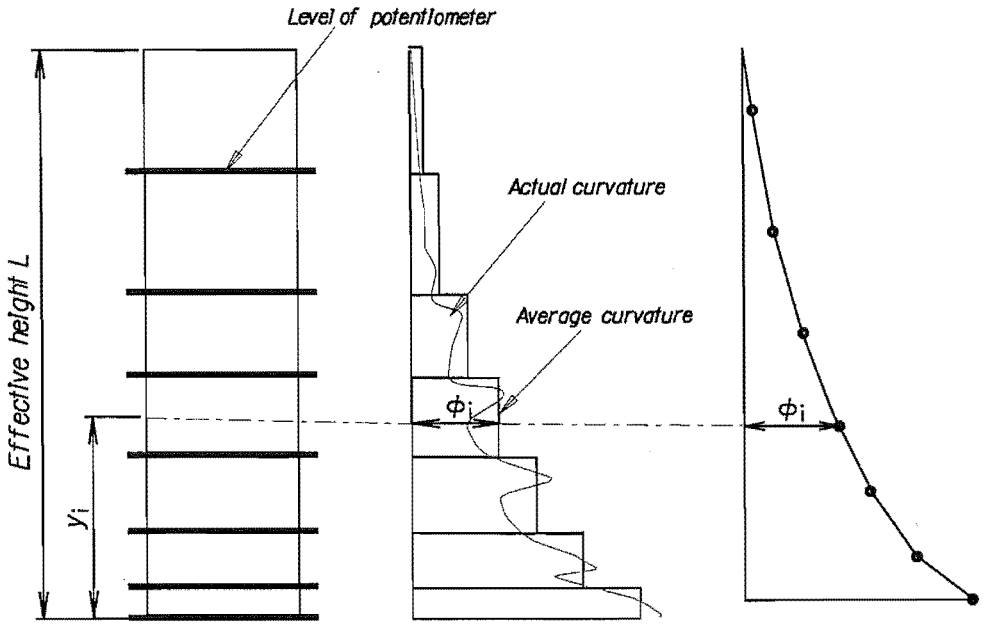

Fig.3.22: Assumed curvature distribution

3.5 SECTION BEHAVIOUR OF THE COLUMN UNITS

3.5.1 Experimental Moment-Curvature Relationships

The column units generally remained in the elastic range during the initial loading cycles to $\pm 0.75H^{+}_{u}$. Once the column was loaded into the post-elastic range, the deformation concentrated in the plastic hinge regions. For further loading, the increase of lateral displacement was mainly due to plastic deformations at the yielding sections. The member ductility mainly depends on the deformation capacity of the plastic hinge regions. It is of interest to examine the moment-curvature relationships since they represent the section behaviour of the column units. Information on the curvature behaviour of the critical sections of the column in the plastic hinge regions is very useful in design.

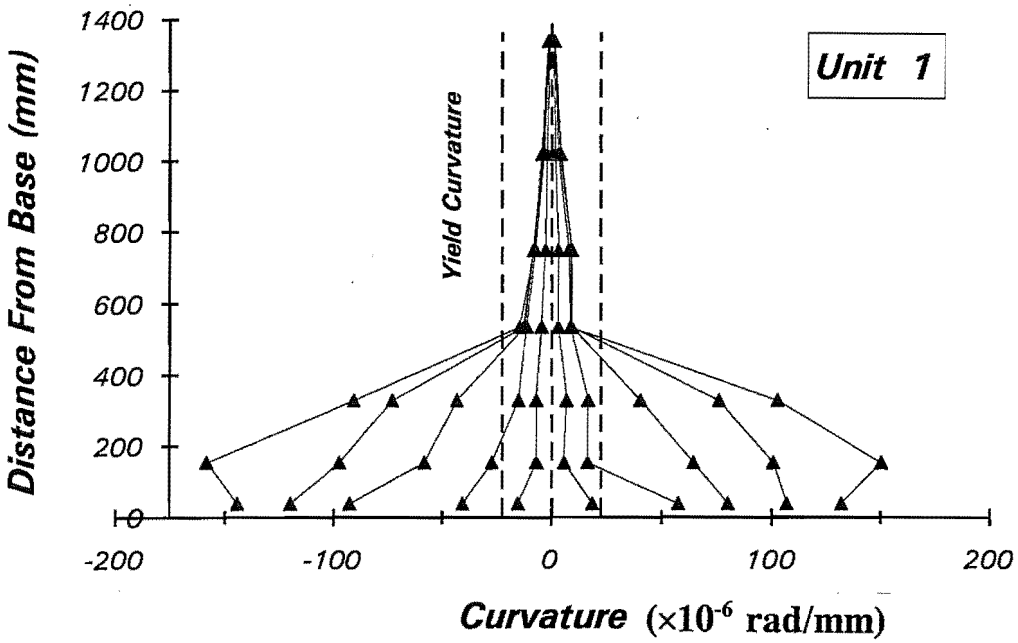

Fig.3.23: Measured Curvature Distribution for Unit 1

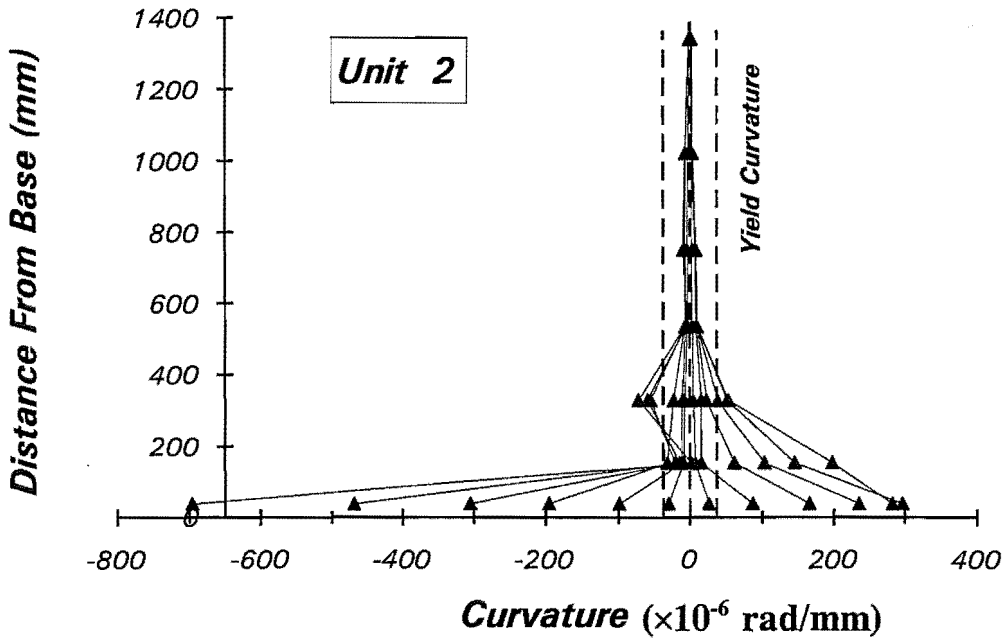

Fig.3.24: Measured Curvature Distribution for Unit 2

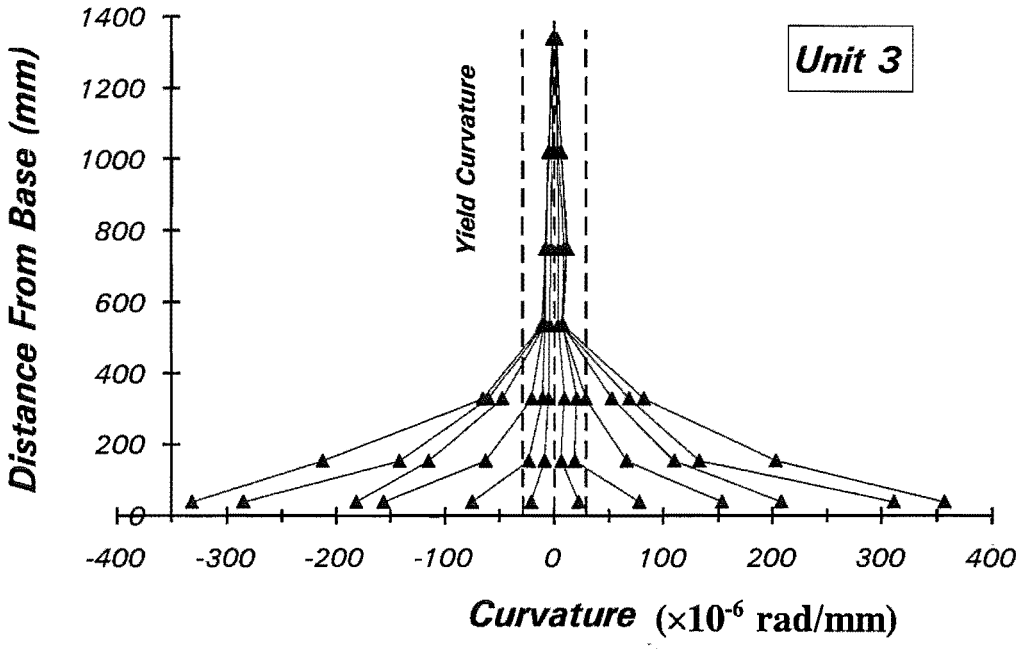

Fig.3.25: Measured Curvature Distribution for Unit 3

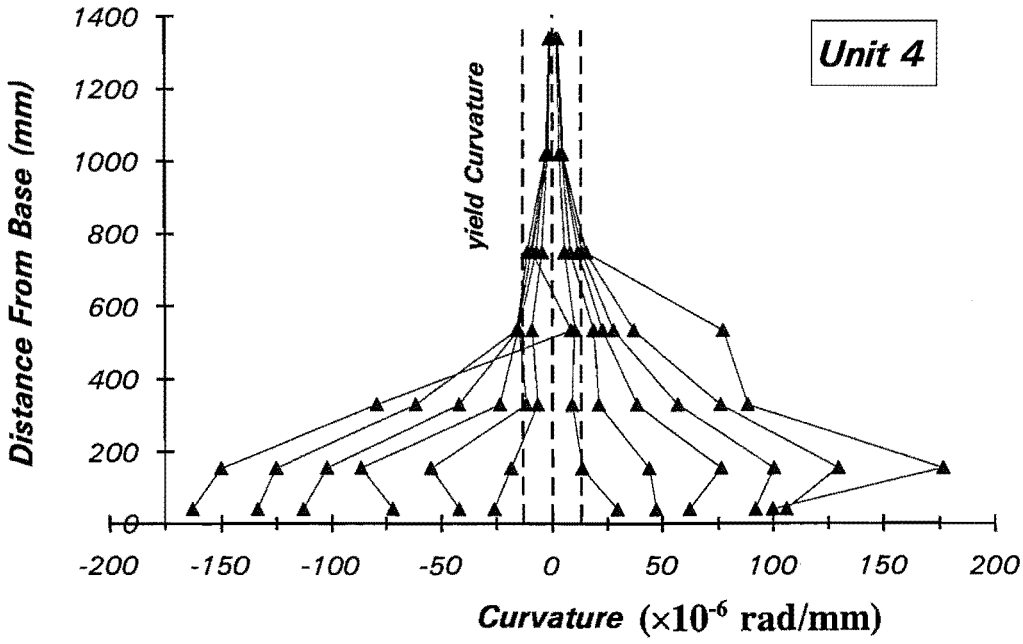

Fig.3.26: Measured Curvature Distribution for Unit 4

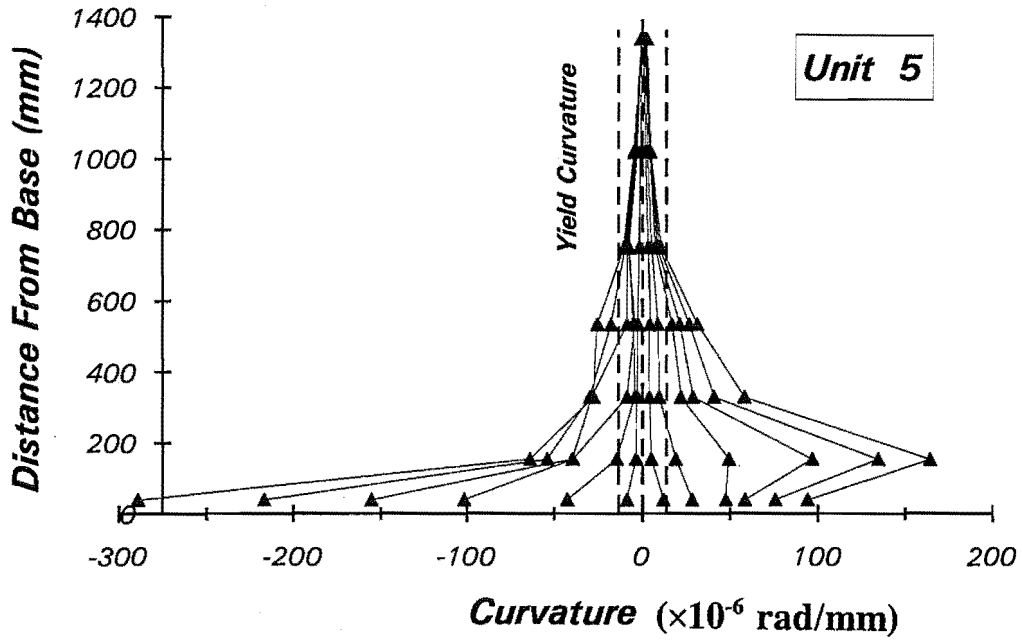

Fig.3.27: Measured Curvature Distribution for Unit 5

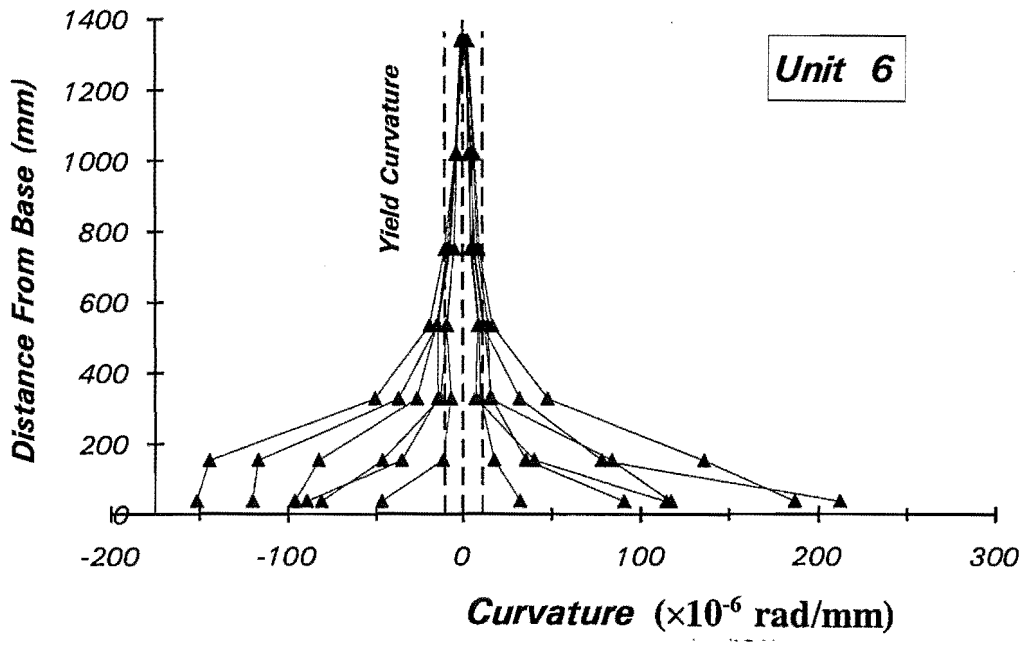

Fig.3.28: Measured Curvature Distribution for Unit 6

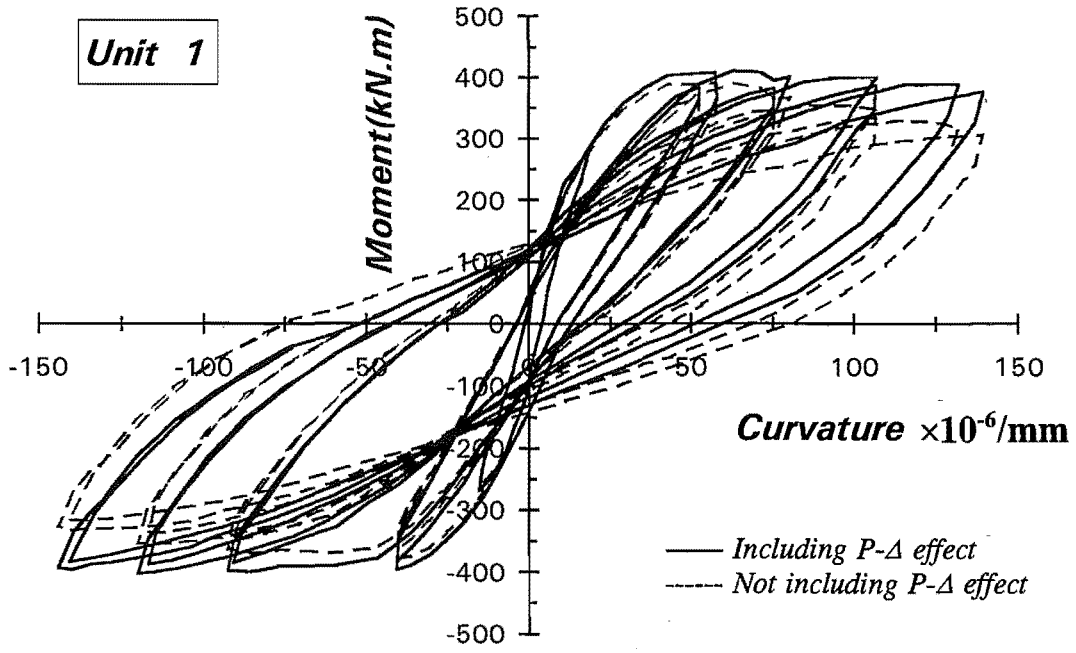

Fig.3.29: Experimental Moment-Curvature Hysteresis Loops for Unit 1

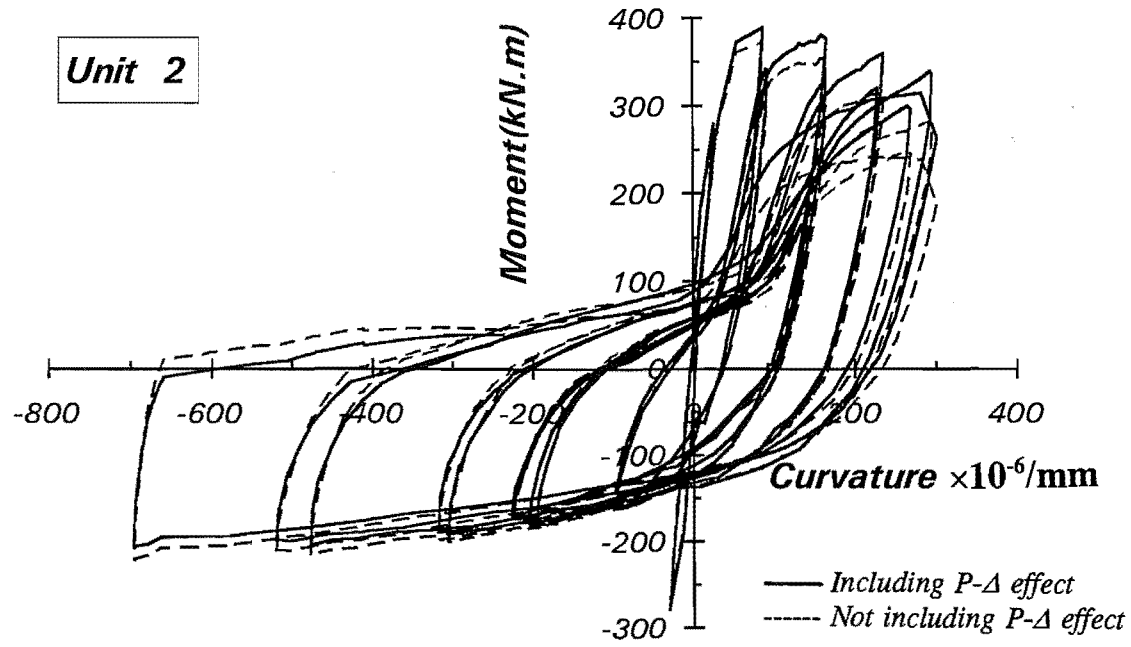

Fig.3.30: Experimental Moment-Curvature Hysteresis Loops for Unit 2

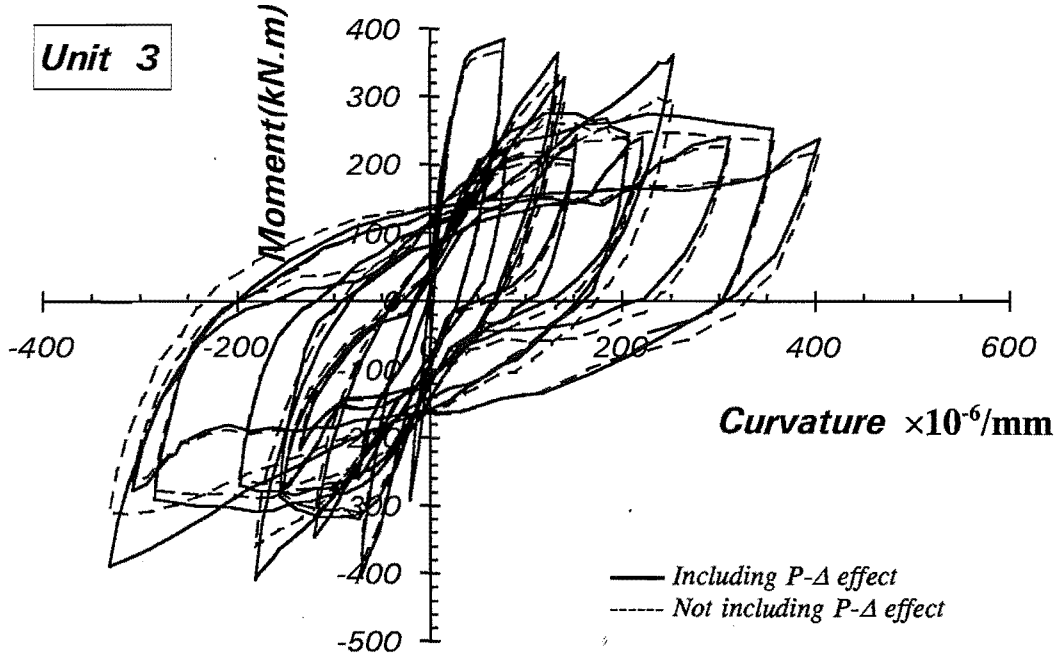

Fig.3.31: Experimental Moment-Curvature Hysteresis Loops for Unit 3

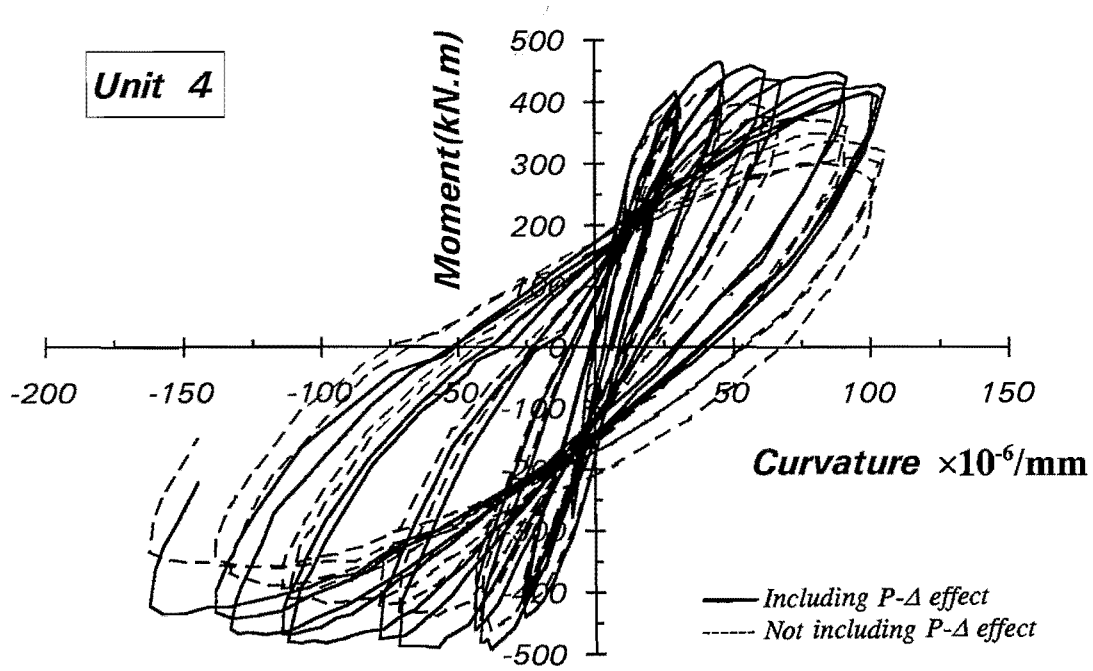

Fig.3.32: Experimental Moment-Curvature Hysteresis Loops for Unit 4

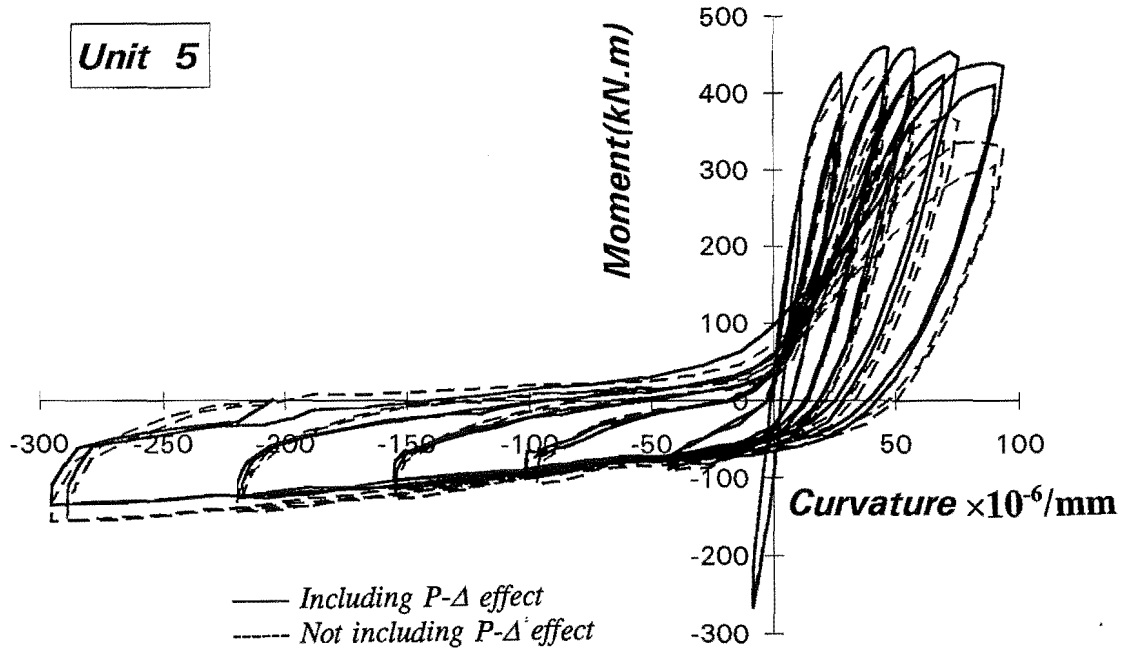

Fig.3.33: Experimental Moment-Curvature Hysteresis Loops for Unit 5

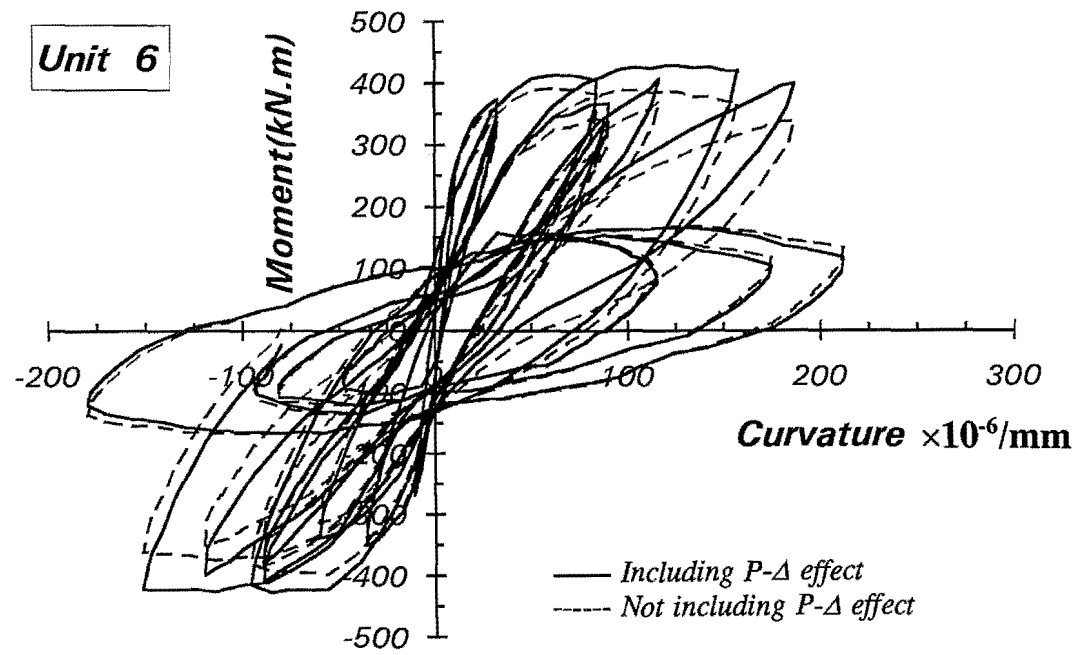

Fig.3.34: Experimental Moment-Curvature Hysteresis Loops for Unit 6

The experimental moment-curvature relations for the six column units are illustrated in Figs.3.29 to 3.34. The column moments shown in these figures were those at the face of the column base calculated from the measured lateral load. The curvatures shown in the figures are those measured at the first potentiometer levels. Hence, these curvatures include the effect of yield penetration of the longitudinal bars into the column base and any tension cracking. The dashed lines represent the moment-curvature relations without including the P-Δ effect in the calculation of the moment. The solid lines represent the moment-curvature relations taking into account the effect P-Δ in the calculation of the moment(see Fig.3.19).

Unit 1 and Unit 4 with constant compression axial load exhibited very stable moment-curvature hysteresis loops with little strength degradation(see Figs.3.29 and 3.32). Also, no pinching of the moment-curvature hysteresis loops occurred for these column units. The moment-curvature responses of the columns subjected to the variations in axial load, however, were significantly different from those of the columns tested under constant compression axial load. The moment-curvature hysteresis loops for the columns with varying axial loading were very asymmetric in shapes with significant changes in the strength and stiffness during the loading and unloading. Pinching of the hysteresis loops occurred at low displacement ductility levels. For Unit 2 and Unit 5, pinching of the moment-curvature hysteresis loops occurred when the axial load was reversed from tension to the compression. For Unit 3 and Unit 6 with uncoupled axial loading, pinching took place in both of the axial loading directions. These characteristics are also observed in the lateral load-displacement hysteresis loops.

The degradation of the section moment capacity of the columns subjected to varying axial load was more significant than that of the columns under constant compression axial load. The strength decay in the columns with alternating tension and compression load(Units 2 and 5) was more severe than that in the columns with uncoupled axial load pattern(Units 3 and 6).

Examination of Figs.3.30 and 3.33 with Figs.3.24 and 3.27 revealed that the presence of the tension axial load caused a concentration of plastic deformation in the end regions adjacent to column base and significantly increased the curvature at the critical section. Hence, the curvatures reached in the tension axial loading direction corresponding to each peak displacement ductility level were much larger than those reached in the compression axial loading direction. Under the tension axial load, the lateral load applied was very small, compared with that imposed under the compression axial load. The column yielded in flexure only in a small regions adjacent to the column base. Most of the column section may remain in elastic or yielded in tension due to tension axial force. The flexural deformation was concentrated in the yielding sections. To achieve the same lateral displacement at the top of the column as that in the compression load direction, the critical section had to experience the larger rotations. This effect was enhanced by the fact that the tension axial load increased the yield penetration of the longitudinal bars into the column base, which produced additional rotation at the critical section. A

similar trend occurred for Unit 3 and Unit 6. For the same displacement, the maximum curvatures attained in the tension axial load cycles was larger than that in the compression axial load cycle.

3.5.2 Effect of Axial Loading Pattern

To investigate the effects of different variable on the section behaviour of the column units tested, the monotonic moment-curvature envelopes for each column unit were constructed from the experimental cyclic moment-curvature relations shown in Figs.3.29 to 3.34 in the same manner as for experimental monotonic lateral load-displacement envelopes described in the Section 3.3.4. For comparative purposes, the section moment capacity, M, and the associated curvature, ϕ, were normalized with respect to the ideal flexural strength, M^+_i, and yield curvature, ϕ_y, respectively. The constructed moment-curvature envelopes for the six column units are shown in Figs.3.35 and 3.36.

The effect of the axial loading pattern on the behaviour of the column units can be found by comparing the constructed monotonic moment-curvature envelopess of the two groups of columns tested, shown in Figs. 3.35. Each of the two groups of column units contained the same amount of transverse reinforcement, and were tested under constant compression axial load, and coupled and uncoupled varying axial load along with the cyclic lateral loading. Unit 1 and Unit 4 with constant axial compression load showed relatively stable moment-curvature responses and achieved the largest moment enhancement ratios over the ideal fleureal strengths, compared with the correspondingly identical specimens with varying axial load. The early deterioration in the section moment capacity can be seen in Fig. 3.35 for Unit 2 and Unit 5. The moment capacity of Unit 1 is about 6% higher than that of Unit 2 and Unit 3 at $\mu_n=2$, and increased to approximately 16% at $\mu_n=8$. It can be seen in Fig.3.35 that the strength deteriorations of the columns subjected to varying axial load were generally more significant than those of the columns subjected to constant compression axial load.

3.5.3 Effects of Axial Load Level and Amount of Transverse Steel

The effects of the axial load level and the amount of transverse reinforcement on the section behaviour of the column were evaluated by comparing the constructed moment-curvature envelopes of the columns subjected to different axial load levels and containing different amounts of transverse reinforcement, as shown in Fig.3.36. Units 1, 2 and 3 had a maximum axial compression load of $0.3f'_cA_g$ contained volumetric transverse reinforcement ratio, ρ_s, of 2.13%. Units 4, 5 and 6 had a maximum axial compression load of $0.5f'_cA_g$ contained volumetric transverse reinforcement ratio, ρ_s, of 2.7%. It is evident that the adverse effect on member ductility of increasing the axial load level was compensated by the increase in the degree of confinement. The closely spaced transverse reinforcement greatly increased the deformation capacity of the column section. The effectiveness of reducing the hoop spacing

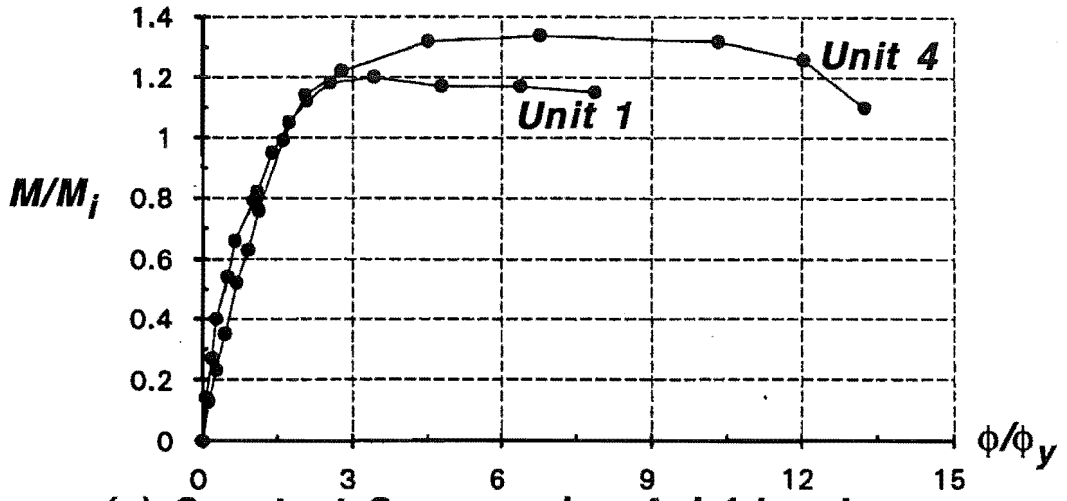

(a) Constant Compression Axial Load

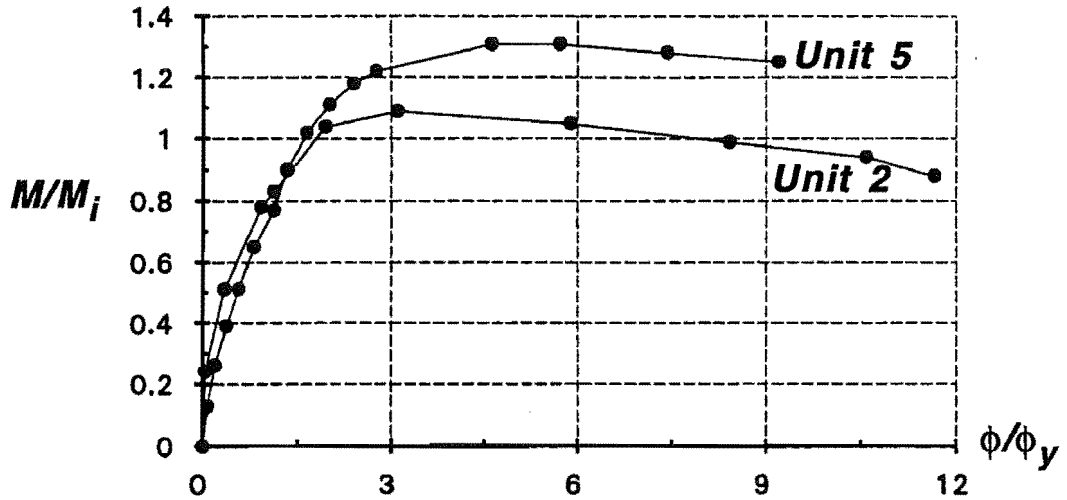

(b) Axial Load Coupled with Bending Moment

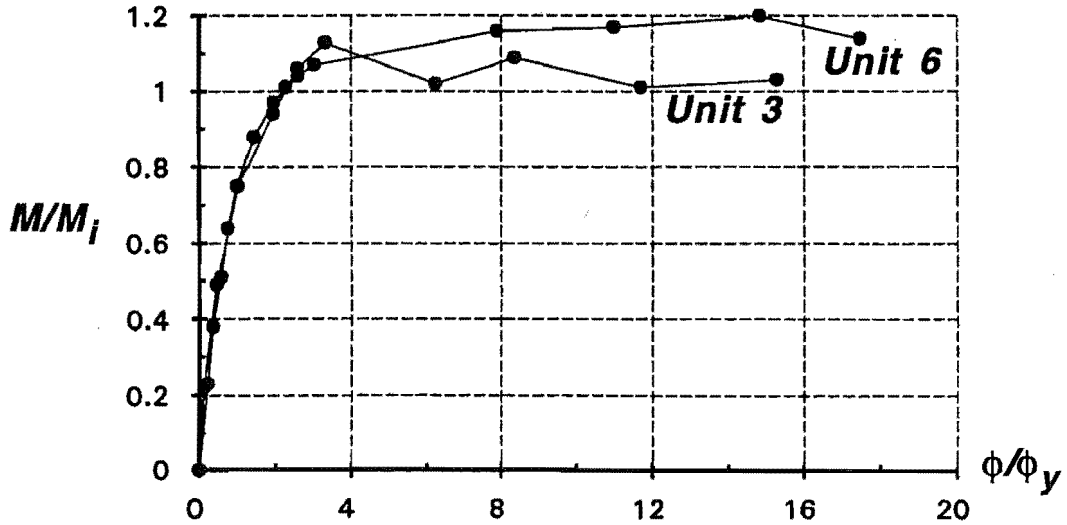

(c) Uncoupled Axial Load

Fig.3.35: Effects of Axial Load Level and Amount of Transverse Reinforcement

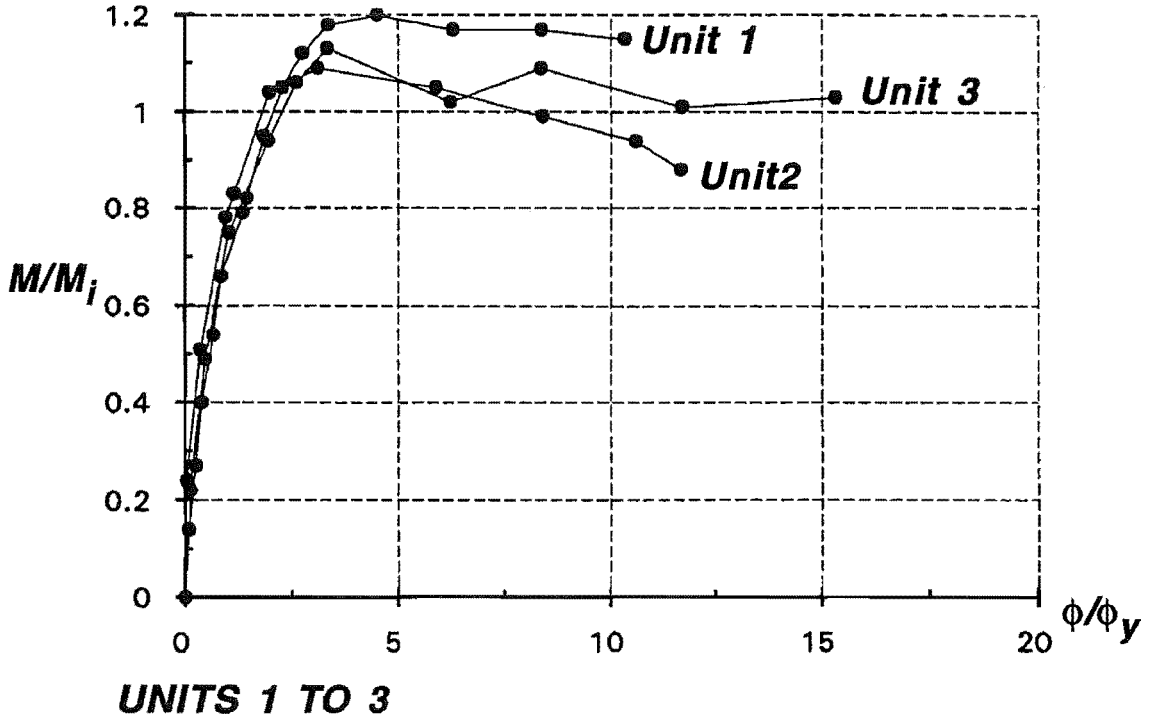

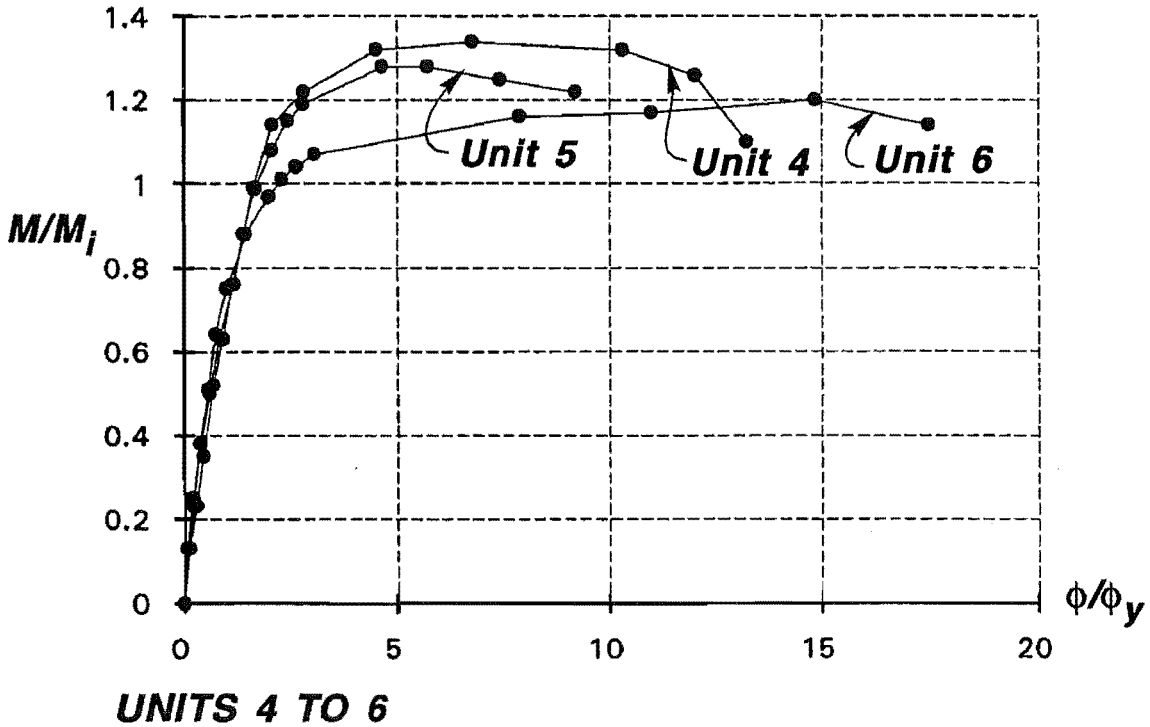

Fig.3.36: Effects of Axial Load Histories on Constructed Monotonic Moment-Curvature Relations

in improving the deformation capacity of the concrete section is especially evident when considering the varying axial loading.

3.6 YIELD CURVATURE AND SECTION RIGIDITY

3.6.1 Definition of Yield Deformation

When calculating ductility factors of a reinforced concrete member, the yield deformation is required to be known. The yield deformation can be defined readily in the case of an elasto-plastic system. For reinforced concrete members, however, the definition of the yield deformation often causes difficulty, since the force-deformation relation of such members does not have a well defined yield point due to the nonlinear behaviour of the materials. Various alternative definitions have been used by investigators to estimate the yield deformation[P2]. Park[P2] has suggested that the most realistic definition for the yield deformation of a reinforced concrete member is to define the yield deformation of the equivalent elasto-perfectly plastic system with reduced stiffness, which includes the effects of cracking and other nonlinear effects, and which has the same ultimate load as the real member. Based on this definition, the yield curvature and yield displacement are defined as described in the following sections.

3.6.2 Theoretical Yield Curvature

Fig.3.37 shows a typical monotonic moment-curvature curve for a reinforced concrete section. The definition of the yield curvature is graphically shown in this figure. The theoretical yield curvature, ϕ_y, is calculated by extrapolating a straight line from the origin($\phi=0$, $M=0$) through the point(ϕ'_y, M'_y) to the theoretical ultimate strength M_i. Therefore

$$\phi_y = \phi'_y \frac{M_i}{M'_y} \qquad (3.3)$$

where ϕ'_y, and M'_y are the curvature and corresponding moment calculated at the instant when the steel closest to the tension face of the section reaches yield or when the strain in the concrete at the extreme compressive fibre reaches 0.002, whichever occurs first. The coordinate(ϕ'_y, M'_y) defines the initial stiffness of the equivalent elasto-plastic system. The above definition takes into account the effects of axial load level on the yield stiffness of reinforced concrete. For the column with high compression axial load, the tension steel will not yield before the strain in the extreme compressive fibre reaches 0.002, at

which stage the column shows reduced stiffness. This definition for ϕ_y has been used at the University of Canterbury. The ideal moment M_i can be determined using code approach[S14] with measured material strengths and assuming a strength reduction factor of unity. To take into account the effects of enhancement of concrete compressive strength due to confinement and strain hardening of the longitudinal bars, the ideal strength M_i has been taken by Zahn[Z3] as the maximum moment reached before the curvature exceeds five times ϕ_y. This definition for the ideal moment is used in this study.

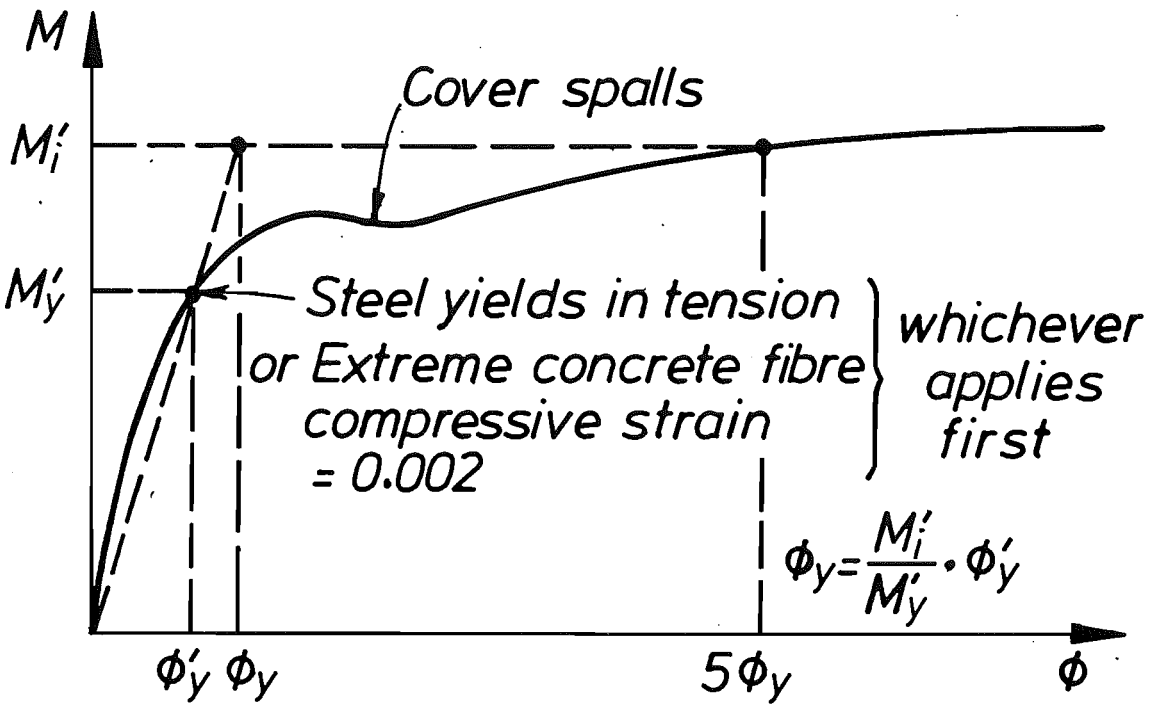

Fig.3.37: Definition of yield curvature, yield moment and ideal moment

The theoretical yield curvature can be obtained by simply carried out a monotonic moment-curvature analysis with the known section properties and material parameters. Analytical studies[L2] have indicated that the yield curvature of a reinforced concrete column is dependent on the axial load level. To demonstrate this effect, the yield curvature was calculated for the section of the column tested in this study, and with a concrete compressive strength of 32 MPa and a transverse reinforcement yield strength of 350 MPa. Fig.3.38 plots the calculated yield curvature against the axial load level. It is evident from Fig. 3.38 that variations in the axial load level can significantly influence the yield curvature. For low axial load levels, the yield of the steel closest to the tension face of the section occurs before the extreme concrete fibre concrete compressive strain reaches 0.002, and the yield curvature increases as the axial load level increases. For high axial load levels, however, the tension steel will not yield before the extreme fibre concrete compressive strain reaches 0.002 and the yield curvature decreases with increase in the axial load level.

The theoretical values of the yield curvature ϕ_y were also calculated for the six column units tested using Eq.3.3 with actual material strengths for each column unit. The results are given in Table 3.2. The maximum compression axial load imposed on each column unit is used for the calculation of ϕ_y in all cases. For all the six column units, the tension longitudinal reinforcement did not yield before the extreme fibre concrete fibre compressive strain reached 0.002.

The flexural stiffness of the section can be determined as the initial slope of the idealized moment curvature relationship; that is, the secant slope of the line from the origin to the first yield point(ϕ'_y, M'_y). Table 3.3 gives the section rigidity for the six column units.

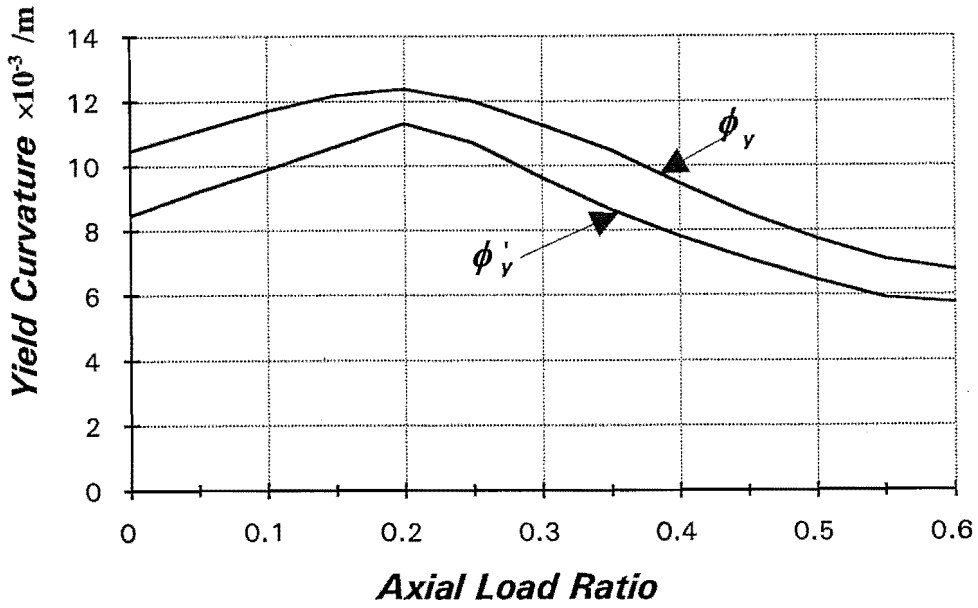

Fig.3.38: Theoretical variation of yield curvature with axial load level

3.6.3 Experimental Yield Curvature and Section Stiffness

The experimental yield curvature was calculated using the similar method as for the theoretical yield curvature given by Eq.3.3. The experimental yield curvature ϕ'_y was found by measuring the curvature at $0.75M^+_i$ for each direction of loading, and extrapolating linearly to M^+_i. The experimental yield curvature was then taken as the average of the yield curvatures found in both the positive and negative lateral loading directions. Fig.3.39 shows the calculation of the experimental yield curvature. The experimental yield curvature measured at the first and second potentiometer levels are compared with the theoretical yield curvature in Table 3.2 for the six column units tested.

It has to be emphasized that the experimental yield curvature was determined corresponding to the maximum compression axial load level, which was imposed on each column unit during the initial loading cycle. As indicated by the theoretical analysis results in Fig.3.38, the yield curvature varies with the axial load level. For Unit 2 and 3 with maximum compression and tension axial load of $0.3f'_cA_g$ and $0.05f'_cA_g$, respectively, the experimental yield curvature determined at the compression axial load of $0.3f'_cA_g$ represented a rough average value of the yield curvatures in the load range applied (see Fig.3.38). For Unit 5 and Unit 6, the experimental curvatures determined corresponding to an axial compression load of $0.5f'_cA_g$ gave a low value. Hence, the use of these yield curvatures would result in the curvature ductility factors of Units 5 and 6 to be overestimated.

The measured flexural stiffness of the column section, calculated as M_i/ϕ_y, is compared with the theoretical values in Table 3.3.

3.7 YIELD DISPLACEMENT AND MEMBER STIFFNESS

3.7.1 Theoretical Yield Displacement

The theoretical yield displacement was defined in a similar way as the yield curvature. The first yield displacement, Δ'_y, which governs the initial stiffness of the elasto-plastic idealization of the load-displacement curve, is the deflection corresponding to the lateral load V'_y, which produces the first yield moment, M'_y, at the critical section of the column. The yield displacement, Δ_y, is obtained by extrapolating a straight line from the origin through the first yield point(Δ'_y, V'_y) to the lateral load $V_i=M^+_i/L$, where L is the effective length of the column. Fig. 3.40 illustrate the calculation of the yield deflection. Thus

$$\Delta_y = \Delta'_y \frac{M_i^+}{M'_y} \qquad (3.4)$$

The theoretical yield displacement, Δ'_y, was obtained by carrying out routine section analysis and integrating the curvature along the column height. The theoretical yield displacement was calculated by the cyclic moment-curvature theory[M2], in which the ideal flexural strength was calculated using the code[S14] approach. A computer program developed by Mander[M2] and recently modified by Dodd[D1] was used to calculate the yield displacement. Table 3.2 includes the theoretical yield displacements for the six column units tested. The maximum compression axial load applied to each column unit was adopted in the calculations for the yield displacement. It will be seen in Table 3.2 that the yield displacement of the column decreases with the increase in compression axial load level.

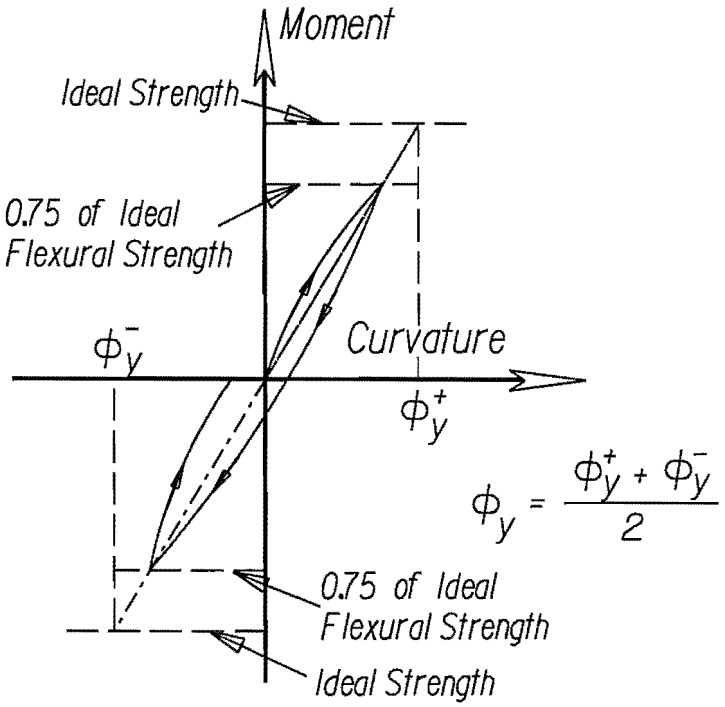

Fig.3.39: Calculation of Experimental Yield Curvature

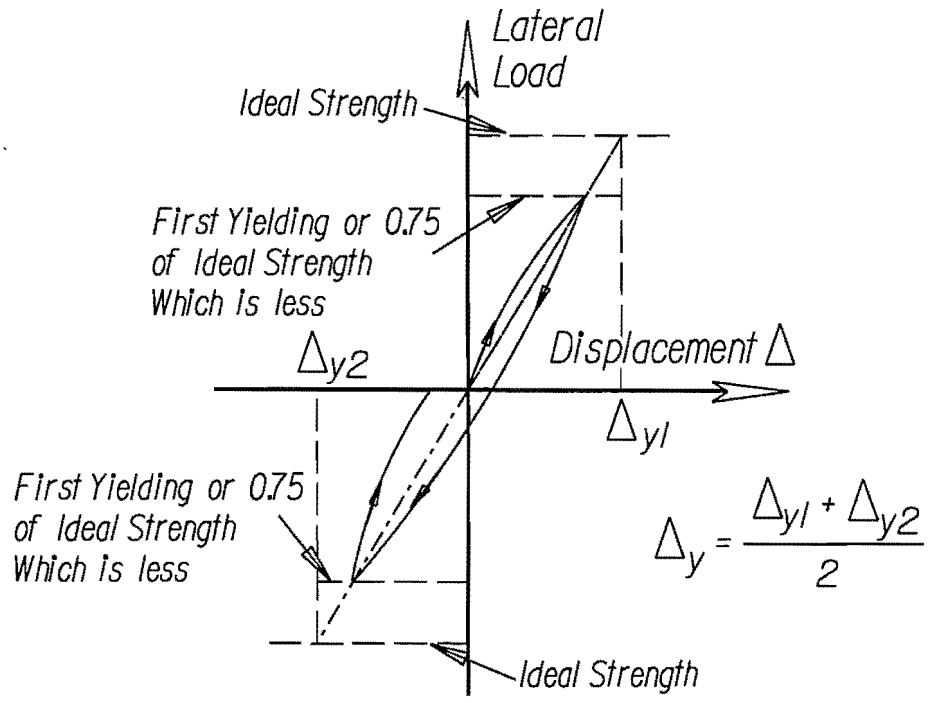

Fig.3.40: Definition of Yield Displacement

3.7.2 Experimental Yield Displacement and Effective Column Rigidity

As with the yield curvature, the experimental yield displacement was the average of the deflections measured in both the directions of the initial loading cycles to a lateral load of 75% of the ideal flexural strength M^+_i calculated using code approach with the measured material strengths and assuming a strength reduction factor of unity. The experimental yield displacement for the six column units tested are given in Table 3.2. It can be seen that the values of Δ_y for Unit 1 to Unit 3 are larger than for Unit 4 to Unit 6. For the purpose of comparison, the compression axial load applied during the initial loading cycle was $0.3f'_cA_g$ for Units 1, 2 and 3, and $0.5f'_cA_g$ for the Units 4, 5 and 6, respectively. These axial load levels are larger than the balanced point axial load, and hence the corresponding moments are smaller than the moments at the balance point. Since the yield displacement of the column decreased as the compression axial load increased, it meant that for the column units tested under varying axial load the yield displacement determined corresponding to the maximum compression axial load level would result in the yield displacement in tension half cycle to be underestimated and the associated displacement ductility factors to be overestimated.

Table 3.2 : Yield Curvature and Yield Displacement

Unit	Yield Curvature ϕ_y ($\times 10^{-6}$ rad/mm)				Yield Disp. Δ_y (mm)	
	Theory		Experiment		Theory	
	(1)	(2)	(3)	(4)	(5)	Experiment
1	11.2	12.2	21.66	8.52	10.24	11.10
2	11.4	12.4	36.58	10.85	10.24	11.96
3	11.4	12.4	28.06	10.32	10.24	11.52
4	7.7	9.7	13.19	7.13	6.82	7.60
5	7.7	9.7	13.57	5.70	6.82	7.79
6	7.7	9.7	14.15	6.80	6.82	7.70

Note:

(1). The ideal flexural strength was calculated using code approach of NZS 3101[S14]

(2). The ideal flexural strength was calculated as the maximum moment reached before $\phi=5\phi_y$

(3). Measured at the first level of potentiometer

(4). Measured at the second level of potentiometer

(5). The ideal flexural strength was calculated using code approach of NZS 3101[S14]

The effective member stiffness can be evaluated from the measured yield displacement. For a cantilever column, the displacement at the first yield due to the flexure alone is

$$\Delta'_{yf} = \frac{M'_y L^2}{3(EI)_e} \qquad (3.5)$$

where $(EI)_e$ is effective flexural stiffness of column section, M'_y is the first yield moment($M'_y=0.75M^+_i$), and L is the effective height of the column.

The shear deformation, Δ'_{ys} at the first yield can be approximated by assuming that the reduction in the shear rigidity caused by cracking is in proportion to the reduction in flexural rigidity[P23]. Hence

$$\Delta'_{ys} = \frac{V'_y L}{A_e(0.4E_c)} \frac{(EI)_g}{(EI)_e} \qquad (3.6)$$

where $(EI)_g$ is the initial stiffness of gross section, the shear area is taken as $A_e = 0.8A_g$, and the shear modulus is taken as $0.4E_c$. The total column displacement at first yield is then given by

$$\Delta'_y = \Delta'_{yf}+\Delta'_{ys} \qquad (3.7)$$

From experimental displacement Δ'_y measured at 75% of theoretical flexural strength, the effective column stiffness was determined for each column unit tested by using preceding equations. The results are given in the Table 3.3.

The effective flexural rigidity $(EI)_e$ of the column section at first yield was found to be about $0.50(EI)_g$ on average for Units 1, 2 and 3 with compression axial load of $0.3f'_cA_g$, and $0.71(EI)_g$ for Units 4, 5 and 6 with compression axial load of $0.5f'_cA_g$.

To investigate the effects of displacement ductility level and axial load pattern on the column stiffness, Eqns.3.5 to 3.7 were also used to calculate the column stiffness at various nominal displacement ductility levels, assuming an average section rigidity over the entire height of the column. The calculated results are shown in Table 3.4.

It can be seen from Table 3.4 that the average flexural stiffness $(EI)_e$ of the column had reduced drastically to $0.27(EI)_g$ on average for Units 1, 2 and 3, and $0.41(EI)_g$ for Units 4, 5 and 6, at nominal displacement ductility factor of $\mu_n=2$. The average stiffness $(EI)_e$ for the column units subjected to varying axial loading was 15 to 21% less than that subjected to constant compression axial load, for

instance, at nominal displacement ductility factor of $\mu_n=4$.

Table 3.3 : Section Stiffness and Member Stiffness

Unit	Section Stiffness (1)		Experimental Member Stiffness (2)	
	Theory ($kN.m^2 \times 10^3$)	Experiment ($kN.m^2 \times 10^3$)	$(EI)_e$ ($kN.m^2 \times 10^3$)	$(EI)_e/(EI)_g$
1	28.28	20.58	29.52	0.51
2	27.50	12.12	28.99	0.50
3	27.50	15.78	27.70	0.48
4	35.88	35.19	43.46	0.72
5	35.88	34.18	42.41	0.70
6	35.88	32.17	42.86	0.72

Notes:

(1) calculated from M_i/ϕ_y

(2) calculated from Eqns. 3.5 to 3.7

Table 3.4: Experimental Column Stiffness at Various Nominal Displacement Ductility Factor

Unit	$\mu_n=2$		$\mu_n=4$		$\mu_n=6$	
	$(EI)_e$ ($kN.m^2 \times 10^3$)	$(EI)_e/(EI)_g$	$(EI)_e$ ($kN.m^2 \times 10^3$)	$(EI)_e/(EI)_g$	$(EI)_e$ ($kN.m^2 \times 10^3$)	$(EI)_e/(EI)_g$
1	16.74	0.29	7.87	0.14	4.94	0.086
2	16.02	0.28	7.12	0.12	4.23	0.073
3	14.00	0.24	6.27	0.11	4.53	0.078
4	26.52	0.44	13.32	0.23	6.42	0.110
5	24.75	0.41	12.73	0.21	5.42	0.090
6	22.77	0.38	11.62	0.19	5.64	0.090

3.8 EQUIVALENT PLASTIC HINGE LENGTH

The equivalent plastic hinge length is theoretically considered as the length over which all plastic curvature takes place with a constant value. This assumption implies a curvature distribution as shown in Fig.3.41. The plastic rotation that occurs in the vicinity of the critical section of a column can be written as $\theta_p=(\phi-\phi_y)L_p$, where $(\phi-\phi_y)L_p$ has the same area as the actual inelastic curvature distribution, shown in Fig.3.41. With this assumption, the ultimate deflection of the column and the relation between the displacement ductility factor and curvature ductility factor can be predicted. In the detailing of a reinforced concrete member, it is important to provide additional transverse reinforcement in the potential plastic hinge regions which is at least as long as the region of the actual inelastic curvature distribution.

The equivalent plastic hinge length, L_p, can be obtained from the measured plastic deformation. For a cantilever column, the displacement beyond the first yield displacement can be obtained by taking the first moment of area of the idealized distribution of plastic curvature, as shown in Fig.3.41, about the end of the column. Thus

$$\Delta_p = \theta_p(L-0.5L_p) = (\phi-\phi_y)\,L_p(L-0.5L_p) \qquad (3.8a)$$

where $(\phi-\phi_y)$ is the plastic curvature measured beyond the first yield curvature, L is the distance from the critical section to the top of the column. Also, the plastic displacement can be written as

$$\Delta_p = (\mu_n-1)\,\Delta_y \qquad (3.8b)$$

where μ_n is the displacement ductility factor and Δ_y is the yield displacement.

By equating Eqns.3.8a and 3.8b, the equivalent plastic hinge length can be expressed as

$$L_p = L\left[1-\sqrt{1-\frac{2\,(\mu_n-1)\,\Delta_y}{L^2\,(\phi-\phi_y)}}\right] \qquad (3.9)$$

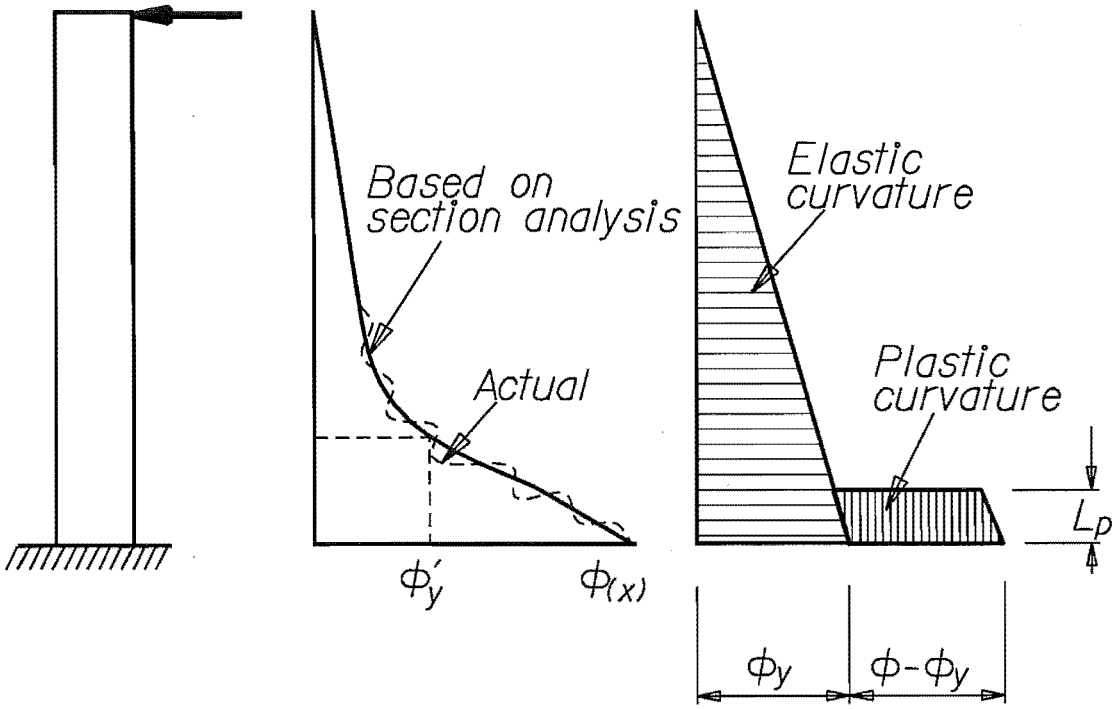

Fig.3.41: Assumed Curvature Distribution for Columns

The experimental values of L_p for the six column units were calculated using Eq.3.9. The measured curvature at the first potentiometer level over a 75 to 80 mm gauge length was used for the value of ϕ, which as noted by Watson[W2] would include the effect of yield penetration of the longitudinal reinforcement into the column base. The values L_p were calculated corresponding to nominal displacement ductility factors $\mu_n \geq 4.0$. The values of L_p corresponding to low displacement ductility are less reliable than those for high displacement ductility because as the level of displacement ductility increases, discrepancies in the yield deflection and yield curvature in Eq.3.9 becomes less significant[D1]. For Units 1 and 4, L_p was calculated for each peak of the loading cycle in both directions. For Units 2 and 5, L_p was calculated only for each peak in the compression axial loading direction. For Units 3 and 6, L_p was calculated for the peak of the loading cycles where compression axial load was applied. The calculated results are shown in Figs.3.42 to 3.47.

As can be seen from these figures, there was a general tendency for L_p to increase with increase in

displacement ductility factor. The effect of increased compression axial load level on L_p can be found by comparing the values of L_p for Unit 1 and Unit 4, in which constant compression axial load was applied(see Figs.3.42 and 3.45). The effect of higher axial compression load is to increase the plastic hinge length. The same trend was also observed for the columns subjected to varying axial load. Compared with their companion specimens, the columns tested under varying axial load had a smaller L_p, except for Unit 5. The average values of L_p for all the load cycles shown in Figs.3.42 to 3.47 are given in Table 3.4. The equivalent plastic lengths for the Units 1 and 4 had a average value of 1.04h, where h=overall section depth. The L_p for all other units had an average value of 0.78h. Also included in this table are the lengths of the regions over which damage(spalling and crushing of concrete) were observed during the testing.

For the comparisons, Table 3.4 also lists the theoretical equivalent plastic hinge length predicted by the equation suggested by Priestley and Park[P22]

$$L_p = 0.08L+6d_b \qquad (3.10)$$

and the equation by Corley[C2]

$$L_p = 0.5d+\sqrt{d}\left(\frac{L}{d}\right) \quad \text{(mm)} \qquad (3.11)$$

in which L = distance from the critical section to the top of the column, d_b = the diameter of longitudinal bar; and d = effective depth of the column.

Eqns.3.10 and 3.11 predicted a smaller equivalent plastic hinge length than were measured for Units 1, 4 and 5. For Units 2, 3 and 6, they gave better estimation of L_p. Eq.3.10 considers the influence of yield penetration of steel and the spreading of plasticity by relating the plastic hinge length to the diameter of the longitudinal reinforcement. Both Eqns.3.10 and 3.11 indicate that the column axial load level has no effect on the equivalent plastic hinge length.

Previous experimental results[W2 and D1] have shown that the axial load level does have an effect on the equivalent plastic hinge length but the data collected showed a great deal of scatter. It is to be noted that using Eq.3.9 to calculate L_p may effected by several factors, including the gauge length. It appears that the axial load level should be considered possible parameter in the theoretical determination of equivalent plastic hinge length.

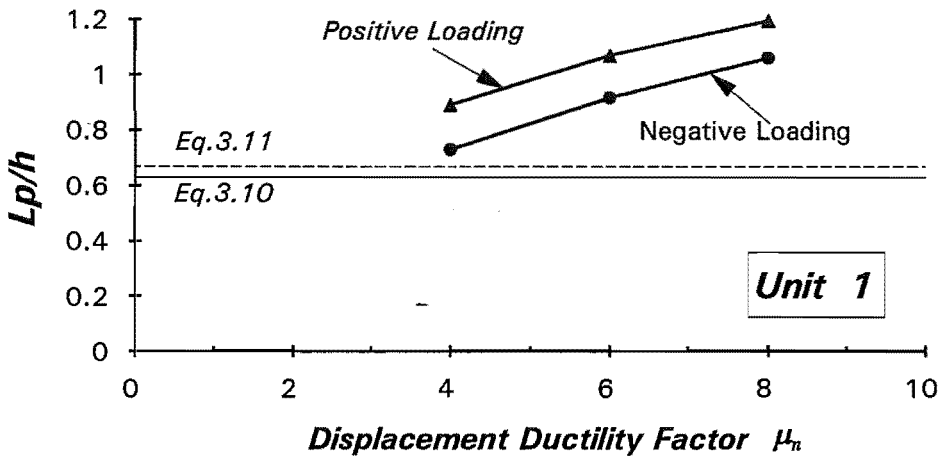

Fig.3.42: Equivalent Plastic Hinge Length for Unit 1

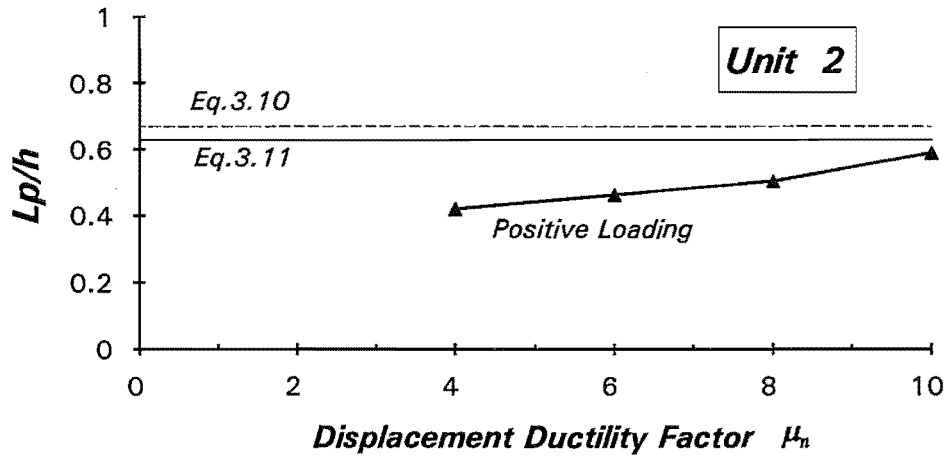

Fig.3.43: Equivalent Plastic Hinge Length for Unit 2

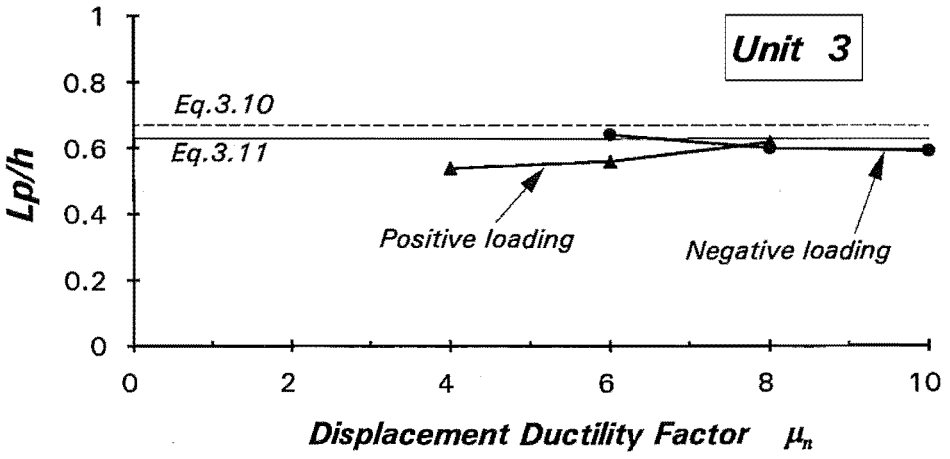

Fig.3.44: Equivalent Plastic Hinge Length for Unit 3

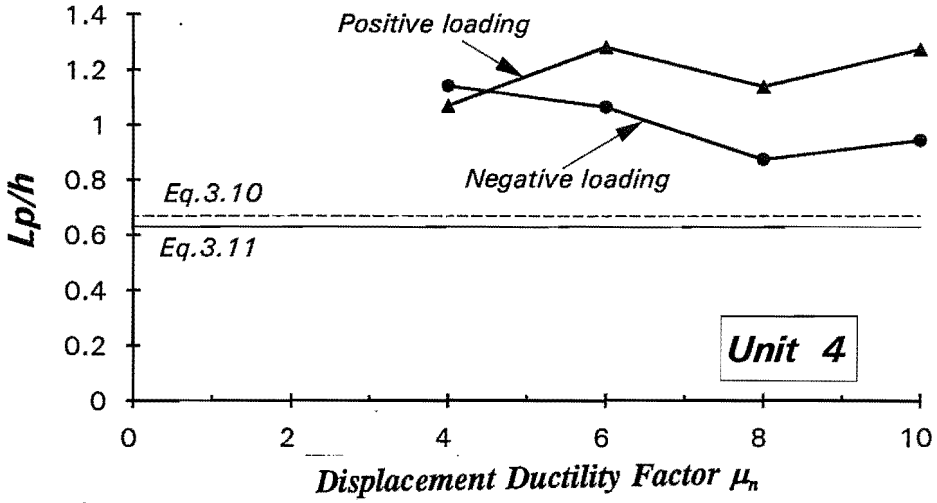

Fig.3.45: Equivalent Plastic Hinge Length for Unit 4

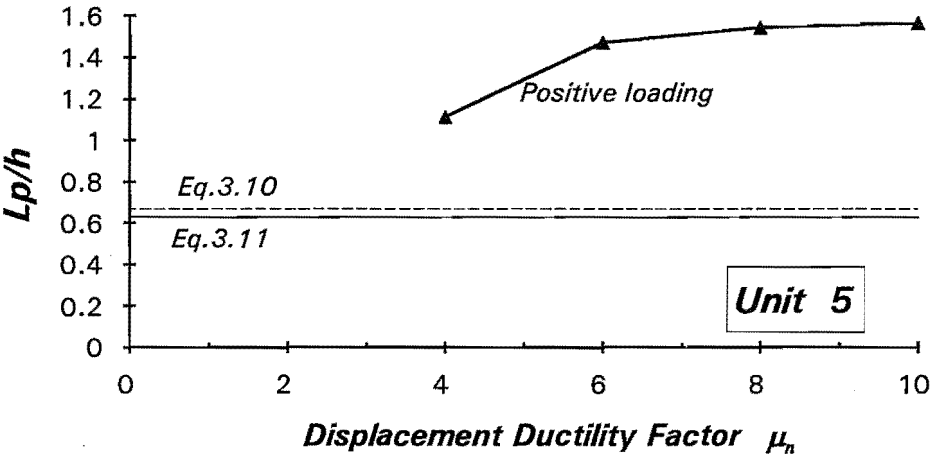

Fig.3.46: Equivalent Plastic Hinge Length for Unit 5

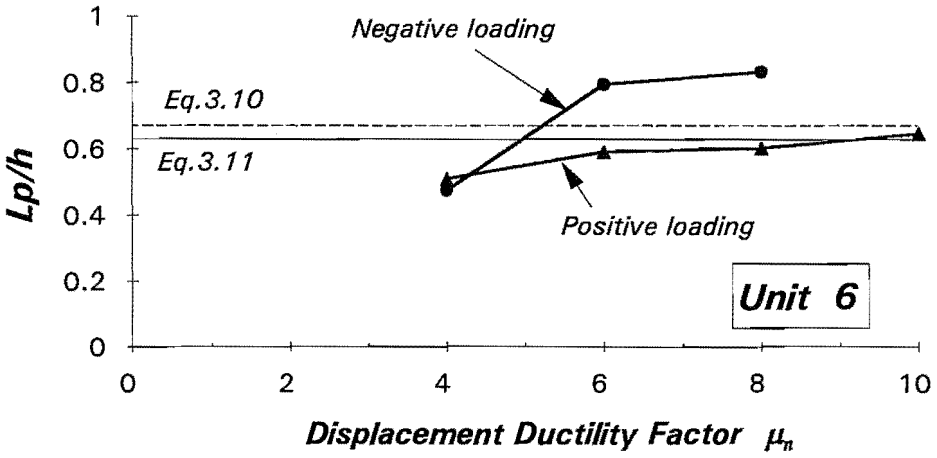

Fig.3.47: Equivalent Plastic Hinge Length for Unit 6

Table 3.5 : Equivalent Plastic Hinge Length

Unit	Experiment Eq.3.9		Observed Length of Damaged Region (mm)	Eq.3.10		Eq.3.11	
	L_p(mm)	L_p/h		L_p(mm)	L_p/h	L_p(mm)	L_p/h
1	390	0.98	420	252	0.63	267	0.67
2	198	0.49	360	252	0.63	267	0.67
3	239	0.60	400	252	0.63	267	0.67
4	440	1.10	490	252	0.63	267	0.67
5	560	1.40	430	252	0.63	267	0.67
6	254	0.64	430	252	0.63	267	0.67

3.9 DISPLACEMENT COMPONENTS

3.9.1 Deflection Components

Under the loading actions, the column unit was deformed into inelastic range. The column deflection, Δ_c, in the inelastic range consisted of three deformation components as follow.

$$\Delta_c = \Delta_f + \Delta_s + \Delta_{slip} \qquad (3.12)$$

Where Δ_f = column deflection due to flexure

Δ_s = column deflection due to shear

Δ_{slip} = column deflection due to bar slip(yield penetration) at the base

With the measurements from the vertical potentiometers placed on the columns, the components of the column deflection due to flexure and bar slip were experimentally determined. Also, the total column

deflection was measured directly from the horizontal displacement transducers at the top and mid-height of the columns. The significance of each deflection component is discussed in the following sections.

3.9.2 Deflection due to Flexure

The deflection due to flexure can be obtained by integrating the curvature along the column height. It was assumed that the flexural deflection is comprised of discrete rotations, θ_i, which occurred at the mid-point of each gauge length. After the curvatures were calculated as described in previous sections, the average rotation at the mid-point of each gauge length can be taken as

$$\theta_i = \phi_i l_i \qquad (3.13)$$

Where l_i = the initial length of the gauge "i". The flexural deflection due to rotation at gauge length "i" is calculated as(see Figs.3.21 and 3.22)

$$\Delta_{fi} = \theta_i (L - y_i) \qquad (3.14)$$

where L is the effective height of the column and y_i is the distance from the centre of the gauge length to the top of the column base. The total flexural deflection is the sum of the deflections from all gauge lengths:

$$\Delta_f = \sum \Delta_{fi} \qquad (3.15)$$

Note the bottom potentiometer readings were those which did not include the bar slip in the column base.

3.9.3 Deflection due to Bar Slip

In order to experimentally estimate the deflection due to the extension and possible slip of reinforcing bar from the anchorage concrete, additional pairs of potentiometers were placed in the plastic hinge regions to measure the deformation at the column-base interface due to bar extension. As shown in Fig.2.10b, the potentiometers marked PA(opposing pairs) were placed with their target relative to the column base. It is apparent the deformation measured by these potentiometers included the effects of yield penetration

into the column base. The other two pairs of opposing potentiometers, marked PB1 and PB2, placed in the same level were made with their target relative to the column critical section. This was achieved by attached a steel stub to the longitudinal bars(see Fig.2.10b). These steel stubs were actually 3-5mm above the column base. The deformation measured from these additional potentiometers can be considered to be the flexural deformation over the first gauge length. Therefore, the difference between deformation measured by potentiometers PA and PB was assumed to be the deformation due to bar slip from column base. Once the bar displacement, δ_{slip}, was determined, the deflection due to additional rotation, Δ_{slip}, was evaluated from

$$\Delta_{slip} = \frac{\delta_{slip}}{d'} L \qquad (3.16)$$

Where d' is the distance between the centre of the reinforcing bar in each side of the column and L is the effective height of the column.

3.9.4 Deflection due to Shear

After the components of deflections due to flexure and bar slip were determined, the deflection due to shear was obtained from Eq.3.12, thus

$$\Delta_s = \Delta_c - (\Delta_f + \Delta_{slip}) \qquad (3.17)$$

where Δ_c = measured deflection at the top of the column.

The accuracy of the method described here in predicting deflection components is testified in Chapter 5 by comparing the calculated and measured deflections.

The three components of the column displacement at the peak of each displacement ductility level and cycle, calculated using above method, are plotted against the nominal displacement ductility factor in Figs.3.48a to 3.53a. The significance of each displacement component, that is, the ratios of the displacement due to flexure, shear and bar slip, to the total column displacement are shown as percentages in Figs. 3.48b to 3.53b. For the Unit 2, the potentiometers were unable to measure the deformation due to bar slip at $\mu_n \geq 6$, because the steel rods debonded from the longitudinal bars. Hence, the displacement components due to the bar slip and shear were only evaluated up to $\mu_n = 6$.

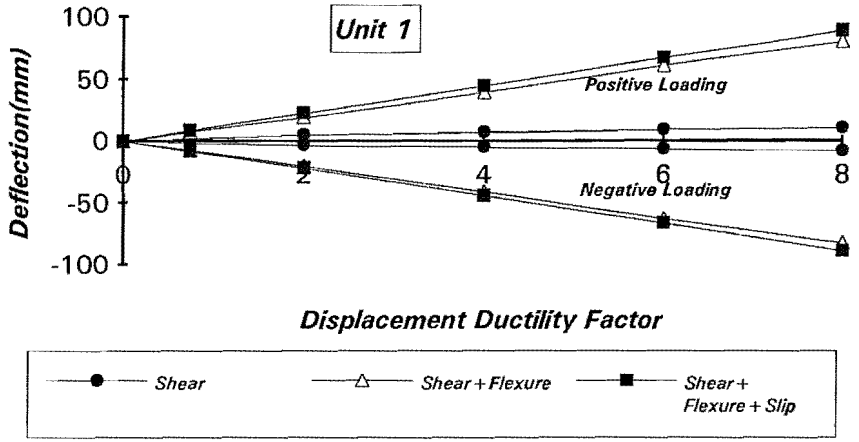

(a) Deflection components

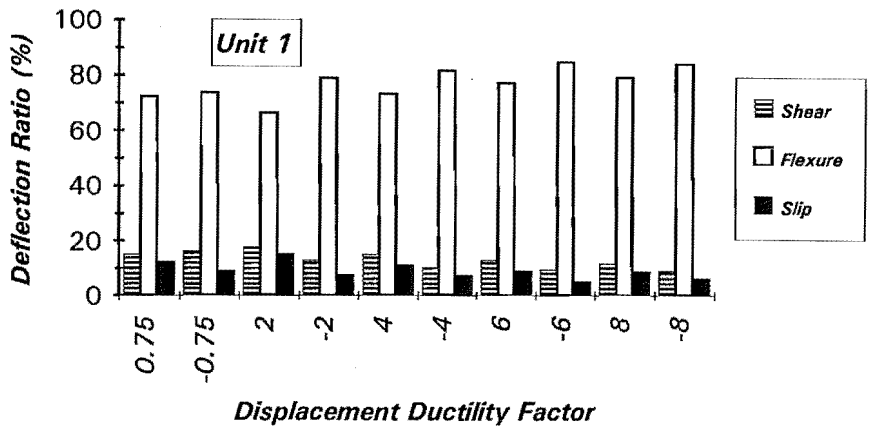

(b) Deflection ratios

Fig.3.48: Lateral Deflections for Unit 1

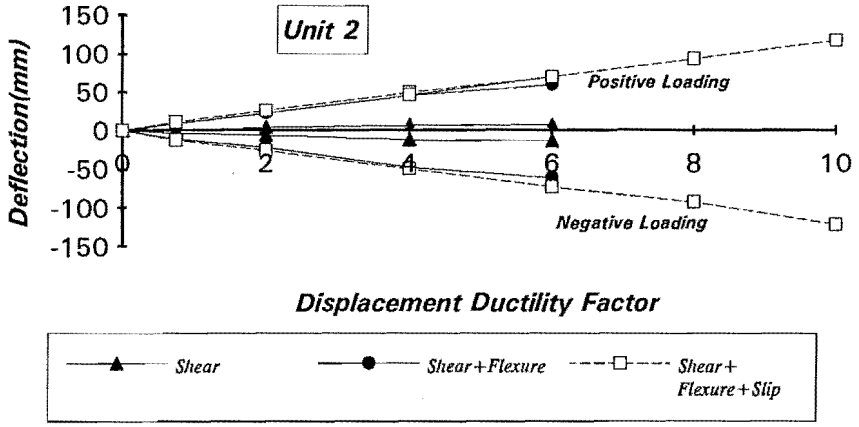

(a) Deflection components

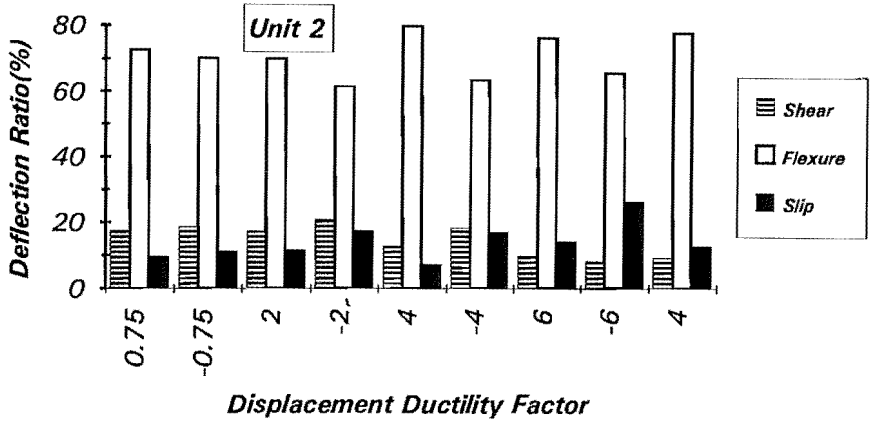

(b) Deflection ratios

Fig.3.49: Lateral Deflections for Unit 2

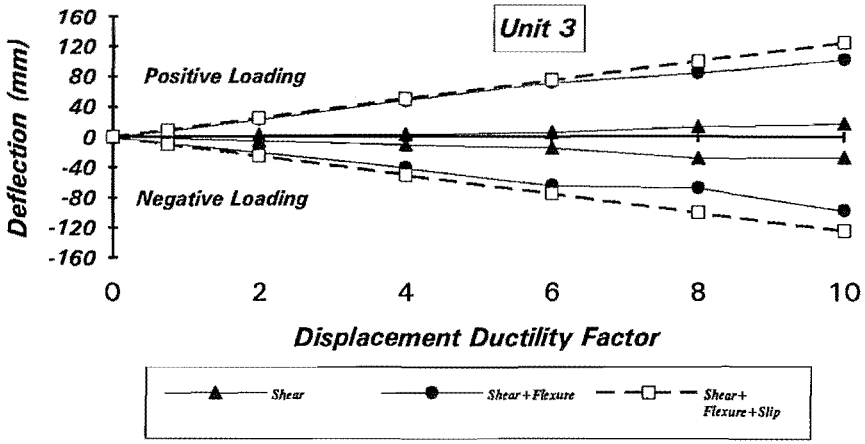

(a) Deflection components

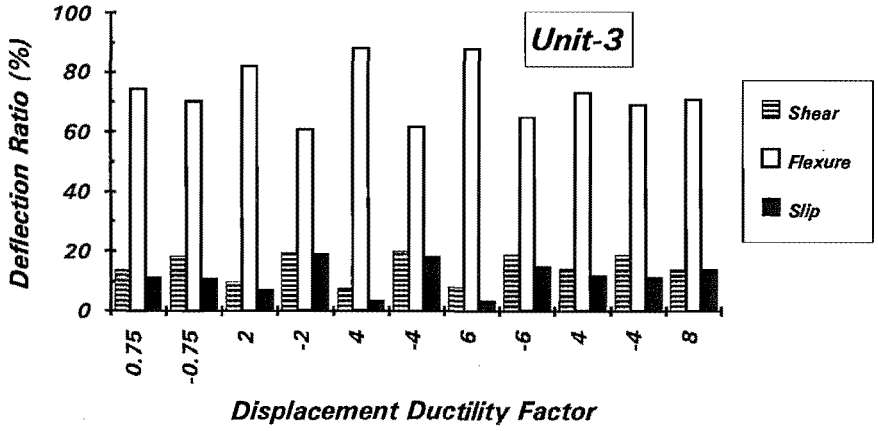

(b) Deflection ratios

Fig.3.50: Lateral Deflections for Unit 3

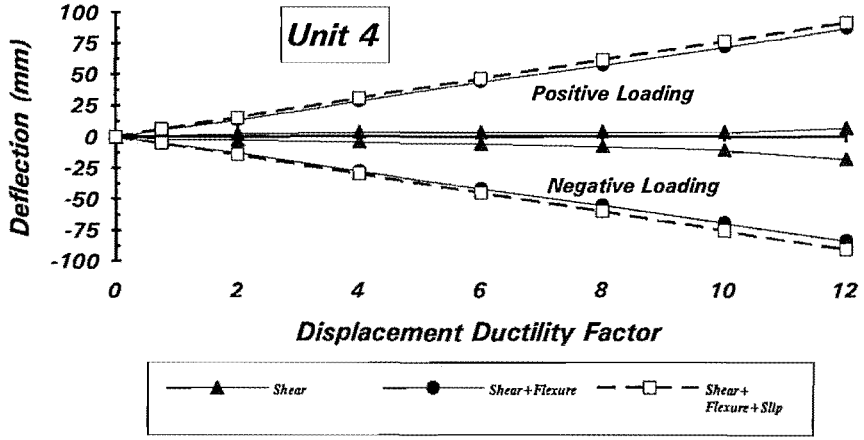

(a) Deflection components

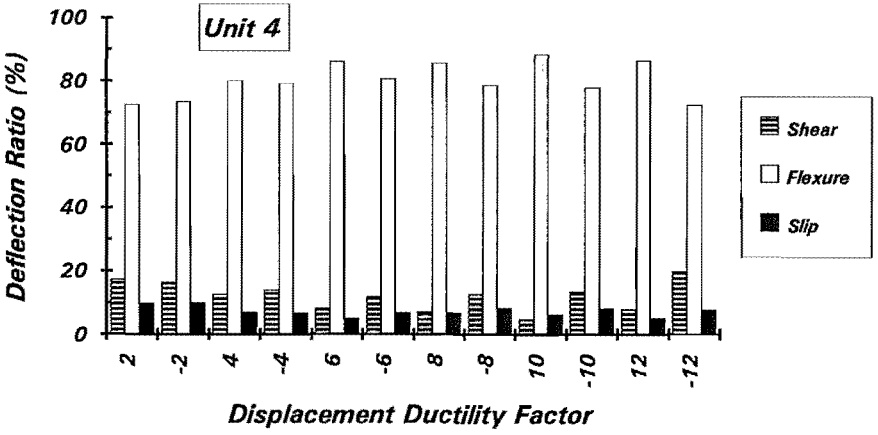

(b) Deflection ratios

Fig.3.51: Lateral Deflections for Unit 4

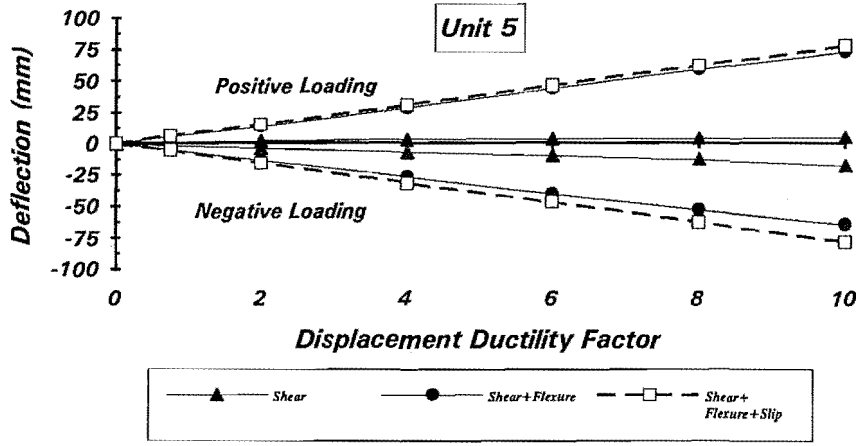

(a) Deflection components

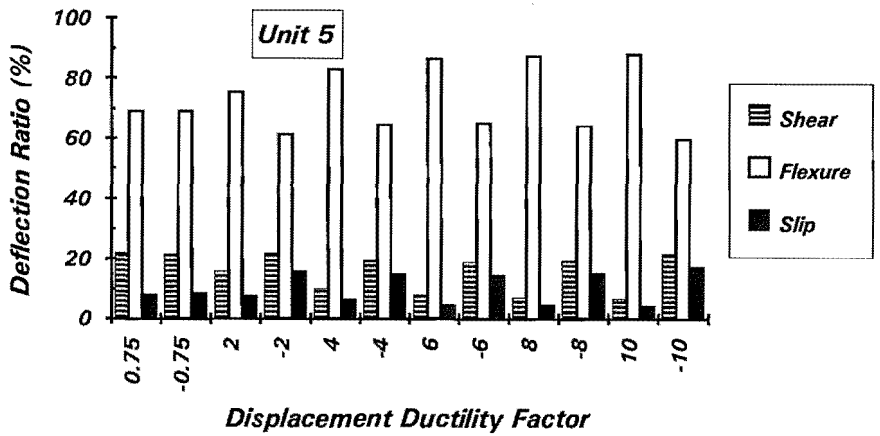

(b) Deflection ratios

Fig.3.52: Lateral Deflections for Unit 5

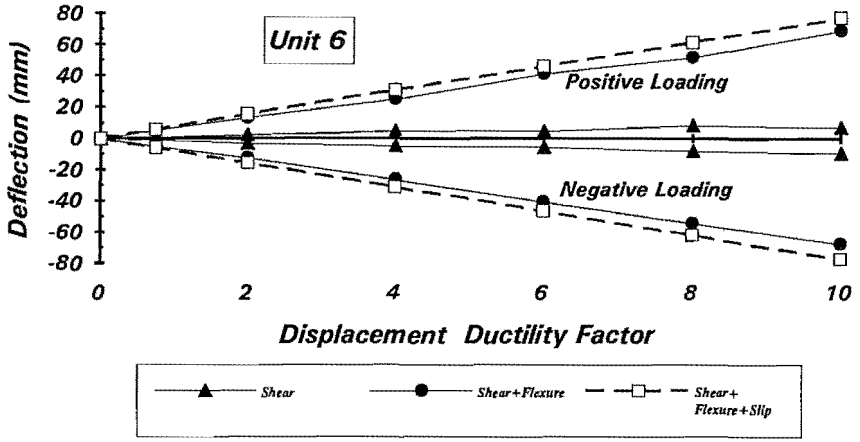

(a) Deflection components

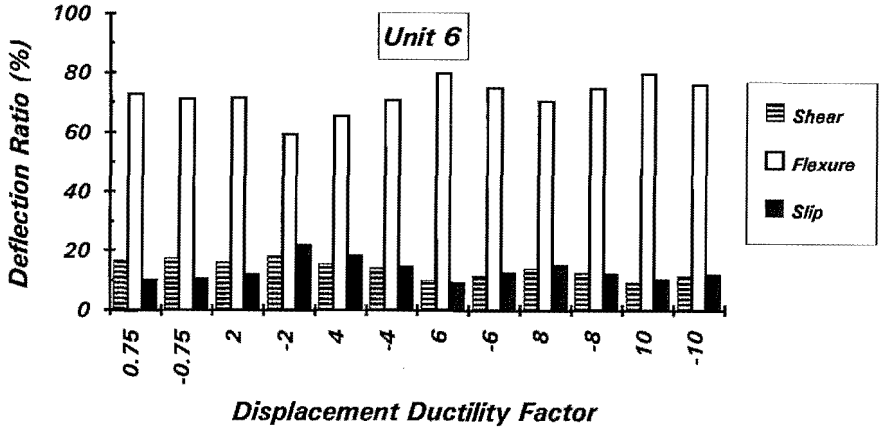

(b) Deflection ratios

Fig.3.53: Lateral Deflections for Unit 6

It can be seen from Figs.3.48 to 3.53, that the displacement of each component generally increased with the increase of the imposed displacement ductility factor. The displacement due to the flexure was the major source of the total displacement in all the column units tested. In the elastic loading cycles, the displacement due to the shear accounted for, on average, about 16% of the total column displacement. This suggested that the yield displacement was significantly effected by the shear deformation in the elastic loading range. The displacement due to the bar slip contributed less than 8% to the total displacement in the elastic loading cycles. It is to note that since the deflection due to shear effect was indirectly obtained by subtracting the deflections due to flexure, Δ_f, and due to bar slip, Δ_{slip}, from the measured total column deflection, Δ_c, it could include errors induced in the estimates of the deflections due to flexure and bar slip.

For the Units 1 and 4 which had constant compression axial load, the deflection ratios remained relatively stable as the imposed displacement increased(Figs.3.48a and 3.51a). The flexural deformation contributed the main column deflection up to final stage of testing, and on average accounted for 81% of the total column displacement. The displacement due to the shear averaged 12% of the total displacement, and the displacement due to the bar slip averaged about 8.5% of the total column displacement.

The displacement components due to the bar slip and due to shear during the tension axial load half cycle were found to be much larger than those during the compression axial loading cycle for Unit 2 and Unit 5, which were subjected to coupled variations in axial load and cyclic flexure. The tension axial load imposed in the negative lateral loading direction obviously increased the bar extension due to yield penetration into the column base, and the extensive cracking under the tension axial load reduced the shear stiffness. The displacement due to the bar slip and shear accounted for about 20% and 19% of the total displacement, respectively, in the negative loading direction. The associated flexural displacement contributed only about 65% of the column deflection in the negative loading direction, compared with 81% in the positive lateral loading direction.

A similar trend was observed for the Unit 3 and Unit 6. For the loading cycles when the tension axial load was applied, the displacement components due to the bar slip and shear increased(see Figs. 3.50 and 3.53).

3.10 LONGITUDINAL STRAIN OF CORE CONCRETE

Using the potentiometer readings, the longitudinal strains in the core concrete were determined using the same method as for the curvature. These strains were calculated for the surface of the concrete core(at

the outside of the perimeter hoops) and were plotted in the same way as for the curvatures. The strain profiles at the peak of each nominal displacement ductility factor are illustrated in Figs. 3.54 to 3.59. In these figures, the tension strains were taken as positive and the compression strains were taken as negative.

The magnitude of the strains at each location generally increased with the increasing displacement ductility factor. The plastic strains for Units 4, 5, and 6, with the magnitude larger than 0.003 which is proposed by various codes for the ultimate concrete strain at the flexural strength, spread over a larger regions than for Units 1, 2, and 3. This may be attributed to the higher compression axial load applied to these column units. The strain profiles for Units 1 and 4, as shown in Figs. 3.54 and 3.57, are seen to be essentially symmetric for the east and west sides of the columns. The compressive strains for Unit 4 are higher than those for Unit 1 and spread over larger regions above the column base. This was apparently the result of the larger compression axial load applied to Unit 4.

The strain profiles for Units 2 and 3 are unsymmetric for the east and west sides of the columns. The large compression strains mainly developed in the west side of the column when the positive lateral loading was applied, in which the west side of the section was in compression. Due to the presence of the tension axial load, the east side of the column was mostly in tension for both the positive and negative loading directions. The compression strains was observed only in the initial loading cycles, and the magnitude of these strains was very small. The tension strains for Units 2 and 5 were generally much larger than those occurring in Units 1 and 4. These high tension strains resulted in slippage between the concrete and the longitudinal reinforcing bars. As a consequence, concrete became very loose and spalling of the concrete followed immediately when these regions were loaded into compression. It was, therefore, observed during the tests that the serious spalling of the concrete occurred at the west side of the column and propagated into the core area at high displacement ductility levels.

At the east side of the column, only minor spalling of concrete took place in Unit 2 and no spalling of concrete was detected in Unit 5, in which the core concrete was confined by more closely placed transverse reinforcement.

In the case of Units 3 and 5, compression strains existed at both sides of the columns. Once again, the compression strains in Unit 6 spread over larger regions than that in the case of Unit 3. The spalling of the concrete, extended into the concrete core to some extent, as was observed at both sides of the column of Unit 3.

The maximum longitudinal compressive strain at the surface of core concrete was approximately 0.02 to 0.04 for Units 1, 2 and 3, and 0.03 to 0.05 for Units 4 , 5 and 6.

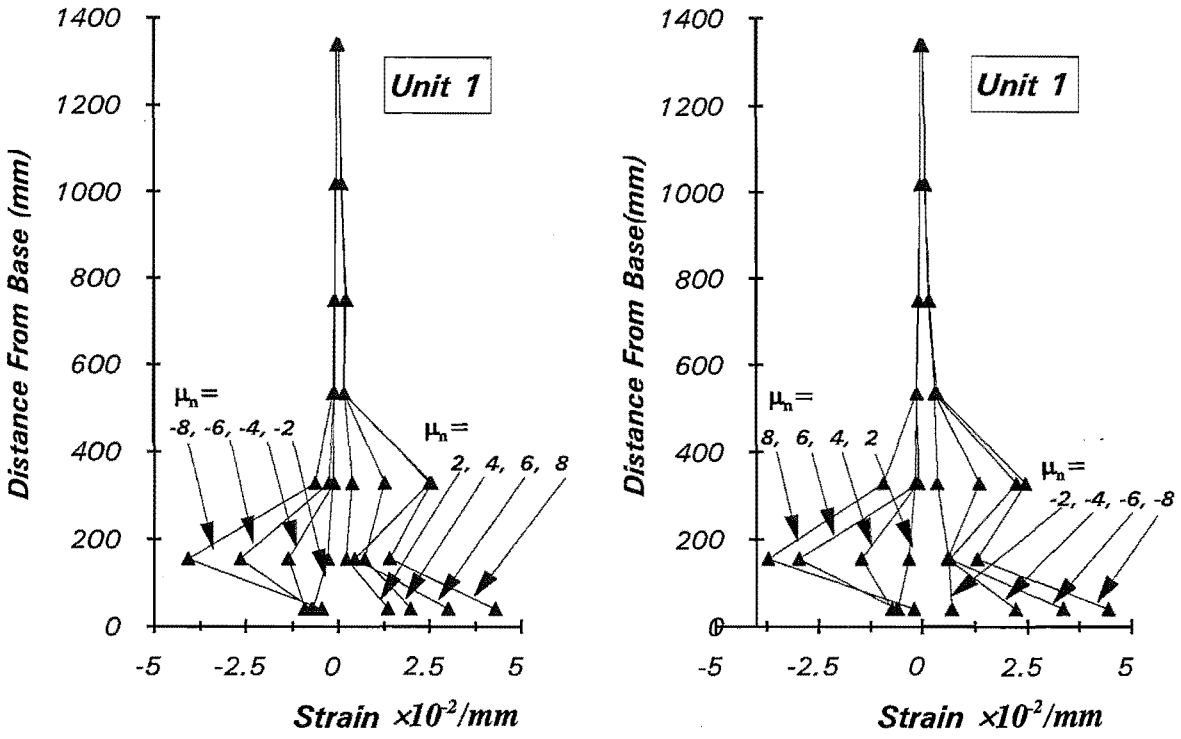

(a) East side of column (b) West side of column

Fig.3.54: Longitudinal Strains at Surface of Concrete Core

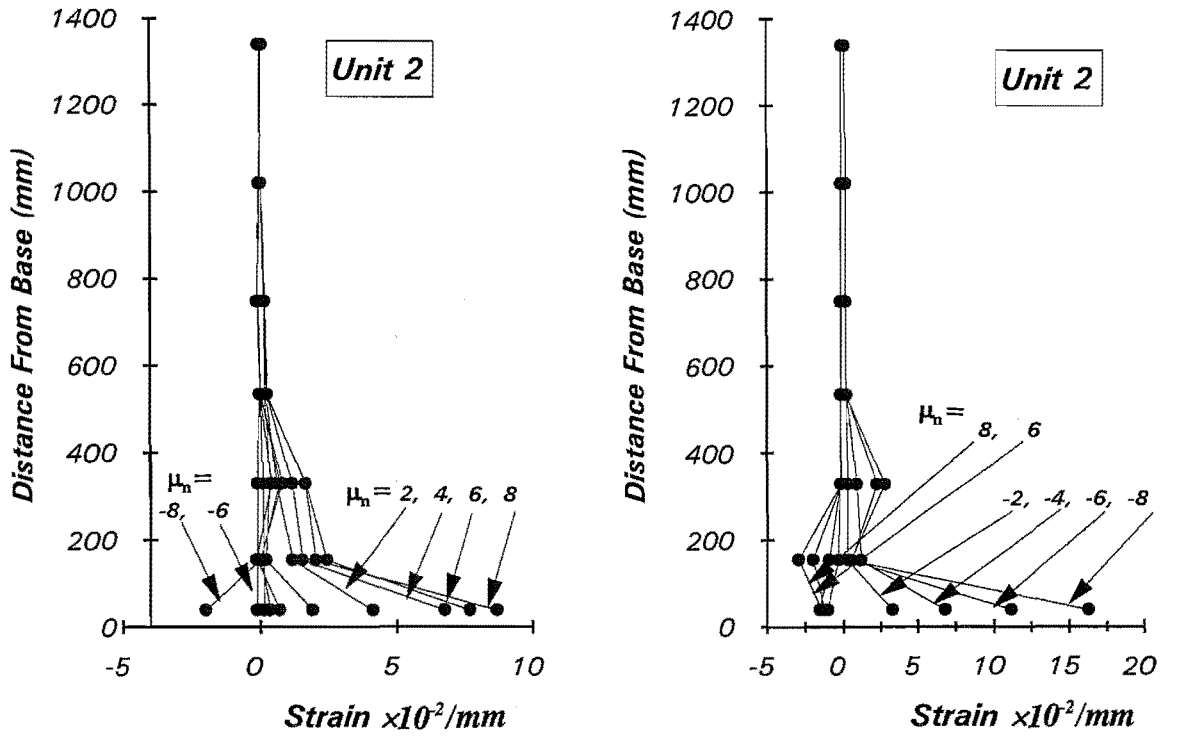

(a) East side of column (b) West side of column

Fig.3.55: Longitudinal Strains at Surface of Concrete Core

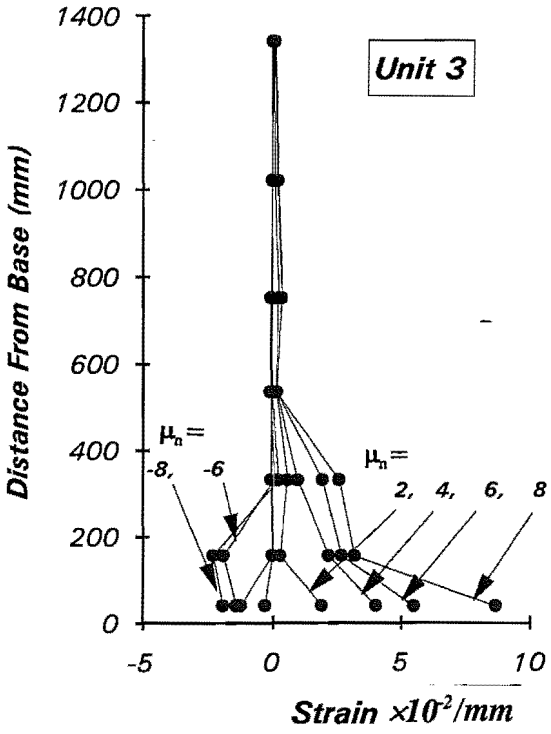

(a) East side of column

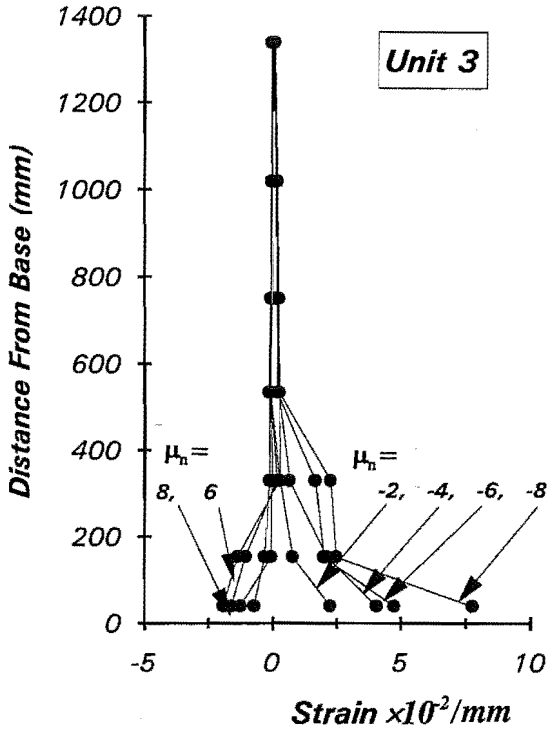

(b) West side of column

Fig.3.56: Longitudinal Strains at Surface of Concrete Core

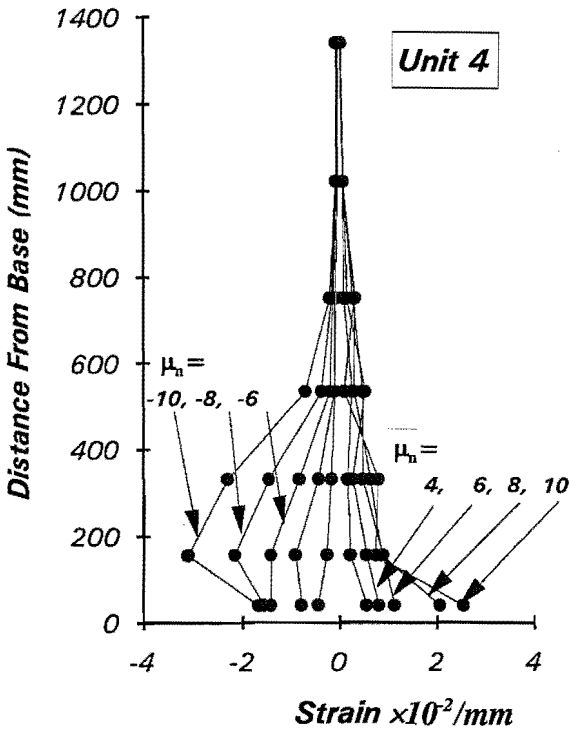

(a) East side of column

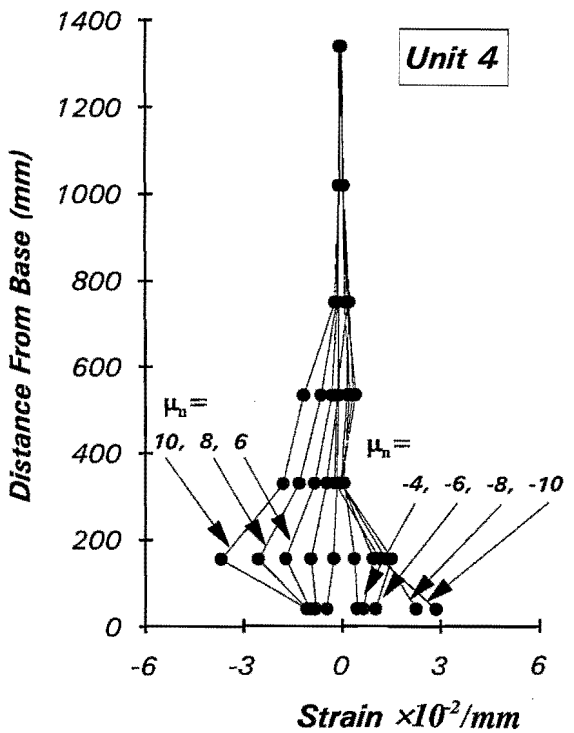

(b) West side of column

Fig.3.57: Longitudinal Strains at Surface of Concrete Core

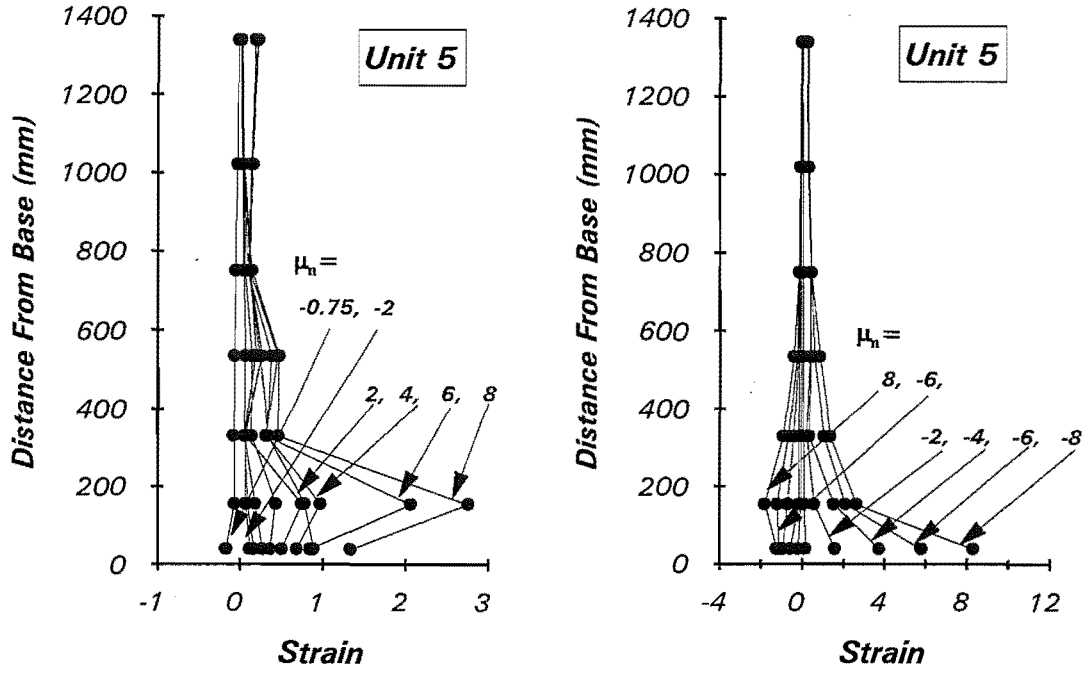

(a) East side of column (b) West side of column

Fig.3.58: Longitudinal Strains at Surface of Concrete Core

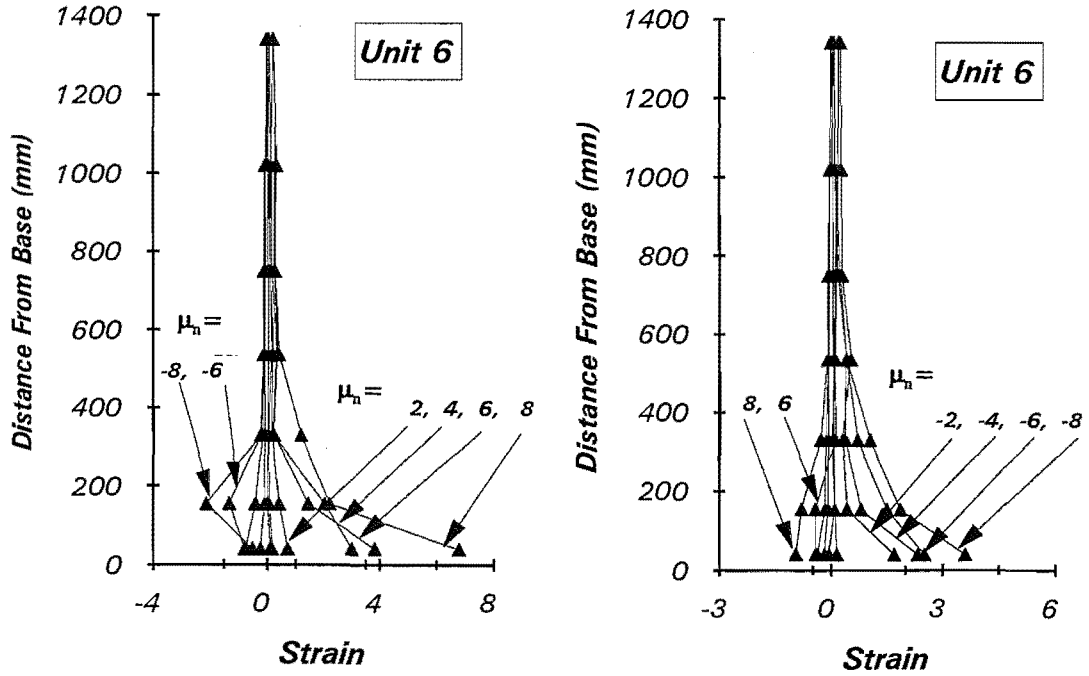

(a) East side of column (b) West side of column

Fig.3.59: Longitudinal strains at surface of concrete core

3.11 MEASURED STRAINS ON LONGITUDINAL REINFORCEMENT

The unsymmetric response of the columns under varying axial load can be found from the longitudinal bar strain histories. Figs.3.60 to 3.65 show the measured strain histories of the longitudinal bars for the six column units. The lateral load-strain relations of the east and west bars of Unit 1 and Unit 4 were basically symmetric. However, the lateral load-strain relations for the east and west bars in the columns subjected to varying axial load were markedly different, despite the lateral displacements being almost the same for each loading direction. For the columns under alternating tension and compression axial load, the reinforcing bar at the east side of the column was in tension for all the loading excursions except for in the initial loading cycle. The longitudinal bars in the west side of the column yielded both in tension and compression.

The distribution of the measured strains at the height of the columns obtained from strain gauge readings on the longitudinal bars are illustrated in Fig.3.66 to 3.71. In these figures the tension strains are taken as positive and the compression strains as negative.

Again, it can be seen that the strain profiles of the longitudinal bars on the east and west sides of Units 1 and 4 are basically symmetric. The asymmetry of the strain distributions for the east and west longitudinal bars in the other column units was caused by the unsymmetric actions in the columns due to varying axial loading. The strains at each location generally increased as the imposed displacement ductility increased. The strains at the first strain gauge level, which were located at the column-base interface, are smaller than those at the second strain gauge level. This indicated that the critical section may move away from the column-base interface, because the regions adjacent to the column base received additional confinement from the relatively rigid column base. The largest strains occurred at the second or third strain gauge level, in the regions between 100 to 250mm above the column base. The longitudinal bars in both sides of the column yielded in tension at low displacement ductility levels. The compressive strains in the east side longitudinal bars of Units 2 and 5 are very small. This occurred because most of the longitudinal bars at the east side of the column were in tension under both positive and negative lateral loading, due to the presence of tension axial load in the negative loading direction. This is especially evident for Unit 5 with high tension axial load in the negative lateral loading direction. In fact, the longitudinal bar strains at the east side of Unit 5 were in compression only in the initial loading cycles(see Figs.3.64 and 3.70).

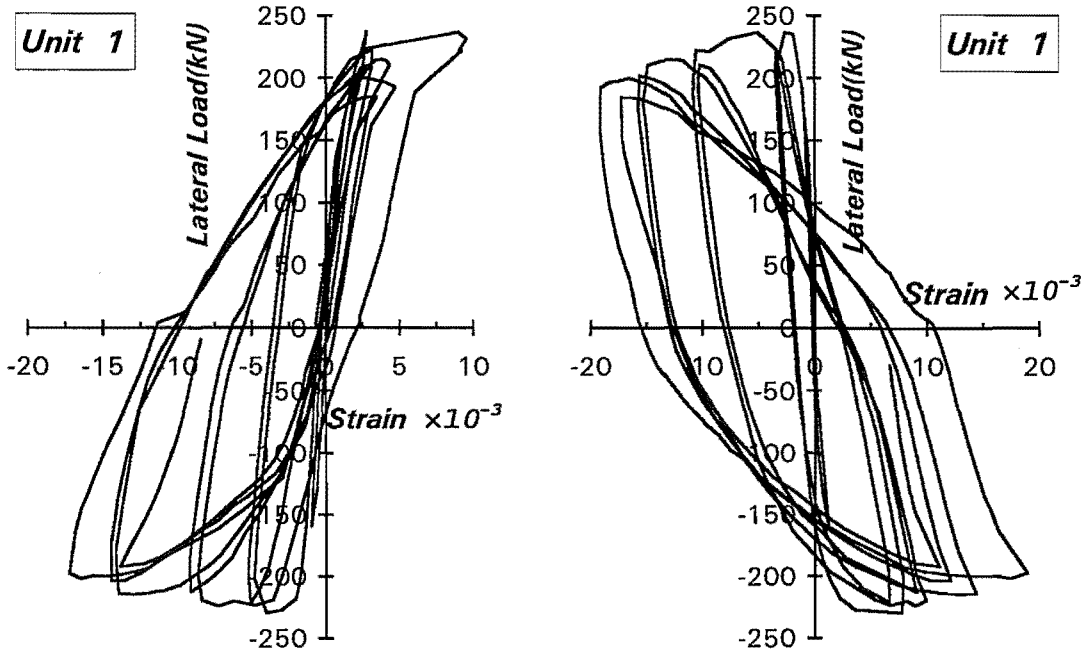

(a) East side 75mm above base (b) West side 75mm above base

Fig.3.60: Strain histories of longitudinal bars for Unit 1

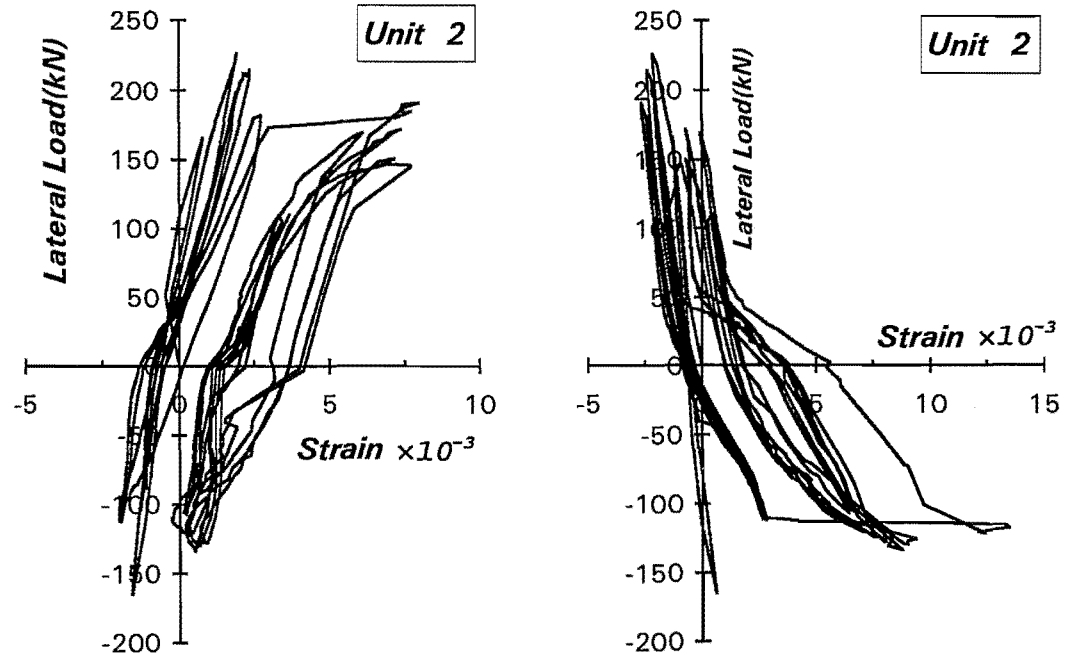

(a) East side 75mm above base (b) West side 355mm above base

Fig.3.61: Strain histories of longitudinal bars for Unit 2

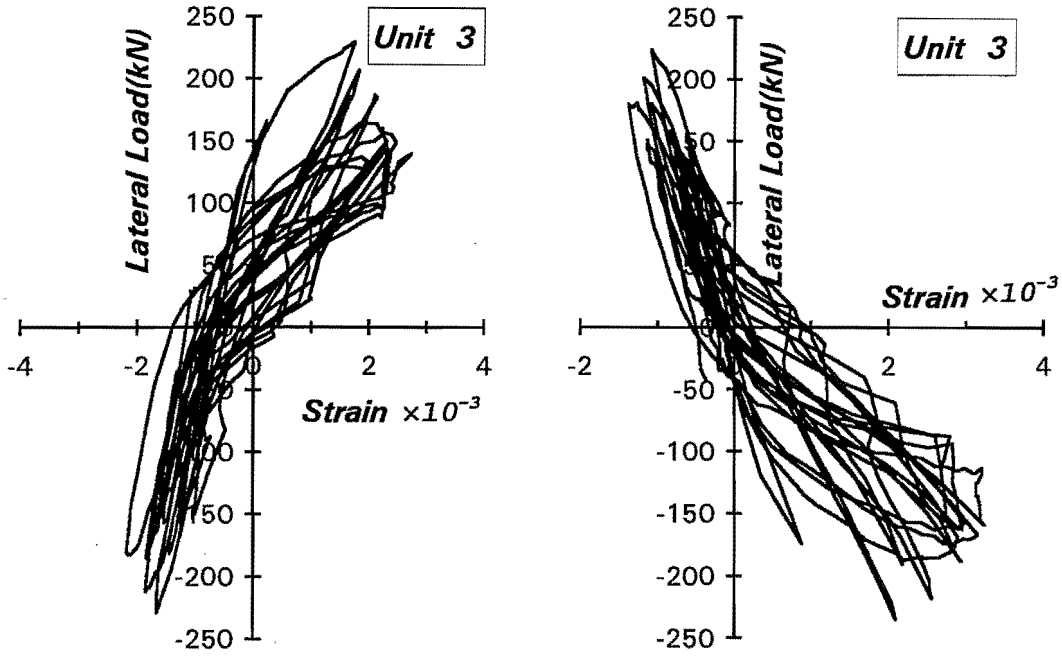

(a) East side 565mm above base (b) West side 565mm above base

Fig.3.62: Strain histories of longitudinal bars for Unit 3

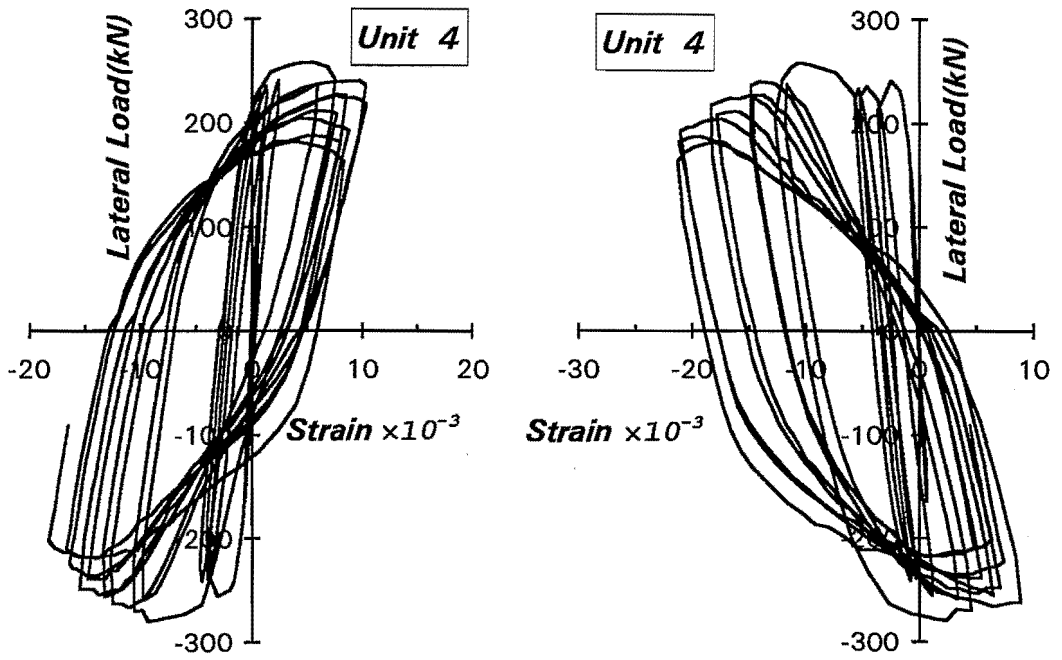

(a) East side 565mm above base (b) West side 565mm above base

Fig.3.63: Strain histories of longitudinal bars for Unit 4

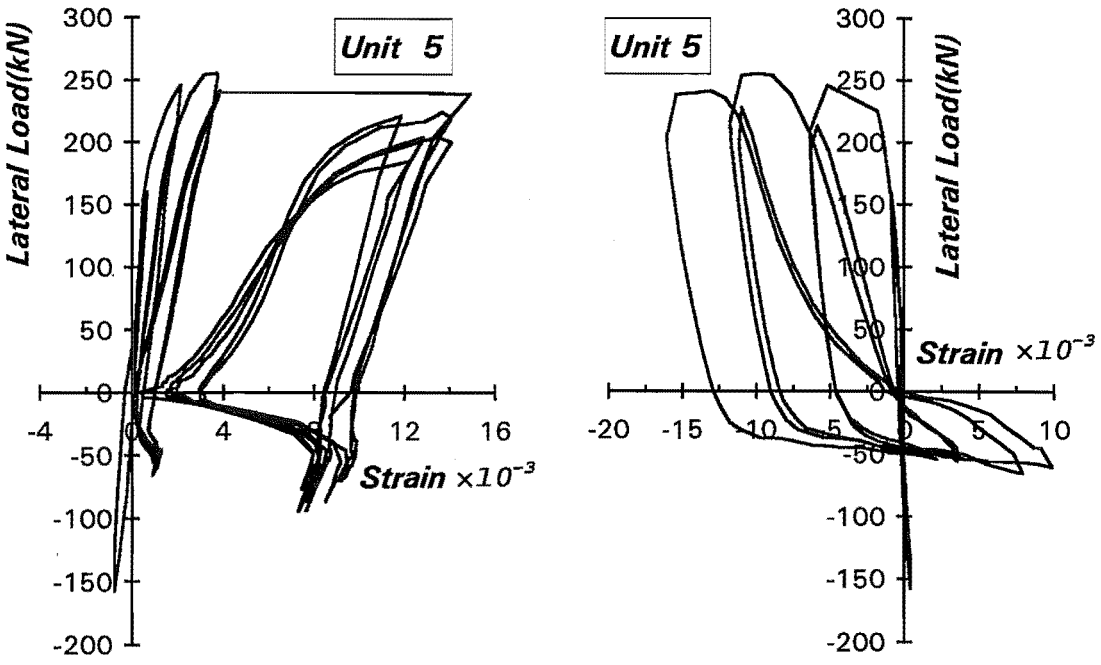

(a) East side 400mm above base (b) West side 400mm above base

Fig.3.64: Strain histories of longitudinal bars for Unit 5

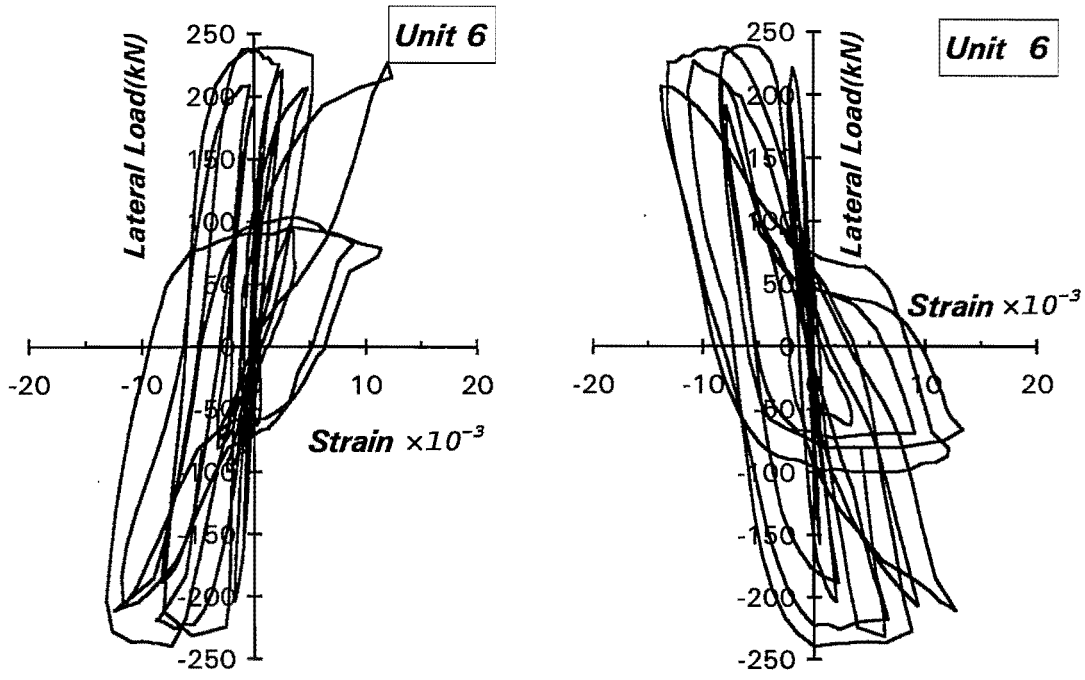

(a) East side 80mm above base (b) West side 80mm above base

Fig.3.65: Strain histories of longitudinal bars for Unit 6

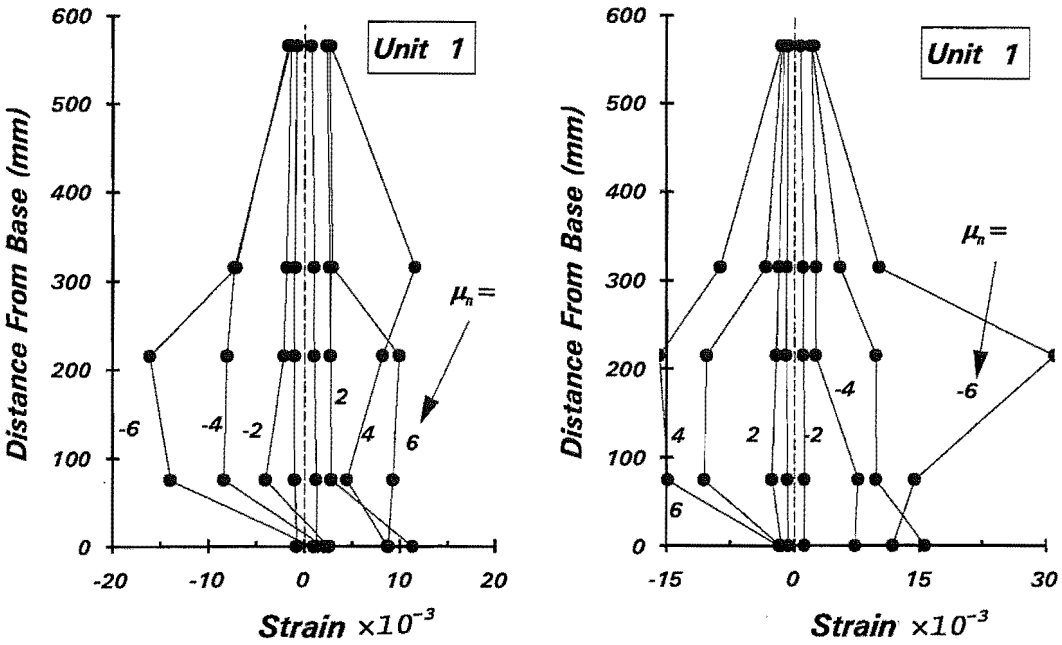

(a) East side of column (b) West side of column

Fig.3.66: Distribution of strains in longitudinal bars for Unit 1

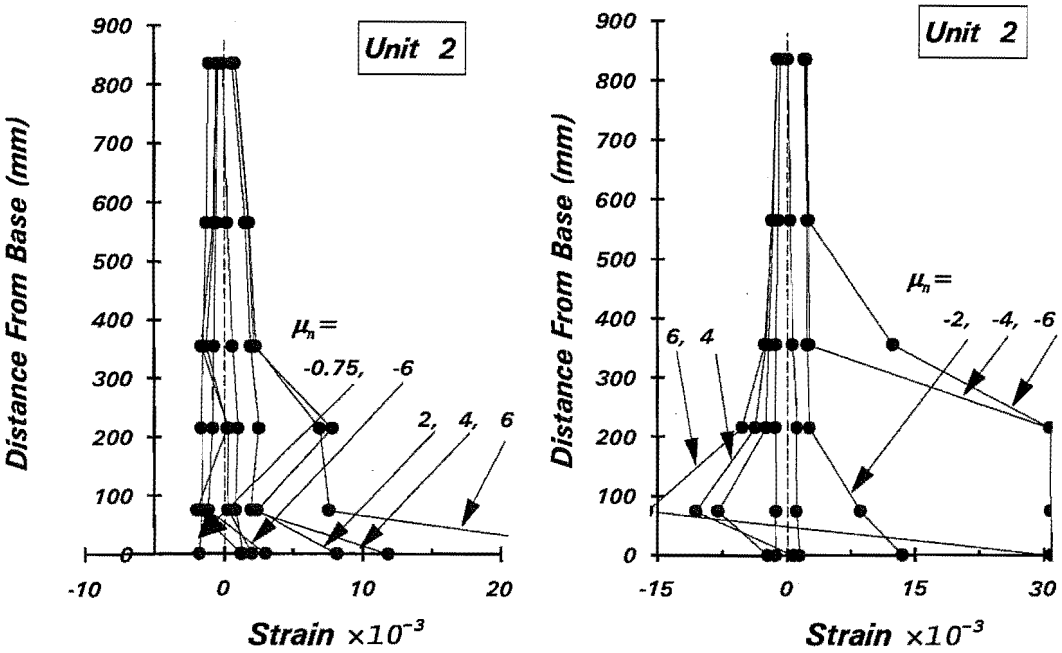

(a) East side of column (b) West side of column

Fig.3.67: Distribution of strains in longitudinal bars for Unit 2

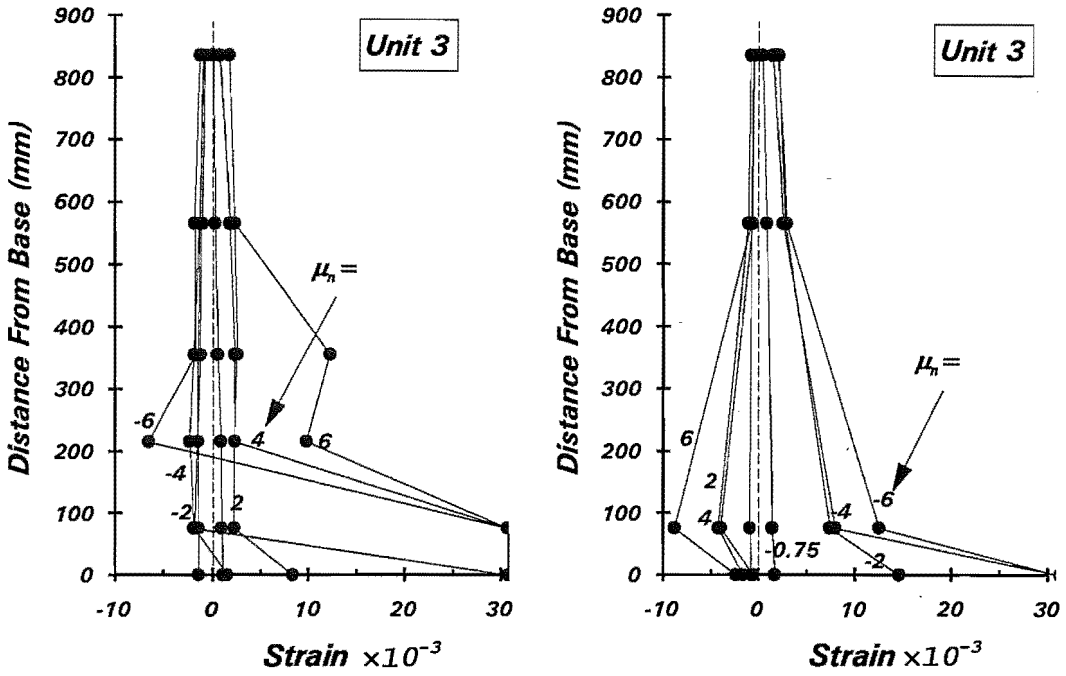

(a) East side of column (b) West side of column

Fig.3.68: Distribution of strains in longitudinal bars for Unit 3

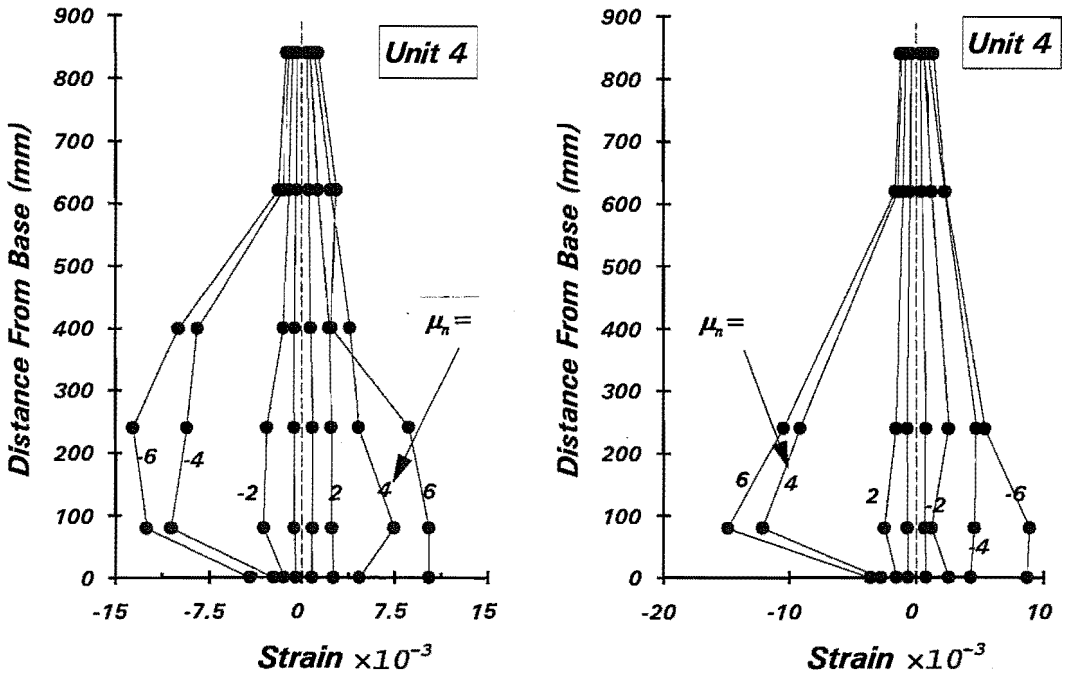

(a) East side of column (b) West side of column

Fig.3.69: Distribution of strains in longitudinal bars for Unit 4

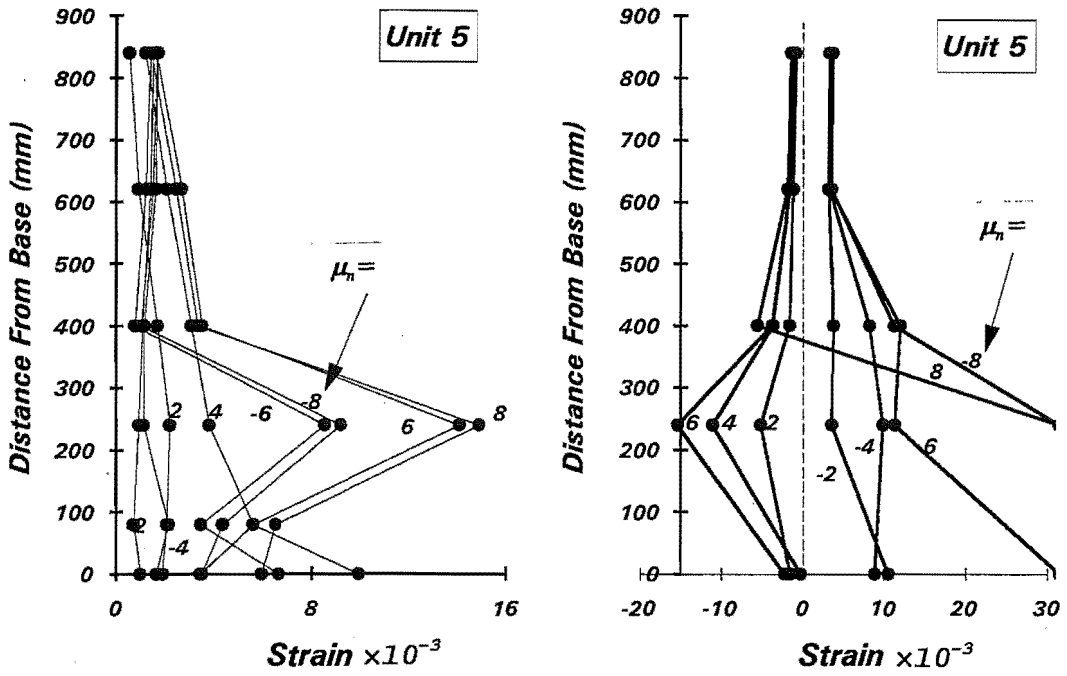

(a) East side of column (b) West side of column

Fig.3.70: Distribution of strains in longitudinal bars for Unit 5

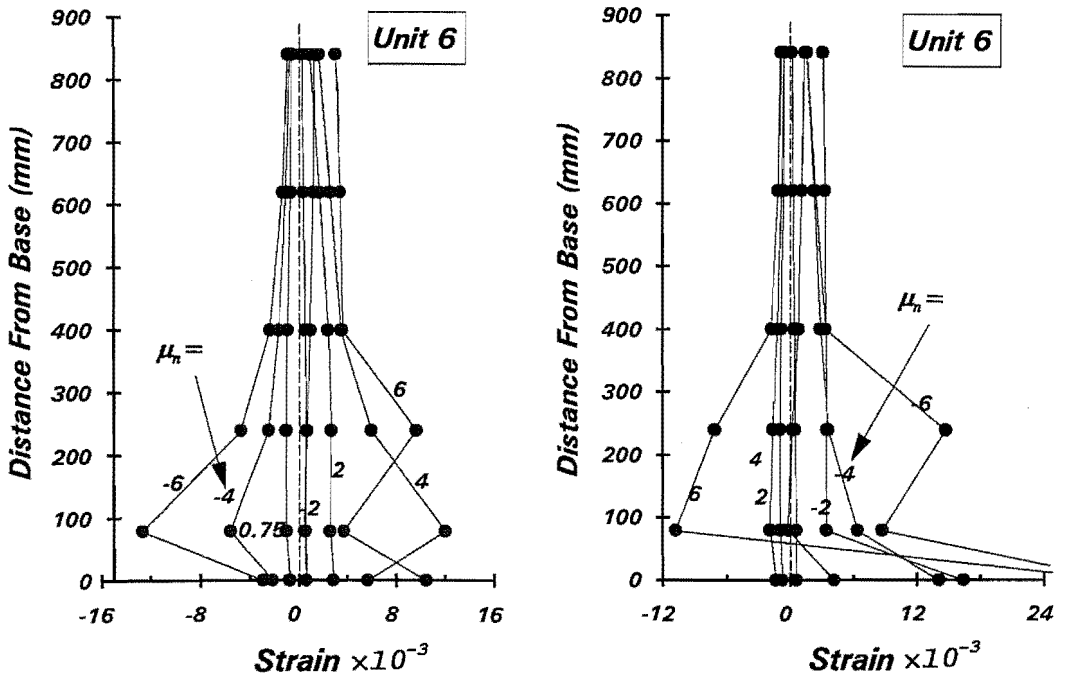

(a) East side of column (b) West side of column

Fig.3.71: Distribution of strains in longitudinal bars for Unit 6

3.12 HOOP STRAINS DUE TO CONFINEMENT OF CORE CONCRETE

The hoop strains measured from the strain gauges, which were attached to the square hoops of the column in the direction perpendicular to the lateral loading direction(see Fig.2.9), were considered to be due to confinement of core concrete. These strain gauges were placed on the west side of the column for Units 1 to 3, and on the east side of the column for Units 4 to 6. For Units 1 and 4 with constant compression axial load, these strain gauges were in compression zone during the loading in one lateral direction, and were in tension zone during the loading in the other direction. For the column units with varying axial load, the hoop strain gauges could be in compression or tension zone, depending on the application of lateral load and the presence of axial load.

The distributions of measured hoop strains due to confinement of concrete at the successive positive and negative lateral loading peaks are illustrated in Figs.3.72 to 3.77. The strains are plotted at the strain gauge positions and joined by straight lines. As can be seen from Figs.3.72 to 3.77, the measured hoop strains due to confinement for Units 1 and 4 reached yield at about nominal displacement ductility factor $\mu_n \geq 6$. The hoop strains for Unit 4 were much larger than that for Unit 1, indicating the effect of compression axial load level on the confinement of core concrete. The hoop strains due to confinement of concrete for Units 2, 3 and 6 reached yielding only in one lateral loading direction. The hoop strains at all levels for Unit 5 remained in elastic range. This was because when the positive lateral loading was applied, the hoop strain gauges were in tension zone, when the negative lateral loading was applied and hence tension axial load was applied, they were also in tension zone.

3.13 ELONGATION OF TEST COLUMNS

The column elongation is defined as the elongation of the column at the centroid of the column section. Column elongation is the result of the tensile strains in the longitudinal reinforcement being larger than the compression strain in the concrete. The column elongation can be readily calculated from the measurements of the linear potentiometers. The deformation of top stub of the column was not measured. It is believed that deformation of the top stub should be extremely small since this region has been greatly strengthened by use of a larger cross section and additional steel reinforcing bolts.

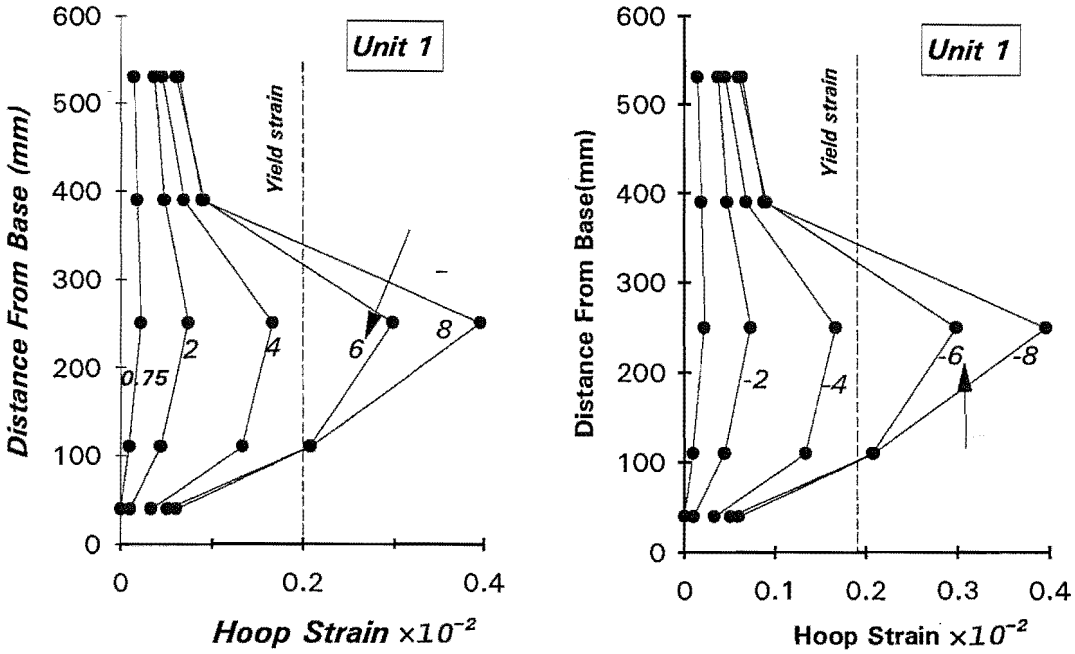

(a) Positive loading (b) Negative loading

Fig.3.72: Distribution of hoop strains due to confinement for Unit 1

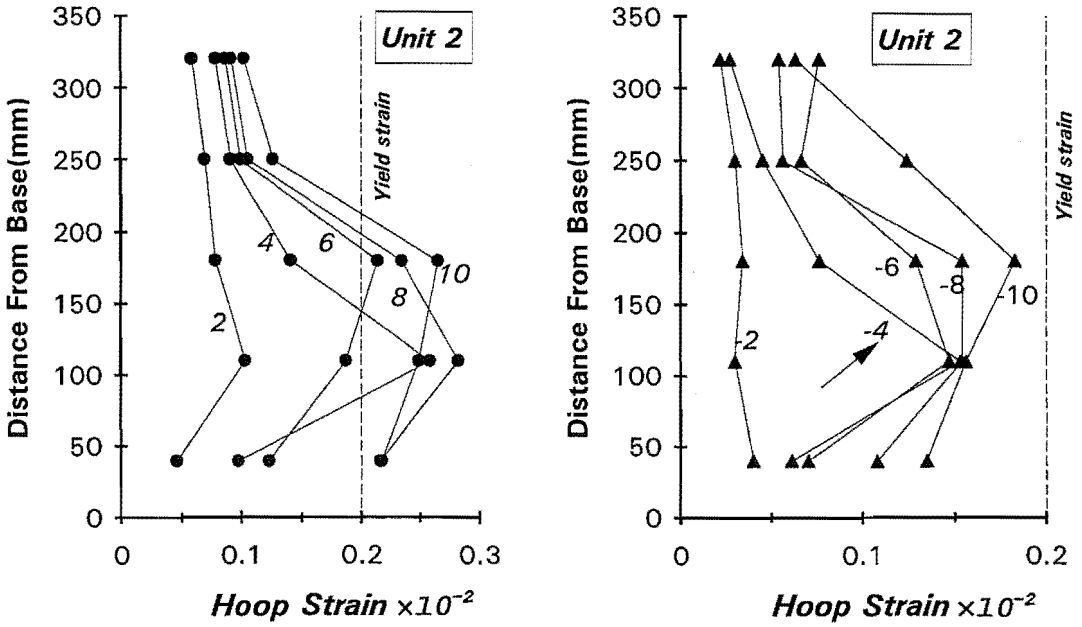

(a) Positive loading (b) Negative loading

Fig.3.73: Distribution of hoop strains due to confinement for Unit 2

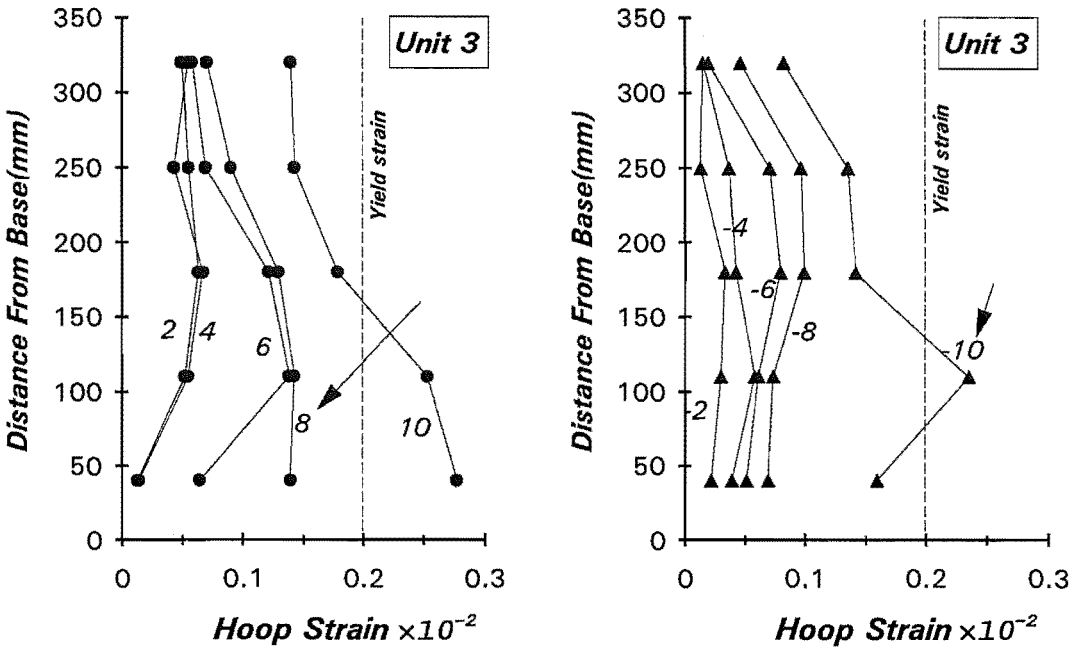

(a) Positive loading (b) Negative loading

Fig.3.74: Distribution of hoop strains due to confinement for Unit 3

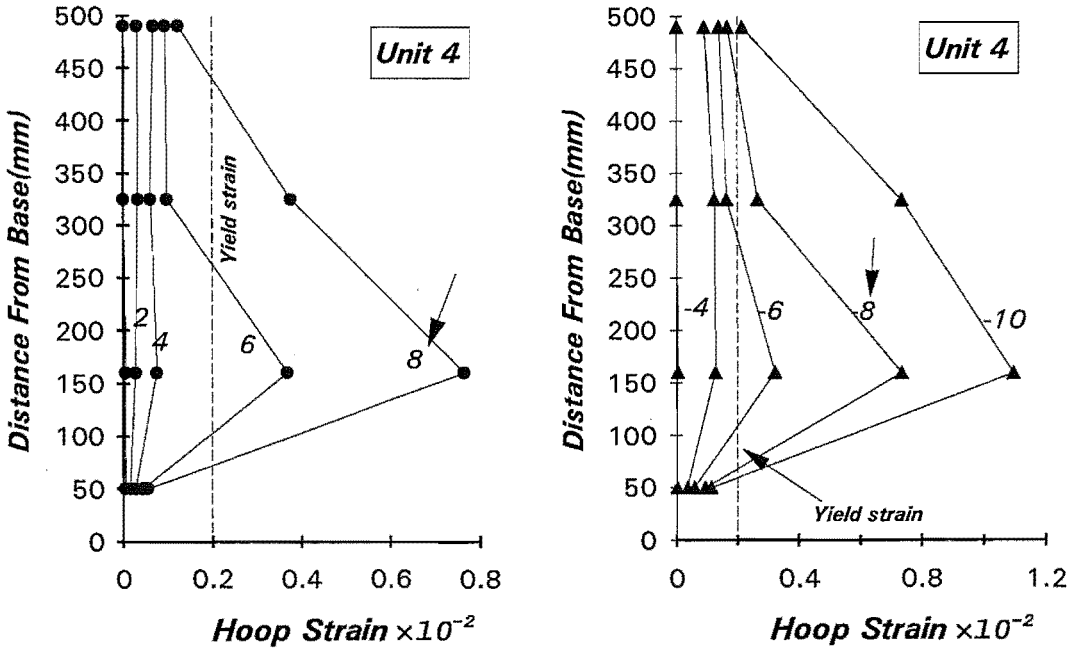

(a) Positive loading (b) Negative loading

Fig.3.75: Distribution of hoop strains due to confinement for Unit 4

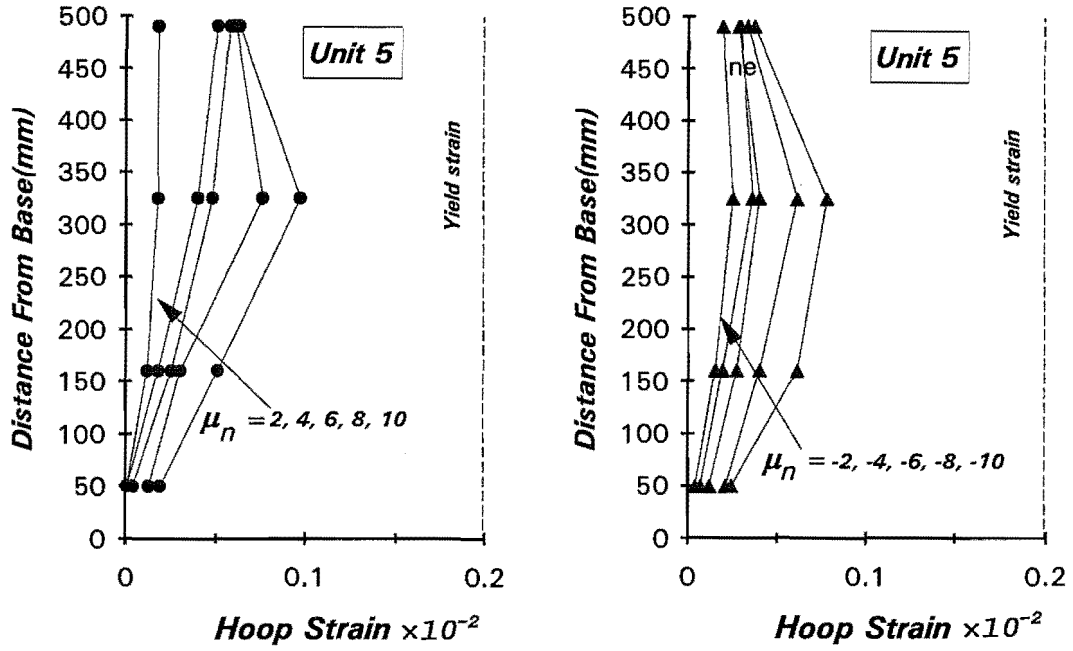

(a) Positive loading (b) Negative loading

Fig.3.76: Distribution of hoop strains due to confinement for Unit 5

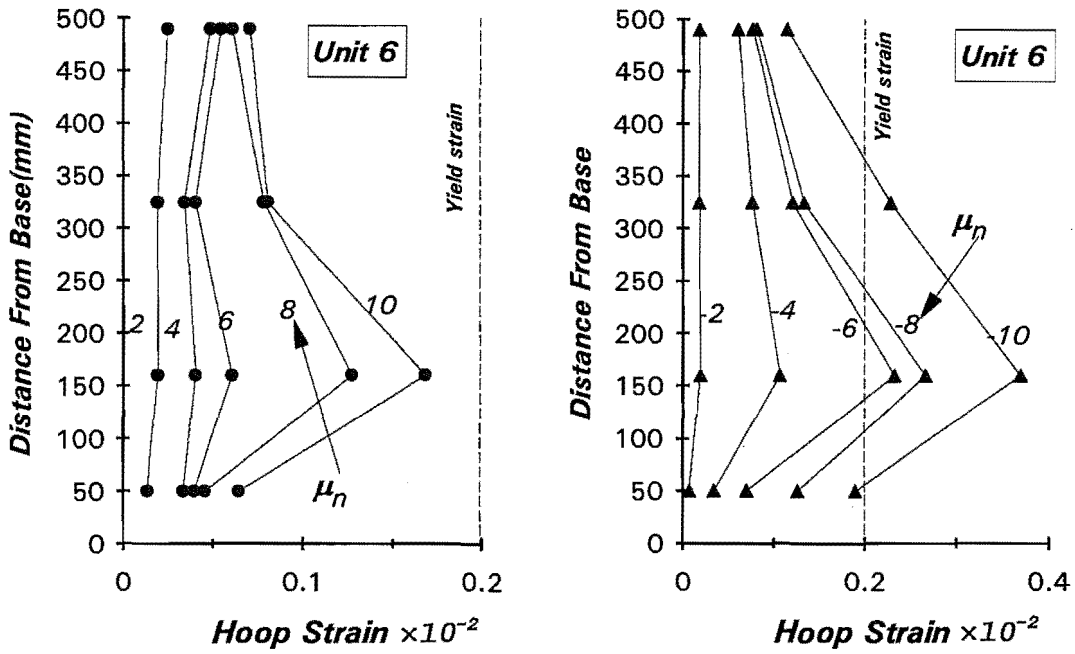

(a) Positive loading (b) Negative loading

Fig.3.77: Distribution of hoop strains due to confinement for Unit 6

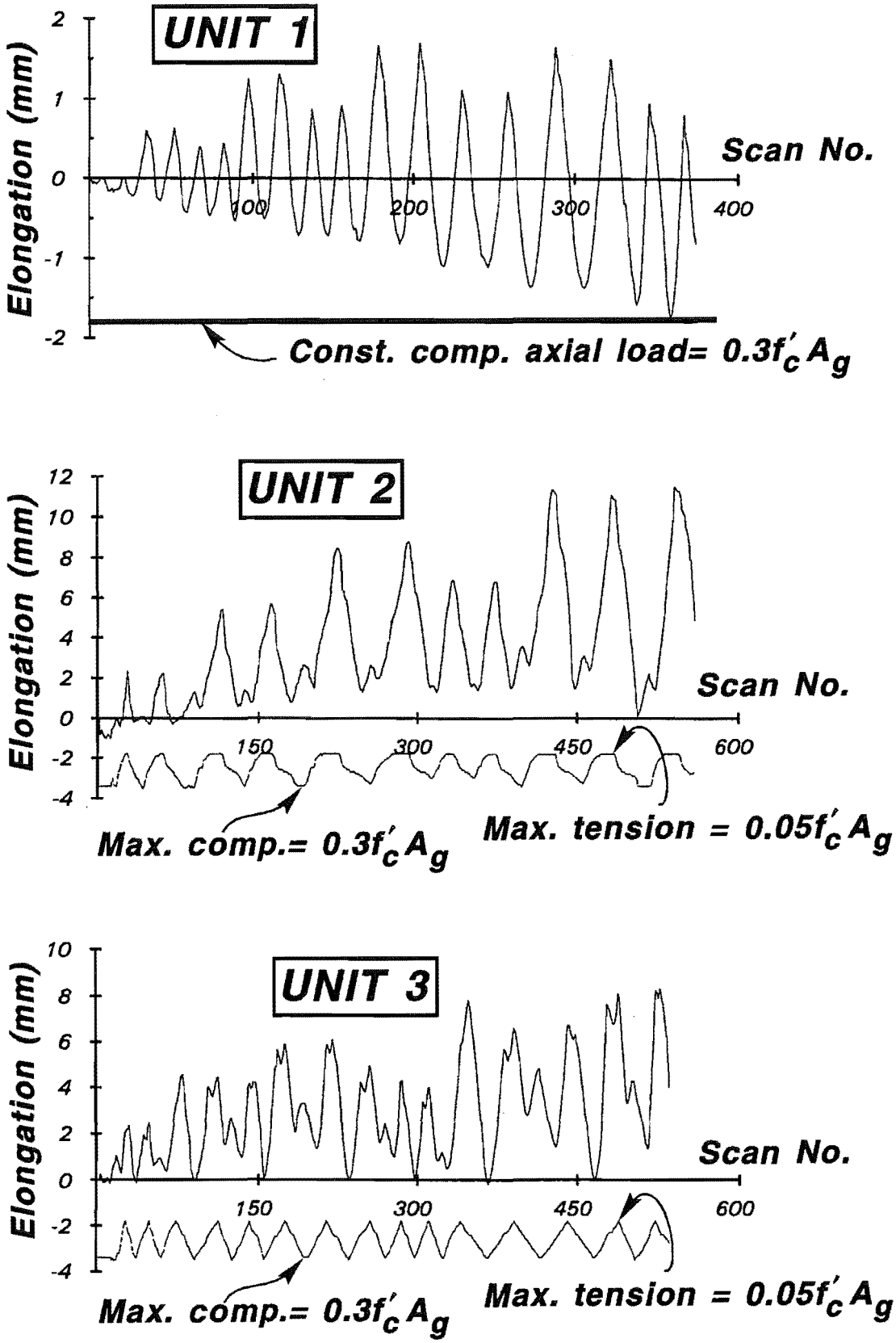

Fig.3.78: Measured Column Elongations of Units 1, 2 and 3

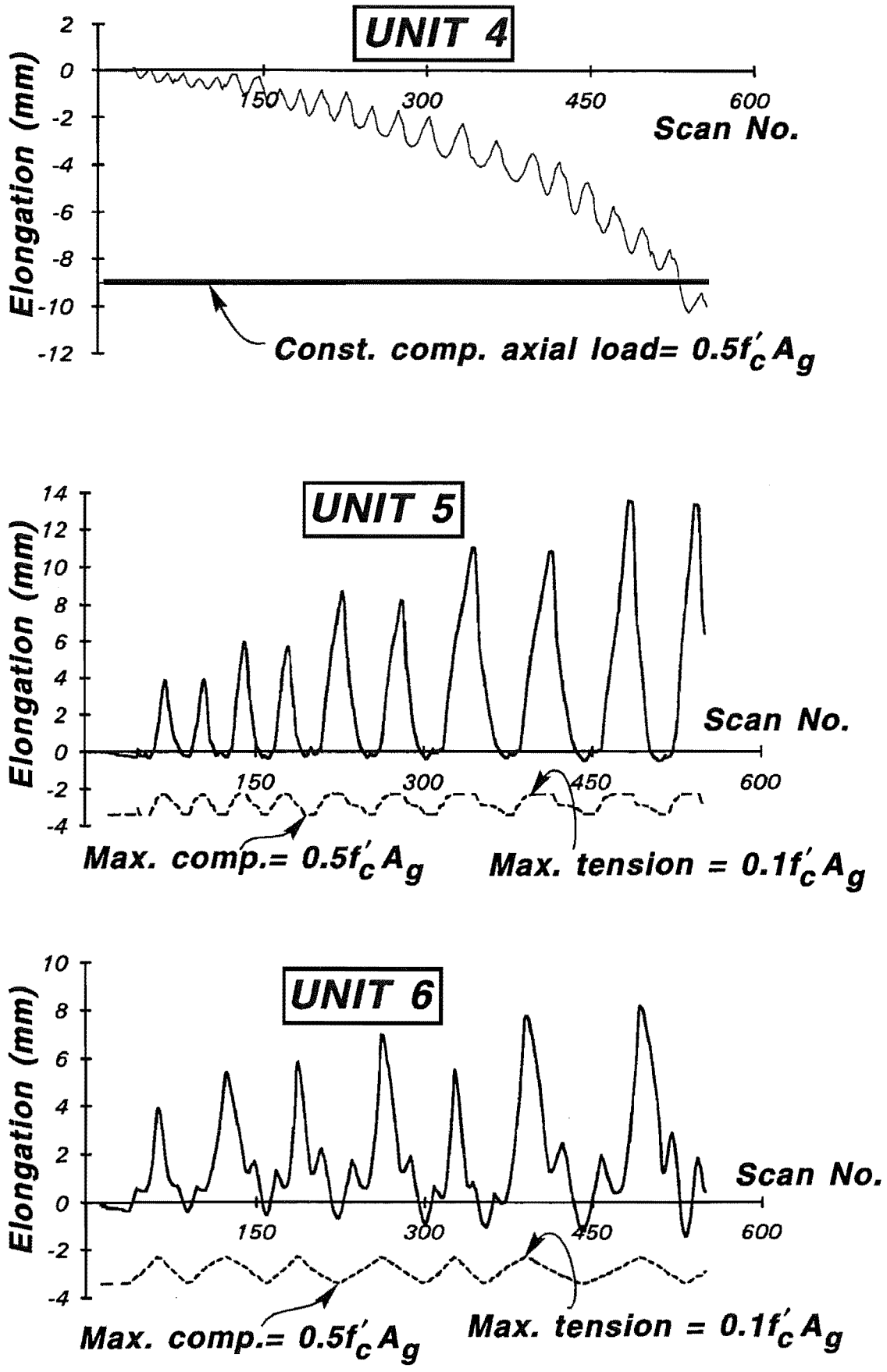

Fig.3.79: Measured Column Elongations for Column Units 4, 5 and 6

The measured column elongations, plotted against the scan number of recorded data, are illustrated in Figs.3.78 and 3.79 for the six column units. The axial load histories, shown as dashed lines, are also included in the figures. In general, the maximum column elongation occurred at the peaks of each lateral loading cycle where the large tension strains were imposed. The column could become elongated or shortened, depending on the intensity of the axial load applied. When the lateral load unloaded to around zero, the lowest value of the column elongation was attained, since most open flexural cracks were closed at this loading instant. The column elongation was also significantly influenced by the axial load histories.

Under a constant compression axial load of $0.3f'_cA_g$, Unit 1 elongated at each peak lateral displacement and shortened upon unloading to zero displacement. Column Unit 4, subjected to a constant compression axial load of $0.5f'_cA_g$, however, continued to shorten as the imposed displacement ductility increased. The elastic recovery was only observed during initial lateral loading cycles. It is evident that large compression strains were induced in the concrete in Unit 4 due to the high compression axial load. The maximum shortening of Unit 4 was 10 mm at $\mu_n=8$.

The presence of tension axial load greatly increased the column elongation. This was more pronounced in Units 2 and 5, since the application of the tension axial load reached maximum value at each displacement peak in the negative lateral loading direction. The column elongations at the peak of negative lateral loading direction were much larger than those during positive lateral loading for Units 2 and 5. For column Units 3 and 6, the peak column elongations corresponded to the application of tension axial load. Large column elongation occurred even when the lateral load was zero should the tension axial load reach the maximum value. This indicated the column elongation was more relied on the axial load level than the level of flexural rotation.

It is clear the maximum elongations for the columns subjected to varying axial loading, ie, Units 2, 3, 5 and 6, were much larger than those for the columns under constant axial load, ie, Units 1 and 4.

3.14 CONCLUSIONS

All six reinforced concrete column units tested had a 400mm square cross section, an aspect ratio(column height/section depth) of 4.12, a longitudinal reinforcement ratio of 1.6% and transverse reinforcement which was placed according to the code provisions of NZS 3101[S14]. Based on the performance of the six column units tested during cyclic lateral loading and varying axial load histories the following conclusions can be drawn.

1. Units 1 and 4, subjected to the cyclic flexure and constant compression axial load levels of $0.3f'_cA_g$ and $0.5f'_cA_g$, respectively, were capable of maintaining very stable lateral load-displacement hysteresis hoops up to a displacement ductility factors of at least eight, which corresponded to an interstorey drift of about 5 percent, before losing their lateral load carrying capacity by more than 20%. The measured flexural strength of the columns exceeded the ideal flexural strength, calculated using the code provisions of NZS 3101[S14] and using the actual material strengths, and with a strength reduction factor of unity, by a considerable margin(18 to 42%). No significant degradation of strength was observed before the end of the testing. The buckling of the longitudinal bars resulted in the termination of the test on Unit 4 at a displacement ductility factor of $\mu_n=12$. However when test on Unit 1 was stopped at displacement ductility factor of $\mu_n=8$, the buckling of longitudinal bars and strength decay were not significant.

2. Units 2 and 5, tested under varying axial compression and tension load between $0.3f'_cA_g$ and $-0.05f'_cA_g$ for Unit 2, and between $0.5f'_cA_g$ and $-0.1f'_cA_g$ for Unit 5, which varied in direct proportion to the bending moment at the critical section of the column, achieved lower flexural strengths than Units 1 and 4, and attained nominal displacement ductility factors of $\mu_n=8$ and $\mu_n=10$, respectively. The observed lateral load-displacement hysteresis loops were unsymmetric. Serious pinching of the lateral load-displacement hysteresis loops occurred at low displacement ductility levels for the both columns. The spacing of transverse reinforcement in the plastic hinge regions played an important role in preventing premature decay of strength. For both column units, spalling of cover concrete took place only at one side of the column. The crushing of the concrete, which propagated into the concrete core, was more pronounced for Unit 2 than for Unit 5, because the latter had the smaller hoop spacing than the former, which provided better confinement of the concrete core. After a few excursions of lateral loading, the effect of the reduced hoop spacing on maintaining confinement in the plastic hinge regions became more important. The degradation of the lateral load strength in the compression axial load direction of Unit 2 was very significant. Both column units showed little deterioration in the lateral load carrying capacity in the tension axial load direction. The hoops reached yield strain, but no fracture of the hoops occurred. Buckling of the longitudinal bars eventually resulted in the termination of the tests on the two column units.

3. Units 3 and 6, tested under cyclic flexure and varying axial load, between the same compression and tension limits as Units 2 and 5 but which was uncoupled with the bending moment, attained nominal displacement ductility factors of six and eight, respectively. Pinching of the hysteresis loops took place for both column units. The strength degradation of Unit 3 was more significant than that of Unit 6. The concrete was damaged on both sides of the columns. The damage appeared more severe for Unit 3 than for Unit 6. Buckling of the longitudinal bars commenced

before the end of the testing.

4. The experimental results indicated that alternating compression and tension axial load has significant effect on the behaviour of reinforced concrete columns subjected to cyclic lateral loading. Under varying axial load, the column exhibited a very different lateral load-displacement response than when subjected to constant compression axial load. Varying axial load resulted in lower strength and stiffness of the column, which was indicated by serious pinching of the hysteresis loops. Considerable change in the column stiffness would result in a significant redistribution of the input forces in the columns of a moment resisting frame. The design forces should be obtained from an analysis which takes into account the effects of variations in the axial load on the stiffness of the columns.

5. Varying axial load caused a more severe degradation in the lateral load carrying capacity. Compared to companion columns with constant compression axial loads, the lateral load strength of the columns subjected to varying axial load levels was reduced by about 8% to 12% at displacement ductility factors of six, and further reduced by about 12 to 17% at displacement ductility factors of eight. The section moment capacity of the columns under varying axial load was reduced by about 8% to 15% , compared to the columns under constant axial load. The amount and spacing of transverse reinforcement played an important role in preventing premature strength decay. Less strength degradation was observed for the column with smaller hoop spacing.

6. The effective flexural rigidity $(EI)_e$ of the column section at first yield was found to be about $0.50(EI)_g$ for Units 1, 2 and 3 with compression axial load of $0.3f'_cA_g$, and $0.71(EI)_g$ for Units 4, 5 and 6 with compression axial load of $0.5f'_cA_g$. These $(EI)_e$ values had reduced to $0.27(EI)_g$ on average for Units 1, 2 and 3, and $0.41(EI)_g$ for Units 4, 5 and 6 at nominal displacement ductility factor $\mu_n=2$. The $(EI)_e$ value for the columns subjetced to varying axial loading was about 15 to 20% less than that subjected to constant compression axial load at nominal displacement levels of $\mu_n\geq 2$.

7. The application of tension axial load caused a concentration of the plasticity over a smaller length of column adjacent to the column base, hence increased the section curvature there. For the same displacement ductility factor the curvature at the critical section of the columns under varying axial load was about 20% larger than that of the column under constant axial load. The effect of varying axial load on the required deformation capacity of the critical section should be considered in seismic design.

Chapter 4

Experimental Investigation of the Shear Strength of Reinforced Concrete Columns Under Varying Axial Load ___ Test Series 2

4.1 INTRODUCTION

It is recognized that the shear strength of reinforced concrete columns is a function of the imposed flexural displacement ductility factor. The degradation in shear strength mainly results from the reduced contribution of the concrete shear resisting mechanisms. This reduction in shear strength is closely associated with the widening of flexure/shear cracks which leads to the loss of the capacity of concrete aggregate interlock. Most of the past research on the shear strength of columns has been conducted on the columns subjected to cyclic flexure and constant axial load level. However, in the event of a major earthquake, variations in axial force will occur in the columns of a moment resisting frame. The test results from the series of six reinforced concrete column units presented in Chapters 2 and 3 indicated that the flexural behaviour of reinforced concrete column is significantly influenced by variations in axial load. When accounting for the variations in axial load, the widening of flexural cracking and deterioration in the strength and stiffness became more significant during the application of the axial tensile load. It is of interest to investigate the effect of varying axial load on the shear strength of reinforced concrete columns.

The main aim of this second series of tests is to experimentally investigate the shear strength of reinforced concrete column under cyclic flexure and varying axial load. The particular emphasis of the investigation was put on the shear strength contributed by concrete shear resisting mechanism.

This chapter describes the design, instrumentation and test procedure of the three reinforced concrete columns of test series 2.

4.2 DESIGN CONSIDERATION

As part of the chosen deformation mechanism in ductile reinforced concrete frames, column plastic hinges at foundation level of the structure are expected to occur. Also, in the bridge structures, the columns will be the primary source of energy dissipation. Flexural yielding in the end regions of bridge piers is desirable. To simulate the first floor column of a building, or a column in a bridge between the adjoining footing and the point of contraflexural. Nevertheless, the test specimen was so designed as a cantilever column and subjected to combined cyclic flexure and varying axial load.

To investigate the shear strength, the test specimen was to be designed so that shear was the dominant mode of behaviour. The results from experiments conducted by Ang et al.[A7] on circular cantilever columns showed that the ratio of ideal shear strength to ideal flexural strength gives a good indication of the column failure mode. When this strength ratio is between 0.65 to 1.1, shear failure with moderate or limited ductility will occur. This strength ratio was taken as guildline in the detailing of reinforcing steel for the three column units tested. The calculations and detailing of the column was carried out based on the current New Zealand concrete design code: NZS 3101:1982[S14].

The main variable investigated in this series of tests is the effect of different axial load histories. Other variables included the axial load levels and the volumetric ratio of transverse reinforcement.

The three reinforced concrete column units were subjected to cyclic flexure and varying axial load. The maximum axial compressive load levels were $0.1f'_cA_g$, $0.2f'_cA_g$ and $0.3f'_cA_g$, and the maximum axial tensile load levels were $0.05f'_cA_g$, $0.1f'_cA_g$ and $0.15f'_cA_g$, for the Units 7, 8 and 9, respectively. All three column units used the same diameter reinforcing bars for the transverse reinforcement. The different content of hoop reinforcement was achieved by varying the hoop spacing, s_h. The plastic hinge length, according to NZS 3101[S14], was 1.5 times the overall depth of the column section, ie 600 mm. The distance from top face of the column base to the point of horizontal loading was 1 m, as shown in

Fig. 4.1. For simplicity, the hoop spacing was kept constant over the entire height of the column.

4.3 DESIGN OF COLUMN UNIT

4.3.1 Details of the Column Units

The three reinforced concrete column units were designated as Units 7, 8 and 9. All column units had a total height of 2.15m and a 400mm square cross section. These dimensions were chosen to suit the existing loading frame. The columns were seated on a 1.2x1.0x0.9 m reinforced concrete block. The distance from column base to the point of application of lateral load was 1.0 m, giving an aspect ratio, M/V*h*, of 2.5(Note: for column units 1 to 6 of series 1 described in Chapters 2 and 3 M/Vh=4.12), where M/V=shear span length and h=overall depth of the column section. The column section represents a scale model of about one-half to two-third of typical columns in a structure. Fig.4.1 shows the overall dimensions of the column units, the cross section, and the arrangement of longitudinal and transverse reinforcement in the column and column base.

Table 4.1: Details of Column Units

Unit	$(\frac{P}{f'_c A_g})^c$ (1)	$(\frac{P}{f'_c A_g})^t$ (2)	$(\frac{P}{f'_c A_g})^i$ (3)	Transverse Steel			Long. Steel	
				d_b mm (4)	s_h mm (5)	ρ_s % (6)	Num-d_b (7)	ρ_t % (8)
7	0.1	0.05	0.05	6	120	0.47	12-HD20	2.36
8	0.2	0.10	0.10	6	110	0.52	12-HD20	2.36
9	0.3	0.15	0.20	6	100	0.57	12-HD20	2.36

(1) The maximum compression axial load ratio

(2) The maximum axial tension load ratio

(3) The axial compression load applied during initial loading cycles.

(4) The diameter of hoop reinforcement

(5) Centre to centre spacing of hoop reinforcement

(6) The volumetric ratio of transverse reinforcement, $\rho_s=7.22A_b/(h"s_h)$, A_b is area of hoop steel.

(7) Total longitudinal reinforcement ratio, $\rho_t=A_s/A_g$.

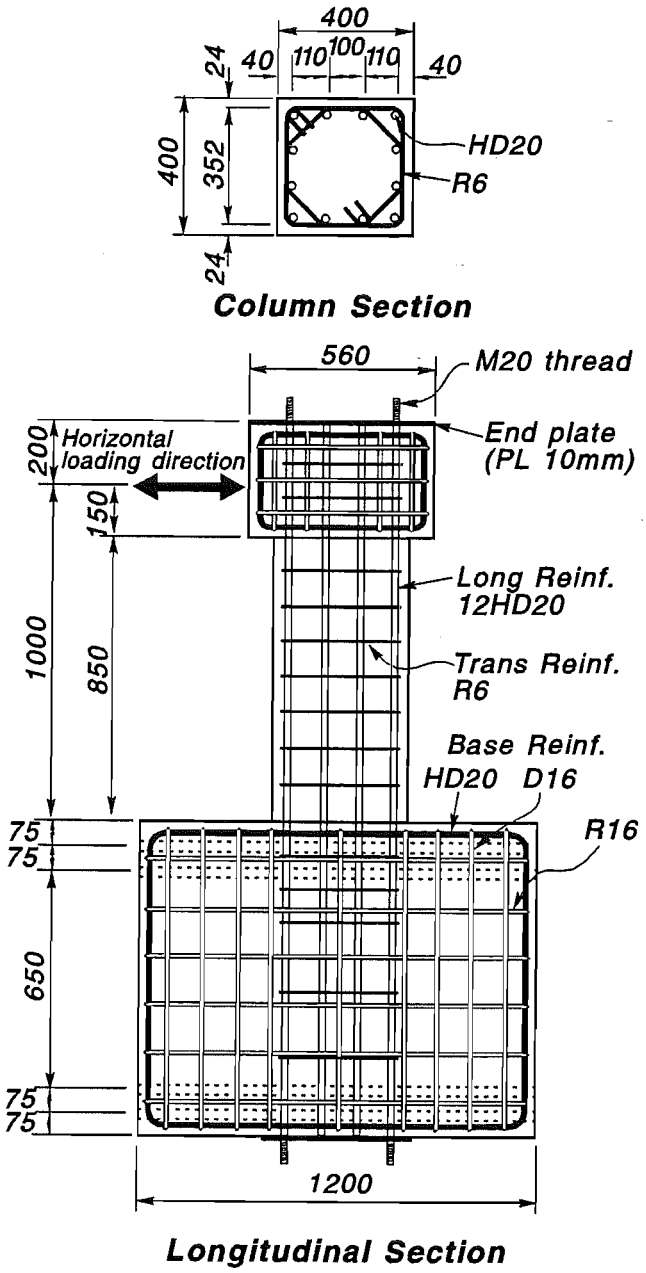

Fig. 4.1: Details of Column Units 7, 8 and 9

Each column unit contained twelve 20mm diameter Grade 430 deformed bars, which were almost evenly distributed around the sides of the column section, giving a total longitudinal reinforcing ratio, ρ_t, of 2.36%. The transverse reinforcement in the column units consisted of 6 mm diameter Grade 300 plain round bars in the form of square and octagonal hoops. The column base was heavily reinforced

with Grade 430 deformed bars, as the main reinforcement, and Grade 300 plain round bars as confinement hoops to ensure it will remain in elastic status during the testing.

Normal weight concrete with target compressive strength of 30 MPa, a maximum aggregate size of 13mm was used for the column portion. For the column base block, the concrete with compressive strength aimed at 45 MPa was used. Table 4.1 lists the details for the three column units.

4.3.2 The Flexural Strength of Column Units

To ensure that the test column failed in desired mode, the shear force corresponding to the development of the probable flexural strength of the column has to be determined. The ideal flexural strength of the column unit, M_i, was calculated by using code approach of NZS 3101:1982[S14] with the strength reduction factor, ϕ, set equal to unity. In the design, the specified material strength was used, while in the analysis after testing the calculations were based on the measured concrete and steel strength. The maximum flexural strength, or overstrength of the column, was also estimated. The flexural overstrength includes the contribution of additional strength enhancement of steel due to strain hardening at large deformations and the strength enhancement of concrete due to confinement. Ang et al[A7] proposed that the flexural overstrength factor of the column can be calculated as

$$For \quad \frac{P}{f_c A_g} < 0.1: \quad \frac{M_{max}}{M_i} = 1.13 \tag{4.1}$$

$$For \quad \frac{P}{f_c A_g} \geq 0.1: \quad \frac{M_{max}}{M_i} = 1.13+2.35\left(\frac{P}{f_c A_g}-0.1\right)^2 \tag{4.1}$$

4.3.3 Shear Strength of the Column Units

The shear forces acting on the column units corresponding to the ideal flexural strength were readily calculated as M_i/L, in which L =the effective height of the column. The shear forces corresponding to the development of flexural overstrength were obtained by multiplying the ideal flexural strength, V_i , by strength enhancement factor M_{max}/M_i given by Eq.4.1. The shear strength of column units was calculated based on the current New Zealand code provisions, as given by Eqns.2.4 to 2.9 in Chapter 2. The flexural strength and shear strength of the three column units listed in Table 4.2 are based on the actual material strengths.

4.3.4 Transverse Reinforcement Required by Shear

To ensure against shear failure, the shear strength of the column units should at least equal to the shear forces corresponding to the development of flexural overstrength. To force the column units to show a shear dominated behaviour, however, it is to provide less transverse reinforcement in the plastic hinge regions than that required by the code provisions[S14] to resist the shear forces corresponding to development of flexural overstrength. The ratios of the shear strength V_i calculated using the code provisions of NZS 3101:1982[S14] for outside potential plastic hinge regions to the shear force V^+_{if} corresponding to the ideal flexural strength M^+_i are 0.91, 0.95 and 1.04 for Units 7, 8 and 9, respectively, where M^+_i is the ideal flexural strength of the column unit calculated using the code approach and corresponding to the maximum compression axial load applied to each column unit. With these relative strength ratios, it was expected that the column units will fail in a shear controlled behaviour with limited or moderate displacement ductility. Table 4.3 lists the details of transverse reinforcement actually provided for each column unit.

Table 4.2: Flexural Strength and Shear Strength of Column Unit Based on Measured Material Strength

Unit	M_i^+ kN.m (1)	V^+_{if} kN (2)	V^+_{io} kN (3)	V_s kN (4)	V_c(kN)		V_i(kN)		V_i/V^+_{if} (7)/(2)	V_i/V^+_{io} (7)/(3)
					non-s (5)	s (6)	non-s (7)	s (8)		
7	331	331	388	111	189	0	300	111	0.91	0.77
8	389	389	456	121	250	198	371	319	0.95	0.81
9	413	413	562	133	300	283	433	416	1.04	0.77

Note:

(1): The ideal flexural strength using code approach based on measured material strength.

(2): The shear corresponding to ideal flexural strength M_i^+.

(3): The shear force corresponding to the development of flexural overstrength.

(4): The ideal shear strength provided by the transverse reinforcement(Eq.2.9)

(5): The ideal shear strength of concrete contribution for outside potential plastic hinge region(Eq.2.6).

(6): The ideal shear strength of concrete contribution for inside potential plastic hinge region(Eq.2.5).

(7): The ideal shear strength of column unit for outside potential plastic hinge region(Eqns.2.6 + 2.9).

(8): The ideal shear strength of column unit for inside potential plastic hinge region(Eqns.2.5 + 2.9).

For all ideal strength calculation the strength reduction factor was taken as unity.

4.3.5 Transverse Reinforcement Required for Confinement and Antibuckling

The amount of transverse reinforcement required by the New Zealand code NZS 3101:1982[S14] to confine the compressed concrete inside the potential plastic hinge regions given by Eq.2.1 increases as the axial compression load level increases. For the column with the moderate to high compression axial load level, this requirement will govern the design. In order to achieve shear dominated behaviour in the tests, the amount of transverse reinforcement provided over the whole height of column was very close to that required by the code[S14] for outside potential plastic hinge regions(see (2) in Table 4.3). This meant that the transverse reinforcement provided in the column units did not follow the code requirements for confinement of concrete in potential plastic hinge regions. The ratios of actually provided transverse reinforcement to that required by code provisions[S14] for concrete confinement were 0.39, 0.31 and 0.29, for Units 7, 8 and 9, respectively, as given in Table 4.3. For the same reason, the code requirement that the centre to centre spacing of transverse reinforcement in the potential plastic hinge regions was to be less than one-fifth of the least lateral dimension of cross section was not satisfied strictly(see Table 4.3). The hoop spacings for the three column units did meet the code requirements for antibuckling of the longitudinal bars; that is, the centre to centre spacing of the hoop did not exceed the smaller of six times longitudinal bar diameter or 200 mm.

Table 4.3: Details of Transverse Reinforcement of Column Unit

Unit	$\frac{P}{f'_c A_g}$ (1)	f'_c (MPa)	dia-s_h (mm)	f_{yh} (MPa)	Transverse Reinforcement for				
					Actual/Code			Spacing	
					Shear	Confine-ment	Anti-buckling		
					(2)	(3)	(4)	(5) s_h/b	(6) s_h/d_b
7	0.1	29.0	R6-120	382	0.91	0.39	1.02	0.30	6.0
8	0.2	33.5	R6-110	382	0.95	0.31	1.12	0.28	5.5
9	0.3	34.1	R6-100	382	1.04	0.29	1.23	0.25	5.0

Note:

1. The maximum compression axial load ratio applied to the column unit
2. Ratio of shear strength for outside potential plastic hinge regions to the ideal flexural strength
3. Ratio of actually provided ρ_s to that required by code[S14] equations for confinement
4. Ratio of tie force $A_{te}f_{yh}$ to 1/16 longitudinal bar force at 100 mm centre

5. Ratio of hoop spacing, s_h, to the section width of the column

4. Ratio of hoop spacing, s_h, to longitudinal bar diameter d_b

4.4 TEST SET-UP, CONSTRUCTION AND INSTRUMENTATION

4.4.1 Test Set-up

Three column units, Units 7, 8 and 9, studied in this series of test had the same overall dimensions as those of Units 1 to 6 described in Chapters 2 and 3, except for the column height. The applied loading histories were also similar. Therefore, the same loading system was used for this second series of tests. The only modification made was to lengthen the bottom end of the loading frame so as to fit the dimension due to the change of column height. Fig. 4.2 shows the test set-up used for the three column units. Fig. 4.3 shows the overall view of test set-up with a column being tested.

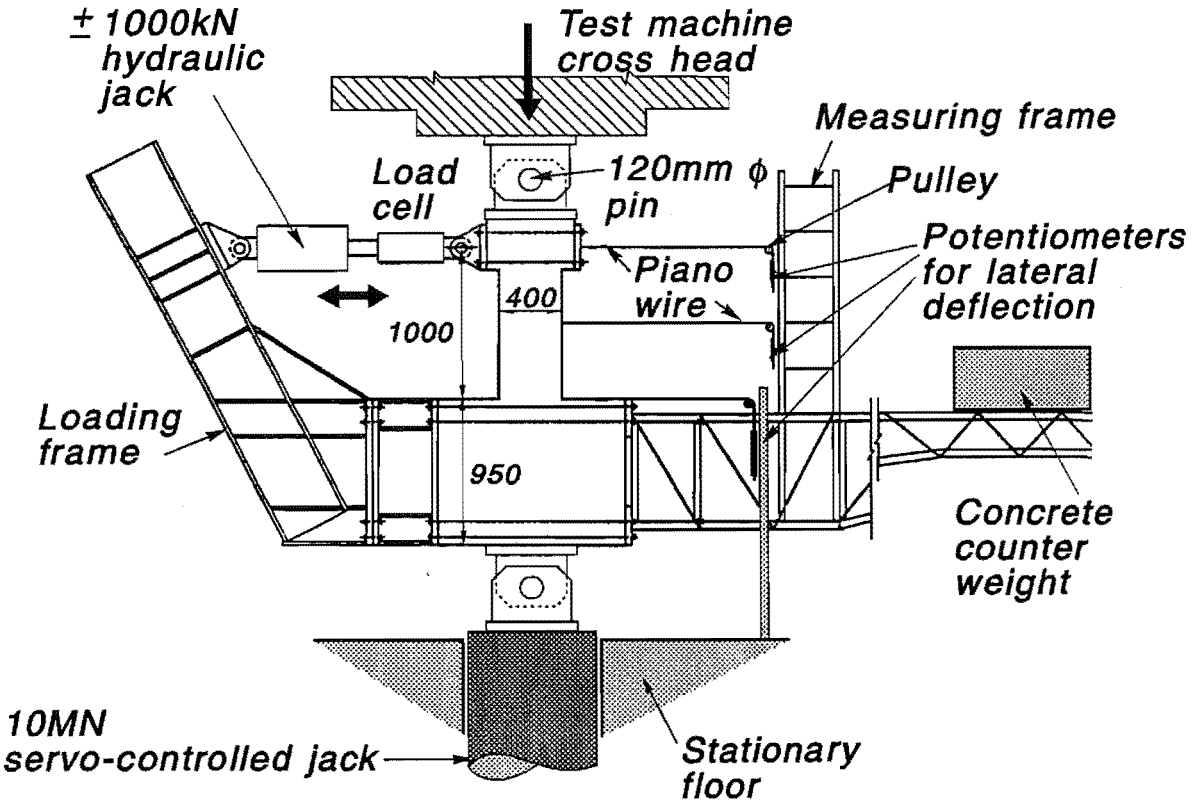

Fig.4.2: Test Set-up for Units 7, 8 and 9

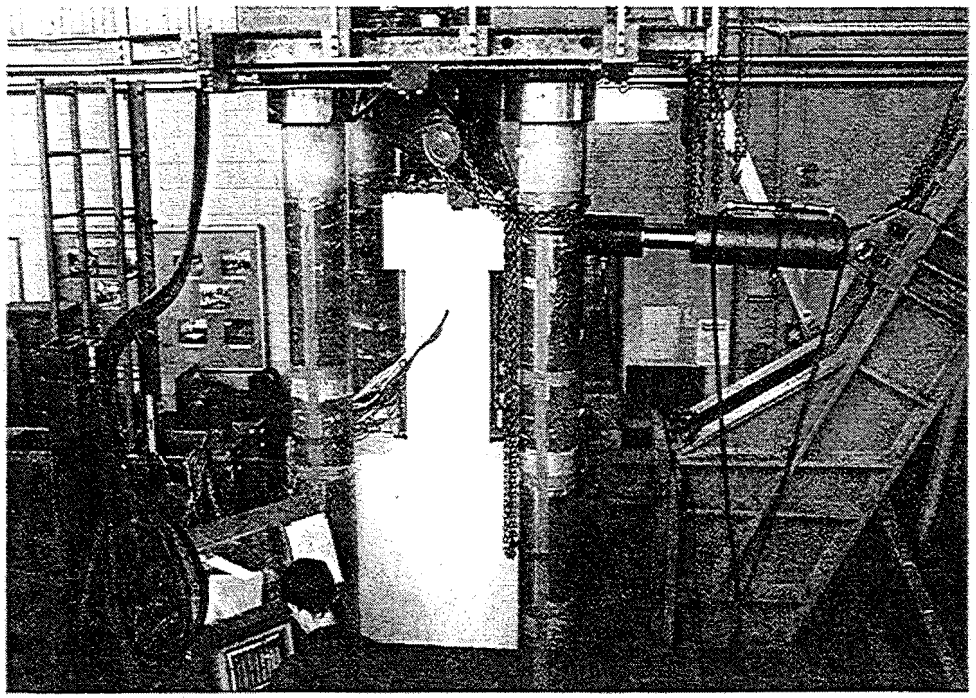

Fig. 4.3: Overall View of the Test Set-up

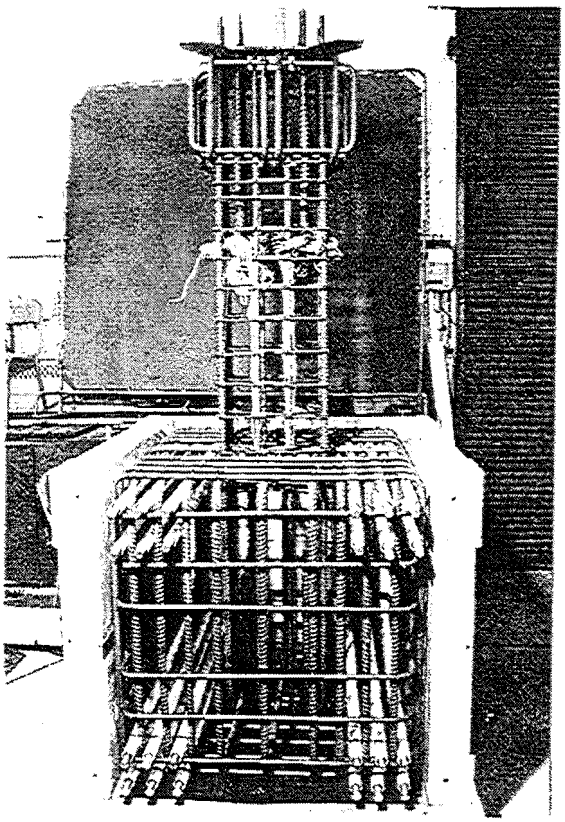

Fig.4.4: Reinforcing Cage Seating in Base Mould

4.4.2 Construction of the Column Unit

Three test specimens were fabricated within the structural laboratory. The procedure of construction of the specimens followed the same steps as that for the column units presented in Chapters 2 and 3.

All reinforcing steel was provided by a local steel supplier. The hoops were cut and bent by the local firm. The extension tails of the 135-deg end hooks of the transverse reinforcement were designed to be 50 mm ($8d_b$) as specified by the concrete design code NZS 3101:1982. The actual length of the extension tails was found to be in the range 48 mm to 60 mm. The hoops were tied to the longitudinal bars before the reinforcing cage was positioned into the mould. The mould was manufactured using 18 mm plywood sheet and stiffened by the steel brackets and bolts. Fig. 4.4 shows a typical reinforcing cage in the plywood mould before casting of the concrete of the column base.

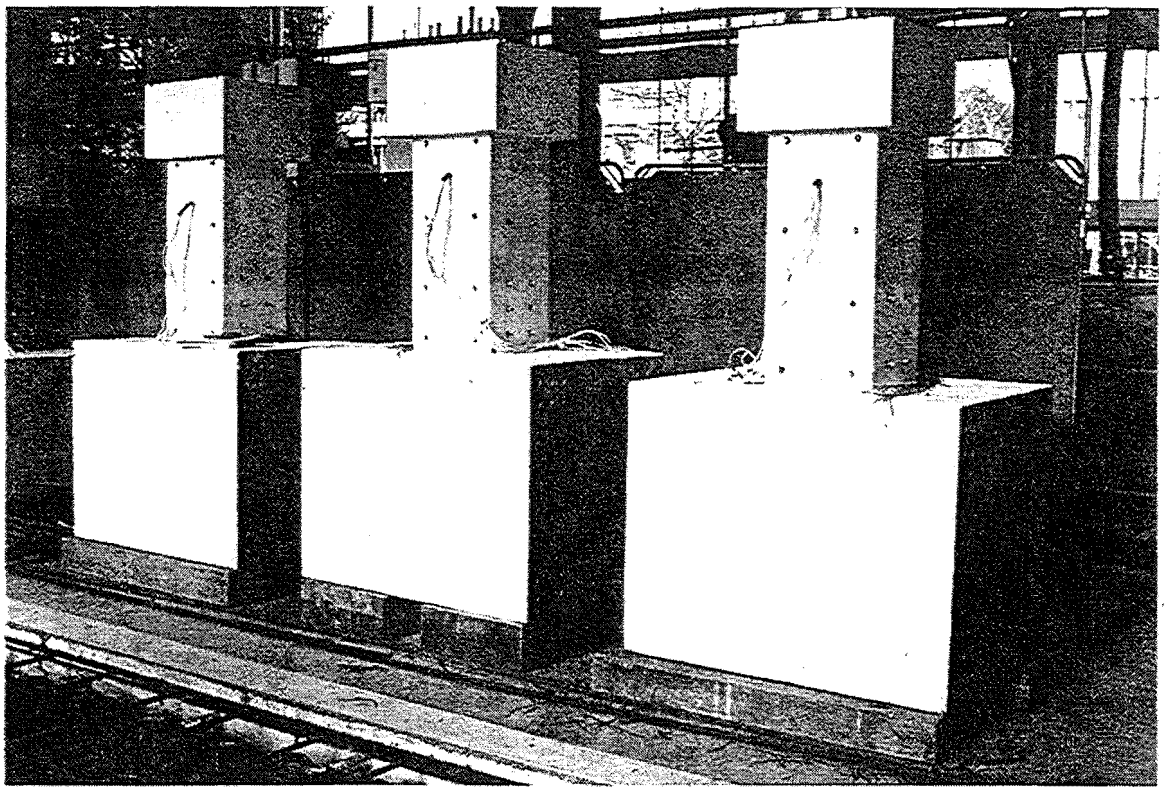

Fig.4.5: Three Column Units Before Testing

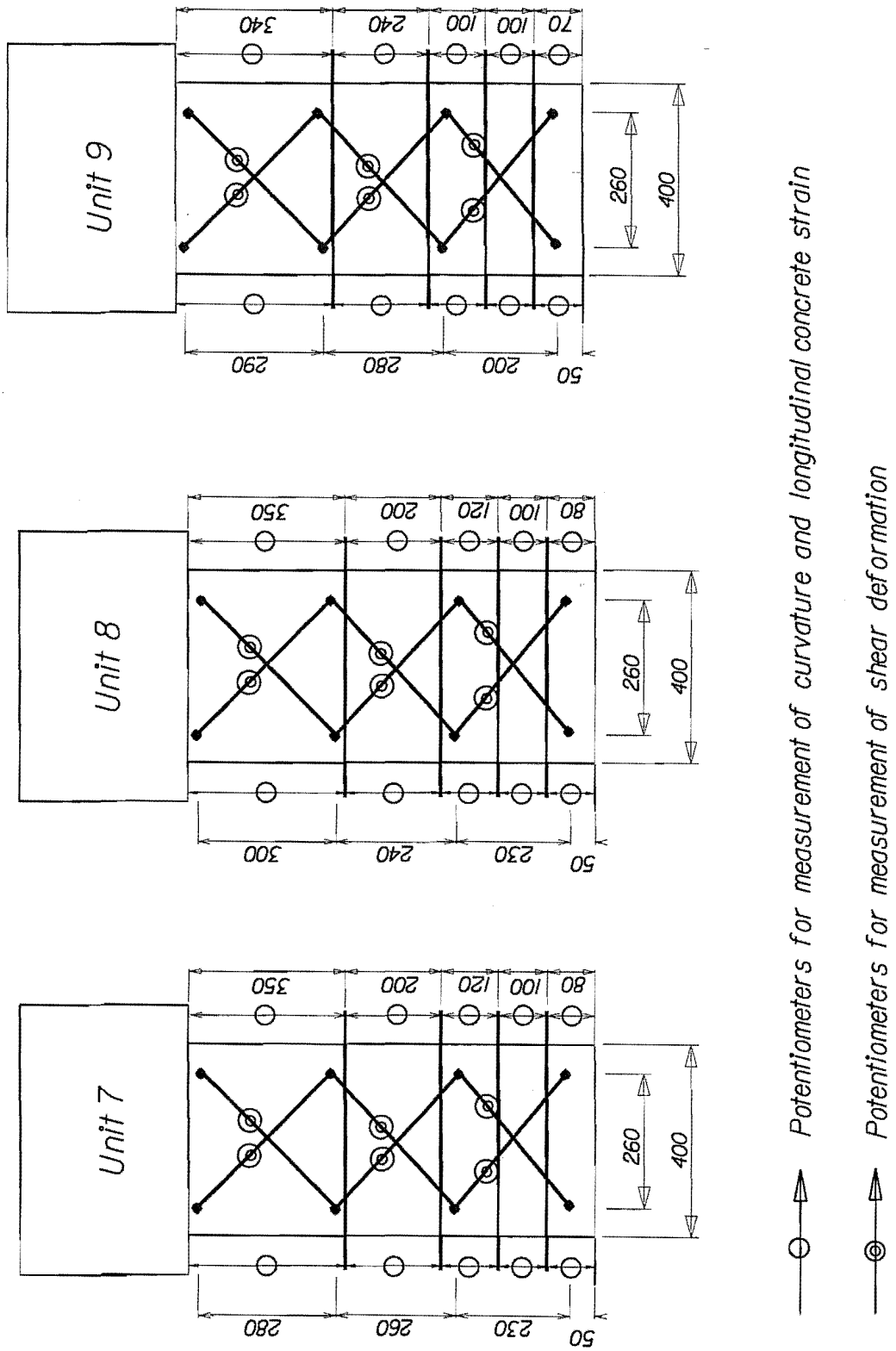

Fig.4.6: Arrangement of Potentiometers for Units 7, 8 and 9.

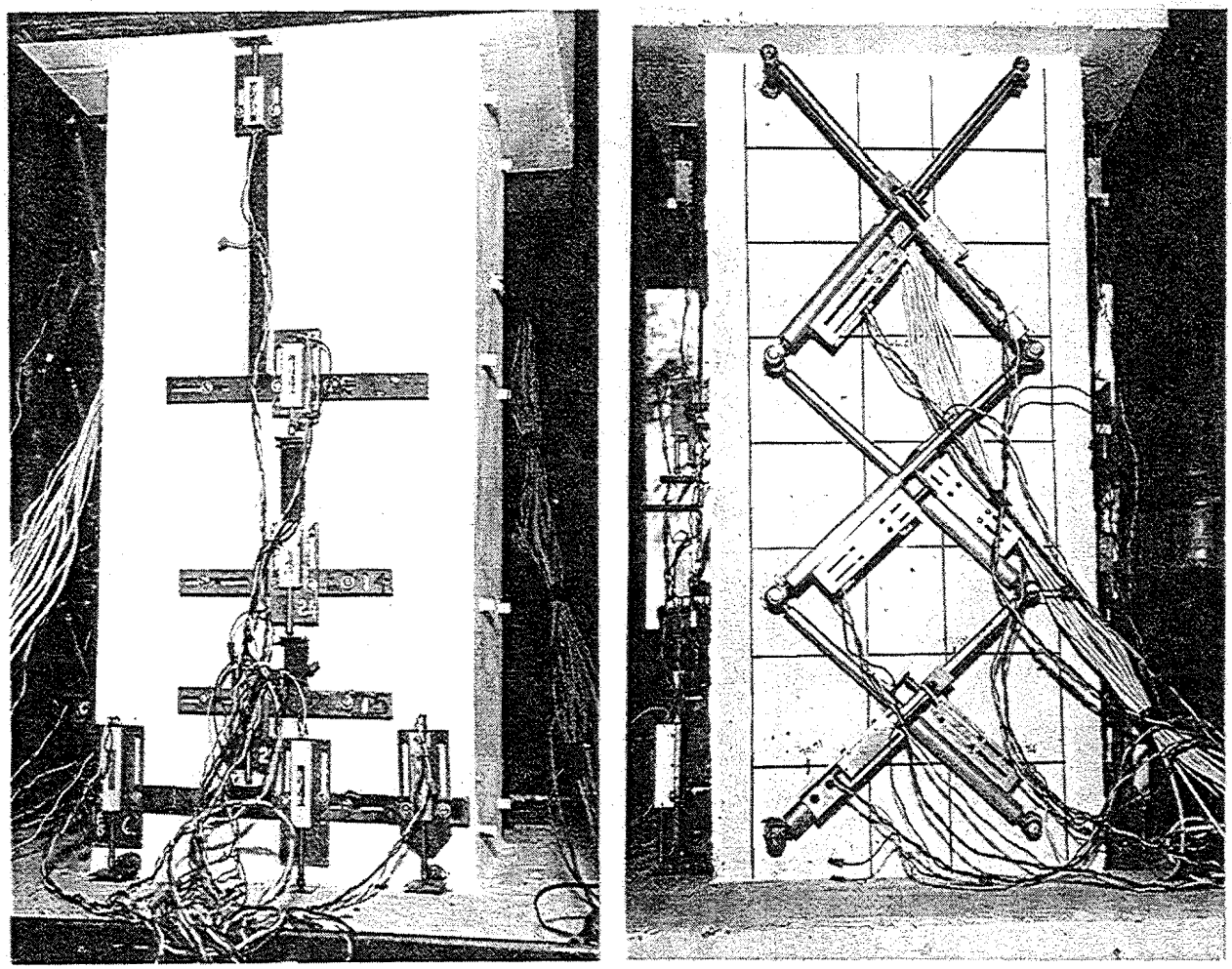

(a) Measurement of curvature (b) Measurement of shear deformation

Fig.4.7: Potentiometers Aligned on the Column

Only one mould was fabricated for the column base, but three moulds were made for the concreting of column portions. This made it possible to cast the concrete of the column portions of the three column units using the same batch of concrete, so as to obtain a similar concrete strength for all three specimens. Each column unit was cast in the vertical position. The concrete was cured at least for ten days before the removal of the mould. Fig.4.5 shows the three column units after removal from the column moulds.

4.4.3 Instrumentation

The instrumentation for the three column units was in most case similar to that for the six column units presented in Chapters 2 and 3. In the following sections a detailed description of the instrumentation is only given where there were differences.

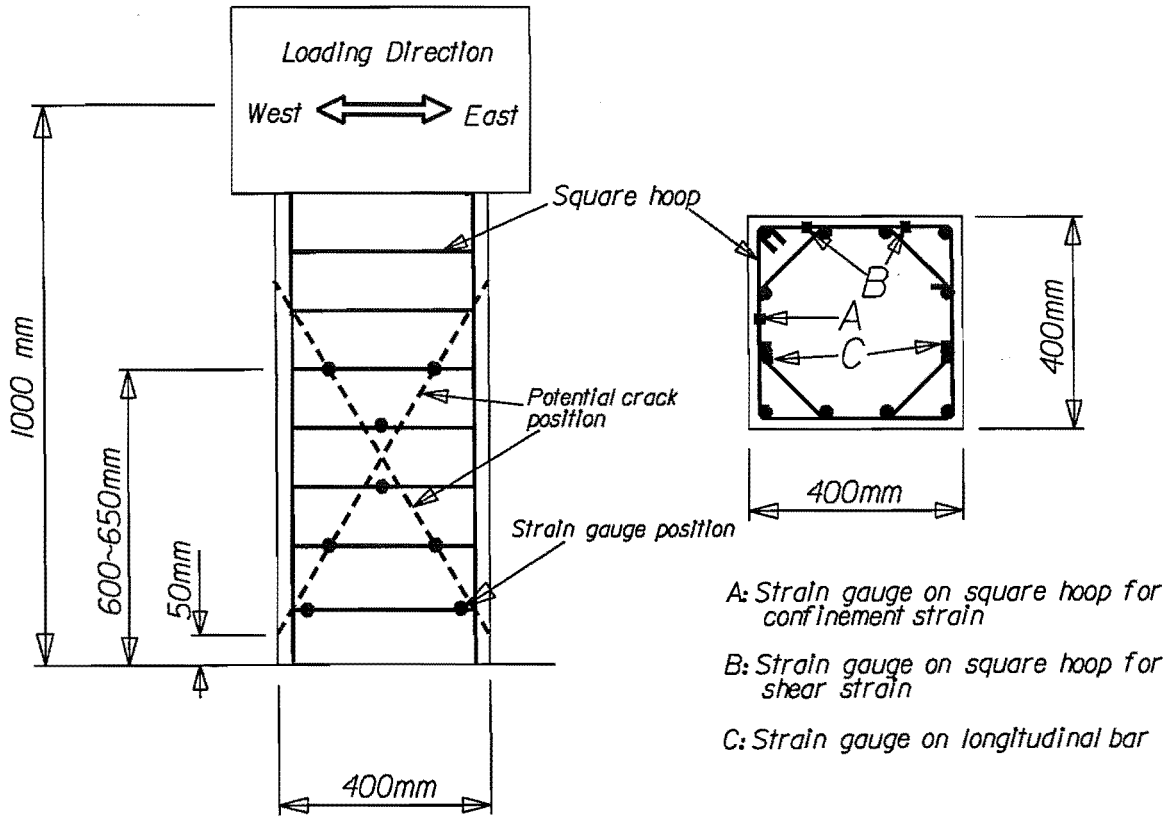

Fig.4.8: Positions of Strain Gauges on The Hoops and Longitudinal Bar of Units 7, 8 and 9

Three linear potentiometers with 300mm travel were installed on a stiff measuring frame to measure the horizontal displacement at the levels of lateral load application, mid-height and bottom of the columns, as shown in Fig.4.2. The arrangement of the linear potentiometers, aligned vertically at various height of the column, which were used for the curvature measurements as well as the measurements of the longitudinal strain of the core concrete, is illustrated in Fig.4.6 and 4.7a.

Strain gauges were placed at various location on the square hoops and longitudinal reinforcement within the potential plastic hinge regions. All gauges were SHOWA-N11-FA-5-120-115mm electrical resistance strain gauges and were used together with Showa SFG-ST self adhesive terminal strips. For each position, the strain gauges were placed in pairs so that the axial stress could be obtained eliminating the effect of bar bending. All gauges were attached to the reinforcing bars prior to the fabrication of reinforcing cages.

The strain gauges marked A in Fig.4.8, which was placed for measuring the strains mainly due to confinement of the concrete, were positioned in the middle portion of the square hoops on the west side of the columns. The strain gauges marked B in Fig.4.8, which were placed for measuring the strains of transverse reinforcement mainly due to shear, were placed on the north face of the column section. These strain gauges were positioned following a likely crack pattern with inclination of about 45-deg with respect to the longitudinal axis of the column, in both loading direction, as shown for a typical column unit in Fig.4.8. The strain gauges on longitudinal reinforcement were positioned at six levels above and below the top face of the column base.

Six linear potentiometers were placed on the north face of the column to measure the diagonal deformations of the column panel, as shown in Fig. 4.6 and 4.7b. These potentiometers were mounted on 12 mm diameter steel rods which passed north-south horizontally through the column. To ensure that these measurement would not be affected by the crushed cover concrete, the same technique used for the potentiometers for the measurement of column curvature and as described in section 2.4.3 was adopted. The measurement of these diagonally placed potentiometers enabled the shear deformation of the column to be experimentally determined.

Before the testing of each column unit, all displacement transducers were calibrated against a known displacement to obtain calibration factors. For the lateral load cell, the same calibration factor was used for all three column units. It is believed that little change in the sensitivity of the load cell would have occurred during the testing of the three column units. The gain for the hydraulic jack in the DARTEC machine was adjusted according to the axial load range to obtain the maximum accuracy of axial load application.

4.5 MATERIALS

Reinforcing steel was supplied by a local commercial steel fabricator. For all columns, 20mm diameter Grade 430 deformed bars were used for the longitudinal reinforcement, and 6mm diameter Grade 300 plain round bars were used for the transverse reinforcement. The steel samples were cut from the same reinforcing bars as used for reinforcement in the columns. Before testing the column units, monotonic tension tests were carried out on the samples in an Avery Universal Testing Machine to obtain the actual mechanical properties of the reinforcement. The steel strain was measured by a Batty extensometer with a gauge length of 52mm. Figs.4.9 and 4.10 show the stress-strain curves for the steel used for the three column units. The measured mechanical properties are also presented in Table 4.4.

Grade 430 deformed bars and Grade 300 plain round bars with different diameters were used in the column bases. Since each column base was heavily reinforced and cast using higher strength concrete, it was expected to remain in elastic range during the testing. It was considered unnecessary to determine the actual mechanical properties of the reinforcing steel used in the column base blocks.

Table 4.4: Measured Properties of Reinforcing Steel

Properties	f_y (MPa)	f_{su} (MPa)	ε_y	ε_{sh}	E_s (MPa)	E_{sh} (MPa)	ε_{su} (estimated)
HD 20	446	615	0.0019	0.016	238000	5200	0.16
R 6	380	465	0.0018	0.015	211100	3600	0.17

The concrete was supplied by a ready mix concrete. Normal weight concrete with target compressive strength of 30 MPa was ordered for the column portion, and the concrete with compressive strength of 45 MPa was for column base. The column portions of all three column units were cast using the same batch of concrete in the same day. The compressive strength for the column portion of each column unit at 28 days and at the stage of testing the column unit was obtained from testing 200×100mm diameter concrete cylinders. Table 4.5 summarise the measured compressive strengths for all specimens. Each result is the average value from three cylinders.

Table 4.5: Measured Concrete Compressive Strengths

Unit	Column		Base Block
	Age at Test (days)	Compressive Strength (MPa)	Compressive Strength (MPa)
7	70	29.0	69
8	88	33.5	60
9	116	34.1	66

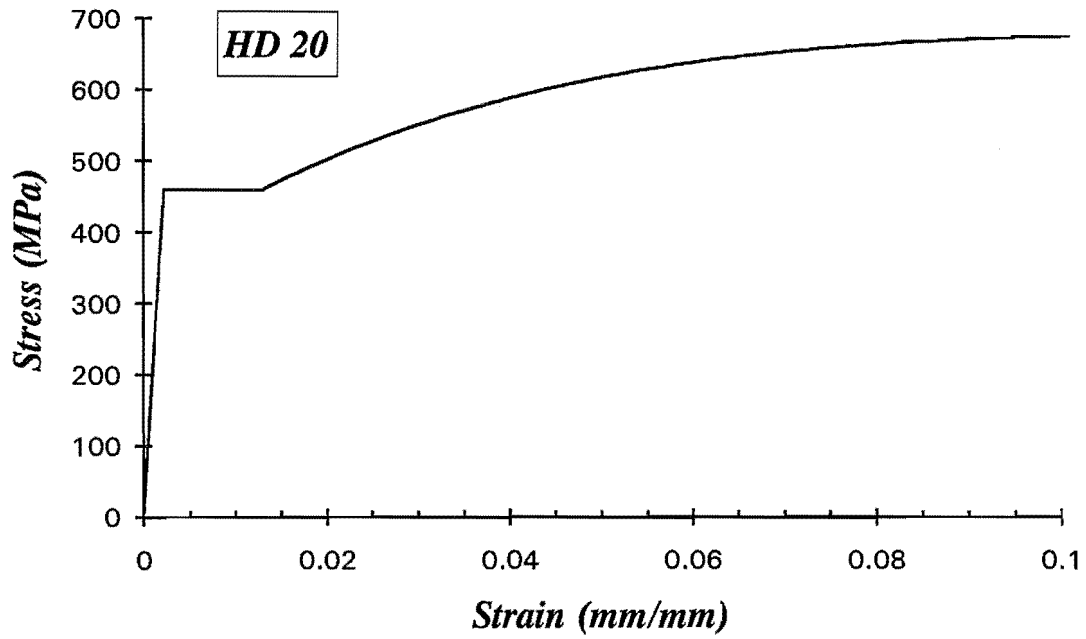

Fig.4.9: Stress-strain Relation for Deformed Bar HD 20

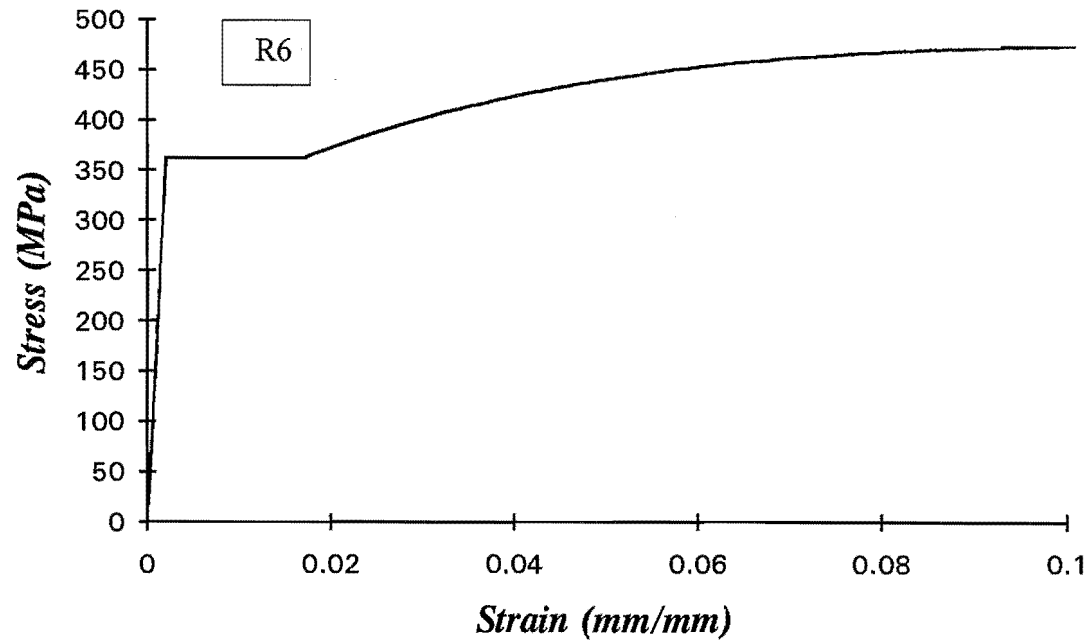

Fig.4.10: Stress-strain Relation for Plain Round bar R6

4.6 LOADING HISTORIES

The three column units were subjected to cyclic lateral loading and varying axial load loading.

Two full cycles of lateral loading were initially applied with the axial load held constant to establish the yield displacement. After the initial loading cycles, the lateral load was controlled by displacement and followed the predetermined displacement pattern. The lateral displacement pattern used for the three columns consisted of three complete cycles to various displacement ductility levels, as shown in Fig.4.11b.

The test results from the six reinforced concrete columns presented in Chapters 2 and 3 showed that the manner of axial load variation had an influence on the behaviour of the column. Although uncoupled axial and lateral load histories resulted in differences in the responses of the column , it was not applied in this series of tests due to the limited number of test specimens. The axial load for the three column units was varied in direct proportion with the bending moment at the critical section of the columns until it reached the predetermined maximum compression or maximum tension axial load. Compression axial load levels of $0.05f'_cA_g$, $0.1f'_cA_g$ and $0.2f'_cA_g$ were chosen to represent the axial forces induced by gravity loads for the Units 7, 8 and 9, respectively. The maximum compressive and maximum tensile axial loads were arbitrarily set for each column unit to simulate the axial forces in the columns due to the effects of overturnning moment or vertical acceleration. Fig.4.12 shows the axial loading histories for the three column units. It was taken into consideration that the variation in the axial load of the columns would become small once a beam yield mechanism forms in a structure. Therefore, the axial load was held constant when $M > 0.85M_i$, where M= applied bending moment at the critical section of the column, and M_i= ideal flexural strength of the column section.

4.7 TEST PROCEDURE

The manner of application of the lateral and axial loads was similar to that for the tests presented in Chapters 2 and 3. The cyclic lateral load was applied by a 1000kN double acting hydraulic jack, which was connected to the cantilever arm of the loading frame and the top stub of the column unit. The concentric axial load was applied to each column unit through pin fittings by the 10MN servo-controlled hydraulic jack in the DARTEC universal testing machine.

The application of axial load was monitored by a computer(DARTEC Apple), which ran on the software incorporating the relationship between axial load and lateral load or bending moment at the critical section of the column. The axial load could be changed to any required value and desired load step. The

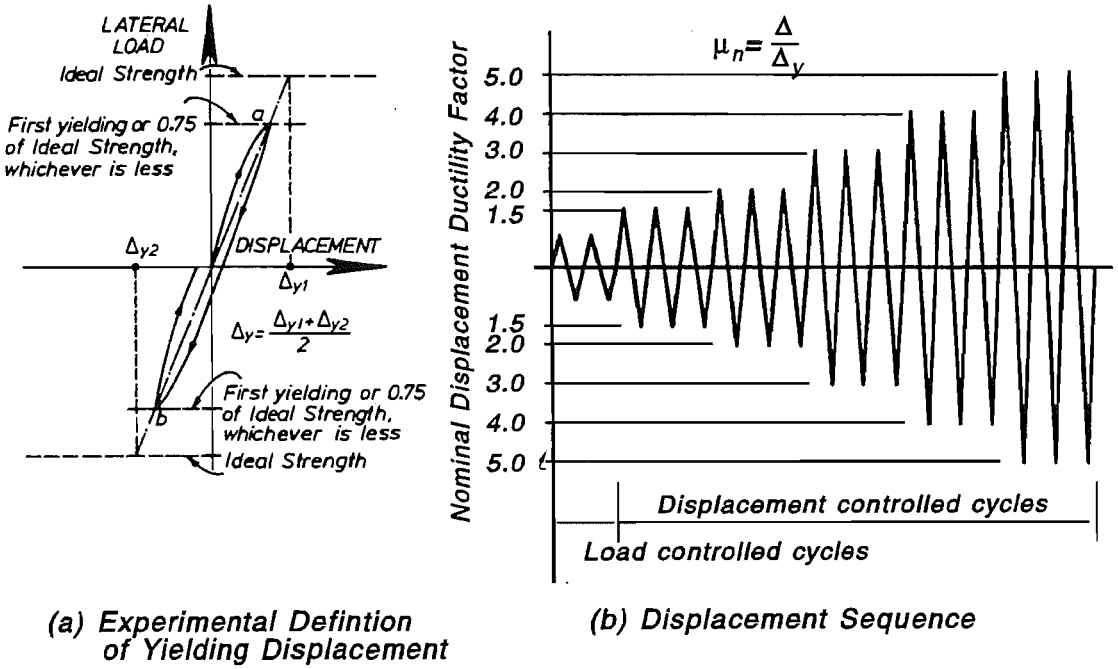

Fig.4.11: Sequence of Imposed Cyclic Lateral Displacements Used for Units 7, 8 and 9

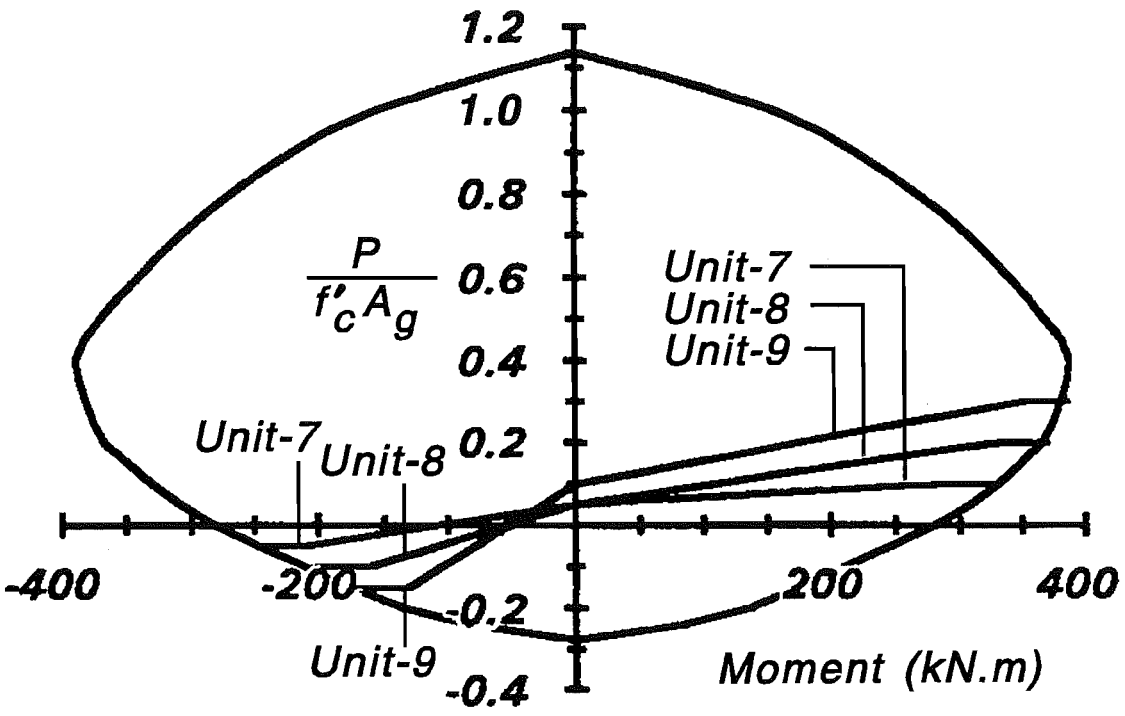

Fig.4.12: Axial Load Versus Moment Histories Used for Units 7, 8 and 9

lateral load ram was operated under displacement control after the initial loading cycles. The output(signal) from the load cell due to the applied lateral load served as the command signal for the application of axial load. When a displacement increment was applied, resulting in an increase or decrease in the required lateral load, the corresponding axial load was then adjusted by operating the computer to the required value. In this way, the applied axial load followed the predetermined loading patterns.

To establish the yield displacement, Δ_y, two cycles of initial lateral load(load controlled) to 75 percent of the ideal flexural strength, V^+_{if}, was carried out. During these initial loading cycles, the axial load was held constant at an average level between the maximum axial compressive load and the maximum axial tensile load. The experimental yield displacement was found by extrapolating a straight line from the origin through 75 percent of V^+_{if} to the ideal flexural strength. The average of the values in two cycles in both the positive and negative lateral loading directions was taken as the yield displacement, Δ_y. The nominal displacement ductility factor, μ_n, was then defined as the ratio of the applied displacement to the yield displacement. Having established the yield displacement, Δ_y, the subsequent loading cycles were displacement controlled to various levels of nominal displacement ductility factor. These consisted of three complete lateral load cycles to displacement ductility factors $\mu_n = \pm 1.5, \pm 2, \pm 4, \pm 6$, etc. For Unit 7, two additional loading cycles at $\mu_n = 2$ and 3 were imposed under constant axial load at the maximum compression axial load level. This was discarded in the Units 8 and 9, as it was considered unnecessary. Since the axial load was varied in direct proportion to the bending moment, the compressive axial load was increased from the stage when the horizontal load was reversed from the negative lateral loading direction. When loading reversed to the negative lateral loading direction, the compression axial load was decreased.

The initial readings of all instrumentation were taken before the application of lateral load. Subsequently, complete readings were taken at every peak displacement ductility factor, zero lateral load, zero displacement and at reasonably small displacement increment intervals.

Chapter 5

Experimental Results and Observations of the Shear Strength of Reinforced Concrete Columns Under Varying Axial Loading ____ Test Series 2

5.1 INTRODUCTION

This chapter presents the experimental results from three reinforced concrete column units, Units 7, 8 and 9, which had an aspect ratio of 2.5 and were tested under cyclic lateral loading while simultaneously subjected to varying axial load. The axial load varied in direct proportion with the moment at the critical section of the column. All column units were designed to fail eventually in shear. The main purpose of this series of tests was to experimentally investigate the shear strength of reinforced concrete columns under cyclic flexure and varying axial loading. Therefore, emphasis was placed on the study of the concrete shear resisting mechanisms. The results of each column unit are discussed individually with reference to its failure behaviour, shear carrying capacity and hysteretic response. Other aspects of behaviour, such as curvature distribution, deformation components, longitudinal strains of core concrete and strains of longitudinal reinforcement, etc, are also examined.

5.2 GENERAL BEHAVIOUR

5.2.1 General Results

The general observations from the tests of three reinforced concrete column units subjected to varying axial load are discussed individually for each test specimen in the following sections. Table 5.1 summarizes the parameters and experimental findings for each column unit. The shear force V^+_{if} corresponding to the development of the ideal flexural strength, M^+_i, determined using code approach of NZS 3101[S14], and corresponding to the maximum compression axial load applied to each column unit is included in Table 5.1. Also listed in Table 5.1 are the ideal shear strengths, V_i and V^s_i, which were calculated using the code[S14] equations(Eqns.2.4 to 2.9) for inside and outside potential plastic hinge regions. The measured material strengths were used in all calculations and the strength reduction factor,ϕ, was taken to be unity. The experimental yield displacement, Δ_y, of each column unit was determined by the procedure described in section 3.7.2. The ratio of the actual displacement to a defined yield displacement is used as an index, known as the nominal displacement ductility factor, to define the deformation capacity of the column.

5.2.2 Unit 7

Unit 7 had an aspect ratio of 2.5 and concrete compressive strength of 29MPa. The centre to centre spacing of transverse reinforcement was 120 mm and the column had a shear strength, calculated using the code equations of NZS 3101:1982[S14] for outside potential plastic hinge regions, of about 90 percent of the shear force corresponding to the development of ideal flexural strength V^+_{if}. The maximum compression and maximum tension axial loads applied during the tests were $0.1f'_cA_g$(462kN) and $0.05f'_cA_g$(232kN), respectively.

The testing commenced by applying two full cycles of loading to 75 percent of the unit's ideal flexural strength V^+_{if}. During these initial loading cycles, the compression axial load applied was held constant at the level of $0.05f'_cA_g$(232kN). The load cycles at this value of axial load were used to establish the yield displacement and thereafter to determine the nominal displacement ductility for the column. The first cracks to appear in the specimen, when the applied load was increased to about 40% of the ideal flexural strength, were short flexural cracks in the bottom portions of the column. These cracks became inclined at about 55 percent of the ideal flexural strength to form flexure-shear cracks. The flexural-shear cracks were not significant until $\mu_n=1.5$. The cracking extended over entire height of the column

between column base and top stub. The angles of the inclination of the diagonal cracks were 40 to 50-deg with respect to the column longitudinal axis. It is to be noted that the compression axial load was held constant during the initial loading cycles. As a result, the crack patterns for both loading directions were very similar during these loading cycles.

When the loading histories shown in Fig.4.12 were next applied to the column, the axial load imposed changed from compression to tension when the lateral load reversed from one loading direction to the other loading direction. Therefore, the column was subjected to compression load in one loading direction and was subjected to tension axial load in other loading direction. For the convenience of discussion, in the following sections, positive loading and negative loading will be referred to as the loading directions in which the compression axial load and tension axial load were applied to the column, respectively.

With further loading, the diagonal cracks lengthened and widened. During the loading to $\mu_n=1.5$, many diagonal cracks propagated further over three quarters of the column depth. The main diagonal crack was not evident at this loading stage. In the positive loading direction, the flexural/shear cracking exhibited a typical fanned pattern. In the negative loading direction, several diagonal cracks were almost parallel to each other. On average, the inclination of the diagonal cracks to the longitudinal axis in the positive loading direction was smaller than that for the negative loading direction.

Fig.5.1 shows the cracking patterns at different stages of testing for the Unit 7. During the third cycle to $\mu_n=2$, one major diagonal crack was formed in the positive loading direction. This main diagonal crack ran nearly from corner to corner of the column, forming the inclined plane of diagonal tension failure in the loading direction. The inclination of main diagonal crack was about 30-deg with respect to the column longitudinal axis. The width of main diagonal crack was about 3mm at $\mu_n=2$, 5mm at $\mu_n=4$, and 7mm at the final stage of the test. In the negative loading direction, three diagonal cracks became distinctive at $\mu_n= 4$. The inclination of these cracks were about 40 to 50-deg to the column longitudinal axis. The difference in crack patterns for the positive and negative loading directions was obviously due to the change of axial load from compression to tension.

No visible cracking was detected in the column base of the three column units, indicating that the column base remained in elastic range and did provide a rigid foundation for the columns.

Incipient of buckling of longitudinal reinforcement was observed at third cycles to $\mu_n=4$, after shear failure has occurred. Serious buckling of longitudinal reinforcement took place at $\mu_n= 5$, at which the test was terminated.

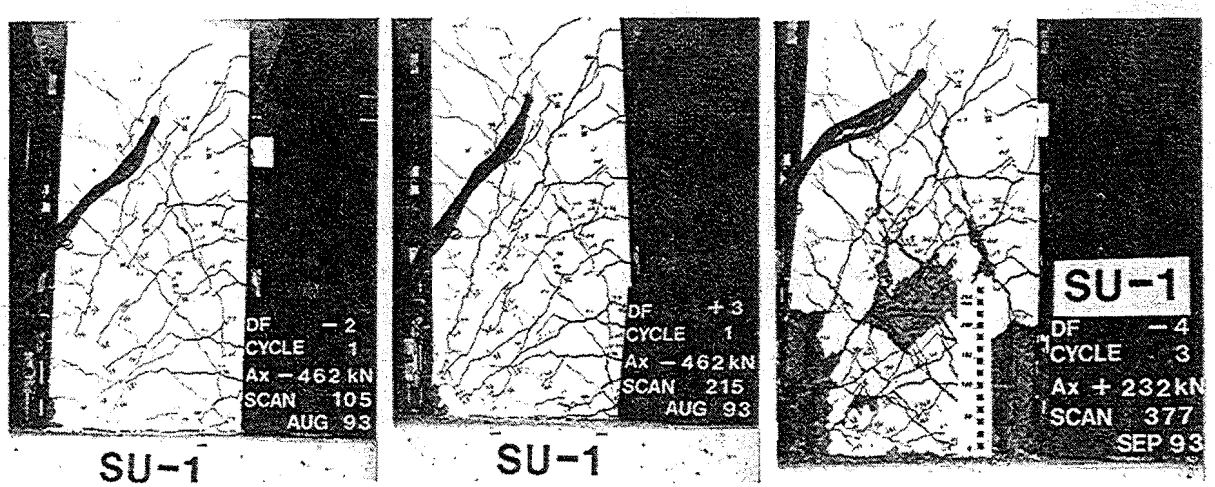

Fig.5.1: Cracking Patterns for Unit 7

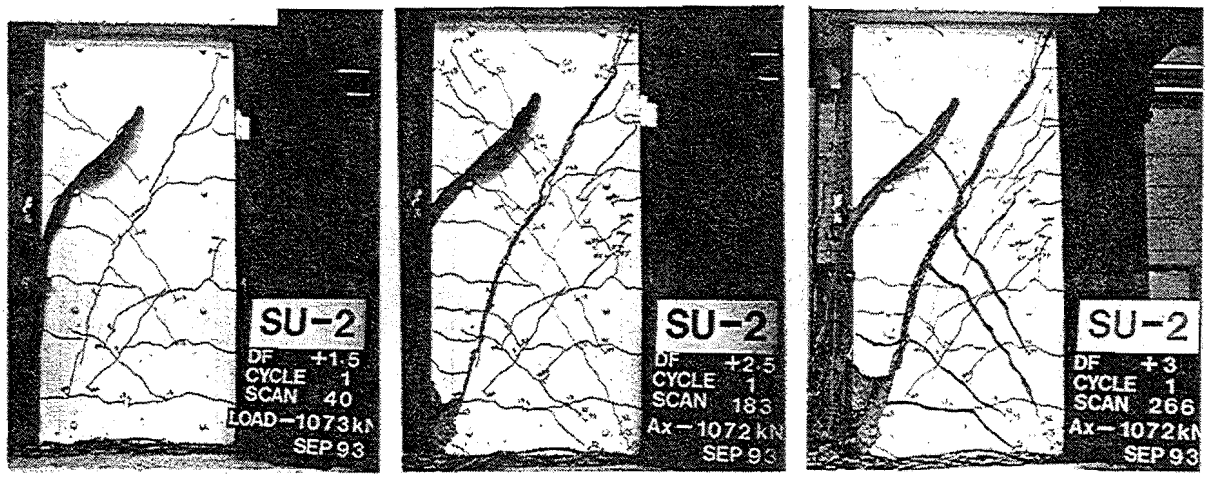

Fig.5.2: Cracking Patterns for Unit 8

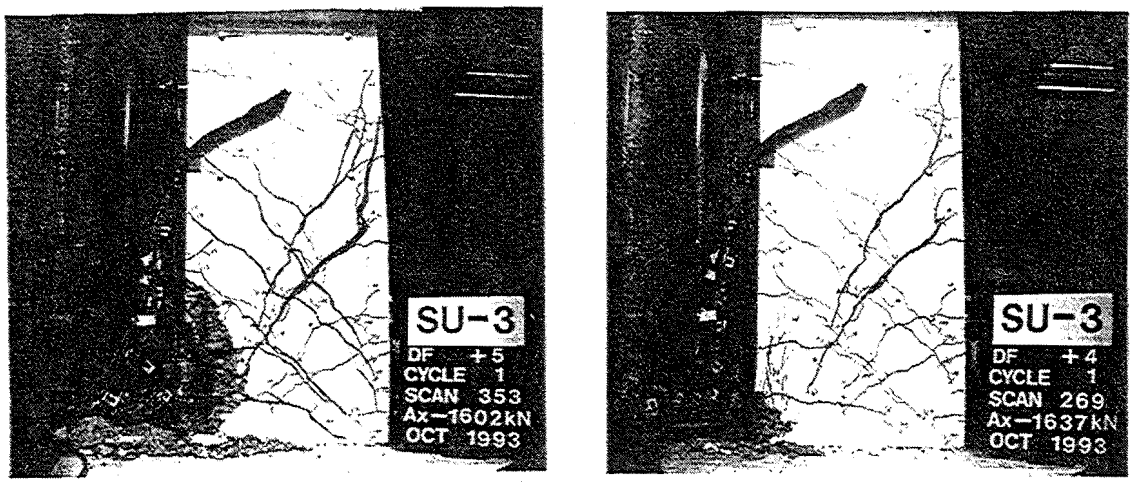

Fig.5.3: Cracking Patterns for Unit 9

Note: *The specimen numbers, SU-1, SU-2 and SU-3 which were used in the tests for the three column units are referred to as Unit 7, Unit 8 and Unit 9 in this thesis, respectively.*

5.2.3 Unit 8

Unit 8 had an aspect ratio of 2.5 and concrete compression strength of 33.5MPa. The centre to centre spacing of the transverse reinforcement was 110mm, which gives a shear strength of $0.96V^{+}_{if}$ calculated using the code equations of NZS3101:1982[S14] for outside potential plastic hinge regions. The ideal flexural strength, V^{+}_{if}, was determined for the case when the column is subjected to the maximum compression axial load. The maximum compression axial load and the maximum tension axial load applied to the column were $0.2f'_cA_g$(1072kN) and $0.1f'_cA_g$(536kN), respectively. The column unit was loaded to 75 percent of its ideal flexural strength V^{+}_{if} during the initial loading cycles with the compression axial load of $0.1f'_cA_g$(536kN) held constant.

Flexural cracks were first formed at the lower portion of the column at about 30 percent of ideal flexural strength. These cracks extended horizontally to about one-half of the column depth. With further loading, the initial horizontal flexural cracks became inclined to the column axis under the influence of shear at about 60 percent of the ideal flexural strength. The flexural-shear cracks fanned up from column corner. The angles of inclination of initial flexural-shear cracks varied between 30 to 45-deg with respect to longitudinal axis of the column.

The crack patterns at different stages of the testing for Unit 8 are shown in Fig. 5.2. In the positive loading direction, several diagonal cracks were formed. During first few cycles of loading, the width of diagonal cracks was small. At first cycle to $\mu_n=2$, a major diagonal crack at about 26-deg to the column axis became evident, which was on a line from corner to corner of the column(see Fig.5.2). In the subsequent loading cycles this main diagonal crack opened significantly. Most transverse reinforcement crossing the main diagonal crack yielded. Once the main diagonal crack was formed, shear deformation concentrated along it. The other diagonal cracks became secondary, indicating a redistribution of internal stress. The shear deformation was noted to be significant. The width of the main diagonal crack observed was 3.4mm at $\mu_n=2$, 6.8mm at $\mu_n=2.5$, and 9.8mm at $\mu_n=3.5$(failure), respectively.

The crack patterns in the negative loading direction were basically similar to those occurred in the positive loading direction, although the inclination of diagonal cracks was generally smaller. At $\mu_n=-2$, three diagonal cracks at about 38-deg to the column axis prevailed. Because the deformations were distributed over several cracks, the width of these diagonal cracks was much smaller than that which occurred in the positive loading direction. Due to the application of axial tension load, the main diagonal crack developed in the compression loading direction remained unclosed when the loading reversed from positive loading direction to negative loading direction. The width of unclosed diagonal crack, for example, was 3mm at $\mu_n=-2.5$.

Buckling of longitudinal reinforcement was observed after significant shear deformation occurred. In fact, buckling was initiated by the bend of the longitudinal bar in the bending moment plane due to diagonal thrust.

5.2.4 Unit 9

Unit 9, with an aspect ratio of 2.5, concrete compressive strength of 34.1MPa and with 100mm centre to centre spacing of transverse reinforcement, had a shear strength, calculated using the code equations of NZS3101:1982[S14] for outside potential plastic hinge regions, of 104 percent of the ideal flexural strength V^{+}_{if}, which was determined using the code approach for the stage at the maximum axial compression load. The maximum axial compression load and maximum axial tension load applied to the column were $0.3f'_cA_g$(1637kN) and $0.15f'_cA_g$(818kN), respectively.

Loading to about 75 percent of ideal flexural strength was carried out initially. A compression axial load of $0.2f'_cA_g$(1091kN) was held constant during the initial loading cycles. In the examination of measured force-deformation curves and longitudinal strain on the completion of initial loading cycles, it was found that the column unit was deformed well into inelastic range during initial loading. It was decided that some adjustment be made in determining the yield displacement. The yield displacement used for subsequent loading cycles was actually that corresponding to about 70 percent of the ideal flexural strength.

The flexural cracks were first observed at about 48% of the ideal flexural strength. Under the influence of flexure and shear, these cracks became inclined to the column axis at about 65% of the ideal flexural strength. Compared with Units 7 and 8, it is apparent that the presence of larger axial compression delayed the onset of diagonal cracking. Similar cracking patterns for both loading directions were observed in the initial loading cycles. The angles of inclination of the initial diagonal cracks varied between 45 to 55-deg to the longitudinal axis.

Fig.5.3 shows the cracking patterns for Unit 9 at different stages of testing. In the positive loading direction, diagonal cracking was not significant at low displacement ductility level. At μ_n=3, two main diagonal cracks became evident at about 35-deg to the column axis. The maximum width of diagonal crack was 1.5mm at μ_n=3. The concrete in west side(see Fig.4.8) of the column started to crush at μ_n=2. Spalling of cover concrete occurred at third cycle to μ_n=3. During following cycles of testing, the spalling of the concrete in west side of the column propagated into core area due to repeated tension and compression strains. No spalling of concrete was detected in the east side(see Fig.4.8) of the column.

It was observed that the 135-deg end hook of a square hoop was gradually opened during the cycle to μ_n=4. This resulted in the loss of shear force carried by the hoop and led to sudden increase of the shear force resisted by the octagonal hoop at the same level, since significant deterioration in the concrete shear mechanisms at this loading stage has taken place and the concrete mechanism could not resist more shear. Soon after straightening of end hook of the square hoop, the octagonal hoop in the same level fractured. Another square hoop fractured before end of testing.

Table 5.1: Test Results

Unit	Axial Comp. Load				Axial Tension Load				At Failure	
	V_{if}^{+} (kN)	$\frac{V_{NZS}}{V_{if}^{+}}$	$\frac{V_{max}^{+}}{V_{if}^{+}}$	θ (Deg)	V_{if}^{-} (kN)	$\frac{V_{NZS}}{V_{if}^{-}}$	$\frac{V_{max}^{-}}{V_{if}^{-}}$	θ (Deg)	μ_n	$\frac{\Delta}{h}$ (%)
7	331	0.91	0.99	32	246	0.65	0.96	40	4	3.6
8	389	0.96	1.01	28	200	0.61	1.02	38	2.5	2.1
9	413	1.04	1.04	35	155	0.86	1.12	48	3	2.3

Note:

V^{+}_{if}, V^{-}_{if}= theoretical shear strength corresponding to the maximum compression and the maximum tension axial load

V_{NZS}= shear strength for outside potential plastic hinge regions calculated by code method

V^{+}_{max}, V^{-}_{max}= maximum experimental shear strength corresponding to the compression and the maximum tension axial load respectively

θ = observed angle of diagonal crack to the longitudinal axis of the column

Δ = lateral displacement of the column at the point of application of lateral load

h = overall depth of the column section

The maximum tension axial load applied to the Unit 9 was 0.15f'cAg(818kN) in the negative loading direction, which was larger than the cracking strength of the column. The diagonal cracks were formed in the lower portion of the column at about 45-deg to the column axis. The inclinations of the diagonal cracks in this loading direction were larger than those in the positive loading direction. A few cracks commencing at upper portion of the column propagated near horizontally through the full depth of the column. The diagonal cracking was not significant in this loading direction, suggesting that the

deformation was not locally concentrated. The maximum width of diagonal cracks observed was about 2.2mm at μ_n=-4.

Buckling of the longitudinal bars at the west side of the column took place at the final stage of testing.

5.3 LATERAL LOAD-DISPLACEMENT RESPONSE

5.3.1 General Results

The performances of the column units are discussed in this section with reference to their lateral force-displacement hysteresis loops. In the plots of hysteresis curves, as shown in Figs.5.4 to 5.8, the ideal flexural strength, V_{if}^+, and V_{if}^-, are shown as horizontal lines. The ideal flexural, V_{if}^+ and V_{if}^-, are calculated using the code approach[S14] with the measured material strengths, and corresponding to the maximum axial compression and the maximum axial tension load applied to each column units, respectively. With the measurement of lateral displacement at the column base, P-Δ effects due to axial load can be determined for various loading stages. Included in these figures are the P-Δ effects at each peak displacement ductility. Table 5.1 summarise the main results from each test unit.

5.3.2 Unit 7

The lateral load-displacement hysteresis loops of Unit 7 in the initial loading cycles are illustrated in Fig.5.4a. The measured load-displacement relationship became nonlinear at μ_n=0.75 due to flexural/shear cracking. Fairly large amount of energy was dissipated in the first cycle of initial loading while the repeated loading cycle exhibited less energy dissipation capacity, indicating that softening of the column occurred due to flexural/shear cracking in previous loading cycle. It is to be noted that the compression axial load assumed in the determination of the ideal flexural strength was $0.1f'_cA_g$. The constant compression axial load applied during the initial loading cycles was $0.05f'_cA_g$. Therefore, the imposed lateral load at μ_n=0.75 was 75% of the ideal flexural strength corresponding to the maximum axial compression load, and was about 80% of the ideal flexural strength corresponding to the axial compression load applied during the initial loading cycle.

The complete lateral load-displacement hysteresis loops for the Unit 7 are shown in Fig.5.4b. In the first cycle to μ_n=1.5, the column reached its flexural strength V_{if}^+. This is also the maximum lateral resistance measured throughout the test. The lateral resistance in subsequent loading cycles to μ_n=2,

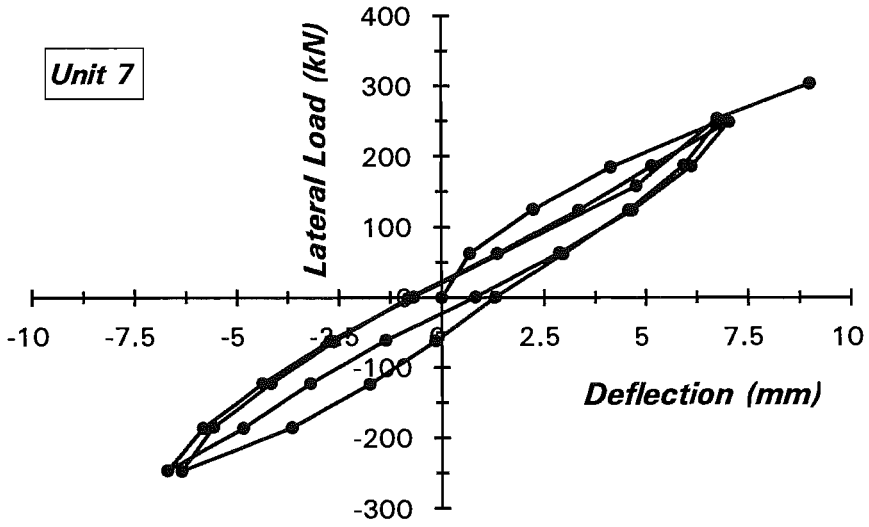

(a) Hysteresis Loops in Initial Loading Cycles

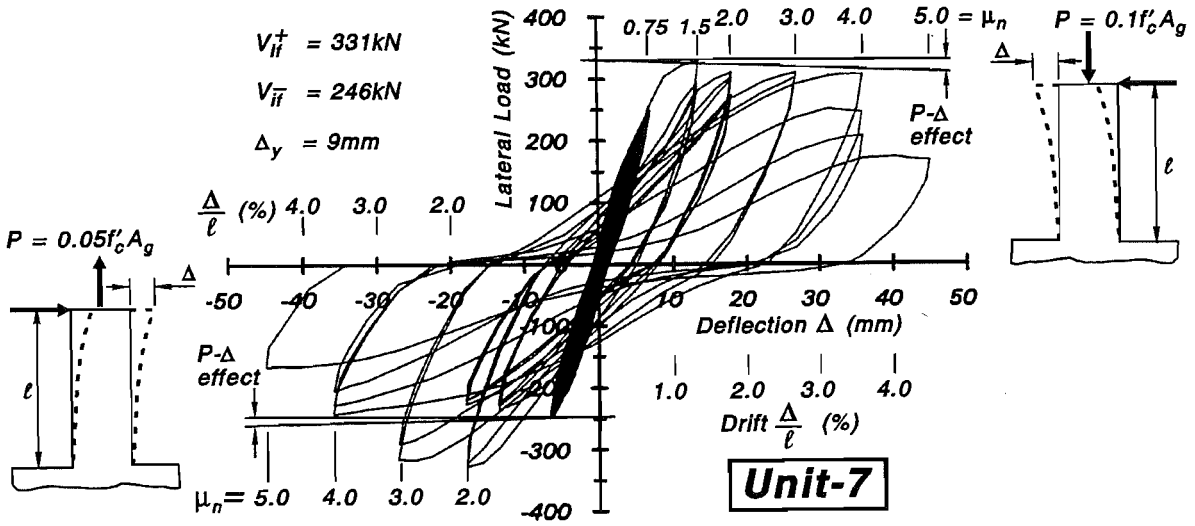

(b) Complete Hysteresis Loops

Fig.5.4: Lateral Load-displacement Hysteresis Loops for Unit 7

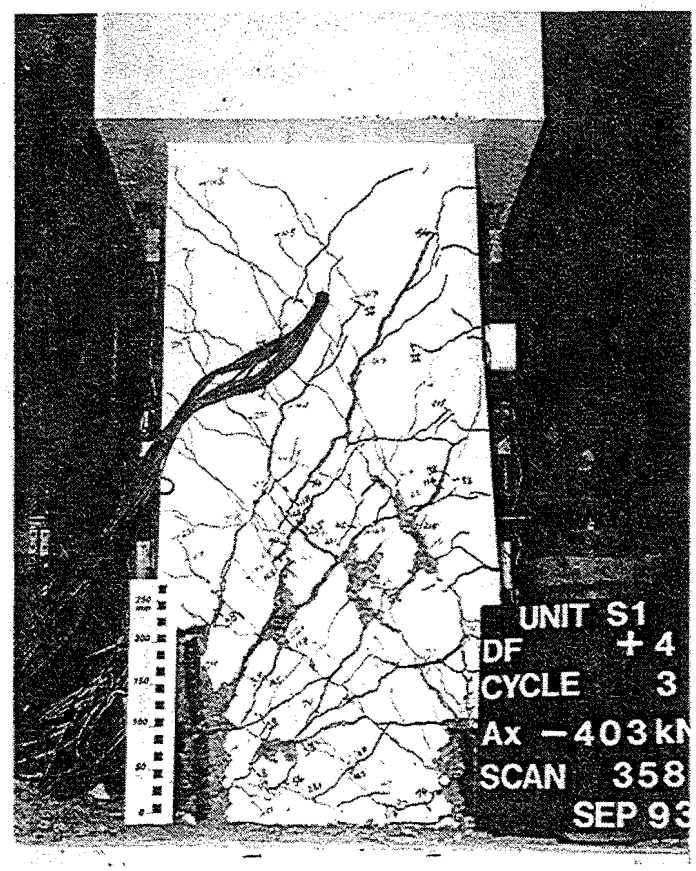

Fig.5.5: Appearance of Unit 7 at the End of Testing

3 and 4, was reduced to about $0.94V_{if}^{+}$. The strength degradation in the repeated loading cycles at $\mu_n < 3$ were within 13% of that developed in the first cycles. The degradation in strength and stiffness became very significant in repeated loading cycle to $\mu_n = 4$, indicating the failure of the column.

During the first two loading cycles to $\mu_n = 2$ and 3, the compression axial load(462kN) was held constant. Hence, as can be seen from lateral load-displacement hysteresis loops(Fig.5.4b), the lateral load attained in the negative loading direction became almost the same as that in the positive lateral direction. The lateral resistance was about $0.94V_{if}^{+}$ in both loading directions.

In the negative loading direction, the column sustained a lateral load very close to the flexural strength, V_{if}^{-}, until $\mu_n = -4$. The strength degradation was minor prior to failure.

Pinching of the load-displacement hysteresis loops was observed at $\mu_n \geq 3$. The pinching was directly associated with the opening and closing of diagonal cracking. It can be seen from Fig.5.4b, the hysteresis responses for both loading directions were reasonably stable up to $\mu_n = 4$. However, once the

column displaced beyond μ_n=4, the stability in lateral load-displacement response could no longer be held. During the second and third cycles to μ_n=4, crushing and spalling of cover concrete became extensive. Crushing and spalling of concrete took place on both sides of the column in the regions up to about 400mm above the column base. This was not the case for Units 8 and 9. It was also observed that spalling of concrete was more severe in the positive loading direction. The test was terminated after serious shear failure and buckling of longitudinal reinforcement took place. The photo shown in Fig5.5 was taken after the testing was completed and the loose concrete was chipped away, to show extent of damage and buckling of longitudinal reinforcement.

Unit 7 attained a nominal displacement ductility factor of μ_n=4, at an interstorey drift of 3.5%, when the shear failure occurred. In terms of available displacement ductility, the overall behaviour of this column was of limited ductility.

5.3.3 Unit 8

Fig.5.6a shows the measured lateral load-displacement hysteresis loops for Unit 8 in the initial loading cycles in the elastic range. The imposed lateral load at μ_n=0.75 was 75% of the ideal flexural strength corresponding to the compression axial load applied in these loading cycles, and was 67% of the flexural strength corresponding to the maximum compression axial load applied during the test. A linear force-displacement relationship was maintained up to 45% of V_{if}^+ during initial loading cycles. Less energy was dissipated during the second cycle than that in the first cycle.

The complete lateral force-displacement hysteresis loops for Unit 8 are illustrated in Fig.5.6b. In the positive loading direction, the lateral resistance of the column exceeded the flexural strength V_{if}^+ at μ_n=1.5. The maximum flexural overstrength of $1.01V_{if}^+$ was recorded at first cycle to μ_n=1.5. The degradation in load carrying capacity, following the formation of the main diagonal crack, took place during the cycles to $\mu_n \geq 2$. At first cycle to μ_n=2.5, the lateral load degraded to $0.8V_{if}^+$, and reduced to $0.72V_{if}^+$ at the second cycle to μ_n=2.5. After the formation of the main diagonal crack, the transverse reinforcement yielded in tension and was unable to effectively restrain the opening of the diagonal crack. This, coupling with the axial tension applied in the negative loading direction, resulted in the opening of diagonal crack developed in the positive loading direction all the time. It is to be noted that sliding occurred along the open diagonal crack when the loading direction reversed. Repeated shear deformation quickly damaged the integrity of the concrete and led to reduced concrete interlock capacity. The load carrying capacity degraded drastically for loading cycles to $\mu_n > 2$. The extensive shear deformation and shear sliding caused large strain in the transverse reinforcement. The lateral load attained when first hoop fractured was 263kN, which was 67% of the ideal flexural strength. Fracture of the square hoop at the location 440mm above the column base took place in the cycle to μ_n=3.0,

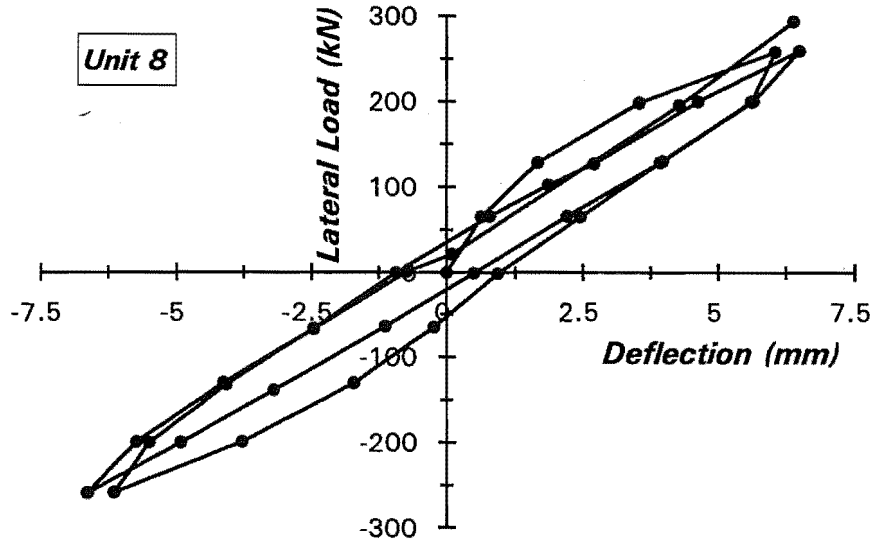

(a) Hysteresis Loops in Initial Loading Cycles

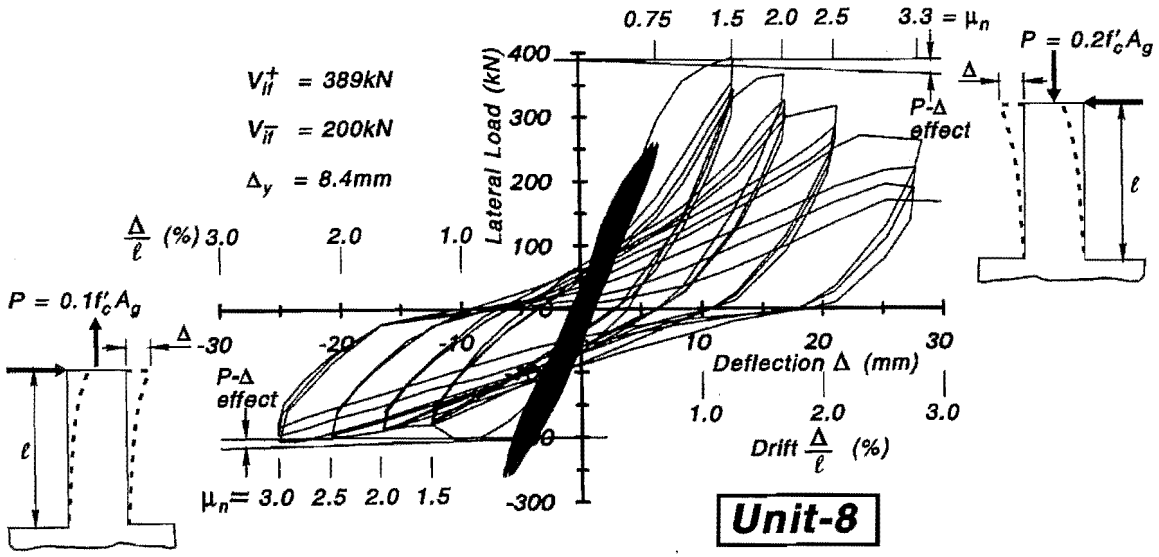

(b) Complete Hysteresis Loops

Fig.5.6: Lateral Load-displacement Hysteresis Loops for Unit 8

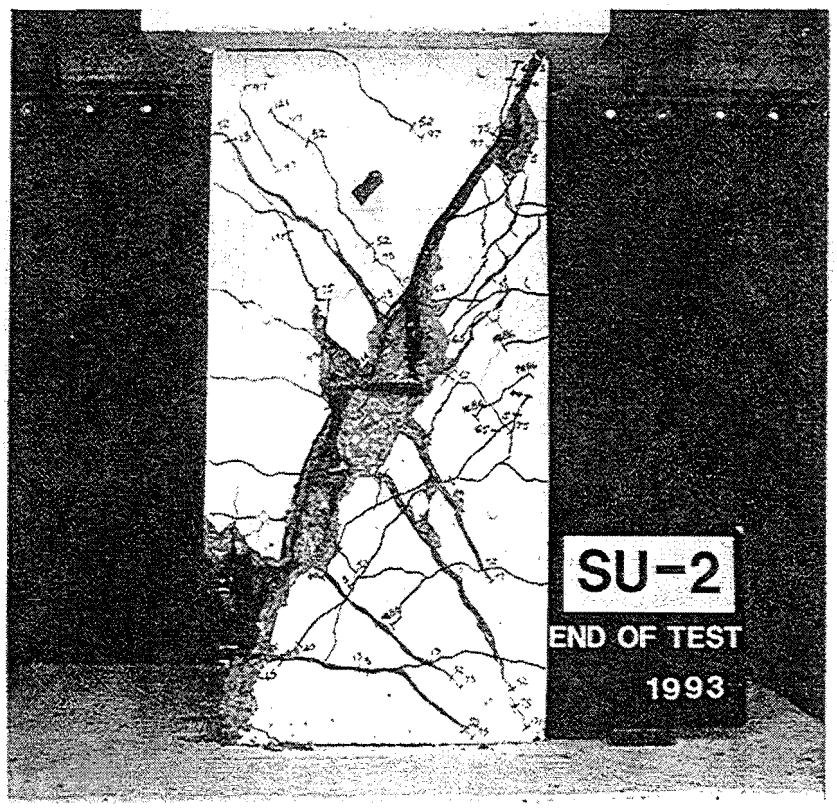

Fig.5.7: Appearance of Unit 8 at the End of Testing

as shown in Fig.5.7. The shear released from the first fractured hoop transferred to the other hoops and resulted in a sudden increase in the shear resisted by these hoops. The square hoop one spacing below fractured during the third cycle to $\mu_n=3$, soon after the first hoop fractured.

The pinching of the hysteresis loops at low displacement ductility level can be seen from Fig.5.6b. The pinching effects became severe during the final stages of testing.

In the negative lateral loading direction, the column sustained a relatively constant strength until the end of the test. The lateral resistance attained was slightly below the flexural strength V_{if}^-. The degradation in strength in the repeated loading cycles was relatively small except in the third loading cycle to $\mu_n=3$. Minor crushing of concrete was detected in the vicinity of the column base. However, no spalling of concrete took place in the east side of the column, as is shown in Fig.5.7.

Before the lateral load capacity reduced to 80% of the ideal flexural strength and the occurance of hoop fracture, Unit 8 attained a nominal displacement ductility factor of 2.5, at an interstorey drift of 2.13%.

The lateral-load displacement performance of Unit 8 can be considered to be of limited ductility. Fig.5.7. shows the Unit 8 at the end of testing, with shear failure mode and fracture of the transverse reinforcement.

5.3.4 Unit 9

Fig.5.8a shows the lateral load-displacement hysteresis loops for Unit 9 in the initial loading cycles. The lateral load imposed at $\mu_n=0.75$ was 75% of the ideal flexural strength corresponding to the compression axial load applied in the initial loading cycles, and was 71% of the flexural strength corresponding to the maximum axial load applied during the test. The load-displacement relationship was linear up to 30% of V_{if}^+ and the column was deformed into inelastic range at $\mu_n=0.75$. More energy was dissipated in the first loading cycle than that in the repeated loading cycle.

Fig.5.8b shows the complete lateral load-displacement hysteresis curves for Unit 9. The column reached the flexural strength, V_{if}^+, for the first time at $\mu_n=1.4$. Prior to the fracture of the hoop reinforcement and the spalling of cover concrete, the lateral load-displacement response remained relatively stable, although pinching of the hysteresis loops was noted at low displacement ductility level. The lateral resistance exceeded V_{if}^+ by about 4% at each peak to $\mu_n=1.5$, 2, and 3.

The maximum lateral load of the column, $V_{max}=1.04V_{if}^+$, was recorded in the first loading cycle to $\mu_n=1.5$. The strength degradation in the repeated loading cycles took place at $\mu_n\geq1.5$, and became significant at $\mu_n\geq3.0$. The lateral load strength in the first cycle of each displacement ductility level started to degrade at $\mu_n>3.0$. At the first cycle to $\mu_n=4$, the lateral resistance decreased to $0.89V_{if}^+$. Remarkable strength degradation took place in the repeated loading cycles to $\mu_n=4$ and $\mu_n=5$. The spalling of concrete propagated into the core area of the column section. As mentioned in the previous section, the 135-deg end hooks of a rectangular hoop opened up during the third cycle to $\mu_n=4$ and the hoop lost its shear resistance. This resulted in the fracture of the octagonal hoop at the same level because the shear released from the fractured rectangular hoop transferred to the octagonal hoop. A drastic degradation in the strength and stiffness followed during the cycle to $\mu_n=5$, implying that failure of the column had taken place.

The test ended after significant degradation in the strength and stiffness had taken place. Fig. 5.9 shows the appearance of the column at the end of the test.

In the negative loading direction, the lateral load resistance slightly increased with increase in displacement ductility level. The column reached V_{if}^- at $\mu_n=4$. No strength degradation was detected in this loading direction. It was also observed that crushing of concrete was very minor at the east

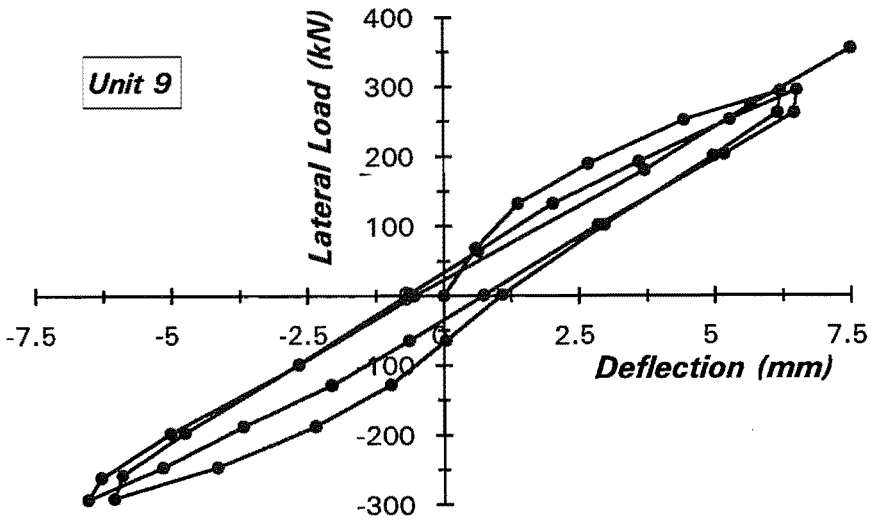

(a) Hysteresis Loops in Initial Loading Cycles

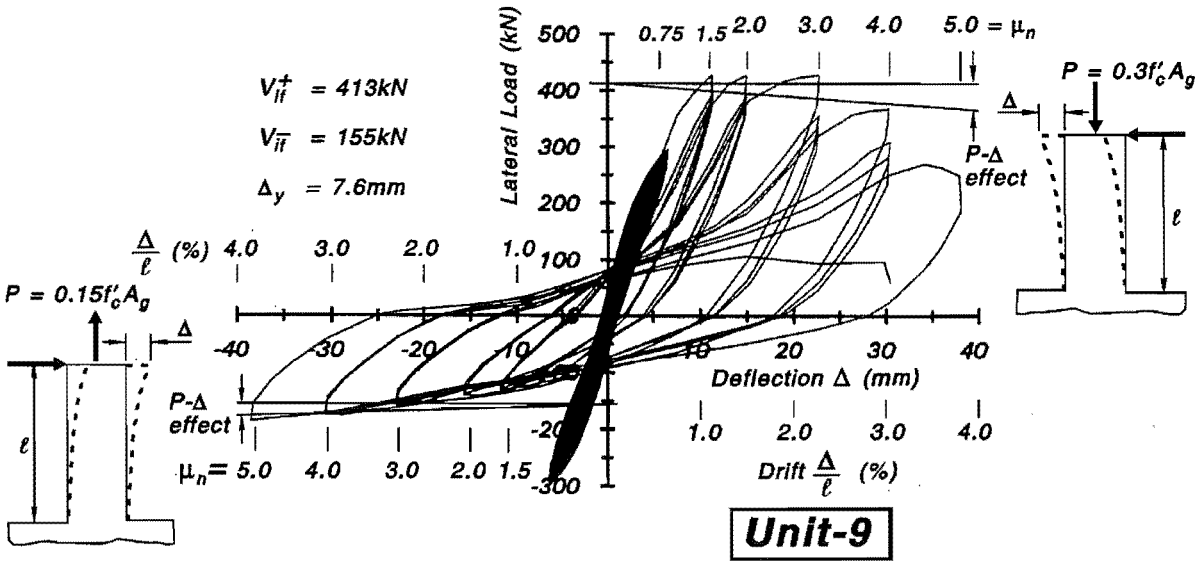

(b) Complete Hysteresis Loops

Fig.5.8: Lateral Load-displacement Hysteresis Loops for Unit 9

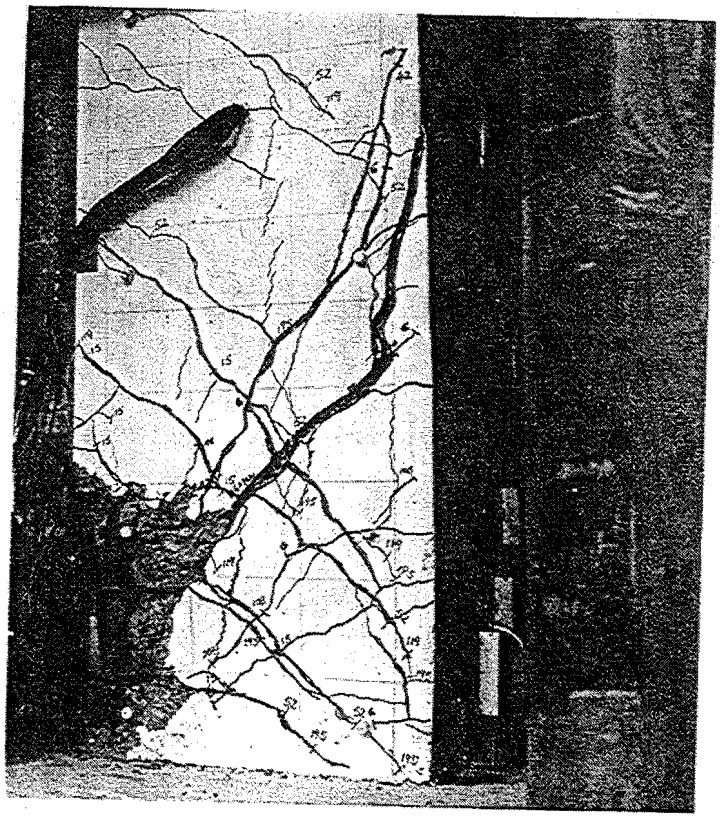

Fig.5.9: Appearance of Unit 9 at the End of Testing

side(see Fig.4.8) of the column. No spalling of concrete took place. Fig.5.9 shows the appearance of critical region of the column after the test was completed. It is to be noted that P-Δ effect in negative loading direction tended to increase the lateral resistance, due to the presence of axial tension applied in this loading direction.

Prior to the fracture of transverse reinforcement, the Unit 9 reached a nominal displacement ductility factor of μ_n=4, at an interstorey drift of 3.03%, and attained the lateral load of $0.89V_{if}^{+}$. Therefore, the displacement performance of Unit 9 can be considered to be of limited ductility.

5.4 YIELD CURVATURE AND YIELD DISPLACEMENT

The yield curvature and yield displacement were calculated using the same method as given in Section 3.6 and 3.7. Table 5.2 lists the theoretical and experimental values of yield curvature and yield

displacement for the three column units. The yield curvature and yield displacement were determined for an axial load level between the maximum compression and the maximum tension axial load applied to each unit. The axial compression load used to establish the yield displacement in the elastic loading cycles is shown in the second column of Table 5.2. The longitudinal compressive concrete strain at the extreme fibre determined from the potentiometer reading and the tension strain of longitudinal steel closest to the tension face of the section obtained from strain gauges at $\mu_n=0.75$ are also given in Table 5.2. For the Unit 7 with compression axial load of $0.1f'_cA_g$, the tension steel yielded before the concrete compressive strain at extreme fibre reached 0.002. The concrete compressive strain in the Unit 9 reached a value of 0.004 before the tension steel yielded.

Table 5.2: Yield Curvature and Yield Displacement

Unit	$\frac{P}{f'_cA_g}$	Yield Curvature $\phi_y \times 10^{-6}$ rad/mm			Yield Displacement Δ_y (mm)		ε_c (exp)	ε_s (exp)
		Theory	Exp.(1)	Exp.(2)	Theory	Exp.		
7	0.05	11.87	35.33	13.10	8.7	9.0	0.0012	0.0025
8	0.10	12.11	33.06	12.98	7.5	8.4	0.0026	0.0021
9	0.20	12.48	42.20	14.47	6.2	7.6	0.0040	0.0017

Note:

(1). Measured at first potentiometer level

(2). Measured at second potentiometer level

ε_c: Longitudinal compressive strain of concrete at the extreme fibre

ε_s: Tension strain of the longitudinal bar closest to tension face of the section

The elastic section stiffness computed as M_y/ϕ_y and the effective member stiffness calculated using Eq.3.7 for each unit are given in Table 5.3. The calculated values of section stiffness are much greater than the experimental values. This is probably because of the larger experimental yield curvature due to the inclusion of yield penetration of longitudinal steel into the base and the effect of shear.

Table 5.3: Section Stiffness and Effective Column Stiffness

Unit	Section Stiffness M_y/ϕ_y		Effective Member Stiffness	
	Theory $kN.m^2 \times 10^3$	Exp. $kN.m^2 \times 10^3$	$(EI)_e$ $kN.m^2 \times 10^3$	$(EI)_e/(EI)_g$
7	20.72	8.35	12.25	0.227
8	23.67	10.47	13.76	0.237
9	25.64	9.29	17.19	0.296

5.5 SHEAR INDUCED HOOP STRAINS AND HOOP FORCES

5.5.1 Hoop Strain Histories

The positions of the strain gauges attached on the square hoops parallel to the loading direction followed a likely 45-deg diagonal crack pattern in both loading directions(see Fig.4.8). The hoop strains measured in this direction were considered to be mainly due to the effect of shear. The locations of the strain gauges were marked on the surface of the concrete. It was observed during the testing that most strain gauges were situated near or/on the critical diagonal cracking plane. The strain gauges generally performed very well. The strain readings were obtained beyond the strain hardening range, up to 2.4%. Occasionally, the strain gauge was found to lose its life, which was probably due to breaking of the wire or debonding of strain gauge from the attached surface. In the reduction of the hoop strain from strain gauge readings, the reliability of these readings were checked and necessary adjustments were made in some cases. The each hoop strain was normally taken as the average of the values from pairs of strain gauges placed on opposite side of the hoop at the same location. In some cases, the strain readings from a strain gauge were discarded once they were suspected to be not reliable.

Fig.5.10 shows typical traces of shear-induced hoop strains with the time of loading histories. The figure exhibits distinctively accumulated and step-wise increased shear strains. In general, the shear-induced strain was negligible before the onset of diagonal cracking. After the initial loading cycles, unloading to zero load or zero displacement did not release all the strains in the hoops and these strain were accumulated as testing proceeded. The inelastic strains induced in the hoops and the strains due

to concrete confinement were probably the main source of the residual strains. Compressed concrete tended to expand transversely and thus induced confinement strains in the hoops. Once the hoops yielded in tension, the inelastic strains remained even when the loading was reversed, since the transverse reinforcement was unlikely to be subjected to compression. After the formation of the main diagonal cracks, incomplete closure of these cracks became the main cause of the residual strain in the hoops. The accumulated strains in hoops were more pronounced after the formation of the main diagonal cracks. Unit 9 had a larger maximum compression axial load than that for Units 7 and 8, and hence the diagonal cracking was not significant at low displacement ductility level. It can be seen from Fig.5.10, that before the final stage of testing, both the peak strains and the residual strains in hoops were smaller than those for Units 7 and 8. The hoop shear strains in Unit 8 were more significant than that in the other units. Once the main diagonal cracks were formed, the shear strains quickly reached yield and peak shear strain and residual strain increased significantly.

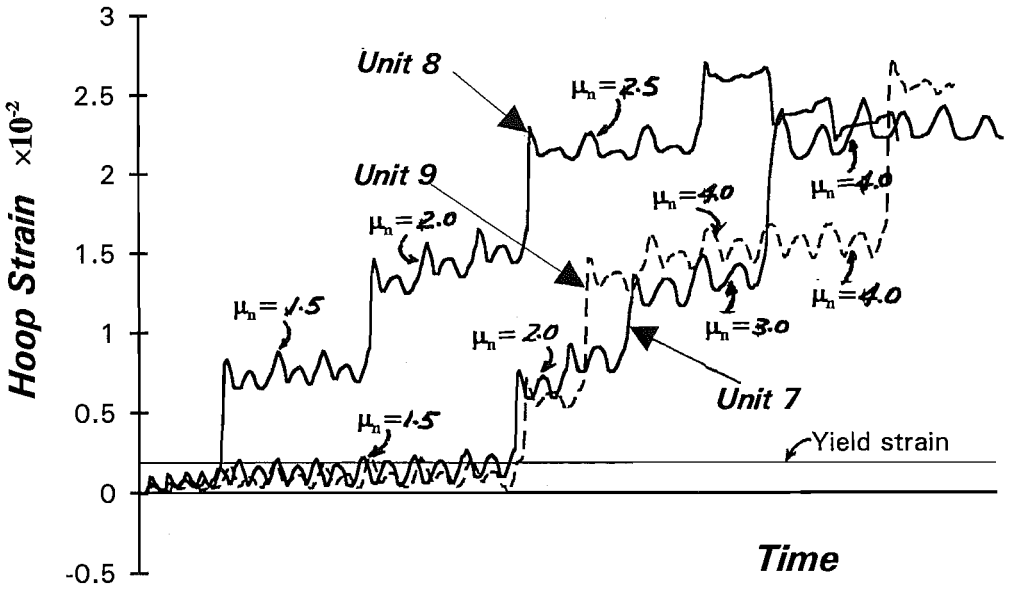

Fig.5.10: Typical Hoop Strain Histories for Units 7 to 9

5.5.2 Distribution of Shear-induced Hoop Strains

The vertical distributions of measured hoop strains mainly due to shear for the three column units are illustrated in Fig. 5.11 to 5.13. The strains plotted in these figures are those in the first cycles to each peak displacement ductility factor. The yield strain and strain hardening are also shown in these figures

by dashed lines.

As was expected, the hoop strains were very small during the initial loading cycles. It can be seen from these strain profiles that most strains for Units 7 and 8 exceeded yield strain at $\mu_n=1.5$, indicating that the shear became significant in these column units at low displacement ductility factor. For Unit 8, the hoop strains at all levels except for at the first level of strain gauge exceeded strain hardening prior to failure. Although the strain gauges only covered the regions about 1.5 times the column depth, the trend of the strain distribution and the pattern of critical diagonal cracking(see Fig.5.7) suggested that the yielding of the hoops would occur over larger regions. It is also noted that once pairs of hoops yielded, they quickly entered the strain hardening range and in some case reached the ultimate strain and fracture took place. The largest strain was measured by the strain gauges situated at the mid-height of the column. In these regions, the main diagonal cracks were more likely to intersect the transverse reinforcement. The development of shear-induced strain was closely associated with the development of the diagonal cracking. The critical diagonal crack was more significant in the Unit 8, so the hoop shear strains were larger. In the Unit 7, the hoop shear strains reached yield in the region about 150mm to 550mm above column base.

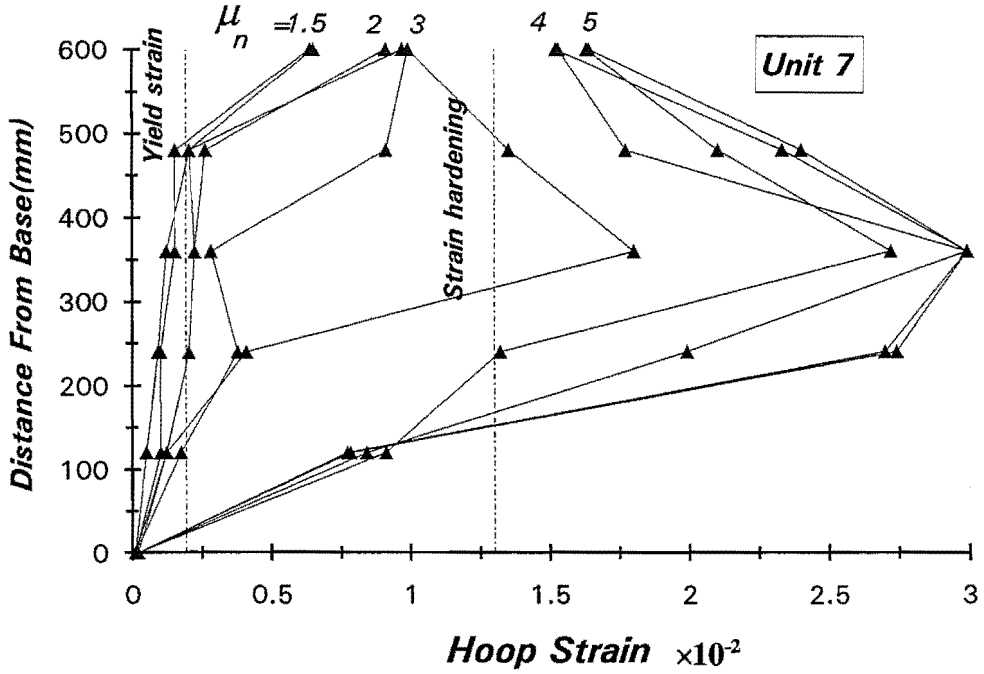

Fig.5.11: Distribution of Mainly Shear Induced Hoop Strains

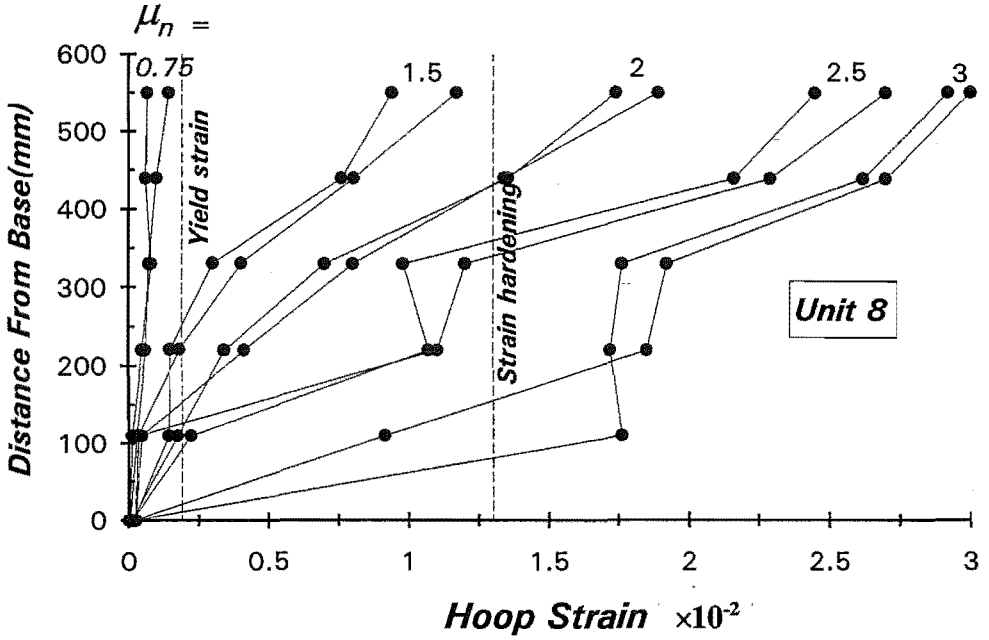

Fig.5.12: Distribution of Mainly Shear Induced Hoop Strains

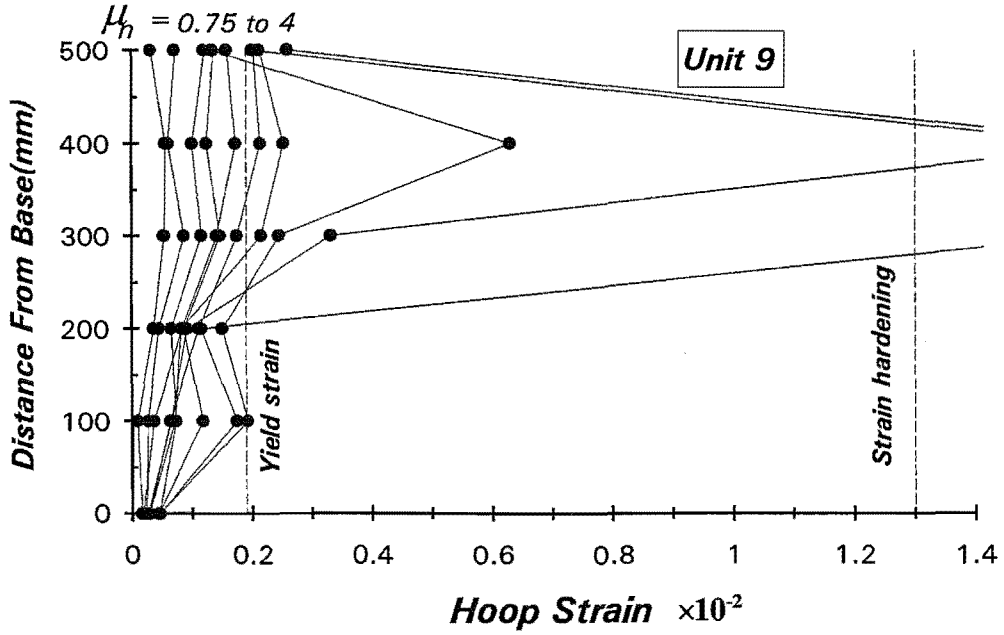

Fig.5.13: Distribution of Mainly Shear Induced Hoop Strains

The hoop shear strains for Unit 9 remained in the elastic range until μ_n=2. The values of shear strains in Unit 9 are generally smaller than those in Units 7 and 8, especially at low displacement ductility levels, and indicated the effect of the larger axial compression force applied which restrained diagonal cracking. With the larger angle of inclination of diagonal cracks in Unit 9, the main diagonal cracks intersected less sets of transverse reinforcement. Only the strains in the upper three strain gauge levels exceeded the yield strain and the others remained in elastic range.

It is appeared from Figs.5.11 to 5.13 that the shear-induced hoop strains in the first strain gauge level, which were at the end of the columns, are almost negligible. The main diagonal cracks generally ran up about 60mm above the column base, and did not cross the transverse reinforcement in the end region of the column. This resulted in the small strains recorded at the first strain gauge level. Therefore, it can be concluded that in the end regions of the column, the transverse reinforcement did not participate significantly in the shear transfer mechanisms.

From the view point of diagonal shear cracking, it appears that the regions of columns requiring extra shear protection are larger than 1.5 times the overall column depth.

5.5.3 Shear Forces Resisted by The Hoops Using the Observed Angle of Diagonal Tension Cracks

It is generally accepted by most concrete design codes that the shear strength of a reinforced concrete member is given by the contributions of the concrete mechanisms and the truss mechanism of the hoop reinforcement and diagonal compression struts inclined at 45 degree to the longitudinal axis of the column. During the tests with axial tension loading a larger angle of inclination θ of the diagonal crack to the column axis was observed than during axial compression(see Table 5.1). Most observed angles θ were less than 45-degree.

From the measurements of hoop strains at various strain gauge levels, as shown in Fig. 5.11 to 5.13, and from the observed angle of inclination of diagonal cracks, the total shear force, V_s, carried by transverse reinforcement can be evaluated by the truss analogy by summing the components of hoop forces cross the diagonal cracks. Thus

$$V_s = \frac{f_s A_v d}{s} \cot\theta \qquad (5.1)$$

where θ is observed inclination of critical diagonal cracks to the longitudinal axis of the column, and f_s is the hoop stress obtained from measured hoop strains.

The measured stress-strain relationship for the hoop steel, as shown in Fig.4.10, was used in the calculation of steel stress f_s. The calculated results for V_s using the observed value for f_s and the measured angle of diagonal cracking are plotted against the displacement ductility factor in Figs.5.14 to 5.16.

As mentioned previously, before the onset of diagonal cracks the shear strains were negligible. Therefore, as indicated in these figures, the shear carried by the transverse reinforcement was very small during early loading. The shear V_s increased as the displacement ductility factor increased. Though Unit 9 had smaller hoop spacing than that in Unit 8, the angle of critical diagonal crack was larger than that in Unit 8. As a result, the maximum shear, V_s, achieved in both column units was approximately the same. Compared with Units 8 and 9, Unit 7 provided with the largest hoop spacing had the largest angle of critical diagonal crack, which resulted in smallest total shear, V_s, carried by hoop steel. The effect of strain hardening was taken into account in the stress-strain relationship. Hence, after yielding of hoop steel the shear V_s slightly increased at high displacement ductility levels.

The applied shear force V is also plotted in Figs.5.14 to 5.16. Graphically, the region between lines for V_s and V in Figs.5.14 to 5.16 represents the shear carried by the mechanisms other than the steel shear resisting mechanisms, ie, commonly known as the "concrete shear resisting mechanisms". Quantitatively, the shear carried by the "concrete mechanisms" can be obtained by subtracting the shear, V_s, carried by transverse reinforcement from the total shear applied, V.

It should be noted that the measured hoop strains in the direction of loading could include the effects of confinement of core concrete and due to wedging action(Fig.5.17). The wedging action was also observed in the tests conducted by Ang et al[A7] and Wong[W4]. It is very difficult to evaluate this effect. It is believed that the confining effects of the core concrete on increasing hoop strains in the direction parallel to the lateral force would be relatively small. However, the hoop strain due to the effect of wedging action could become important when at large inelastic displacement the wedging action along the opening produced additional deformation. Therefore, the use of entire hoop strains to calculate the hoop stress will inevitably result in overestimate of the shear carried by the transverse reinforcement and the associated shear carried by the concrete mechanisms will be underestimated.

The regions between the lines for V and V_s based on the observed angle of diagonal cracking in Figs.5.14 to 5.16 narrowed with increasing displacement ductility factor because of the degradation in the concrete shear resisting mechanisms. In the negative loading direction, the concrete contribution suddenly dropped after initial loading cycle. On the application of the axial tension load, tension-shear cracks extended extensively over the section, especially under high intensity tension force, for example, in Unit 9. This resulted in the loss of concrete in shear resistance.

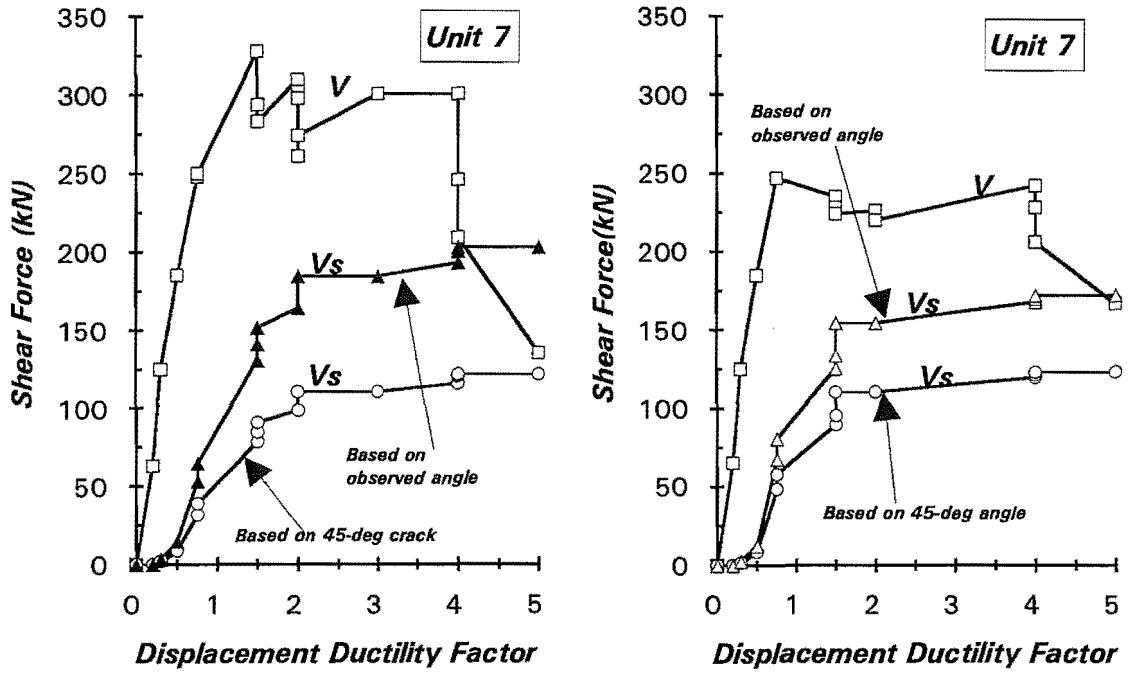

(a) Compression axial loading cycle (b) Tension axial loading cycle

Fig.5.14: Shear Force Versus Imposed Displacement Ductility Factor for Unit 7

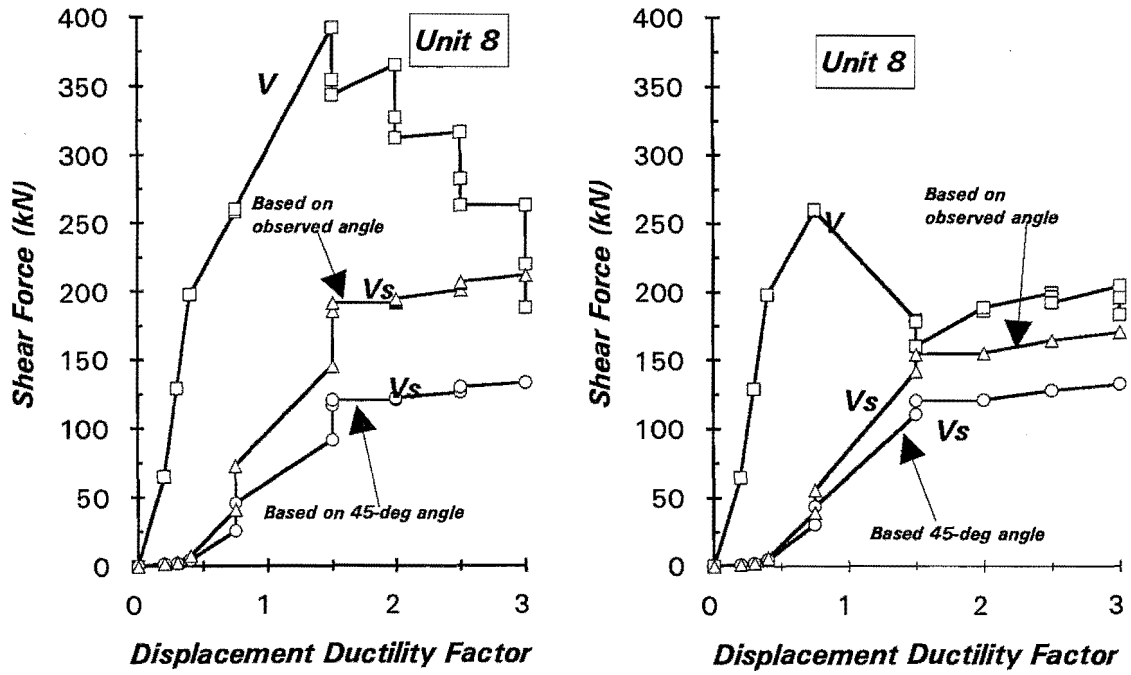

(a) Compression axial loading cycle (b) Tension axial loading cycle

Fig.5.15: Shear Force Versus Imposed Displacement Ductility Factor for Unit 8

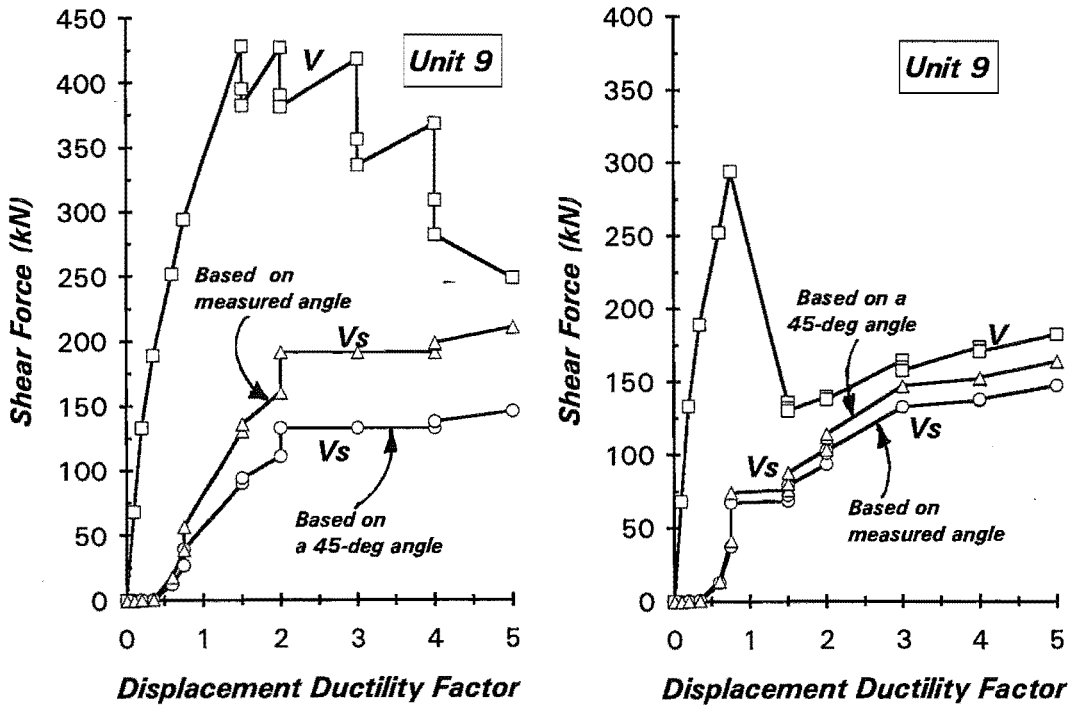

(a) Compression axial loading cycles (b) Tension axial loading cycles

Fig.5.16: Shear Force Versus Imposed Displacement Ductility Factor for Unit 9

5.5.4 Shear Forces Resisted by the Hoops Assuming a 45 degree Truss Mechanism

The new Zealand concrete design code NZS 3101:1982[S14] and the building code for reinforced concrete of the American Concrete Institute ACI 318:1989[A3] assume that the shear force resisted by the hoops is given by a 45 degree truss mechanism. To compare the experimental shear forces carried by the concrete with the code specified concrete shear strength in the following sections, the shear V_s resisted by the hoops was also calculated using a 45 degree truss mechanism. The calculated results for V_s are also shown in Figs.5.14 to 5.16.

Since the observed inclinations of the critical diagonal cracks were less than 45 degree except for Unit 9 when the tension axial load was applied, the shear V_s calculated using observed angle of diagonal cracks was larger than that calculated assuming a 45 degree truss mechanism.

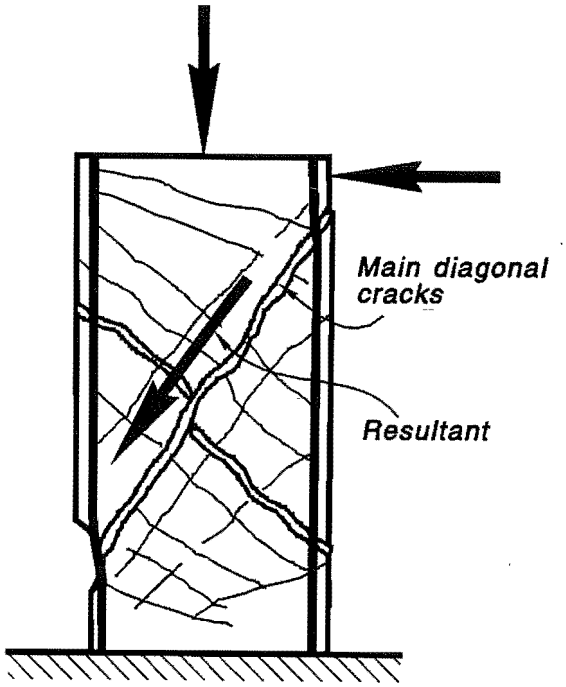

Fig.5.17: Wedging Action of Column Under Compression Axial Load

5.6 CONCRETE SHEAR RESISTANCE

The shear carried by the concrete mechanisms was obtained by subtracting the shear carried by the transverse reinforcement from the total shear applied. To further examine the change of concrete contribution to the shear strength with the imposed displacement ductility , the shear force ,V_c, carried by the concrete was normalized by dividing by the effective shear area, $b_w d$, and the square root of the concrete compressive strength, f'_c. The quantity, $\sqrt{f'_c}$, is commonly related to the concrete shear strength by many codes. In the calculations of the shear V_c the associated shear forces V_s determined using the observed inclination of diagonal cracks and a 45 degree angle of diagonal crack were used.

The values, $v_c/b_w d\sqrt{f'_c}=v_c/\sqrt{f'_c}$,attained in the first loading cycle of each peak displacement factors for the three column units when the compression axial load was applied are plotted against the displacement ductility factors, μ_n, in Figs.5.18 to 5.20. The concrete shear strengths determined using code provisions of NZS 3101:1982[S14] for inside and outside potential plastic hinge regions are also illustrated in these figures.

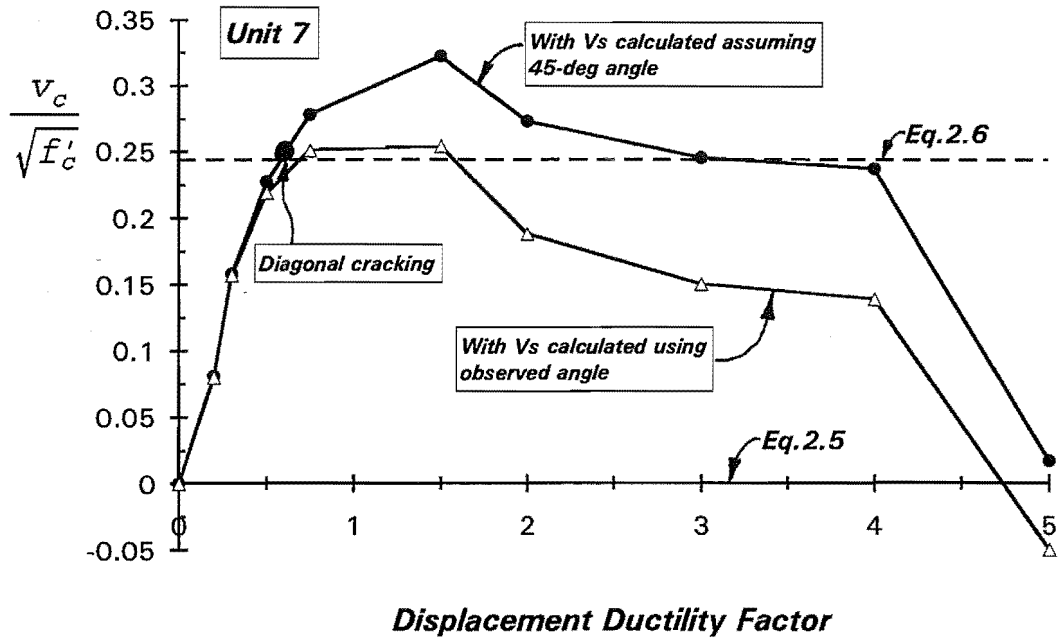

Fig.5.18: Shear Stress Resisted by Concrete Mechanisms When Compression Axial Load was Applied for Unit 7

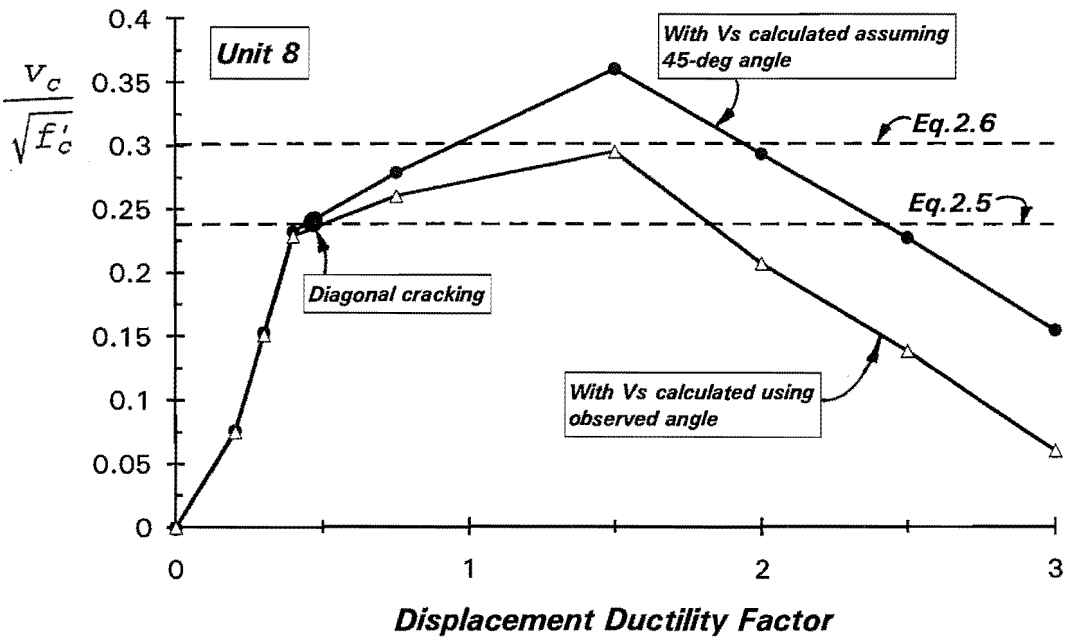

Fig.5.19: Shear Stress Resisted by Concrete Mechanisms When Compression Axial Load was Applied for Unit 8

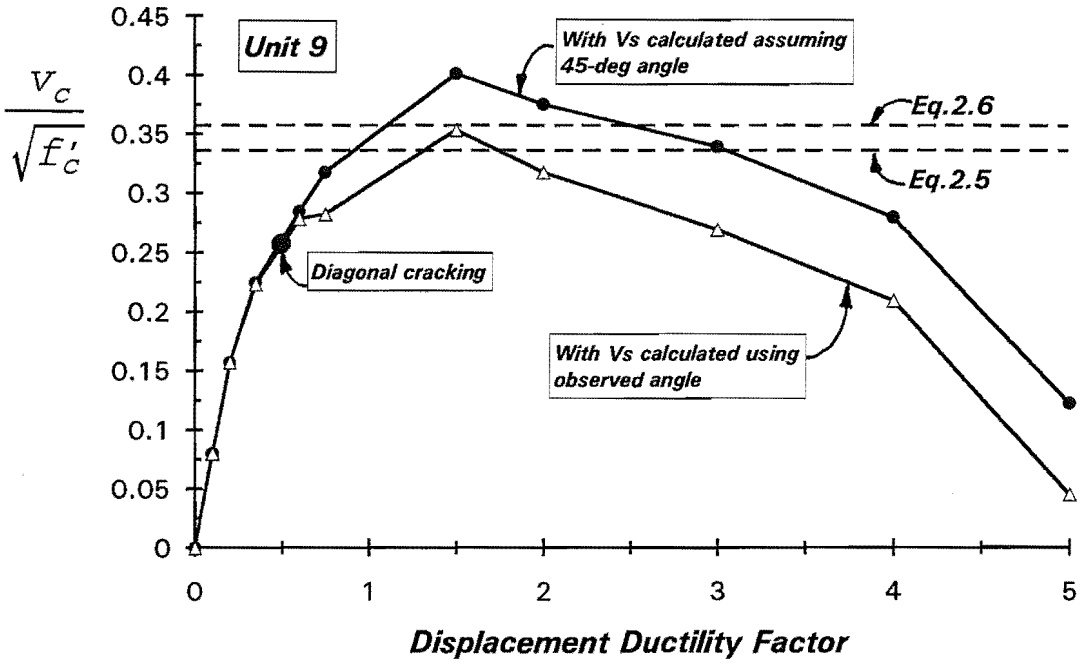

Fig.5.20: Shear Stress Resisted by the Concrete Mechanisms When Compression Axial Load was Applied for Unit 9

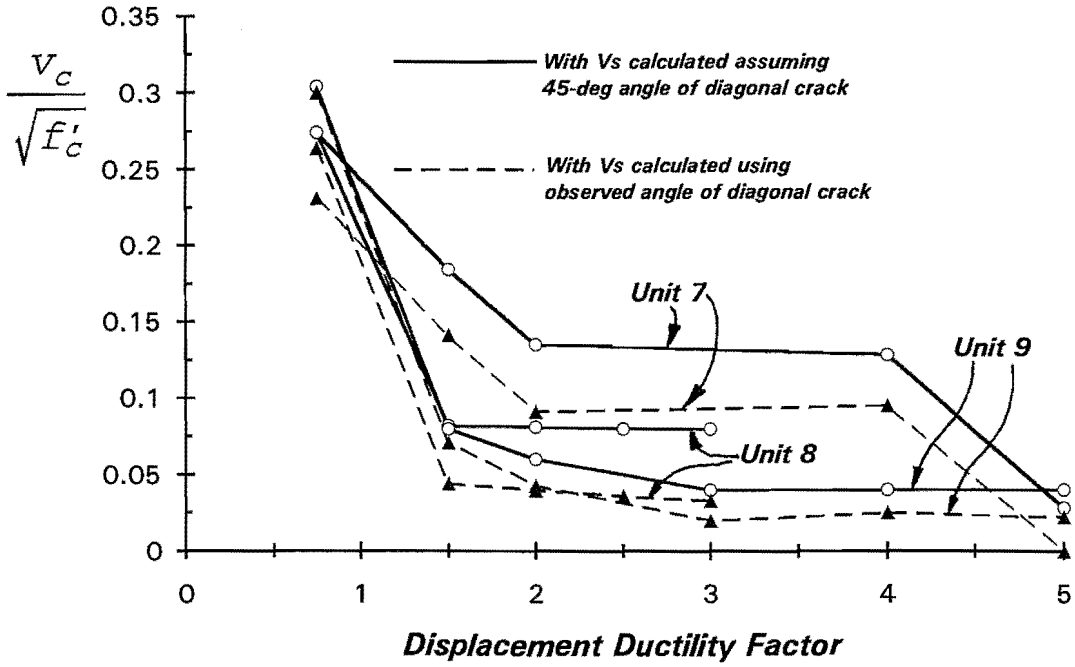

Fig.5.21: Shear Stress Resisted by the Concrete Mechanisms When Tension Axial Load was Applied for Units 7, 8 and 9

Figs.5.18 to 5.20 indicated a distinctive interaction between the shear stress resisted by the concrete mechanisms under compression axial load and imposed displacement ductility factors. Prior to the onset of diagonal cracking, shear carried by the transverse reinforcement was negligible, the shear force was primarily carried by the concrete mechanisms and hence the concrete shear stress, $v_c/\sqrt{f'_c}$, increased almost in proportion with displacement ductility factors. As can be seen in these figures, that concrete shear stress continued to increase after the formation of diagonal cracks.

In the positive lateral loading direction, the maximum value of $v_c/\sqrt{f'_c}$ for the three column units all reached in the first loading cycle to $\mu_n=1.5$. The degradation in concrete shear strength followed the cycle in which the axial tension force was first applied. After attainment of the maximum value, the concrete shear strength decreased with increasing displacement ductility. The widening of flexure/shear cracks reduced the capacity for the shear transfer by aggregate interlock, and shear strength reduced. The tension axial force encouraged the widening and delayed the closure of the diagonal cracks. This probably was also the main cause of earlier formation of the major diagonal crack and premature degradation of concrete shear strength. The deterioration in the concrete shear mechanism could be the result of several factors. The axial tension force was applied to the column in the negative loading direction immediately after initial loading cycles. The application of the tension axial force caused large tension strain in the concrete. Due to repeated tension and compression strains, concrete became very loose and deterioration of bond strength between the concrete and reinforcing steel was also expected. This directly degraded the concrete shear resisting capacity. During the negative loading cycle, the diagonal cracks which had opened in the positive loading direction were unable to close because of tension axial force, and the cracked surface along diagonal cracks tended to slid towards the opposite direction when the loading was reversed. This repeated grinding and abrasion under unsymmetric strain histories led to progressive disintegration of the concrete. The concrete interlock capacity, which is believed to contribute a large portion in the concrete shear mechanism, degraded greatly with increasing loading cycles and increasing displacement ductility level. Spalling of concrete, especially when it extended into the core region of the section at high displacement ductility as observed during the tests, reduced the effective shear area of the column and therefore the concrete shear capacity.

The effect of the compression axial load level on both the concrete shear stress at the onset of diagonal cracking and the maximum shear strength can be seen in Fig5.18 to 5.20. It is noted that decrease of the concrete shear strength for Unit 9 was not significant in early stage due to the larger axial compression restraining the widening of diagonal cracks. Once hoop steel yielded, diagonal cracking became important and the drop of concrete shear strength was drastic. The concrete shear strength in Unit 9 actually vanished at $\mu_n=5$, as shown in Fig.5.20.

It is to be remembered that the shear carried by the hoops calculated using measured inclination of critical diagonal cracks was to some extent overestimated due to the reasons stated in section 5.5.3. Therefore, the estimated concrete shear stress would represent a conservative boundary strength.

The shear stress resisted by the concrete in the first loading cycle of each peak displacement ductility factor for the three column units when the tension axial load was applied is shown in Fig.5.21. In the tension axial loading direction, the shear stress resisted by the concrete mechanisms was dependent on the intensity of the tension axial load level(see Figs.5.21). For Unit 7 with the maximum axial tension of $0.055f_c'A_g$, a large portion of the shear was still able to be transmitted by the concrete. For Units 8 and 9 with higher axial tension, the concrete shear strength was very small. For the axial tension greater than $0.2f_c'A_g$ the concrete shear strength could be neglected in the design.

5.7 SHEAR CARRYING CAPACITY

5.7.1 Shear Strength Envelope

In the previous section, the overall behaviour of each column unit was discussed with reference to its lateral load-displacement hysteresis loops. It was indicated that the degradations in the strength and stiffness took place in all three column units at some stage. To further investigate the strength decay characteristics of the columns with increasing displacement ductility, the shear strength envelopes were constructed. The lateral load attained at each of peak displacement ductility factors was expressed in the non-dimensional form, $\frac{V}{A_e\sqrt{f_c'}} = \frac{v}{\sqrt{f_c'}}$, where the effective shear area $A_e=b_wd$, where b_w = width of column section and d = 0.9h. The shear stress in each loading cycle was joined by straight lines and then plotted against the displacement ductility factor, in Figs.5.22 to 5.24. The shear strengths given by the code equations of NZS 3101:1982 based on a 45-deg truss mechanism for inside and outside potential plastic hinge regions are also included in these figures, as indicated by the horizontal dashed lines.

Figs.5.22 to 5.24 displayed the characteristics of the shear strength with distinctive ascending and descending branch of strength envelopes. The ascending branch of the strength envelope were characterized by the cracking in the concrete due to flexure/shear and the yielding of the longitudinal reinforcement. The slope of the envelope curve before diagonal cracking gives direct indication of the elastic stiffness of the column. This slope was greatly influence by the presence of axial load level. The

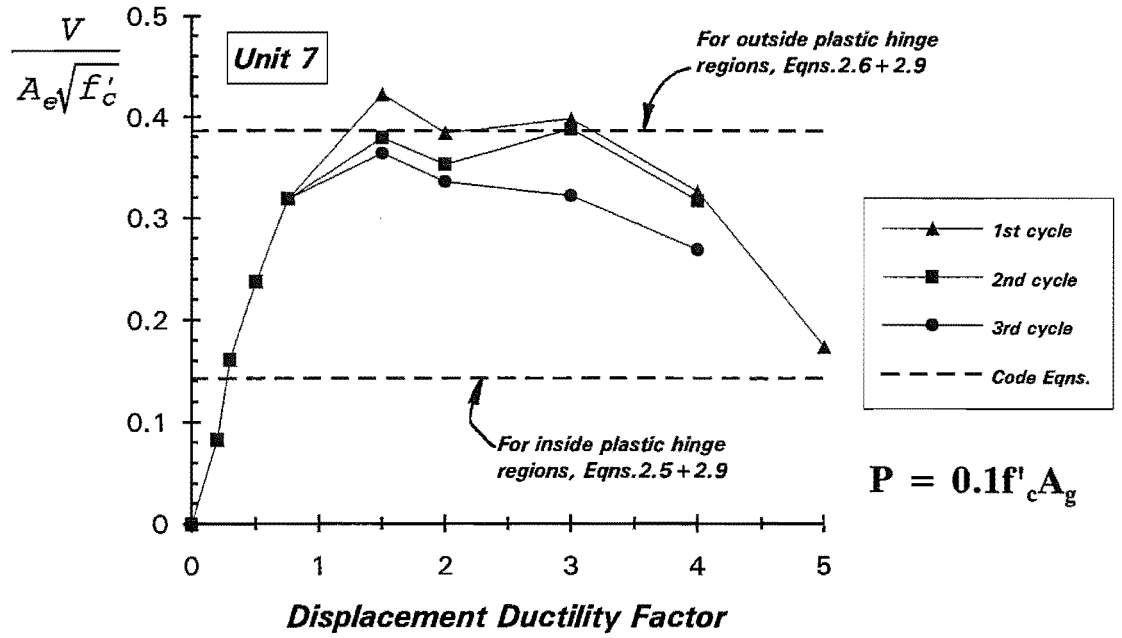

(a) Under compression axial load

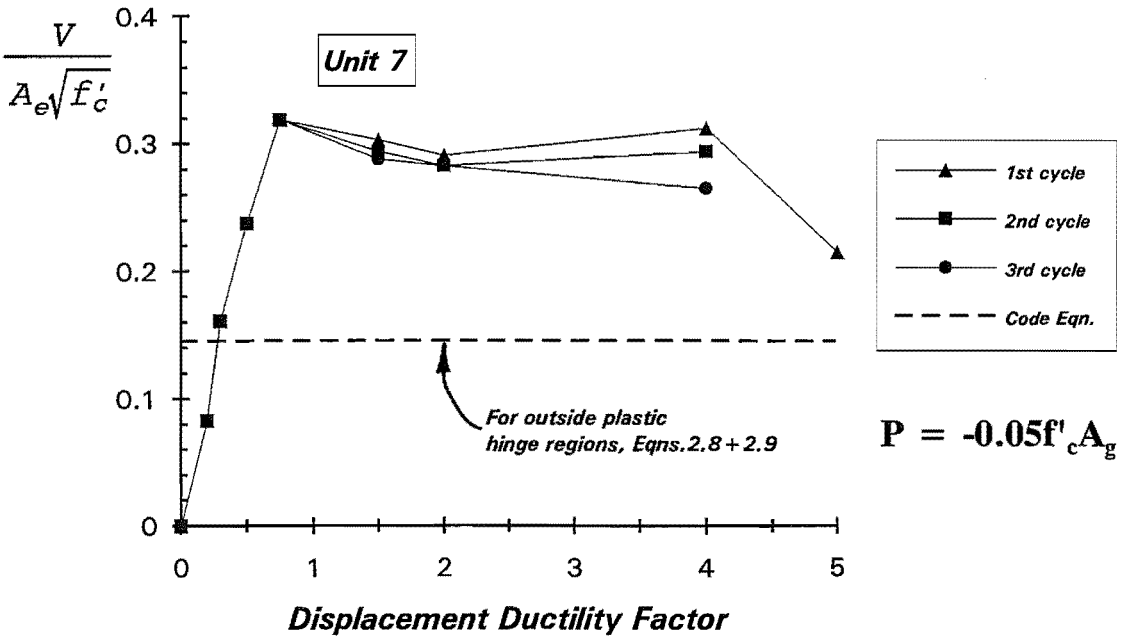

(b) Under tension axial load

Fig.5.22: Shear Stress Envelopes for Unit 7

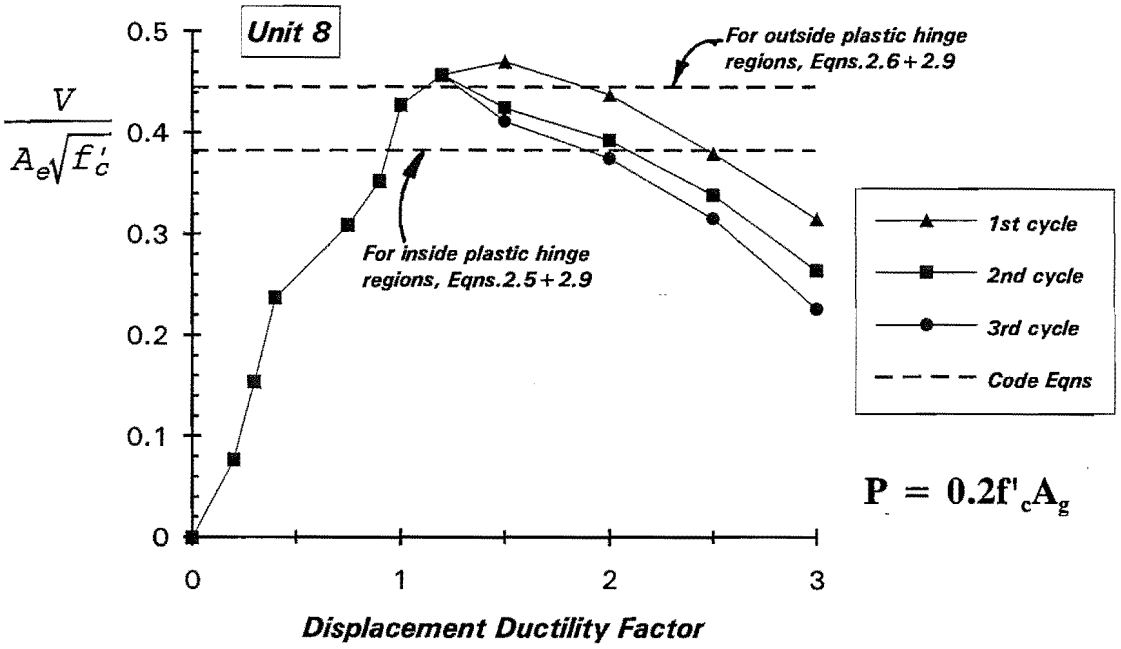

(a) Under compression axial load

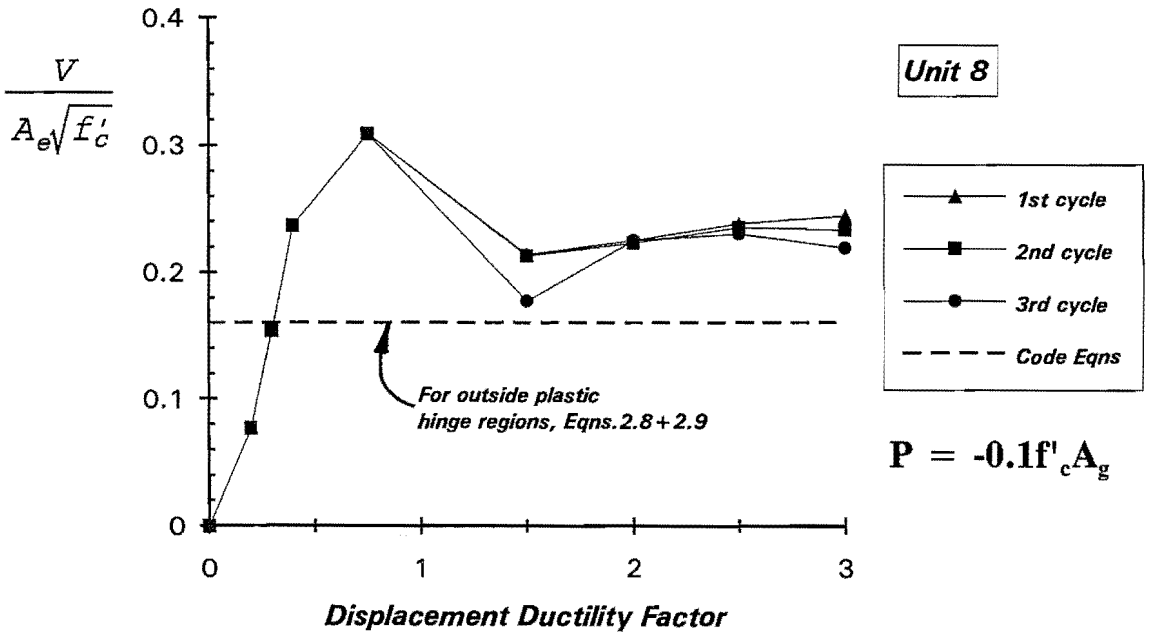

(b) Under tension axial load

Fig.5.23: Shear Stress Envelopes for Unit 8

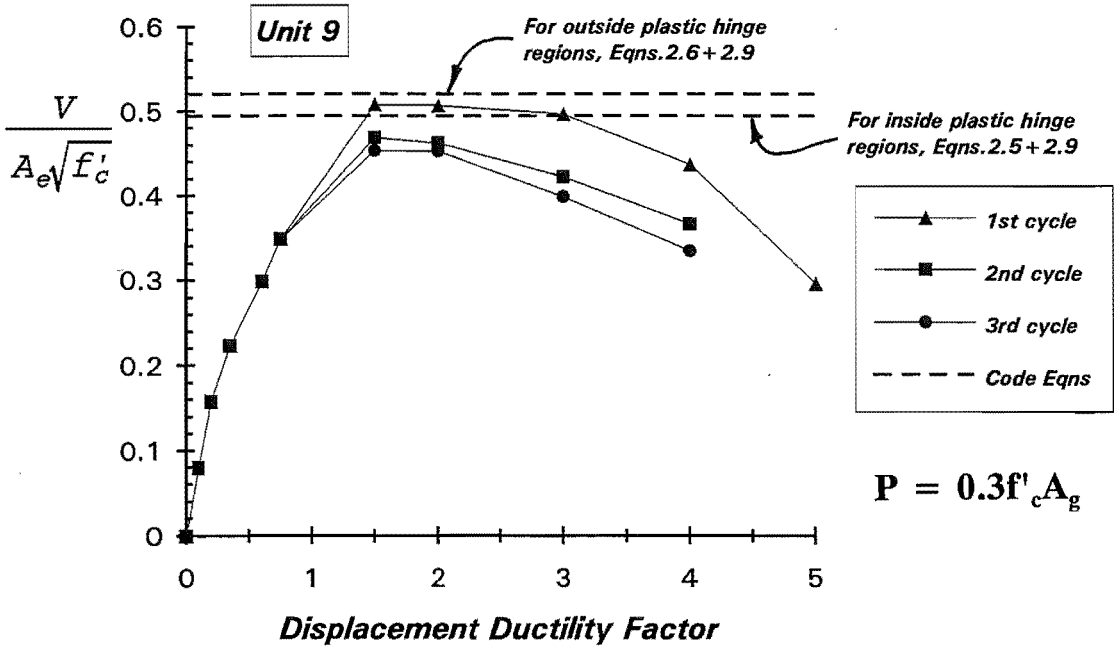

(a) Under compression axial load

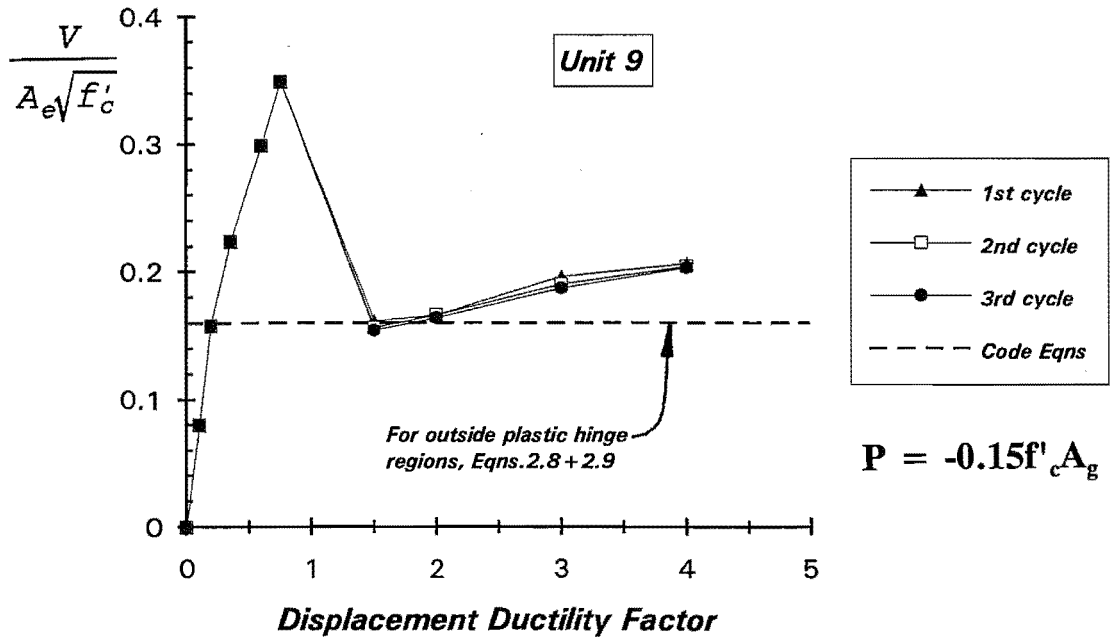

(b) Under tension axial load

Fig.5.24: Shear Stress Envelopes for Unit 9

larger compression axial load delayed the onset of diagonal cracking and maintained the elastic stiffness of the column.

It is evident that Unit 9, with a compression axial load of $0.2f'_cA_g$ during the initial loading cycles, exhibited a steeper slope of its envelope curve on ascending branch than those for Units 7 and 8. Sudden softening of stiffness in Unit 8 took place after diagonal cracking. This was due to the premature formation of a major diagonal crack as observed during the testing. The hoop reinforcement reached yielding soon after onset of diagonal cracking.

The envelope curves during the initial loading cycles are quite similar for both the loading directions. The descending portions of the envelope curves are completely different for the positive and negative lateral loading directions. In the positive lateral loading direction, the shear stress continued to increase beyond the diagonal cracking. All the three column units reached their maximum shear strength at $\mu_n=1.5$. The magnitude of the maximum shear strength was dependent on the axial compression load level and the content of transverse reinforcement. Although the shear actually carried by the transverse reinforcement across the diagonal crack still slightly increased after $\mu_n=1.5$ due to strain hardening, the decrease in the shear taken by the concrete was larger than the increase in the shear carried by hoops. As a result, the total shear capacity decrease once the degradation of concrete contribution to the shear strength started.

In the negative lateral loading direction, the shear strength remained very stable with increased displacement ductility. A slight increase of shear strength can be attributed to P-Δ effect since it tend to increase lateral load capacity. Figs.5.22 to 5.24 show that the column sustained a fairly large portion of shear even under large tension axial load up to $0.15f'_cA_g$, as for example in the case of Unit 9. Examination of Figs.5.22 to 5.24 indicated a obvious tendency of shear strength under tension axial loading on the intensity of axial load level applied.

5.7.2 Shear Strength At Onset of Diagonal Cracking

The diagonal cracking commences when the principle tensile stress in concrete exceeds the concrete tension strength. The lateral load at which the diagonal cracking first occurs mainly depends on the axial load applied and the concrete compressive strength.

During the testing in the initial loading cycles, particular care was paid to observe the development of flexural and shear cracking. The lateral load at which the visible diagonal cracks first appeared in both the loading directions was recorded. The corresponding increment of the lateral load was checked against the measured hoop strains, since the load at which the hoop strains became significant would

give good indication of the onset of diagonal cracking[A7]. The lateral load at the onset of diagonal cracking was determined based on the assessment of the recorded cracking load and the measured hoop strains. It was found that the observed diagonal cracking loads were very close to the load at which the hoop strains became significant. The onset of diagonal cracking for the three column units all took place during initial loading cycles. The average shear stress at the onset of diagonal cracking expressed in dimensionless form, $v_{cr}/\sqrt{f'_c}$, and shear stress of concrete contribution, $v_c/\sqrt{f'_c}$, calculated using code equations of NZS 3101:1982[S14] for outside potential plastic hinge regions are listed in Table 5.4. Also listed in this table are the angles of inclination of initial diagonal cracks to the column axis. The axial load ratios given in Table 5.4 are that applied during the initial loading cycles.

Fig.5.25 shows the plot of average shear stress at the onset of diagonal cracking for the three column units versus the axial load ratio. It can be seen in Fig.5.25 that the shear stress at the onset of diagonal cracking increased with the compression axial load level. This was expected since higher compression axial load allows larger shear stress to be transferred before the principle tensile stress exceeds the concrete tensile strength and therefore results in a larger diagonal cracking load. The relation between the shear stress at the onset of diagonal cracking and the compression axial load ratio appears to be linear, as demonstrated by the best-fit straight line in Fig.5.25. It will be seen in Table 5.4 that the average shear stress for the three column units is less than code specified values for outside potential plastic hinge regions.

Table 5.4: Shear Stress at Onset of Diagonal Cracking

Unit	$\frac{P}{f'_c A_g}$	V_{cr} (kN)	$\frac{v_{cr}}{\sqrt{f'_c}}$ (1)	$\frac{v_c}{\sqrt{f'_c}}$ (2)	Inclination of Cracks θ(deg)	
					Positive Loading	Negative Loading
7	0.05	185	0.239	0.244	48	50
8	0.10	210	0.252	0.301	36	42
9	0.20	250	0.298	0.357	45	48

Note:

(1). experimental average shear stress at onset of diagonal cracking

(2). shear stress of concrete contribution by code equations for outside potential plastic hinge regions(Eq.2.6).

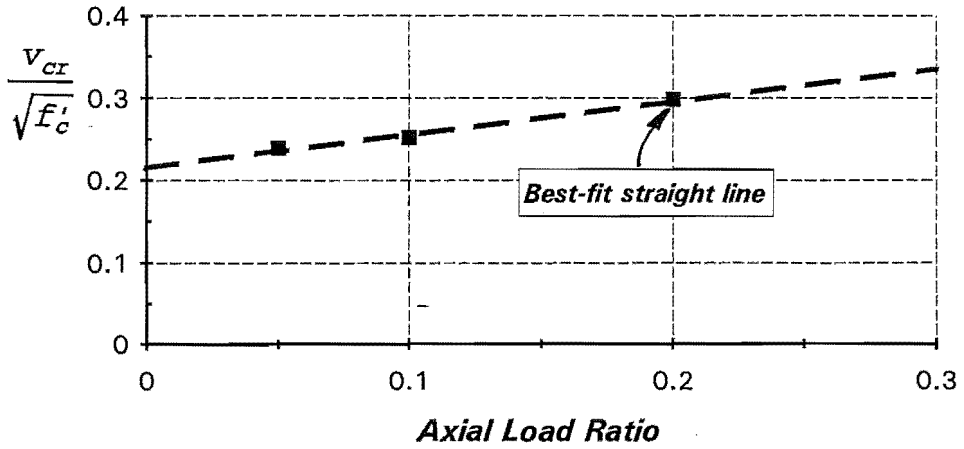

Fig.5.25: Average Shear Stress at Onset of Diagonal Cracking Versus Axial Load Ratio

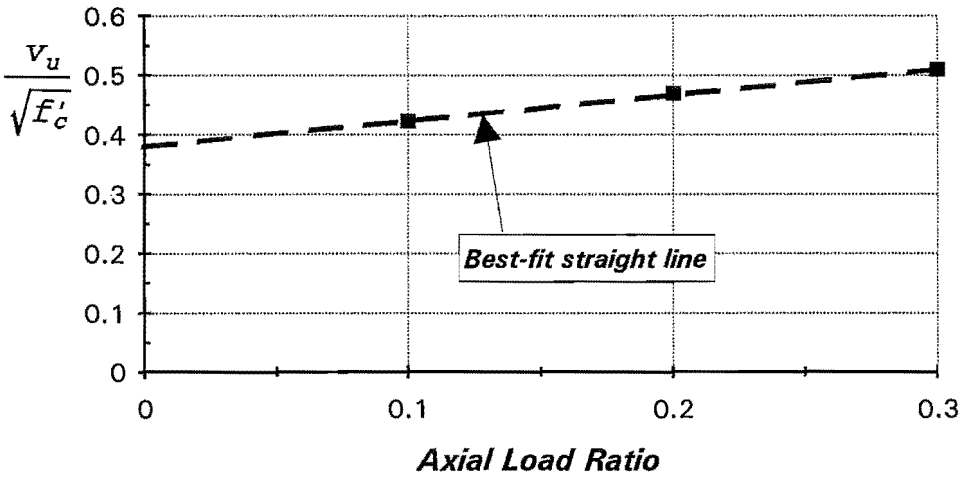

Fig.5.26: Maximum Shear Stress Versus Axial Load Ratio

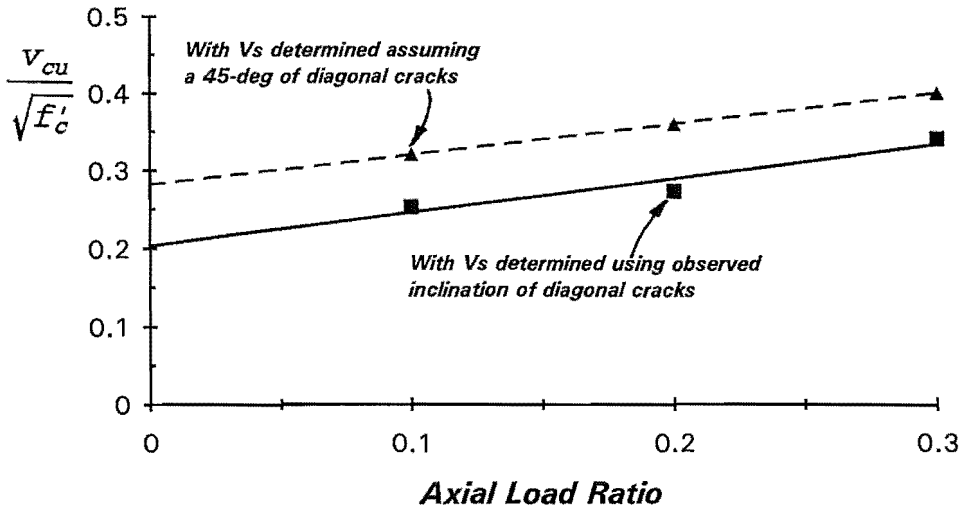

Fig.5.27: Concrete Shear Stress at Ultimate

5.7.3 The Maximum Shear Strength

The maximum shear strengths achieved during the tests are further examined as they served as upper bound strengths for the column units. Table 5.5 lists the maximum shear strengths for the three column units. The shear strength calculated using code equations[S14] for outside potential plastic hinge regions are also included in this table. The plot showing the maximum shear stress for the three column units versus the axial load ratio is shown in Fig.5.26.

It can be seen in Table 5.5, the maximum shear strength of the column units increases as the compression axial load ratio increases. The rate of increase, however, became less for higher axial load levels. The calculated shear strengths for Units 7 and 8 using the code equations of NZS 3101:1982 for outside potential plastic hinge regions are less than the experimental shear strength. For Unit 9, code specified value is slightly greater than experimental shear strength. Fig.5.26 indicates that the maximum experimental shear stress increased almost linearly with the increase in the compression axial load ratio. The interstorey drift of the column unit corresponding to the maximum shear strength, as given in Table 5.5, decreases with the increase in the compression axial load ratio.

It has to be emphasized that the column can be considered to develop its shear strength when the transverse reinforcement reaches yielding or physically when diagonal cracks become significant. This was the case for the three tested columns. Hence, the experimental maximum lateral forces at μ_n=1.5 were considered to be the maximum shear resistance for the three column units.

Table 5.5: The Maximum Shear Strength of Column Units

Unit	$\frac{P}{f'_c A_g}$	V_u (kN)	$\frac{v_u}{\sqrt{f'_c}}$ (1)	$\frac{v_i}{\sqrt{f'_c}}$ (2)	$\frac{V_u}{V_i}$	μ_n	Drift (%)
7	0.1	328	0.423	0.387	1.18	1.5	0.136
8	0.2	392	0.470	0.444	1.14	1.5	0.127
9	0.3	428	0.509	0.514	1.07	1.5	0.114

Notes:

(1) experimental average shear stress at maximum lateral load

(2) shear strength given by the code equations of NZS 3101:1982 for outside potential plastic hinge regions(Eq.2.6).

5.7.4 Concrete Shear Stress at Maximum Lateral Load

It was shown in the Section 5.6 that concrete shear component continues to increase after the onset of diagonal cracking. The shear stress resisted by the concrete at the maximum lateral load was further examined, since these values can be considered as the initial shear strength of the concrete resisting mechanisms. The shear carried by the concrete was obtained by subtracting the shear, V_s resisted by hoops, from the total shear applied. The non dimensional concrete shear stresses with the shear V_s determined using observed inclination of diagonal cracks and a 45 degree diagonal crack at the maximum lateral load are given in Table 5.6 and 5.7. For the comparison, the concrete shear strength determined by code[S14] equations for outside potential plastic hinge regions are also included in these tables. The shear stress actually resisted by the concrete for Units 8 and 9(see Table 5.6) are less than shear strengths given by the code equations of NZS 3101:1982 for outside potential plastic hinge regions.

Fig.5.27 plots the concrete shear stress, $v_{cu}/\sqrt{f'_c}$, at the maximum lateral load for the three column units versus axial load ratio. It can be seen that the concrete shear stress has a strong dependence on the axial load ratio.

Table 5.6 Concrete Shear Stress at the Maximum Lateral Load With V_s Calculated using Observed Inclination of Diagonal Cracks

Unit	$\frac{P}{f'_c A_g}$ (1)	V_u (kN) (2)	V_{cu} (kN) (3)	V_s (kN) (4)	$\frac{V_{cu}}{\sqrt{f'_c}}$ (5)	$\frac{V_c}{\sqrt{f'_c}}$ (6)	$\frac{(5)}{(6)}$	μ_n
7	0.1	328	197	131	0.254	0.244	1.04	1.5
8	0.2	392	228	164	0.274	0.301	0.92	1.5
9	0.3	428	287	141	0.341	0.357	0.96	1.5

Notes:

(1) maximum compression axial load ratio

(3) shear resisted by the hoops

(4). shear resisted by the concrete, $V_{cu}=V_u-V_s$.

(6). concrete shear strength given by the code equations of NZS 3101:1982 for outside potential plastic hinge regions(Eq.2.6).

Tabel 5.7 Concrete Shear Stress at the Maximum Lateral Load With V_s Calculated a 45-deg Inclination of Diagonal Cracks

Unit	$\frac{P}{f'_c A_g}$ (1)	V_u (kN) (2)	V_s (kN) (3)	V_{cu} (kN) (4)	$\frac{V_{cu}}{\sqrt{f'_c}}$ (5)	$\frac{V_c}{\sqrt{f'_c}}$ (6)	$\frac{(5)}{(6)}$	μ_n
7	0.1	328	79	249	0.322	0.244	1.32	1.5
8	0.2	392	92	300	0.360	0.301	1.19	1.5
9	0.3	428	90	338	0.401	0.357	1.12	1.5

Notes:

(1) maximum compression axial load ratio

(3) shear resisted by the hoops

(4). shear resisted by the concrete, $V_{cu}=V_u-V_s$.

(6). concrete shear strength given by the code equations of NZS 3101:1982 for outside potential plastic hinge regions(Eq.2.6).

5.7.5 Concrete Shear Stress at Failure

It was noted in the Section 5.6.1 that the total shear strength of the columns degraded with the increased displacement ductility, although a slight increase in the shear carried by the hoops was expected due to strain hardening. The reduction in the shear strength was caused by the degradation of concrete shear resisting mechanisms. It is of importance to assess the shear stress carried by the concrete at available displacement ductility level, since they provide a lower bound for the concrete contribution to the shear strength.

The residual concrete shear strength, V_{cf}, was taken as the shear corresponding to the lateral load at which significant shear deformation or fracture of the transverse reinforcement occurred. The residual concrete shear stress was calculated in the same manner as for concrete shear stress at the maximum lateral load. Tables 5.8 lists the shear stress, $v_{cf}/\sqrt{f'_c}$, carried by the concrete at failure when the

associated shear V_s was calculated using observed inclination of diagonal cracks and a 45 degree diagonal crack. The shear strengths of concrete contribution calculated using code[S14] equations for inside potential plastic hinge regions are also included in this table. It is apparent from the Table 5.8 that at failure the shear resistance of concrete contribution reduced to less than the code specified values for inside potential plastic hinge regions except for Unit 7, in which the shear strength of concrete component was ignored for the compression axial load of $0.1f'_cA_g$, according to the code provisions of NZS 3101:1982[S14]. The strain hardening effects, which became evident before failure, were included in determining the hoop stress. This effect may be slightly overestimated due to use of the stress-strain relationship of reinforcing steel obtained from monotonic tension tests.

The influence of axial load level on the degraded concrete shear stress appeared to be less significant than was the case for the concrete shear stress at the onset of diagonal cracking and at the maximum lateral load.

Table 5.8 Residual Concrete Shear Stress With V_s Calculated using Observed Inclination of Diagonal Crack

Unit	$\frac{P}{f'_cA_g}$ (1)	V_r (kN) (2)	With a 45-deg diagonal crack		With measured angel of diagonal crack		$\frac{v_c}{\sqrt{f'_c}}$ (3)	μ_n (4)
			V_{cf} (kN)	$\frac{v_{cf}}{\sqrt{f'_c}}$	V_{cf} (kN)	$\frac{v_{cf}}{\sqrt{f'_c}}$		
7	0.1	252	126	0.16	60	0.08	0	4
8	0.2	316	189	0.23	115	0.14	0.238	2.5
9	0.3	368	235	0.28	176	0.21	0.336	4

Note:

(1). Maximum compression axial load ratio

(2). Experimental shear force at failure

(3) Shear strength of concrete contribution given by the code equation for inside potential plastic hinge regions

V_{cf} = Shear resisted by the concrete at failure

5.7.6 Shear Carrying Capacity With Tension Axial Load

The development of shear resisting mechanisms in a reinforced concrete column is associated with the cracking patterns. The shear force which can be transmitted across the diagonal failure plane by the truss mechanism is dependent on the inclination of critical crack and the amount of transverse reinforcement crossing the critical diagonal crack. It was observed during the tests that crack patterns of the column under the tension axial load were basically similar to those under compression axial load. The measured angles of inclination of main diagonal cracks were about 38 to 48-deg to the longitudinal axis, indicating they were not noticeably effected by the presence of tension axial force.

The shear force transferred through either the truss mechanisms or concrete mechanisms is also relied on the development of diagonal compression strut. Although extensive cracking in the tension axial loading direction was observed, the shear/tension deformation was distributed over more cracks instead of one or two major diagonal cracks, and thus the crack width was generally small. The worst situation occurred when the crack extended over full depth of the section. This was noted, for example for Unit 9. When unloading to zero displacement from the positive loading direction, the axial force changed from its maximum compression load to tension axial load. The previously opened cracks in the tension side of the section were unable to close due to inelastic strains and reduced compression axial load. These cracks merged with tension-flexure cracks on the other side of the section to form fully open cracks, taking place in some loading instant, most likely around zero displacement. These cracks may close as lateral load increased, depending on the intensity of tension axial force. Under low to moderate tension axial load, it appeared that the aggregate particles along the cracked interface, which extended over the full depth of the section, still engaged to some extent, at least in the confined core concrete. Therefore, the truss mechanism and concrete aggregate interlock shear transfer could remain operative

.

The shear strength of each column unit in the negative lateral loading direction was evaluated in this section. The shear, V^-_s, carried by the hoops was determined using truss analogy with the measured hoop strains and measured inclination of critical diagonal crack. The difference between lateral force V^- and V^-_s was assumed to be the associated shear carried by the concrete mechanisms. The shear strength was calculated at nominal displacement ductility factors $\mu_n = 1.5$ and at failure. The results are given in Tables 5.9 and 5.10. The shear strengths specified by the code equations of NZS 3101: 1982 for outside potential plastic hinge regions are also provided in these Tables.

It can be seen from Tables 5.9 and 5.10 that even under large tension axial load up to $0.15f'_cA_g$ the column unit was still capable of carrying a rather large portion of shear until failure. According to the current New Zealand concrete code[NZS 3101: 1982], for the column with tension axial load the shear strength of the concrete contribution for inside potential plastic hinge regions is taken to be zero. For outside potential plastic hinge regions, the shear strength of concrete contribution decreases with the

increase in the tension axial load. It can be shown From Eq.2.8 that the shear strength of the concrete contribution will be reduced to zero when the tension axial load exceeds $0.083f'_cA_g$.

Table 5.9: Measured Shear Strength Under Tension Axial Load at $\mu_n=1.5$

Unit	$(\frac{P}{f'_cA_g})^t$ (1)	V^-_u (2)	(3)		(4)		$\frac{v_c}{\sqrt{f'_c}}$ (5)
			V^-_{cu}	$\frac{v^-_{cu}}{\sqrt{f'_c}}$	V^-_{cu}	$\frac{v^-_{cu}}{\sqrt{f'_c}}$	
7	0.05	235	145	0.186	127	0.163	0.063
8	0.10	179	69	0.083	38	0.051	0.00
9	0.15	136	68	0.081	73	0.087	0.00

Note:

(1) Maximum tension axial load ratio

(2) Experimental shear force at $\mu_n=1.5$

(3) Shear resisted by the concrete with the associated shear V_s carried by the hoops determined using a 45 degree truss mechanism

(4) Shear resisted by the concrete with the associated shear V_s carried by the hoops determined using observed inclination of critical diagonal cracks

(5) Shear strength of concrete contribution given by the code equation for inside potential plastic hinge regions

Table 5.10: Measured Shear Strength Under Tension Axial Load at Failure

Unit	$(\frac{P}{f'_cA_g})^t$ (1)	V^-_r (2)	(3)		(4)		$\frac{v_c}{\sqrt{f'_c}}$ (5)
			V^-_{cf}	$\frac{v^-_{cf}}{\sqrt{f'_c}}$	V^-_{cf}	$\frac{v^-_{cf}}{\sqrt{f'_c}}$	
7	0.05	235	104	0.13	79	0.11	0.063
8	0.10	179	71	0.08	34	0.04	0.00
9	0.15	136	37	0.04	48	0.06	0.00

Note:

(1) Maximum tension axial load ratio

(2) Experimental shear force at failure

(3) Shear resisted by the concrete with the associated shear V_s carried by the hoops determined using a 45 degree truss mechanism

(4) Shear resisted by the concrete with the associated shear V_s carried by the hoops determined using observed inclination of critical diagonal cracks

(5) Shear strength of concrete contribution given by the code equation for inside potential plastic hinge regions

5.8 COMPARISONS OF MEASURED AND PREDICTED SHEAR STRENGTH

5.8.1 Introduction

In the following sections, the experimental results from three columns tested are compared with the shear strengths specified by various code equations and available predictive models. The comparisons are made in terms of the ratio of experimental shear strengths to the code specified shear strengths or predicted shear strengths by available methods. The results are presented in Table 5.11 to 5.14. The shear strengths were in all cases calculated using measured concrete strength and measured steel yield strength. The strength reduction factor in the code equations was taken to be unity.

5.8.2 The New Zealand Code NZS 3101: 1982[S14]

The shear strengths specified by the code[S14] equations for inside potential plastic hinge regions(Eqns.2.4, 2.5 and 2.9) and the equations for outside potential plastic hinge regions(Eqns.2.4, 2.6 and 2.9) were computed and compared in Table 5.11 with the maximum experimental shear strengths, V_{exp}, obtained from the three column units tested when the compression axial load was applied. As noted previously, the maximum values of shear strength were reached at $\mu_n=1.5$ for all the three column units. It can be seen in Table 5.11, in all cases, that the calculated shear strengths using code equations, either for outside or inside potential plastic hinge regions, are smaller than the maximum experimental shear strengths, except for Unit 9, in which the code specified shear strength

for outside potential plastic hinge region is slightly higher than experimental shear strength. There is a tendency for the code predicted shear strength to become more close to the test values as the axial load level increases. The average ratios of the maximum experimental shear strength to the shear strength based on code equations for inside and outside plastic hinge regions are 1.74 and 1.05, respectively. The ratio of the maximum experimental shear strength to the computed strength, V_{exp}/V^{p}_{NZS}, is extremely high for Unit 7, because the shear strength of concrete contribution is ignored for a column with compression axial of $0.1f_c'A_g$ or less, according to the code provisions[S14]. The code equations for outside potential plastic hinge regions also conservatively predicted the maximum experimental shear strengths.

Table 5.11: Comparison of Maximum Experimental Shear Strength With the Code Values When Axial Compression is Applied

Unit	$\frac{P}{f_c'A_g}$	V_{exp} (kN)	V_s Eq.2.9 (kN)	V_c Eq.2.5 (kN)	V^{p}_{NZS} (kN)	$\frac{V_{exp}}{V^{p}_{NZS}}$	V_c Eq.2.6 (kN)	V_{NZS} (kN)	$\frac{V_{exp}}{V_{NZS}}$
7	0.1	328	111	0	111	2.95	189	300	1.10
8	0.2	392	121	198	319	1.23	250	371	1.06
9	0.3	428	133	283	416	1.03	300	430	0.99

V^{p}_{NZS}: code specified shear strength for inside potential plastic hinge region.

V_{NZS}: code specified shear strength for outside potential plastic hinge region.

Table 5.12: Comparison of Maximum Experimental Shear Strength With the Code Values When Axial Tension is Applied

Unit	$\frac{P}{f_c'A_g}$	V_{exp} (kN)	V_s Eq.2.9 (kN)	V_c Eq.2.5 (kN)	V^{p}_{NZS} (kN)	$\frac{V_{exp}}{V^{p}_{NZS}}$	V_c Eq.2.6 (kN)	V_{NZS} (kN)	$\frac{V_{exp}}{V_{NZS}}$
7	0.05	235	111	0	111	2.12	49	160	1.47
8	0.1	179	121	0	121	1.48	0	121	1.48
9	0.2	136	133	0	133	1.02	0	133	1.02

V^{p}_{NZS}: code specified shear strength for inside potential plastic hinge region.

V_{NZS}: code specified shear strength for outside potential plastic hinge region.

In Table 5.12, the maximum experimental shear strengths obtained in the tension axial loading direction are compared with the shear strength given by the code[S14] equations. From Eq.2.8, it can be shown that the shear strength V_c of concrete contribution will be reduced to zero when the axial tension exceeds $0.083f_c'A_g$. For Units 8 and 9, with axial tension of $0.1f_c'A_g$ and $0.15f_c'A_g$, respectively, the concrete shear V_c is equal to zero and hence equations for inside and outside potential plastic hinge regions give the same shear strength. It is apparent in Table 5.12 that when the axial tension is less than $0.1f_c'A_g$, the code equations gave a very conservative prediction of the shear strength. For larger axial tension, such as for Unit 9, the predicted shear strength compares reasonably well with the experimental results.

Table 5.13: Comparisons of Shear Strengths at Different Imposed Displacement Ductility Levels When Axial Compression was Applied

Unit	$\frac{P}{f_c'A_g}$	At μ_n=2			At Failure			
		V_{exp} (kN)	$\frac{V_{exp}}{V_{NZS}}$	$\frac{V_{exp}}{V_{NZS}^P}$	V_{exp} (kN)	$\frac{V_{exp}}{V_{NZS}}$	$\frac{V_{exp}}{V_{NZS}^P}$	μ_n
7	0.1	310	1.03	2.80	252	0.84	2.27	4.0
8	0.2	365	0.98	1.14	316	0.85	0.99	2.5
9	0.3	427	0.99	1.03	367	0.85	0.88	4.0

V^P_{NZS}: code specified shear strength for inside potential plastic hinge region.

V_{NZS}: code specified shear strength for outside potential plastic hinge region.

The shear strengths predicted by the code equations are further compared with the shear strengths measured at different displacement ductility levels when the compression axial load was applied in Table 5.13. These values represent the degrading shear strengths corresponding to the imposed displacement ductility level. It will be seen in Table 5.13 that the calculated shear strengths are fairly close to the measured shear strengths at μ_n=2.0 for the three column units except that in Unit 7 the calculated shear strength for inside potential plastic hinge region is much less than the measured values at μ_n=2.0 and at failure, due to neglect of concrete component V_c in the code equations. At shear failure, however, the experimental shear strengths reduced to less than code specified values.

5.8.3 The American Concrete Institute Code ACI 318-89

The building code requirements for reinforced concrete of the American Concrete Institute ACI 318-89[A3] also adopts the additive equations for the shear strength of reinforced concrete column.

$$V_n = V_c + V_s \qquad (5.2)$$

The simplified expression for the shear strength carried by the concrete, V_c, for the gravity design load is as follow

$$V_c = \left(1+\frac{N}{14A_g}\right)\frac{\sqrt{f'_c}}{6}b_w d \qquad (5.3)$$

The shear strength provided by the transverse reinforcement perpendicular to axis of member takes the same form of Eq.2.9.

The shear strengths calculated using the American Concrete Institute code equations for the three columns tested are compared with the maximum experimental shear strengths in Table 5.14. The average strength ratio, V_{exp}/V_{ACI}, is 1.19, indicating the ACI equations conservatively predict the experiments.

Table 5.14: Comparisons of the Maximum Measured and Predicted Shear Strength

Unit	$\frac{P}{f'_c A_g}$	V_{exp} (kN)	V_{ACI} (kN)	$\frac{V_{exp}}{V_{ACI}}$	V_{Ang} (kN)	$\frac{V_{exp}}{V_{Ang}}$	$V_{Priestley}$ (kN)	$\frac{V_{exp}}{V_{Priestley}}$
su-1	0.1	328	267	1.23	443	0.74	453	0.72
su-2	0.2	392	326	1.20	560	0.70	553	0.71
su-3	0.3	428	376	1.14	658	0.65	618	0.69

5.8.4 Shear Strength Model By Ang et al[A7]

Based on their test results on circular reinforced concrete columns under cyclic loading and constant axial load, Ang et al[A7,A8] developed a degrading shear strength model for evaluating the shear strength of reinforced concrete columns. The method of the predictive equations was based on the additive principle, similar to code approach of Eq.2.4. The initial shear strength of the concrete

mechanisms is defined by

$$V_{ci} = 0.37\alpha\left(1+3\frac{P}{f'_c A_g}\right)\sqrt{f'_c}\ A_e \qquad (5.4)$$

where $\alpha=2/(M/VD) \geq 1.0$, in which M and V are the moment and shear at the critical section of the column, D is the overall section depth. The effective shear area is taken as $A_e=0.8A_g$.

The initial shear strength provided by the transverse reinforcement was based on a 45-deg truss mechanism, which for the rectangular columns has the same form as Eqn. 2.9.

The initial shear strengths predicted by Ang's model are included in Table 5.14. The predicted shear strengths for the three column units far exceeded the maximum experimental shear strengths, with an average ratio, V_{exp}/V_{Ang}, of 0.70. The application of the method proposed by Ang et al. to the rectangular columns was confirmed to be suspectable, since this predictive model for the shear strength was derived from the tests on circular columns.

5.8.5 Shear Strength Model By Priestley et al[P23]

The experimental results were compared with the initial shear strengths predicted by the model recently proposed by Priestley et al.[P23]. This model is a simplification to the method developed by Ang et al[A7] and was refined based on the assessment of a large number of test results both from rectangular and circular columns. In this method, the shear strength enhancement provided by axial compression is separated from the "concrete contribution" to the shear strength and considered to result from arch action(see Fig.5.28). The shear strength of the column is considered to consist of three independent components: a concrete component V_c, an axial load component V_p, and a truss component V_s. Thus

$$V = V_c + V_p + V_s \qquad (5.5)$$

The magnitude of concrete component is dependent on the flexural displacement ductility level. For both rectangular and circular column the initial shear strength is given by

$$V_c = 0.29\sqrt{f'_c}A_e \qquad (5.6)$$

where the effective shear area is taken as $A_e=0.8A_g$ for both circular and rectangular columns, A_g is gross section area. The enhancement of axial compression to the shear strength is taken to be the horizontal component of the diagonal compression strut, as shown in Fig.5.27 . Thus

$$V_p = P \tan\alpha = \frac{D-c}{2a} P \qquad (5.7)$$

where D is the overall section depth, c is the depth of the compression zone and a is height of the column. The contribution of transverse reinforcement to the shear strength is calculated based on a truss mechanism which recognizes that the observed inclination of critical diagonal cracks were smaller than 45-deg as conventionally used by various codes. An inclination angle of 30-deg to the column axis is assumed for the truss analogy. Both the initial and residual strength of truss mechanism are given by

$$V_s = \frac{A_v f_{yh} D'}{s_h} \cot 30 \qquad (5.8)$$

where D', is the distance between centres of the peripheral hoops. The predicted shear strengths for three column units are listed in Table 5.14.

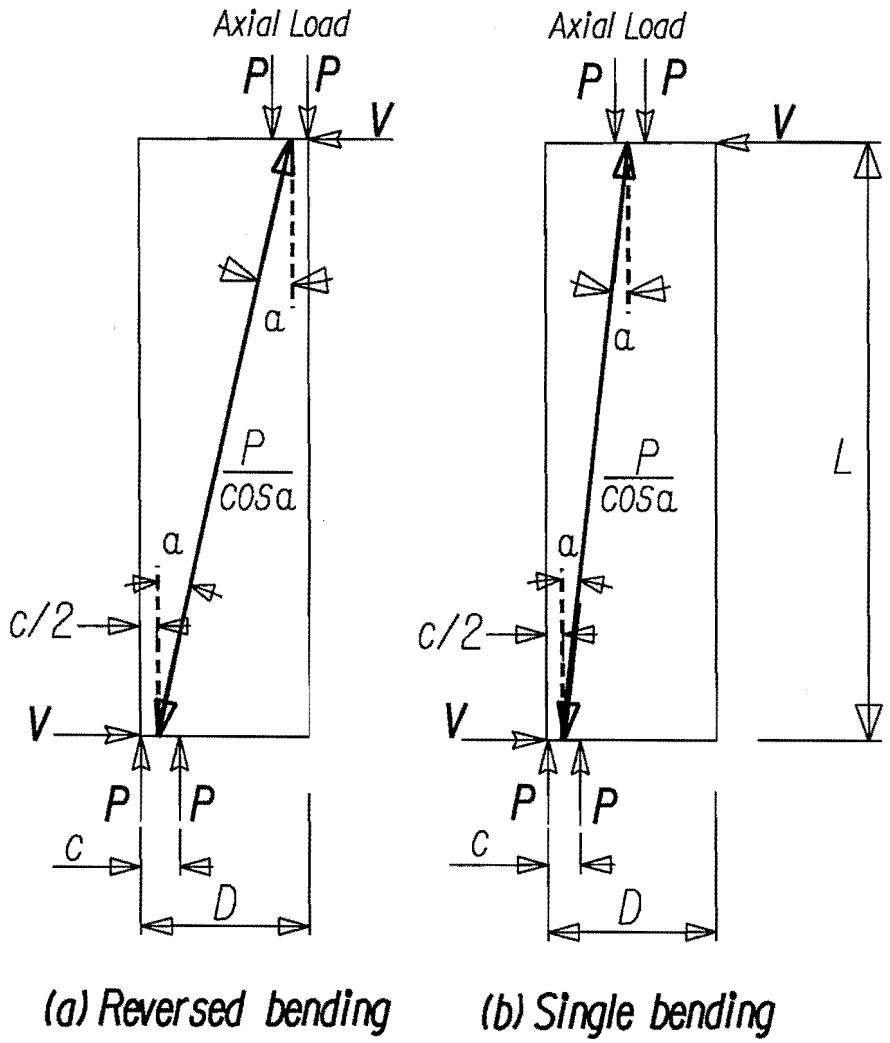

Fig.5.28: Contribution of Axial Force to Column Shear Strength According to Priestley[P23]

Priestley et al.[P23] reported that the ratio of the maximum experimental shear strength from tests on rectangular columns to the predicted shear strength by above equations was 1.041. However, the ratio of experimental shear strength from three column units to the shear strength predicted by above equations is 0.71 on average. This indicated that the shear strength of the columns under varying axial load was significantly reduced

5.9 DISPLACEMENT COMPONENTS

As discussed in the Section 3.9, the column deflection consisted of three deformation components, the deflection due to flexure, the deflection due to shear, and the deflection due to bar slip. The disposition of linear potentiometers on the column units presented in this Chapter, including vertical and diagonal gauges, enabled all these deflection components to be experimentally determined at various loading stages.

5.9.1 Deflection due to Flexure

The deflection due to flexure was determined as described in section 3.9.1 by Eq.3.15. The flexural deflection was calculated at each peak displacement ductility.

5.9.2 Deflection due to Bar Slip

Similarly, the component due to bar slip was obtained by Eq.3.16 at each peak displacement ductility.

5.9.3 Deflection due to Shear Distortion

It was expected that the shear deformation of the column would be significant for the three column units presented in this Chapter. Therefore, the three columns were instrumented to obtain the shear deformation. Six pairs of linear potentiometers were set to measure the diagonal displacement of the column panel, as shown in Fig.4.6 and 4.7b. Fig.5.29 shows the shape of the column panel before and after deformation. From the geometry of the column panel, the shear deformation of each column panel can be estimated as follows.

$$\gamma_i = \gamma_1 + \gamma_2 = \frac{\delta_1 - \delta_2}{2l_j}\left(\tan\alpha + \frac{1}{\tan}\alpha\right) \qquad (5.9)$$

where δ_1 and δ_2 are diagonal displacements of the column panel and were obtained from readings of diagonal potentiometers(they are taken as positive when diagonal length of the column panel elongated and as negative when it shorted), and l_j is the initial diagonal length of each column panel. The component of deflection due to shear is then calculated as follows:

$$\Delta_s = \sum \gamma_i h_i \qquad (5.10)$$

Having determined the deflections of each component, the total column deflection was then calculated by Eq.3.12. On the other hand, the deflection at the top of the column was measured directly by a displacement transducer placed at the tip of column. The accuracy of the method used here to calculate the deflection component can be found by comparing the deflections predicted by Eq.3.12 with the measured deflections.

The variations of deflection components with increasing displacement ductility factors are shown in Figs.5.30 to 5.32 for the three column units. The contribution of each component generally increased with increasing displacement ductility. The magnitude of the shear deformation under tension axial load was seen to be larger than that under compression axial load. A sudden increase in the shear deflection component, for example, at a nominal displacement ductility factor of μ_n =2.5 in the Unit 8, gave a good indication of shear failure of the column, since deterioration of the shear resisting mechanism resulted in significant shear deflection and shear sliding along the diagonal crack.

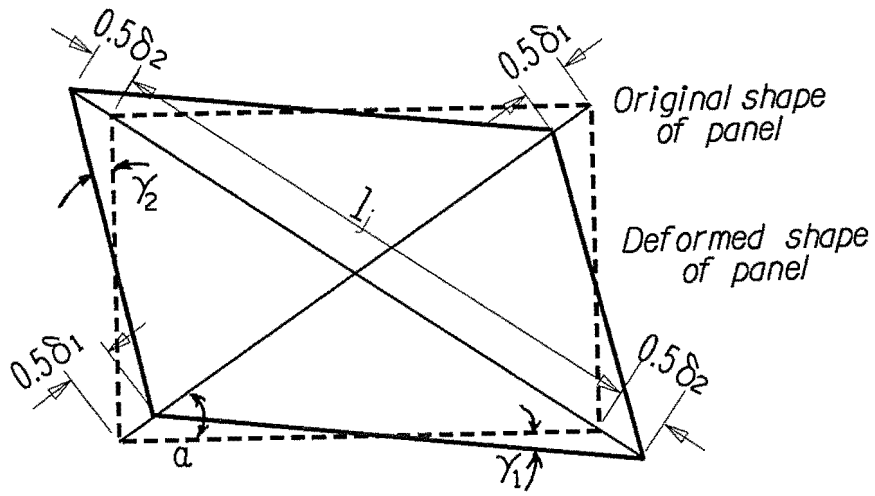

Fig.5.29: Shear Deformation of Column Panel

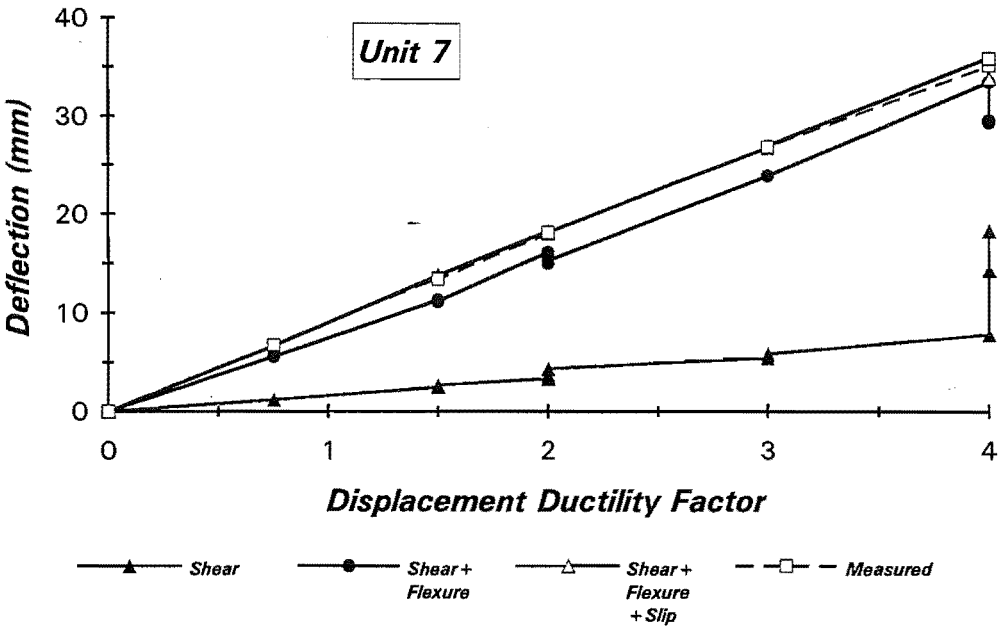

(a) Positive loading(compression axial load)

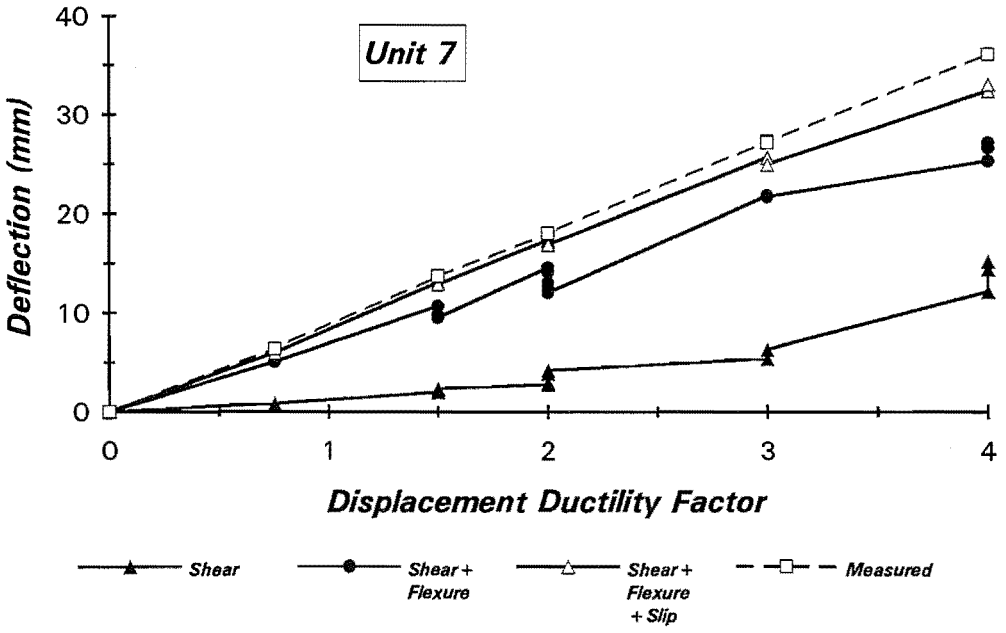

(b) Negative loading(tension axial load)

Fig.5.30: Deflection Components for Unit 7

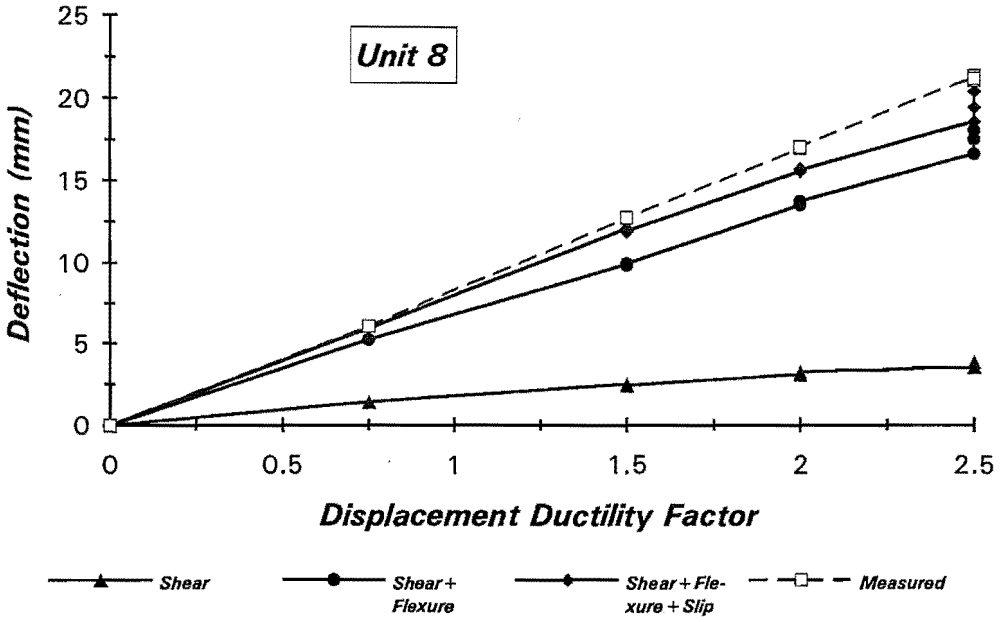

(a) Positive loading(compression axial load)

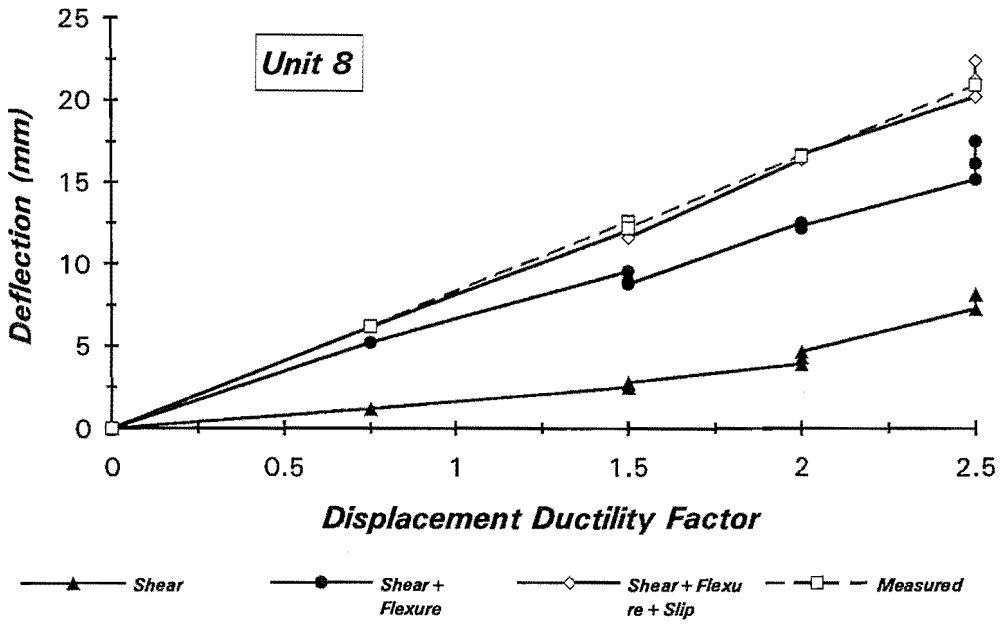

(b) Negative loading(tension axial load)

Fig.5.31: Deflection Components for Unit 8

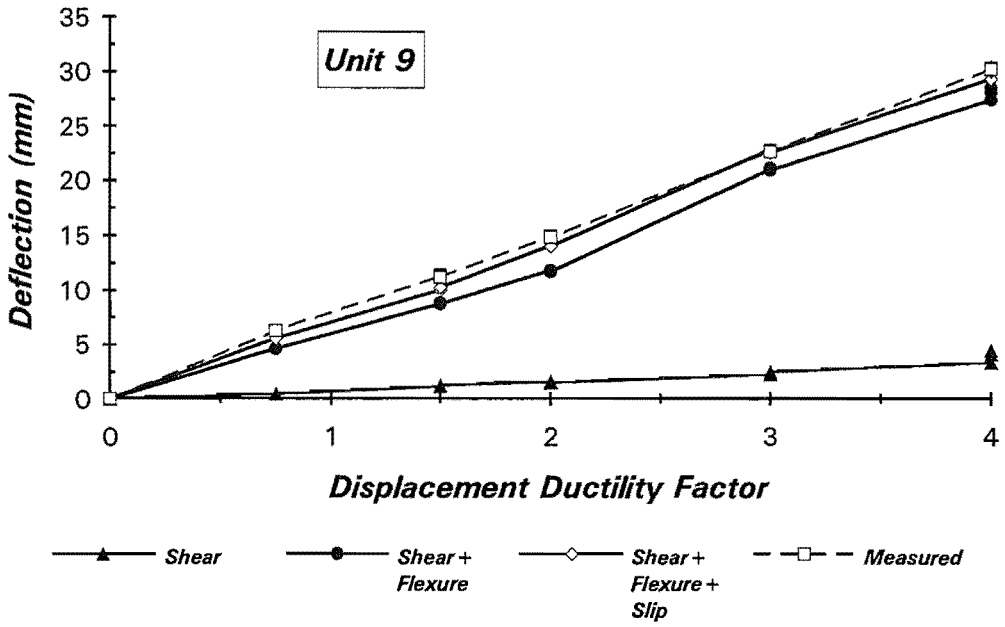

(a) Positive loading(compression axial load)

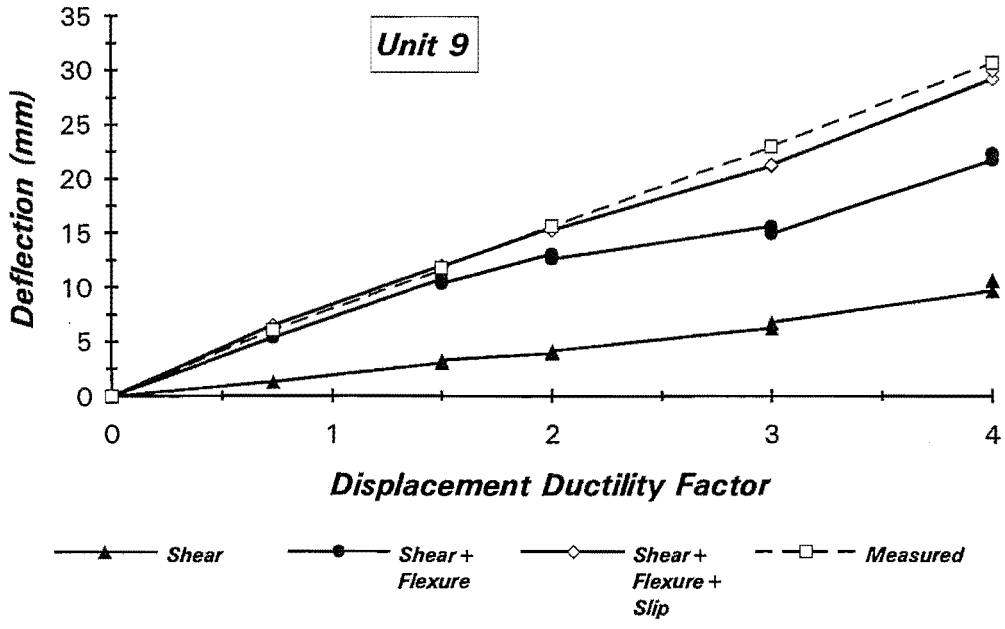

(b) Negative loading(tension axial load)

Fig.5.32: Deflection Components for Unit 9

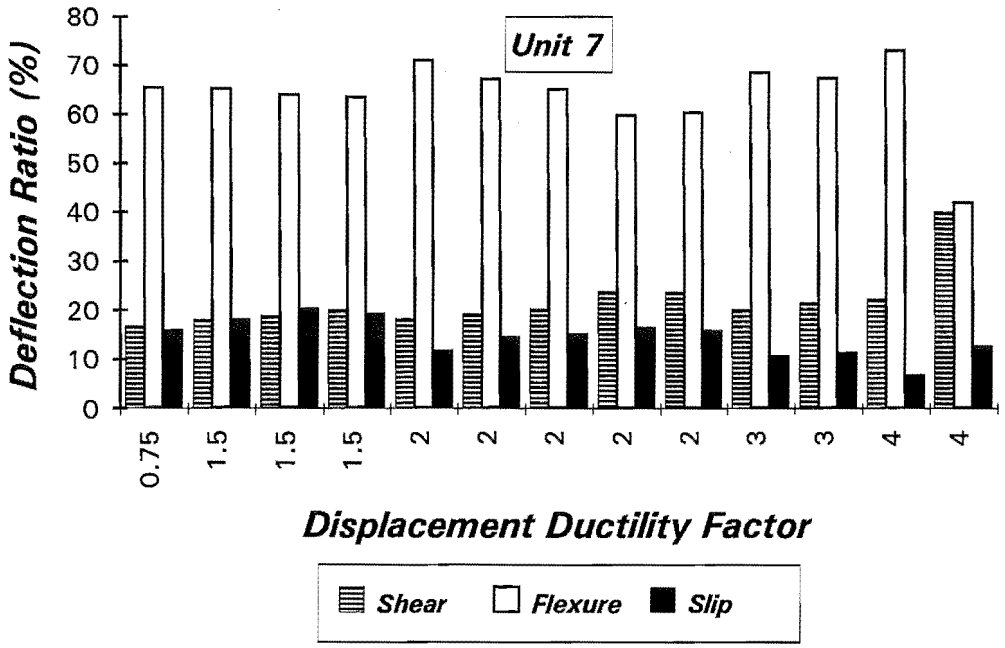

(a) Positive loading(compression axial load)

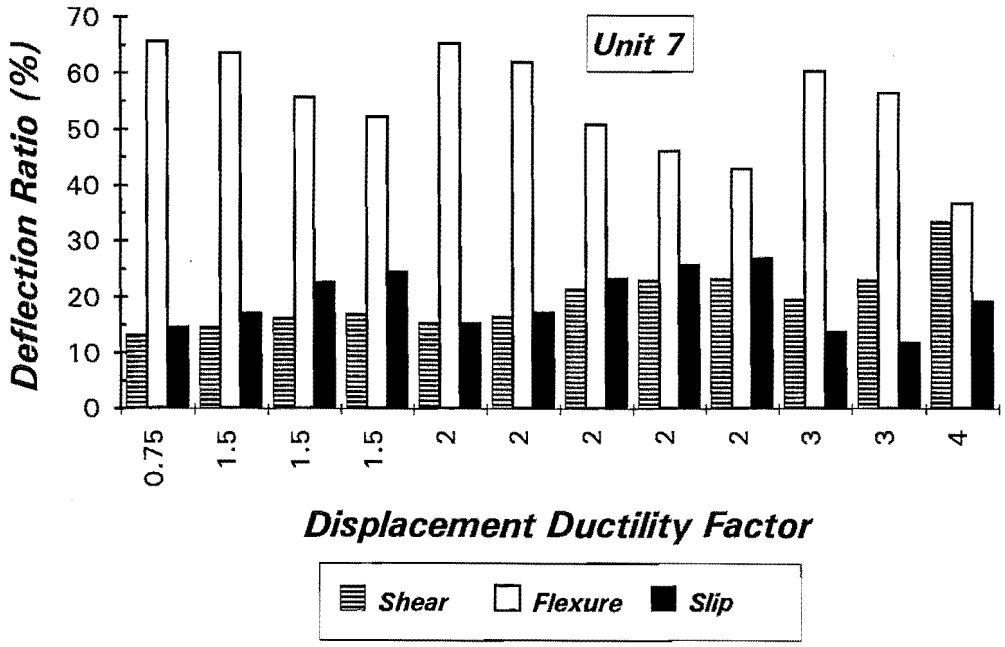

(b) Negative loading(tension axial load)

Fig.5.33: Deflection Components as Percentage of Total Deflection for Unit 7

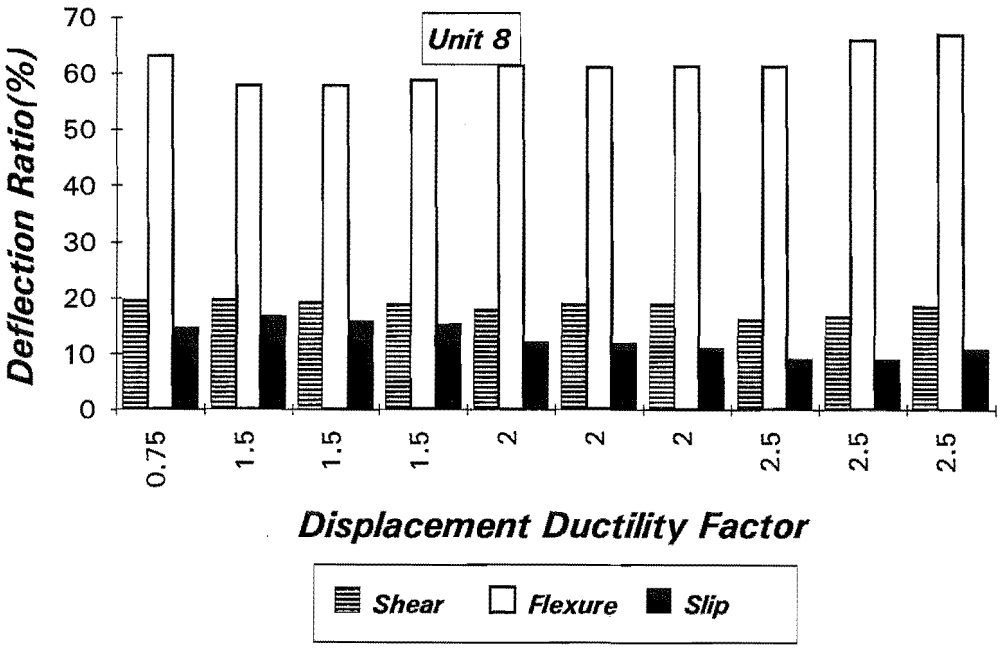

(a) Positive loading(compression axial load)

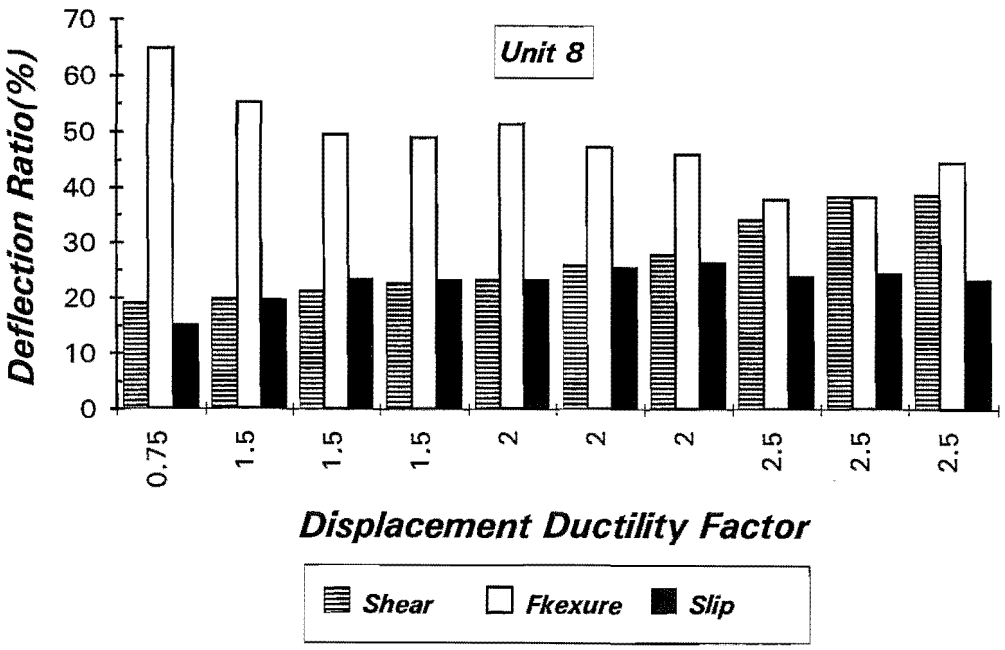

(b) Negative loading(tension axial load)

Fig.5.34: Deflection Components as Percentage of Total Deflection for Unit 8

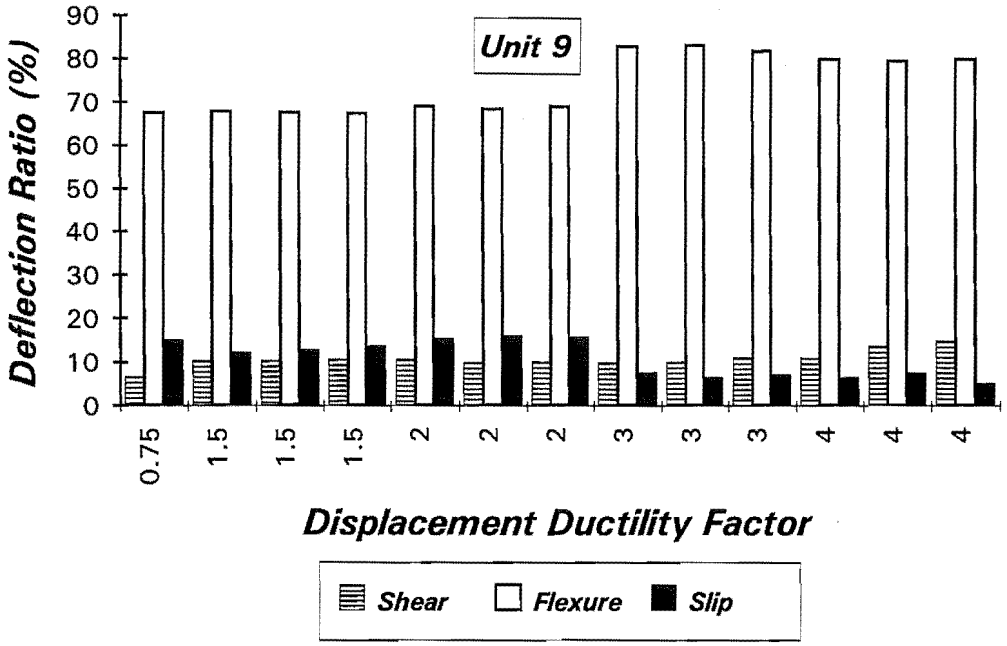

(a) Positive loading(compression axial load)

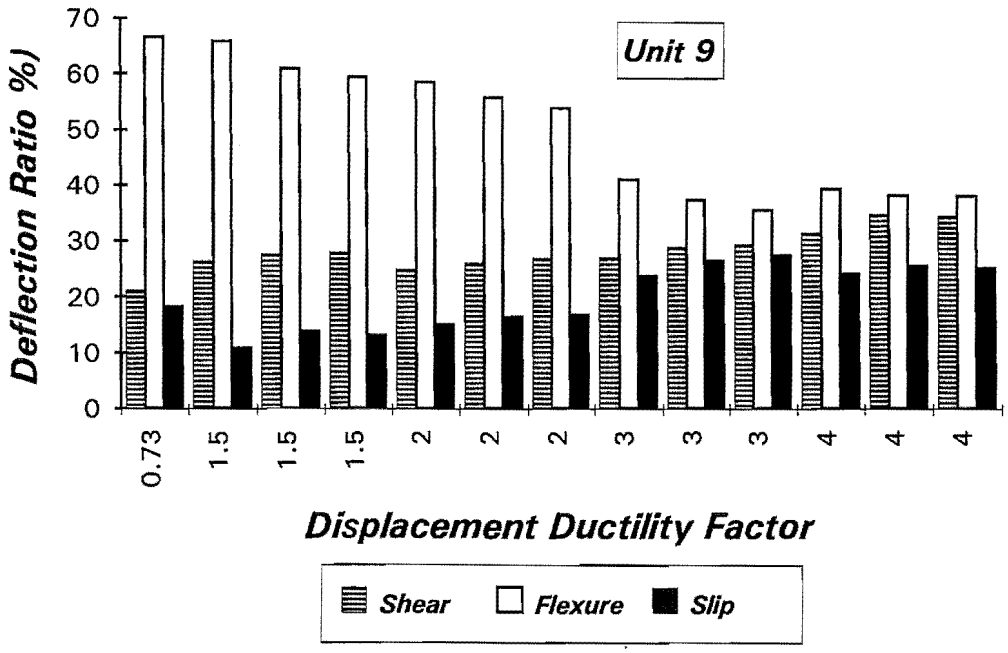

(b) Negative loading(tension axial load)

Fig.5.35: Deflection Components as Percentage of Total Deflection for Unit 9

The predicted column deflections from each component were compared with the measured column displacement in Fig.5.30 to 5.32. The discrepancy between the calculated and measured deflection is shown in these figures as the closure error. The agreement between the predicted column deflection and the measured deflection is seen to be fairly good. In general, the calculated deflection from Eq.3.12 is slightly smaller than the measured column deflection. The error was within 7%. This is probably because Eq.3.12 did not include the possible contribution of the deflection due to shear sliding. It was observed that shear sliding did occur, particularly after the formation of the main diagonal cracks. Another source of error would probably come from using the average curvature distribution over the gauge length in predicting flexural deflection, since the curvature distribution was non-linear after yielding.

The deflection components were further examined to assess the significance of each component of deflection. The ratios of the deflections due to shear, flexure and yielding extension of the longitudinal bars from column base to the measured column deflection were calculated and plotted against displacement ductility factors in Figs.5.33 to 5.35. They are shown separately for the positive and negative loading directions, respectively.

It can be seen that flexural deflection was initially the main source of the column deflection at low displacement ductility level. In the positive lateral loading direction, the ratio of flexural deflection remained relative stable until final loading stage. In the negative lateral loading direction, however, the ratio of deflection due to flexure decreased significantly with the increase in displacement ductility level.

Shear deflection was present as early as in the initial loading cycles. The shear deflection was up to 23% of the column deflection recorded for Unit 8 at μ_n=0.75. The shear deflections became more significant with the progression of the tests, particularly after the formation of main diagonal cracks. Shear deflections occurring in the negative loading direction were much higher than those occurring in positive loading direction, accounting for about 35% of the total deflection in the negative loading direction at the final stage of testing.

The deflection due to bar slip in the three column units appeared to be less significant, compared with those of the six column units presented in Chapter 2 and Chapter 3. The deflection due to bar slip accounted for about 15% of total deflection in the early stage of testing, and increased to about 25% before failure.

It has to be emphasized that Eq.6.2 calculates the shear deformation from change in length of the diagonals of column panel. It simulates the idealized shear deformation in the member subjected to pure shear stress. The use of Eqns.6.2 and 6.3 to obtain the shear deflection components could lead to errors, because the change in length of the diagonal of each column panel is also effected by sliding

shear and flexural bending. In a member with shear dominant behaviour, shear sliding along the critical diagonal cracks is significant, as observed during the tests. Fig.5.36 shows the shear deformation due to the effect of shear sliding along a diagonal crack crossing through the column panel.It was difficult to evaluate the shear sliding effect in the test, since is was dependent on the sliding displacement and the position of the diagonal crack. With regard the bending effects, Ma et al[M1] pointed out that shear deformations in the span of a short member are coupled with flexural deformations. Restrepo[R1] has quantatively demonstrated the shear deflection due to the effect of flexure in the beam-column subassembly. This effect may not so significant in columns, compared to the that caused by shear sliding.

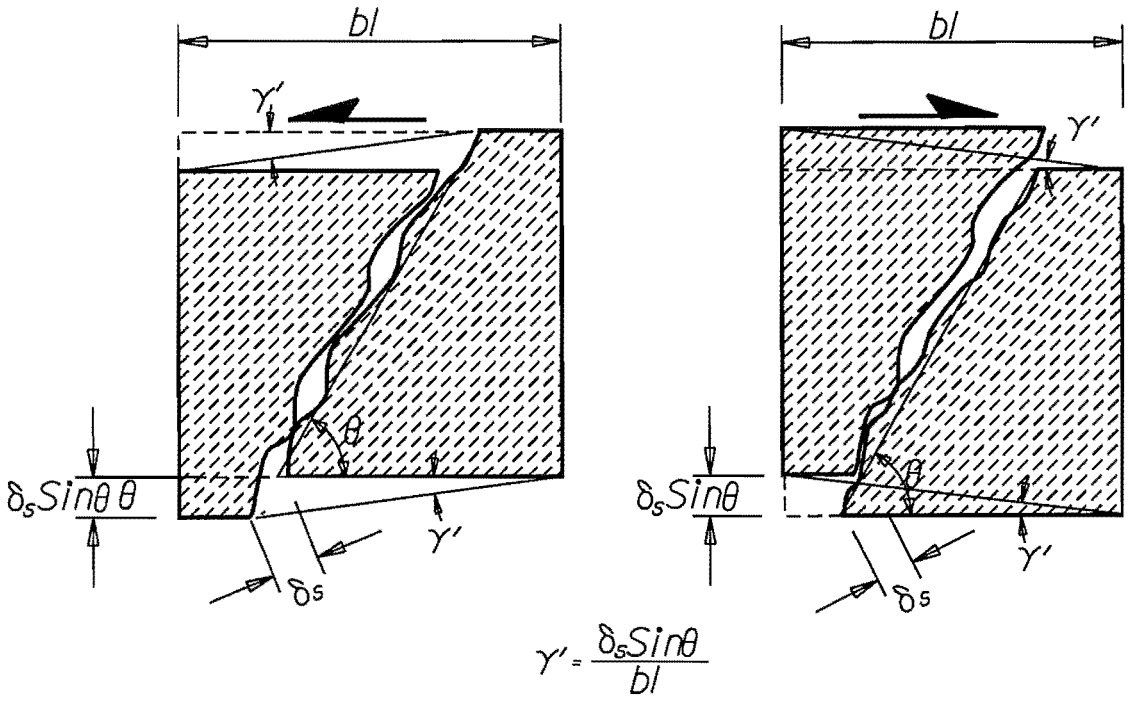

(a) Under compression axial load (b) Under tension axial load

Fig.5.36: Shear Deformation due to Sliding

5.10 CURVATURE DISTRIBUTIONS

The experimental curvatures at various locations for each column unit were calculated in the same manner as described in the Section 3.4. The average curvatures at discrete gauge level were plotted at the mid-point of each gauge length and straight line was drawn between the two successive points to obtain curvature distribution. The curvature distributions for the three column units are illustrated in

Figs.5.37 to 5.39. Also included in these figures are the experimental yield curvature, ϕ_y, which was calculated at the first potentiometer level(80 mm) corresponding to about 75% of ideal flexural strength, and when the column was subjected to a constant compression axial load.

It can be seen that the curvature distribution were unsymmetric with respect to the two loading directions for the three column units. This was expected because of unsymmetric actions induced from the variations in axial force applied in the two loading directions. In general, the magnitude of the curvature at each gauge level increased as the displacement ductility was increased. It was indicated in section 3.4 that, for flexural dominated column the experimental curvature at first gauge level was unproportionally larger than those at other gauge levels. Examination of Figs.5.37 to 5.39, however, indicates the curvatures at first gauge length for the three columns were almost proportionally increased, indicating the effect of bar slip was not significant. The magnitude of curvature in the end regions was greatly influenced by the axial load level. These figures also show that the regions where the plastic curvature occurred were within 300mm above the column base, indicating the flexural deformation was concentrated in these regions.

In the calculations of average curvature over the gauge length, it was assumed that plane sections remain plane after bending. That is, that steel rods passing through the section and supporting the potentiometers will remain straight. In some cases, however, this assumption could no longer be held due to the effect of wedging actions and led to abnormally of curvature distribution. For example in Unit 8, the calculated curvature at the third gauge length became negative during the positive loading

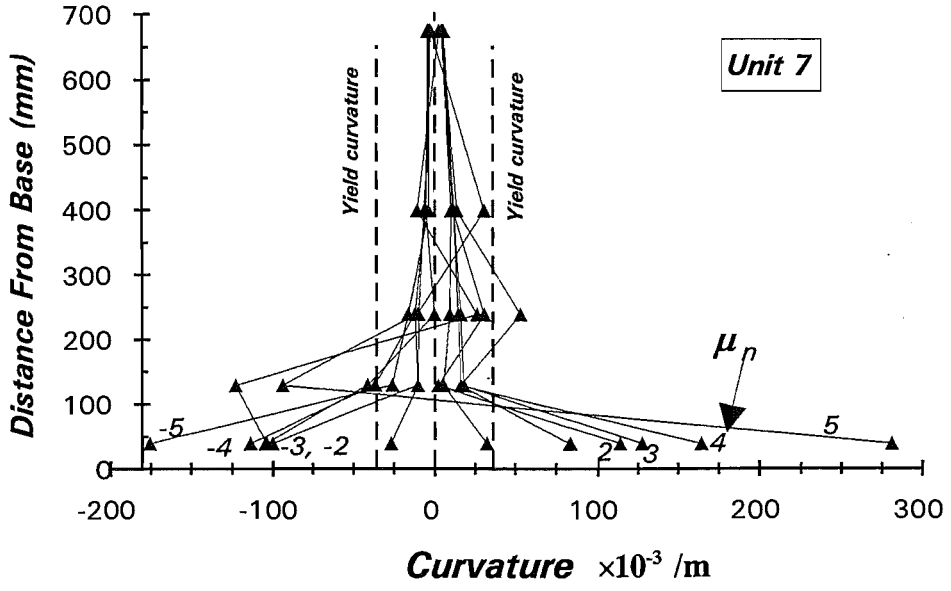

Fig.5.37: Curvature Distribution Versus Column Height for Unit 7

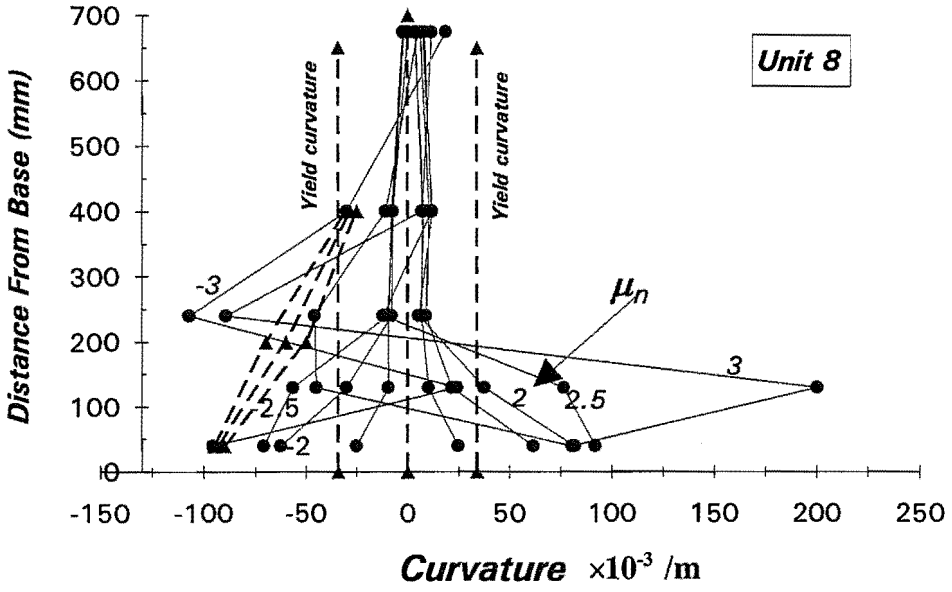

Fig.5.38: Curvature Distribution Versus Column Height for Unit 8

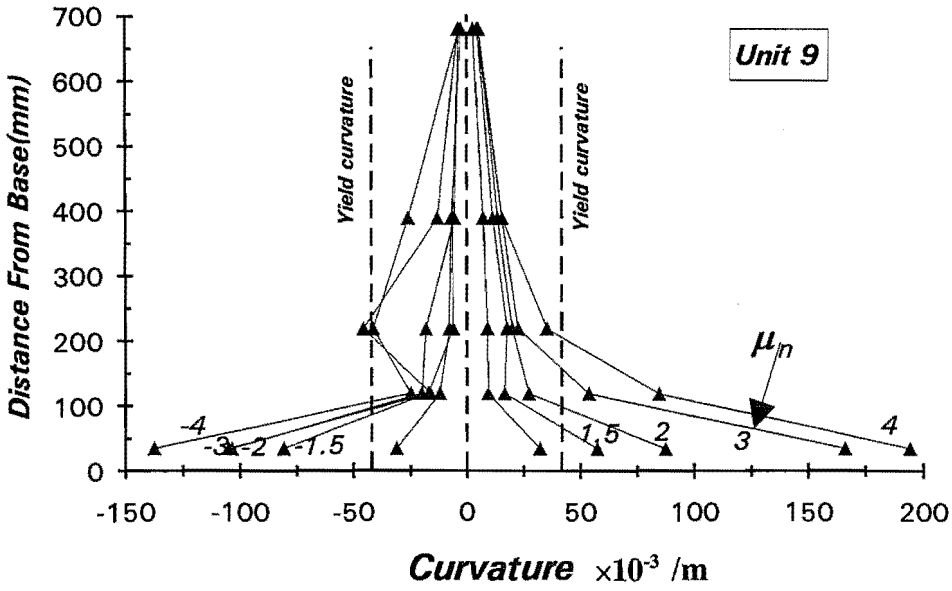

Fig.5.39: Curvature Distribution Versus Column Height for Unit 9

cycle at $\mu_n \geq 2$, while the curvature at the second gauge level was unproportionally large. This can be explained as follows. At high ductility level, it was observed that potentiometer rod at second gauge level were bent down at their west ends under the diagonal thrust due to shear and axial compression force. The readings of potentiometers at the second and third gauge level did not represent the actual deformation for each gauge length. In the positive loading action, the deformation at the second gauge level became very large and the deformation at the third gauge level became negative. However, if the average curvature was computed over two gauge length, reasonable results could be obtained. These values were shown in Fig.5.38, indicated by inclined dashed lines. For the same reason, the negative curvature at second gauge level and positive value at third gauge level occurred when the negative loading was applied.

A similar phenomenon took place in Unit 7. The potentiometer rods at the west end were slightly bent down at first gauge level at $\mu_n \geq 3$.

5.11 LONGITUDINAL STRAIN PROFILE OF CORE CONCRETE

From the measurements of the vertical potentiometers, the longitudinal compressive strains in the concrete core were calculated assuming a linear strain distribution over the section depth. The strain profiles, showing the measured longitudinal strains of the core concrete at outside of perimeter hoop and at the successive positive and negative loading peaks are illustrated in Figs.5.40 to 5.42. In these figures, tension strain is taken as positive and compression strain as negative.

The strain profiles for the three column units are seen to be unsymmetric for the east and west side of the columns. When the positive lateral loading was applied, the east side of the column was in tension and the west side was in compression. When the tension axial load was applied, most of the regions of the column sections were in tension, depending on the magnitude of applied tension axial load. Therefore, the compressive strain mainly took place in the west side of the column sections. The tension strains with large magnitude were recorded for the three column units and were more significant in the west side of the column.

The compressive strains of the core concrete in the east side of the column were negligible, except that at the first gauge level adjacent to the column base small compression strains were still observed because the compression zone could be maintained there under tension axial loading.

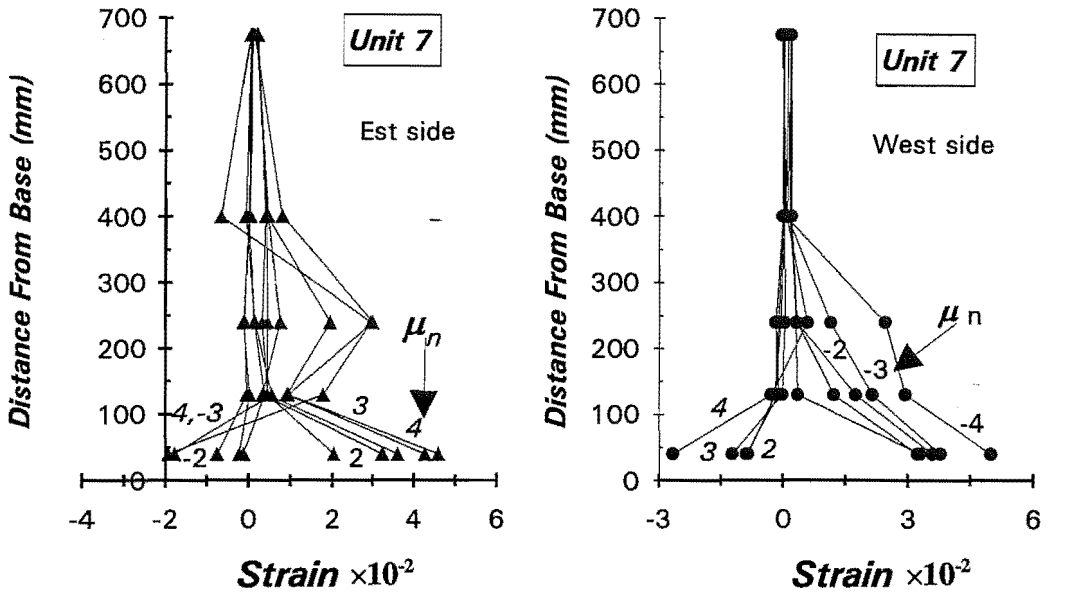

(a) At east side of section (b) At west side of section

Fig.5.40: Measured Concrete Compressive Strains of Core Concrete for Unit 7

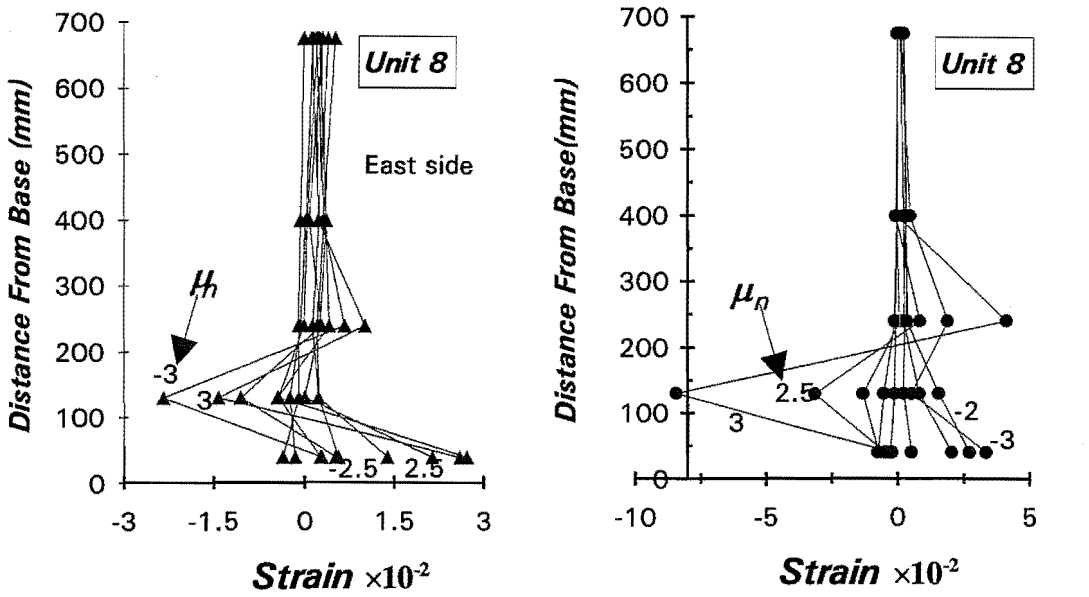

(a) At east side of section (b) At west side of section

Fig.5.41: Measured Concrete Compressive Strains of Core Concrete for Unit 8

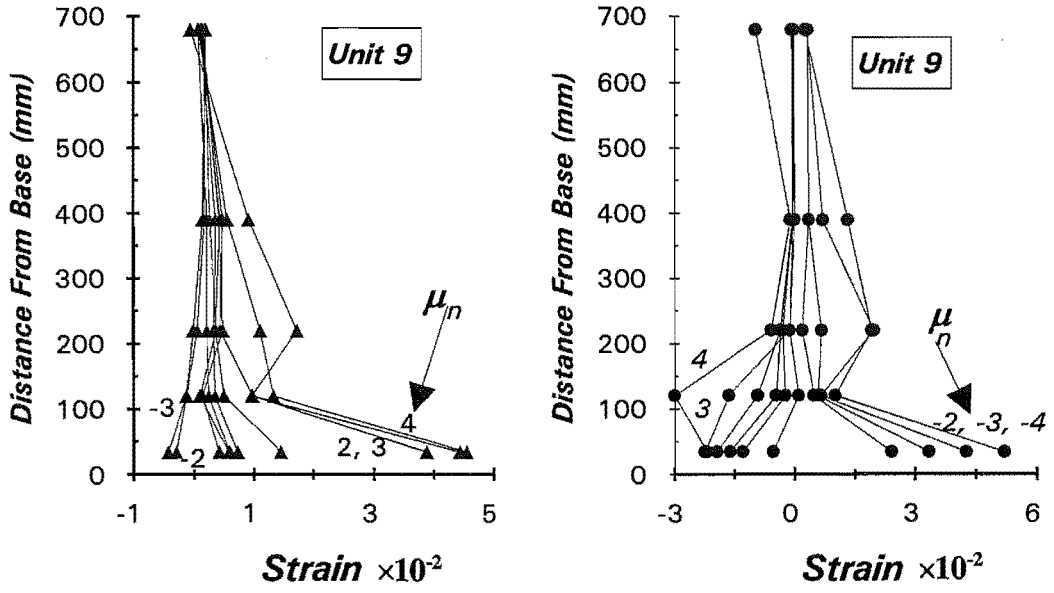

(a) At east side of section

(b) At west side of section

Fig.5.42: Measured Concrete Compressive Strains of Core Concrete for Unit 9

As indicated in the previous section, the steel rods which supported the potentiometers were bent at large inelastic displacements. The deformation measured from these potentiometers could not represent the average deformation of each gauge length for these loading cycles. This caused the abnormal distribution of concrete strains.

5.12 CONFINEMENT STRAIN PROFILES

The electric resistance strain gauges, which were attached on the square hoops perpendicular to the loading direction, were used to measure the strains mainly due to confinement of the core concrete. These strain gauges were only placed to the square hoops on the west side of the columns, as shown in Fig.4.8. When the positive lateral loading was applied, they were in the compression zone of the column while when negative loading was applied they were in tension zone. The east side of the column was in tension for both positive and negative loading, because of the application of the axial tension in the negative loading direction. Therefore, the strains due to confinement on the east side of the column were relative small. The vertical distributions of the hoop strains due to confinement along the column height are shown in Figs.5.43 to 5.45, in which the tension strain was taken as positive and compression strain as negative. The hoop yield strain is also shown in these figures.

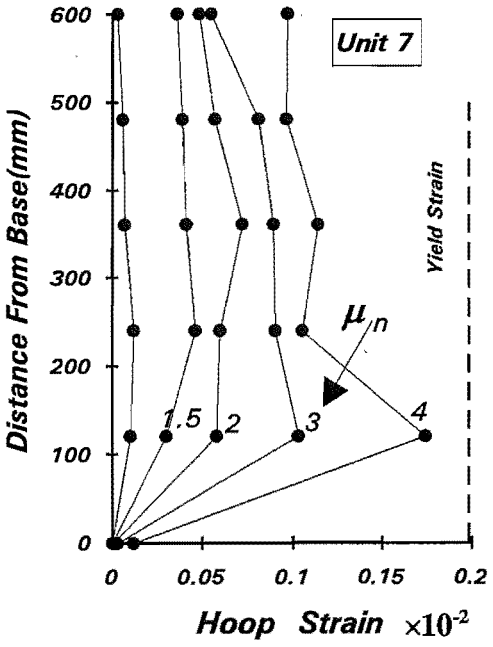

(a) Positive lateral loading

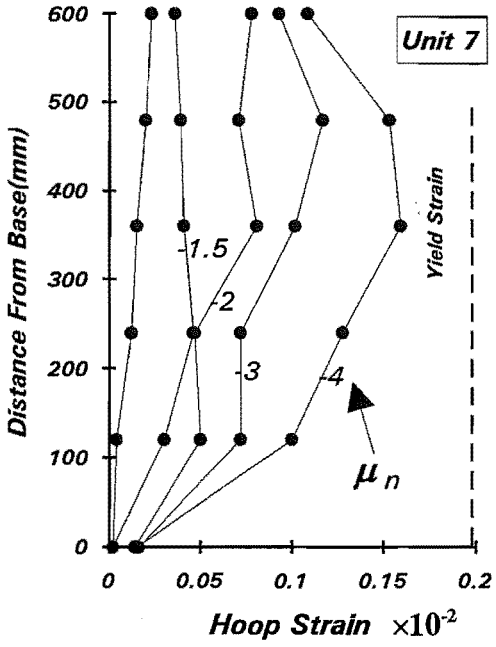

(b) Negative lateral loading

Fig.5.43: Measured Hoop Strains due to Confinement for Unit 7

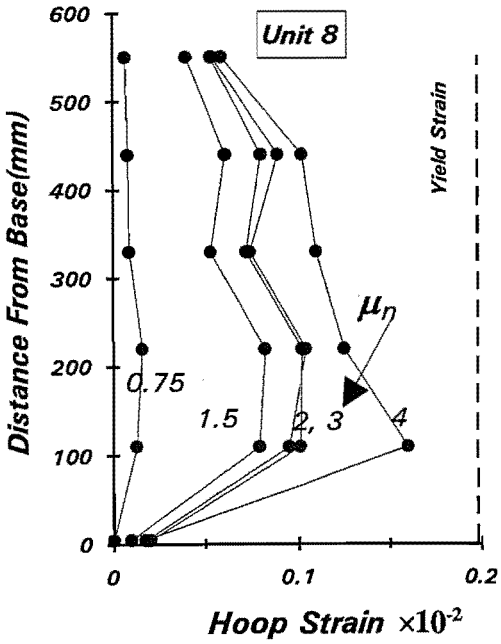

(a) Positive lateral loading

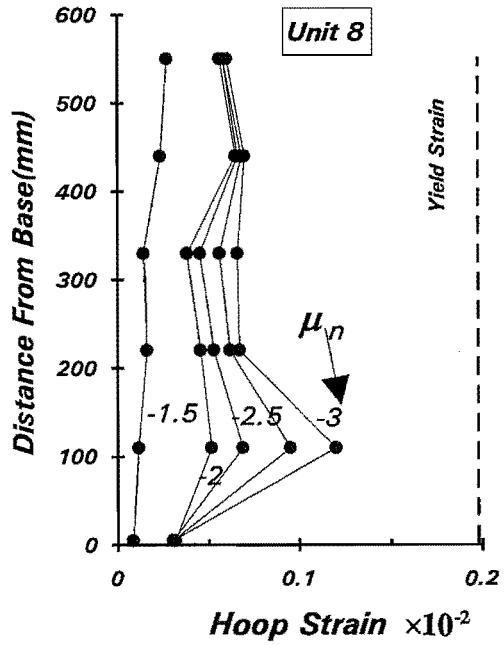

(b) Negative lateral loading

Fig.5.44: Measured Hoop Strains due to Confinement for Unit 8

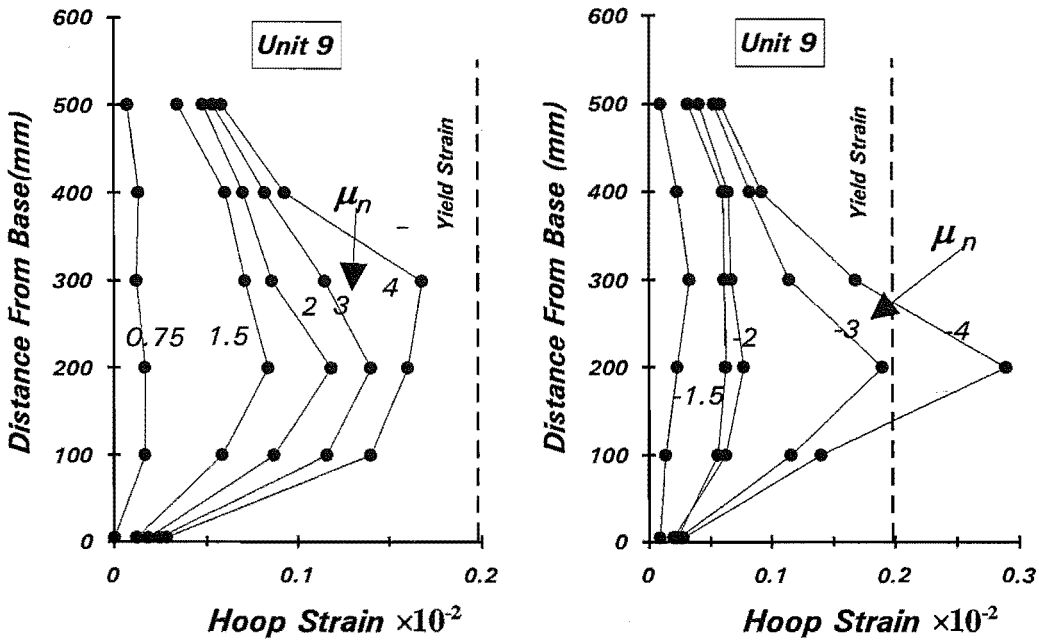

(a) Positive lateral loading

(b) Negative lateral loading

Fig.5.45: Measured Hoop Strains due to Confinement for Unit 9

The hoop strains due to the effect of confinement generally increased as the displacement ductility increased. All the strains remained within the elastic range in both loading directions, except that for Unit 9, the strain at the third level reached yielding in the negative loading direction at μ_n=4.

The hoop strains in the direction perpendicular to the loading direction are caused mainly by the passive confining stress due to expansion of compressed concrete. The presence of tension force significantly reduced the confinement hoop strains. Compared with those measured from the six columns tested presented in the Chapters 2 and 3, the confinement strains in the three column units presented in this chapter are much smaller.

5.13 STRAIN DISTRIBUTIONS IN THE LONGITUDINAL REINFORCEMENT

Figs.5.46 To 5.48 show the shear force versus strain in longitudinal bars in the end region of the columns. These figures are presented in pairs to show the strains on the longitudinal bars at symmetric

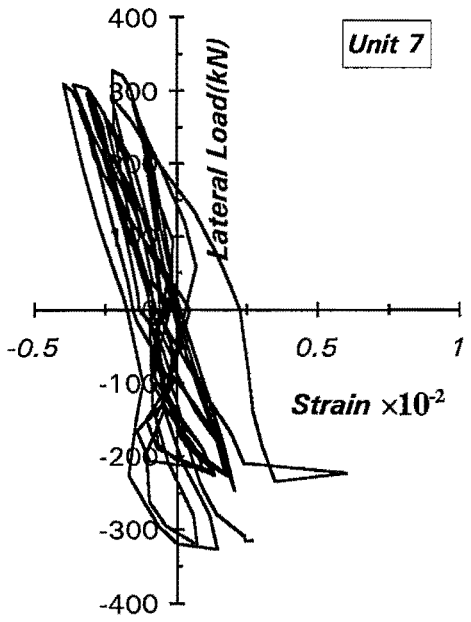

(a) West side 50mm above base

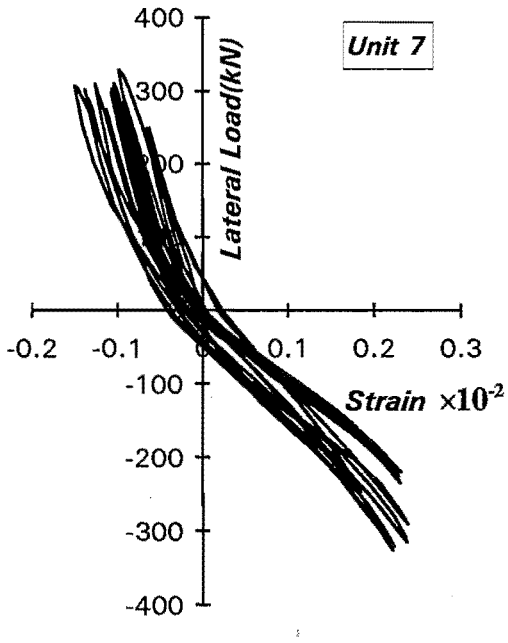

(b) West side 350mm above base

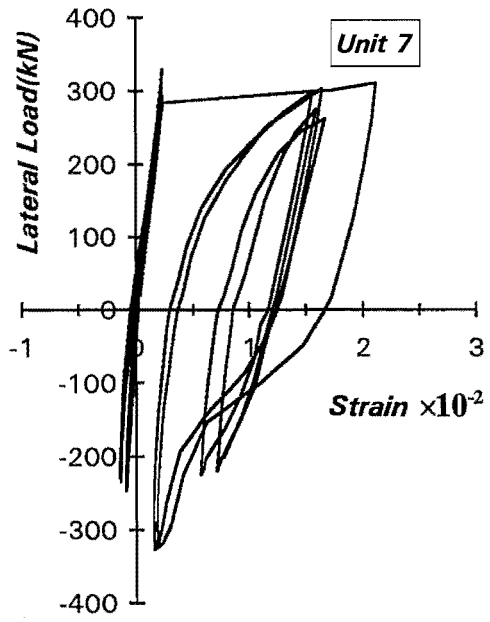

(a) Eest side 50mm above base

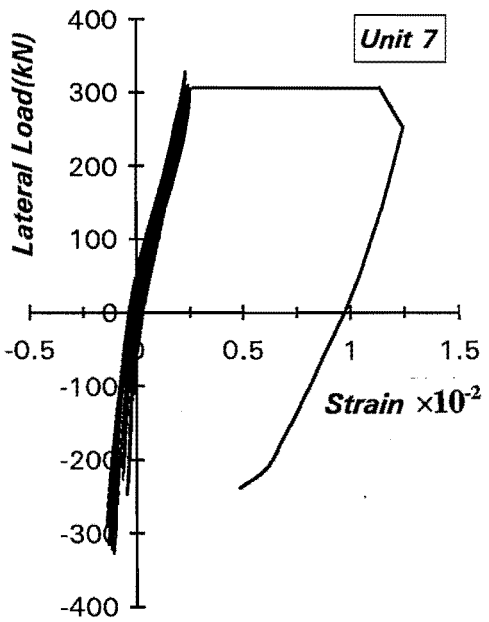

(b) Eest side 350mm above base

Fig.5.46: Longitudinal Bar Strain Histories for Unit 7

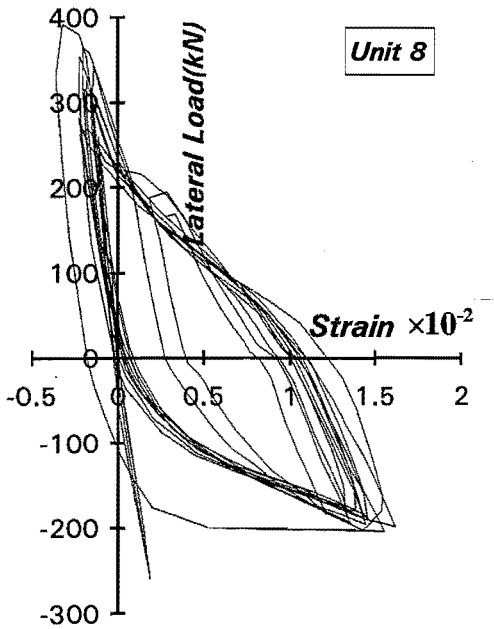

(a) West side 50mm above base

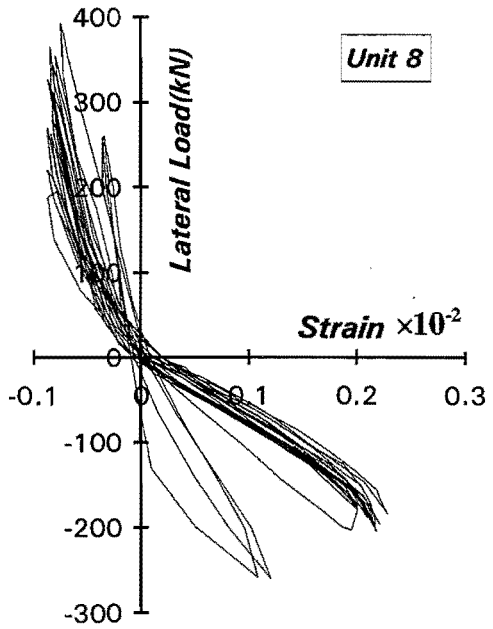

(b) West side 600mm above base

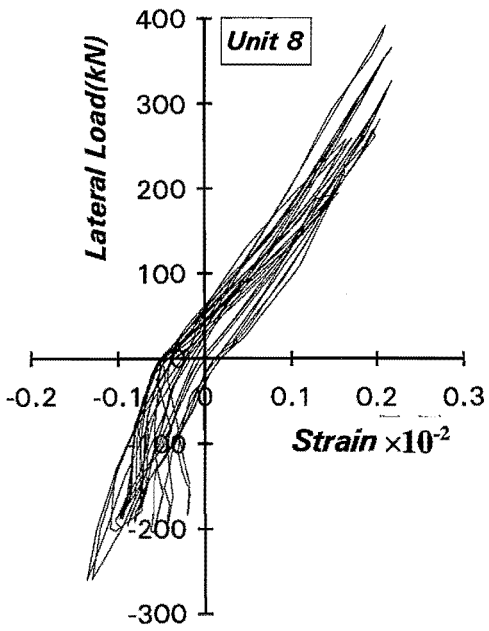

(a) Eest side 50mm above base

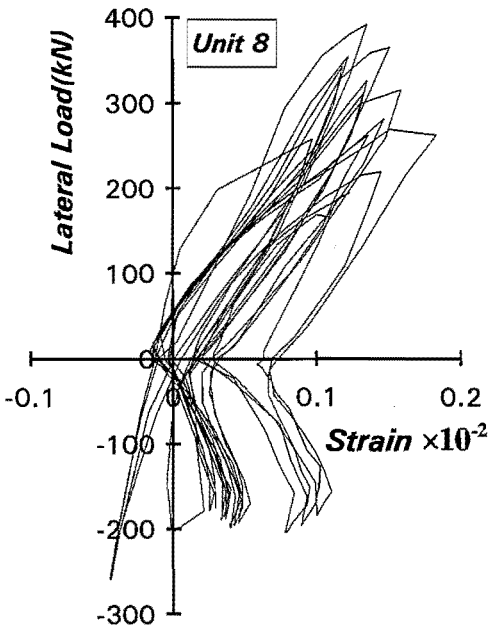

(b) Eest side 600mm above base

Fig.5.47: Longitudinal Bar Strain Histories for Unit 8

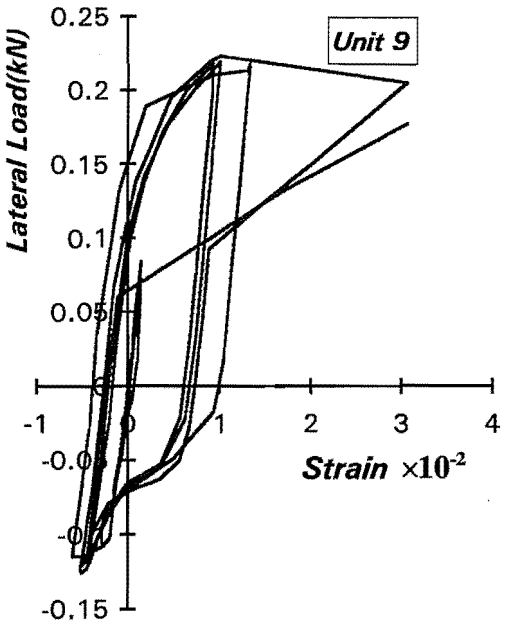

(a) West side 50mm above base

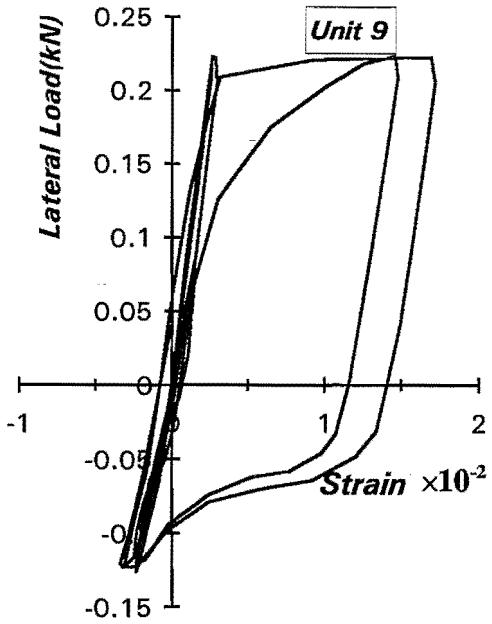

(b) West side 350mm above base

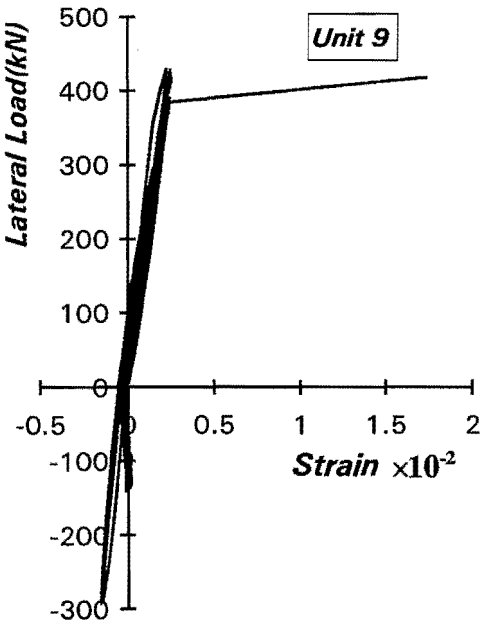

(a) Eest side 50mm above base

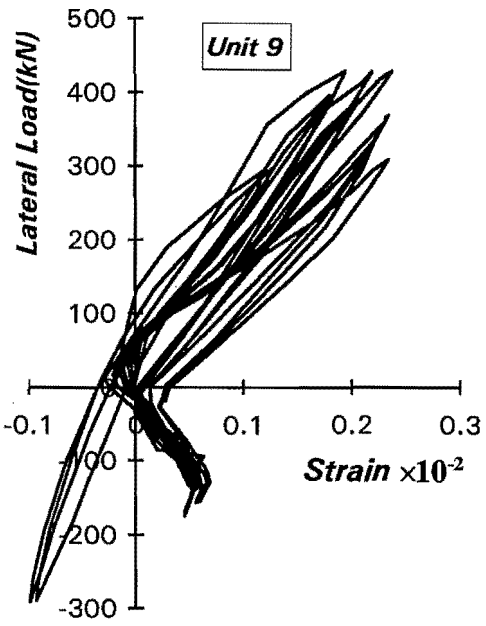

(b) Eest side 350mm above base

Fig.5.48: Longitudinal Bar Strain Histories for Unit 9

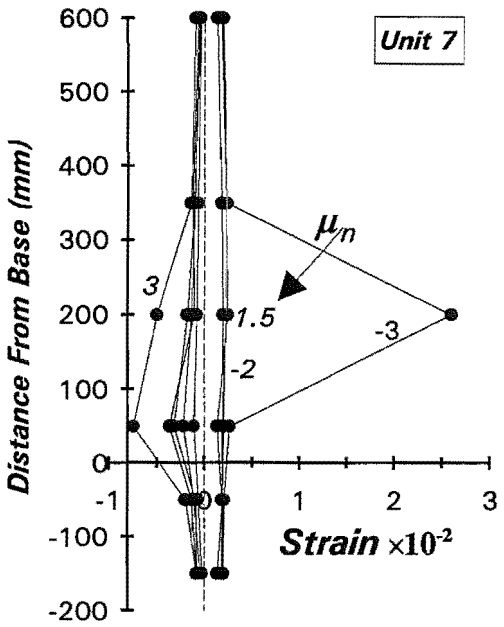

(a) West longitudinal bar

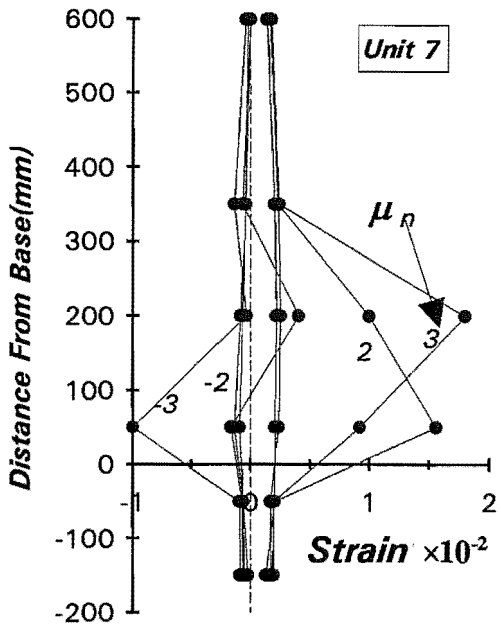

(b) East longitudinal bar

Fig.5.49: Distribution of Longitudinal Bar Strains for Unit 7

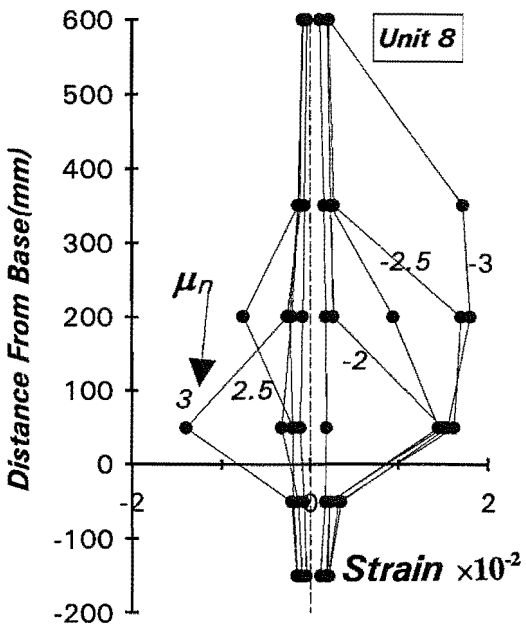

(a) West longitudinal bar

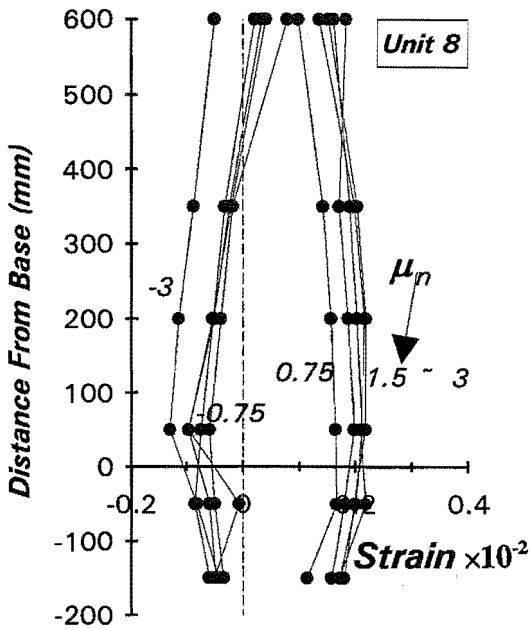

(b) East longitudinal bar

Fig.5.50: Distribution of Longitudinal Bar Strains for Unit 8

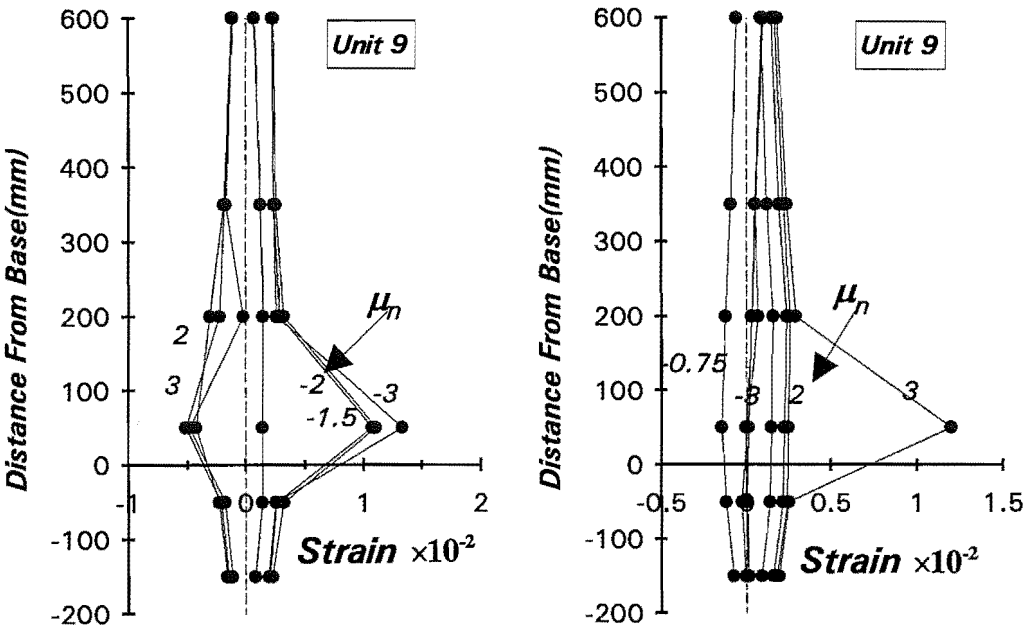

(a) West longitudinal bar

(b) East longitudinal bar

Fig.5.51: Distribution of Longitudinal Bar Strains for Unit 9

locations with respect to the section axis. Asymmetric shear force-longitudinal bar strain relations for the east and west longitudinal bars indicate the unsymmetric responses of the columns under alternating tension and compression axial load

The distribution of longitudinal bar strains along the column height are illustrated in Figs.5.49 to 5.51. The tension strains are taken as positive and compression as negative in these figures. The strain distributions are seen to be unsymmetric for the east and west side longitudinal bars. The longitudinal bars in the west side of the section yielded both in tension and compression. For the east longitudinal bars the compression strains only took place during the initial loading cycles. The longitudinal bars 50 mm below the column base in Units 7 and 8 yielded in tension. The yielding penetrated into 150 mm below the column base in Unit 9.

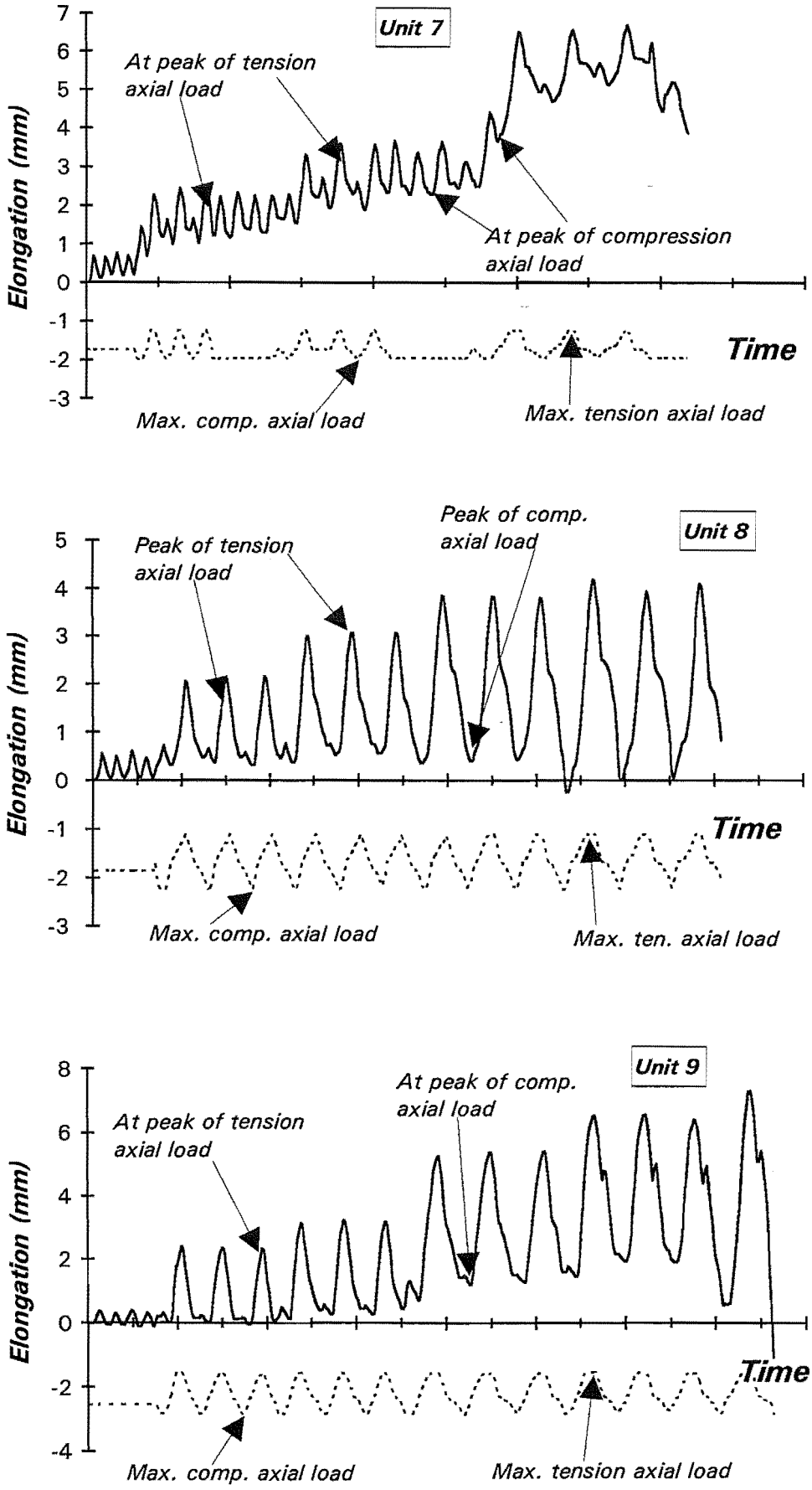

Fig.5.52: Column Elongation for Units 7, 8 and 9

5.14 ELONGATION OF THE COLUMN

The plots, showing the histories of the measured column elongations with scan number of the recorded data for the three column units are given in Fig.5.52 as full lines. The measured column elongations were calculated at the centre of the column section. Also included in the figure are the axial loading histories applied during the tests, shown as dashed lines. It can be seen from the figure that the patterns of column elongation for the three column units are very similar. They displayed a step-wise increase of column elongation with the increase in the displacement ductility. The presence of axial tension force induced large tension strains and hence resulted in significant elongation of the columns. As a result, the column elongations at each peak load in the negative lateral loading direction are much larger than those in the positive lateral loading direction. The elastic recovery of the column elongation was observed only in initial loading cycles. After the initial loading cycles, the column units elongated even at zero lateral load or zero displacement. This indicated the inelastic tension strains in the column were larger than the inelastic compression strains.

The effect of the compression axial load level on the column elongation can be found by comparing the elongations of the three column units at the peaks of load cycles.At the final stage of testing, the column elongation decreased significantly, indicating that buckling of the longitudinal bars was taking place.

5.14 CONCLUSIONS

Based on the experimental results of the three reinforced concrete columns subjected to cyclic flexure and varying axial loading, the following conclusions can be drawn.

1. Three reinforced concrete column units with the shear strengths calculated using code equations of NZS 3101:1982[S14] for outside potential plastic hinge regions of about 91, 96 and 104 percent of the shear force corresponding to the development of the ideal flexural strengths failed eventually in shear dominant modes and attained nominal displacement ductility factors of 4, 2.5 and 4.0 for Units 7, 8 and 9, respectively.

2. The test results indicated that varying axial load applied with cyclic flexure had a significant effect on the response of the reinforced concrete columns tested. Although direct comparison of the results with those of the columns tested under a constant applied compression axial load was not available in this study, it appears that a varying axial loading pattern will result in a more severe degradation in the shear strength. This was indicated by the formation of a major

diagonal crack and the deterioration of the concrete shear carrying capacity, since the axial tension load encouraged the opening and delayed the closure of the diagonal cracks due to large inelastic tension strains. The onset of the shear strength degradation for the three test columns took place in the compression loading direction, following the cycle immediately after the application of the tension axial load. The effect of tension axial load on the degradation of shear strength in the compression load direction is self evident.

3. The experimental results further confirmed the interaction between the shear strength and the imposed displacement ductility factors. The reduction in the shear strength was caused by the degradation of the concrete shear resisting mechanisms during reversed cyclic loading. The application of tension axial load accelerated the onset of degradation of the concrete contribution to the shear strength. No obvious trend of the rate of strength degradation related to the axial load intensity was found due to limited number of test specimens. The presence of tension axial force during the axial load variation reduced the shear strength of the column in the compression axial load direction, but little degradation in the shear carrying capacity was observed in the tension axial load direction.

4. The comparisons revealed that the current New Zealand concrete design code[S14] for the shear strength gave a conservative prediction for the peak shear force resisted by the concrete mechanisms at a displacement ductility factor of 1.5, even using design equation for outside potential plastic hinge regions. However, the shear carried by the concrete mechanisms rapidly degraded to less than the code specified shear strength for outside potential plastic hinge regions when the imposed displacement ductility factor exceed about 2. Neglect of the shear strength of the concrete contribution for columns with axial load of $0.1f'_cA_g$ or less in the code equations appears extremely conservative. It was found that a fairly large portion of the total shear was able to be transferred by the concrete mechanisms even under small tension axial force. None of the existing models is able to successfully predict the maximum experimental shear strength of the columns under varying axial loading. For example, the most recently developed model by Priestley et al. overestimated the shear strength of the test specimens, giving a ratio, $V_{exp}/V_{Priestley}$ of 0.71.

5. The truss mechanism was operative under both tension and compression axial load until failure of the column, provided no bond failure or anchorage failure occurred. Based on the current New Zealand code provisions using a 45-deg truss analogy, the shear carried by the transverse reinforcement was also found to be underestimated. That is because the measured angle of inclination to the column axis of the critical diagonal crack under compression axial load was smaller than 45-deg. The diagonal cracks became steeper when they propagated further into the compressed concrete zone. Even with the smaller tension axial load applied to Units 7 and 8 the observed angle was less than 45-deg.

6. The shear strength of the columns was closely associated with the axial load ratio and the transverse reinforcement content. An increase in compression axial load delayed the onset of diagonal cracking and hence increases the diagonal cracking load. Higher axial compression load also increases the shear stress carried by the concrete mechanisms. The rate of increase of the enhanced strength due to axial compression load became less as the axial load level increased. The transverse reinforcement content had little effect on the shear carrying capacity before diagonal cracking but it increased the shear strength of the column and improve the performance of the column during the post-yielding range.

7. Opening of the 135-deg end hooks of the transverse reinforcement was observed to take place in the three column units. The extension tails of these end hooks complied with the New Zealand code requirement and in some cases was slightly larger than code specified value. It is felt that code specified extension length of $8d_b$ for 135-deg end hook of plain round bars, especially for the hoops with small diameter, was insufficient to ensure reliable anchorage of transverse reinforcement when severe crushing and spalling of concrete is expected. A minimum extension length of 70mm from centre of the bent should be provided for the hoop with diameter $d_b \leq 10$mm.

Chapter 6

Shear Failure Mechanisms and Design Equations for Shear Strength

6.1 INTRODUCTION

this chapter considers the mechanisms of shear resistance and the factors affecting the shear strength of column. In particular, the effects of alternating tension and compression axial load on the shear resisting mechanisms are studied. On the basis of experimental results proposals are made for predicting shear strength of reinforced concrete column of ductility and limited ductility.

6.2 SHEAR FAILURE MECHANISMS

6.2.1 Modes of Shear Failure

Test column Units 7, 8 and 9 of the second series all experienced significant inelastic deformation prior to significant strength degradation and failed in shear. Physically, the shear failure was indicated by significant diagonal cracking. The column displayed different failure mechanism. Three failure modes

were observed during the testing, a shear-flexure failure, a diagonal-tension failure, and a shear-compression failure. The failure modes are related to the magnitude of axial forces , the shear span to section depth ratio and the amount of transverse reinforcement.

(a) Shear-Flexure Failure

A shear-flexure failure mechanism is initiated by the yielding of the longitudinal reinforcement due to flexure. The column then develops inclined diagonal tension cracks which stabilize and further shear force can be sustained before failure. The failure is associated with crushing of concrete in the compressed region, preceded by yielding of transverse reinforcement.

The failure of the Unit 7 was characteristic of a shear-flexure failure. The first diagonal crack occurred at a lateral displacement of 4.18mm and widened significantly at a displacement of 13.57mm(nominal displacement ductility factor of $\mu_n=1.5$) when a hoop at the middle height of the column reached yield. At a lateral displacement of 26.8mm(nominal displacement ductility factor of $\mu_n=3.0$), all transverse reinforcement crossing the critical diagonal crack had reached yield. Failure was reached when the concrete crushed at a displacement of 35.2mm(nominal displacement ductility factor of $\mu_n=4.0$ and a rotation angle of about 1/30)(see Fig.6.1). The rotation angle here is defined as the lateral displacement at the tip of the column divided by the height of the column.

(b) Diagonal-Tension Failure

A diagonal-tension failure is characterized by a sudden propagation of the critical diagonal crack. Once the diagonal cracking commences, the hoop strains increase drastically since the hoops are unable to restrain the opening of the diagonal cracks. The shear resisting mechanism becomes unstable and inclined crack propagates through the compression zone causing failure of the column.

The Unit 8 failed in a diagonal-tension mode. The diagonal crack was significant at a lateral displacement of 16.9mm(nominal displacement ductility factor of $\mu_n=2.0$, and rotation angle of 1/60) associated with the yielding of nearly all hoops crossing the main diagonal crack. The critical diagonal crack propagated through the compression zone at a displacement of 21.3mm($\mu_n=2.5$ and rotation angle of about 1/50) and formed a clear cut tension crack(see Fig.6.2), resulting in the failure of the column. Little crushing of core concrete occurred but there was minor spalling of cover at the failure.

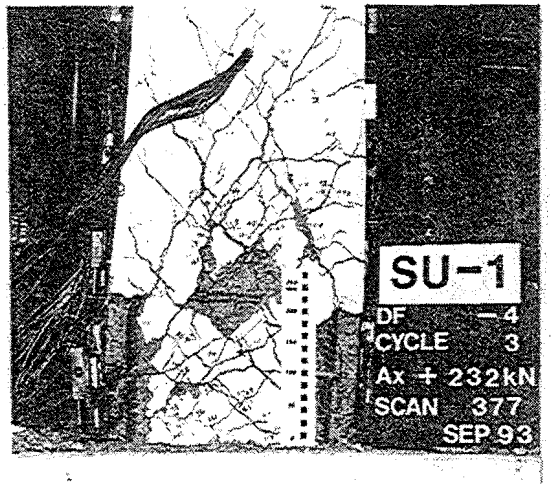

(a) at μ_n= -4.0, south face

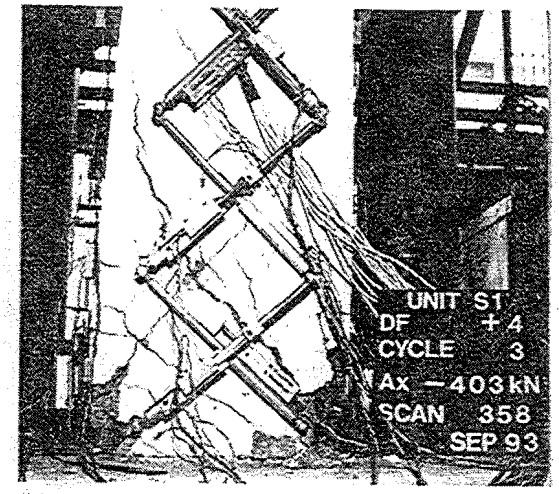

(b) at μ_n= 4.0, north face

Fig.6.1: Shear Failure Mode for Unit 7

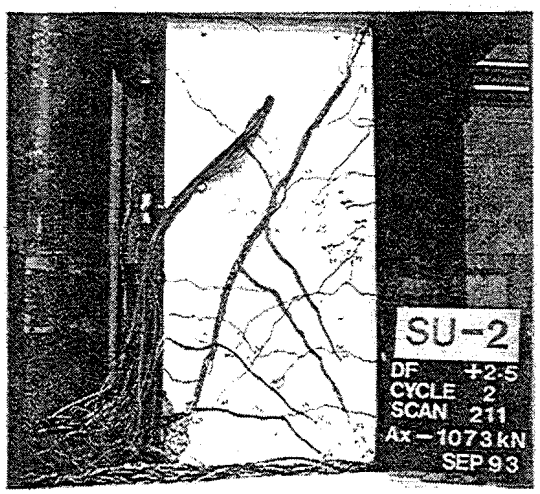

(a) at μ_n= 2.5

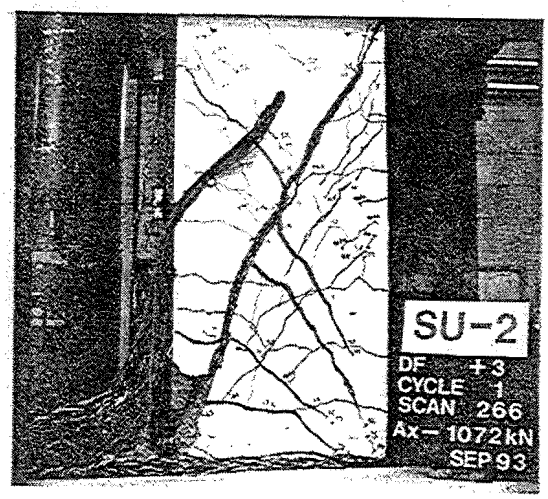

(b) at μ_n= 3.0, north face

Fig.6.2: Shear Failure Mode for Unit 8

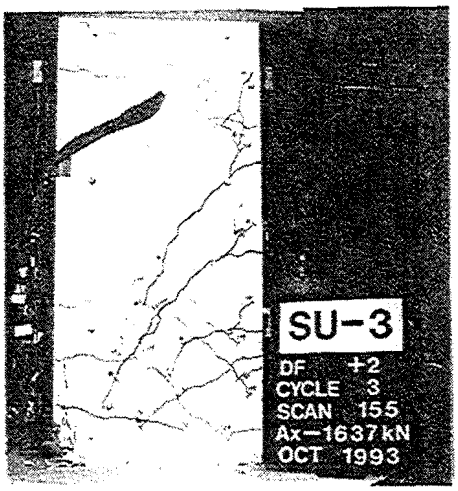

(a) at μ_n= 2.0

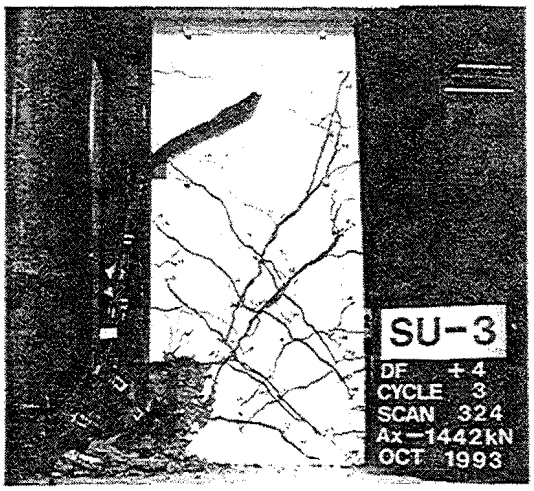

(b) at μ_n= 4.0

Fig.6.3: Shear Failure Mode for Unit 9

Note: *The specimen numbers, SU-1, SU-2 and SU-3 which were used in the tests for the three column units are referred to as Unit 7, Unit 8 and Unit 9 in this thesis, respectively.*

(c) Shear-Compression Failure

Shear-compression failure is characterised by the crushing or diagonal splitting of concrete, following the yielding of transverse reinforcement. The inclined crack is evident but the compression strut is stable with further loading cycles.

Unit 9 failed in a shear-compression mode. The main diagonal cracks became evident and extended over two-thirds of the section depth with yielding of transverse reinforcement occurring at a lateral displacement of 15.7mm(nominal displacement ductility factor of μ_n=2.0 and rotation angle of 1/64). The diagonal cracks stabilized until a lateral displacement of 22.8mm(nominal displacement ductility factor of μ_n=3.0 and rotation angle of 1/44). The column failed at a lateral displacement of 30.5mm(nominal displacement ductility factor of μ_n=4.0 and rotation angle of about 1/33), at which stage serious crushing of compressed concrete occurred accompanied by significant distress along the critical diagonal crack(see Fig.6.3).

6.2.2 The Effect of Axial Load on the Shear Failure Mechanisms

In a reinforced concrete beam with relative large shear span ratio and without web reinforcement, the beam may fail immediately at the diagonal cracking load. Fenwick and Paulay[F3] found that there exists a critical shear span depth ratio, a/d, which separates the beams that fail at diagonal cracking from those that may sustain further shear forces after diagonal cracking, where a = shear span length and d = effective section depth. They suggested that this critical shear span ratio a/d be in the range of 2 to 3 for the beams without web reinforcement and may be larger for the beams with higher transverse reinforcement content. Russo[R3] used an analytical model to demonstrate that the critical a/d ratio was dependent on the longitudinal reinforcement content and concrete compressive strength.

In a reinforced concrete column with usual(current) amount of transverse reinforcement, it is unlikely that the column would fail at the diagonal cracking load. The formation of a diagonal crack results in a change in the shear resisting mechanisms. That is, the shear previously carried by the uncracked concrete is now carried by the transverse reinforcement, aggregate interlock and dowel action. The shear failure mode can be identified by the stage at which yielding of transverse reinforcement occurs, which depends on the amount of transverse reinforcement provided. Furthermore, the magnitude of axial force applied has a significant effect on the failure model of the column. The three column units tested were identical in geometric shape(aspect ratio M/VD=2.5) and had the same longitudinal reinforcement content(2.36%). The variations in the transverse reinforcement content were not significant(volumetric ratio of 0.47 to 0.57, see Table 4.1). Hence the difference in the failure modes of the three column units must have been due to the difference in the applied compression axial load

level. The failure mode changed from shear-flexure to diagonal-tension to shear-compression failure as the compression axial load increased.

From an examination of the equilibrium and compatibility conditions in the shear span of the columns, it was found that the change in failure mode is related to the ratio of the axial force, P, to the shear force, V, applied. There appeared to exist some dependence of the inclination of the critical diagonal crack on the ratio, P/V, which determines the direction of the thrust line of the external actions. Fig.6.4 shows the effect of axial load ratio on the shear transfer mechanism of the three column units. It is to be noted that for the column subjected to a constant axial load, the angle of the resultant of lateral load

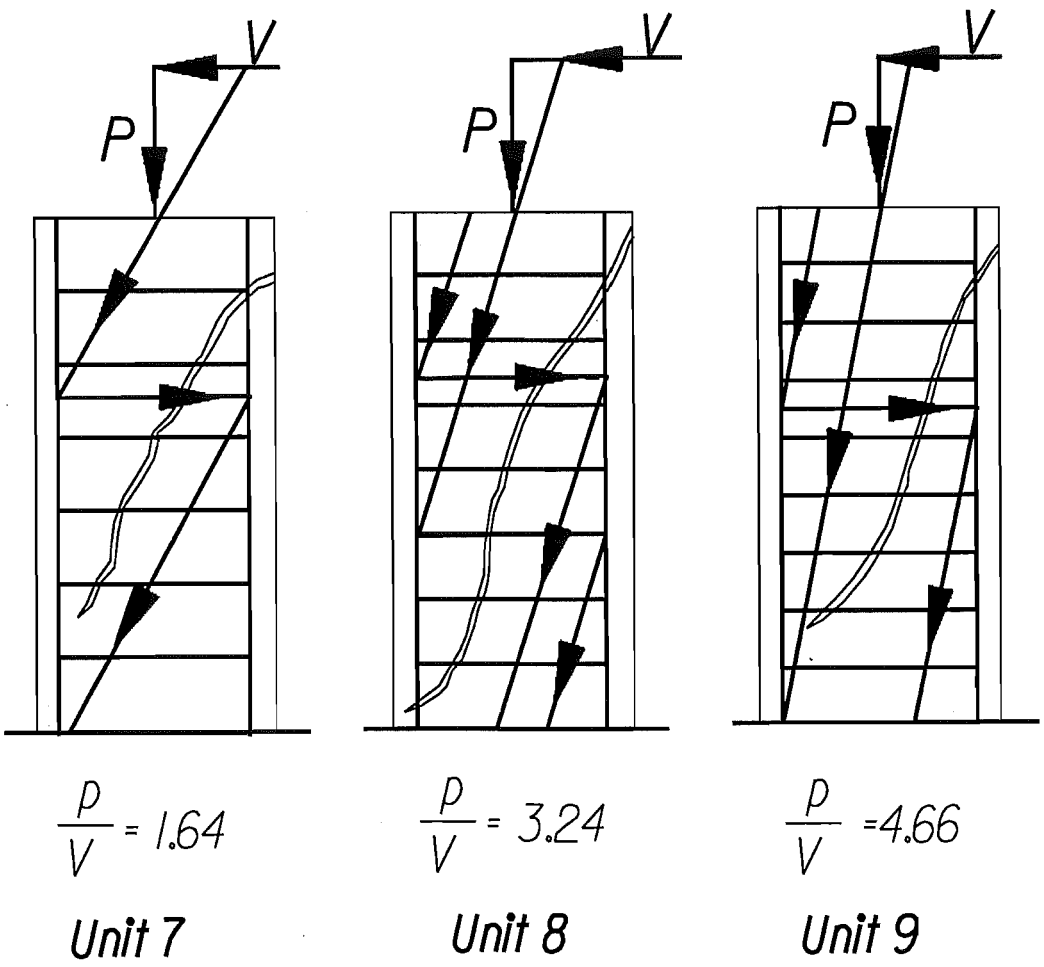

Fig.6.4: Effect of Axial Load on Shear Transfer Mechanisms

and axial load varies as the lateral load increases. The direction of the thrust line in the three column units is unchanged during the compression axial loading cycle, because the applied axial load was in direct proportion to the lateral load. It can be seen in Fig.6.4 that as the maximum axial compression level increases the line of thrust becomes steeper. The critical diagonal crack formed under the compression strut band.

When the axial compression load is low, the thrust can not be transferred to the base block by a straight path. The diagonal forces have to be transferred through the tension ties(hoops) to the next diagonal strut. In this case, the beam mechanism governs. The failure is controlled by the tension capacity of transverse reinforcement along the critical diagonal crack. The formation of the main diagonal crack requires greater participation of transverse reinforcement in the shear transfer, which results in a sudden increase in the hoop strains. The inclined strut then becomes unstable and inclined cracks propagate through the compression zone after yielding of the transverse reinforcement, resulting in diagonal tension failure. An increase in the axial compression load up to the balanced point also increases the flexural capacity and so reduces the possibility of flexural failure.

When the ratio P/V is high, the thrust line is able to reach directly to the column base, forming an arch mechanism(see Fig.6.4). Direct shear transfer through the arch mechanism alone becomes possible. As the shear span to the section depth ratio is small diagonal cracks may also form but do not extend deeply. However, the inclined strut is stable even after yielding of transverse reinforcement since a high compression axial load requires a large compression depth and hence a small rotation angle at the diagonal cracking load. The failure is controlled by the crushing or vertical splitting of the compressed concrete. A shear-compression failure will most likely take place if $P/V > 2h/d$, where h/d is column aspect ratio. When $P/V < 2h/d$, the column could fail in either a diagonal-tension or shear-compression mode, depending on the transverse reinforcement content.

6.3 SOME ASPECTS INFLUENCING THE SHEAR BEHAVIOUR OF REINFORCED CONCRETE COLUMN

6.3.1 Effect of Compression Axial Load

The magnitude of column axial load has an important influence on the performance of a reinforced concrete column. It effects the initial stiffness, the flexural strength and the shear strength, as well as the deformation capacity of the column. The column failure mode can be changed by change in

compression axial load level.

Due to the combined effects of lateral force and axial load, the concrete in the column is subjected to a multiaxial state of stress. Flexural or flexure-shear cracking occurs when the principal tensile stress exceeds the tensile strength of the concrete. Before the onset of diagonal cracking, the shear stress is mainly resisted by the concrete. The presence of compression axial load will reduce the principal tensile stress and delay the cracking. The normal stress induced by the axial compression force also increases the ultimate value of the shear stress[B1]. This allows a larger shear force to be transferred across the section before the principal tensile stress reaches the value at the first cracking. The observed lateral force when diagonal cracking first occurs is obviously increased with increase in compression axial load level, as shown in Fig.5.25. The increase in lateral load at diagonal cracking appears to be in proportion to the compression axial load level. Fig.6.5 shows the variations of the ratios of experimental column flexural rigidity to gross section flexural rigidity with axial load level. It is evident that the higher compression axial load increases the flexural rigidity of the column before diagonal cracking.

After diagonal cracking occurs, the tensile stress that was carried by the concrete is mainly carried by the longitudinal reinforcement. The presence of compression axial load enhances the shear strength of the column. Since a higher compression axial load requires a larger compression depth of the section, the shear transferred by the compressed concrete increases due to increased area of uncracked concrete. It can be seen in Fig.6.4 that arch action becomes more significant as the compression axial force increases. More shear force can be transmitted through arch action. The compression axial load also restrains the opening of diagonal cracks and this improves the interlock capacity of concrete. As shown in Fig.5.26, the maximum experimental lateral load increases with increase in compression axial load level. The maximum compressive axial load applied to these test columns is below or near the balanced point axial load level. It has to be emphasized that the rate of enhanced shear resistance due to axial compression will change as axial load level increases. At low axial loads the shear strength is enhanced by the increased arch action. At high axial loads, however, shear compression failure is expected and the shear strength is governed by the ultimate capacity of compressed concrete. Then increase in compression axial load can no longer increase the shear strength.

The maximum lateral load was reached for all three columns at nominal displacement ductility factors of $\mu_n=1.5$, when the corresponding rotation angles were 1.35, 1.26 and 0.93%(or 1/74, 1/80, 1/107), for Units 7, 8 and 9, respectively. These values indicate that an increase in compression axial load reduces the deflection at which the maximum shear strength of the column is reached. The shear deformation when the maximum shear strength was reached accounted for about 17% of the total deflection for Unit 7, 22% for Unit 8, and only 12% for Unit 9. The larger shear deformation of Unit 8 was associated with more extensive shear cracking and deterioration of stiffness at that loading stage.

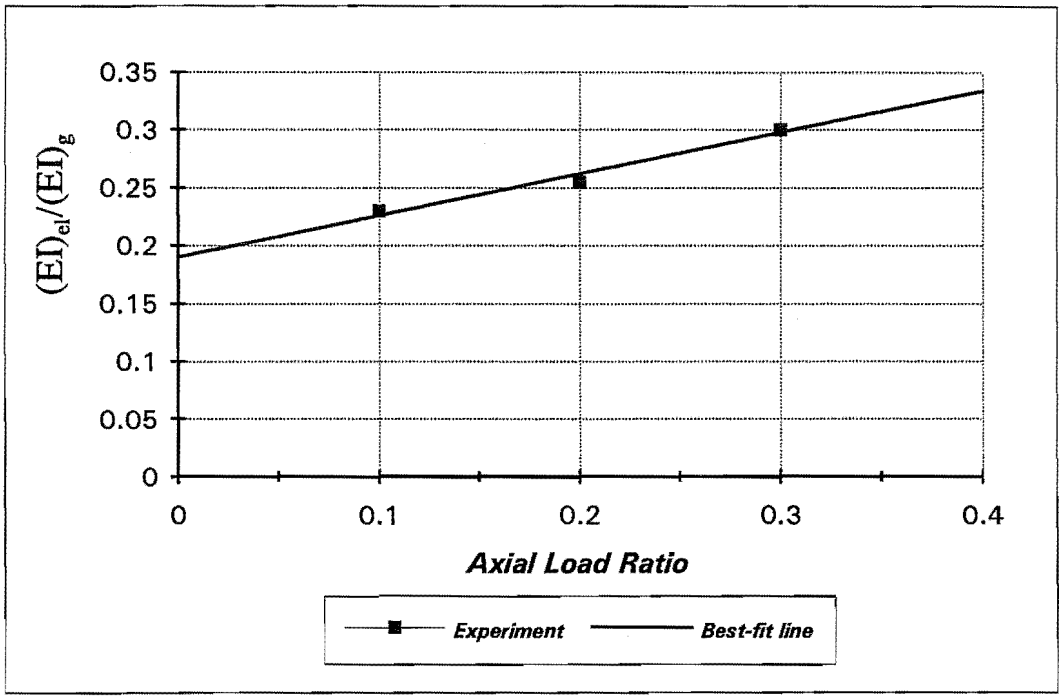

Fig.6.5: Variations of Elastic Flexural Rigidity With Axial Load Level

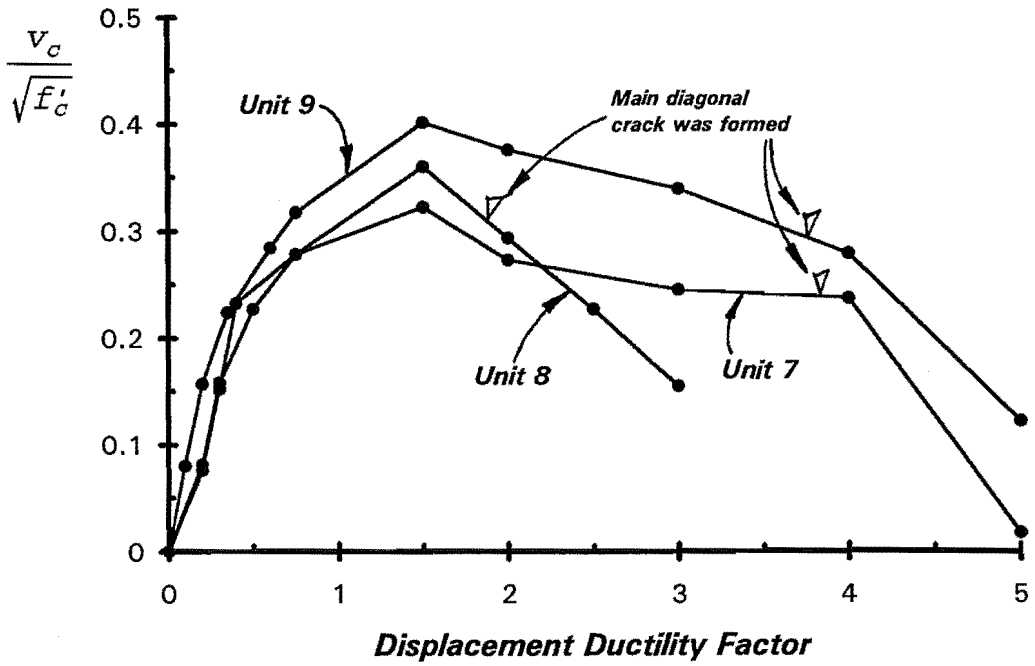

Fig.6.6: Effect of Axial Load Level

The maximum experimental shear strength was reached when transverse reinforcement yielded. The yielding of transverse reinforcement permitted the diagonal cracks to widen and propagate. A major diagonal crack was formed. The shear resistance of aggregate interlock and dowel force decreased and the shear strength of the column commenced to degrade. The beneficial effect of compression axial load on the shear strength is valid until the formation of a major diagonal crack. After the major diagonal crack becomes evident, the presence of compression axial load appears to increase the rate of degradation of the shear resistance of the column(Fig.6.6). The presence of compression axial load increases the shear deformation along the critical diagonal crack and degrades the aggregate interlock. For the column with low compression axial load, arch action is not so significant as indicated by the flat line of thrust in the column(Fig.6.4) while beam action becomes more significant. The shear force and axial load shown in Fig.6.4 are the maximum lateral load and corresponding axial load applied. The widening of the critical diagonal crack could lead to the tension shear failure, as was the case in column Unit 8. For the column with higher compression axial load, the line of thrust became steeper and arch action is more significant and shear compression failure may occur.

The presence of compression axial force may also be responsible for the fracture of transverse reinforcement. Shear deformation along diagonal cracks invokes the vertical dowel action of transverse reinforcement. The steel shear stress induced by dowel action changes direction when the loading reversed as shown in Fig.6.7. This could degrade the tension strength of the transverse reinforcement and may be one of the reasons caused the fracture of transverse reinforcement.

The effect of compressive axial load on the shear strength is recognized by many design codes. The current New Zealand code[NZS 3101: 1982] uses two separate equations for the shear strength of the concrete mechanisms for inside and outside potential plastic hinge regions. The American code ACI 318-89[A3] specifies the shear strength of the column regardless of whether inside or outside the plastic hinge regions. Fig.6.8 shows the variations of shear stress resisted by the concrete mechanisms, $V_c/b_w d\sqrt{f'_c}$, based on NZS 3101[S14] equations as a function of the axial load level. In the calculation, the tension reinforcing steel content was assumed to be the same as used in the test column($\rho_w = 1.18\%$). The concrete shear strength for inside potential plastic hinge regions for a column with axial load less than $0.1f'_cA_g$ is assumed to be zero, as for beams without axial load, according to the New Zealand code[S14]. This results in an abrupt increase in the calculated shear strength V_c in the range of axial load of $P > f'_cA_g$(see Fig.6.8). Large difference between the shear strengths for inside and outside potential plastic hinge regions can be seen in Fig.6.8 for low axial loads. This difference becomes less as the axial load increases. For the given steel content, concrete shear strength given by the equations of NZS 3101:1982 for inside potential plastic hinge region is actually slightly larger than those for outside potential plastic hinge regions when the compression axial load is around $0.5f'_cA_g$. The rate of enhancement of the shear strength due to the presence of axial load in the provisions of NZS 3101 is maintained at high axial load levels.

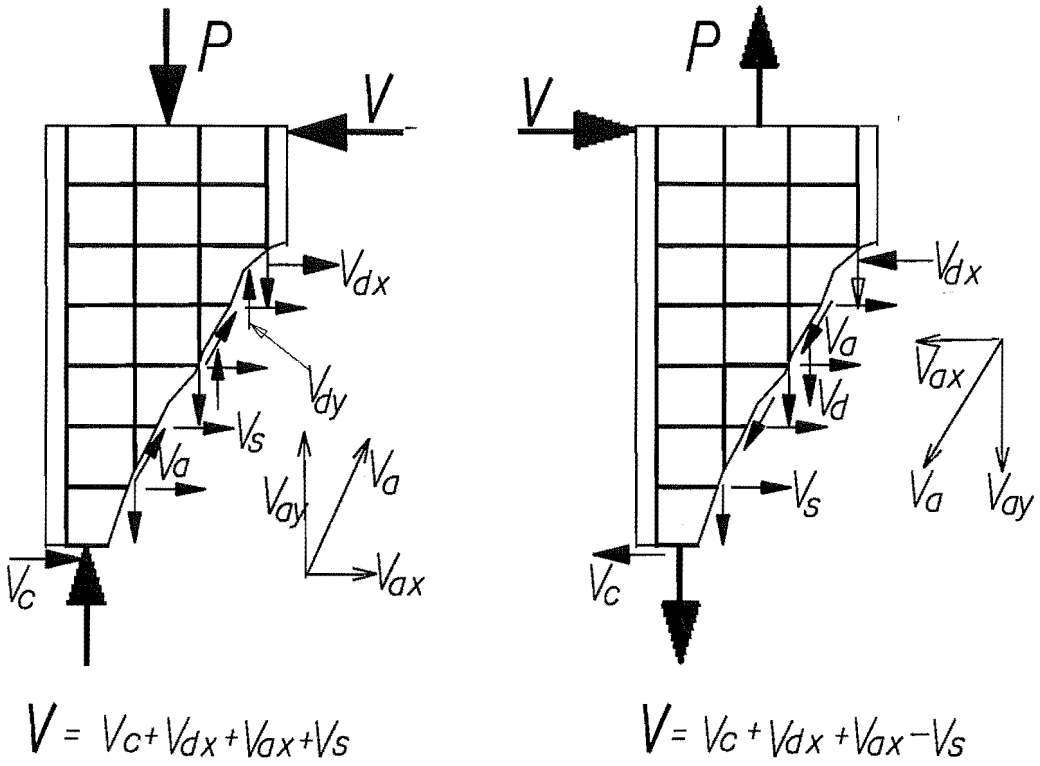

Fig.6.7: Shear Resistance Along Diagonal Crack and Dowel Action of Transverse Reinforcement

Fig.6.8 also shows (the black squares) the experimental shear stress, $V_c/b_w d\sqrt{f'_c}$, obtained by subtracting the shear V_s carried by hoop reinforcement assuming a 45-deg inclination of critical diagonal crack from the total shear applied V. It can be seen that measured shear stress carried by the concrete mechanisms increased as the axial load increased, and was greater than the code specified values for outside potential plastic hinge regions. The calculated shear strength became more close to the test results as the axial load level increased. The experimental results(Fig.6.8) also indicated that the enhancement of shear strength due to axial load becomes less as the axial load increases. As noted before, the code design equations for shear strength are based on the results of numerous beams tests without axial load, and a few tests on the columns with relatively small axial load[M10]. The extrapolation of these same equations to columns with medium to high axial compressive force may result in an overestimate of enhancing effect of axial compressive load on the shear strength.

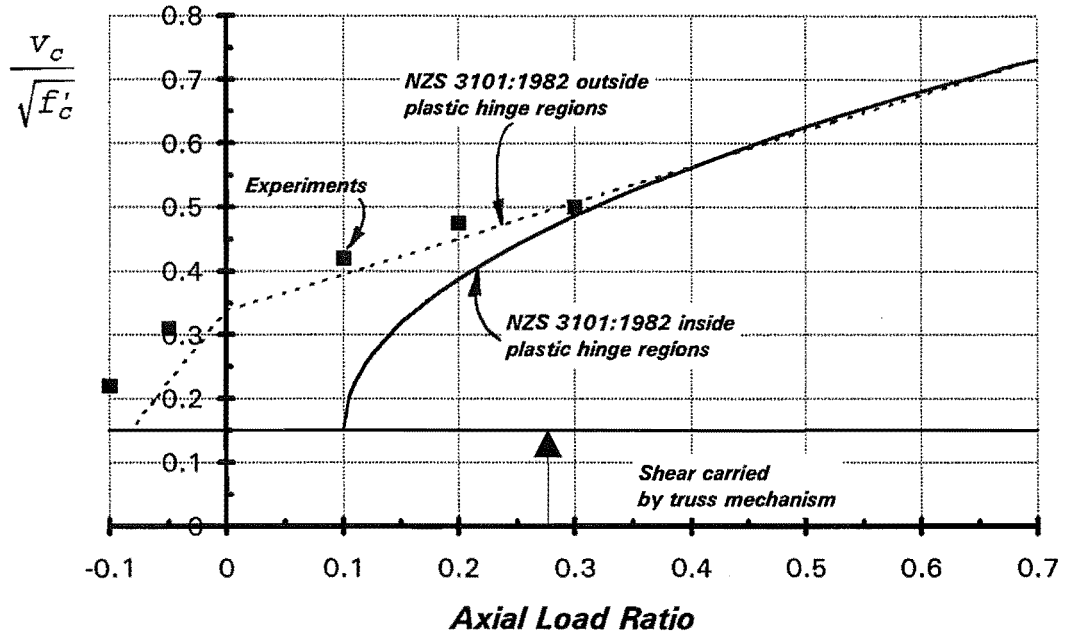

Fig.6.8: Shear Strength Specified by the Code Equations of NZS 3101:1982

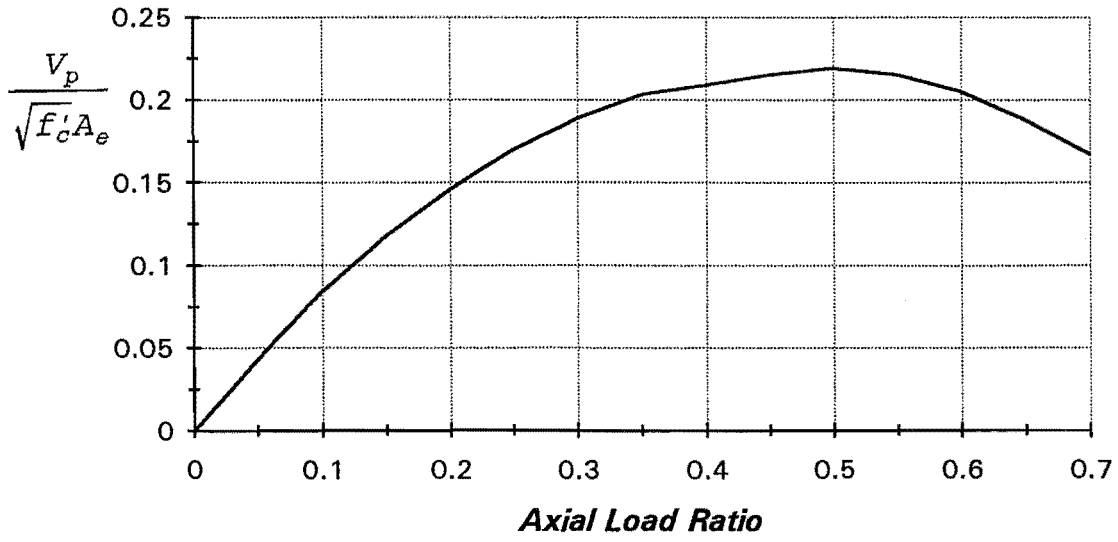

Fig.6.9: Enhancement of Shear Strength Due to Axial Force Postulated by Priestley et al[P23]

Priestley et al[P23] use an inclined strut to determine the enhancement of the shear strength due to column axial load. The enhanced shear strength, V_p, is taken as the horizontal component of the diagonal compression strut, as shown in Fig.5.28. The value of V_p is given by Eq.5.7. Fig.6.9 illustrates the enhanced shear strength, $V_p/b_w d\sqrt{f'_c}$, so calculated due to increased axial load level. This figure indicates that the shear stress continues to increase until about an axial load level of $0.5f'_cA_g$ and decreases thereafter due to reduced strut angle.

6.3.2 Effect of Transverse Reinforcement

The most important functions of the transverse reinforcement in a column are to resist shear, to provide the confinement to the compressed concrete and to prevent premature buckling of longitudinal bars. The action of transverse reinforcement in resisting shear has been conventionally modeled by a truss mechanism. Acting as the tension web members of an idealized truss, the transverse reinforcement transmits the shear across the plane of diagonal cracks. The compression web members are formed by concrete struts, and the longitudinal chords of the truss are formed by the compressed concrete and the tension reinforcement, respectively. The shear transferred by the truss is directly related to the amount of transverse reinforcement which crosses the diagonal cracks. The truss mechanisms is mobilized after diagonal cracks occur in the column. The capacity of the truss is fully developed when the transverse reinforcement yields. The propagation of inclined cracks reduces the depth of the compressed concrete and the shear resistance of the concrete compression region decreases. The decrease in the shear resistance of the uncracked concrete and aggregate interlock can be compensated for by an increase in the shear force resisted by the transverse reinforcement. The sudden increase in the hoop strains indicates when the diagonal crack initially develops and the stage when the shear resistance of the compressed concrete and concrete aggregate decreases. When insufficient transverse reinforcement is provided to resist the transition shear force, diagonal tension failure may occur at the diagonal cracking load.

Previous studies[O1,P14] have shown that the spacing of transverse reinforcement has little influence on the shear resistance of reinforced concrete members, provided at least one set of hoops can be crossed by the diagonal crack. However, it is believed that smaller spacings of hoops can enhance the shear strength by improving the bond strength and increasing the efficiency of concrete confinement. Scott et al[S8] noted that an increase in the hoop spacing, while maintaining a constant volumetric ratio of transverse reinforcement by the use of larger diameter hoop steel, tended to reduce the efficiency of concrete confinement. It has to be emphasized that the development of the truss mechanism relies on the ability to transfer stress from reinforcement to concrete through bond and mechanical anchorage. Closely placed transverse reinforcement can decrease the shear strength decay. Under cyclic loading, bond deteriorates and slip between the concrete and the longitudinal reinforcement occurs due to extensive cracking. Closely spaced hoops can effectively prevent the core concrete from spalling.

Transverse reinforcement plays an important role in controlling the width of the inclined cracks. The shear strength of columns before inclined cracking is dependent mainly on the capacity of concrete. After the formation of diagonal cracks, the shear resisted by the concrete mechanisms is strongly related to the effectiveness of aggregate interlock along the diagonal cracks. An important function of transverse reinforcement is to control the width of the inclined cracks and so to maintain the aggregate interlock capacity. The aggregate interlock capacity is dependent on the width of diagonal cracks. The propagation of diagonal cracking will reduce the shear resistance of the compressed concrete. Before yielding of transverse reinforcement, the decrease in the shear resistance of the concrete and the increase in the external shear can be accommodated by the increase in the tensile stress of the transverse reinforcement. Once the transverse reinforcement yields, its stiffness drops suddenly. Any increase in external shear can only be resisted by the increase in shear resistance of dowel action or by a change in the inclination of diagonal concrete compression stresses. The development of dowel action requires large shear deformations, which in turn to reduces the shear resistance of interlock and compressed concrete. The yielding of transverse reinforcement signals the commencement of degradation in the shear strength of the column. The shear strength degradation initiated by yielding of transverse reinforcement is amplified by cyclic deformations. The inclined cracks widen and the shear deformation increases with each loading cycle, resulting in degradation of the shear resisting mechanism, in particular aggregate interlock.

In short, the yielding of transverse reinforcement results in (1) the elimination in the ability of transverse reinforcement to compensate for the shear loss of the other components of shear resisting mechanisms, and (2) a loss of restraint due to crack widening which leads to a reduction in the effectiveness of aggregate interlock and dowel action. Transverse reinforcement also interacts with the other shear transfer mechanisms by supporting the longitudinal bars and enhancing dowel action. It can increase the efficiency of dowel action by preventing dowel cracking and by supporting dowel[O1]. It is clear that decreased hoop spacing improves the overall behaviour of the column.

Another important function of transverse reinforcement in the potential plastic hinge regions of column is to provide confinement to the compressed concrete in the core of the section. Recent research, for example[P9], has shown that use of closely spaced lateral reinforcement with sufficient quantity will result in improved ductility of column. The research conducted in New Zealand has resulted in the design of confining steel based on the curvature ductility factor expected in a column and the level of axial load[Z3]. The confining stress exists even at the zero shear condition, because of the residual transverse deformation after the removal of lateral force. The major source of residual confining stress may come from the lack of fit between the rugged faces of diagonal cracks. The transverse reinforcement provides the confinement in the direction of external shear and in the direction perpendicular to the external shear to the diagonal concrete struts. Previous experimental studies have indicated that an increase in the amount of transverse reinforcement due to decrease in spacing will

increase substantially both the concrete strength and the ultimate strain. Consequently, this will enhance the compressive strength of the concrete in the diagonal struts in the plastic hinge zone.

6.3.3 Effect of Alternating Tension and Compression Axial Load

The shear strength of reinforced concrete columns under tension axial load has been studied previously by O'Leary[O1]. It was found that constant tension axial load reduces the shear strength. That is, the shear strength of reinforced concrete when a tension force acts across a shear plane decreases with the tension stress[M9]. This effect is recognised by many codes. For example, the current New Zealand code provisions[S14] assumes that the shear strength of reinforced concrete members inside potential plastic hinge regions is zero when subjected to flexure and tension axial load. Outside potential plastic hinge regions it is assumed that the shear strength reduces to zero as the tension axial load increases to $0.087f'_cA_g$. The ACI code[A3] specifies that V_c shall be reduced linearly to zero as the average concrete axial tension stress on the member increases to 3.34MPa.

Little attention has been paid to the influence of tension axial load on the shear strength of columns when subjected to tension alternating with compression axial force. The test results from the three columns tested in this study indicate that tension axial load can significantly effect the shear strength of reinforced concrete columns in the compression axial loading half cycle. One major effect is that tension axial load encourages the opening of diagonal cracks developed during the compression axial load half cycle. The width of diagonal cracks becomes larger due to the inelastic tension strain induced in the tension axial loading half cycle. The aggregate interlock capacity then reduces significantly, since the effectiveness of interlock action is directly related to the width of diagonal cracks. Consequently the shear strength decreases.

The shear resisting mechanism of reinforced concrete members is associated with the deformation behaviour, which in a loading cycle is influenced by the strain histories. Alternating tension and compression axial force induces an unsymmetric strain, and hence affects the shear resistance. This effect is further explained with the aid of Fig.6.10 which shows laterally loaded deformed column during tension and compression axial load application. Under the actions of lateral load and compression axial load, most regions of the column are under compression. As the shear increases, the diagonal crack may propagate and extend into the initially compressed concrete. After the transverse reinforcement yields, the main diagonal crack can widen extensively and a weak shear plane is formed along the diagonal crack. The thrust of lateral and compression axial load then tends to push the top wedging block down and outward along the diagonal cracking plane. Large shear deformation can occur along this plane. When loads reversed, the main diagonal crack may not close because of the residual inelastic strains and change in direction of the axial load.

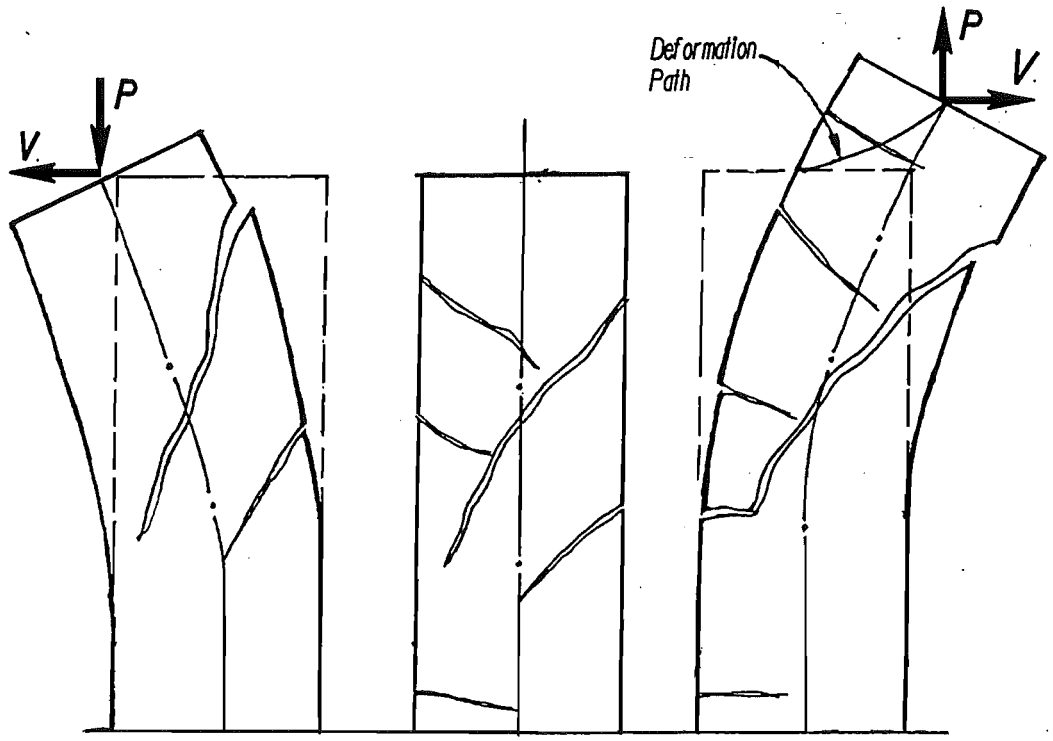

Fig.6.10: Deformed Column Subjected to Lateral Load and Axial Load

Under the action of shear and tension axial load, the new tension and flexural crack joins with the previously formed diagonal tension crack, and forms a full depth open crack. This crack remains open during the tension axial loading half cycle. The plastic deformation concentrates along this crack, as was observed in the tests. The diagonal thrust tends to pull the top wedging block up and outwards. Large shear sliding occurs along the diagonal crack during lateral loading when the axial loading changes from compression to tension. This relative movement greatly diminishes the shear transferred by the concrete aggregated interlock. The shear resisting mechanism along this major diagonal crack is quite different under tension and compression axial loads.

Under compression axial load, the shear is resisted by the compressed concrete, aggregate interlock and dowel force, in addition to the transverse reinforcement(Fig.6.7). The free body shown in Fig.6.7 indicates that under tension axial load, shear transfer can only be resisted by aggregate interlock and dowel action and the tension stress in the transverse reinforcement acts in the same direction as the

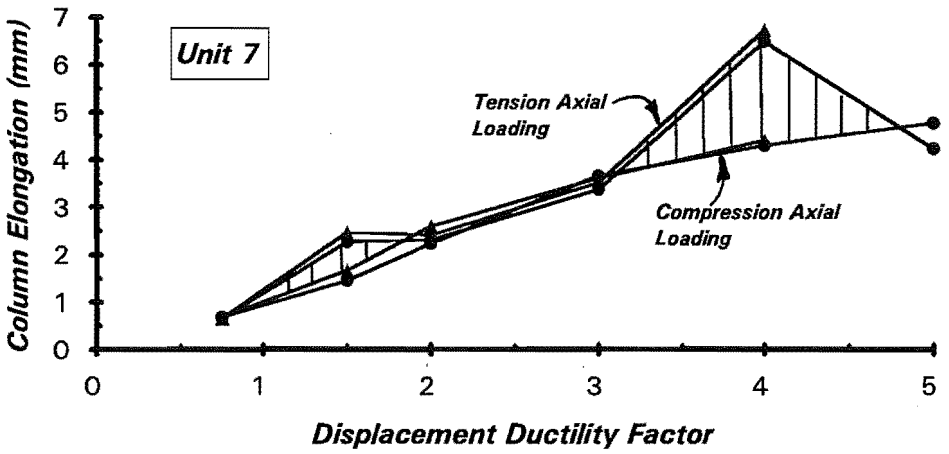

(a) Column elongation of Unit 7

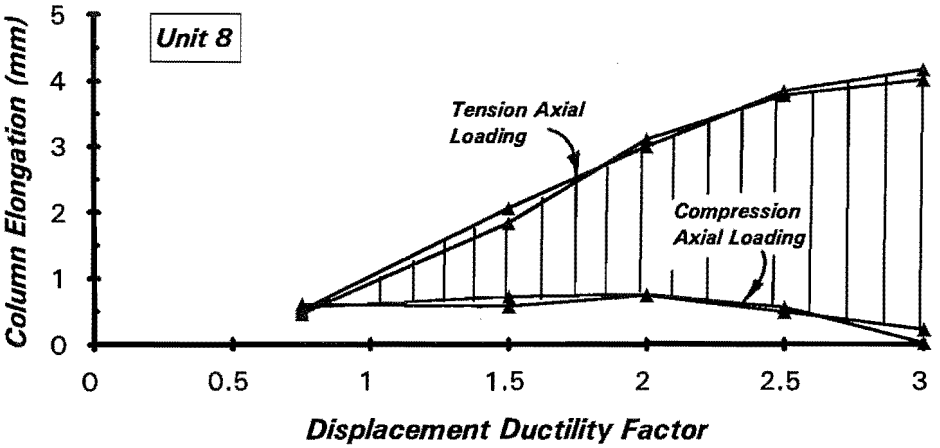

(b) Column Elongation of Unit 8

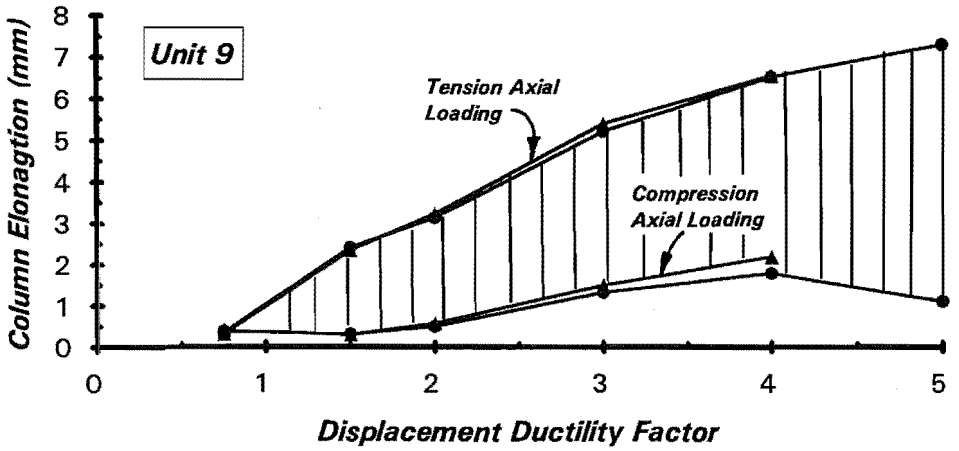

(c) Column Elongation of Unit 9

Fig.6.11: Axial Elongation Measured on the Three Column Units

external force. It is to be noted that shear sliding also mobilized the dowel force of transverse reinforcement. High dowel stresses, associated with large shear displacement along the crack, can lead to local tension failure. This was indicated by the splitting crack and secondary tension cracks observed in the columns tested.

The effect of tension axial load on the deformation characteristic of the column is indicated by the column elongation as shown in Fig.6.11. In this figure, the column elongations at each peak displacement in tension and compression axial loading direction are plotted against the displacement ductility factor. The shaded area represents the relative elongation of the column at peak displacement between the tension and compression axial loading half cycle. It can be seen in this figure that the relative elongation of the column increases with the increase in displacement ductility level. The longitudinal elongation combined with lateral displacement leads to the movement of the column tip in the directions shown in Fig.6.10. This movement mainly occurs along the critical diagonal crack developed in the compression axial loading direction, because this crack remains open during the change from the compression loading half cycle to the tension loading half cycle. Fig.6.11 also indicates that the relative column elongation is dependent on the magnitude of tension axial load.

Under constant axial load, the relative elongation of the column during reversed lateral loading would become zero theoretically. This was confirmed by the elongation of Unit 7 at displacement ductility factor of μ_n=2 and 3(Fig.6.11a). During these lateral loading cycles, the compression axial load was held constant.

It has to be emphasized that the shear deformations in the compression and tension axial loading half cycles are unsymmetric. The effect of unsymmetric shear deformations on the fit between worn aggregate particles in the diagonal cracks is very significant. It was observed that unsymmetric shear deformations with repeated abrasion quickly destroy the aggregate interlock capacity.

The adverse effect of tension axial load on the deterioration of bond strength was also evident. Vertical cracks running along the longitudinal reinforcement were observed during the tests, as can be seen in Figs.6.1 to 6.3. This indicates a significant deterioration in the bond stress transfer mechanism between the reinforcement and concrete.

6.3.4 Effect of Longitudinal Reinforcement

The longitudinal reinforcement ratio was not a variable studied in these tests. The ratio of total longitudinal reinforcement to the gross section was 2.36% for the three column units.The longitudinal

bars were evenly distributed around the perimeter of the column section(see Fig.4.1). Considering one-half of the longitudinal reinforcement as tension steel gives a tension reinforcement ratio of 1.18% with respect to the gross section area.

The longitudinal reinforcement participates in the shear transfer as part of the truss mechanism. Another important role of longitudinal reinforcement in shear transfer is its dowel force capacity. Dowel action may be an effective means of resisting shear both before and after the yielding of transverse reinforcement. The contribution of dowel action and aggregate interlock are interdependent[S15]. Aggregate interlock and dowel action are both initiated by shear displacement along the diagonal crack. In the initial stage of diagonal cracking, the shear transfer by aggregate interlock predominates. The aggregate interlock force transferred is dependent on the length and width of the crack, and the shear displacement along the crack. The interlocking aggregate diminishes when the crack width is large. At this stage the dowel force prevails.

Significant dowel action can only be generated when considerable shear displacement occurs along the diagonal crack. The magnitude of the dowel force increases with the bar diameter and the concrete strength[P16]. Taylor[T5] has pointed out that the shear force carried by dowel action in a typical reinforced concrete beam accounted for about 15 to 25% of the applied shear, depending on the layout of the tension reinforcement, the width of dowel failure surface and the tensile strength of concrete. It has been observed that the shear displacement across inclined cracks in a beam occurs by the flexural rotation of the compression zone between adjacent concrete cantilevers[F3]. In a column, larger shear sliding is expected to occur under the combined actions of lateral load and axial load. After the formation of a major diagonal crack, considerable relative movements between the faces of this diagonal crack occurs, which effectively mobilizes the dowel forces. Also, intermediate longitudinal reinforcement is normally provided in columns. The bearing strength and stiffness of the concrete under these intermediate longitudinal bars are greater than those for the extreme bars. Dowel action diminishes when splitting of concrete occurs along the longitudinal bars as a result of the dowel forces. Transverse reinforcement can effectively maintain dowel action after splitting if present in adequate quantity. It can be concluded that an increase in longitudinal reinforcement content can increase the shear strength of adequately tied columns. The dowel force available to resist shear in a column where the longitudinal bars are distributed around the perimeter of the section should be greater that in a beam where longitudinal bars are normally located only at the top and bottom faces of the section.

In a column with alternating tension and compression axial load, the diagonal crack developed in the compression axial loading direction may not close and may merge with tension and flexural cracks formed in the tension axial loading direction, so as to form a fully opened diagonal crack. The dowel force capacity of longitudinal reinforcement may in this case become the main source of shear transfer across the diagonal plane.

The stiffness provided by the longitudinal reinforcement is very important in maintaining the stability of the diagonal tension cracks. For columns containing low longitudinal reinforcement, shear failure could occur along the inclined crack after yielding of the transverse reinforcement.

6.4 PROPOSED EQUATIONS FOR THE PREDICTION OF SHEAR STRENGTH

6.4.1 Basic Considerations

On the basis of the experimental results presented in the preceding chapters, a proposal for predicting the shear strength of reinforced concrete columns is made in this section. The proposal is developed based on the following considerations.

The experimental results revealed that the traditional approach based on a 45-deg truss mechanism and a supplemental component known as the "shear carried by the concrete" is unable to accurately predict the shear strength of reinforced concrete column under seismic actions. The current provisions of the New Zealand code NZS 3101:1982[S14] for shear strength gives a very conservative prediction for the shear force resisted by the concrete at low displacement ductility levels, even using the equations for outside potential plastic hinge regions. Several factors may be responsible for this conservatism and deficiency in the code equations. The approximation for the roles played by some parameters, such as axial load level may result in an overestimate of the column shear strength in some cases, and in the other cases may give an unduly conservative prediction of shear strength. It has to be emphasized that the deficiency in the code equations due to overoptimism of the effect of axial compressive force in some cases may have been shaded by the requirements for confinement and anti-buckling of longitudinal bars in the code provisions. The requirements for confining the compressed concrete will govern the amount of transverse reinforcement required for columns with relatively high axial compression load.

Under seismic actions, causing cyclic loading in the inelastic range, the shear strength of reinforced concrete columns decreases with increased flexural displacement ductility. The reduction in the shear strength is caused by the deterioration of the shear resisting mechanisms other than the truss mechanism as the column experiences inelastic deformations. At low displacement ductility level, each shear resisting mechanism effectively maintains its capacity and contributes to the shear strength of the column. As the displacement increases, especially with the yielding of transverse and longitudinal reinforcement, the widening of flexure-shear cracks and shear grinding along diagonal cracks during reversed cyclic loading, reduces the capacity for shear transfer by the aggregate interlock as well as by

the compressed concrete. The shear strength of the column therefore degrades with the increased displacement ductility level. The lower the ductility demand, the higher is the shear strength of the member. Neglect of the shear strength of the concrete contributions in the code provisions of NZS 3101:1982 for the plastic hinge regions of column, with axial compression of $0.1f'_cA_g$ or less appears unnecessarily conservative. The measured shear force resisted by the concrete in the tests on Units 7, 8 and 9 was much greater than that given by the equations of NZS 3101:1982 for columns with low axial compression load, but reduced to less than the code specified values for the column with relatively high axial compression even using equations for inside potential plastic hinge regions at moderate displacement ductility(see Figs.5.18 to 5.20).

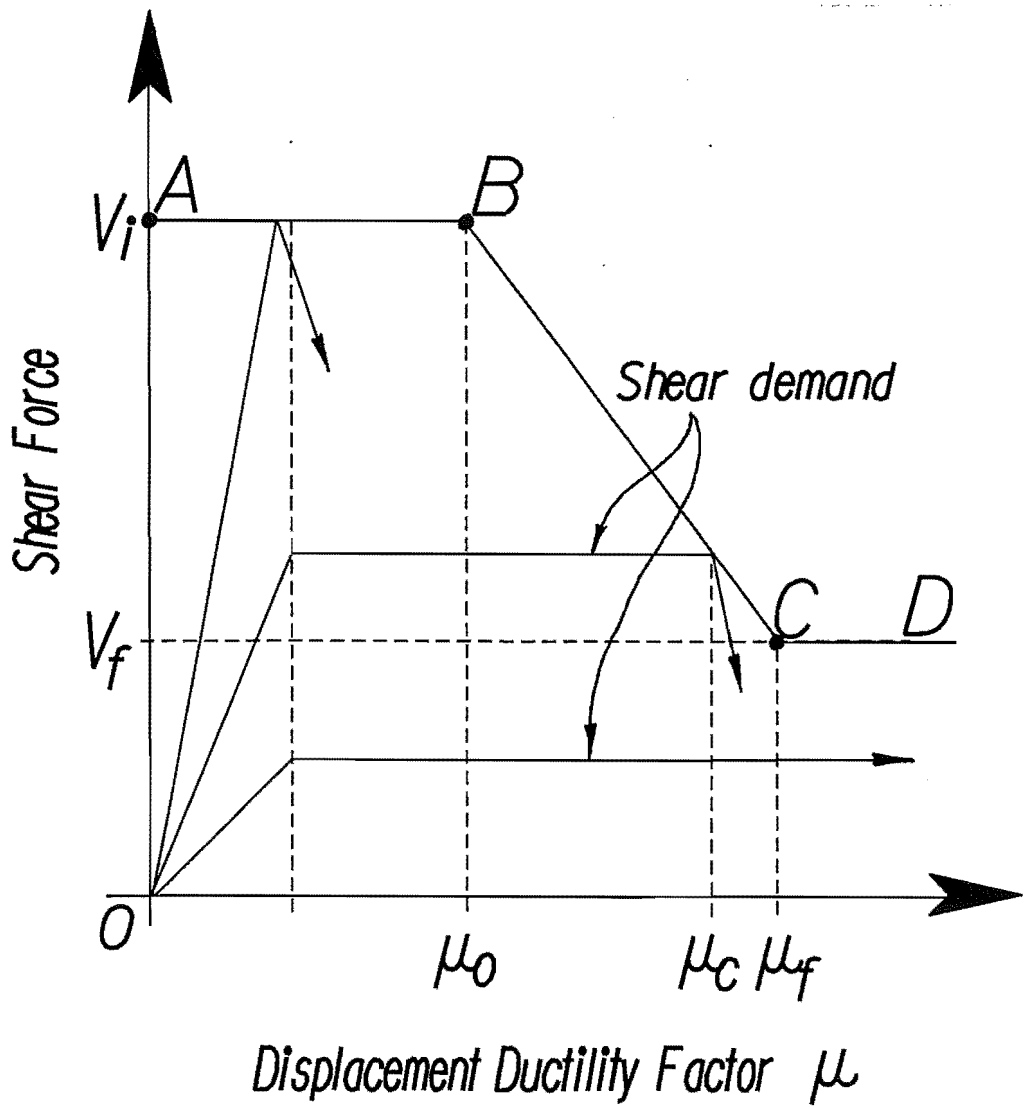

Fig.6.12: Relationship Between Available Shear Strength and Displacement Ductility Capacity

Under complex loading histories, the degradation of shear strength becomes more severe. Wong[W4] demonstrated that the shear strength decay in columns subjected to bi-directional displacement patterns occurred at a displacement ductility level one unit less than that of identical columns under uni-directional loading patterns. The test results from this present study indicated that an alternating tension and compression axial load pattern will result in even more severe degradation in the shear strength and stiffness. This is because, as discussed in previous sections, the tension axial load greatly increases the inelastic tension strain and encourages the widening of diagonal cracks. This directly degrades the capacity of shear transfer by aggregate interlock and dowel action. Also, unsymmetric strain histories due to varying axial load accelerates the shear strength decay.

The proposed equations for the shear strength followed the model developed by Ang et al[A7]. In this model, the shear strength is represented by a trilinear skeleton curve to reflect the interaction between the shear strength and flexural displacement ductility factor, as shown in Fig.6.12. The shear carrying capacity of the column is given by the line ABCD and is considered to remain constant at the initial shear strength, V_i, until a displacement ductility factor, μ_0 is reached. The shear strength is then assumed to reduce linearly from the initial value V_i at a displacement ductility $\mu=\mu_o$ to the residual shear strength V_f at a displacement ductility factor $\mu=\mu_f$. The residual shear strength is assumed to be maintained at displacement ductility factor greater than μ_f.

If the applied shear force corresponding to the flexural overstrength, V_{if}, and the imposed displacement ductility fall between the skeleton relation ABCE(see Fig.6.12), a ductile flexural failure can be ensured. Otherwise a shear failure will occur. The displacement ductility,μ_0, at which the degradation of shear strength commences, is assumed to be 1.5. The required displacement ductility, μ_f, can be obtained by the procedure suggested by Priestley and Park[P22].

The shear strength of the column is considered to consist of two components: a concrete component, V_c, whose magnitude depends on the level of the imposed displacement ductility factor, and a truss component, V_s, whose magnitude depends on the amount of transverse reinforcement. Thus

$$V_n = V_c + V_s \qquad (6.1)$$

6.4.2 Truss Component V_s

The test results indicated that under a compression axial load, the inclination of the critical diagonal crack to the column axis was about 35 to 45-deg when the shear strength was reached. Although a smaller inclination of the diagonal cracks was observed when the diagonal cracks propagated further into the compressed region, at that stage the failure may have already occurred. Under tension axial

load, the truss mechanism was still operative and the inclination of the critical diagonal tension crack was close to 45-deg. Therefore the shear strength of the truss component may be calculated assuming an angle of 45-deg for the inclination of the critical diagonal crack. Then both the initial and the residual shear strength provided by the truss component with either tension or compression axial load is given by

$$V_s = \frac{A_v f_{yh} d}{s_h} \qquad (6.2)$$

Priestley et al[P23] have proposed that a smaller angle(30-deg) of inclination of diagonal cracks to the column axis than 45-deg be used. However 45-deg is preferred here because: (a) an angle of 45-deg is traditionally used for beams and a smooth transition of the shear equations for members with or without axial load is desirable, (b) an angle of 45-deg is fairly close to that observed in the tests, and (c) in any case the V_c contribution is found from V_n-V_s, and hence an appropriate V_c for a particular V_s can be determined and no accuracy is lost.

6.4.3 Initial Shear Strength of Concrete Component V_{ci}

It is proposed that the initial shear strength of the concrete component when compression axial force is present can be calculated from

$$V_{ci} = \alpha_1 \alpha_2 \left[0.45 + 2.6 \sqrt{0.1 + \frac{P}{f'_c A_g}} \right] v_b b_w d \qquad (6.3)$$

where:

(a) The factor α_1 is to allow for the reduction in shear strength due to loading histories. It is suggested that for a column subjected to varying axial loading and biaxial bending, α_1=0.90. For a column subjected to constant axial load and uniaxial bending, α_1=1.0.

(b) The factor α_2 is to allow for increase in shear strength due to a low aspect ratio of the column. Ang[A7] suggested, based on his test results, that this effect can be estimated from

$$\alpha_1 = \frac{2.0}{\frac{M}{VD}} \geq 1.0 \qquad (6.4)$$

where M and V are the applied bending and the corresponding shear force, D is overall section dimension in the direction of applied lateral load.

(c) The longitudinal reinforcement content can influence the shear strength by increasing the dowel force and enhancing the stiffness of the column. No data was available from this study to evaluate this effect. The basic shear stress v_b as given by the current New Zealand design code NZS 3101:1982[S14] includes the factor ρ_w.

$$v_b = (0.07+10\rho_w)\sqrt{f'_c} \qquad (6.5)$$

where ρ_w=ratio of tension steel area to gross concrete area.

The value of basic shear stress v_b is limited to $0.2\sqrt{f'_c}$ for ρ_w=0.013 or more according to NZS 3101:1982[S14]. This limit was determined mainly from beam tests in which the longitudinal reinforcement was located at the top and bottom faces of the section and the reinforcement ratio was normally low. For columns, in which the longitudinal bars are evenly distributed around the section, this limit appears to be too restrictive. Ang[A7] suggested that the limit on v_b could be increased to $0.37\sqrt{f'_c}$.

Under tension axial load, the truss mechanism is still operative. The shear carried the transverse reinforcement can be calculated using the truss analogy and assuming a 45-deg inclination of diagonal crack as given by Eq.6.2. Moderate tension axial force does reduce the shear strength of the member. The test results demonstrated that a large portion of the shear was still able to be transferred by the concrete even under an axial tension force up to $0.1f'_cA_g$. The magnitude of the shear stress sustained by the concrete component was dependent on the intensity of the tension axial load level(see Fig.5.21). It can be conservatively assumed that the shear strength of concrete component, V_{ci}, will reduce to zero when the tension axial force exceeds $0.1f'_cA_g$. It is proposed that the shear strength of the concrete component with tension axial force is given by

$$V_{ci} = 3.9\alpha_1\alpha_2\sqrt{0.1+\frac{P}{f'_cA_g}}\,v_bb_wd \qquad (6.6)$$

where P is taken as negative, and α_1 and α_2 have the same values as in Eqn.6.3.

6.4.4 Residual Shear Strength of the Concrete Component V_{cf}

As shown in Figs.5.22 to 5.24, the total shear strength of the column decreased with increase in displacement ductility factor. The shear resistance provided by the truss mechanism can be maintained providing no anchorage or bond failure occurs. Hence the value of V_s after strength degradation is still given by Eq.6.2. The reduction in the shear strength is caused by the degradation of the concrete shear

resisting mechanisms. The degrading characteristic is associated with the effectiveness of aggregate interlock and dowel action. The concrete shear stress obtained by subtracting the shear V_s carried by hoop reinforcement assuming a 45-deg inclination of the diagonal crack from the total shear V applied in the tests indicated an approximately linear reduction of the shear force carried by the concrete with increase in displacement ductility factor during cyclic loading. It was assumed that the shear strength of concrete component, V_c, decreases linearly from an initial strength, V_{ci}, to a residual strength, V_{cf}. The rate of shear strength decay appears to depend on the failure mode, as indicated by a more rapid degradation of shear strength in the case of Unit 8, which failed in a diagonal-tension mode, than observed for Units 7 and 9, which failed in shear-flexure and shear-compression modes, respectively.

The test results indicated that the residual concrete shear strength is influenced by the axial load level. Also, after substantial deterioration, the participation of dowel action in shear strength may become more significant. Hence a larger longitudinal reinforcement content would increase the residual shear strength. Furthermore the varying axial loading pattern also increased the severity of the degradation. Insufficient data was available from the tests to fully define these effects. Based on the limited data, following equation for the residual shear strength for both compression and tension axial load is tentatively suggested.

$$V_f = 2.23\sqrt{0.1+\frac{P}{f'_c A_g}}\, v_b b_w d \qquad (6.7)$$

where the axial load P is taken as positive when it is in compression, and as negative when it is in tension. When the tension axial force exceeds $0.1f'_cA_g$, the residual shear strength V_f is assumed to be zero.

6.5 COMPARISONS OF MEASURED AND PREDICTED SHEAR STRENGTHS

6.5.1 Tests of the Three Columns Reported in Chapter 5

The shear strength of the three columns tested, Units 7, 8 and 9, were computed using the proposed equations(Eqns.6.1 to 6.7). The calculated strength values are listed in Table 6.1 and 6.2. The ratio of the mean experimental to predicted shear strength when compression is applied for both the initial shear strength and residual shear strength is 1.01 with a standard deviation of 0.10. When the tension axial

load is applied, the proposed equations give conservative predictions, with a mean strength ratio of 1.16 for the initial shear strength and 1.4 for the residual shear strength.

6.5.2 Tests by Previous Researches on Rectangular and Square Columns

The predictions using the proposed equations were also compared with experimental results obtained by other researches. These include the tests reported by Priestley et al[P23] on three rectangular columns, by Woodward and Jirsa[W6] and Umehara and Jirsa[U1] at the University of Texas on square columns under uniaxial and biaxial bending, and by Mattock and Wang[M10] on rectangular members with high axial compressive stress. The details of the tested columns, together with the predicted shear strengths using the proposed equations are listed in Table 6.3 to 6.6. The columns tested at the University of Texas were conducted in double curvature bending. In determining the shear strength of the columns tested by Woodward and Umehara subjected to biaxial bending, the reduction factor α_1 in Eq.6.3 was taken as 0.9. The average strength ratio of V_{exp}/V_n for these columns is 0.96. The rectangular column(406×610mm) tested by Priestley et al[P23] contained twenty-two 19mm(#6) diameter deformed bars, which were evenly distributed around the sides of the column section. A small compression axial load of $0.06f'_cA_g$ was applied to these three columns. The tension longitudinal reinforcement ratio, ρ_w, in Eq.6.5 for these column was taken to be 2/3 of the total longitudinal reinforcement ratio with respect to the gross section area.

Fig.6.13 illustrate the ratios of V_{exp}/V_n for all rectangular and square columns considered. The maximum and minimum ratios are 1.24 and 0.80, respectively. The average strength ratio is 1.02 with a standard deviation of 0.11.

The shear strength of the columns were also computed using the current New Zealand code provisions[S14] for outside potential plastic hinge regions. The results are listed in the last two columns of Table 6.1 to 6.6. The agreement between the experimental shear strengths and that calculated using the proposed equations is very satisfactory.

6.5.3 Tests on Circular Columns

The proposed equations for the shear strength were also used to predict the results of the experiments conducted by Ang et al[A7] and Priestley et al[P23] on circular short columns. When determining the shear strength of the concrete component for these columns, the effective section area in Eq.6.3 is taken as $b_wd=0.8A_g$. The tension reinforcement ratio, ρ_w, in Eq.6.5 is taken as two-third of the total longitudinal reinforcement ratio.

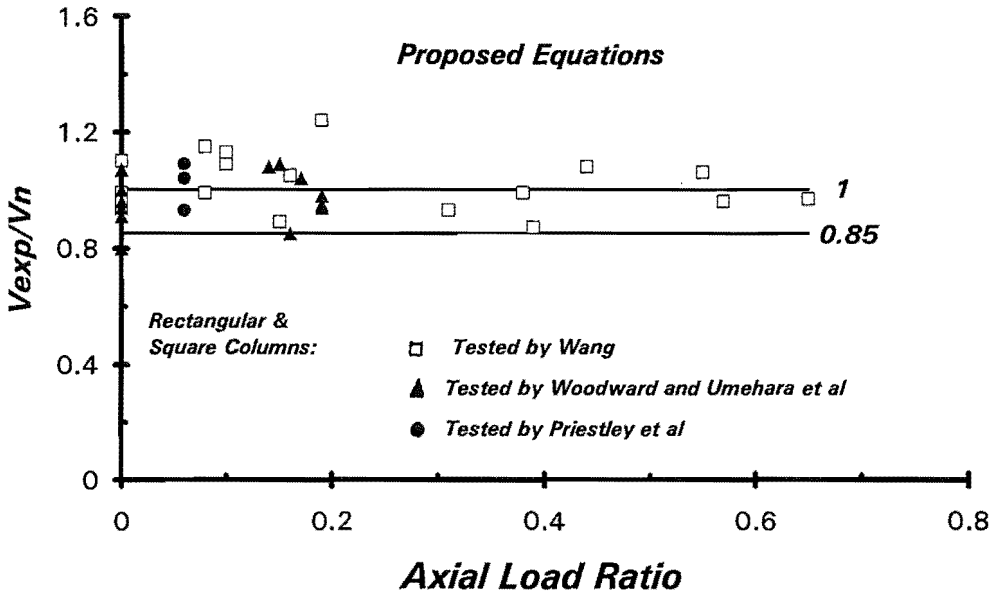

(a) Ratio of Vexp/Vn for various axial load ratios

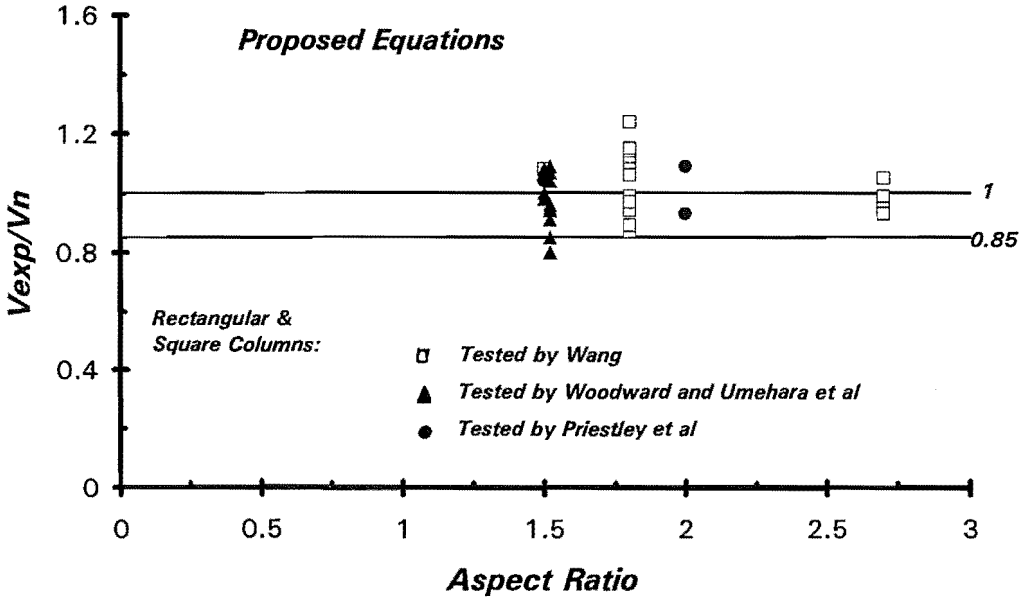

(b) Ratio of Vexp/Vn for various aspect ratios

Fig.6.13: Proposed Equations Compare With Experimental Results

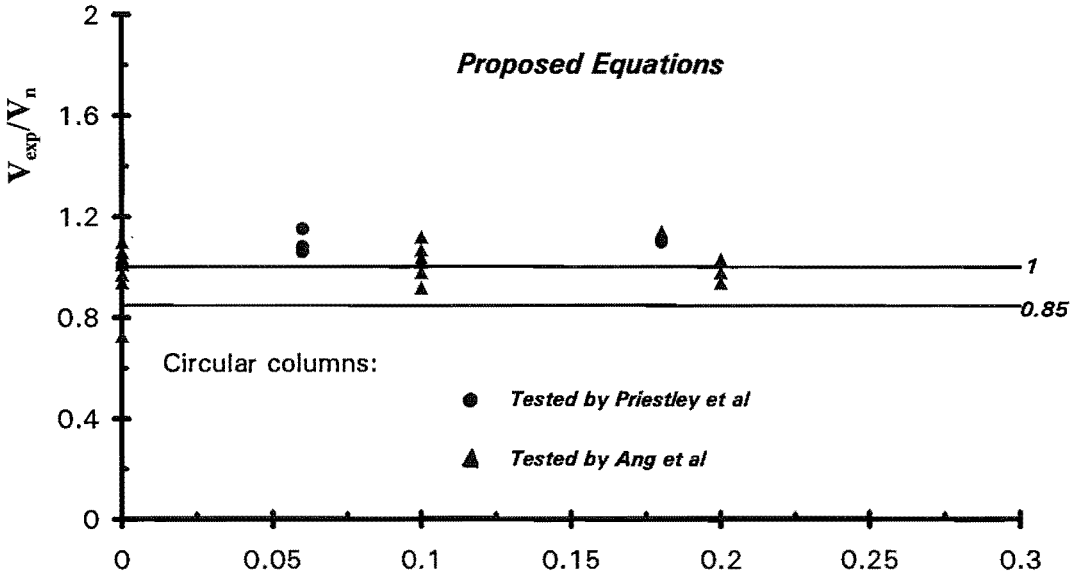

(a) Ratio of Vexp/Vn for various axial load ratios

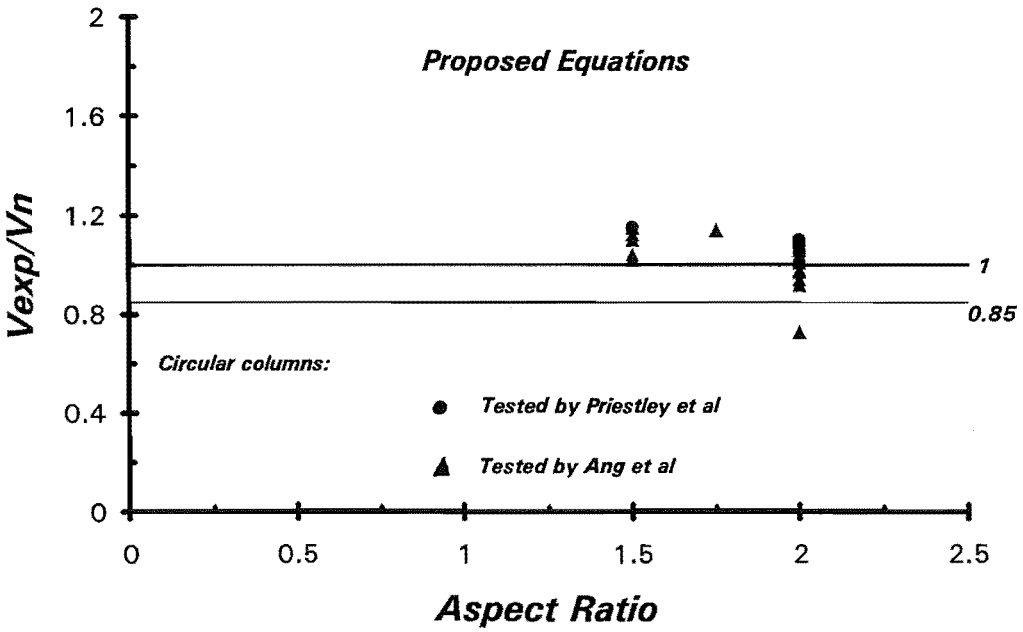

(b) Ratio of Vexp/Vn for various aspect ratios

Fig.6.14: Proposed Equations Compare With Experimental Results

The computed results are given in Tables 6.7 and 6.8. The shear strength ratios of V_{exp}/V_n are illustrated in Fig.6.14. It can be seen the agreement between the predictions and experiment is very good for all columns. The maximum strength ratio is 1.12 and the minimum is 0.90, except for Unit 2 tested by Ang[A7], which had the lowest ratio, V_{exp}/V_n, of 0.73. It is to be noted that the longitudinal reinforcement used in this column was from Grade 275 deformed bars with measured yield strength of 296 MPa. The strength of the column might have been controlled by flexure instead of by shear. The average strength ratio for the 28 circular columns compared is 1.01 with a standard deviation of 0.11.

Figs.6.15 and 6.16 illustrate the ratios of the experimental shear strengths to the predictions made by the proposed equations and by the current New Zealand code equations[S14] for all the columns considered. It can be seen that the proposed equation has resulted in a greatly improved predictions.

6.5.4 Comparison of NZS 3101 and Proposed Equations

Like the code provision, the proposed approach also employs a 45-deg truss mechanism to determine the shear resistance of the transverse reinforcement. The difference between the NZS 3101:1982 approach and the proposed equations arises only from the shear strength assigned to the concrete component. The difference between the shear strength of concrete component given by the provisions of NZS3101:1982 and proposed equations are plotted in non-dimensional form, $v_c/\sqrt{f'_c}$, against the axial load level in Fig.6.17. The measured concrete shear stresses for the three columns tested are also illustrated in this figure.

It is clear that the current New Zealand code provision is generally conservative at low axial load levels. The neglect of the concrete contribution for columns with axial compression of $0.1f'_cA_g$ or less in the code equation for inside potential plastic hinge regions is especially unduly conservative. On the other hand, the code equations may become non-conservative at higher axial load levels. The shear force carried by the concrete as shown in Fig.6.17 for the three column units indicates that the rate of enhanced shear stress with increasing axial load becomes less at higher axial loads. The proposed equation for the initial shear strength becomes less than that given by the code equations for both inside and outside potential plastic hinge regions at relatively high axial load levels.

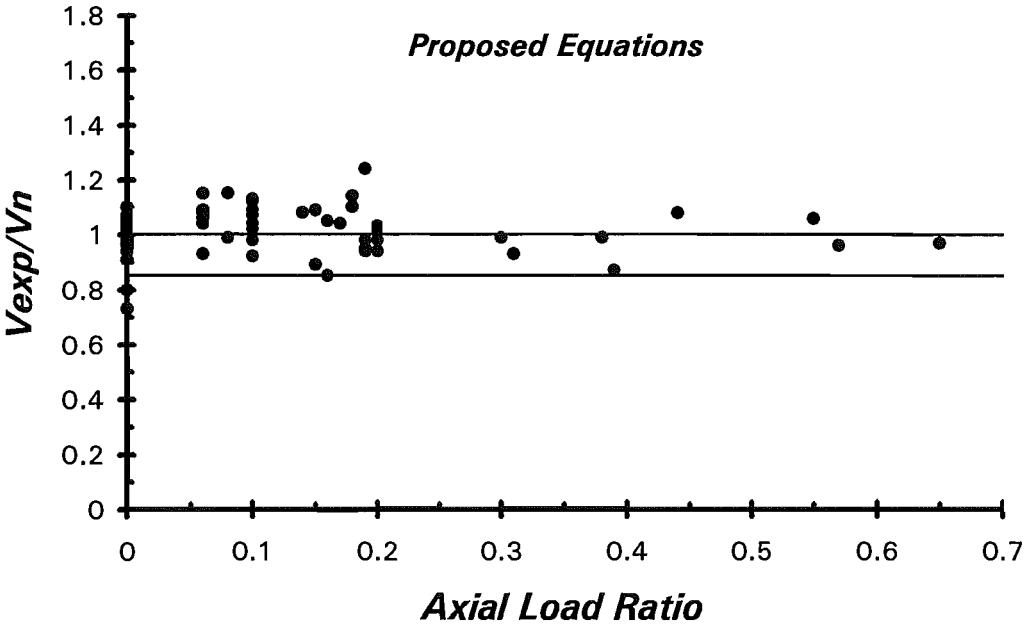

(a) Ratio of Vexp/Vn for Various Axial Load Ratios

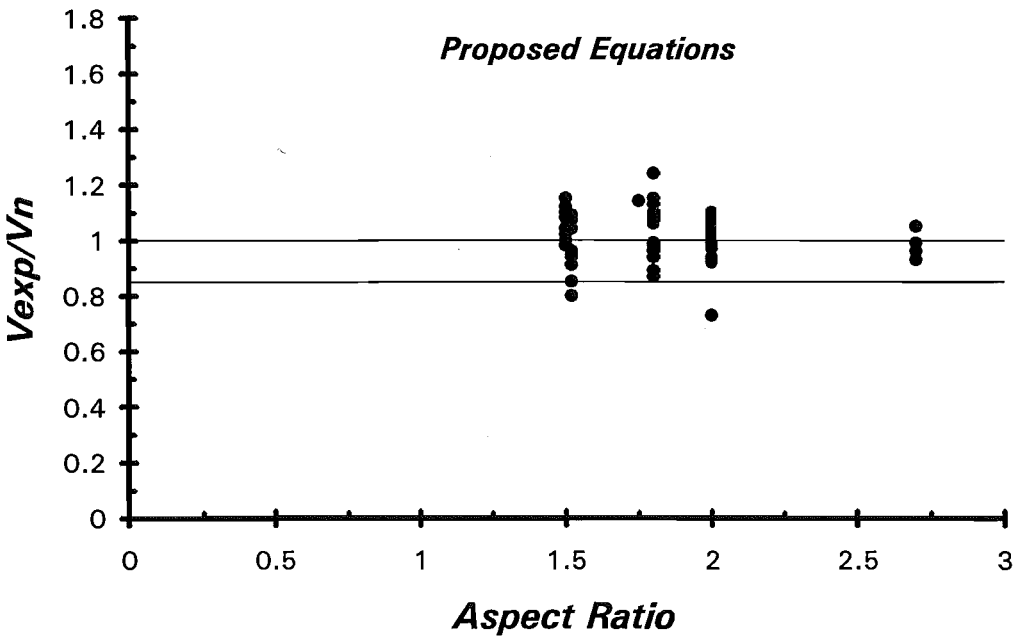

(b) Ratio of Vexp/Vn for Various Aspect Ratios

Fig.6.15: Proposed Equations Compare With Experimental Results

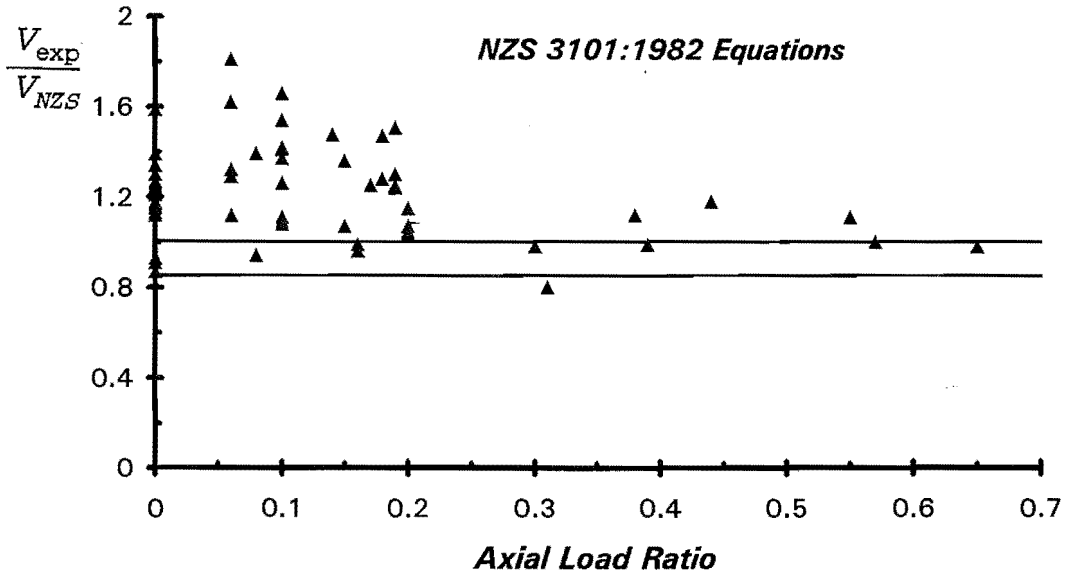

(a) Ratio of Vexp/Vnzs for Various Axial Load Ratios

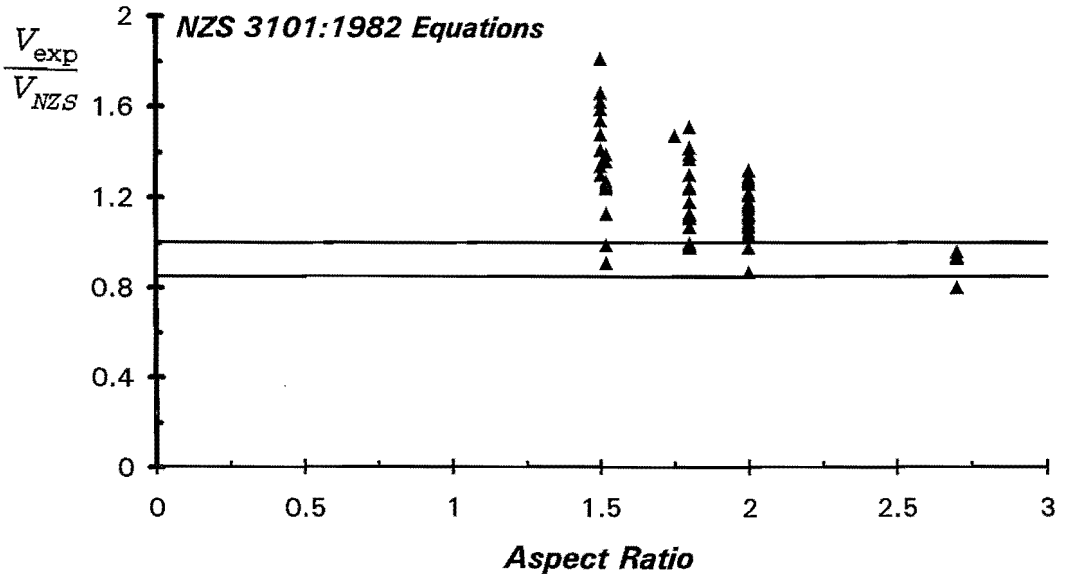

(b) Ratio of Vexp/Vnzs for Various Aspect Ratios

Fig.6.16: New Zealand Code Equations Compare with Experimental Results

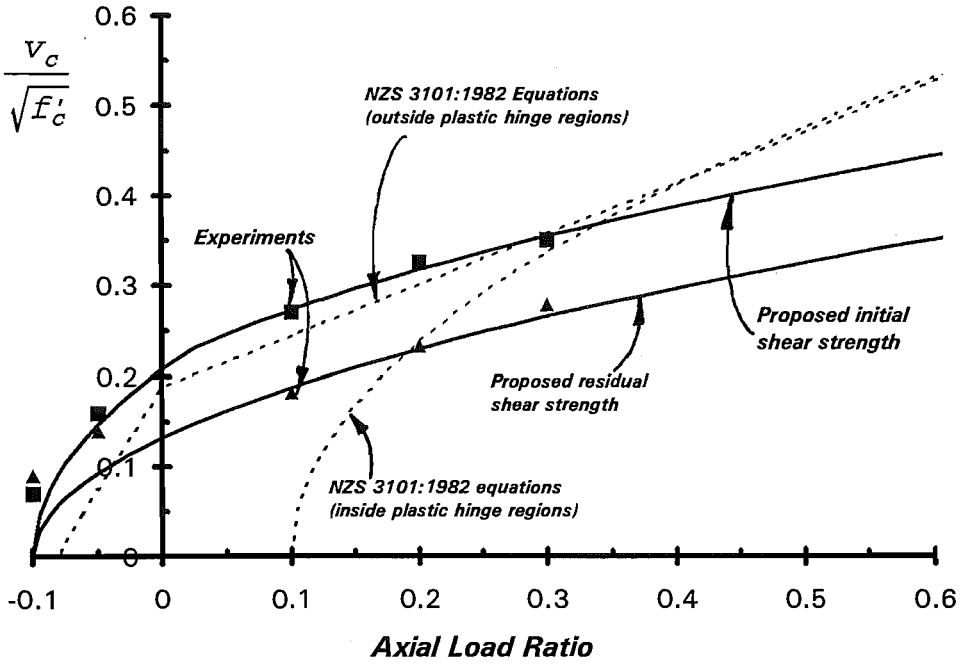

Fig.6.17: Comparisons Between the Proposed and the Code Equations

6.6 THE SHEAR STRENGTH OF THE COLUMNS IN STRUCTURES OF LIMITED DUCTILITY

Reinforced concrete structures designed for ductile flexural yielding will be the subject of capacity design. The elements in such structures should have adequate ductility, achieved by means of providing appropriate longitudinal reinforcement and sufficient transverse reinforcement in the regions where the energy dissipation is expected to take place. The ductile detailing of potential plastic hinge regions can

result in the presence of large quantities of transverse reinforcement to confine the compressed concrete, to prevent premature buckling, and to prevent shear failure[P4].

There are many structures which, because of their structural configuration, inherently possess strength considerably in excess of the strength required for fully ductile structures[P17], or due to architectural requirements and/or gravity load domination, have beams which are larger than columns and are difficult to design for strong column-weak beam behaviour[P4]. Such structures can be more practically designed for limited ductility. In this situations, the designer may take advantage of the available excess strength and use simplified detailing for the reduced ductility demand.

The limited ductility demand implies that such structures will be designed for higher seismic design forces than ductile structures. That is, the seismic design force used could be part way between the level for a ductile structure and an elastically responding structure. Structures which have an available displacement ductility factor between 4 to 6 are considered to be ductile. When the available displacement ductility factor is between 2 to 3, the structures can be deemed to have limited ductility. The seismic design loading for the frames of limited ductility may be 2 to 3 times that used for ductile frames. Since the ductility demand reduces, the requirements for the detailing of the potential plastic hinge regions in the structure of limited ductility can be considerably relaxed.

As noted before, the degradation of shear strength of the concrete mechanisms in the plastic hinge regions is due to the deterioration of the concrete as a result of flexural yielding during reversed cyclic loading. For the columns in the structures of limited ductility, the ductility demand decreases as the design seismic loading increases, and hence degradation will be reduced.

Very few experimental studies have been conducted on the shear strength of reinforced concrete with limited ductility. The current design code NZS 3101:1982[S14] simply specifies that the contribution to shear strength by the concrete in the designed end regions of columns of structures of limited ductility is one-half that for the gravity load design(Eq.2.6), and not less than

$$v_c = 0.4\sqrt{\frac{P}{A_g}} \qquad (6.8)$$

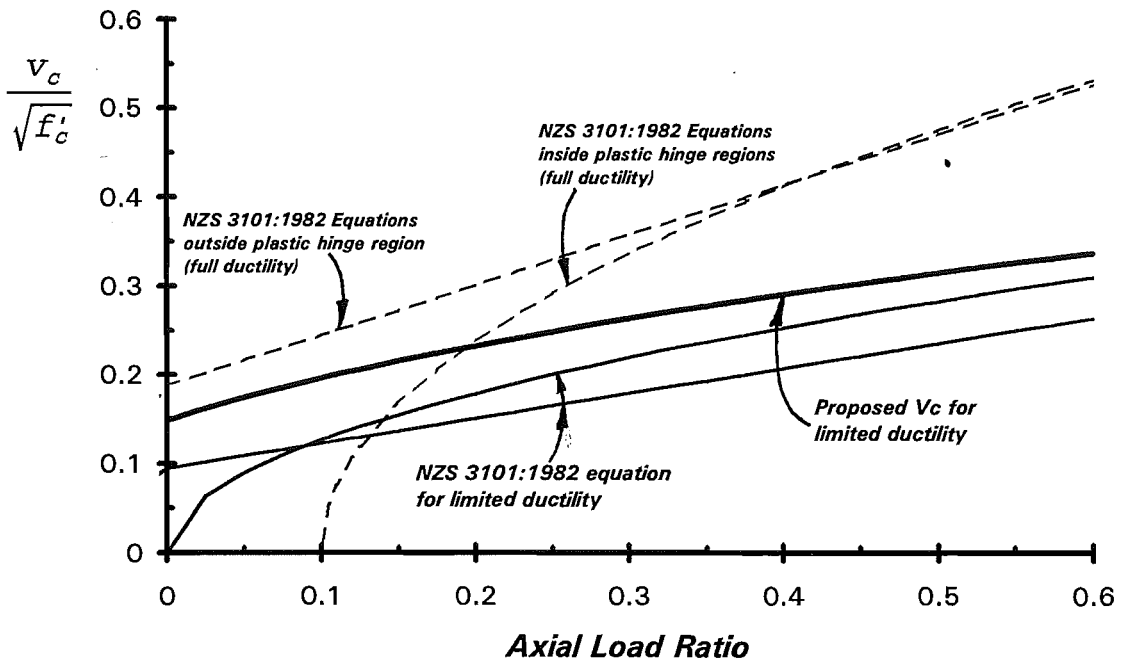

Fig.6.18: Comparisons of the Code[S14] Specified and the Proposed Shear Strength

As noted in the section 6.3.1, the code[S14] specified shear strength for the concrete mechanisms for inside potential plastic hinge regions will be increased to close to the shear strength for gravity load design when the axial compression load increases to larger than about $0.3f'_cA_g$. Clearly, the code specified fraction of one-half of the concrete contribution given by the code equations for outside potential plastic hinge regions will be less than that given by the code equations for inside potential plastic hinge regions at high axial load level(see Fig.6.18). This is obviously not logical. As the shear resistance of the concrete mechanisms degrades with the imposed displacement ductility factor, a reasonable value for the concrete shear strength of the column with limited ductility should be that which lies between the initial concrete shear resistance(elastic strength) and residual shear resistance(ductile strength).

The column tests conducted by Ang[A7] and by Priestley et al[P23] indicated that the concrete contribution to the shear resistance could maintained its initial value until a flexural displacement ductility factor of about 2.0. The results from the three column tests under varying axial load in this study and those tested by Wong[W3] under multi-direction loading histories indicated that shear resistance of the concrete mechanisms commenced to degrade at a displacement ductility factor of about

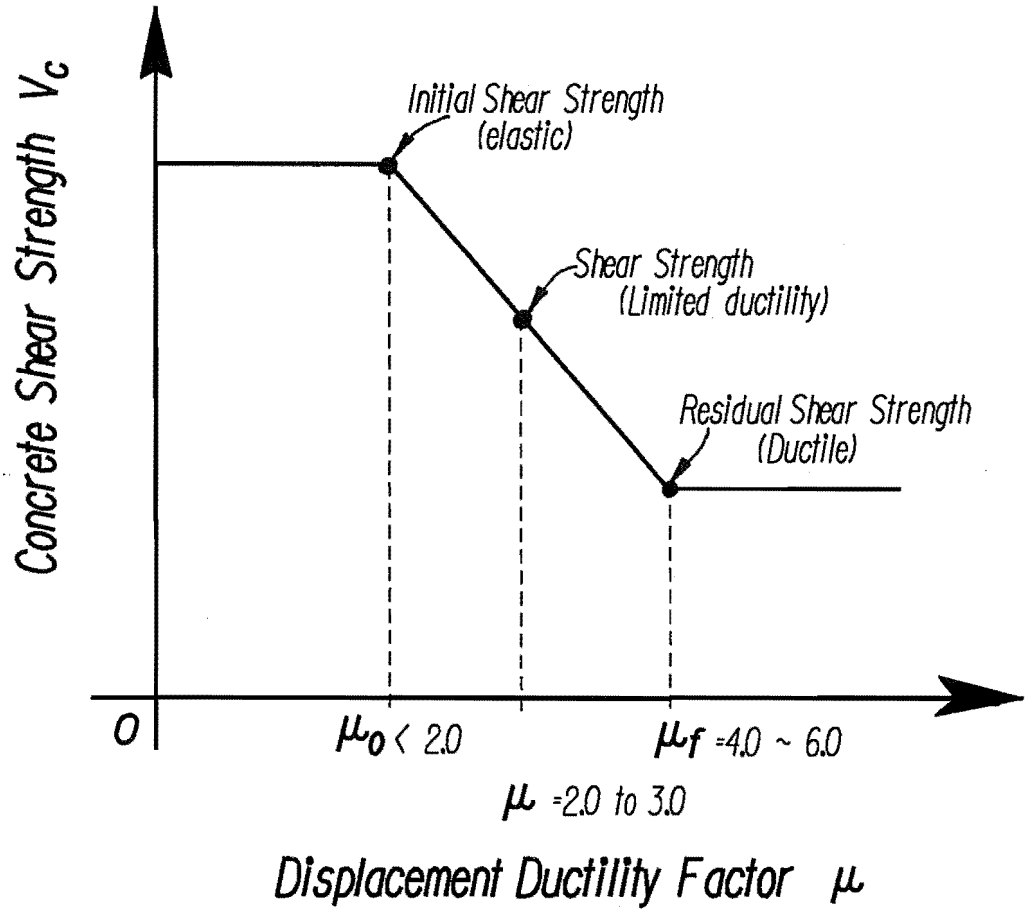

Fig.6.19: Relationship Between Shear Strength and Ductility Demand

1.5. Since the shear strength of the concrete mechanisms for columns with displacement ductility factor of 4 to 6 attains the residual shear strength, V_{cf}, the concrete shear strength for columns with displacement ductility factor of 2 to 3 should be part way between the initial shear strength and residual shear strength, as shown in Fig.6.19. Hence the shear resistance of the concrete mechanisms in the end regions of columns of structures with limited ductility could be taken as

$$V_{cl} = \left[0.22+2.4\sqrt{(0.1+\frac{P}{f'_c A_g})}\right] v_b b_w d \qquad (6.9)$$

Fig.6.18 compares the proposed shear strength of the concrete contributions(Eq.6.9) with the code[S14] specified value for the columns of structures with limited ductility.

6.7 CONCLUSIONS

1 The three reinforced concrete columns tested under cyclic lateral loading and varying axial loading failed in either shear-flexure, diagonal-tension or shear-compression modes. It appears that the type of shear failure mode is related to the ratio of axial force P to the shear force V applied, since the ratio P/V determined the direction of the thrust line of the external actions. A low P/V ratio tends to result in shear flexure failure. When the ratio P/V is high, the column will be more likely to fail in diagonal-tension or shear-compression mode.

2 On the basis of experimental results, equations for predicting the shear strength of reinforced concrete column are proposed. The proposed equations are based on the degrading shear strength model developed by Ang et al. Comparisons with experimental results indicate that the proposed equations result in a greatly improved prediction of the shear strength. The ratio of experimental maximum shear strength V_{exp} to the shear strength V_n predicted by proposed equations(Eqns.6.1 to 6.5) is 1.01.

3 Based on the limited experimental results, a tentative equation for determining the shear strength of the concrete mechanisms for columns with limited ductility is also suggested.

Table 6. 1 : Comparisons of Measured and Predicted Shear Strength When Compression Axial Load is Applied

Unit	M/VD	P/f'_cA_g	Initial Shear Strength					Residual Shear Strength						V_{NZS}	V_{exp}/V_{NZS}
			V_{exp} (kN)	V_{ci} (kN)	V_s (kN)	V_i (kN)	V_{exp}/V_i	V_{exp} (kN)	V_{cf} (kN)	V_s (kN)	V_f (kN)	V_{exp}/V_f	μ_n		
7	2.5	0.1	328	210	111	321	1.02	252	145	111	256	0.98	4.0	300	1.10
8	2.5	0.2	392	264	121	385	1.01	316	191	121	312	1.01	2.5	371	1.06
9	2.5	0.3	428	297	133	430	0.99	367	223	133	356	1.03	4.0	433	0.99

Note:

V_{NZS} is the shear strength given by the code provisions[NZS 3101: 1982] for outside potential plastic hinge regions.

Table 6.2 : Comparisons of Measured and Predicted Shear Strength When Tension Axial Load is Applied

Unit	M/VD	P/f'_cA_g	Initial Shear Strength					Residual Shear Strength						V_{NZS}	V_{exp}/V_{NZS}
			V_{exp} (kN)	V_{ci} (kN)	V_s (kN)	V_i (kN)	V_{exp}/V_i	V_{exp} (kN)	V_{cf} (kN)	V_s (kN)	V_f (kN)	V_{exp}/V_f	μ_n		
7	2.5	0.05	235	126	111	236	0.99	224	73	111	184	1.22	4.0	160	1.47
8	2.5	0.10	179	0	121	121	1.48	204	0	121	121	1.68	2.5	121	1.48
9	2.5	0.15	136	0	133	133	1.02	174	0	133	133	1.32	4.0	133	1.02

Note:

V_{NZS} is the shear strength given by the code provisions[NZS 3101: 1982] for outside potential plastic hinge regions.

Table 6.3: Details of Square Column By Woodward and Jirsa[W6]

Unit	M/VD	P/f'_cA_g	f'_c (MPa)	s_h (mm)	f_{yh} (MPa)	A_v (mm^2)	b_w (mm)	h (mm)	ρ_w	V_{exp} (kN)	V_n (kN)	V_{exp}/V_n	V_{NZS}	V_{exp}/V_{NZS}
O-86-14	1.52	0.00	41.1	65.3	450	56.6	300	300	0.0126	245	260	0.95	194	1.26
C-86-14	1.52	0.19	36.2	65.3	450	56.6	300	300	0.0126	303	321	0.95	241	1.25
O-86-32*	1.52	0.00	31.4	28.6	450	56.6	300	300	0.0126	280	347	0.80	304	0.91
C-86-32*	1.52	0.16	37.6	28.6	450	56.6	300	300	0.0126	356	417	0.85	357	0.99
C-86-21*	1.52	0.17	39.7	44.5	450	56.6	300	300	0.0126	360	346	1.04	286	1.25

Table 6.4: Details of Rectangular Columns By Umehara and Jirsa[U1]

Unit	M/VD	P/f'_cA_g	f'_c (MPa)	s_h (mm)	f_{yh} (MPa)	A_v (mm^2)	b_w (mm)	h (mm)	ρ_w	V_{exp} (kN)	V_n (kN)	V_{exp}/V_n	V_{NZS}	V_{exp}/V_{NZS}
O-PM	1.52	0.00	31.0	64	469	56.6	300	300	0.0126	267	249	1.07	192	1.39
O-PU	1.52	0.00	34.5	64	469	56.6	300	300	0.0126	249	257	0.97	196	1.27
C-PU	1.52	0.19	30.7	64	469	56.6	300	300	0.0126	298	313	0.95	239	1.24
O-PB*	1.52	0.00	41.3	64	469	56.6	300	300	0.0126	232	254	0.92	205	1.13
C-PB*	1.52	0.15	41.0	64	469	56.6	300	300	0.0126	338	309	1.09	248	1.36

Note for Table 3 and Table 4:

* the columns subjected to biaxial displacement.

V_{NZS} is the shear strength given by the code provisions[NZS 3101: 1982] for outside potential plastic hinge regions.

V_n is the shear strength predicted by proposed equations(Eqns.6.1 to 6.5)

Table 6.5: Details of Rectangular Columns By Wang[M10]

Unit	M/VD	P/f'_cA_g	f'_c (MPa)	s_h (mm)	f_{yh} (MPa)	A_v (mm^2)	b_w (mm)	h (mm)	ρ_w	V_{exp} (kN)	V_n (kN)	V_{exp}/V_n	V_{NZS}	V_{exp}/V_{NZS}
1	1.8	0.00	23.4	152	352	58.1	152	356	0.0233	138	139	0.98	110	1.25
2	1.8	0.10	23.4	152	352	58.1	152	356	0.0233	182	166	1.08	131	1.37
3	1.8	0.39	23.4	152	352	58.1	152	356	0.0233	191	217	0.88	192	0.99
4	1.8	0.00	24.1	152	352	58.1	152	356	0.0187	125	126	1.00	100	1.24
5	1.8	0.10	24.1	152	352	58.1	152	356	0.0187	169	148	1.13	118	1.42
6	1.8	0.19	24.1	152	352	58.1	152	356	0.0187	205	164	1.24	135	1.51
7	1.8	0.38	24.1	152	352	58.1	152	356	0.0187	191	1912	1.00	169	1.12
8	1.8	0.57	24.1	152	352	58.1	152	356	0.0187	205	213	0.96	204	1.00
9	1.8	0.00	27.6	76	352	58.1	152	356	0.0233	178	188	0.94	157	1.13
10	1.8	0.15	27.6	76	352	58.1	152	356	0.0233	205	229	0.89	191	1.10
11	1.8	0.00	27.6	76	352	58.1	152	356	0.0233	196	178	1.10	150	1.30
12	1.8	0.08	22.7	76	352	58.1	152	356	0.0233	231	200	1.15	166	1.39
13	1.8	0.44	22.7	76	352	58.1	152	356	0.0233	285	262	1.08	240	1.18
14	1.8	0.55	22.7	76	352	58.1	152	356	0.0233	294	276	1.06	264	1.11
15	1.8	0.65	22.7	76	352	58.1	152	356	0.0233	280	288	0.97	285	0.98
16	2.7	0.00	26.2	152	352	58.1	152	356	0.0233	107	110	0.96	114	0.93
17	2.7	0.08	26.2	152	352	58.1	152	356	0.0233	125	125	0.99	132	0.94
18	2.7	0.16	26.2	152	352	58.1	152	356	0.0233	145	137	1.05	150	0.96
19	2.7	0.31	26.2	152	352	58.1	152	356	0.0233	147	156	0.93	183	0.80

Note: V_{NZS} is the shear strength given by the code provisions[NZS 3101: 1982] for outside potential plastic hinge regions.

V_n is the shear strength predicted by proposed equations(Eqns.6.1 to 6.5)

Table 6.6: Details of Rectangular Columns By Priestley et al[P23]

Unit	M/VD	P/f'_cA_g	f'_c (MPa)	s_h (mm)	f_{yh} (MPa)	A_v (mm^2)	b_w (mm)	h (mm)	ρ_w	V_{exp} (kN)	V_n (kN)	V_{exp}/V_n	V_{NZS}	V_{exp}/V_{NZS}
R1A	2.0	0.06	38.0	127	358	63.3	406	610	0.0168	566	606	0.93	501	1.12
R3A	2.0	0.06	34.5	127	324	63.3	406	610	0.0168	627	573	1.09	473	1.32
R5A	1.5	0.06	32.4	127	324	63.3	406	610	0.0168	748	714	1.04	461	1.62

Note: V_{NZS} is the shear strength given by the code provisions[NZS 3101: 1982] for outside potential plastic hinge regions.

V_n is the shear strength predicted by proposed equations(Eqns.6.1 to 6.5)

Table 6.7: Details of Circular Columns By Priestley et al[P23]

Unit	M/VD	P/f'_cA_g	f'_c (MPa)	s_h (mm)	f_{yh} (MPa)	A_{sp} (mm^2)	D (mm)	ρ_w	V_{exp} (kN)	V_n (kN)	V_{exp}/V_n	V_{NZS}	V_{exp}/V_{NZS}
C1A	2.0	0.06	31.0	127	358	31.6	610	0.0253	574	540	1.06	444	1.29
C3A	2.0	0.018	34.5	127	324	31.6	610	0.0253	734	667	1.10	573	1.28
C5A	2.0	0.06	35.8	127	324	31.6	610	0.0253	614	567	1.08	464	1.32
C7A	1.5	0.06	30.7	127	324	31.6	610	0.0253	792	685	1.15	436	1.81

Note: V_{NZS} is the shear strength given by the code provisions[NZS 3101: 1982] for outside potential plastic hinge regions.

V_n is the shear strength predicted by proposed equations(Eqns.6.1 to 6.5)

Table 6.8 : Details of Circular Columns By Ang et al[A7]

Unit	M/VD	P/f'_cA_g	f'_c (MPa)	s_h (mm)	f_{yh} (MPa)	A_{sp} (mm^2)	D (mm)	ρ_w	V_{exp} (kN)	V_n (kN)	V_{exp}/V_n	V_{NZS}	V_{exp}/V_{NZS}
1	2.0	0.0	37.5	60	328	28.3	400	0.032	320	315	1.03	263	1.21
2	2.0	0.0	37.2	60	296	28.3	400	0.032	228	314	0.73	262	0.87
3	2.5	0.0	36.0	60	328	28.3	400	0.032	298	310	0.97	259	1.15
4	2.0	0.0	30.6	165	316	78.5	400	0.032	295	290	1.03	243	1.21
5	2.0	0.0	31.1	40	328	28.3	400	0.032	340	337	1.02	290	1.17
6	1.5	0.0	30.1	60	328	28.3	400	0.032	390	359	1.08	244	1.59
7	2.0	0.0	29.5	80	372	28.3	400	0.032	280	275	1.01	229	1.22
8	2.0	0.2	28.7	30	372	28.3	400	0.032	475	490	0.96	443	1.07
10	2.0	0.2	31.2	120	332	113.1	400	0.032	450	480	0.93	431	1.04
11	2.0	0.2	29.9	60	372	28.3	400	0.032	404	398	1.01	350	1.15
12	0.1	0.1	28.6	30	328	28.3	400	0.032	527	509	1.03	373	1.41
13	2.0	0.1	36.2	30	326	28.3	400	0.032	443	456	0.97	397	1.11
14	2.0	0.0	33.7	60	326	28.3	400	0.0324	311	303	1.02	253	1.22
15	2.0	0.0	34.8	60	326	28.3	400	0.0192	230	238	0.96	203	1.13
16	2.0	0.1	33.4	60	326	28.3	400	0.032	379	357	1.06	300	1.26
17	2.5	0.1	34.3	60	326	28.3	400	0.032	329	361	0.91	303	1.08
18	1.5	0.1	35.0	60	326	28.3	400	0.032	507	456	1.11	305	1.66
19	1.5	0.1	34.4	80	326	28.3	400	0.032	436	432	1.00	282	1.54
20	1.8	0.18	36.7	80	326	28.3	400	0.032	487	433	1.12	331	1.47
21	2.0	0.0	33.2	80	326	28.3	400	0.032	258	278	0.92	229	1.12
22	2.0	0.0	30.9	220	310	78.5	400	0.032	280	268	1.04	220	1.27
23	2.0	0.0	32.3	160	308	78.5	400	0.032	339	334	1.01	286	1.18
24	2.0	0.0	33.1	110	310	78.5	400	0.032	338	338	1.00	289	1.16

Note: V_{NZS} is the shear strength given by the code provisions[NZS 3101: 1982] for outside potential plastic hinge regions.

V_n is the shear strength predicted by proposed equations(Eqns.6.1 to 6.5)

Chapter 7

Modelling the Flexural Hysteretic Relationship of Reinforced Concrete Columns

7.1 INTRODUCTION

Reinforced concrete structures subjected to strong earthquake excitation will sustain inelastic deformations at certain critical regions. The inelastic dynamic analysis of reinforced concrete structures requires realistic analytical models which can represent the strength, stiffness and energy dissipation characteristics of the members. Various hysteretic models have been proposed in recent years to describe the behaviour of reinforced concrete members. These models range from quite simple ones, such as elasto-plastic and bi-linear models, to more sophisticated ones, such as degrading stiffness models. While each of these models can reasonably predict different characteristics of the structural response, none of model can accurately simulate every aspect of reinforced concrete hysteretic response.

This chapter considers a number of issues that effect the hysteretic response of reinforced concrete columns. First, the local contact effects of cracked concrete is studied. In reinforced concrete members

subjected to cyclic flexure, with or without axial load, concrete which was cracked previously in tension can carry some compression across cracks before they close.

Next, the experimental evidence for the enhancement of flexural strength of columns is examined. An empirical equation for flexural strength enhancement due to Ang et al[A7] is examined. That equation considers axial load level as the only variable. The equation is modified to take into account the effect of degree of concrete confinement and the ratio of area of cover to core concrete on the flexural strength enhancement.

Finally, the effect of varying axial load on the flexural hysteretic behaviour of reinforced concrete column is studied. The effect of constant axial load on the flexural behaviour has been thoroughly investigated previously[A6, M2, S12 and Z3]. However, varying axial load introduces additional complication of variable yield moment and yield deformation.

One of the most significant aspect of hysteretic modelling is the construction of the primary curve, since it serves as the envelope for the strength and conveniently reflects the interactive effects of flexure-axial force and reinforcement slippage. It is therefore essential to determine the main stiffness parameters, that is, the initial stiffness and post-yield stiffness of the member section, in order to construct the primary hysteretic curve. Although the parameters used to determine the hysteretic behaviour can be computed through section analysis based on the section properties and reliable stress-strain laws of materials, the computation of the stiffness parameters can be cumbersome for the analyst, especially if concrete confinement and steel strain hardening are to be considered. As a result, rough approximations of section stiffness are often made in the inelastic response analysis, which has possibly reduced the accuracy of the analysis. There is a need to develop a simple and more accurate method to calculate the flexural stiffness of reinforced concrete column sections.

In this section of this chapter parametric study of a full range of variables on the flexural stiffness of reinforced concrete column sections is carried out and the significant variables are determined. Simple equations are developed to evaluate the initial elastic and post-yield stiffness of column sections. Comparisons of the calculated stiffness are made with the results of experiments conducted in recent years at the University of Canterbury. Also, based on the experimental results of the columns tested, a hysteretic model for reinforced concrete column including the effect of varying axial loading histories is proposed.

7.2 LOCAL CONTACT EFFECTS OF CRACKED CONCRETE ON THE HYSTERETIC RESPONSE

Theoretical moment-curvature analysis can provide a basis for the assessment of the flexural strength and ductility available from the reinforced concrete sections. Moment-curvature analysis can be conducted providing that the stress-strain relationships for the concrete and steel are known. It is essential to have accurate information concerning the complete stress-strain models in order to obtain reliable moment-curvature relationships. The available material models for the confined or unconfined concrete are capable of simulating many phases of the monotonic and cyclic response of reinforced concrete section. However, there are still some phenomena that could affect the moment-curvature response, such as the post-cracking effect described below, as well as bond deterioration and inelastic shear effects, which are not well modeled.

In current moment-curvature analysis, it is commonly assumed that cracked concrete in the compression zone does not carry any compression until the cracks completely close[K1,M2, M3]. This is shown, for example. in the stress-strain relation for concrete employed in moment-curvature analysis by Mander et al[M3], as shown in Fig.7.1. When reloading occurs after cracking in tension the concrete stress is assumed to be zero until the strain reversal reaches the plastic strain ε_{pl}. With the above assumption, over a large proportion of the theoretical moment-curvature hysteresis curve, the moment is carried by a steel couple alone[P5,M2]. As a result, the theoretical moment-curvature hysteretic curve displays a marked pinching which was different from what was observed from experimental tests by Kent[K1]. The observed moment-curvature hysteresis loops are fatter than theoretical predictions. This is due to the fact that some compression can be carried across cracks before they completely close. The results of an experimental test conducted by Zhu et al[Z5] also indicate that cracked concrete in the compression zone does carry some compressive stress before the cracks close. The mechanism by which the compression can be transferred across the cracks is discussed below.

In reality, clean cracks do not exist since the particles of concrete that flake off during cracking lodge in the cracks. This enables the crack faces to make local contact and compression force to be transferred across cracks before complete closure of cracks occurs. Small relative shear displacements along the crack also causes high spots on the crack faces to come into contact gradually rather than suddenly and this causes compression to be transferred across the cracks gradually. Friction may develop along the rough surface of aggregate particles that pull out during cracking and this friction also contributes to compression carried across unclosed cracks.

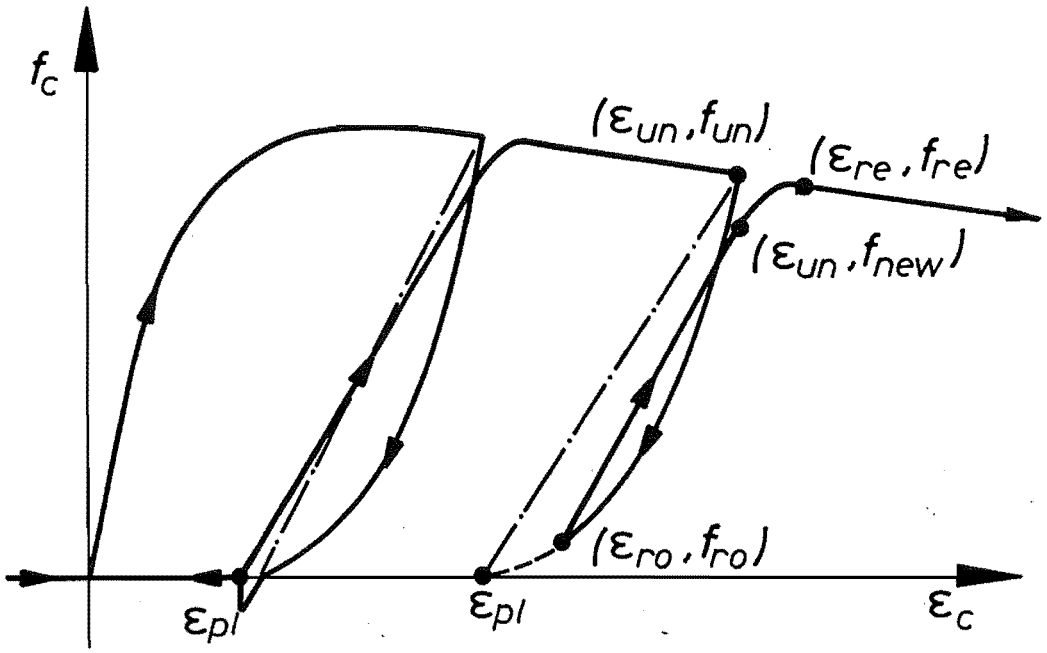

Fig.7.1 Stress-Strain Model for Concrete due to Mander[M3]

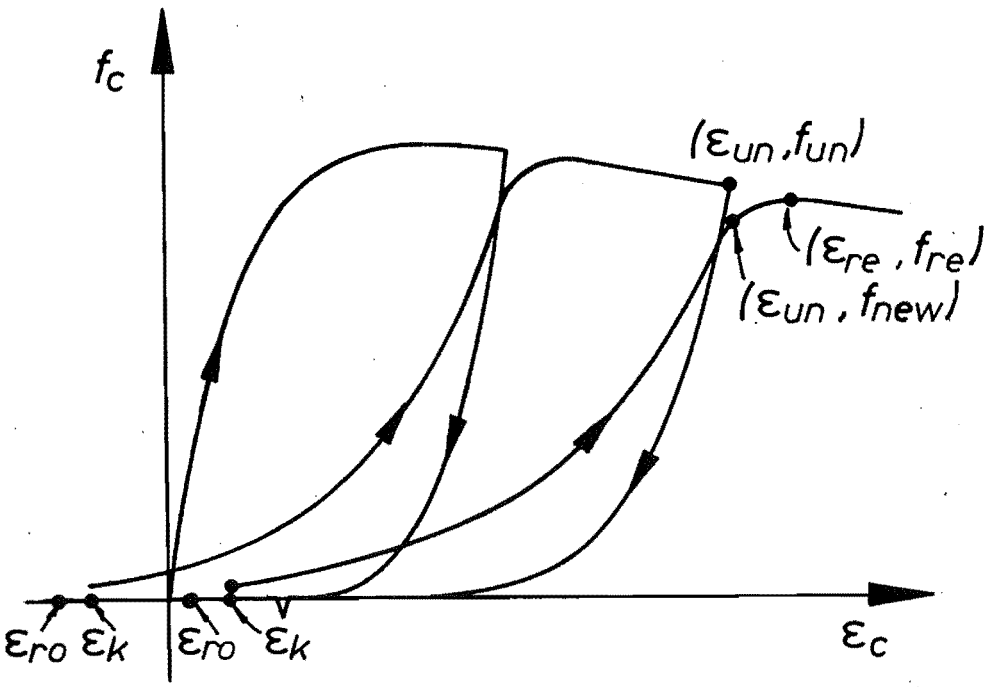

Fig.7.2: Stress-Strain Model for Concrete Including the Proposed Reloading Brance

In order to model the above phenomenon, an equivalent stress-strain reloading branch is proposed in this study. This reloading branch is integrated with the skeleton curve proposed by Mander et al[M2]. Fig.7.2 shows the stress-strain relation including the skeleton curve, the unloading and the herein proposed reloading branches. The definitions for the skeleton curve and unloading branch can be found elsewhere[M2,M3].

When strain reversal occurs from the tension state, a contact strain point ε_k is determined. The value of ε_k is given by $\varepsilon_k=\alpha_1\varepsilon_{ro}$, where ε_{ro}= the strain at the reloading reversal(see Fig.7.2); and α_1= a coefficient that is related to the maximum crack width experienced during the previous loading sequences and the size of concrete aggregate. The value of α_1 can be determined from experimental data. In this study, the value of the coefficient α_1 was taken as 0.8 when $\varepsilon_{ro}\leq 0$ and as 1.0 when $\varepsilon_{ro}>0$, taking compression strain as positive. It is assumed that the cracked concrete commences to carry compression when the contact strain ε_k is reached. The reloading curve between ε_k and unloading strain ε_{un} is then defined as a modified form of the relation for the unloading curve given by Mander[M3] as

$$f_c = f_{new} - \frac{f_{new}\, Xr}{r-1+X^r} \qquad (7.1)$$

in which

$$X = 0.6\frac{\epsilon_c-\epsilon_{un}}{\epsilon_k-\epsilon_{un}} \qquad r = \frac{E_u}{E_u-E_{sec}}$$

$$E_{sec} = \frac{f_{new}}{\epsilon_{un}-\epsilon_k} \qquad E_u = 0.8bcE_c \qquad (2)$$

$$b = \frac{f_{new}}{f'_c} \qquad c = \left(\frac{\epsilon_{cc}}{\epsilon_{un}}\right)^{\frac{1}{2}} \leq 1$$

and E_c = modulus of elasticity of concrete and f_{new} = new concrete stress on reloading at strain of ε_{un}.

To assess the validity of the proposed stress-strain reloading branch, in improving the accuracy of cyclic moment-curvature analysis, the experimental results obtained by Park et al[P5] from a reinforced concrete beam subjected to cyclic bending moment, and by Soesianawati[S12] from a reinforced concrete column under axial compression load and reversed cyclic lateral loading, were checked against the results from theoretical predictions. The stress-strain relationship for concrete with the proposed reloading branch was used in the computer program to calculate the theoretical moment-curvature hysteresis loops. The computed results are compared with experimental data in Fig.7.3 for the beam and in Fig.7.4 for the column, respectively. Theoretical predictions using original concrete model due to Mander[M3] were also obtained and are shown in Figs.7.3 and 7.4 as well. The results indicate that the proposed reloading branch is quite effective in improving the accuracy of moment-curvature analysis.

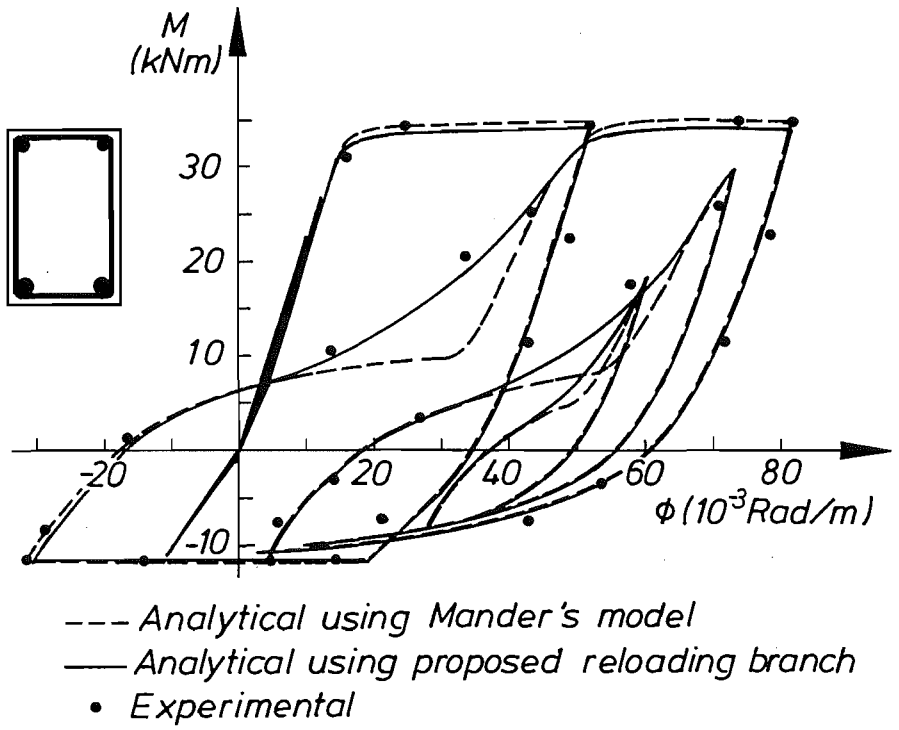

Fig.7.3: Moment-Curvature Relations for Unsymmetrically Reinforced Concrete Beam

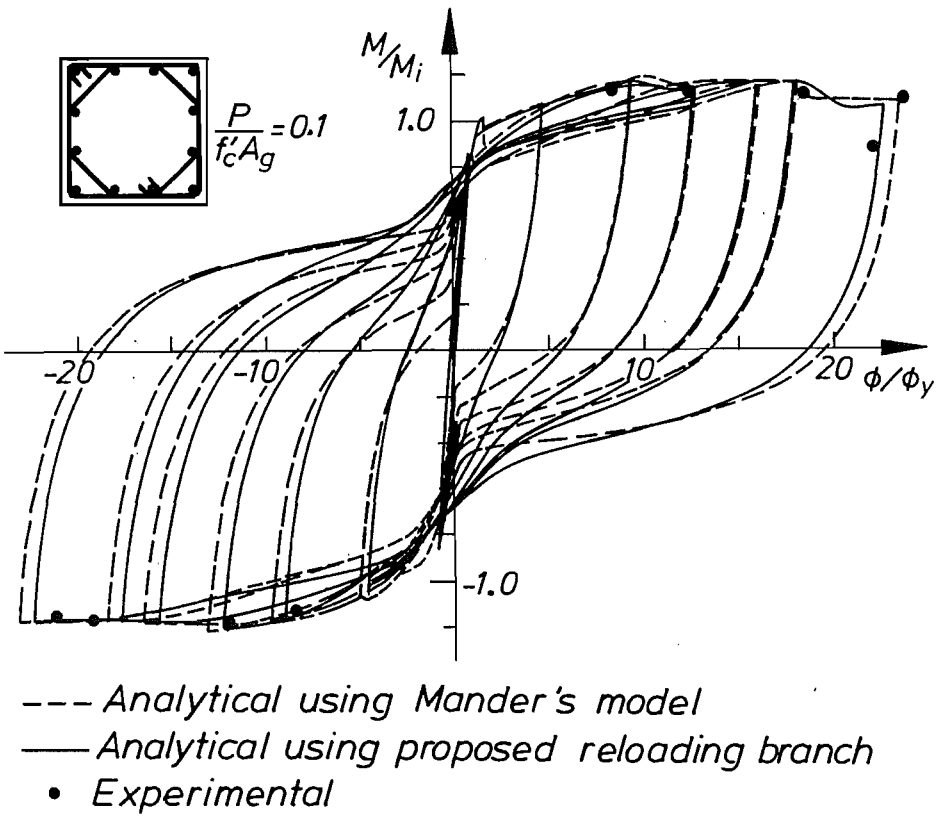

Fig.7.4: Moment-Curvature Relations for Symmetrically Reinforced Concrete Column

7.3 FLEXURAL OVERSTRENGTH OF CONFINED CONCRETE COLUMN

The theoretical flexural strength of a reinforced concrete column section, as specified by many codes, is calculated by assuming a rectangular compressive concrete stress block with mean stress of $0.85f'_c$, an extreme fibre concrete compressive strain of 0.003, and specified material strengths f'_c and f_y. The experimental results from previous researches[P7,P21] have indicated that the conventional code approach gives a very conservative prediction of the flexural strength of reinforced concrete columns designed for ductile flexural response. The conservative prediction of the flexural strength by the code approach is mainly because the transverse reinforcement provided to improve the ductility of the column also results in an enhancement of the concrete compressive strength and ultimate strain due to confining stress. The increased ultimate concrete compressive strain results in larger deformation capacity. In addition, strain hardening of the longitudinal reinforcement causes flexural strength enhancement. Strain hardening of longitudinal reinforcement was observed to occur in the tests when column was subjected to large inelastic deformation at high displacement ductility levels. In the design of reinforced concrete columns shear failure must be avoided. Hence it is required that the shear strength of the column be not less than the shear force corresponding to the development of probable flexural strength of the column. It follows that an accurate estimate of the flexural overstrength is essential to obtain the maximum shear acting on the column based on which the shear capacity of the column can be provided.

The test results indicated that the flexural strength enhancement of columns is strongly dependent on the axial load level. Based on the experimental results on the confined concrete columns tested at the University of Canterbury in recent years, Ang et al[A7] derived an empirical formula(Eq.4.1) for estimating the flexural overstrength factor. In this formula, the axial load ratio was taken as the only parameter which effects the flexural strength enhancement. The equation predicts the general trend of the measured flexural overstrength, but less satisfactory results were found in some cases, especially for columns with high compression axial load.

It has to be emphasized that the reinforced concrete columns tested at the University of Canterbury during recent years all had a heavily reinforced concrete stub or base block that was adjacent to the critical region of the column. The heavily reinforced concrete stub or column base provide additional confinement in the regions of the column adjacent to the stub. Sheikh and Khoury[S10] have demonstrated that a heavy stub provided additional confinement to the adjacent section and increased section moment capacity by more than 20%. This moves the failure to a section away from the stub where the stub restraining effect is minimal. However, the columns tested at the University of

Canterbury with stubs are realistic for bridge piers or columns in a framed structure[D1], because the plastic hinge region of such members will form adjacent to beams of the foundation or footing.

As stated before, the enhancement of the flexural strength over the theoretical flexural strength based on code approach mainly come from the increase in concrete compressive strength over the specified concrete strength due to confinement. The strain hardening of longitudinal reinforcement may further increase the flexural strength but this occurs only when the column experiences significant inelastic deformation. The enhanced concrete compressive strength is directly related to the degree of confinement. Mander[M2] in evaluating test results of confined columns expressed the confined concrete strength ratio, f'_{cc}/f'_c, as the function of confining stress f'_l provided by confining reinforcement, whose magnitude is mainly dependent on the volumetric ratio and yield strength of the confining reinforcement. Furthermore, the ideal flexural strength is normally calculated on the basis of the gross section dimensions. However the confinement due to the transverse reinforcement can only increases the concrete compressive strength in the core of the section. At the maximum flexural strength, the cover concrete in compression zone generally has shown distress or spalled. Therefore, the enhanced flexural strength should be related to the proportion of core concrete area to the gross section area.

To improve the its accuracy in predicting the flexural overstrength, Ang's Eq.4.1 can be modified to include above factors. The following modified equations were found by trial and error in this present study for the ratio of the maximum flexural strength to the theoretical flexural strength based on the conventional code approach.

$$For \quad P/(f'_c A_g) < 0.1 : \qquad \frac{M_{max}}{M_i} = 1.16 \tag{7.2a}$$

$$For \quad P/(f'_c) \geq 0.1 :$$

$$\frac{M_{max}}{M_i} = \alpha\left[1.16 + 2.6\left(0.8\frac{A_c}{A_g}R^{\frac{1}{2}}\frac{P}{f'_c A_g} - 0.1\right)^2\right] \tag{7.2b}$$

In which, M_i is the flexural strength given by conventional US or New Zealand code approach using the actual f'_c and f_y values and assuming a strength reduction factor $\phi = 1$; A_c/A_g is the core concrete area ratio, where A_c = area of core concrete, A_g = gross section area, $R = f'_{cc}/f'_c$ is concrete strength ratio, where f'_c = unconfined concrete compressive strength and f'_{cc} = confined concrete compressive strength. The value of f'_{cc} can be determined by the model developed by Mander et al[M2] and later

modified by Zahn et al[Z3]. The factor α is introduced to allow for the reduction in the flexural overstrength due to loading histories. For the columns tested in this study which were subjected to varying axial tension and compression load, the flexural overstrength was reduced about 15%. For these columns, it is assumed that $\alpha=0.85$.

The comparisons between the experimentally obtained flexural overstrength factors for the column units and those obtained from the proposed Eq.7.2a and b are given in Table 7.1. The flexural overstrength factors predicted by Ang's Eq.4.1 are also included in this table. Fig.7.5 plots the ratio, M_{max}/M_j, against axial load level for the experimental results and Eqns.4.1 and 7.2. It was found that all experimental results fall within the shaded area which represents a variation of ±8% from the average enhancement values given by Eq.7.2.

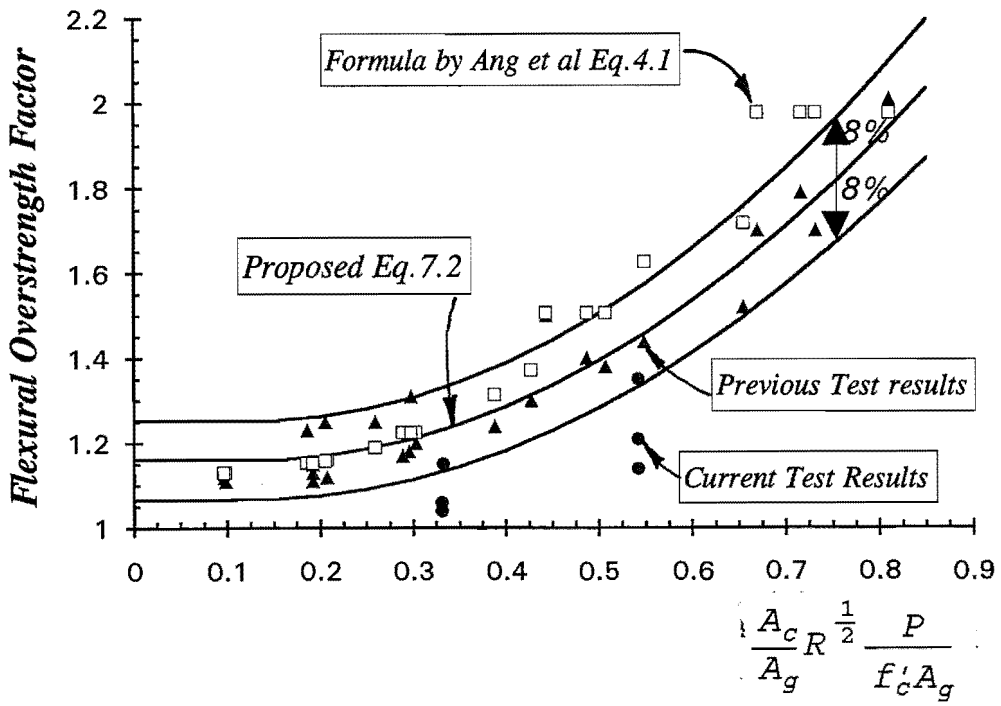

Fig.7.5: Prediction of the Strength Enhancement Factor of Confined Concrete Column

Table 7.1: Comparisons of experimental and predicted flexural overstrength factors

Unit	$\frac{P}{f'_c A_g}$	$\frac{A_c}{A_g}$	$\frac{f'_{cc}}{f'_c}$	M_{ACI} (kN.m)	M_{EXP}	$\frac{M_{EXP}}{M_{ACI}}$	Eq.4.1	Eq.7.2	Reference
G1	0.26	0.855	1.36	691	863	1.25	1.19	1.19	Gill[G1]
G2	0.21	0.855	1.34	905	1013	1.12	1.16	1.17	
G3	0.42	0.855	1.41	646	839	1.30	1.37	1.31	
G4	0.60	0.855	1.63	598	908	1.52	1.72	1.62	
S1	0.10	0.935	1.11	302	335	1.11	1.13	1.16	Soesianawiti[S12]
S2	0.30	0.935	1.17	405	486	1.20	1.23	1.21	
S3	0.30	0.935	1.11	406	479	1.18	1.23	1.20	
S4	0.30	0.935	1.06	383	448	1.17	1.23	1.20	
S5	0.50	0.935	1.18	381	525	1.38	1.51	1.40	
S6	0.50	0.935	1.09	376	626	1.40	1.51	1.37	
S7	0.70	0.935	1.25	304	516	1.70	1.98	1.77	
S8	0.70	0.935	1.20	293	524	1.79	1.98	1.74	
S9	0.70	0.935	1.53	298	598	2.01	1.98	1.94	
S10	0.50	0.935	1.24	259	388	1.50	1.51	1.34	
S11	0.70	0.935	1.33	214	363	1.70	1.98	1.65	
A1	0.20	0.875	1.26	216	265	1.23	1.15	1.16	Ang[A6]
A1	0.56	0.875	1.40	215	309	1.44	1.63	1.50	
A3	0.38	0.875	1.37	269	333	1.24	1.32	1.27	
A4	0.21	0.875	1.25	258	322	1.25	1.16	1.17	
T1	0.20	0.855	1.27	251	278	1.11	1.16	1.16	Tanaka [T3]
T2	0.20	0.855	1.27	251	283	1.13	1.16	1.16	
T3	0.20	0.855	1.27	251	288	1.15	1.16	1.16	
T4	0.20	0.855	1.27	251	283	1.13	1.16	1.16	
T5	0.10	0.855	1.27	601	673	1.12	1.13	1.16	
T6	0.10	0.855	1.27	601	679	1.13	1.13	1.16	
T7	0.30	0.855	1.35	797	1044	1.31	1.22	1.20	
T8	0.30	0.855	1.35	797	1044	1.31	1.22	1.20	
Unit 1	0.30	0.93	1.32	345	408	1.18	1.23	1.23	Series 1
Unit 2	0.30	0.93	1.34	356	389	1.09	1.23	1.05	
Unit 3	0.30	0.93	1.34	356	405	1.13	1.23	1.05	
Unit 4	0.50	0.93	1.47	348	493	1.42	1.51	1.49	
Unit 5	0.50	0.93	1.47	348	446	1.28	1.51	1.27	
Unit 6	0.50	0.93	1.47	348	429	1.22	1.51	1.27	
Unit 7	0.10	0.93	1.12	331	333	1.01	1.13	0.99	Series 2
Unit 8	0.21	0.93	1.12	389	402	1.03	1.16	0.99	
Unit 9	0.31	0.93	1.13	413	442	1.10	1.23	1.02	

7.4 CHARACTERISTICS OF CONFINED REINFORCED CONCRETE COLUMN SECTIONS

As is well known, a beam section is generally designed such that its reinforcing steel yields in tension. Ductile behaviour of a beam section can be achieved by limiting its tension reinforcement content. Due to the increase in neutral axial depth caused by compressive axial load, the longitudinal reinforcing steel in a column section does not yield in tension when the axial compression is high. For such a column, sufficient transverse reinforcement has to be provided to confine the core concrete of the section to achieve ductile behaviour. The quantity of confinement steel required in the column section to achieve certain ductility level is related to the axial load level. A confined column section possesses specific features of strength and stiffness, which to some extent, are different from those of a beam section.

One of important features of reinforced concrete columns is the variation of the section stiffness under different axial load level. Variation of section stiffness at a range of deformation levels is directly related to the cracking of the concrete and the possible strain softening of the concrete. Hence the extent of variation in section stiffness is significantly influenced by axial compression load and transverse reinforcement. For a section subjected to low axial compression, extensive cracking of concrete and tension yielding of longitudinal reinforcement are expected. On the other hand, for a column with high axial compression, the cracking of concrete is not extensive and the longitudinal reinforcement may not yield in tension. The higher the axial compression on the column, the higher the elastic stiffness of the section.

The results of the experiments indicated that the flexural strength of reinforced concrete column sections is significantly increased due to the enhancement of the concrete strength caused by confinement and the strain hardening of the longitudinal reinforcement. The post-yield behaviour of a reinforced concrete column is greatly influenced by the degree of confinement, which depends on several factors including the spacing of longitudinal and transverse reinforcement, and the amount, arrangement and yield strength of the confining steel. These features of confined column sections have to be considered in order to evaluate the post-yield stiffness.

When a column is loaded into inelastic range with flexural cracking in the end regions, the moment of inertia will vary along the column height(Fig.7.6). The moment of inertia, I, at any section will be influenced by the magnitude of the moment, and axial load and the amount of reinforcing steel, as well as the section geometry. The tension stiffening will cause further stiffness variations between cracked sections and the sections between cracks[P6,P17]. The section stiffness varies from section to section along the column height.

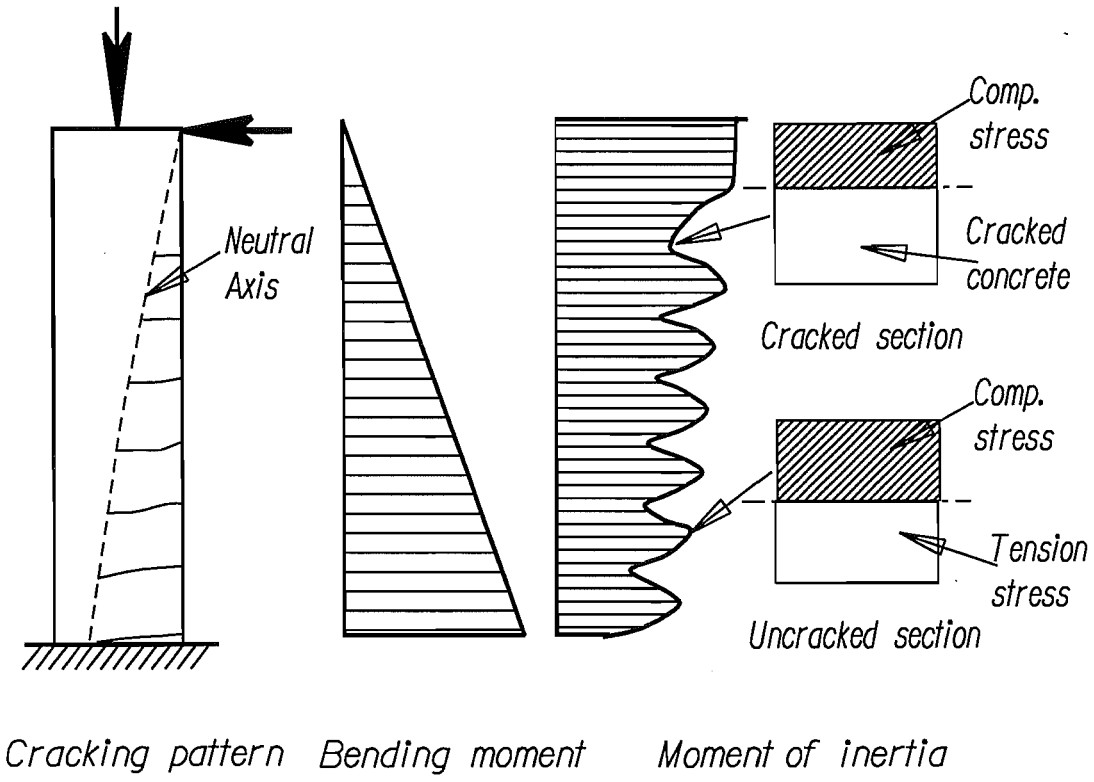

Fig.7.6: Variation of Sectional Propoties Along Column Height

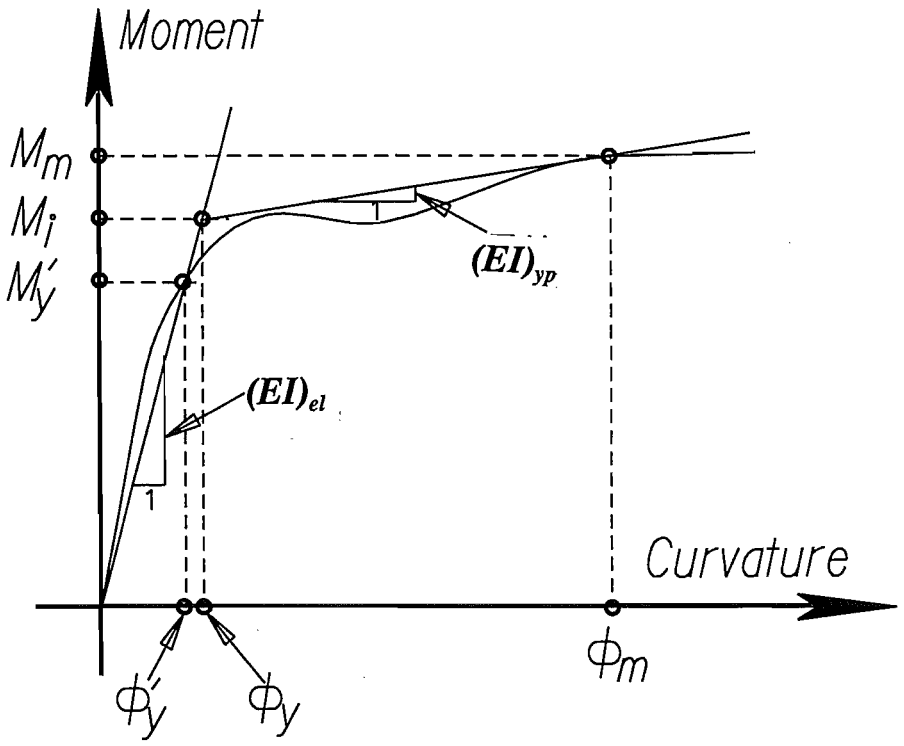

Fig.7.7: Moment-Curvature Relationship for Reinforced Concrete Column Section

For the purpose of design, the stiffness of a column in the elastic range is generally obtained from an average value of the section flexural rigidity along the length of the member, known as the effective stiffness. For inelastic response analysis of reinforced concrete frames, a member is generally modelled as single-spring element or finite element model, which requires the additional information of the moment-curvature relations in the end regions where the inelastic rotation is expected to occur.

7.5 INITIAL AND POST-YIELD STIFFNESS OF REINFORCED CONCRETE SECTIONS

Hysteretic models can generally be expressed in the form of moment-curvature relationships. Fig7.7 shows a typical moment-curvature relationship for a reinforced concrete column section which experiences inelastic deformation. Most hysteretic models are defined on the basis of the primary moment-curvature curve which can be idealized as a bilinear relationship. The first line segment on the primary curve represents the elastic flexural rigidity of a critical section. The second line segment characterizes the post-yield section rigidity.

The elastic flexural rigidity, $(EI)_{el}$, at a cracked section can be defined as(see Fig.7.7):

$$(EI)_{el} = \frac{M'_y}{\phi'_y} \qquad (7.3)$$

where ϕ'_y and M'_y can be defined as the curvature and corresponding moment calculated at the instant when the steel at the extreme tensile fibre of the section reaches yield or when the concrete compressive strain at the extreme fibre reaches 0.002, whichever occurs first. This dual definition of the yield curvature is because in columns with high axial load the tension steel will normally not yield before the section has lost considerable flexural rigidity. Then the curvature when the extreme fibre reaches a compressive strain of 0.002 is similar to that at first yield of the tension steel in the columns with low axial load.

The post-yield(second slope) line segment is assumed to start at the defined theoretical yield point (ϕ_y, M_i) of moment-curvature relationship. The post-yield flexural rigidity of the section is then defined as(see Fig.7.7):

$$(EI)_{py} = \frac{M_m - M_i}{\phi_m - \phi_y} \qquad (7.4)$$

where M_i is the ideal flexural strength of the column section calculated using conventional code approach and the theoretical yield curvature ϕ_y is calculated by extrapolating a straight line from the origin through the point(ϕ'_y,M'_y), so that $\phi_y=\phi'_yM_i/M'_y$. The post-yield line segment of the primary moment-curvature relation characterizes the general behaviour of the column section after yielding. The flexural strength of reinforced concrete column sections generally continue to increase after yielding due to strain hardening of the longitudinal reinforcement and the concrete strength enhancement due to confinement. The strain hardening of the longitudinal bars normally occurs at around curvature ductility factor of about 10, depending on the axial load level. The results of reinforced concrete columns tested under cyclic loading[P22] indicated that column sections designed according to the current New Zealand concrete code[S14] are able to achieve a curvature ductility factor of 10 or more without significant reduction in flexural strength. Therefore, ϕ_m and M_m in Eq.7.4 can be assumed to be the curvature and associated moment when the curvature reaches $10\phi_y$.

7.6 MOMENT-CURVATURE ANALYSIS

7.6.1 The Approach

Moment-curvature analysis was carried out to obtain the main flexural stiffness parameters of reinforced concrete column sections as defined in Section 7.5. The discrete element(fibre) model was adopted to compute moment-curvature relationships based on the assumptions that plane sections before bending remain plane after bending and that stress-strain relations for concrete and steel are known. The stress-strain relations proposed by Mander et al[M2] for longitudinal steel and for concrete were employed in this analysis. It is known that these stress-strain models are capable of successfully simulating the characteristics of reinforced concrete sections[M2, W2, Z3]. The tensile strength of the concrete is neglected.

In the analysis, the concrete strain corresponding to the compressive strength of unconfined concrete f'_c was taken as 0.002 and the initial tangent modulus E_c was taken to $4700\sqrt{f'_c}$ (MPa).

The values used to define the stress-strain curve for the longitudinal steel both in tension and compression are summarized in Table 7.2, based on the previous studies in New Zealand[W2,Z3].

Table 7.2: Parameters Assumed for the Stress-Strain Curve of Reinforcing Steel

	f_y (MPa)	f_{su} (MPa)	ε_{sh}	ε_{su}	E_s (MPa)	E_{sh} (MPa)
Grade300	350	460	0.015	0.16	190000	4500
Grade430	450	650	0.013	0.15	200000	6500

7.6.2 The Parameters Investigated

Theoretical moment-curvature analyses were conducted on a full range of variables to determine the influence of each variable on the section rigidity. The variables selected in the analysis included the axial load ratio P/f'_cA_g, the longitudinal reinforcement ratio ρ_t, the concrete compressive strength f'_c, the core concrete ratio c/h, where c=concrete cover thickness, and h=column depth, and the yield strength of the longitudinal reinforcing steel f_y. The range of variables considered is shown in Table 3.

The range of axial compression loads investigated was from 0.0 to $0.7f'_cA_g$. The lower and upper limits of the ratio of longitudinal reinforcement to gross section area, according to the New Zealand concrete design code[S14], are of 0.008 and 0.06. In the analysis, a longitudinal reinforcement ratio, ρ_t, from 0.01 to 0.045 was examined. The longitudinal reinforcement was considered to be distributed uniformally around the perimeter of the column. A range of concrete compressive strength of from 25 MPa to 45 MPa was investigated, which covered the commonly used values.

Table 7.3: Range of Variables Investigated

Variables	Description	Range Investigated
P/f'_cA_g	Axial Load Ratio	0.0 to 0.7
ρ_t (%)	Longutudinal Reinforcement Content, distributed uniformally around the perimeter of column	1.0 to 4.5
f'_c (MPa)	Concrete Compressive Strength	25,30,35,40,45
c/h	Cover Concrete Ratio	0.02,0.045,0.064,0.082
⊠	Section Demensions	400×400, 550×550, 700×700

The minimum concrete cover thickness required by the New Zealand concrete design code[S14] for ties, hoops and stirrups in the columns is 40 mm or 25 mm depending on whether or not the concrete is exposed to weather. The most commonly used size of column section in design is between 350 mm and 1200 mm. Thus, the lower and upper limits of the cover ratio are 0.021 to 0.11. In this study, the range of cover concrete ratio c/h varied from 0.02 to 0.082, and the corresponding ratio of core concrete area A_c to the gross section area A_g were from 0.92 to 0.70.

The transverse reinforcement provided in the sections was assumed to be in accordance with the requirements of the New Zealand concrete design code[S14] for the plastic hinge regions of reinforced concrete columns of ductile structures, that is, full code confinement, when investigating the effects of variable on the section flexural rigidity.

A 550 mm square section with concrete compressive strength of 35MPa, steel yield strength of 450 MPa, cover concrete ratio of 0.036 and longitudinal reinforcement ration of 1.8 percent, was chosen as the basic section. The different variables were then changed to investigate their effects on the section stiffness.

7.7 DISCUSSION OF COMPUTED RESULTS

7.7.1 The Manner of Presentation of the Results

The moment-curvature analyses were performed to obtain the elastic flexural rigidity at a cracked section and the post-yield second slope flexural rigidity of the reinforced concrete column sections as given by Eqns.7.3 and 7.4. The computed results for the elastic flexural rigidity and post-yield second slope flexural rigidity were presented in the forms of $(EI)_{el}/(EI)_g$ and $(EI)_{py}/(EI)_{el}$, where I_g is the moment of inertia of the gross concrete section, neglecting the longitudinal reinforcement.

7.7.2 The influence of Axial load Level on the Yield Curvature

The investigation was first conducted to examine the influence of axial load level on the first yield curvature ϕ_y, since this was considered important in understanding the effects of the various parameters on the variation of section stiffness. Fig.7.8 plots the yield curvature obtained from the moment-curvature analysis against the axial load ratio with various longitudinal reinforcement contents. It is evident from Fig.7.8 that variation in the axial load level can significantly influence the yield curvature.

The variation of the yield curvature shown in Fig.7.8 can be explained as follows. It was found from the analysis, for low axial load levels(P less than about $0.2f'_cA_g$), that yielding of the steel closest to the tension face of the section occurs before the extreme concrete fibre compression strain reaches 0.002. In this axial load range, the yield curvature increases as the axial load level increases, since a higher axial load requires a larger compression depth of the section and consequently a larger yield curvature. For the high axial load level(P greater than about $0.2f'_cA_g$), however, the tension steel does not yield before the extreme concrete fibre compression strain reaches 0.002. The yield curvature then decreases with the increase in axial load level because a higher axial load means larger compression depth and a smaller yield curvature in this axial load range. Fig.7.8 also indicates that a higher longitudinal reinforcement content results in a larger yield curvature.

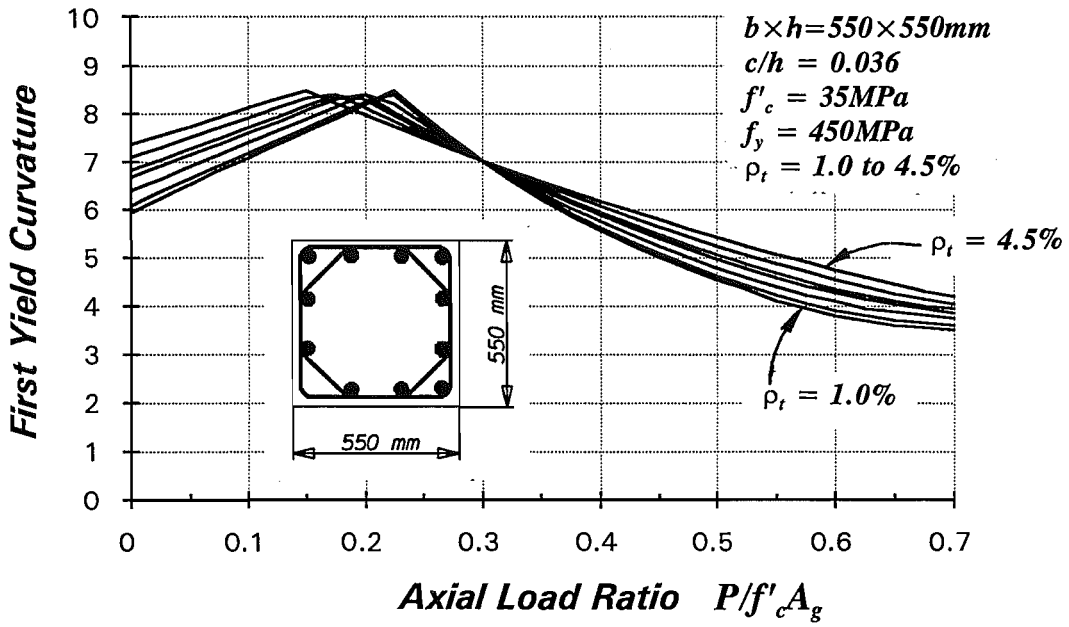

Fig.7.8: Variation of Yield Curvature With Axial Load Level

7.7.3 The Effects of Axial Load Ratio on the Elastic Flexural Rigidity

The effects of axial load levels on the flexural rigidity at cracked section are shown in Figs.7.9 and 7.10. The elastic flexural rigidity and the post-yield second slope flexural rigidity ratios are plotted in these figures against the axial load ratio with various longitudinal reinforcement contents and concrete compressive strengths.

The elastic flexural rigidity ratio, $(EI)_{el}/(EI)_g$, as shown in Fig.7.9, generally increases with the increase in axial load level. The reduction of section stiffness is caused by the development of cracks and the possible nonlinear behaviour of the concrete. For lightly loaded column sections, the neutral axis depth is small and hence a large portion of the section is cracked. For heavily loaded sections, the longitudinal reinforcement will not yield in tension and the concrete cracking will not be so extensive but some inelastic behaviour of the concrete occurs before reaching a compressive strain of 0.002. The higher the compression axial load level, the greater is the elastic flexural rigidity. The variation of elastic flexural rigidity ratio changes its trend in the vicinity of an axial load level of about $0.2f'_cA_g$.

The post-yield second slope flexural rigidity ratio, as shown in Fig.7.10, decreases slightly as axial load level increases when the axial load is less than about $0.2f'_cA_g$. The variation with increasing axial load when P is greater than about $0.2f'_cA_g$ is more pronounced. In this axial load range, the ratio of $(EI)_{py}/(EI)_{el}$ increases significantly with increase in axial load ratio. This indicates the effect of confinement on the flexural strength enhancement of the column section. It is to be noted that the sections investigated contained the amount of transverse reinforcement required for concrete confinement by the New Zealand concrete design code[S14]. The quantity of transverse reinforcement provided, according to the code[S14], increases with the axial load level, as indicated by Eq.2.1. Also, a high axial load means a large neutral axis depth, which in return means that the flexural strength of the column section is more dependent on the contribution of concrete compressive stress distribution. Therefore, the higher the axial load level, the larger the flexural overstrength of the section in the post-yield range, and hence the higher the post-yield second slope flexural rigidity.

The flexural overstrength of reinforced concrete sections at high axial load levels is mainly due to concrete strength enhancement as a result of confinement. The proportion of the flexural strength enhancement due to strain hardening of longitudinal reinforcement actually decreases with the increase in compression axial load level. The strain at which strain hardening commences for the New Zealand manufactured steel is about 1.2 to 1.5%. Fig.7.11 shows the curvature ductility factor, ϕ/ϕ_y, at which the strain hardening in the longitudinal bar closest to the tension face of the section starts to occur for the case that the column section is subjected to monotonic loading. As can be seen in this figure, the strain hardening occurs at higher curvature ductility factor when the compression axial load level increases. Fig.7.12 illustrates the tensile strain in the longitudinal bar closest to the tensile face of the section at curvature ductility factor $\phi/\phi_y=10$ and 15. For the same curvature ductility factor, the strain in the longitudinal reinforcement decreases as the axial load level increases. For the given section, the strain hardening will not occur at curvature ductility factor $\phi/\phi_y=10$, when axial load is increased to $P=0.5f'_cA_g$(see Fig.7.12).

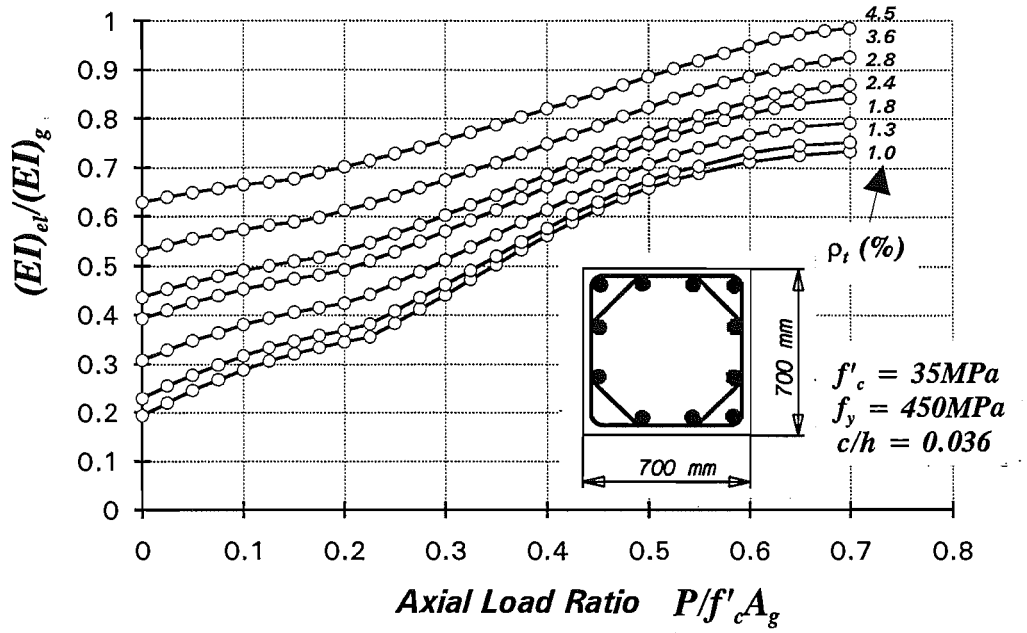

(a) With various longitudinal reinforcement content

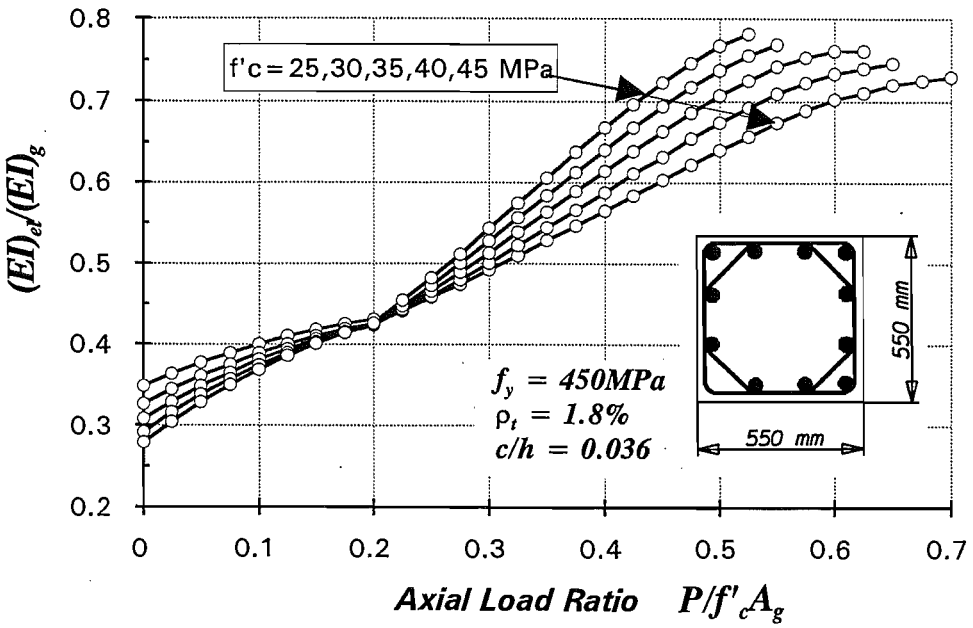

(b) With various concrete compressive strength

Fig.7.9: Effect of Axial Load Level on the Elastic Flexural Rigidity

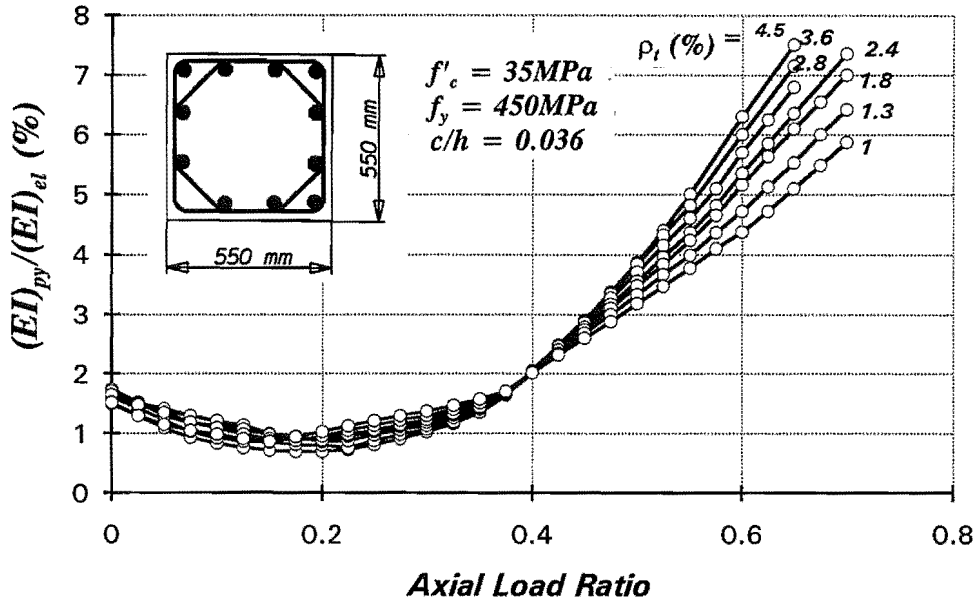

(a) With various longitudinal reinforcement content

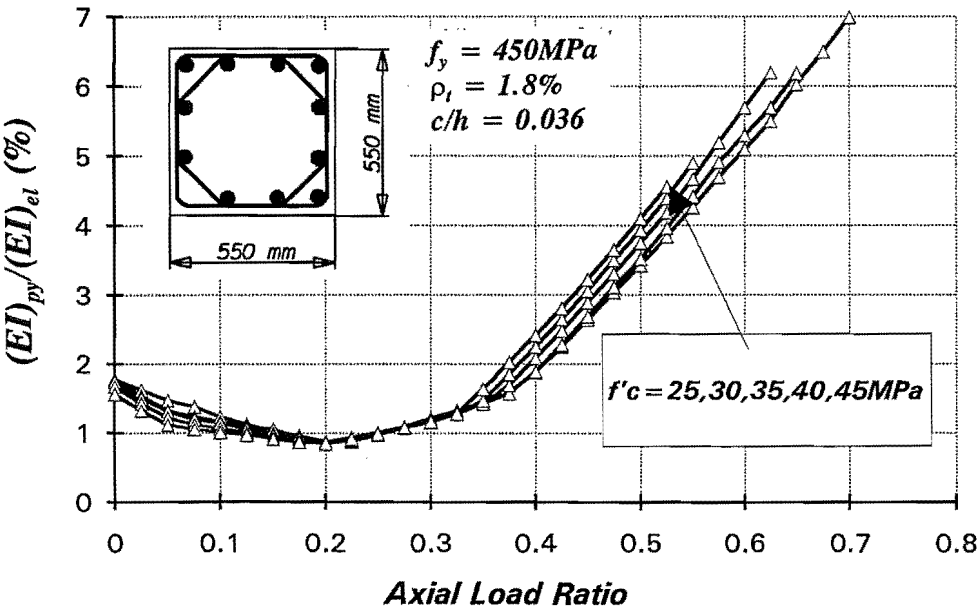

(b) With various concrete compressive strength

Fig.7.10: Effect of Axial Load Level on the Post-yield Flexural Rigidity

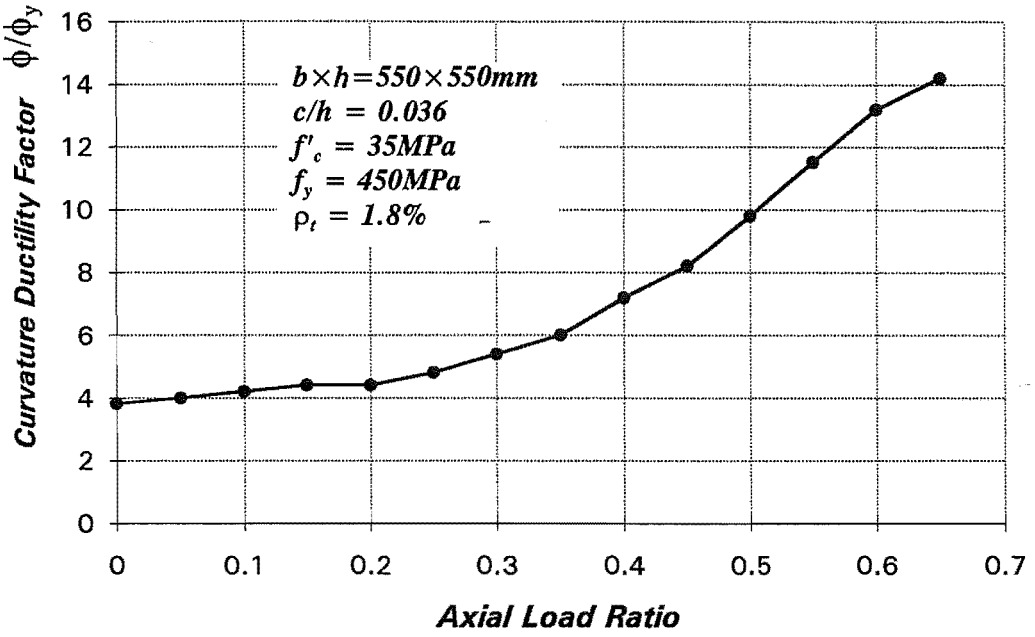

Fig.7.11: Curvature Ductility Factor at Onset of Strain Hardening

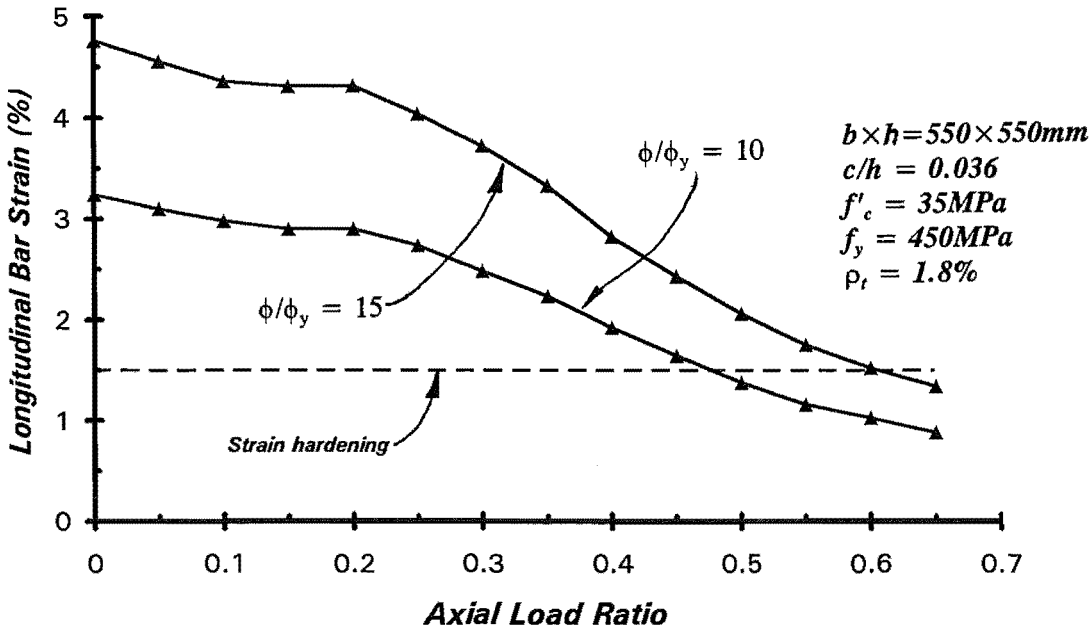

Fig.7.12: Tension Longitudinal bar Strain at Curvature Ductility Factor ϕ/ϕ_y = 10 and 15

7.7.4 The Effects of Longitudinal Reinforcement Content

Figs.7.13 and 7.14 plot the flexural rigidity ratios against the longitudinal reinforcement ratios with various axial load levels. It can be seen from Fig.7.13 that a higher longitudinal reinforcement content results in a larger $(EI)_{el}/(EI)_g$ ratio. Fig.7.13 indicates that this ratio increases almost linearly with increase in the longitudinal reinforcement ratio. The slope of this variation is dependent on the axial load level.

The contribution of the enhanced concrete compressive stress due to confinement to the flexural strength of the column section is greater than that of longitudinal bars due to strain hardening in the post-yield range. The post-yield second slope flexural rigidity of the section decreases slightly with the increase in longitudinal reinforcement content when axial load is high, as shown in Fig.7.14.

7.7.5 The Effect of Concrete Strength

Effects of concrete compressive strength on the elastic and post-yield flexural rigidities are illustrated in Figs.7.15 and 7.16, which plot these variables for various axial load levels. These figures indicate that flexural rigidity ratios vary linearly with the increased concrete strength. The trend of the variation changes at the vicinity of an axial load level of about $0.25f'_cA_g$. For the section subjected to an axial load larger than $0.25f'_cA_g$, the ratios plotted increase as concrete compressive strength increases. For the section with axial load less than about $0.25f'_cA_g$, the ratios decrease as the concrete strength increases. It is to noted that for the same axial load ratio, the axial compression load applied to the section is actually increased with increase in concrete compressive strength. For example, the axial compression load applied to a 550mm square section with axial load ratio of $0.1f'_cA_g$ will be increased from 756kN when f'_c=25MPa to 1210kN when f'_c=40MPa. For axial load ratios less than about $0.25f'_cA_g$, the yielding of steel will govern the calculation of yield curvature and corresponding moment. However, for axial load ratio greater than about $0.25f'_cA_g$ the extreme concrete fibre compression strain reaches 0.002 before the tension steel yields, and a larger axial compression results in a smaller yield curvature. While the yield moment does not vary significantly with increased axial compression, the elastic flexural rigidity increases with increased axial compression.

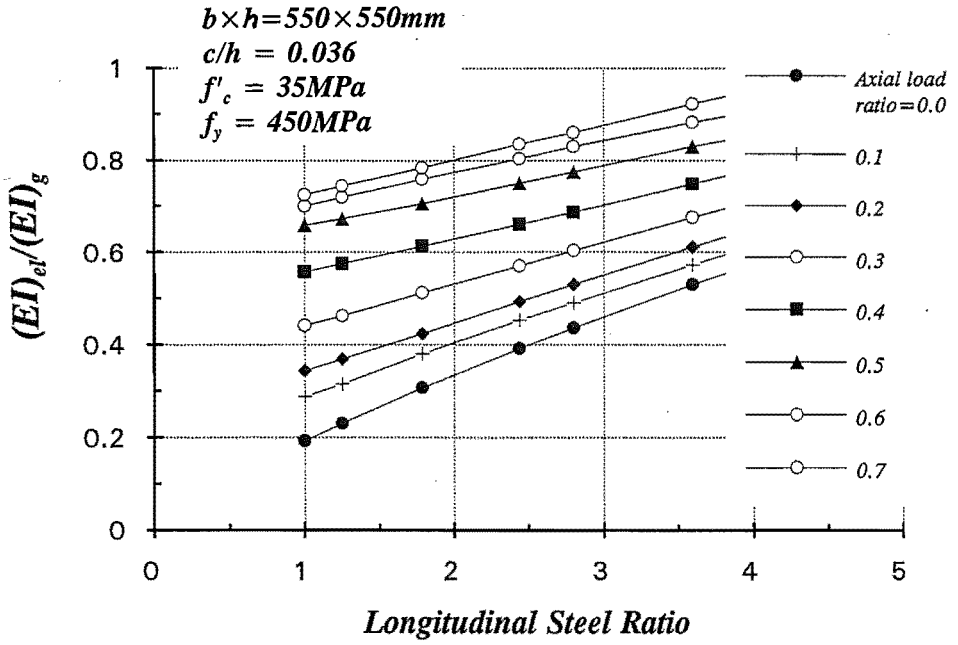

Fig.7.13: Effect of Longitudinal Reinforcement Ratio on the Elastic Flexural Rigidity

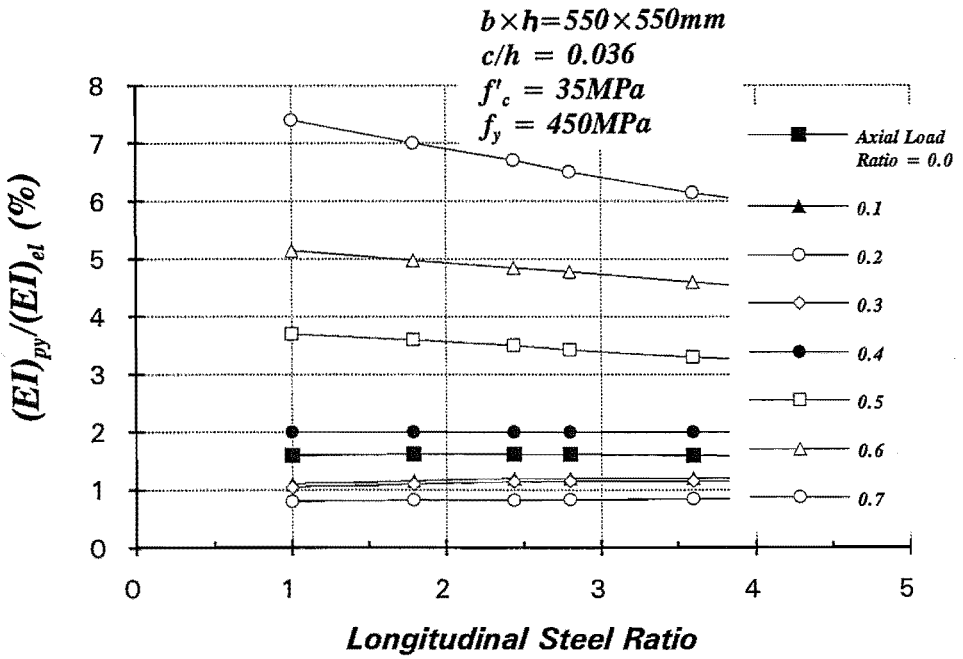

Fig.7.14: Effect of Longitudinal Reinforcement Ratio on the Post-yield Flexural Rigidiry

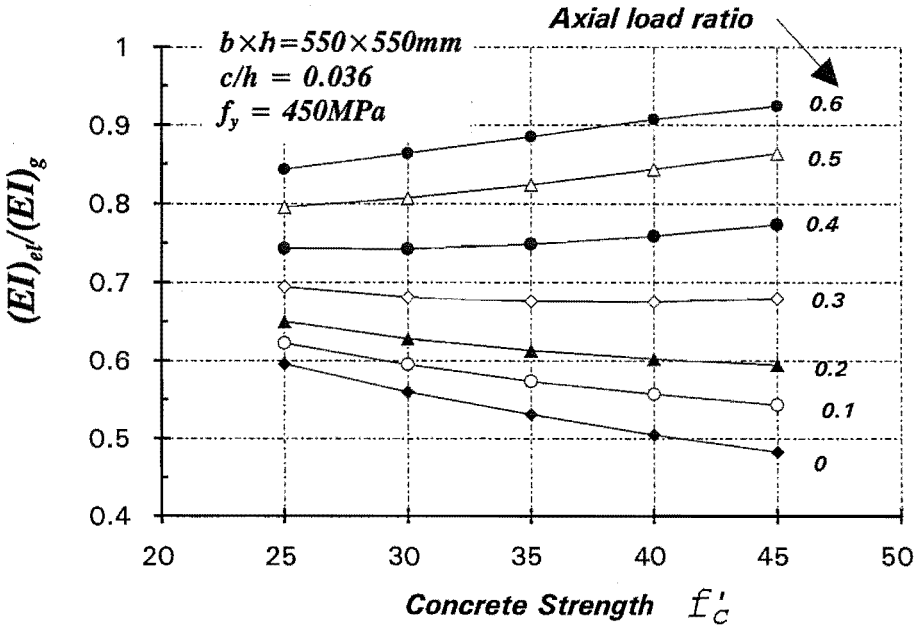

(a) Longitudinal reinforcement ratio ρ_t = 1.8%

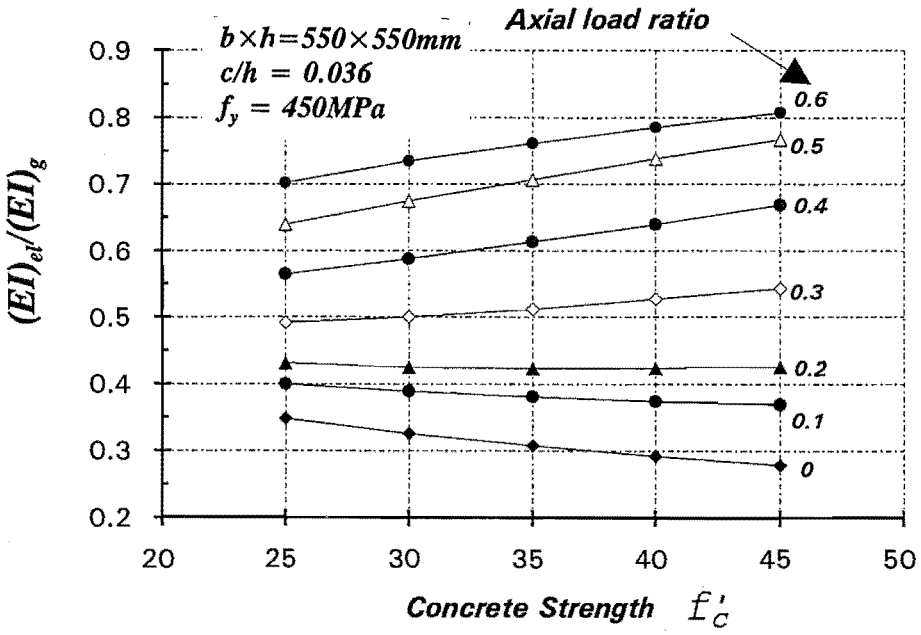

(b) Longitudinal reinforcement ratio ρ_t = 3.6%

Fig.7.15: Effect of Concrete Compressive Strength on the Elastic Flexural Rigidity

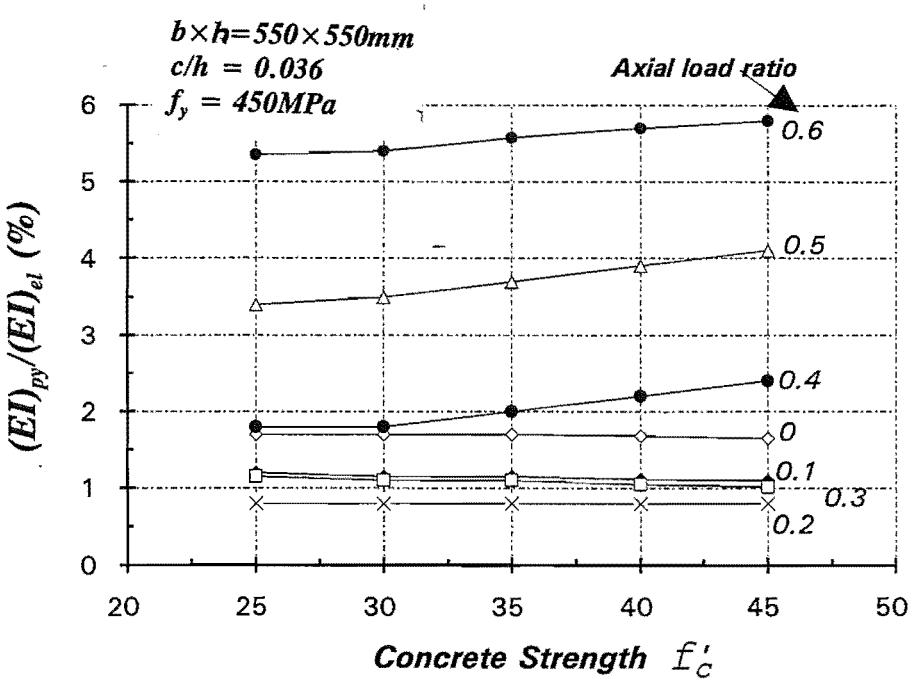

(a) Longitudinal reinforcement ratio ρ_t = 1.8%

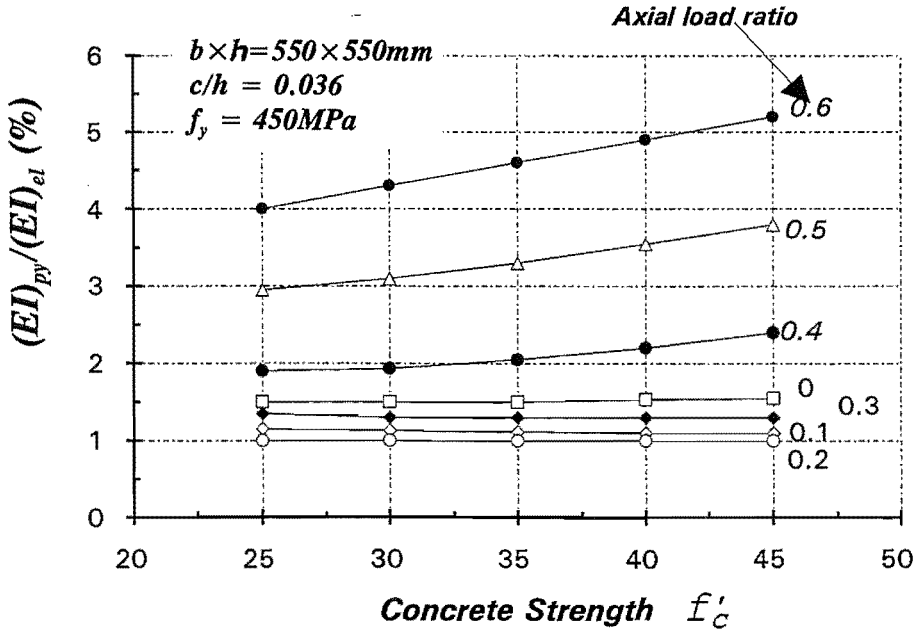

(b) Longitudinal reinforcement ratio ρ_t = 3.6%

Fig.7.16: Effect of Concrete Compressive Strength on the Post-yield Flexural Rigidity

7.7.6 The Effect of Cover Concrete

The effects of the cover concrete ratio, c/h, on the flexural rigidities are demonstrated in Figs.7.17 and 7.18. It can be seen from Fig.7.17 that the cover concrete ratio has little influence on the elastic flexural rigidity. This was expected, since the stress in the core concrete(confined concrete) was only a little larger than that in the cover concrete(unconfined concrete) prior to the yielding of the section. This is especially the case for the section with low axial compression, in which the extreme fibre concrete compressive strain was smaller than 0.002 before yielding.

The post-yield second slope flexural rigidity of the section, however, is significantly influenced by the cover concrete ratio, as shown in Fig.7.18. It was observed in the experiments that the cover concrete started to spall off at compressive strain around 0.006 to 0.014. In the moment-curvature analysis, the spalling strain for unconfined concrete was assumed to be 0.01. When the curvature of the section reaches ten times yield curvature ϕ_y, the concrete compressive strain in most of the cover concrete in the compression region has normally exceeded the assumed spalling strain for unconfined concrete. Hence the concrete contribution to the flexural strength was mainly from the core concrete in the post-yield range. Therefore, the larger the cover concrete ratio, the smaller the concrete section which can sustain the flexural strength after yielding. Consequently, the post-yield flexural rigidity ratio of the sections decreases with the increase in cover concrete ratio. This effect was more pronounced when the axial load is high, due to the larger contribution to flexural strength of the compressive fibre in the concrete.

7.8 DEVELOPMENT OF EQUATIONS FOR THE EVALUATION OF THE FLEXURAL RIGIDITY OF SECTIONS

7.8.1 The Approach

From the computed data for the flexural rigidity of 650 reinforced concrete sections, expressions were developed for estimating the flexural rigidities of reinforced concrete column sections.

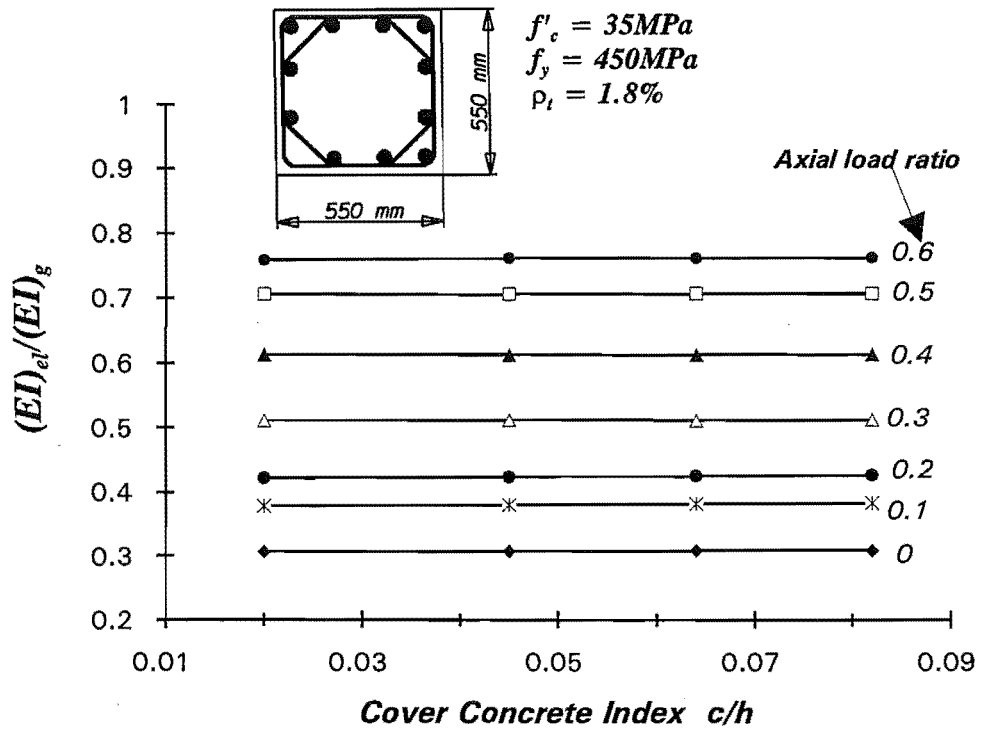

Fig.7.17: Effect of Cover Concrete on the Elastic Flexural Rigidity

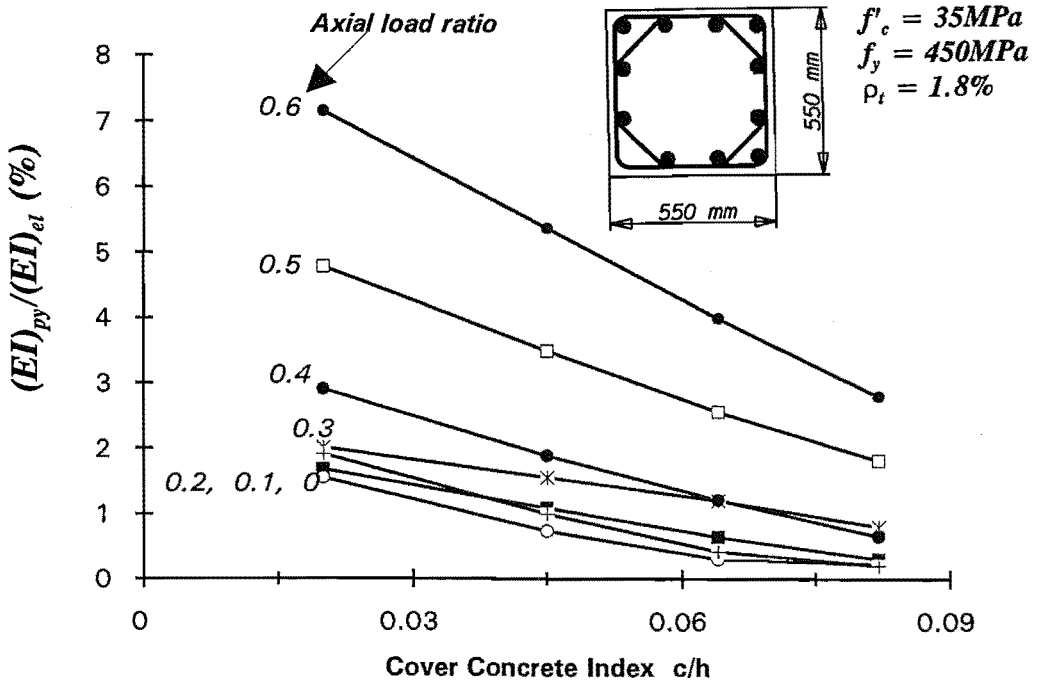

Fig.7.18: Effect of Cover Concrete on the Post-yield Flexural Rigidity

In the development of equations for the flexural rigidity of reinforced concrete sections, to be used in design, it needs to be considered that such equations should be able to evaluate the section rigidity with adequate accuracy, and yet the equations should be simple to use so as to avoid unnecessary computation effort.

7.8.2 Elastic Flexural Rigidity Ratio

From the discussion of the previous sections, it is clear that the variables which affect the elastic flexural rigidity ratio $(EI)_{el}/(EI)_g$ most significantly are the axial load level, the longitudinal reinforcement content and the concrete compressive strength. The influence of other variables including cover concrete is not remarkable and can be neglected. This assumes that the yield strength of the longitudinal reinforcement is around 450MPa. It was decided that the elastic flexural rigidity ratio should be taken as a function of the axial load ratio, P/f'_cA_g, the longitudinal reinforcement content, ρ_t, and the concrete compressive strength, f'_c. The examination of Figs.7.13 and 7.15 reveals that a linear relation exists between the elastic flexural rigidity ratio and the longitudinal reinforcement content as well as the concrete compressive strength. The gradient of these relations is affected by the axial load level. The elastic flexural rigidity ratio generally increases with increase in axial load level. A trial regression analysis showed that very reasonable accuracy can be achieved by linear relations, although higher-order equations may be more appropriate. For the purpose of simplicity, linear relations were also assumed and the elastic flexural rigidity was written as:

$$\frac{(EI)_{el}}{(EI)_g} = \left(a_1\frac{P}{f'_cA_g}+a_2\right)\rho_t + \left(a_3\frac{P}{f'_cA_g}+a_4\right) f'_c + a_5\frac{P}{f'_cA_g} + a_6 \qquad (7.5)$$

A least-squared method[W7] was used to determine the coefficients in Eq.7.5. Rearranging the Eq.7.5, with the coefficients determined from regression analysis, gives

$$\frac{(EI)_{el}}{(EI)_g} = (0.35+0.019f'_c-0.115\rho_t)\frac{P}{f'_cA_g}+0.125\rho_t-0.004f'_c+0.197 \qquad (7.6)$$

where f'_c = concrete compressive strength in MPa and ρ_t = total longitudinal reinforcement content in %. Figs.7.19 to 7.21 compare the elastic flexural rigidity ratio found from the analyses of the column sections with the values given by the proposed equation Eq.7.5.

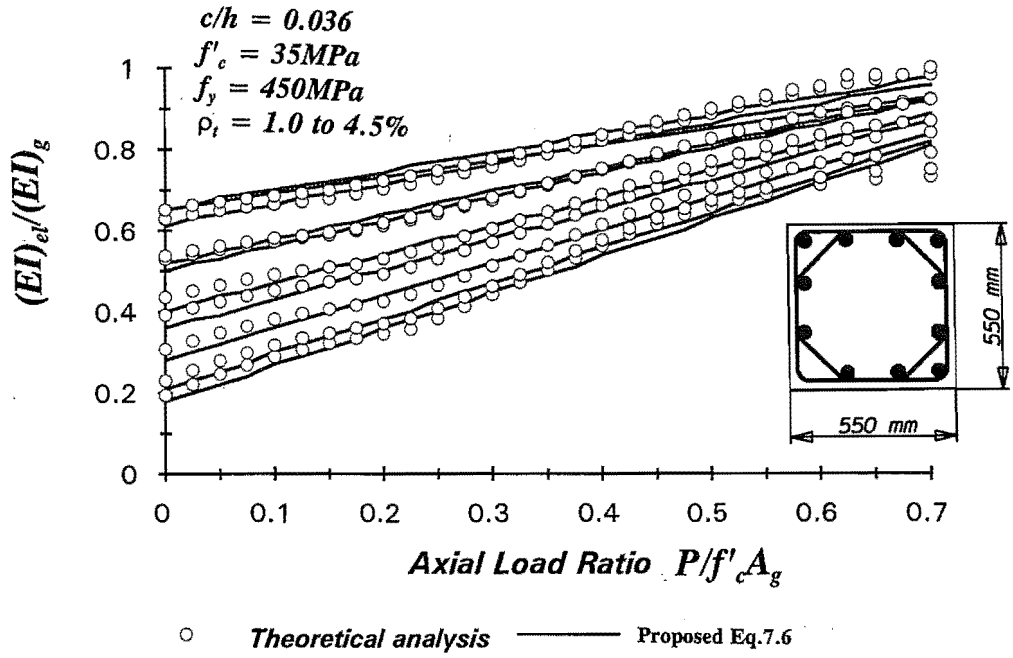

Fig.7.19: Regression Analysis Results for the Elastic Flexural Rigidity

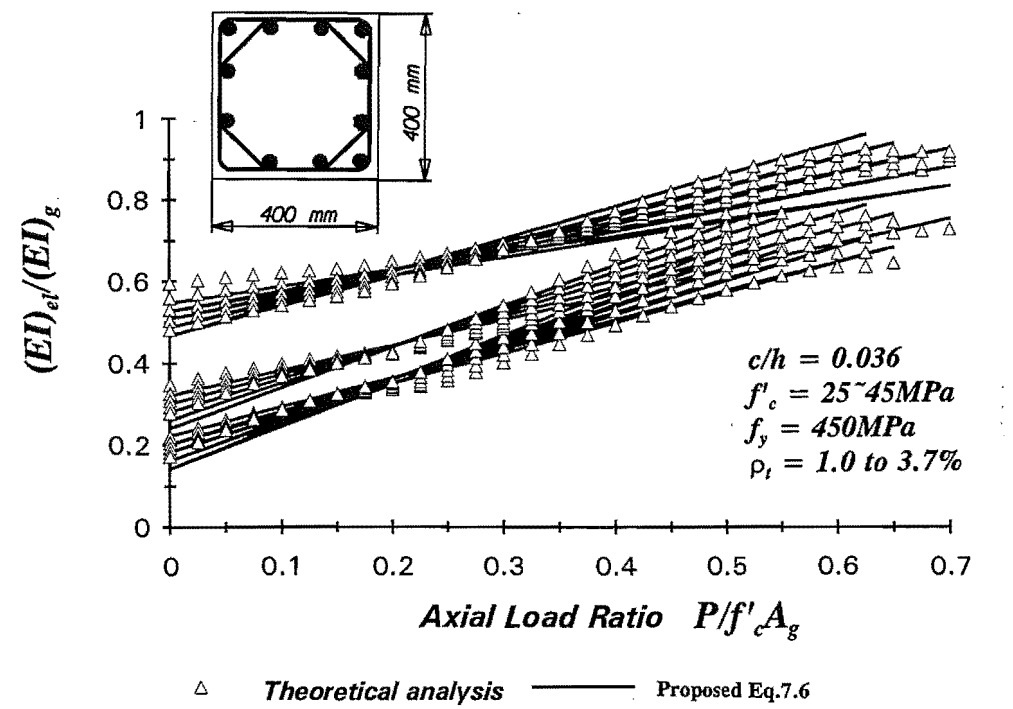

Fig.7.20: Regression Analysis Results for the Elastic Flexural Rigidity

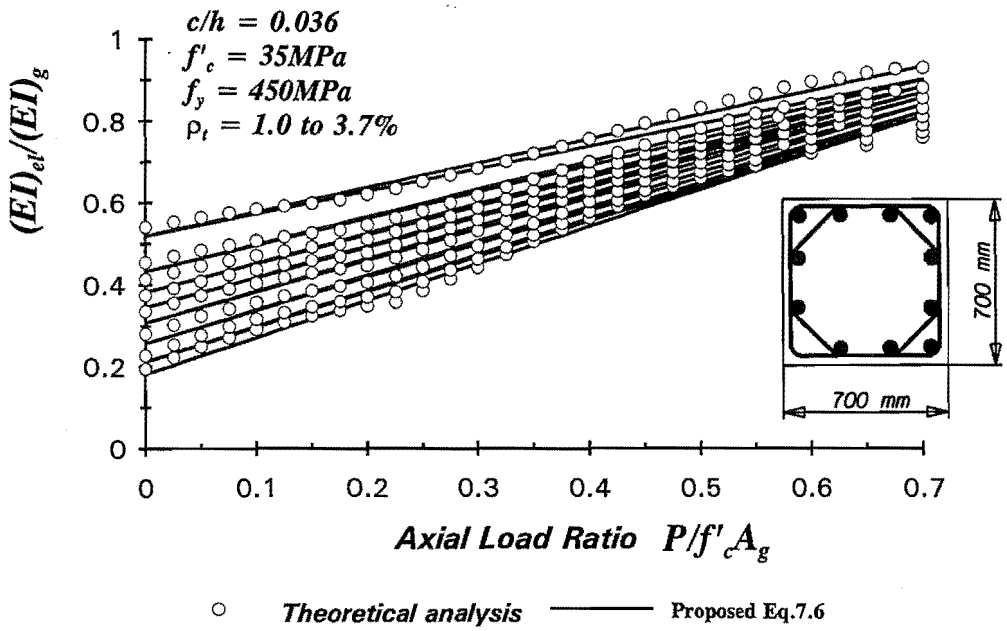

Fig.7.21: Regression Analysis Results for the Elastic Flexural Rigidity

It has be to emphasized that the Eq.7.6 is derived from analytical results of cracked concrete sections. Hence Eq.7.6 represents an average rigidity of cracked concrete section up to yielding stage. For a member section which has not reached yield, the flexural rigidity of the section will be greater than given by Eq.7.6 since the section rigidity is dependent on the moment applied to the section. For example, the flexural rigidity of a section before cracking would at least 20% greater than that at first yielding.

7.8.3 Post-yield Section Stiffness Ratio

The post-yield second slope flexural rigidity is mainly dependent on the axial load levels. For low axial load levels, the strength enhancement due to confinement and strain hardening is not significant. For high axial load levels, significant increase in the flexural strength in the post yielding range is expected. It is emphasized that the column sections studied were assumed to contain the amount of transverse reinforcement required by the current New Zealand code provisions[S14]. Based on regression analysis

of the analytical results of the reinforced concrete column sections, following equations are suggested for the estimate of post-yield second slope flexural rigidify ratio.

$$\text{When } P/f'_cA_g < 0.2: \quad \frac{(EI)_{py}}{(EI)_{el}} = 0.01 \tag{7.7a}$$

$$\text{When } P/f'_cA_g \geq 0.2: \quad \frac{(EI)_{py}}{(EI)_{el}} = \left[0.01+0.25\left(\frac{P}{f'_cA_g}-0.2\right)^2\right] \tag{7.7b}$$

Fig.7.22 compares the results obtained from the analysis of many reinforced concrete sections with the proposed Eq.7.7.

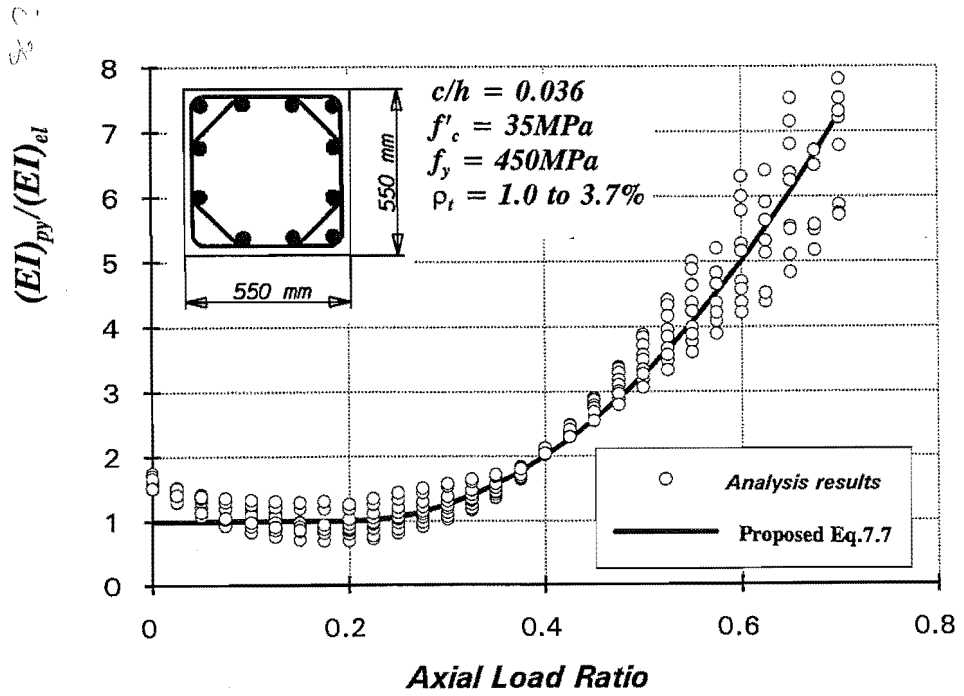

Fig.7.22: Comparison Between the Proposed Equation and Analysis Results

7.9 COMPARISON OF THE COMPUTED FLEXURAL RIGIDITIES WITH EXPERIMENTS

The elastic flexural rigidity of a reinforced concrete column section can be evaluated from the measured yield curvature and the corresponding moment using Eq.7.3. As discussed in Chapter 3, the experimental yield curvature was obtained from the change in the gauge length measured by potentiometers at various levels along the column height. The curvatures measured at the first potentiometer level included the effects of yield penetration of the longitudinal bars into column base. A more realistic value of the curvature for the critical section could be obtained from the curvatures measured at the second potentiometer level. Hence, the computed elastic flexural rigidity for the critical section calculated using the yield curvature at the first potentiometer level may give an lower bound to the real section flexural rigidity while the flexural rigidity calculated using the yield curvature measured at the second potentiometer level may give an upper bound to the real section flexural rigidity.

For the purpose of comparison, both yield curvatures measured at the two levels were used to calculated elastic flexural rigidity. In determining the moment corresponding to the yield curvature, the P-Δ effect due to axial load was taken into account.

The computed elastic flexural rigidity obtained using Eq.7.3, and based on the experimental yield curvature from the nine reinforced concrete columns presented in Chapter 2 to 5 is plotted in Fig.7.23, along with the elastic flexural rigidity ratio calculated using Eq.7.6. The elastic flexural rigidity was also computed using other available experimental data[S12,T3,W2] and is compared with the elastic flexural rigidity given by Eq.7.6 in Fig.7.24. The yield curvature measured at the second potentiometer level was not available for some columns described in the reference S12, T3 and W2. For these columns, the elastic flexural rigidity was computed using only the yield curvatures measured at the first potentiometer level. It can be seen, from Figs.7.23 and 7.24, that the elastic flexural rigidity ratio calculated by Eq.7.6 lies between those computed using the experimental yield curvatures measured at the first and second potentiometer levels, except for two columns in which the elastic flexural rigidity ratio computed using the yield curvature at the first potentiometer level was larger than that given by Eq.7.6. This indicates that Eq.7.6 can be used to evaluate the elastic flexural stiffness ratio of cracked section of reinforced concrete columns with confidence.

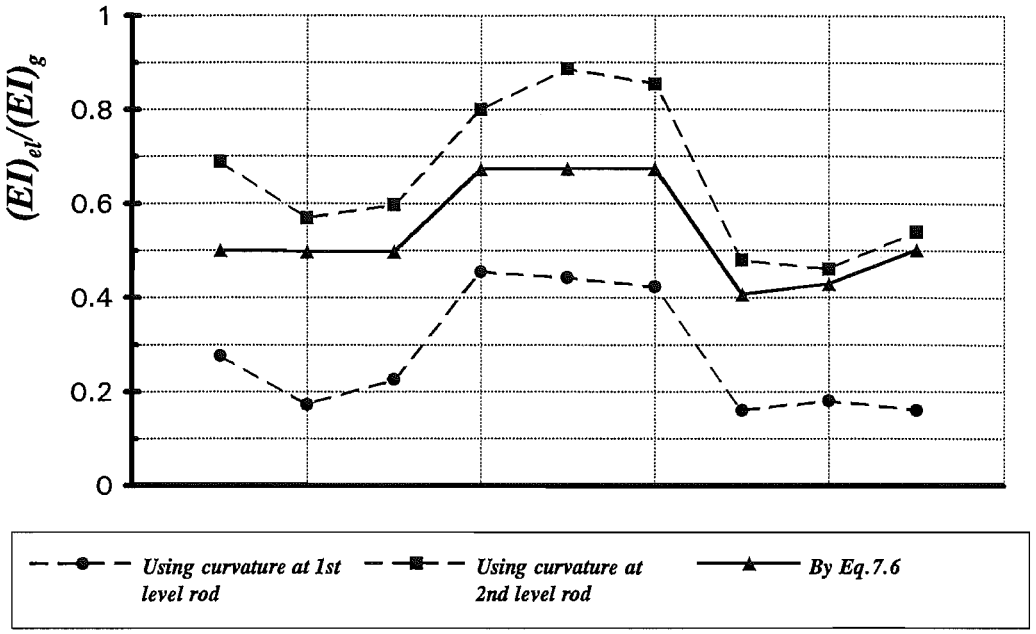

Fig.7.23: Experimental and Computed Section Rigidity Ratio

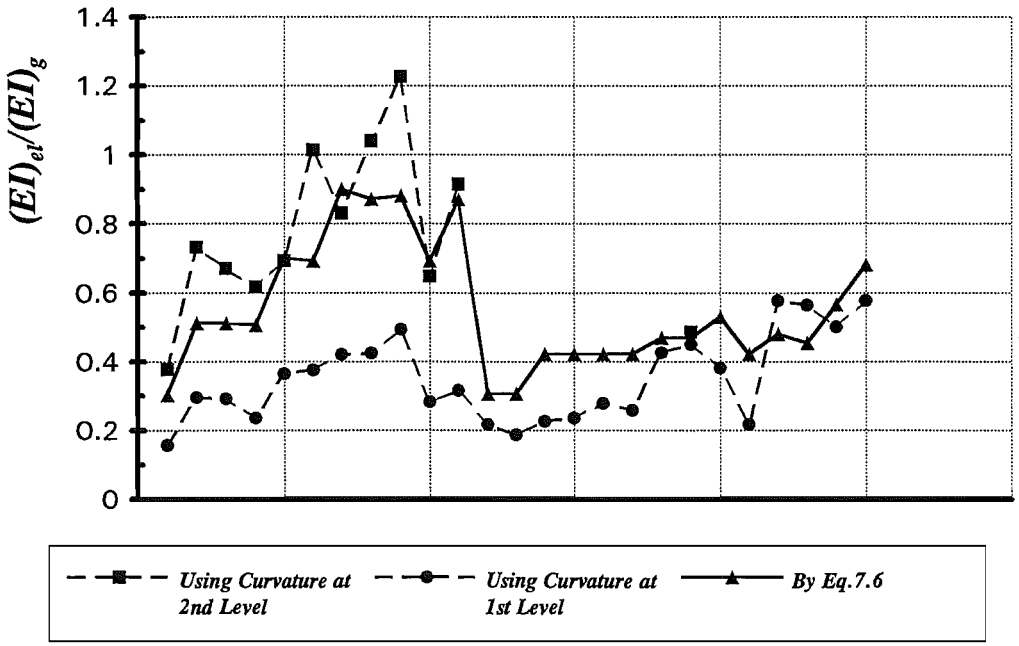

Fig.7.24: Experimental and Computed Section Rigidity Ratio

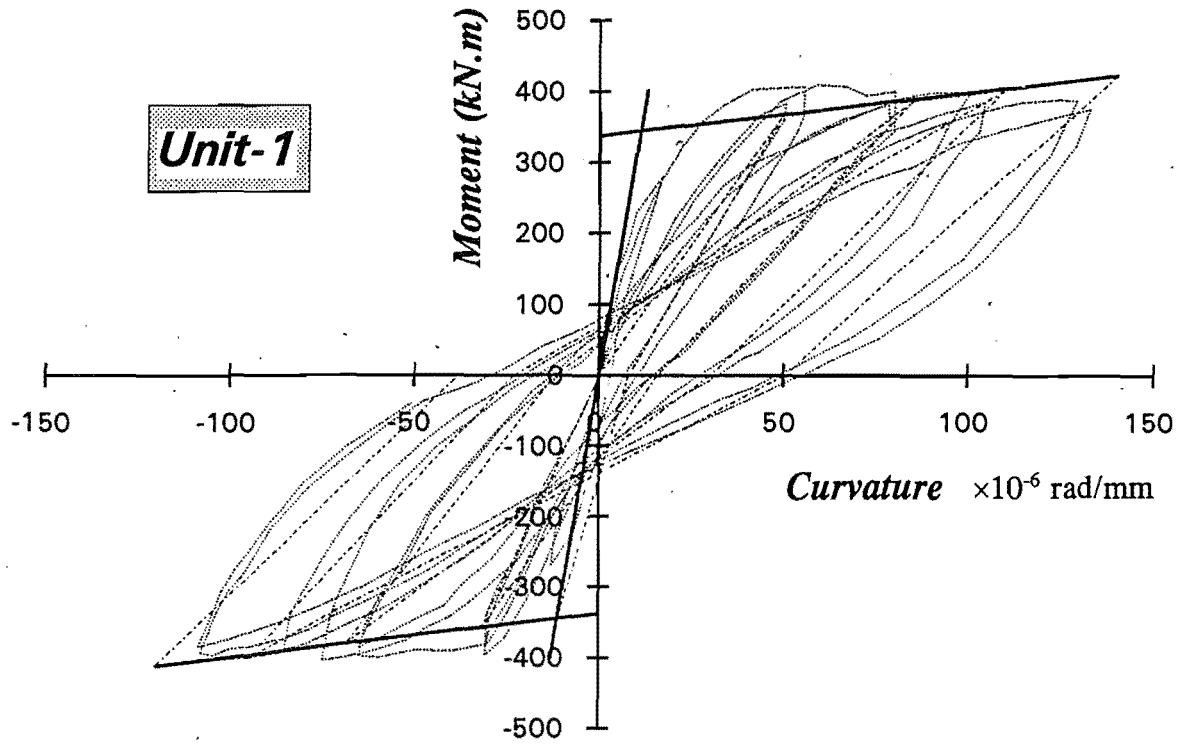

Fig.7.25: Moment-Curvature Hysteresis Loops With Bilinear Curve Determined by Eqns.7.6 and 7.7 for Column Unit 1

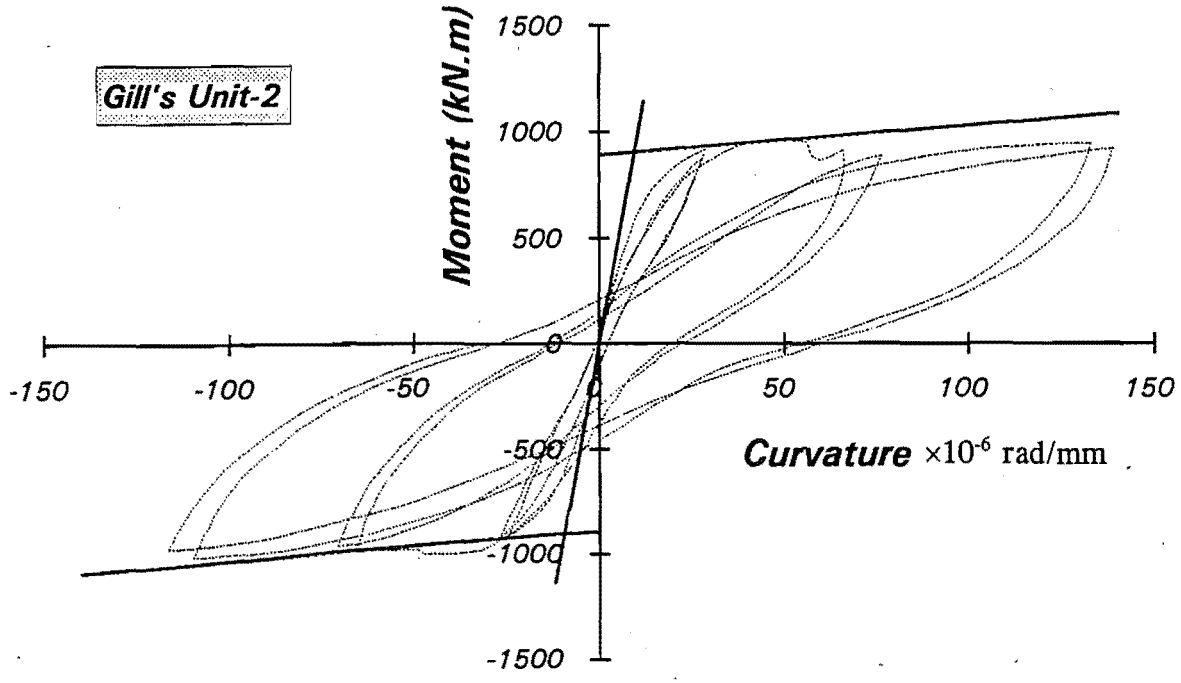

Fig.7.26: Moment-Curvature Hysteresis Loops With Bilinear Curve Determined by Eqns.7.6 and 7.7 for Specimen Two Tested by Gill et al[G1]

It was not possible to evaluate the post-yield second slope flexural rigidity from the previous test results by Eq.7.4 due to the unavailability of the curvature at ten times the theoretical yield curvature and the corresponding moment. For the tests presented in Chapter 2, four of the columns were tested under varying axial loading. The post-yield behaviour of these columns was found to be greatly different from that under constant axial load. Instead of determining the post-yield stiffness from the limited test data, the primary moment-curvature curves were established based on the section properties of tested columns, and using the elastic and post-yield flexural rigidity ratios given by Eqns.7.6 and 7.7. The bilinear primary moment-curvature curves thus obtained were compared with the experimental moment-curvature relationship, as shown in Figs.5.25 and 5.26. These figures demonstrate the applicability of Eqns.7.6 and 7.7 for estimating the elastic and post-yield flexural rigidities for reinforced concrete rectangular sections.

7.10 Modelling of Moment-Curvature Relationships of Reinforced Concrete Column

7.10.1 The Approach

Under load reversal into inelastic range, the flexural rigidity of a column section experiences progressive reduction due to cracking of the concrete and bond deterioration at the steel-concrete interface. The changing of axial load level causes a variation in the yield moment and in the flexural rigidity during loading and unloading. A moment-curvature hysteresis model is proposed in this section based on the experimental results. While using the Takeda type model[T2] to describe the hysteretic moment-curvature relationship in the inelastic regions of the column, the proposed model takes into account the effects of varying axial load on the flexural yielding and rigidity. The proposed model has the four different branches which are identified in Fig.7.27. The determinations of the flexural rigidity of each branch is described below.

7.10.2 Loading and Unloading in the Elastic Range

When the moment has not exceeded the yield moment, the section is loaded and unloaded with the initial elastic flexural rigidity, $(EI)_{el}$. The initial elastic flexural rigidity, $(EI)_{el}$, including the effect due to varying axial load level, is given by Eq.7.6. The yield moment can be determined from the axial force-moment interaction surface(Fig.7.28). Determination of the axial force-moment interaction diagram based on the section properties is straightforward. The interaction surface can be further

approximated with sufficient accuracy by several straight lines, as shown in Fig.7.28. The yield moment, M_y, in each axial load range can be calculated as follows.

$$For\ P_t \le P < 0: \quad M_y = M_o - \frac{M_o}{P_t} P \tag{7.8a}$$

$$For\ 0 \le P < P_b: \quad M_y = \frac{M_b - M_o}{P_b} P + M_o \tag{7.8b}$$

$$For\ P_b \le P < P_{up}: \quad M_y = M_b - \frac{M_b - M_{up}}{P_b - P_{up}} (P_b - P) \tag{7.8c}$$

where P_t is the axial tension capacity of the column section, P_b and M_b are axial load and moment at the balanced yield point, P_{up} and M_{up} are the axial load and the corresponding moment at two-third of the concentric compression capacity, respectively. The yield curvature is then given by

$$\phi_y = \frac{M_y}{(EI)_{el}} \tag{7.9}$$

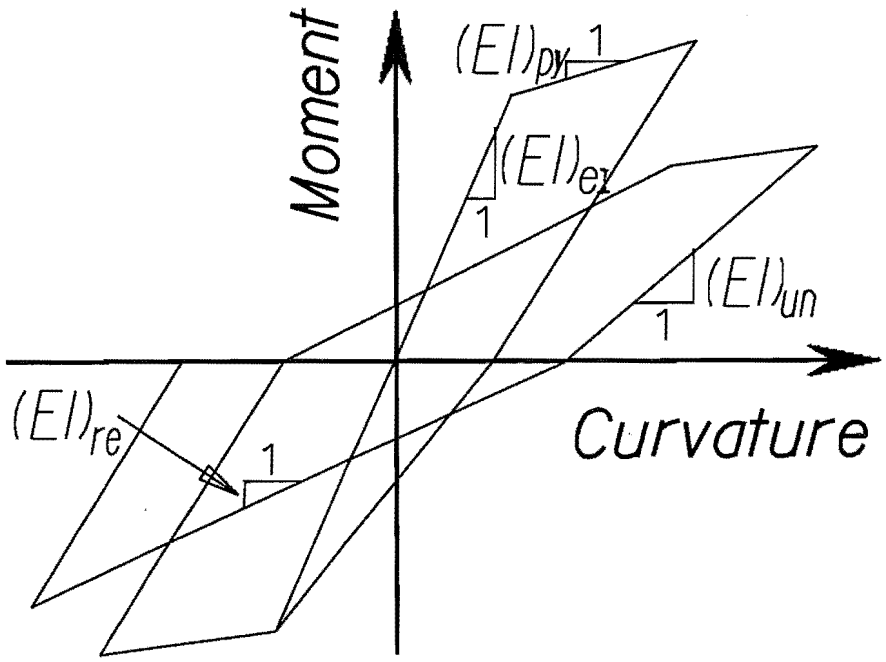

Fig.7.27: Definition of Loading, Unloading and Reloading Flexural Rigidity

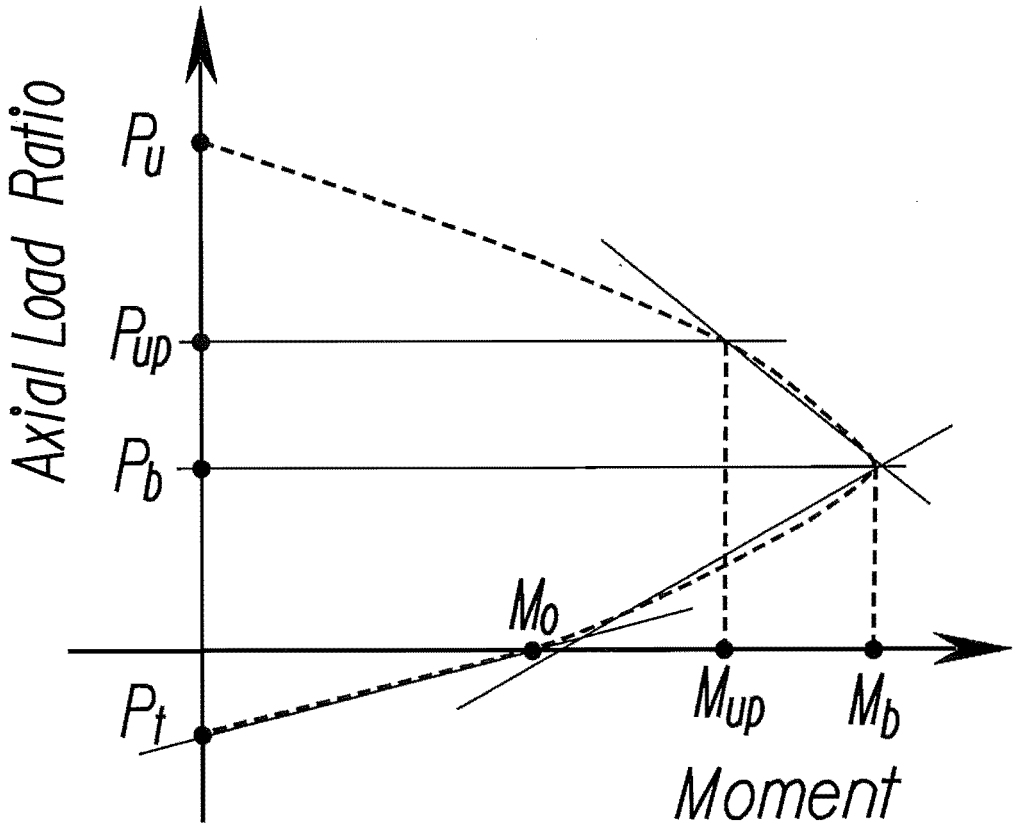

Fig.7.28: Axial Force-Moment Yield Surface

7.10.3 Loading in the Inelastic Range(Post-yield Loading)

When the yield capacity has been exceeded during loading in a direction, the flexural rigidity of the section is reduced to a given percentage of the initial elastic flexural rigidity. Both analytical and experimental results have shown that the post-yield slope of the primary moment-curvature curve lies in the range of 3 to 10 percent of the initial elastic slope. Thus

$$(EI)_{py} = k_1 (EI)_{el} \qquad (7.10)$$

The post-yield flexural rigidity ratio, k_1, can be determined by Eq.7.7. When the axial load reduces during inelastic loading, k_1 can be taken as zero.

7.10.4 Unloading in the Inelastic Range

When unloading occurs after the yield moment has been exceeded in that direction, the member is unloaded with a reduced flexural rigidity. Flexural rigidity during unloading reflects the nature of the softening of the section. For a column section with constant axial load, the unloading curve follows the slope controlled by the ratio of the yield deformation, ϕ_y, to the maximum deformation, ϕ_m, in the direction of loading and the elastic flexural rigidity, $(EI)_{el}$, given by the following equation

$$(EI)_{un} = \left(\frac{\phi_y}{\phi_m}\right)^{\alpha} (EI)_{el} \qquad (7.11)$$

where α is a coefficient determined from experimental data with the value ranging between 0.5 to 0.9. Fig.7.29 shows the variation of flexural rigidity ratio, $(EI)_{un}/(EI)_{el}$, given by Eq.7.11, with the ratio of the yield deformation to the maximum deformation reached at unloading point. Also shown in this figure are the ratios of $(EI)_{un}/(EI)_{el}$, obtained from experimental moment-curvature hysteretic relationships of reinforced concrete column tests conducted by Gill[G1] and Soesianawati[S12], as well as from the Units 1 and 4 tested in this study. These columns were tested under cyclic flexure with a constant compression axial load. It was found that a straight line, $(EI)_{un}=(c_1\phi_y/\phi_m+c_2)(EI)_{el}$, will give better estimate than a exponential curve(Eq.7.11) for the unloading stiffness ratio $(EI)_{un}/(EI)_{el}$. From experimental results, the unloading flexural rigidity for the column section with constant axial load can be determined by the following equation.

$$(EI)_{un} = \left(C_1\frac{\phi_y}{\phi_m}+C_2\right)(EI)_{el} \qquad (7.12)$$

where c_1 and c_2 are the coefficients obtained from test results. To be consistent with the unloading in the elastic range requires that $c_1+c_2=1.0$. In this study, these coefficients are taken as $c_1=0.92$, $c_2=0.08$.

The experimental results indicated that unloading flexural rigidity was affected by the variation in axial load. This effect can be found from the measured moment-curvature relationships of the columns tested under cyclic flexure and varying axial load shown in Figs.3.29 to 3.34. Fig7.30 shows a few cyclic moment-curvature hysteresis loops for Unit 6. The dashed lines shown in this figure indicate the variations in the applied axial load, with the compression axial load being taken as positive and tension axial load as negative. As can be seen in Fig.7.30, upon unloading an increase in the axial compression

load decreased the unloading flexural rigidity, or the reverse. This effect can be related to the change in the axial load. In general, the unloading flexural rigidity(See Fig.7.31) can be determined from

$$(EI)_{un} = \left(C_1 \frac{\phi_y}{\phi_m} + C_2\right)\left(1 - \frac{P - P^*}{P_b}\right)(EI)_{el} \qquad (7.13)$$

where P^* is the axial force applied in previous load step, taking compression axial load as positive, P_b is the balanced point axial load, and P is the currently applied axial load. To prevent excessive drop in the stiffness due to sudden change in axial load, it was suggested that unloading stiffness should satisfy following limit.

$$\frac{M^*}{\phi^*} \leq (EI)_{un} \leq (EI)_{el} \qquad (7.14)$$

where ϕ^* and M^* are the curvature and corresponding moment in previous loading step(see Fig.3.31).

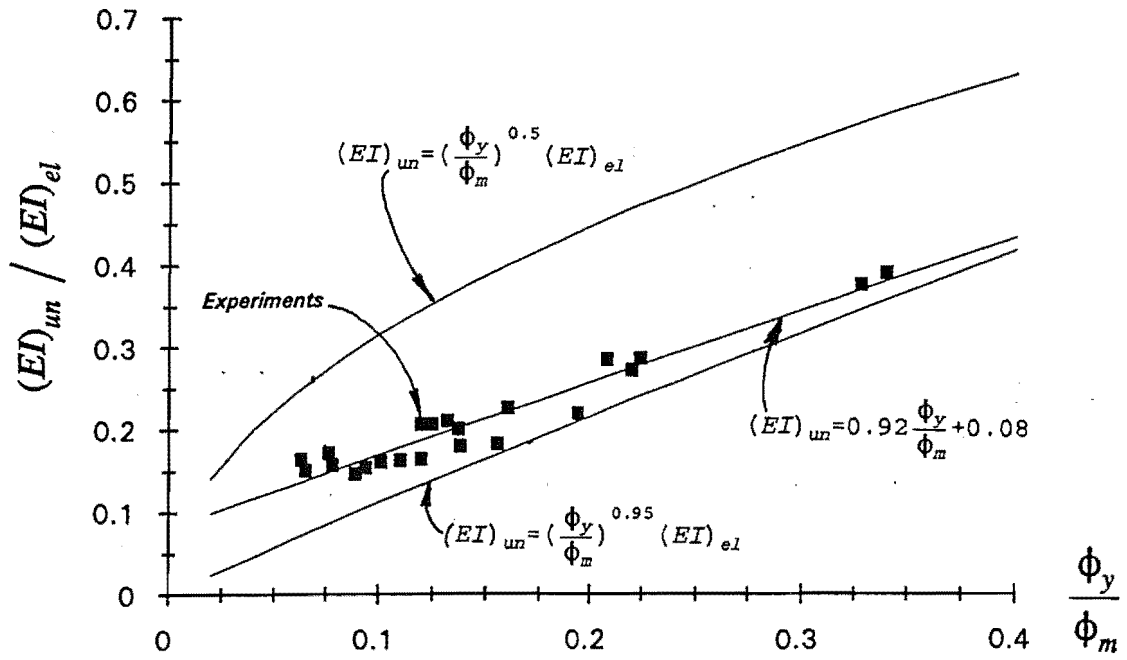

Fig.7.29: Variation of Unloading Flexural Rigidity

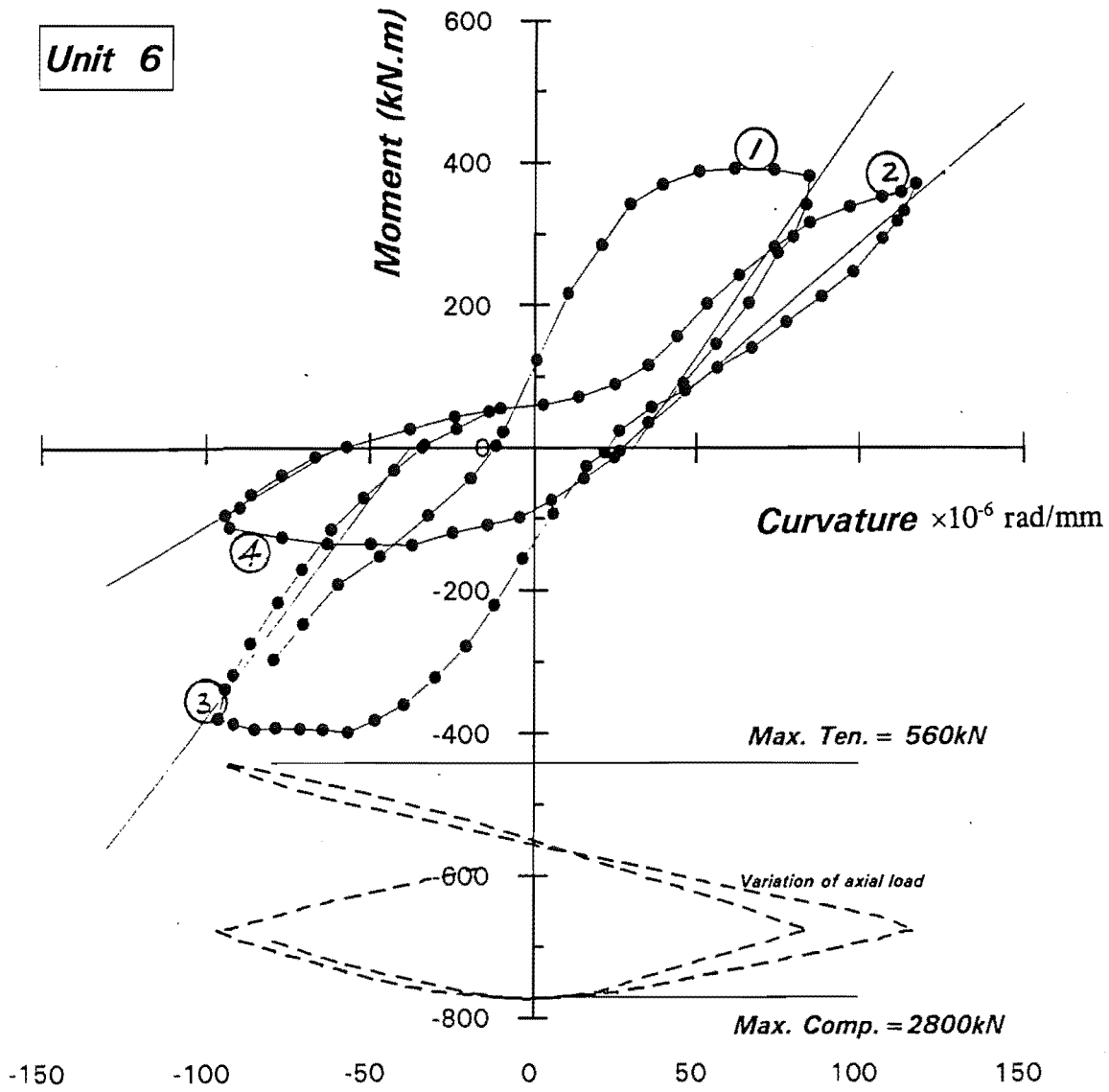

Unloading cycle	Variation of Axial Load (kN)	Secant unloading Stiffness (kN.m2×103)
1	1762 decreased to 895	6.46
2	1771 increased to 2659	3.91
3	1757 decreased to 1082	6.11
4	-564 increased to 0.0	2.67

Fig.7.30: Effect of Varying Axial Load Level on the Unloading Flexural Rigidity

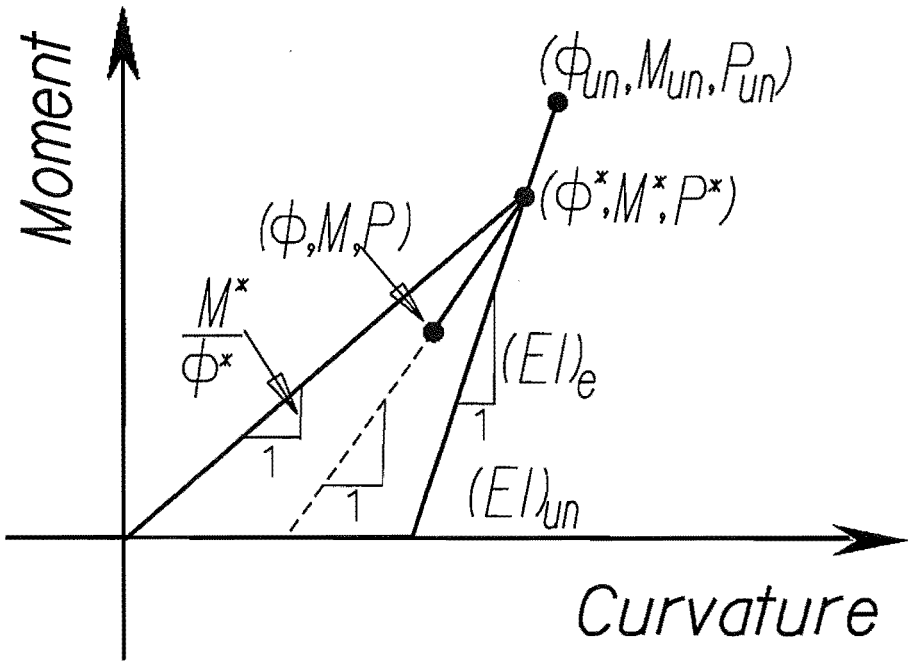

Fig.7.31: Determination of Unloading Flexural Rigidity

7.10.5 Reloading Stiffness in the Inelastic Range

When reloading in a direction in which the yield capacity of the section has been previously exceeded, the member reloads with the flexural rigidity $(EI)_{re}$. The reloading flexural rigidity reflects the pinching effect due to flexural cracking and the effect of variations in the axial load. In the previous hysteretic models, such as the Takeda model[T2] and the modified Takeda model[R1,S6], it is assumed that the member is reloaded towards the point at the onset of previous unloading. Examination of experimental moment-curvature relationships at the critical section of the columns indicates that variations in the axial load level not only caused the change of flexural yield capacity but may also result in curvature shifts.

Fig.7.32 illustrates an example of the measured moment-curvature hysteresis loops found from the test on Unit 3. The column was unloaded at point A with compression axial load of 343kN. During the following reloading excursion, the axial load increased from 163kN in tension at point B to 1538kN in compression at point C. The flexural strength increased from 231kN.m at previous unloading point A to 297kN.m at reloading point C. Also the member picked up the strength quickly and reached yielding at point C with a smaller curvature than previous maximum unloading curvature, ϕ_m. A similar trend can also be found in moment-curvature relations shown in Fig.7.33.

The yield moment reached in each loading cycle appears to mainly depend on the axial load present and can be approximated by the relation given by the axial force-moment interaction diagram. The corresponding yield curvature is associated with the maximum curvature reached in the previous loading excursion and the magnitude of change in axial load.

At a reloading step, an auxiliary yield point (ϕ^*_m, M^*_m) is introduced as shown in Fig.7.34. The coordinates of the point, (ϕ^*_m, M^*_m), can be calculated by following equations.

$$\phi_m^* = \left(1-\lambda_1 \frac{P-P_{un}}{P_b}\right)\phi_{un} \qquad (7.15)$$

and

$$M_m^* = M_y + k_1 (\phi_m^* - \phi_y)\ (EI)_{el} \qquad (7.16)$$

where ϕ_{un} and P_{un} are the curvature and axial load at the onset of previous unloading in the other direction, λ_1 is a coefficient determined from test data with value ranging between 0.5 to 1.0. The yield moment, M^*_y, can be determined from axial force-moment interaction diagram(Eqn.7.8). The inelastic unloading flexural rigidity is then given by the slope of the line joining the points of (ϕ, M) and (ϕ^*_m, M^*_m)(see Fig.7.34).

$$(EI)_{re} = \left(1-\lambda_2 \frac{P_{un}-P}{P_b}\right)\frac{M_m^*-M}{\phi_m^*-\phi} \geq 0 \qquad (7.17)$$

where λ_2 is a coefficient determined from test data.

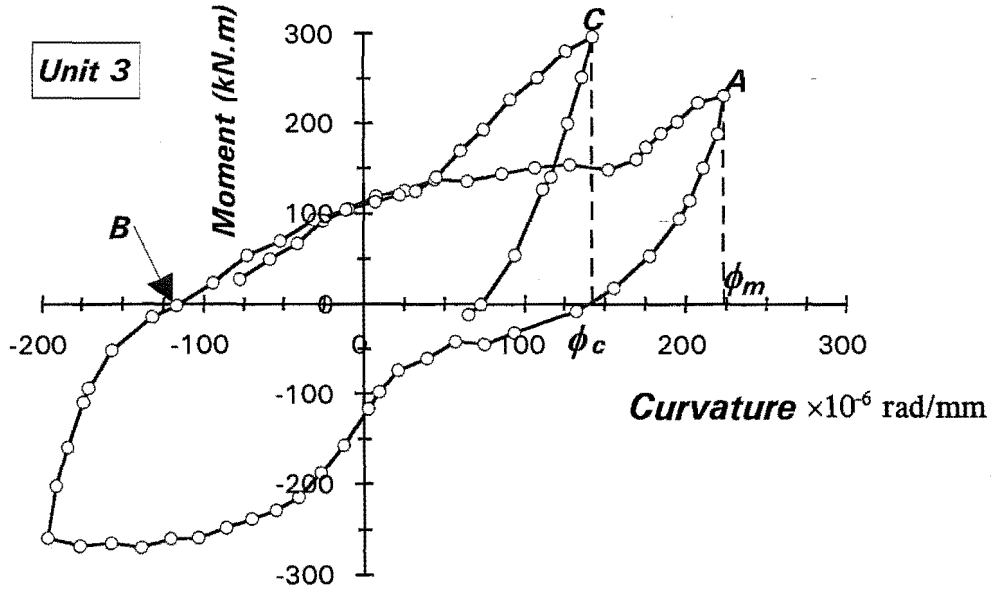

Fig.7.32: Experimental Moment-Curvature Hysteresis Loops for Unit 3

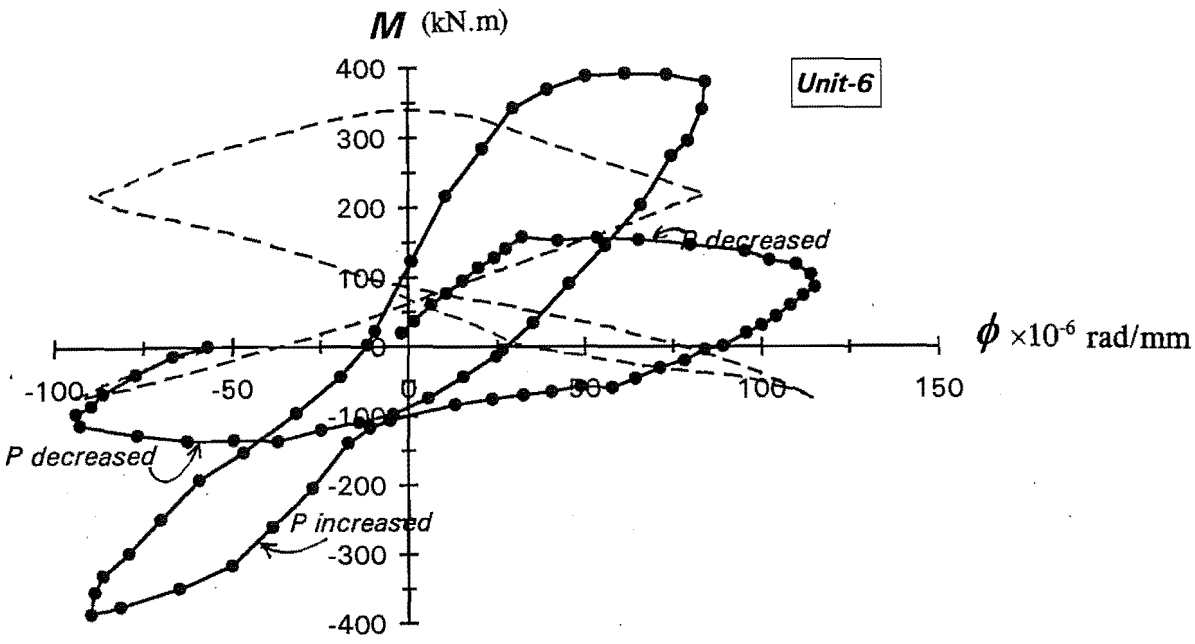

Fig.7.33: Experimental Moment-Curvature Hysteresis Loops for Unit 6

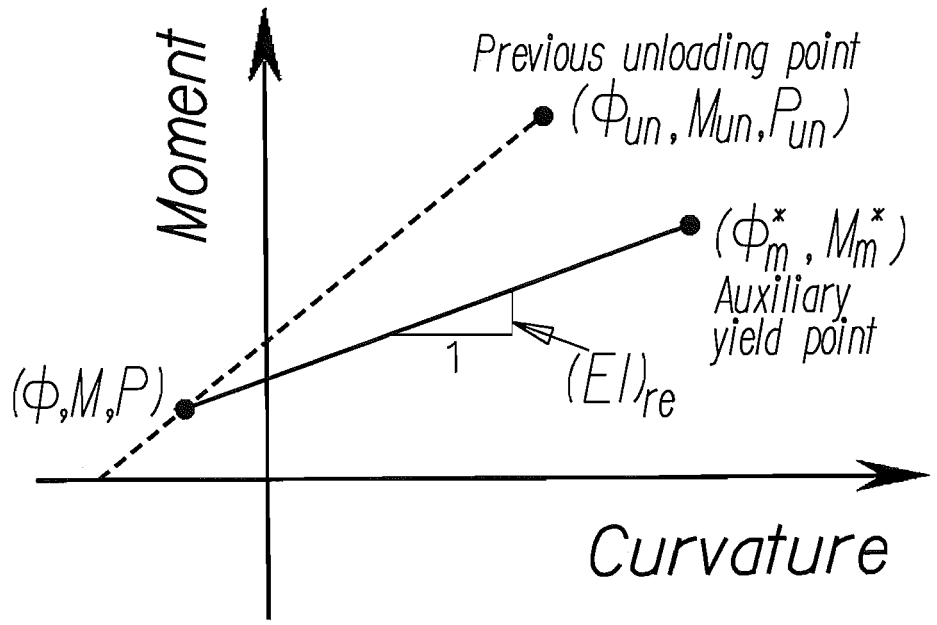

Fig.7.34: Calculation of Reloading Flexural Rigidity

7.11 COMPARISON OF EXPERIMENTAL AND PREDICTED MOMENT-CURVATURE HYSTERETIC RELATIONSHIPS

Moment-curvature hysteretic model described above has been compiled into a Fortran code program called the subroutine HYST(see the Appendix). The model was used to reproduce the experimental moment-curvature hysteretic relations of the columns tested under constant and varying axial loading. The parameters used in the calculation are given in Table 7.4.

Figs.7.35 to 7.40 illustrate the predicted moment-curvature hysteresis loops for Units 1 to 6. Fig.7.41 shows the predicted moment-curvature hysteresis relationship for the column tested under constant compression axial load by Gill et al[G1]. It can be seen from Figs.7.35 to 7.41 that the proposed model can satisfactorily reproduce the experimental moment-curvature hysteretic relationship.

Table 7.4: Parameters Used in Moment-curvature Modelling

Unit	P_b (kN)	P_{up} (kN)	P_t (kN)	M_b (kNm)	M_{up} (kNm)	M_o (kNm)	k_1 (%)	c_1	c_2	λ_1	λ_2
Units 1 to 6	1960	3360	1120	380	319	196	3	0.9	0.1	0.8	0.8
Gill's Specimen two[W1]	5009	6262	1880	1025	970	482	3	0.9	0.1	0.8	0.8

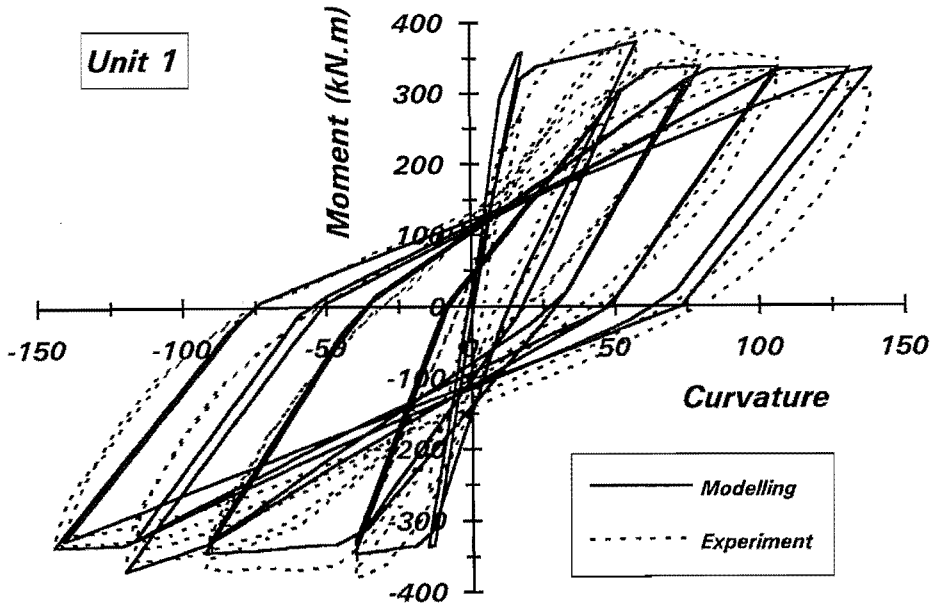

Fig.7.35: Comparison of Experimental and Predicted Moment-Curvature Hysteresis Loops for Unit 1

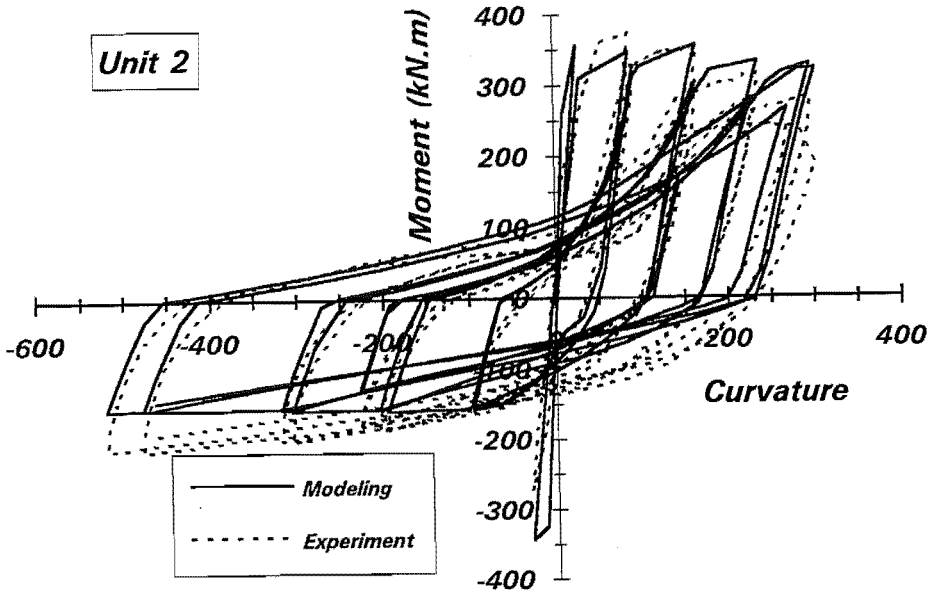

Fig.7.36: Comparison of Experimental and Predicted Moment-Curvature Hysteresis Loops for Unit 2

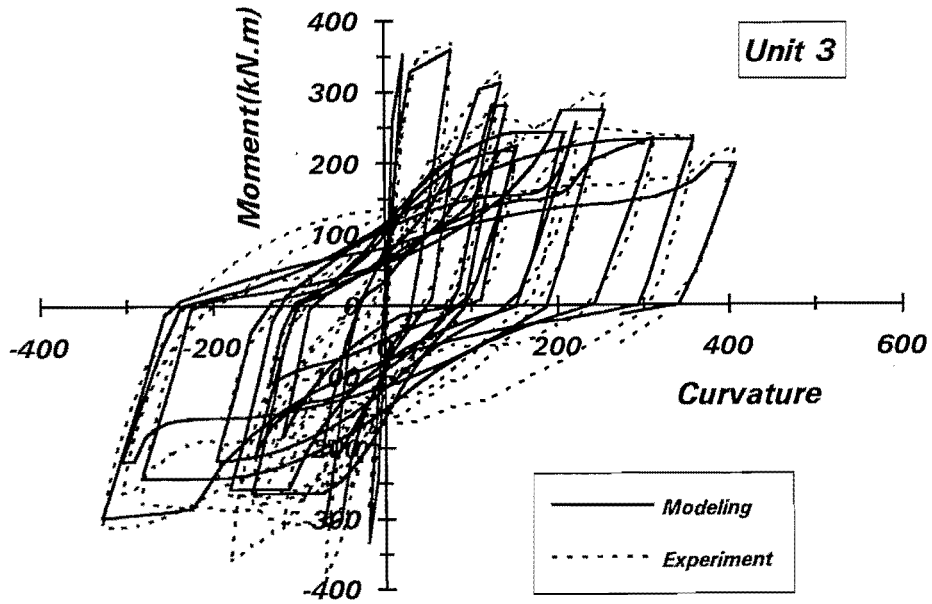

Fig.7.37: Comparison of Experimental and Predicted Moment-Curvature Hysteresis Loops for Unit 3

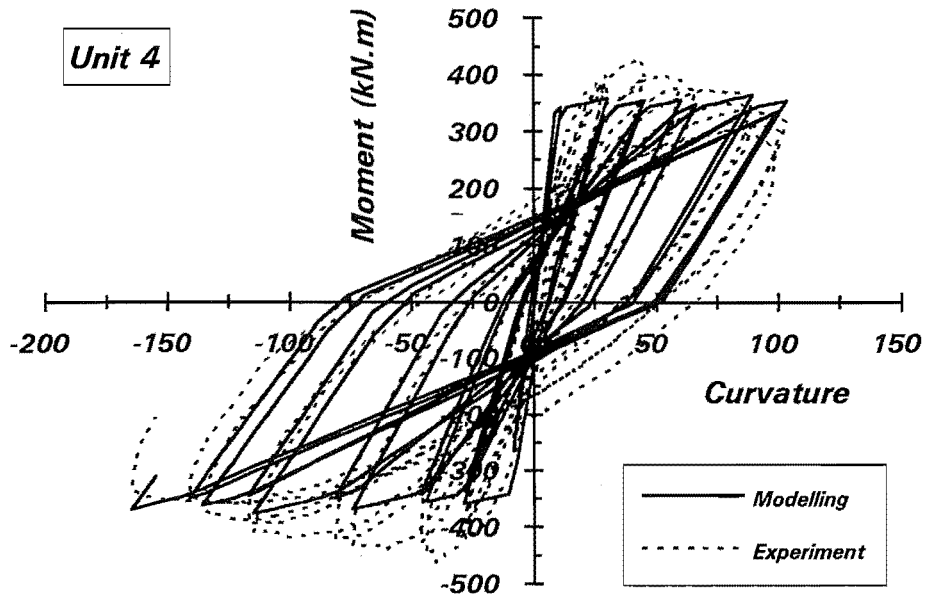

Fig.7.38: Comparison of Experimental and Predicted Moment-Curvature Hysteresis Loops for Unit 4

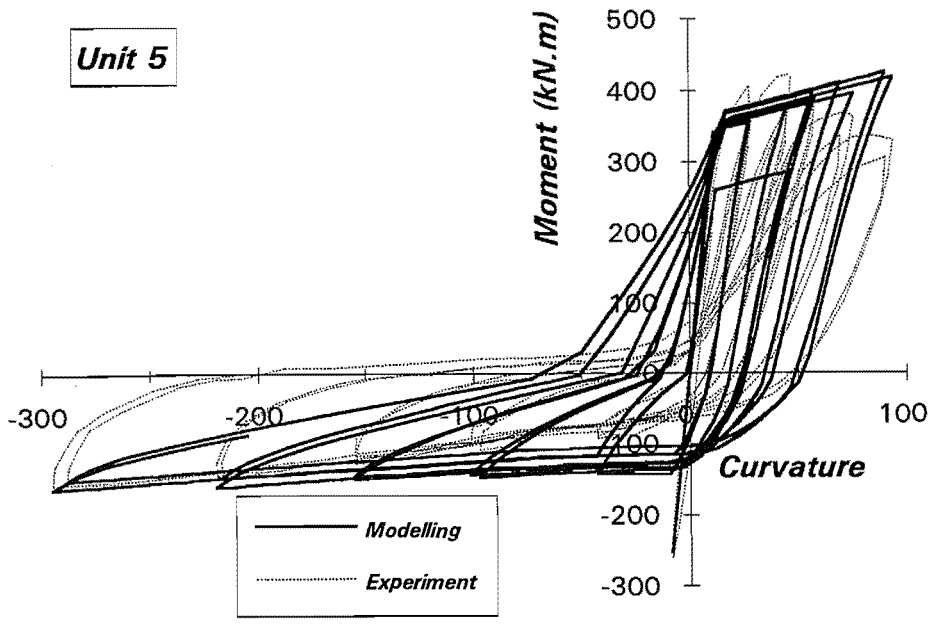

Fig.7.39: Comparison of Experimental and Predicted Moment-Curvature Hysteresis Loops for Unit 5

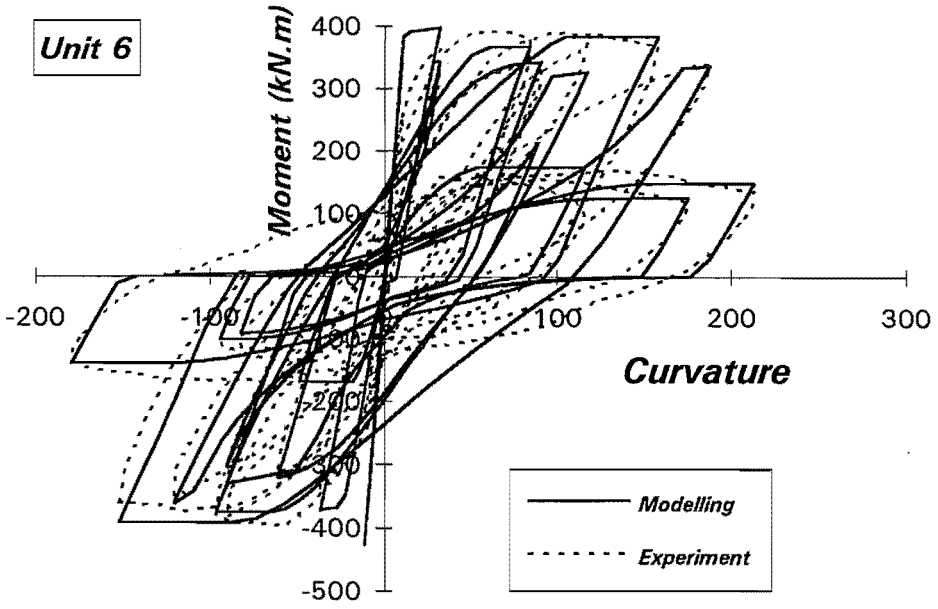

Fig.7.40: Comparison of Experimental and Predicted Moment-Curvature Hysteresis Loops for Unit 6

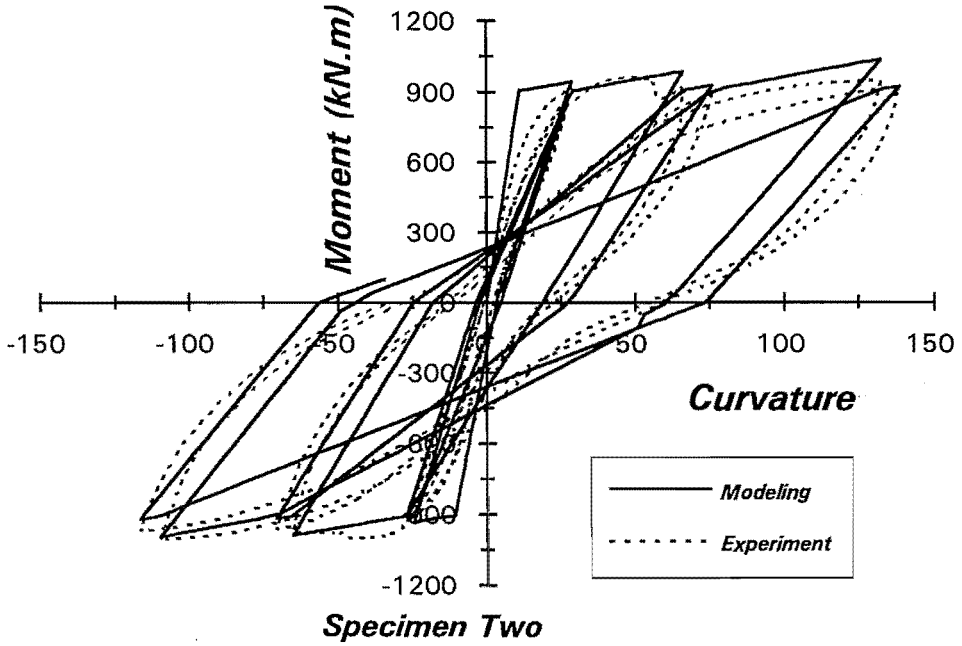

Fig.7.41: Comparison of Experimental and Predicted Moment-Curvature Hysteresis Loops for Specimen Two Tested by Gill[G1]

7.12 CONCLUSION

1 The transfer of compression stress across cracks before crack closure, due to local contact of high points at the crack faces and the presence of debris in the cracks, can be modelled by an equivalent stress-strain reloading branch. Comparisons of moment-curvature relationship from analysis and experiment indicated that proposed stress-strain reloading branch(Eq.7.1) effectively improves the accuracy of cyclic moment-curvature analysis.

2 The strength enhancement factor of reinforced concrete columns, which indicates the increase in strength over the ideal flexural strength determined from the code approach, was found to depend on the degree of confinement and the cover to core concrete ratio, in addition to the axial load ratio. The empirical formula derived by Ang et al[A7] can be modified to include the effect of the degree of confinement and cover to core concrete ratio. It was shown that the experimentally obtained strength enhancement factors fall within ±8% of that given by the proposed Eq.7.2 determined to include the effects of two extra factors.

3 Based on the results of monotonic moment-curvature analysis of 650 reinforced concrete sections, the theoretical elastic and post-yield flexural rigidities of reinforced concrete column section defined by Eqns.7.3 and 7.4 were found to be mainly influenced by the axial load level, the longitudinal reinforcement content and the concrete compressive strength. Theoretical elastic and post-yield flexural rigidity ratios can be estimated by the proposed Eqns.7.6 and 7.7. The elastic flexural rigidity ratio, $(EI)_{el}/(EI)_g$, determined by Eq.7.6 lies between the ratios calculated from experimental curvature measured at the first level of potentiometer (critical section) and the second level of potentiometers.

4. Experimental moment-curvature hysteretic relationships indicate that variation in the axial load can significantly influence the flexural rigidity of reinforced concrete sections at various loading stages. A moment-curvature hysteretic model for reinforced concrete column section, which takes into account the effect of varying axial load on loading and unloading flexural rigidity of reinforced concrete column section, is proposed. The comparisons indicated that the proposed model is capable of satisfactorily predicting experimental moment-curvature hysteresis relationships.

Chapter 8

An Example of Inelastic Dynamic Response Analysis

8.1 INTRODUCTION

Many force-deformation hysteresis models have been developed to represent the elastic and inelastic behaviour of reinforced concrete members for use in dynamic response analyses during the past. Although some models consider the influence of axial load level on yield moment using an axial force moment interaction surface, the basic stiffness of the member is kept constant without considering the effect of the varying axial load which may occur in some members of the structures.

In this chapter, an example is given of inelastic dynamic response analysis of a reinforced concrete frame using the proposed moment-curvature hysteresis model which includes the effects of varying axial load on the yield moment, and the loading and unloading stiffness of the member. The responses are compared with those obtained from analysis using the modified Takeda type model.

8.2 EQUIVALENT LATERAL STATIC ANALYSIS

8.2.1 Gravity Loads of Frame

The computation of the gravity load of the example frame included the followings items:

Floor slab(120 mm thick, at 24kN/m^3)	2.88 KPa
Floor finish, ceiling, services, and movable partition	1.20 KPa
Unreduced live load on all floor and roof	2.50 KPa
Curtain walls, glazing, etc., supported by periphery beams only, extending over floor height of 3.60m	0.50 KPa

8.2.2 Frame Period

The natural period of vibration the frame needs to be estimated in order to compute the equivalent static earthquake loading from design response spectrum. The preliminary estimate of first mode period of the frame is obtained by using the empirical equation[U2].

$$T = 0.061H^{0.75} \qquad (H \text{ in } m) \tag{8.1}$$

where H is the building height.

According to NZS 4203[S16], the natural period may be computed from the Reyleigh formula.

$$T = 2\pi \sqrt{\frac{\sum_{i=1}^{N} W_i \Delta_i^2}{g \sum_{i=1}^{N} F_i \Delta_i}} \tag{8.2}$$

where F_i is the lateral force applied at level i=1 to N, Δ_i are the corresponding lateral displacements, and W_i are the floor weights.

8.2.3 Member Properties

In determination of the member stiffness used for elastic analysis, the allowances were made for the effects of cracking on the stiffness of the members. The assumed properties of the structural members are shown in Table 8.1.

Table 8.1: Assumed Member Properties

Properties	Beams	Column 2	Column 1, 3
Area	$0.5A_g$	$0.75A_g$	$0.6A_g$
Shear Area	$0.5A_g$	$0.6A_g$	$0.6A_g$
Second Moment of Area	$0.5I_g$	$0.75I_g$	$0.75I_g$

Note: A_g and I_g are the area and second moment of area of the gross section, respectively.

8.2.4 Equivalent Seismic Design Forces

The horizontal seismic force acting at the base of the structure in the direction being considered, according to the NZS 4203:1992[S16], V is calculated from

$$V = C_h(T_1, \mu) S_p RZL\ W_t \qquad (8.3)$$

where

$C_h(T_1,\mu)$ = a basic seismic acceleration coefficient, which depends on the fundamental period of vibration of the structure T, the required structure ductility factor μ, and the soil condition. The value of C_h can be determined from one of the sets of normalised curves, as shown in Fig8.1.

S_p = a structural performance factor

R = a risk factor for structure varying between 0.6 and 1.3, which modifies the design load when either diminished failure risk or enhanced failure risk is acceptable.

Z = a zone factor to take into account regional seismicity, derived from appropriate figure given by the loading code, varying between 0.6 and 1.2, for the range of New Zealand site locations.

L = a limit state factor, L=1.0 for ultimate state and L=0.17 for serviceability state.

W_t = seismic weight of structure considered to be present during the earthquake, which is calculated by adding the dead load D and seismic live load(about one third of the unreduced live load).

The equivalent static lateral force, F_i , applied at level i of the structure is obtained from

$$F_i = 0.92V\frac{W_i h_i}{\sum_{i=1}^{N} W_i h_i} \qquad (8.4)$$

where W_i = seismic weight at level i including the dead load and seismic live loads between the mid-heights of adjacent storeys, and h_i = height of level i above the base of the structure.

At the top of the structure an additional horizontal force of 0.08V is added to the value given by Eq.8.3.

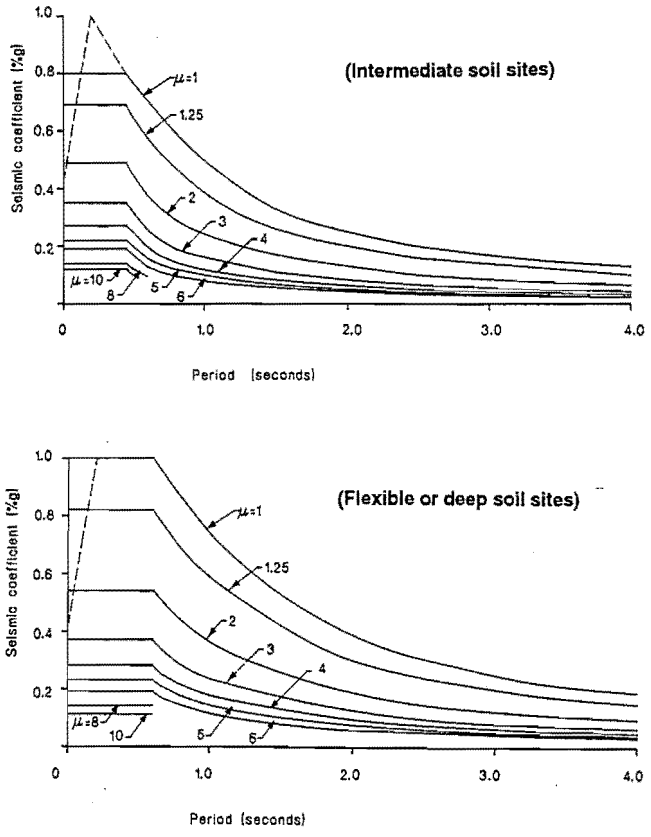

Fig.8.1: Basic Seismic Coefficient Proposed in the New Zealand Code of NZS 4203:1993[S16]

8.3 DESIGN OF PROTOTYPE FRAME

8.3.1 General

A twelve storey reinforced concrete ductile frame was designed. According to the New Zealand code[S14], such a structure shall be the subject of the capacity design. The capacity design approach proposed by Park and Paulay[P6] was used to design the ductile frame. In the capacity design of structure for earthquake resistance, the plastic hinges are designed to form at the beam ends, with inelastic flexural action of the column members avoided by use of the weak beam-strong column approach. Thus the desired mechanism of inelastic deformation under severe earthquake is assured. Other undesired mechanism such as beam or column shear failure, or joint failure, must be avoided since these mechanisms do not possess the fundamental requisite of ductile response, namely the ability to deform inelastically during repeated cyclic displacement response without significant strength or stiffness degradation. The procedure is intended to provide a high degree of protection against the formation of undesirable failure mechanism.

A moment redistribution technique developed by Paulay[P24] was applied to the beam moments obtained from elastic frame analysis. The use of moment redistribution can reduce the absolute maximum moment and utilize as much as possible the positive beam moment capacity required by the code, and therefore to achieve an efficient structural design. Redistribution of beam moments at the column centerlines was carried out leading to reduction of up to 30% of the maximum negative moments.

8.3.2 Beam Design Moment

The design moments for the beams were obtained from elastic frame analysis for code lateral force and factored gravity loads, and moment redistribution. The strength requirements were provided following the design procedure described in detail in the code[S14].

After the beam reinforcement was proportioned, the flexural overstrength of the beams with reference to the column centerlines including the strength enhancement of the beam section can be evaluated. The flexural overstrength factor ϕ_o, at the column centerline at each floor and in each direction of loading, which was used as an index to determine the probable maximum moment input into the adjacent columns, was calculated in terms of the design moments resulted from the analysis for the code specified lateral forces.

The design shear forces for the beams were found from the consideration of the gravity load with appropriate load factors and the simultaneous development of flexural overstrength at both ends of the beams due to lateral forces.

8.3.3 Column Design Moments

A method for the evaluation of column actions in ductile multistorey frames due to Paulay[P12] has been placed in the Commentary of the code[S14]. In the procedure, the column bending moments found from elastic analysis for the code specified lateral load are amplified to take into account the effects of the probable flexural overstrength of the plastic hinges in beams, higher modes of vibration of the structure and the concurrent earthquake loading effects.

Magnification of Column Moments due to Beam Flexural Overstrength

The aim of the capacity design of columns is to eliminate the likelihood of the simultaneous formation of plastic hinges in top and bottom of the columns. Therefore, the column must be capable of resisting the probable largest moment input from the adjacent beams. Using the beam overstrength factor ϕ_o, this moment can be calculated as

$$M_C = \phi_o M_E \qquad (8.5)$$

Magnification of Column Moment due to Dynamic Effects

The bending moment pattern of frame structure under higher modes of vibrations will differ significantly from those derived from the code static lateral static forces. To allow for such dynamic effects, further amplification of column moments resulting from lateral static force is needed to prevent plastic hinging of columns. This is achieved by using dynamic magnification factor

The code suggests that the dynamic moment magnification may be estimated as follows:

For one-way frame

$$\omega = 0.6T + 0.85 \qquad (8.6)$$

but not less than 1.3 nor more than 1.8.

For two-way frame

$$\omega = 0.5T + 1.0 \qquad (8.7)$$

but not less than 1.5 or more than 1.9, where T_1 = fundamental period of vibration of the structure.

The critical column section is assumed to be at the top or bottom of the beams. Accordingly, the centerline column moment M_E is reduced by $0.3h_bV_{col}$, which is based on an estimated gradient of the column bending moment, where h_b = the depth of the beam. With above consideration, the New Zealand concrete design code[S14] suggests that for ductile frames the column design moment in each principle direction, and to be used with the appropriate axial load for the determination of the ideal strength of the column, be taken as

$$M_{col} = \phi_o \omega M_E - 0.3h_bV_{col} \qquad (8.8a)$$

When the total axial compression on the column section does not exceeded $0.1f'_cA_g$, and hence column yielding is more accetable, the design column moment may be reduced and taken as

$$M_{col,red} = R_m(\phi_o \omega M_E - 0.3h_bV_{col}) \qquad (8.8b)$$

where M_E = column bending moment derived from elastic analysis for the code specified seismic forces; and V_{col} = column design shear force given in Section 8.5.

The reduction factor R_m has the value between 1.0 and 1.3, depending on the axial load level on the column and the value of factor ω.

8.3.4 Column Design Axial Force

The design axial forces in columns to be used with M_{col} given by Eq.8.8 for the design of column sections are derived from the earthquake induced axial load input in the adjacent beams at the development of flexural overstrengths, and from factored gravity loads. A reduction in the moment induced shear is allowed to take into account the increasing number of stories above the level to be considered. This is because the number of beam plastic hinges at which the full flexural overstrength will develop is likely to be reduced as the number of stories increases. Thus, the earthquake induced axial force in a column is taken as

$$P_{EO} = R_v \sum V_{EO} \qquad (8.9)$$

where ΣV_{EO} is the sum of the earthquake induced beam shear forces from all floors above the level

considered, developed at all sides of the columns, taking into account the beam overstrengths and the appropriate sense of the shear forces. The axial load reduction factor R_v varies between 0.54 and 0.97, depending on the number of floors above the level concerned and the value of ω.

8.3.5 Column Design Shear Forces

The column design shear forces are derived from the elastic analysis for code specified force, V_E. The New Zealand concrete design code[S14] suggests that design shear forces, acting in each principle direction of the structure, can be taken for the colums of a one-way frame as:

$$V_{col} = 1.3\phi_o V_E \qquad (8.10)$$

In first storey columns, in addition to satisfying the requirement given by Eq.8.10, the following design shear force should also be considered:

$$V_{col} = \frac{\phi_o^* M_E^* + 1.3\phi_o M_{E,T}}{l_n + 0.5h_b} \qquad (8.11)$$

where $\phi^*_o M^*_E$ = flexural overstrength capacity at the base section of the column, $M_{E,top}$ = column moment at the centerline of the beam at level 2 with beam depth h_b, derived from the code static seismic forces, and l_n = clear height of the first storey column.

8.4 DESCRIPTION OF THE TWELVE STOREY FRAME

8.4.1 Structural Layout

A twelve storey reinforced concrete frame under seismic attack is investigated. This moment resisting frame was designed by Jury[J4] and recently modified by Paulay[P25] in accordance with the requirements for ductility specified in the current New Zealand code[S14]. The floor plan and the basic dimensions of the frame are shown in Fig.8.2 and Table 8.2.

Table 8.2: Member Dimensions

Member	Floor		
	1-6	7-8	9-12
Main Beams	900x400	850x400	900x400
Secondary Beams	750x400	750x400	750x400
Column 1 and 3	700x500	650x500	600x500
Column 2	725x725	675x675	625x625
Slab	160	160	160

8.4.2 Material Properties

Concrete Compressive Strength $f'_c = 30MPa$

Yield Strength of Steel Used in

Deformed longitudinal bars in beams $f_y = 300Mpa$

Plain bars for stirrup and ties $f_y = 300MPa$

Deformed longitudinal bars in columns $f_y = 430Mpa$

8.4.3 Load Factors

The load factors used in the design as specified in the NZS 4203: 1992[S16] were as follows:

$$U = 1.4G$$

$$U = 1.2G + 1.6Q$$

$$U = G + Q_u + E$$

where G = dead load, Q = reduced live load, Q_u = live load for ultimate limit state, E = earthquake load. The reduced live load is obtained from unreduced live load multiplied by a reduction factor ψ_a.

$$\psi_a = 0.4 + 2.7\sqrt{A}$$

where A = tributary area per floor in square metres.

The strength reduction factor ϕ, recommended by NZS 3101:1982[S14] corresponding to above load factors are $\phi=0.85$ for the design of beam sections for flexure, and $\phi=1.0$ for the design of column sections for flexure, axial load and shear with the design actions derived in accordance with capacity design.

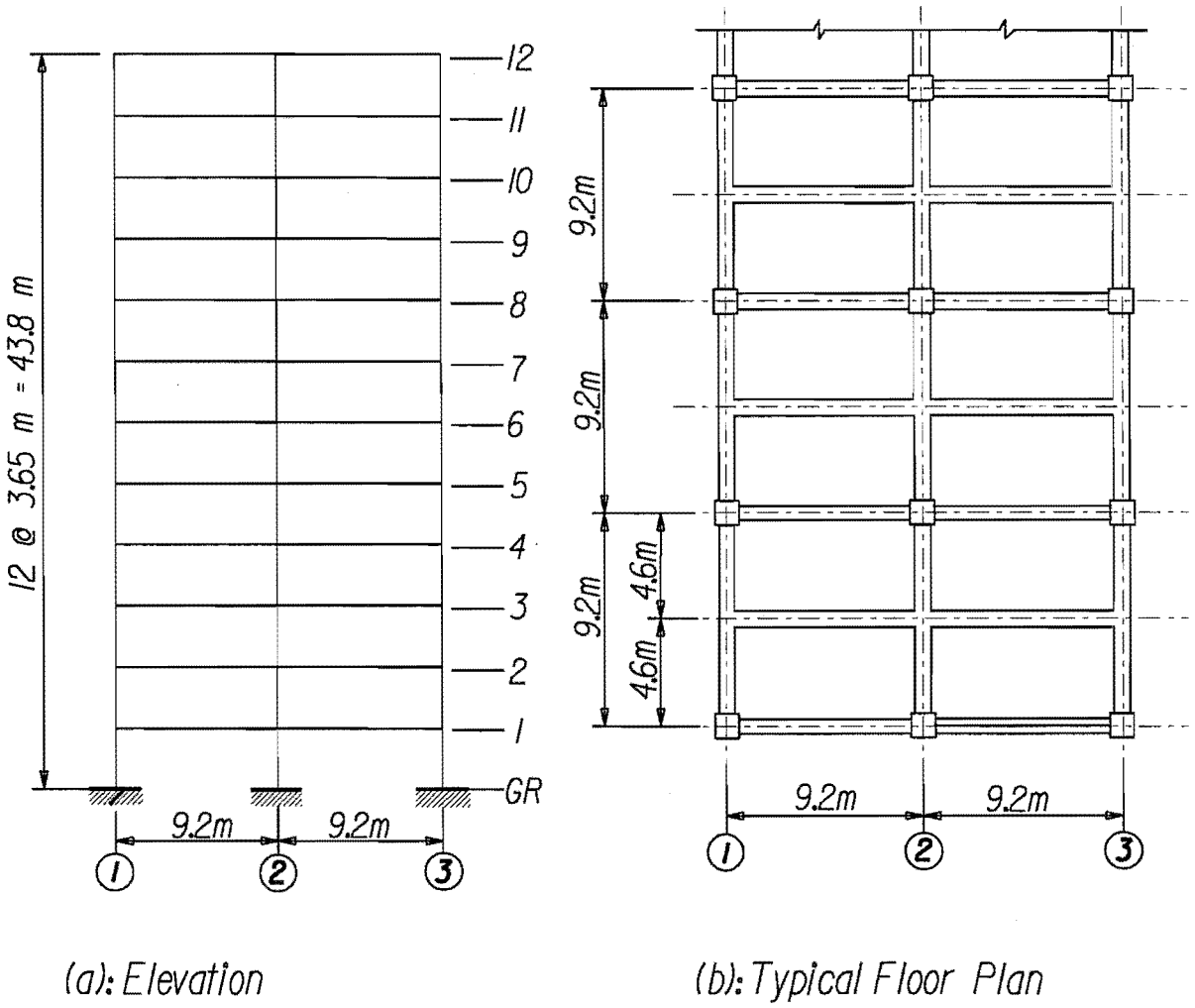

(a): Elevation

(b): Typical Floor Plan

Fig.8.2: Principle Dimensions of Twelve Storey Frame

8.5 COMPUTER PROGRAM, HYSTERESIS MODEL AND GROUND ACCELERATION RECORD

8.5.1 Computer Program-RUAUMOKO

The two dimensional inelastic time-history analysis program RUAUMOKO, written originally by Sharpe[S17] and extensively developed by Carr[C2] over the past two decades, was used to investigate the response of the designed structure under simulated seismic attack.

8.5.2 Modelling Member

In the RUAUMOKO, the components of the structure are modelled by a general two dimensional beam member which covers truss, beam and beam-column members. Truss member carries only axial load and the nonlinear load-displacement characteristics of the member may be represented by the chosen hysteresis rules. The beam member may have bi-linear axial load-displacement hysteresis and any of the hysteretic rules governing the behaviour of the plastic hinges that may form at each end of the member. The beam-column member may include the interaction between the axial load and moment yield states govern by the interaction diagram. The structural element is assumed to be consist of two types of regions, an elastic central region and an inelastic region at each end of the member. The inelastic deformation is confined to the end region. That is, the inelastic behaviour of the member is represented by a possible plastic hinge at one or both ends of the member, and the stiffness of the hinge regions is controlled by the tangent stiffness of the current point on the appropriate hysteresis rule.

Many different hysteresis rules are available in this program to represent the inelastic behaviour of structural members. The range covers from the simple elasto-plastic and bi-linear rules to computationally more expensive rules which may requires over thirty parameters to keep track of the current stiffness parameters. The basic stiffness of the member in these models is held constant throughout the analysis regardless of the influence of varying axial load.

To consider the effect of varying axial load level on the stiffness and yield moment of structural members, the moment-curvature hysteresis model proposed in this study, as described in Chapter 7, was used. The proposed hysteresis model has been written in Fortran code and incorporated as a subroutine into the program RUAUMOKO. The model modifies the section stiffness at each time step based on

the change in member axial load. Compared with other models, such as the Takeda or the modified Takeda type models, the proposed model requires only two extra parameters, f'_c and ρ_t, to define the elastic stiffness, where f'_c = concrete compressive strength, and ρ_t = longitudinal reinforcement ratio. These two parameters are considered to influence the elastic stiffness of the column member.

8.6 INELASTIC DYNAMIC RESPONSE OF TWELVE STOREY DUCTILE FRAME

8.6.1 Response Analyses

To assess the significance of varying column stiffness due to variation in axial load on the seismic response of a structure, by means of time history analysis, a twelve storey reinforced concrete ductile frame was analyzed twice, with and without varying axial load effects being included. The proposed moment-curvature hysteresis model which includes the effects of varying axial load on the loading and reloading stiffness was used in the first analysis. Since the beam axial load is generally negligible and also the variations of axial load in the columns of the top storey of the frame are relatively small, the proposed model was used only for modelling the columns in the first to ninth storey of the frame. The elastic flexural stiffness for the first floor columns is determined by Eq.7.6. For the upper storey columns, plastic hinging is not expected to occur. The elastic flexural stiffness was assumed to be 20% greater than that determined by Eq.7.6.

In the second analysis, the modified Takeda stiffness rule was used in which the basic stiffness of modelled members was held constant throughout the analyses.

In both the analyses, the Pacoima Dam earthquake record(February 1971 SW component record) was used. The Pacoima Dam ground motion was recorded at 9km from the epicentre and had a maximum ground acceleration of 1.15g and long duration pulses.

The response of the frame for the two cases are compared in the following sections.

8.6.2 Variations in Column Axial Load at the Base of the Columns

Fig.8.3 and 8.4 show the variation of axial load at the base of the columns obtained from the dynamic analyses when the proposed moment-curvature hysteresis model and the modified Takeda model were

used, respectively. These figures indicate that large variation in axial load occurs in the exterior columns of the moment resisting frame under earthquake excitation. At the instant of about 3 second, for example, the axial load in the column 3(right column) reached $0.77f'_cA_g$ while the axial load in column 1(left column) was $0.22f'_cA_g$. The axial load in the interior column underwent little change during the excitation, since the shear forces in the beams at the column faces tend to cancel each other out. Comparisons of Fig.8.3 with 8.4 indicate that the variation in column axial load when proposed hysteresis model was used were very similar to those when modified Takeda model was used.

Fig.8.5 shows the variation of axial load in the exterior columns of levels 2 to 4 of the frame obtained from analysis using the proposed hysteresis model. It can be seen that even in the middle levels of the frame, the variations in column axial load were also significant.

8.6.3 Moment-Curvature Relationship and Moment Response Waveform at the Base of Columns

The moment-curvature relationships at the base of the exterior columns obtained during the seismic excitation are shown in Figs.8.6 and 8.7 for the cases using the proposed hysteresis model and the modified Takeda model, respectively. The effect of change of axial load on the moment-curvature response of exterior columns can be found in these figures. When using the proposed hysteresis model, an increase or decrease in axial load will cause change in the loading and unloading stiffness(Fig.8.6). While using the modified Takeda model, the interaction between axial load and yield moment was considered but the basic stiffness of the member was kept unchange regardless of the change of column axial load. The moment-curvature curves for two exterior columns when using the modified Takeda model are very similar(Fig.8.7).

Figs.8.8 and 8.9 show the moment response waveforms obtained from the analyses using the proposed hysteresis model and the modified Takeda model, respectively. When using the proposed hysteresis model, the moment response waves in the two exterior columns are very similar during the early stage of excitation. After the column has yielded at about 3 second of excitation, the moment in column 1 is significantly different from that of column 3. This causes the unsymmetric shear response in the exterior columns. The moments at the base of exterior columns from analysis using the modified Takeda model are nearly the same during the whole excitation, indicating the symmetric response in the exterior columns of the frame.

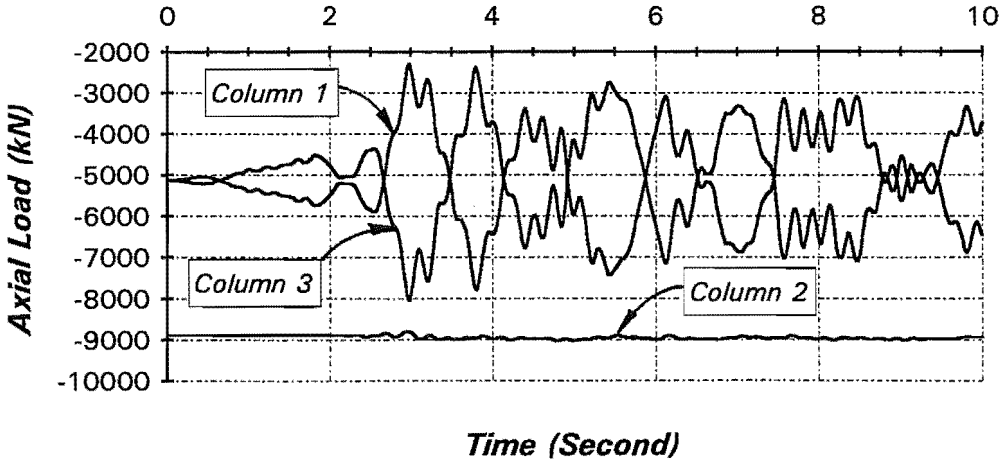

Fig.8.3: Variation of Axial Load at the Base of Columns Using Proposed Hysteresis Model

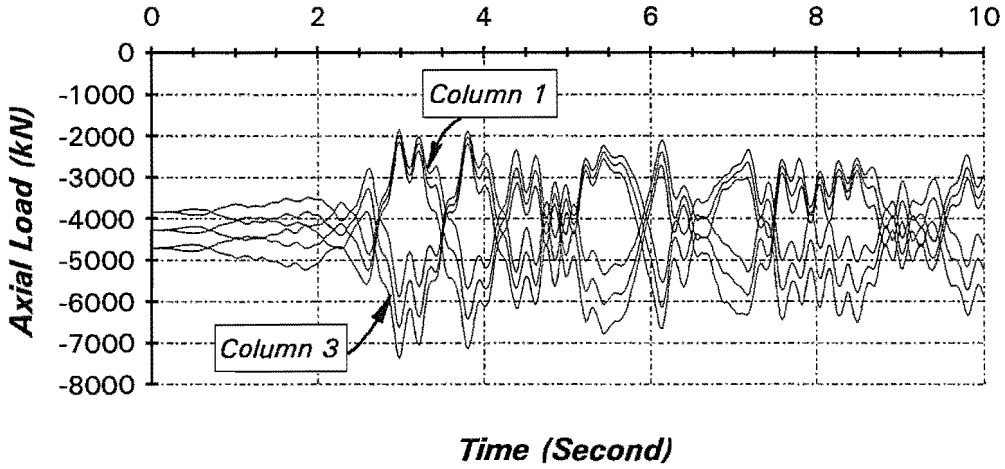

Fig.8.4: Variation of Axial Load at the Base of Columns Using Modified Takeda Model

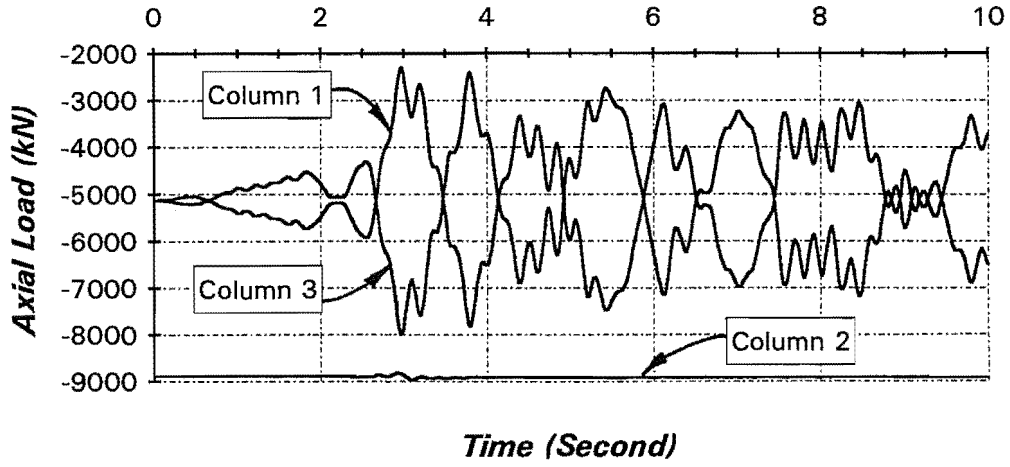

Fig.8.5: Variations of Axial Load in the Exterior Columns of Levels 2 to 4 of Frame Using Proposed Hysteresis Model

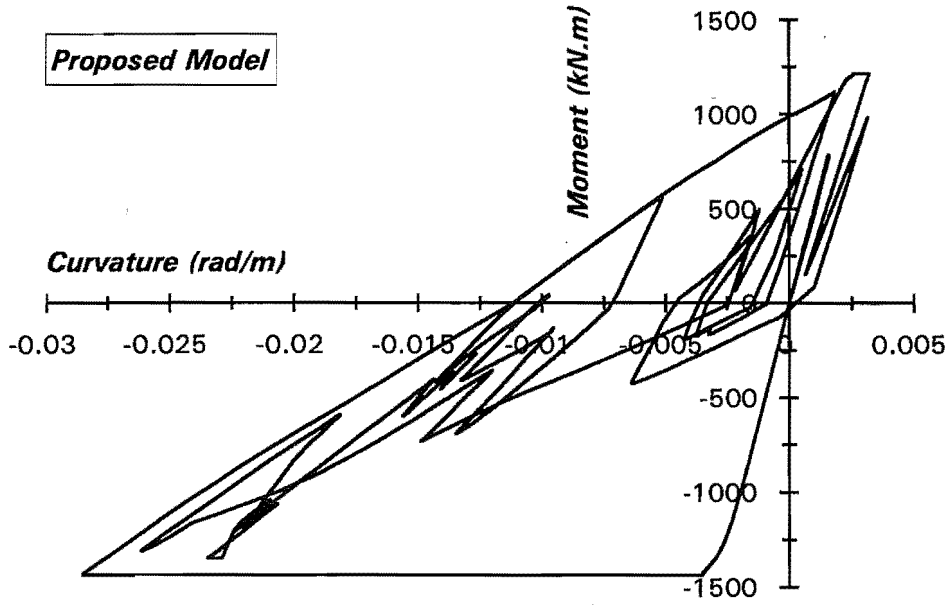

(a) Column 1(left column)

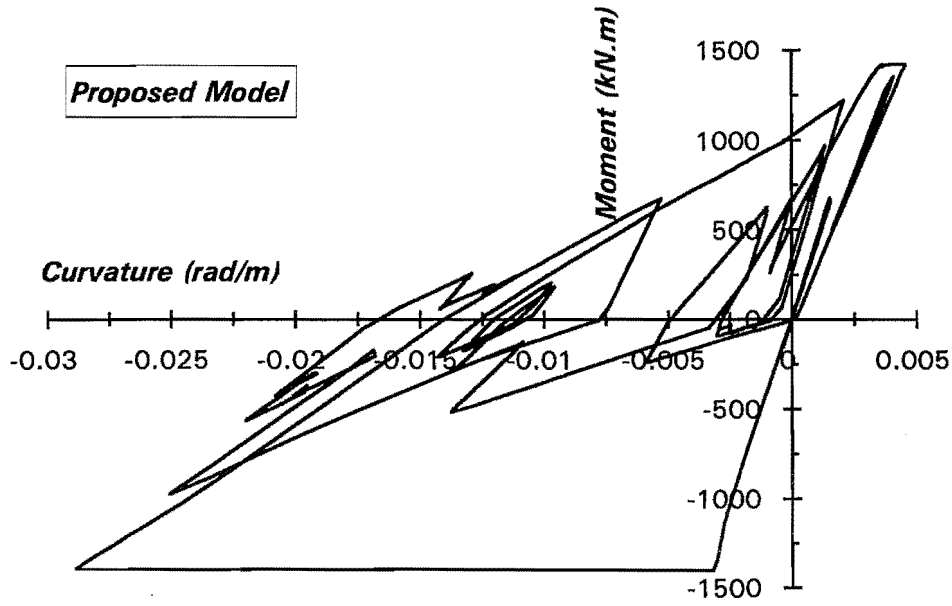

(a) Column 3(right column)

Fig.8.6: Moment-Curvature Relationships at the Base of Exterior Columns Using Proposed Hysteresis Model

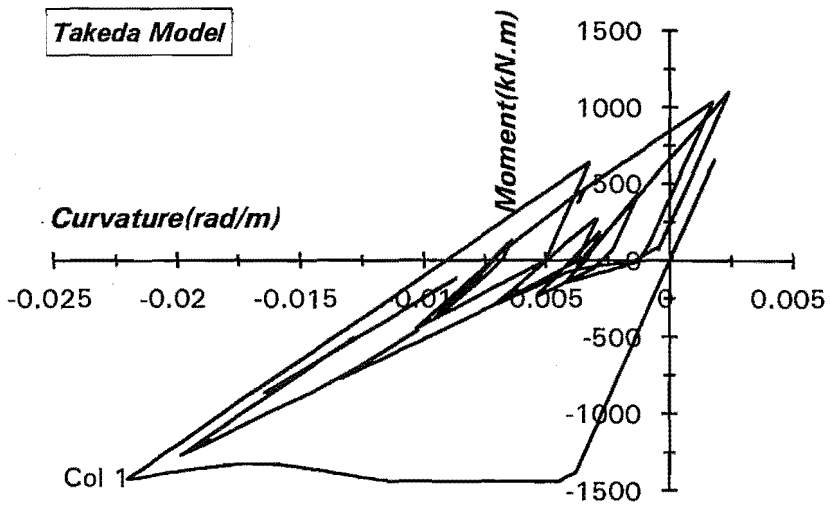

(a) Column 1(left Column)

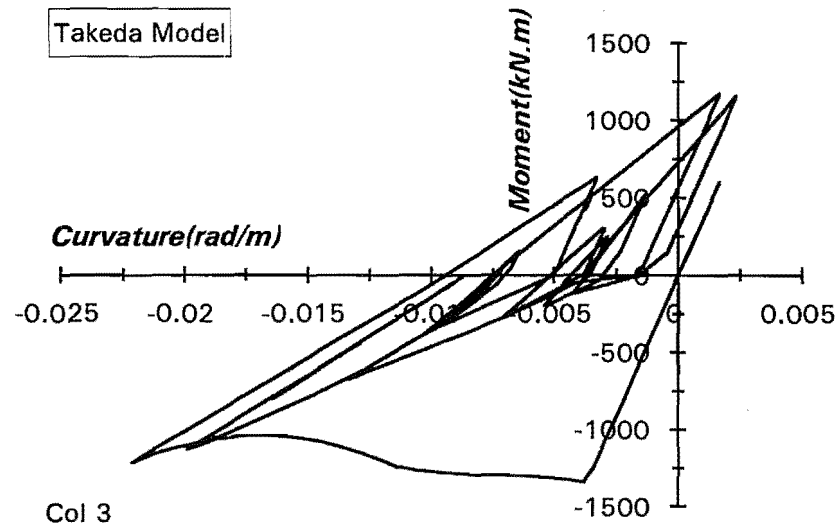

(b) Column 3(right column)

Fig.8.7: Moment-Curvature Relationships at the Base of Exterior Columns Using Modified Takeda Model

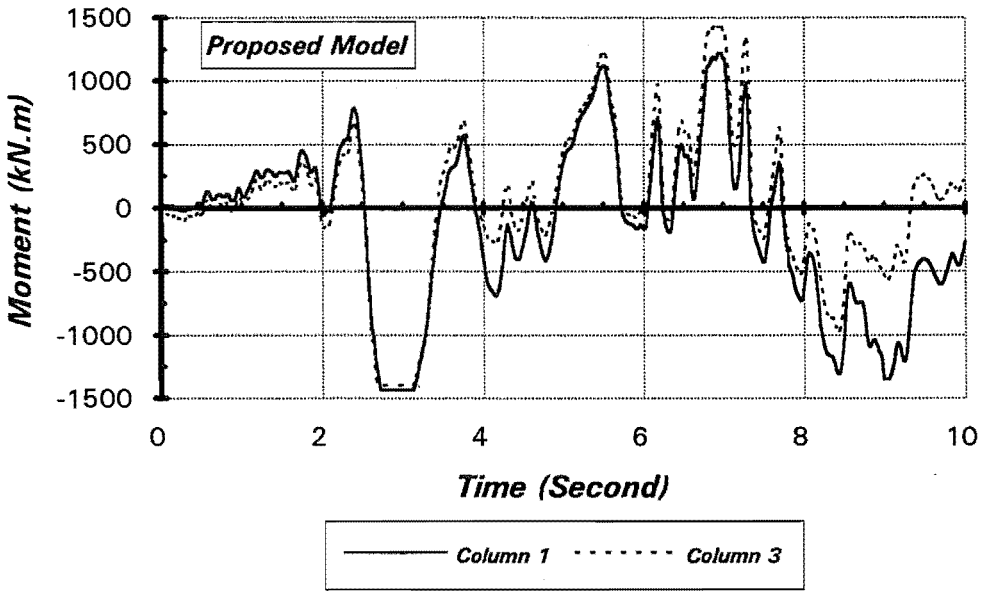

Fig.8.8: Moment Response Waveform at the Base of Exterior Columns Using the Proposed Hysteresis Model

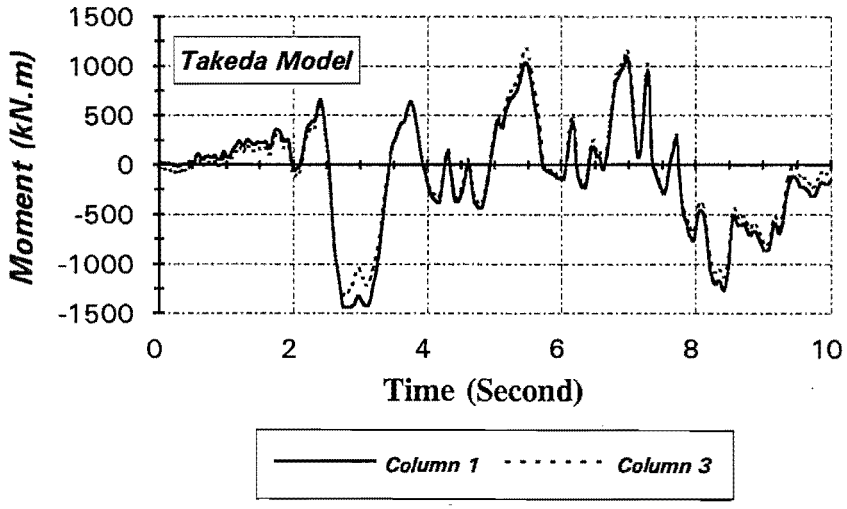

Fig.8.9: Moment Response Waveform at the Base of Exterior Columns Using the Modified Takeda Model

8.6.4 Development of Plastic Hinges

The graphs illustrating the sequence of the formation of plastic hinges in the structure members at the instants when major change in the formation of plastic hinges are shown in Fig.8.10 and 8.11 for the analyses when proposed hysteresis model and modified Takeda model were used, respectively.

Figs.8.10 and 8.11 show that a column sidesway mechanism did not occur during the excitation. This indicated that the columns are effectively protected against plastic hinging using the capacity design approach.

The formations of plastic hinges appear very similar for the analyses using the proposed hysteresis model and the modified Takeda model.

8.6.5 Shear Force Response Waveforms

The shear response waveforms in the columns of the frame observed during the seismic excitation are shown in Figs.8.12 and 8.13 for the cases using the proposed hysteresis model and the modified Takeda model, respectively. The shears in the two exterior first floor columns using the modified Takeda model are almost the same(Fig.8.13). The difference in the shear forces in the two exterior columns can be found in the shear response waveforms obtained using the proposed hysteresis model(Fig.8.12). After the formation of beam plastic hinges, the beam stiffness is significantly reduced, and the joint deformation(rotation) is mainly dependent on the stiffness of the columns which enter that joint. The variations of axial load cause a change of column stiffness. While one exterior column becomes stiffer the opposite exterior column becomes softer. This results in an unsymmetric rotation and hence the moment at the ends of the opposite exterior columns. This effect appears to be more significant in the second floor columns than that in the first floor columns, since the deformations at the both ends of the columns in the upper floor columns are affected by the change of column stiffness while at the base of the frame a fixed end condition was assumed in the analyses.

Fig.8.14 and 8.15 show the base shear for the analysis using the proposed hysteresis model and using the modified Takeda model, respectively. It can be seen from these figures that the total shear inputs due to seismic excitation are very similar for the cases using the proposed hysteresis model and using the modified Takeda model.

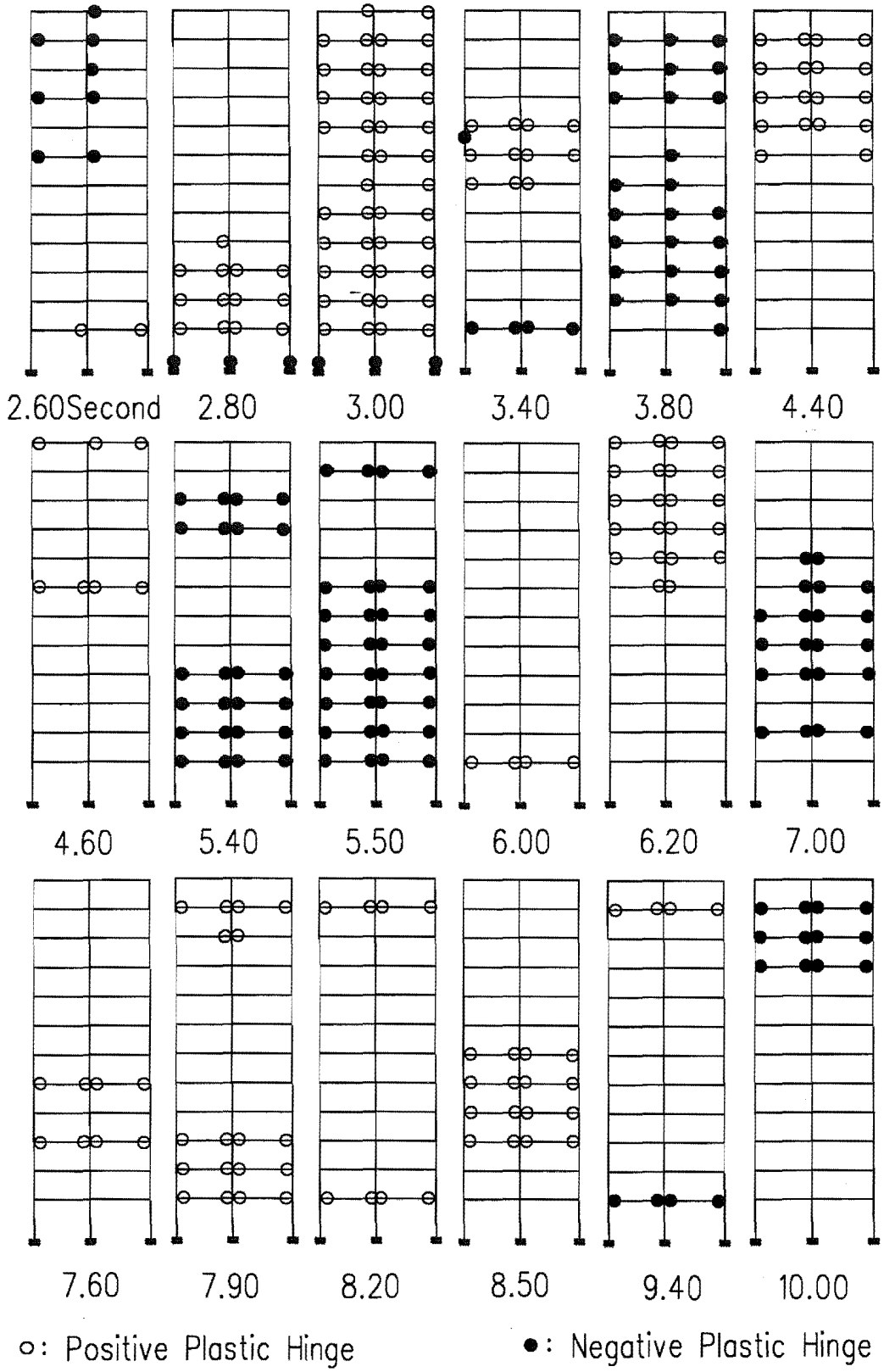

Fig.8.10: The Sequence of the Development of Plastic Hinge Formation in Twelve Storey Frame During the Pacoima Dam Excitation Using the Proposed Hysteresis Model

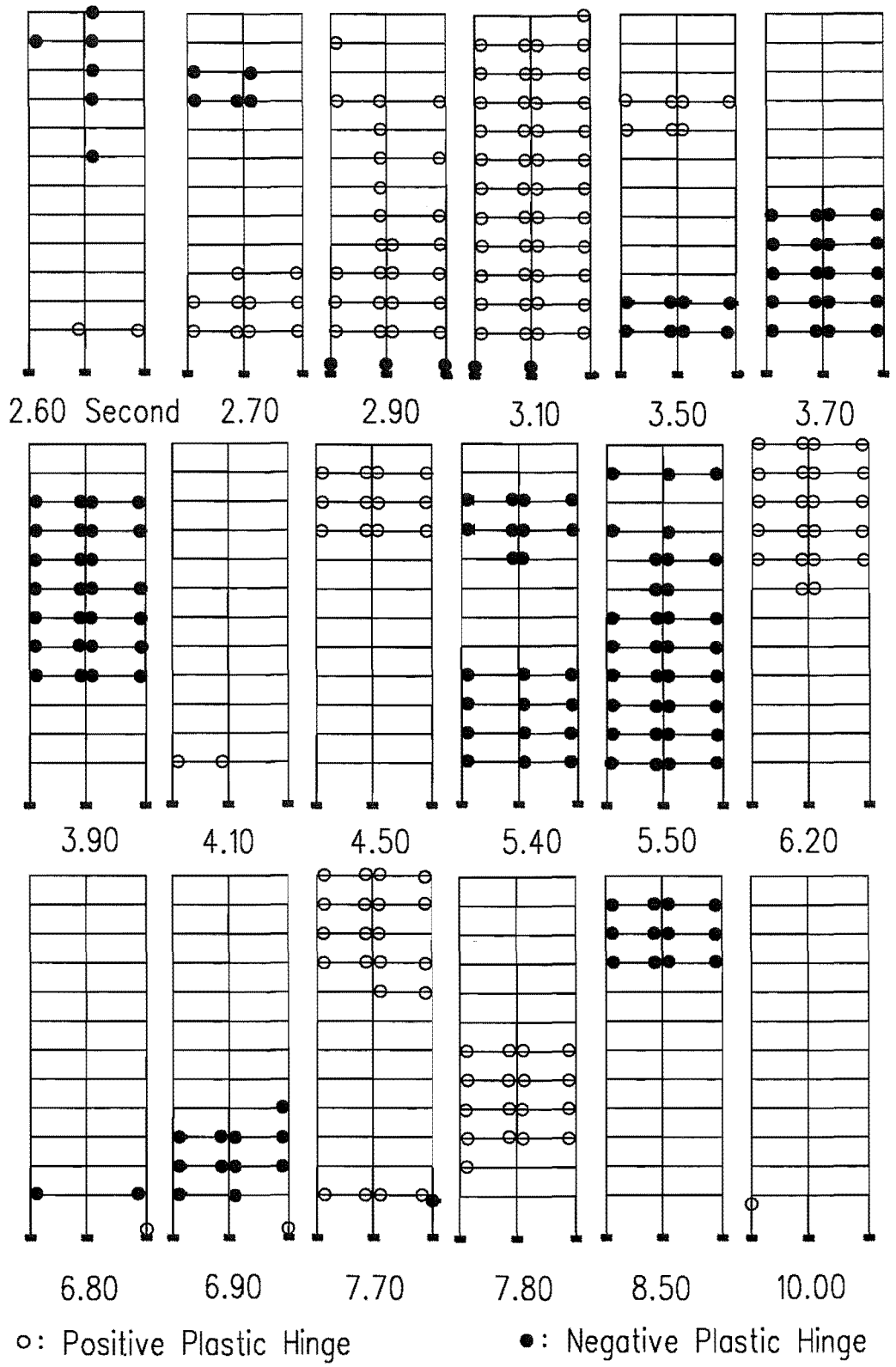

Fig.8.11: The Sequence of the Development of Plastic Hinge Formation in Twelve Storey Frame During the Pacoima Dam Excitation Using the Modified Takeda Model

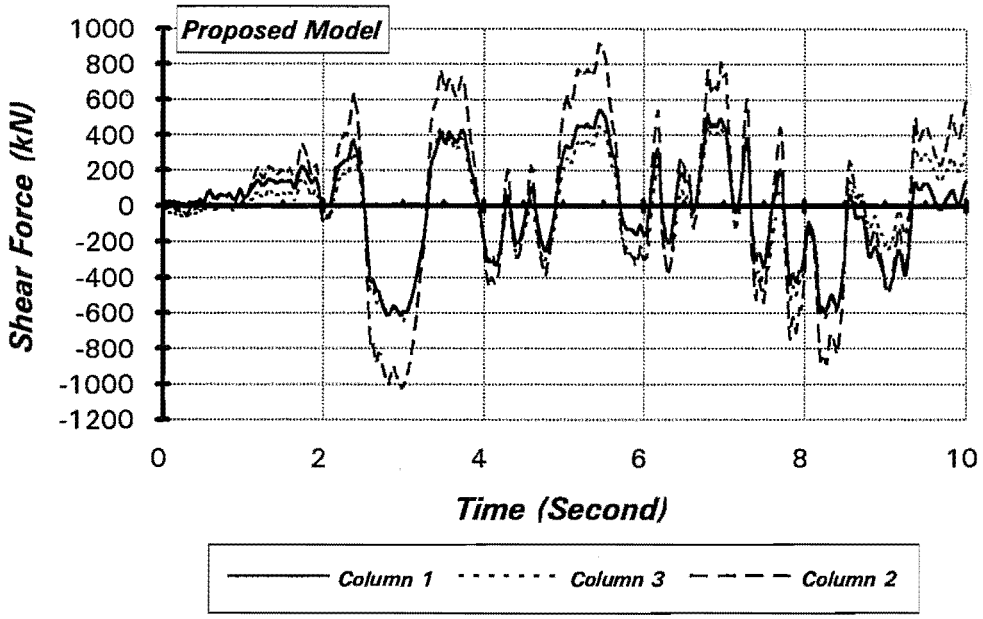

(a) At the first floor of the frame

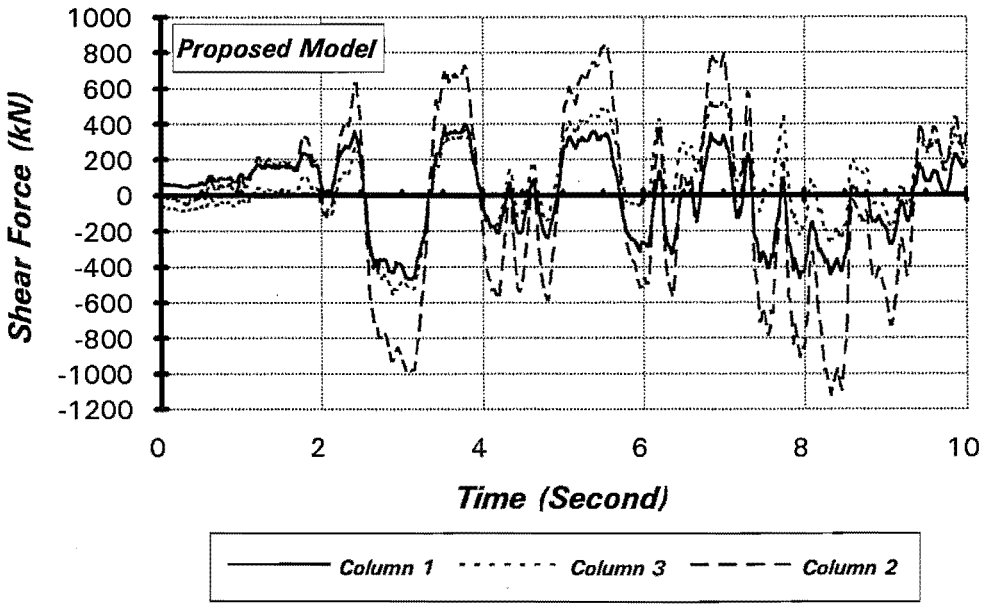

(b) At the second floor of the frame

Fig.8.12: Shear Forces in the Columns of Frame Using the Proposed Hysteresis Model

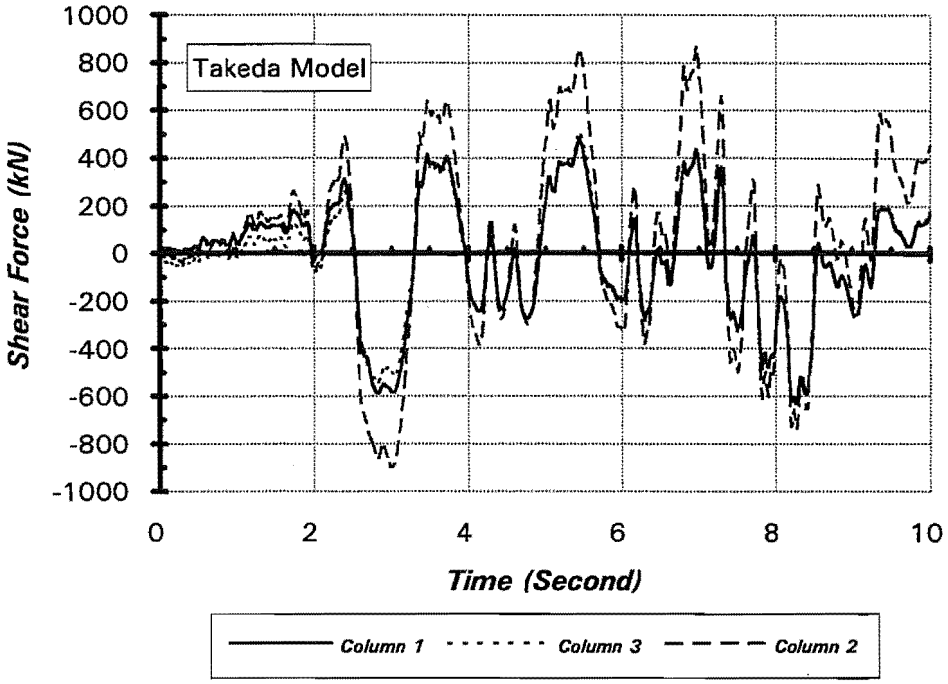

(a) At the first floor of the frame

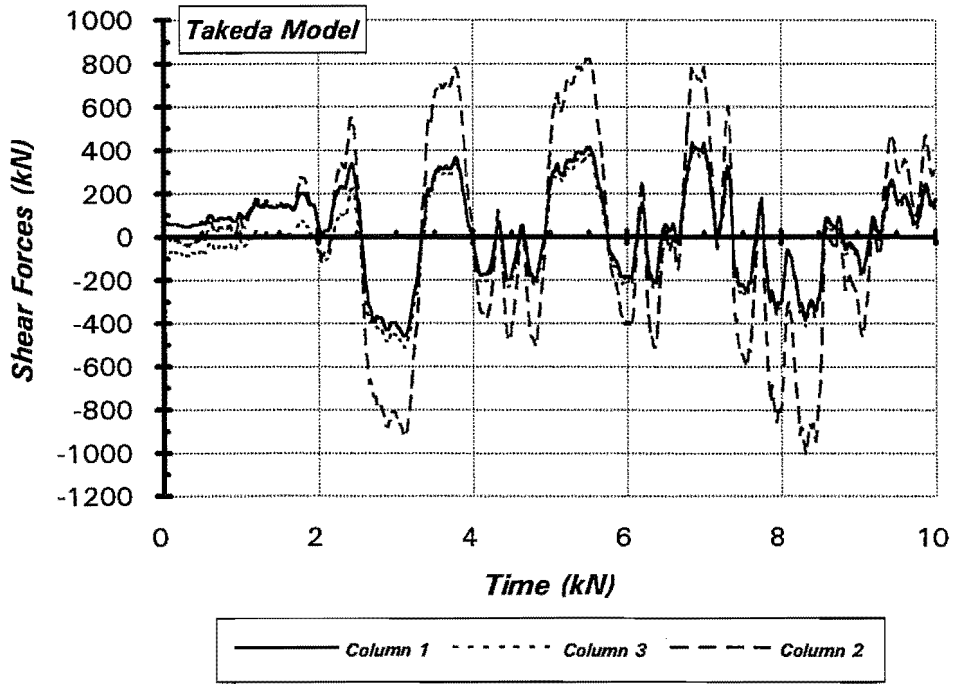

(b) At the second floor of the frame

Fig.8.13: Shear Forces in ther Columns of Frame Using the Modified Takeda Model

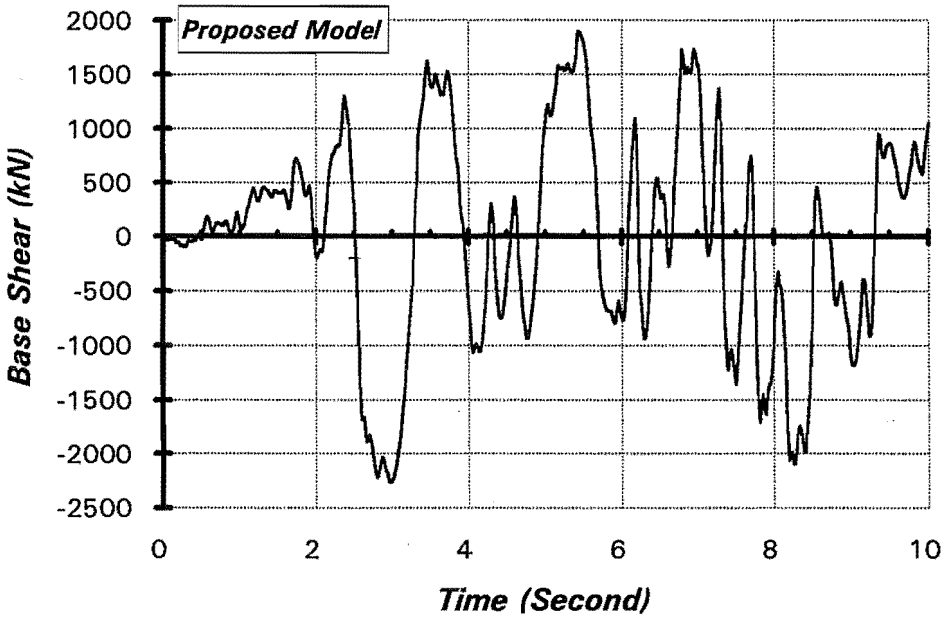

Fig.8.14: Base Shear of the Frame Using the Proposed Hysteresis Model

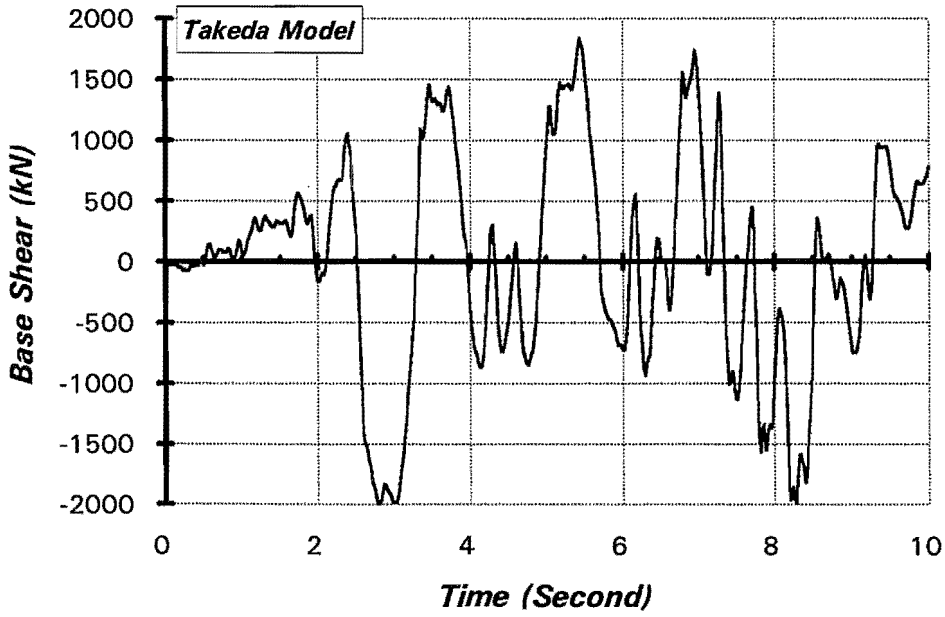

Fig.8.15: Base Shear of the Frame Using the Modified Takeda Model

8.7 CONCLUSIONS

An example is given of the inelastic dynamic response analysis of a two bay twelve storey reinforced concrete frame using the proposed moment-curvature hysteresis model and the modified Takeda model. From this analysis, following preliminary conclusions can be drawn.

1 The results from inelastic dynamic response analyses indicate that large variations of axial load at the base of exterior columns of a moment resisting frame subjected to seismic excitation can occur. Tension axial force was not observed to occur in the columns of the example frame during the seismic excitation. The maximum and minimum compression axial force at the base of exterior columns of the frame obtained in the analysis are $0.72f'_cA_g$ and $0.22f'_cA_g$.

2 The change of column stiffness due to variation in column axial load can effect the dynamic response of the structure. The moment and shear response are unsymmetric in the exterior columns of a symmetric frame when the variation of column stiffness is taken into account.

Chapter 9

Major Conclusions and Recommendations for Future Research

9.1 CONCLUSIONS

Concluding remarks drawn as the results of experimental and theoretical study carried out have been generally given at the end of each chapter. A summary of those findings is as followings.

1. An experimental study was carried out to investigate the flexural behaviour of reinforced concrete columns under simulated seismic lateral loading and varying axial loading patterns. The six columns tested had a 400mm square cross section, an aspect ratio of 4.12, a longitudinal reinforcement content of 1.6% and transverse reinforcement which was placed in accordance with the New Zealand code provisions of the New Zealand concrete design code NZS 3101:1982[S14] for ductile behaviour. The main conclusions from this series of tests are:

(a) Units 1 and 4 were subjected to the cyclic flexural and constant compression axial load levels of $0.3f'_cA_g$ and $0.5f'_cA_g$, respectively, and were capable of maintaining stable lateral load-displacement hysteresis loops up to a displacement ductility factor of at least eight. No significant degradation of strength was observed before the end of testing. The buckling of longitudinal bars resulted in the

termination of the test on Unit 4. The buckling of longitudinal bars was not significant when the test on Unit 1 was stopped at displacement ductility factor of $\mu_n=8$.

(b) Units 2 and 5 were tested under varying axial compression and tension load between $0.3f'_cA_g$ and $-0.05f'_cA_g$ for Unit 2, and $0.5f'_cA_g$ and $-0.1f'_cA_g$ for Unit 5, which varied in direct proportion to the bending moment at the critical section of the column, were capable of achieving nominal displacement ductility factors of $\mu_n=8$ and $\mu_n=10$, respectively. The degradation of lateral load strength in the compression axial load direction of Unit 2 was very significant. Both columns showed little deterioration in load carrying capacity in the tension axial load direction. Buckling of longitudinal bars occurred before the end of testing.

(c) Units 3 and 6 were tested under cyclic flexural and varying axial load, between the same compression and tension limits as Units 2 and 5 but which was uncoupled with the bending moment, and were capable of attaining nominal displacement ductility factors of $\mu_n=6$ and $\mu_n=8$, respectively. The strength degradation of Unit 3 was more significant than that of Unit 6. The buckling of longitudinal bars was observed before the end of testing.

(d) The experimental results indicated that alternating compression and tension axial load has significant effect on the behaviour of reinforced concrete column subjected to cyclic lateral loading. The load carrying capacity of the columns subjected to varying axial load levels was about 10 to 15% lower than those subjected to constant compression axial load at moderate displacement ductility levels. This increased to 15 to 20% at higher displacement ductility levels. The varying axial load pattern resulted in serious pinching of the hysteresis loops. Considerable change in the column stiffness was observed. The flexural rigidity of the columns subjected to varying axial loading was about 20% less than that subjected to constant compression axial load at nominal displacement ductility level of $\mu_n\geq2.0$.

2. An experimental study was carried out to investigate the shear strength of reinforced concrete under reversed flexure and varying axial load. Three reinforced concrete columns had shear strength calculated using New Zealand code equations of NZS 3101: 1982[S14] for outside potential plastic hinge regions of 91, 96 and 104% of the shear force corresponding to the development of ideal flexure strength, and contained 39, 31 and 29% of the NZS 3101:1982[S14] specified quantity of confining reinforcement in the potential plastic hinge regions. Three columns were tested under alternating compression and tension axial load between $0.1f'_cA_g$ and $-0.05f'_cA_g$ for Unit 7, $0.2f'_cA_g$ and $-0.1f'_cA_g$ for Unit 8, and $0.3f'_cA_g$ and $-0.15f'_cA_g$ for Unit 9, respectively, which varied in direct proportion to the bending moment at the critical section of the column.

All three columns failed in a shear dominant mode. The test results indicated that alternating tension and compression axial loading patterns resulted in a more severe degradation in the shear strength and stiffness in the compression axial loading cycle. Tension axial load encouraged the opening and delayed the closure of diagonal cracks. The formation of a major diagonal crack and deterioration of the concrete shear carrying capacity were observed during compression axial loading cycles. The experimental results further confirmed the interaction between the shear strength and the imposed displacement ductility factors. The reduction in the shear strength was caused by the degradation of the concrete shear resisting mechanism during reversed cyclic loading.

The presence of tension axial load degraded the shear strength of the column in the compression axial load direction, but little degradation in shear strength was observed in the tension axial load direction. It was found that a fairly large portion of total shear was able to be transferred by the concrete mechanism even under small tension axial force.

3. Comparisons revealed that the current New Zealand concrete design code[S14] equations for the shear strength gave a conservative prediction for the peak shear force resisted by the concrete mechanisms at a displacement ductility factor of $\mu_n=1.5$, even using the code equations for outside potential plastic hinge regions. Neglect of shear strength of concrete component in the code equations of NZS 3101:1982 for the column with axial compression axial load of $0.1f'_cA_g$ or less appears unnecessarily conservative in terms of requirements for the shear strength. The shear strength carried by the concrete mechanisms rapidly degraded to less than the code specified shear strength for outside potential plastic hinge regions when the imposed displacement ductility factor exceed about 2.

On the basis of experimental results, proposals are made for predicting the shear strength of reinforced concrete column of full ductility(Eqns.6.1 to 6.7) and limited ductility(Eq.6.9). Comparisons of the shear strengths predicted by the proposed equations(Eqns.6.1 to 6.7) with experimental results indicate that the proposed equations result in a greatly improved accuracy of prediction of the shear strength.

4. An analytical investigation using moment-curvature theory was conducted to determine the elastic flexural rigidity and post-yield second slope rigidity of cracked reinforced concrete sections. It was found that the theoretical elastic flexural rigidity and post-yield flexural rigidity of reinforced concrete sections were mainly influenced by the axial load level, the longitudinal reinforcement content and the concrete compressive strength. From regression analysis of the results of 650 reinforced concrete sections containing NZS 3101 specified quantity of confining reinforcement, the equations for the elastic and post-yield flexural rigidity ratio are proposed(Eqns.7.6 and 7.7). These equations are

applicable to the reinforced concrete column sections where the yielding is expected. The elastic flexural rigidity ratio given by Eq.7.5 is reasonably comparable with that obtained from experimentally measured average curvature in the plastic hinge regions.

5 The experimental results indicated that the unloading and reloading stiffness of reinforced concrete column were significantly influenced by the variation in axial loading pattern. An investigation was carried out to model the moment-curvature hysteresis loops of reinforced concrete column section. Based on the experimental results, a moment-curvature hysteresis model including the effect of varying axial load level on the inelastic unloading and reloading stiffness was developed. Comparisons indicate that the proposed moment-curvature hysteresis model is capable of satisfactorily predicting experimentally obtained moment-curvature hysteresis loops in plastic hinge regions.

6. The results from inelastic dynamic response analysis indicate that large variation of axial load in the exterior columns of a moment resisting frame under seismic excitation can occur. The structural response when the effect of varying axial load on the column stiffness is considered is significantly different from that when this effect is ignored.

9.2 RECOMMENDATIONS FOR FUTURE RESEARCH

1. The number of tests on the shear strength of reinforced concrete columns in this study was very limited. It appeared that columns with varying axial loading patterns will undergo a more severe degradation of concrete shear resisting mechanisms than columns with constant axial load. Further investigation is recommended to confirm the findings from this study.

2. More tests are needed to investigated the shear strength of reinforced concrete columns which contain low longitudinal reinforcement content when the axial load ratio is high.

3. The first series of six reinforced concrete column units tested under varying axial loading patterns contained the NZS 3101:1982 specified quantity of confining reinforcement for full ductility. The behaviour of columns which contains less transverse reinforcement, such as the columns designed for limited ductility, needs to be examined.

4. Further research is recommended to systematically investigate the inelastic response of structural frames and coupled structural walls, taking into account the influence of varying axial load on the member stiffnesses.

References

[A1] Abrams, D.P., "Influence of Axial Force Variation on Flexural Behaviour of Reinforced Concrete Columns", Structural Journal, ACI, Mar-June, 1987, pp246-254.

[A2] ACI-ASCE Committee 426, Shear and Diagonal Tension, "The Shear Strength of Reinforced Concrete Members," Journal of Structural Division, ASCE, Vol. 99, No. ST6, June 1973, pp1091-1187.

[A3] ACI Committee 318, "Building Requirements for Reinforced Concrete(ACI 318-89),' American Concrete Institute, Detroit, 1989, 353pp.

[A4] Ahmad, S.H., Khaloo, A.R. and Poveda, A., "Shear Capacity of Reinforced High-Strength Concrete Beams," ACI Journal, March-April, 1986, pp297-305.

[A5] Aktan, A. E. and Bertero, V. V., "RC Structural Walls: Seismic Design for Shear," Journal of Structural Engineering, ASCE, Vol. 111, No. 8, August, 1985, pp 1775-1791.

[A6] Ang, B.G., Priestley, M.J.N. and Park, R., "Ductility of Reinforced Concrete Bridge Piers Under Seismic Loading," Research Report 81-3, Department of Civil Engineering, University of Canterbury, Feb. 1981, 109pp.

[A7] Ang, B.G., Priestley, M.J.N. and Paulay, T., "Seismic Shear Strength of Circular Bridge Piers," Research Report, 85-5, Department of Civil Engineering, University of Canterbury, July, 1985, 408pp.

[A8] Ang, B.G., Priestley, M.J.N. and Paulay, T., "Seismic Shear Strength of Circular Reinforced Concrete Columns," ACI Structural Journal, January-February, 1989, pp45-60.

[A9] Aoyama, H., et al., "A Study on the Cause of Damage to the Hachinohe Technical College Due to 1968 Tokachi-Oki Earthquake(part 1)," Proceedings of the US-Japan Seminar on Earthquake Engineering With Emphasis on the Safety of School Buildings, The Japan Earthquake Engineering Promotion Society, Tokyo, Japan, 1971, pp199-212.

[A10] Aschheim, M. and Moehle, J.P., "Shear Strength and Deformability of RC Bridge Columns Subjected to Inelastic Cyclic Displacements," UCB/EERC 92/04, University of California, Berkeley, 1992, 93pp.

[A11] Azizinamini, A., Corley, W.G. and Paul Johal, L.S., "Effects of Transverse Reinforcement on Seismic Performance of Columns," ACI Journal, V. 89, No. 4, July-August, 1992, pp442-450.

[B1] Bhide, S. B. and Collins, M. P., "Influence of Axial Tension on the Shear Capacity of Reinforced Concrete Members," ACI Structural Journal, V. 86, No. 5, September-October, 1989, pp570-581.

[B2] British Standards Institute, "Methods for tensile Testing of Metals," BS, 18:1971, Part 2: Steel, London.

[B3] Brown, R. and Jirsa, J.O., "Reinforced Concrete Beams Under Load Reversals," ACI Journal, Vol.68, No.5, May, 1971, pp380-390.

[B4] Bull, D., "Los Angeles Earthquake Relevant to NZ," Journal of the Cement & Concrete Association of New Zealand, Vol.38, April-May, 1994, pp42-45.

[C1] Clough, R.W., "Effect of Stiffness Degradation on Earthquake Ductility Requirements", Structural Engineering Laboratory, University of California, Berkley, Report No. 66-16, 1966.

[C2] Carr, A.J., RUAUMOKO, Computer Program Library, Department of Civil Engineering, University of Canterbury, Christchurch, May 1986.

[D1] Dodd, L.L., "The Dynamic Behaviour of Reinforced Concrete Bridge Piers Subjected to New Zealand Seismicity," Research Report 92-04, Department of Civil Engineering, University of Canterbury, New Zealand, 1992, pp460.

[D2] DZ 3101:1978 "Draft Code of Practice for the Design of Concrete Structure," Standards Association of New Zealand, Wellington, 1978.

[E1] Elzanaty, A.H., Nilson, A.H. and Slate, F.O., "Shear Capacity of Reinforced Concrete Beams Using High Strength Concrete," ACI Journal, March-April, 1986, pp290-296.

[F1] Fenwick, R.C., "The Shear Strength of Reinforced Concrete Beams," Ph.D Thesis, University of Canterbury, Christchurch, New Zealand, 1966.

[F2] Fenwick, R.C., "Shear Deformation in Seismic Frame Structures," Journal of Structural Engineering, ASCE Vol. 109, No. 4, April, 1983, pp965-977.

[F3] Fenwick, R.C. and Paulay, T., "Mechanisms of Shear Resistance of Concrete Beams," Proceedings of the American Society of Civil Engineer, Vol.94, No. ST10, October, 1968, pp2235-2350.

[G1] Gill, W.D., Park, R. and Priestley, M.J.N., "Ductility of Rectangular Reinforced Concrete Columns With Axial Load," Research Report, 79-1, Department of Civil Engineering, University of Canterbury, February, 1979, 136pp.

[G2] Gosain, N. K., Brown, R. H. and Jirsa, J. O., "Shear Requirements for Load Reversals on RC Members," Journal of Structural Division, ASCE Vol. 103, No. ST7, July, 1977, pp1461-1476.

[H1] Haddadin, M. J., Hong. S. T., and Mattock. A. H., "Stirrup Effectiveness in Reinforced Concrete Beams With Axial Force," Journal of Structural Division, ASCE Vol. 97, No. ST9,

September, 1971, pp 2277-2297.

[H2] Hirosawa, M. and Goto, T., "Strength and Ductility of Reinforced Concrete Members Subjected to Axial Load," Summaries of Technical Papers of Annual Meeting, AIJ, Nov., 1971, pp817-820.

[H3] Hsiung, W. and Frantz, G.C., "Transverse Stirrup Spacing in R/C Beams," Journal of Structural Engineering, ASCE Vol. 111, No. 2, February, 1985, pp 353-362.

[H4] Hudson, D.E., "Some Recent Near-source Strong Motion Acceleration", Proceedings of 9th Wold Conference on Earthquake Engineering, Vol.2, Tokyo-Kyoto, Aug., 1988, pp271-271.

[J1] Jennings, P.C., "Engineering Features of the San Fernando Earthquake," California Institute of Technology, Pasadena, California, 1971, 512pp.

[J2] Jirsa, J.O., Maruyama, K. and Ramirez, H., "The Influence of Load History on the Shear Behaviour of Short RC Columns," Proceedings of 7th World Conference on Earthquake Engineering, Istanbul, Turkey, Sept. 1980, Vol.6, pp339-346.

[J3] Joint Reconnaissance Team, "Damage Report on 1992 Erzincan Earthquake, Turkey", Joint Reconnaissance Team of Architectural Institute of Japan, Japan Society of Civil Engineers and Bogazici University, Istanbal, Turkey, 1992.

[J4] Jury, R.D., "Seismic Load Demand on Columns of Reinforced Concrete Multistorey Frames", Research Report 78-12, Department of Civil Engineering, University of Canterbury, 1978, pp109.

[K1] Kent, D.C., "Inelastic Behaviour of Reinforced Concrete Members With Cyclic Loading," Ph.D Thesis, Department of Civil Engineering, University of Canterbury, New Zealand, 1969.

[K2] Keshavarzian, M. and Schnobrich, W.C., "Inelastic Analysis of Coupled Shear Walls", Earthquake Engineering and Structural Dynamics, Vol.13, 1985, pp.427-448.

[K3] Kreger, M.E. and Linbeck, L., "Behaviour of R.C. Columns Subjected to Lateral and Axial Load Reversals", Proceedings of 3rd United States National Conference on Earthquake Engineering, Vol.2, 1986, pp1475-1486.

[L1] Li, K.N., Aoyama, H. and Otani, S., "Reinforced Concrete Columns Under Varying Axial Load and Bi-directional Lateral Load Reversals", Procs. of 9th Wold Conference on Earthquake Engineering, Tokyo-Kyoto, Vol.8, 1988, pp537-542.

[L2] Li, X.R., Park, R. and Tanaka, H., (1990), "Effects of Variations in Axial Load Levels on the Strength and Ductility of Reinforced Concrete Columns," Proceedings of Pacific Conference on Earthquake Engineering, November, Auckland, Vol 1990, pp.

[L3] Li, X.R., Park, R. and Tanaka, H., "Shear Strength of Reinforced Concrete Columns Under Varying Axial Load," New Zealand National Society for Earthquake Engineering, Technical Conference, Taupo, New Zealand, March, 1994.

[L4] Loeber, P.J., "Shear Transfer by Aggregate Interlock," M.E. Thesis, University of Canterbury, Christchurch, New Zealand, 1970.

[M1] Ma, S., Bertero, V.V. and Popov, E.P., "Experimental and Analytical Studies on the Hysteretic Behaviour of Reinforced Concrete Rectangular and T-Beams," Report No. EERC 76-2, Earthquake Engineering Research Centre, University of California, Berkeley, 1976, 241pp.

[M2] Mander, J.B., Priestley, M.J.N., and Park, R., " Seismic Design of Bridge Pier," Research Report 84-2, Department of Civil Engineering, University of Canterbury, February, 1984, 483pp.

[M3] Mander, J.B., Priestley, M.J.N., and Park, R., "Theoretical Stress-Strain Model for Confined Concrete," Journal of Structural Division, ASCE Vol.114, No.8, August, 1984, pp1804-1826.

[M4] Mander, J.B., Priestley, M.J.N., and Park, R., "Observed Stress-strain Behaviour of Confined Concrete", Journal of Structural Engineering, ASCE, Vol.114, No.8, August, 1988, pp1827-1849.

[M5] Maruyama, K., Ramirez, H. and Jirsa, J. O., "Short RC Columns Under Bilateral Load Histories," Journal of Structural Engineering, ASCE, Vol. 110, No. 1, January, 1984, pp 120-137.

[M6] Mattock, A.H., "Diagonal Tension Cracking in Concrete Beams With Axial Forces", Proceedings of the American Society of Civil Engineer, Vol 95, No. ST9, Sept. 1969, pp1887-1900.

[M7] Mattock, A.H. and Hawkins, N.M., "Shear Transfer in Reinforced Concrete- Recent Research", Journal, Prestressed Concrete Institute, Vol.17, No.2, March-April, 1972, pp55-75.

[M8] Mattock, A.H., Hofbeek, J.F. and Ibrahim, I.O., "Shear Transfer in Reinforced Concrete," ACI Journal, Vol.66, No.2, Feb., 1969, pp119-128.

[M9] Mattock, A.H., Johal, L. and Chow, H.C., "Shear Transfer in R.C. With Moment or Tension Acting across the Shear Plane", Journal, Prestressed Concrete Institute, Vol.20, No.4, July-Aug., 1975, pp76-93.

[M10] Mattock, A.H. and Wang, Z.H., "Shear Strength of Reinforced Concrete Members Subjected to High Axial Compression Stress," ACI Journal, May-June, 1984, pp287-298.

[O1] O'Leary, A.J., "Shear, Flexure and Axial Tension In Reinforced Concrete Members," A Thesis Presented in Partial Fulfillment of the Requirements for the Degree of Doctor of Philosophy in Civil Engineering at the University of Canterbury, Christchurch, 1971.

[O2] Otani, S., "Hysteresis Models of Reinforced Concrete for Earthquake Response Analysis," Journal of the Faculty of Engineering, The University of Tokyo, Vol.2, No.2, 1981,pp125-159.

[P1] Park, R., "Ductile Design Approach for Reinforced Concrete Frames", Earthquake Spectra,

Earthquake Engineering Research Institute, Vol.2, No.3, 1986, pp565-619.

[P2] Park, R., State-of-Art Report, "Ductility Evaluation From Laboratory and Analytical Testing," Proceedings of Ninth World Conference on Earthquake Engineering, Tokyo-Kyoto, Japan, Vol.8, 1988, pp605-616.

[P3] Park, R., "The Paulay Years," Proceedings of the Tom Paulay Symposium: Recent Developments in Lateral Force Transfer in Building, Sept. La Jolla, California, 1993, pp1-29.

[P4] Park, R., "Proposed Changes to the Seismic Provisions of the Concrete Design Standard NZS 3101," New Zealand National Society for Earthquake Engineering, Technical Conference, Taupo, New Zealand, 1994, pp110-121.

[P5] Park, R., Kent, D.C. and Sampson, R.A., "Reinforced Concrete Members With Cyclic Loading," Structural Division, Proceedings, ASCE, Vol.98, ST7, 1972, pp1341-1359.

[P6] Park, R. and Paulay, T., "Reinforced Concrete Structures," John Wiley, New York, 1975, 769pp.

[P7] Park, R. and Paulay, T., "Strength and Ductility of Concrete Substructures of Bridges." Road Research Unit Bulletin 84 Vol. 1, Christchurch, 1990.

[P8] Park, R. and Priestley, M.J.N., "Code Provisions for Confining Steel in Potential Plastic Hinge Regions of Columns in Seismic Design", Bulletin of New Zealand National Society for Earthquake Engineering, Vol.3, No..1, March, 1988, pp60-70.

[P9] Park, R. and Priestley, M.J.N. and Gill, W.D., "Ductility of Square-Confined Concrete Columns", Proceedings, ASCE, Vol.108, ST.4, April, 1982, pp929-950.

[P10] Park, R. and Sampson, R.A., "Ductility of Reinforced Concrete Column Sections In Seismic Design", ACI Journal, Vol.69, No.9, Sept., 1972, pp543-551.

[P11] Park, R., Zahn, F.A. and Falconer, T.J., "Strength and Ductility of Reinforced and Prestressed Concretes and Piles Under Seismic Loading", Proceedings of 8th Wold Conference on Earthquake Engineering, Vol.6, San Francisco, July, 1984, pp513-520.

[P12] Paulay, T., "Seismic Design of Ductile Moment Resisting Reinforced Concrete Frame, Columns: Evaluation of Actions," Bulletin of the New Zealand National Society for Earthquake Engineering, Vol.10, No.2, June, 1977, pp69-105.

[P13] Paulay, T., "The Design of Ductile Reinforced Concrete Structural Walls for Earthquake Resistance", Earthquake Spectra, Vol.2, No.4, 1986, pp783-823.

[P14] Paulay, T. and Loeber, P.J., "Shear Transfer by Aggregate Interlock," shear in Reinforced Concrete, ACI Publication SP-42, Vol. 1, 1974, pp1-15.

[P15] Paulay, T. and Park, R., "Strength and Ductility of Concrete Bridge Column Under Seismic Loading", Structural Journal, ACI, Vol.84, No.1, Jan-Feb., 1987, pp61-76.

[P16] Paulay, T., Park, R. and Phillips, M.H., "Horizontal Construction Joints in Cast in Place Reinforced Concrete," Shear in Reinforced Concrete, ACI Special Publication SP-42, Detroit, Vol.2, 1974, pp599-616.

[P17] Paulay, T. and Priestley, M.J.N, "Seismic Design of Reinforced Concrete and Masonry Building", John Wiley & Sons, 1992, pp744.

[P18] Placas, A. and Regan, P.E., "Shear Failure in Reinforced Concrete Beams," ACI Journal, Proceedings, Vol.68, No.10, Oct., 1971, pp763-773.

[P19] Potangaroa, R.T., Priestley, M.J.N. and Park, R., "Ductility of Spirally Reinforced Concrete Columns Under Seismic Loading," Research Report, 79-8, Department of Civil Engineering, University of Canterbury, Christchurch, 1979, 116pp.

[P20] Priestley, M.J.N. and Park, R., "Strength and Ductility of Bridge Substructures," Road Research Unit Bulletin 71, National Roads Board, Wellington, 1984, pp120.

[P21] Priestley, M.J.N. and Park, R., "Strength and Ductility of Concrete Bridge Substructures," Research Report, 84-20, Department of Civil Engineering, University of Canterbury, Christchurch, New Zealand, 1984.

[P22] Priestley, M.J.N. and Park, R., "Strength and Ductility of Concrete Bridge Columns Under Seismic Loading," ACI Structural Journal, Vol.84, No.1, Jan-Feb., 1987, pp61-76.

[P23] Preistley, M.J.N., Seible, F., Verma, R. and Xiao, Y., "Seismic Shear Strength of Reinforced Concrete Columns," Report SSRP-93/06, Department of Applied Mechanics and Engineering Science, University of California, San Diego, July 1993.

[P24] Paulay, T., "Moment Redistribution in Continues Beams of Earthquake Resistant Multistorey Reinforced Concrete Frames", Bulletin of the New Zealand Society for Earthquake Engineering, Vol. 9, No.4, 1976, pp205-212.

[P25] Paulay, T., (1994), Private Communication.

[R1] Riddel, R. and Newmark, N.M., "Statistical Analysis of the Response of Nonlinear Systems subjected to Earthquakes", Structural Research Series No. 468, University of Illinois, Urbana, 1979, pp19-79.

[R2] Roufaiel, M.S.L. and Meyer, C., "Analytical Modelling of Hysteretic Behaviour of R/C Frames", Journal of Structural Engineering, ASCE, Vol.113, No.3, March, 1987, pp429-444.

[R3] Russo, G., Zingone, G. and Puleri, G., "Flexure-Shear Interaction Model for Longitudinally Reinforced Beams," ACI Structural Journal, V.88, No. 1, January-February, 1991, pp60-68.

[S1] Saadeghvaziri, M.A. and Foutch, D.A., "Behaviour of RC Columns Under Nonproportionally Varying Axial Load", Journal of Structural Engineering, ASCE, Vol.116, No.7, 1990, pp1835-1856.

[S2] Saadeghvaziri, M.A. and Foutch, D.A., "Dynamic Behaviour of R/C Highway Bridge Under

the Combined Effect of Vertical and Horizontal Earthquake Motions", Earthquake Engineering and Structural Dynamics, Vol.20, 1991, pp535-549.

[S3] Saatcioglu, M.,(1991) "Modelling Hysteretic Force-Deformation Relationship for Reinforced Concrete Elements," ACI SP-127: Earthquake Resistant Concrete Structures- Inelastic Response and Design, American Concrete Institute, Detroit, pp.153-198.

[S4] Saatcioglu, M., Derecho, A.T. and Corley, W.G., "Modelling Hysteretic Behaviour of Coupled Walls for Dynamic Analysis", Earthquake Engineering and Structural Dynamics, Vol. 11, 1983, pp711-726.

[S5] Saiidi, M., "Hysteresis Models for Reinforced Concrete," Journal of the Structural Division, ASCE, Vol.108, No. ST5, May, 1982, pp1077-1087.

[S6] Saiidi, M. and Sozen, M.A., "Simple and Complex Models for Nonlinear Seismic Response of Reinforced Concrete Structures", Structural Research Series No.465, University of Illinois, Urbana,1979.

[S7] Sakai, K. and Sheikh, S.A., "What Do We Known About Confinement in Reinforced Concrete Columns? (A Critical Review of Previous Work and Code Provisions)," ACI Structural Journal, March-April, 1989, pp192-207.

[S8] Scott, B.D., Park, R. and Priestley, M.J.N., "Stress-Strain Behaviour of Concrete Confined By Overlapping Hoops at Low and High Strain Rate," ACI Journal, Jan-Feb, 1982, pp13-27.

[S9] SEAOC, "Recommended Lateral Force Requirements and Commentary," Seismology Committee, Structural Engineers Association of California, California, 1975, 21pp plus commentary and appendices.

[S10] Sheikh, S. A. and Khoury, S. S., "Confined Columns With Stubs," ACI Structural Journal, V.90, No.4, July-August, 1993, pp414-431.

[S11] Sheikh, S.A., Yeh, C.C. and Menzies, D., "Confined Concrete Columns," Proceedings, Pacific Conference on Earthquake Engineering, New Zealand, Vol 1, Aug., 1987, pp177-188.

[S12] Soesianawati, M.T., Park, R. and Preistley, M.J.N, "Limited Ductility Design of Reinforced Concrete Columns," Research Report 86-10, Department of Civil Engineering, University of Canterbury, March, 1986, 208pp.

[S13] Standards Association of New Zealand, "Specification for Methods of Test for Concrete," NZS 3112: 1980, Part 2: Test Relating to the Determination of Strength of Concrete, Wellington, 1982.

[S14] Standards Association of New Zealand, "Code of Practice for the Design of Concrete Structures," NZS 3101, 1982, Wellington.

[S15] Swamy, R.N. and Andriopoulos, A.D., "Contribution of Aggregate Interlock and Dowel Forces to the Shear Resistance of Reinforced Concrete Beams With Web Reinforcement," American

Concrete Institute, Publication SP-42, Vol.1, Detroit, 1974, pp129-166.

[S16] Standards Association of New Zealand, "Code of Practice for General Structural Design and Design Loadings for Building", NZS 4203: 1992, Loading Standard, 1992, Wellington.

[S17] Sharpe, R.D., "The Seismic Response of Inelastic Structures", Research Report 74-13, Department of Civil Engineering, University of Canterbury, 1974.

[T1] Takayanagi, T. and Schnobrich, W.C., "Computed Behaviour of Reinforced Concrete Coupled Shear Walls", Structural Research Series No.434, University of Illinois, Urbana, 1976.

[T2] Takeda, T., Sozen, M.A., and Nielsen, N.N., "Reinforced Concrete Response to Simulated Earthquakes", Journal of the Structural Division, ASCE, Vol.96, No. ST12, December, 1970, pp2557-2573.

[T3] Tanaka, H. and Park, R., "Effect of Lateral Confining Reinforcement on the Ductile Behaviour of Reinforced Concrete Columns," Research Report, 90-2, Department of Civil Engineering, University of Canterbury, June, 1990, 458pp.

[T4] Tanaka, H., Park, R. and McNamee, B., "Anchorage of Transverse Reinforcement in Rectangular Reinforced Concrete Columns in Seismic Design," Bulletin of New Zealand National Society for Earthquake Engineering, Vol.18, June, 1985, pp165-190.

[T5] Taylor, H.P.J., "The Fundamental Behaviour of Reinforced Concrete Beams in Bending and Shear," Shear in Reinforced Concrete, ACI, Publication SP-42, Vol.2, Detroit, 1974, pp43-77.

[U1] Umehara, H. and Jirsa, J. O., "Short Rectangular RC Columns Under Bidirectional Loadings," Journal of Structural Engineering, ASCE, Vol. 110, No. 3, March, 1984. pp 605-619.

[U2] Uniform Building Code, International Conference of Building Officials, Whittier, Calif., 1988, 926pp.

[V1] Viest, I.M. and Baldwin, J.W., "Effect of Axial Compression on Shear Strength of Reinforced Concrete Frame Members," ACI Journal, Proceedings, Vol.55, No.11, Nov. 1958, pp635-654.

[W1] Wang, Z.H., "An Experimental Study of the Influence of Axial Compressive Force on the Shear Strength of Concrete Members Under Eccentric Loading," Chongqing Institute of Architecture & Engineering, Chongqing, China, 1980, 26pp(in Chinese).

[W2] Watson, S. and Park, R., "Design of Reinforced Concrete Frame of Limited Ductility", Research Report, 89-4, Department of Civil Engineering, University of Canterbury, Christchurch, Jan. 1989, 227pp.

[W3] Wight, J.K. and Sozen, M.A., "Strength Decay of RC Columns Under Shear Reversals," Journal of the Structural Division, ASCE, Vol.101, No. ST5, May, 1975, pp1053-1065.

[W4] Wong, Y.L., Paulay, T. and Priestley, M.J.N., "Squat Circular Bridge Piers Under Multi-Directional Seismic Attack," Research Report 90-4, Department of Civil Engineering, University of Canterbury, June, 1990, 276pp.

[W5] Wong, Y.L., Paulay, T. and Priestley, M.J.N., "Response of Circular Reinforced Concrete Columns to Multi-Directional Seismic Attack," ACI Structural Journal, Vol. 90, No. 2, March-April, 1993, pp180-191.

[W6] Woodward, K.A. and Jirsa, J.O., "Influence of Reinforcement on RC Short Column Lateral Resistance," Journal of Structural Engineering, ASCE, Vol.110, No.1 Jan., 1984, pp90-104.

[W7] Wall, F.J., "Statistical Data Analysis Handbook", McGraw-Hill Book Company, 1986, 576pp.

[Y1] Yamada, M., (1974), Shear in Reinforced Concrete "Shear Strength, Deformation and Explosion of Reinforced Concrete Short Columns," American Concrete Institute, Publication SP-42, Vol.2, Detroit, pp 617-638.

[Y2] Yamada, M. and Furui, S., "Shear Resistance and Explosive Cleavage Failure of Reinforced Concrete Members Subjected to Axial Load," Final Report, Eight Congress of International Association for Bridge and Structural Engineering, New York, 1968, pp1091-1102.

[Z1] Zagajeski, S.W., Bertero, V.V. and Bouwkamp, J.G., "Hysteretic Behaviour of R.C. Columns Subjected to High Axial and Cyclic Shear Forces," Report No UCB/EERC-78/05, University of California, Berkeley, 1978.

[Z2] Zahn, F.A., Park, R. and Priestley, M.J.N., "Strength and Ductility of Reinforced Concrete Piers- A Summary Report," Research Report 83-7, Department of Civil Engineering, University of Canterbury, December, 1983, 43pp.

[Z3] Zahn, F.A., Park, R. and Priestley, M.J.N., "Design of Reinforced Concrete Bridge Columns for Strength and Ductility," Research Report 86-7, Department of Civil Engineering, University of Canterbury, March, 1986, 402pp.

[Z4] Zahn, F.A., Park, R., Priestley, M.J.N. and Chapman, H.E., "Development of Design Procedures for the Flexural Strength and Ductility of R.C. Bridge Columns", Bulletin, New Zealand National Society for Earthquake Engineering, Vol.10, No.3, Sept., 1986, pp200-212.

[Z5] Zahn, F.A., Park, R. and Priestley, M.J.N., "Strength and Ductility of Square Reinforced Concrete Column Sections Subjected to Biaxial Bending", Structural Journal, ACI, Vol.86, No.2, March-April, 1989, pp123-131.

[Z5] Zhu B.L., Wu, M. S. and Zhang K.L., "A Study of Hysteretic Curve of Reinforced Concrete Members Under Cyclic Loading," Research Journal of TongJi University, China, Vol.1, pp63-75.

[Z6] Zsutty, T.C.,"Beam Shear Strength Prediction By Analysis of Existing Data," ACI Journal, Proceedings, Vol.65, No.11, Nov., 1968, pp943-951.

Appendix A

```
      SUBROUTINE HYST(F,DF,MOMENT,XS,R,EIN,MY,H,PP,EIG,AG,FPC,RHO,PB,
     *               U,ALFA,BETA,PINCH,FLAST,FOLD,POLD,MUN1,MUN2,M1,
     *               M2,FUN1,FUN2,F1,F2,TPFUN1,TPFUN2,PUN1,PUN2,EIP1,
     *               EIP2,EIU1,EIU2,EIR1,EIR2,EI,FY,N)
C
C     ****************************************************************
C     Reinforced Concrete Beam-column
C
C       F        = Curvature
C       DF       = Increment in Curvature
C       MOMENT   = Moment
C       R        = Stiffness Factor
C       XS       = Moment Overshoot
C       EIN      = Moment of Inertia of Reduced Section
C       MY       = Yield Moment at P
C       H        = Strain Hardening Coefficient
C       P        = Applied Axial Load, (Positive => Compression)
C       EIG      = Moment of Inertia of Gross Section
C       AG       = Gross Section Area
C       FPC      = f'c Concrete Compressive Strength (MPa)
C       RHO      = Longitudinal Reinforcement Content (%)
C       PB       = Balance Axial Load, (Compression)
C       U        = Unloading Coefficient
C       ALFA     = Factor for Unloading Stiffness
C       BETA     = Factor for Relocation of FUN at Unloading Point
C       PINCH    = Factor for Pinching
C       FLAST    = Curvature at the Last Increment
C       FOLD     = Curvature at the Second to Last Increment
C       POLD     = Applied Axial Load at Last Increment
C       MUN1,MUN2 = Moment at Unloading Point
C       FUN1,FUN2 = Curvature at Unloading Point
C       PUN1,PUN2 = Axial Load at Unloading Point
C       EIR1,EIR2 = Reloading Stiffness
C       EIU1,EIU2 = Unloading Stiffness
C       EIP1,EIP2 = Post-yield Stiffness
C       EI       = Flexural Stiffness at axial load P
C       FY       = Curvature at axial load P
C       N        = Status of Loading on Moment-Curvature Curve
C
C     Input:  F,DF,EIN,EIG,AG,FPC,RHO,MY,P,PB,ALFA,BETA,PINCH,H,U
C     Output: MOMENT,R,XS,MUN1,MUN2,M1,M2,FLAST,FOLD,POLD,FUN1,FUN2,
C          F1,F2,TPFUN1,TPFUN2,PUN1,PUN2,EIP1,EIP2,EIU1,EIU2,EI,N
C
C     PROGRAMMED BY :  Li Xinrong
C     DATA/VERSION  :  04-SEP-1994/1.0
C     ****************************************************************
C
      INTEGER        N
CS    REAL           F,DF,MOMENT,XS,R,EIN,MY,H,PP,EIG,AG,FPC,RHO,PB,U
CS    REAL           BETA,PINCH,FLAST,FOLD,POLD,MUN1,MUN2,FUN1,FUN2
```

```
CS   REAL          PUN1,PUN2,M1,M2,F1,F2,EIR1,EIR2,EIU1,EIU2,EIP1
CS   REAL          EIP2,TPFUN1,TPFUN2,EI,FY,FPL1,FPL2,MTEP,EITAN
CS   REAL          ALFA,ZERO,P,ONE,P05,P18,TOL
CD   DOUBLE PRECISION F,DF,MOMENT,XS,R,EIN,MY,H,PP,EIG,AG,FPC,RHO,PB,U
CD   DOUBLE PRECISION BETA,PINCH,FLAST,FOLD,POLD,MUN1,MUN2,FUN1,FUN2
CD   DOUBLE PRECISION PUN1,PUN2,M1,M2,F1,F2,EIR1,EIR2,EIU1,EIU2,EIP1
CD   DOUBLE PRECISION EIP2,TPFUN1,TPFUN2,EI,FY,FPL1,FPL2,MTEP,EITAN
CD   DOUBLE PRECISION ALFA,ZERO,P,ONE,P05,P18,TOL
     DATA          ZERO,ONE,P05,P18,TOL/0.0,1.0,0.5,1.8,0.000001/
C
     P    = -PP
     F    = F+DF
     XS   = MOMENT+R*EIN*DF
     MTEP = MY
C
     IF(N.EQ.0) N=11
     IF(N.EQ.11.OR.N.EQ.12) THEN
       EI    = (0.35+0.02*FPC-0.115*RHO)*P/(1000.0*FPC*AG)
       EI    = (EI+0.13*RHO-0.004*FPC+0.2)*EIG
       EITAN = EI
       FY    = MY/EI
       MUN1  = MY
       MUN2  = -MY
       FUN1  = FY
       FUN2  = -FY
       PUN1  = P
       PUN2  = P
       EIP1  = H*EI
       EIP2  = H*EI
       M1    = MUN1
       M2    = MUN2
       F1    = FUN1
       F2    = FUN2
       TPFUN1 = FUN1
       TPFUN2 = FUN2
     ENDIF
C
     IF(ABS(F-FLAST).LE.TOL) F = 1.0001*FLAST
     IF((F-FLAST)*(FLAST-FOLD).GT.0.0) THEN
       IF(N.EQ.21) THEN
         IF(P.LT.POLD) EIP1 = (1.0+10.0*(P-POLD)/PB)*EIP1
         EITAN  = EIP1
         MOMENT = MOMENT+EIP1*(F-FLAST)
         N      = 21
       ELSEIF(N.EQ.11) THEN
         IF(F.GT.FUN1) THEN
           EITAN  = EIP1
           MOMENT = M1+EIP1*(F-F1)
           N      = 21
         ELSEIF(F.LT.FUN2) THEN
           EITAN  = EIP2
           MOMENT = M2+EIP2*(F-F2)
           N      = 22
         ELSEIF(F.LT.0.0.AND.F.GE.FUN2) THEN
           EITAN  = EI
           MOMENT = F*EI
           N      = 12
         ELSEIF(F.LT.FLAST) THEN
```

```
      FLAST  = MAX(FLAST,TOL)
      EITAN  = MOMENT/FLAST
      MOMENT = EITAN*F
      N      = 11
    ELSE
      EITAN  = (MUN1-MOMENT)/(FUN1-FLAST)
      MOMENT = MOMENT+EITAN*(F-FLAST)
      N      = 11
    ENDIF
  ELSEIF(N.EQ.22) THEN
    IF(P.LT.POLD) EIP2 = (1.0+10.0*(P-POLD)/PB)*EIP2
    EITAN  = EIP2
    MOMENT = MOMENT+EIP2*(F-FLAST)
    N      = 22
  ELSEIF(N.EQ.12) THEN
    IF(F.GT.FUN1) THEN
      EITAN  = EI
      MOMENT = M1+EIP1*(F-F1)
      N      = 21
    ELSEIF(F.GE.0.0.AND.F.LE.FUN1) THEN
      EITAN  = EI
      MOMENT = F*EI
      N      = 11
    ELSEIF(F.LT.FUN2) THEN
      EITAN  = EIP2
      MOMENT = M2+EIP2*(F-F2)
      N      = 22
    ELSEIF(F.GT.FLAST) THEN
      EITAN  = EI
      MOMENT = EI*F
      N      = 12
    ELSE
      EITAN  = (MUN2-MOMENT)/(FUN2-FLAST)
      MOMENT = MOMENT+EITAN*(F-FLAST)
      N      = 12
    ENDIF
  ELSEIF(N.EQ.31) THEN
    EIU1 = MIN(EI,MAX((ONE-ALFA*(P-POLD)/PB)*EIU1,MOMENT/FLAST))
    FPL1 = FLAST-MOMENT/EIU1
    IF(F.GE.FPL1) THEN
      EITAN  = EIU1
      MOMENT = MOMENT-EIU1*(FLAST-F)
      N      = 31
    ELSE
      FUN2   = MIN(P18,MAX(P05,ONE-BETA*(P-PUN2)/PB))*TPFUN2
      MTEP   = MTEP-H*(FY+FUN2)
      EIR2   = MTEP/(FPL1-FUN2)
      IF(F.GT.0.0) EIR2 = MIN(ONE-PINCH*(PUN2-P)/PB,ONE)*EIR2
      EITAN  = MAX(EIR2,ZERO)
      MOMENT = EITAN*(F-FPL1)
      N      = 42
    ENDIF
  ELSEIF(N.EQ.32) THEN
    EIU2 = MIN(EI,MAX((ONE-ALFA*(P-POLD)/PB)*EIU2,MOMENT/FLAST))
    FPL2 = FLAST-MOMENT/EIU2
    IF(F.LE.FPL2) THEN
      EITAN  = EIU2
      MOMENT = MOMENT-EIU2*(FLAST-F)
```

```
          N      = 32
        ELSE
          FUN1   = MIN(P18,MAX(P05,1.0-BETA*(P-PUN1)/PB))*TPFUN1
          MTEP   = MTEP+H*(FUN1-FY)
          EIR1   = MTEP/(FUN1-FPL2)
          IF(F.LT.0.0) EIR1 = MIN(ONE-PINCH*(PUN1-P)/PB,ONE)*EIR1
          EITAN  = MAX(EIR1,ZERO)
          MOMENT = EITAN*(F-FPL2)
          N      = 41
        ENDIF
      ELSEIF(N.EQ.41) THEN
        FUN1   = MAX(P05,MIN(P18,ONE-BETA*(P-PUN1)/PB))*TPFUN1
        IF(ABS(FUN1-FLAST).LE.TOL) FUN1 = 1.0001*FLAST
        MTEP   = MTEP+H*(FUN1-FY)
        EIR1   = (MTEP-MOMENT)/(FUN1-FLAST)
        IF(F.LT.0.0) EIR1 = MIN(ONE-PINCH*(PUN1-P)/PB,ONE)*EIR1
        EIR1   = MIN(0.8*EI,MAX(EIR1,ZERO))
        IF(F.LE.FUN1) THEN
          EITAN  = EIR1
          MOMENT = MOMENT+EIR1*(F-FLAST)
          N      = 41
        ELSE
          F1     = FUN1
          M1     = MOMENT+EIR1*(FUN1-FLAST)
          EIP1   = H*EI
          IF(P.LT.POLD) EIP1=(1.0+10.0*(P-POLD)/PB)*EIP1
          EITAN  = EIP1
          MOMENT = M1+EIP1*(F-F1)
          N      = 21
        ENDIF
      ELSEIF(N.EQ.42) THEN
        FUN2   = MIN(P18,MAX(P05,ONE-BETA*(P-PUN2)/PB))*TPFUN2
        IF(ABS(FUN2-FLAST).LE.TOL) FUN2 = 1.0001*FLAST
        MTEP   = MTEP-H*(FY+FUN2)
        EIR2   = (MTEP+MOMENT)/(FLAST-FUN2)
        IF(F.GT.0.0) EIR2 = MIN(ONE-PINCH*(PUN2-P)/PB,ONE)*EIR2
        EIR2   = MIN(0.8*EI,MAX(EIR2,ZERO))
        IF(F.GE.FUN2) THEN
          EITAN  = EIR2
          MOMENT = MOMENT+EIR2*(F-FLAST)
          N      = 42
        ELSE
          F2     = FUN2
          M2     = MOMENT+EIR2*(FUN2-FLAST)
          EIP2   = H*EI
          IF(P.LT.POLD) EIP2=(1.0+10.0*(P-POLD)/PB)*EIP2
          EITAN  = EIP2
          MOMENT = M2+EIP2*(F-F2)
          N      = 22
        ENDIF
      ENDIF
C                 *Loading Reverse
    ELSE
      IF(N.EQ.11) THEN
C                 *Loading Reverse from Descending
        IF(F.GE.FLAST) THEN
          IF(F.GE.FUN1) THEN
            EIP1   = H*EI
```

```
            EITAN  = EIP1
            MOMENT = M1+EIP1*(F-FUN1)
            N      = 21
          ELSE
            EITAN  = EI
            MOMENT = EITAN*F
            N      = 11
          ENDIF
C               *Loading Reverse from Ascending
        ELSE
          IF(F.GE.0.0) THEN
            EITAN  = EI
            MOMENT = EITAN*F
            N      = 11
          ELSEIF(F.LT.FUN2)THEN
            EIP2   = H*EI
            EITAN  = EIP2
            MOMENT = MUN2+EIP2*(F-FUN2)
            N      = 22
          ELSE
            EITAN  = EI
            MOMENT = EITAN*F
            N      = 12
          ENDIF
        ENDIF
      ELSEIF(N.EQ.21.AND.F.GE.FLAST) THEN
        EITAN  = EIP1
        MOMENT = MOMENT+EIP1*(F-FLAST)
        N      = 21
      ELSEIF(N.EQ.21.AND.F.LT.FLAST) THEN
        FUN1   = FLAST
        TPFUN1 = FUN1
        MUN1   = MOMENT
        PUN1   = POLD
        M1     = MOMENT
        F1     = FUN1
        EIU1   = (U*ABS(FY/FUN1)+0.1)*(1.0-ALFA*(P-POLD)/PB)*EI
        EIU1   = MIN(EI,MAX(EIU1,M1/F1))
        FPL1   = MAX(F1-M1/EIU1,ZERO)
        IF(F.GE.FPL1) THEN
          EITAN  = EIU1
          MOMENT = M1-EIU1*(F1-F)
          N      = 31
        ELSE
          FUN2   = MIN(P18,MAX(P05,1.0-BETA*(P-PUN2)/PB))*TPFUN2
          MTEP   = MTEP-H*(FY+FUN2)
          EIR2   = MTEP/(FPL1-FUN2)
          IF(F.GT.0.0) EIR2 = MIN(1.0-PINCH*(PUN2-P)/PB,ONE)*EIR2
          EIR2   = MAX(EIR2,ZERO)
          IF(F.GE.FUN2) THEN
            EITAN  = EIR2
            MOMENT = EIR2*(F-FPL1)
            N      = 42
          ELSE
            F2     = FUN2
            M2     = EIR2*(FUN2-FPL1)
            EIP2   = H*EI
            EITAN  = EIP2
```

```
      MOMENT = M2+EIP2*(F-F2)
      N      = 22
    ENDIF
  ENDIF
ELSEIF(N.EQ.41) THEN
  M1     = MOMENT
  F1     = FLAST
  EIU1   = (U*ABS(FY/F1)+0.1)*EI
  EIU1   = MIN(EI,MAX(EIU1,M1/F1))
  FPL1   = F1-M1/EIU1
  IF(F.GE.FPL1) THEN
    EITAN  = EIU1
    MOMENT = M1-EIU1*(F1-F)
    N      = 31
  ELSEIF(F.LT.(FUN2+FPL1)) THEN
    EITAN  = EIP2
    MOMENT = M2+EIP2*(F-(FUN2+FPL1))
    N      = 22
  ELSE
    EIR2   = MUN2/(FUN2-FPL1)
    EITAN  = MAX(EIR2,ZERO)
    MOMENT = EITAN*(F-FPL1)
    N      = 42
  ENDIF
ELSEIF(N.EQ.32) THEN
  IF(F.GE.FUN2) THEN
    MOMENT = MOMENT+EITAN*(F-FLAST)
    N      = 42
  ELSE
    MOMENT = M2+EIP2*(F-F2)
    N      = 22
  ENDIF
ELSEIF(N.EQ.31) THEN
  IF(F.LE.FUN1) THEN
    MOMENT = MOMENT+EITAN*(F-FLAST)
    N      = 41
  ELSE
    MOMENT = M1+EIP1*(F-F1)
    N      = 21
  ENDIF
ELSEIF(N.EQ.12) THEN
  IF(F.LT.FLAST) THEN
    IF(F.LT.FUN2) THEN
      EIP2   = H*EI
      EITAN  = EIP2
      MOMENT = M2+EIP2*(F-FUN2)
      N      = 22
    ELSE
      EITAN  = EI
      MOMENT = EITAN*F
      N      = 12
    ENDIF
  ELSE
    IF(F.LE.0.0) THEN
      EITAN  = EI
      MOMENT = EITAN*F
      N      = 12
    ELSEIF(F.GT.FUN1) THEN
```

```
      EIP1   = H*EI
      EITAN  = EIP1
      MOMENT = MUN1+EIP1*(F-FUN1)
      N      = 21
    ELSE
      EITAN  = EI
      MOMENT = EITAN*F
      N      = 11
    ENDIF
  ENDIF
ELSEIF(N.EQ.22.AND.F.LE.FLAST) THEN
  EITAN  = EIP2
  MOMENT = MOMENT+EIP2*(F-FLAST)
  N      = 22
ELSEIF(N.EQ.22.AND.F.GT.FLAST) THEN
  FUN2   = FLAST
  TPFUN2 = FUN2
  MUN2   = MOMENT
  PUN2   = POLD
  M2     = MOMENT
  F2     = FLAST
  EIU2   = (U*ABS(FY/FLAST)+0.1)*(1.0-ALFA*(P-POLD)/PB)*EI
  EIU2   = MIN(EI,MAX(EIU2,ABS(MOMENT/FLAST)))
  FPL2   = MIN(FLAST-MOMENT/EIU2,ZERO)
  IF(F.LE.FPL2) THEN
    EITAN  = EIU2
    MOMENT = MOMENT-EIU2*(FLAST-F)
    N      = 32
  ELSE
    FUN1   = MIN(P18,MAX(P05,ONE-BETA*(P-PUN1)/PB))*TPFUN1
    MTEP   = MTEP+H*(FUN1-FY)
    EIR1   = MTEP/(FUN1-FPL2)
    IF(F.LT.0.0) EIR1 = MIN(ONE-PINCH*(PUN1-P)/PB,ONE)*EIR1
    EIR1   = MAX(EIR1,ZERO)
    IF(F.LE.FUN1) THEN
      EITAN  = EIR1
      MOMENT = EIR1*(F-FPL2)
      N      = 41
    ELSE
      F1     = FUN1
      M1     = EIR1*(FUN1-FPL2)
      EIP1   = H*EI
      EITAN  = EIP1
      MOMENT = M1+EIP1*(F-F1)
      N      = 21
    ENDIF
  ENDIF
ELSEIF(N.EQ.42) THEN
  M2     = MOMENT
  F2     = FLAST
  EIU2   = (U*ABS(FY/F2)+0.1)*EI
  EIU2   = MIN(EI,MAX(EIU2,ABS(MOMENT/FLAST)))
  FPL2   = FLAST-MOMENT/EIU2
  IF(F.LE.FPL2) THEN
    EITAN  = EIU2
    MOMENT = MOMENT-EIU2*(FLAST-F)
    N      = 32
  ELSEIF(F.GT.(FUN1+FPL2)) THEN
```

```
          EITAN  = EIP1
          MOMENT = M1+EIP1*(F-(FUN1+FPL2))
          N      = 21
        ELSE
          EIR1   = MUN1/(FUN1-FPL2)
          EITAN  = MAX(EIR1,ZERO)
          MOMENT = EITAN*(F-FPL2)
          N      = 41
        ENDIF
      ENDIF
    ENDIF
C
C    WRITE(3,'(1X,'**'I3,F11.2,2X,5F9.2)') N,EI,FY,FPL1,FUN1,FPL2,FUN2
C
    IF(ABS(F).LE.0.0) F = 0.00001
    FOLD  = FLAST
    FLAST = F
    POLD  = P
    XS    = XS-MOMENT
    R     = EITAN/EIN
C
    RETURN
    END
```

Classn:

REINFORCED CONCRETE COLUMNS UNDER SEISMIC LATERAL FORCE AND VARYING AXIAL LOAD

Xinrong Li

ABSTRACT: An experimental investigation on two series of reinforced concrete columns under simultaneously cyclic lateral loading and varying axial load is presented. The first series of six specimens were tested to obtain the variations in flexural hysteretic behaviour with fluctuation in axial load level. The second phase of three specimens were tested to study the degrading concrete shear resistance. A research on moment-curvature hysteretic model including varying axial load effect was also conducted.

Department of Civil Engineering, University of Canterbury
Doctor of philosophy Thesis, 1994